Multiscale derivation, analysis and simulation of collective dynamics models: geometrical aspects and applications

A dissertation presented for the degree of Doctor of Philosophy by

Antoine Nicolas Diez

under the advice of

Prof. Pierre Degond
Prof. Sara Merino-Aceituno
Dr. Amic Frouvelle

Department of Mathematics
Imperial College London

February 2022

Declaration of originality

I certify that this dissertation, and the research to which it refers, are the product of my own work, and that any ideas or quotations from the work of other people, published or otherwise, are fully acknowledged in accordance with the standard referencing practices of the discipline.

Antoine Nicolas Diez

Copyright declaration

Abstract

This thesis is a contribution to the study of swarming phenomena from the point of view of mathematical kinetic theory. This multiscale approach starts from stochastic individual based (or particle) models and aims at the derivation of partial differential equation models on statistical quantities when the number of particles tends to infinity. This latter class of models is better suited for mathematical analysis in order to reveal and explain large-scale emerging phenomena observed in various biological systems such as flocks of birds or swarms of bacteria. Within this objective, a large part of this thesis is dedicated to the study of a body-attitude coordination model and, through this example, of the influence of geometry on self-organisation.

The first part of the thesis deals with the rigorous derivation of partial differential equation models from particle systems with mean-field interactions. After a review of the literature, in particular on the notion of propagation of chaos, a rigorous convergence result is proved for a large class of geometrically enriched piecewise deterministic particle models towards local BGK-type equations. In addition, the method developed is applied to the design and analysis of a new particle-based algorithm for sampling. This first part also addresses the question of the efficient simulation of particle systems using recent GPU routines.

The second part of the thesis is devoted to kinetic and fluid models for body-oriented particles. The kinetic model is rigorously derived as the mean-field limit of a particle system. In the spatially homogeneous case, a phase transition phenomenon is investigated which discriminates, depending on the parameters of the model, between a "disordered" dynamics and a self-organised "ordered" dynamics. The fluid (or macroscopic) model was derived as the hydrodynamic limit of the kinetic model a few years ago by Degond et al. The analytical and numerical study of this model reveal the existence of new self-organised phenomena which are confirmed and quantified using particle simulations. Finally a generalisation of this model in arbitrary dimension is presented.

Acknowledgments

First and foremost, I thank my supervisors, Pierre, Sara and Amic. The three of them warmly welcomed me in the team, introduced me to many fascinating topics in collective dynamics and have always shown trust and support during these (almost) four years. It goes without saying that not all the perfect conditions for a normal PhD were met during the last two years. Nevertheless, from the beginning and til the end, the three of them have always found time and patience to share their infinite knowledge and brilliant thoughts. Their kindness and dedication have pushed me always further, both helping me to stay on track and encouraging me to explore new areas. For all the mathematics I learned and for all the rest, I am infinitely grateful.

I thank Greg Pavliotis and Thierry Goudon for having accepted to review this manuscript and to conduct the viva. Greg Pavliotis followed the embryonic development of this work for the Early and Late Stage Review processes, alongside Jose Carrillo and Jeroen Lamb. I am thankful to them for their useful and supportive comments. I would also like to thank Pierre-Emmanuel Jabin who hosted me four weeks in Maryland.

While my sole name is on the front page of this thesis, the outcome would have been much different without the co-authors I had the pleasure to work with, and who have become good friends. I have learned a lot thanks to Louis-Pierre's constant enthusiasm, his sparking mathematical creativity and highly transmissible curiosity. Coding was not something I was comfortable with before, but I hope to have made progress thanks to Jean's deep expertise, his pedagogical and always encouraging advice. For both of them, we may have met somehow unexpectedly, but it has finally changed and improved much more of this thesis that I could have imagined initially. Finally, I also co-authored an article with Grégoire but I would feel a bit strange to describe, and compliment, him as a co-author here. First he would not like that, but mostly, he already knows that he is much more than a co-author.

I did not have the chance to collaborate with the following researchers, but we shared a lunch, a dinner, a discussion or a tea, which is perhaps just as important: thank you Anna, Lorenzo, Sophie, Ariane, Pedro, Angelika, Rafa, Matt and Lifan.

Finally, I thank my other friends, in academia or not, and my family, who, consciously or not, have had a positive influence on this thesis and on my life in general. I am thankful to them, regardless of whether they can, will, cannot or can no longer read this thesis.

This thesis was funded by EPSRC-Roth schorlarship jointly by the Department of Mathematics at Imperial College London and the Engineering and Physical Sciences Research Council. In addition to these two institutions and since I am almost sure that these funds are, ultimately, public funds, I would also like to transparently acknowledge the society for offering me this opportunity. As a young scientist, during these last four years, I am conscious that I had the chance to work on a subject that I chose, with a freedom that many people could envy, and in a rather privileged environment. Beyond the financial aspect and maybe even more importantly, my work also significantly contributed to the carbon debt that we all globally share[1].

[1]To give a very partial but striking example of the specific impact of research, I found enlightening to look at the carbon emissions coming from plane *only* and taken only for research purposes (which is likely to be the largest share of the carbon footprint). In the case of my work, these carbon emissions are roughly equivalent to the annual *total* carbon footprint of a British citizen living with an income in the first quintile group. This is already well above the estimated total annual carbon budget per capita compatible with the 1.5°C goal. Note that all my plane trips were concentrated in one year and that in normal circumstances, this carbon footprint would probably have been at least doubled (it would be equivalent to the total annual carbon emissions of a median British citizen).

Sources:

- The carbon emissions due to plane are estimated using `https://flightfree.org/flight-emissions-calculator` which is based on the computations of the International Council on Clean Transportation.
- The per capita carbon emissions for different income levels are estimated by Oxfam in the technical report attached to the 2015 briefing on *Extreme Carbon Inequality* accessible at `https://oxfamilibrary.openrepository.com/bitstream/handle/10546/582545/tb-carbon-emissions-inequality-methodology-021215-en.pdf?sequence=2`
- The per capita carbon emissions in relation with the 1.5°C goal are analysed by Oxfam in the report *Carbon Inequality in 2030* accessible at `https://oxfamilibrary.openrepository.com/bitstream/handle/10546/621305/bn-carbon-inequality-2030-051121-en.pdf`.

Contents

Introduction

Chapter 1

Background

1.1 Active particle systems and kinetic theory

The starting point of all the subjects discussed in this work will always be a large system of interacting particles and most often, a system of *active* particles. Taking its roots in the kinetic theory of gas due to Boltzmann [44], the notion of *particle* is understood as a convenient elementary modelling entity which can represent for instance an atom, a molecule, a cell in a living organism and even the organism itself: a bird in a bird flock or a human being in a crowd. The interactions can be dictated by the laws of physics, for instance for the molecules in a gas. But in the case of the so-called active particles, the interactions mostly depend on social or behavioural rules commonly found in the living world: e.g. the response of bacteria to chemical signals, the tendency of an animal in a herd to stay close to its fellow animals or the evolution of the opinion of an individual in a debate. When the number of particles in the system grows to infinity, the numerous elementary interactions between the particles can create large-scale complex *swarming* structures which motivate this work (see Figure 1.1). Since these phenomena could not be predicted only by looking at the individual behaviour of the particles (due to their large number), these phenomena are often said to *emerge* or to be *self-organised*.

The study of large particle systems in physics (in thermodynamics typically) is an old (but still active) problem and the pioneering works of Boltzmann and Maxwell have stimulated the development of mathematical concepts and techniques, in particular in stochastic analysis and Partial Differential Equations (PDE). One of the main ideas of the so-called mathematical *kinetic theory* is that a *high-dimensional linear* problem given by a system of $N \gg 1$ ordinary or stochastic differential equations can be turned into only one *nonlinear* PDE. This idea will be largely detailed in Part I of this thesis.

However, the study of active particle systems is much more recent and mainly driven by biological or socio-economical questions. The main difference with classical physical systems is that active particle systems are not bound to physical laws such as the conservation of energy or momentum. It does not mean that biological systems break the laws of physics but that at this modelling scale we simply consider that the particles (bacteria, animals, etc) can use their own energy to interact: we do not really take into consideration this energy loss but only take into account e.g. the evolution of their positions and velocities or the kind of forces which result from the interactions. In this context, the classical results, sometimes, still apply and lead to the study of new types of nonlinear PDEs. However the lack of conservation laws makes the analysis much different and requires new ideas and techniques. In the present work, another layer of difficulty will be added by addressing the influence of *geometry* in active particle systems. Examples of PDE models of swarming with geometrical constraints will be the subject of Part II of this thesis.

Stimulated by these ideas, the last two decades have seen the active development of the *mathematics of swarming*, in particular in the kinetic theory community. Since then, these ideas have been applied to many systems in various contexts. Beyond the seminal biological motivations, one recent trend, which will also be developed in this thesis, is the study of artificial particle systems introduced in data science algorithms.

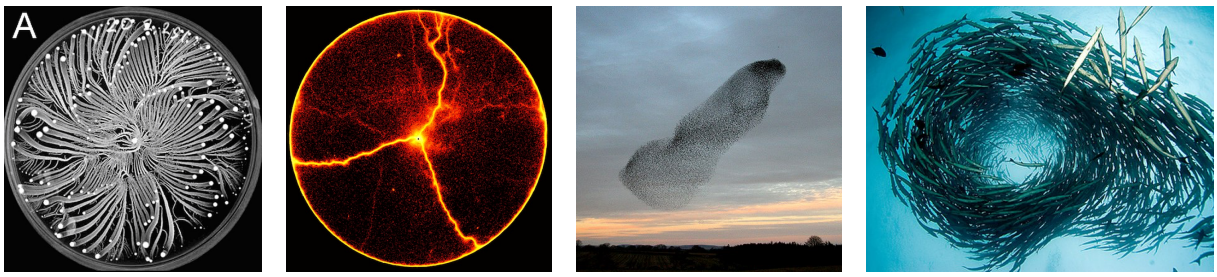

(A) (B) (C) (D)

FIGURE 1.1: Various examples of self-organised phenomena in the living world. (A) A colony of *Paenibacillus vortex* bacteria. Each bright dot is made of many individuals swarming collectively by rotating [204]. *(Colin J. Ingham and Eshel Ben Jacob, CC BY 2.0, via Wikimedia Commons).* (B) Pheromone trails formed by Argentine ants [279]. *(Andrea Perna, Roehampton University, CC BY 2.5, via Wikimedia Commons).* (C) Murmuration of starlings. *(Walter Baxter, CC BY-SA 2.0, via Wikimedia Commons).* (D) A mill of schooling barracuda. *(Robin Hughes, CC BY-SA 2.0, via Wikimedia Commons).*

In a broader perspective, the concept of emergence and self-organisation across scales is actually one of the most fundamental questions in life sciences. Almost all living creatures are made of an aggregate of cells of different sizes and shapes, often interacting with other

symbiotic or adversary microorganisms. During the early embryonic development, the growth, division and spatial organisation of the cells create a very structured mature organism with various specialised organs. This highly complex biological process runs through extended space and time scales. Nevertheless, at the macroscopic scale, living organisms are characterised by both a great variability of traits among the individuals and a great reproducibility of shapes and functions. This remarkable macroscopic robustness, in spite of the inherent microscopic stochasticity, naturally raises fundamental questions about the mechanisms which rule this multiscale development and cause these biological phase transitions. Within this perspective, the development of rigorous mathematical models is of primary importance: on the one hand, to understand how the living world and its constituent systems work and interact together, and, on the other hand, to identify the dysfunctions, their cause and potential treatments. Classically, energy exchanges and chemical signalling have been basic and key modelling components. At an even more fundamental level, mechanical, geometrical and topological constraints certainly also play an important role that may not have been so extensively studied.

The present thesis remains, of course, only a modest contribution to the mathematical formalisation and conceptualization of all these issues. While the present work is mostly based on mathematical kinetic theory, there is nowadays an intense research effort across all mathematics to study the fundamental principles of biology. To cite a few: reaction-diffusion equations, fluid dynamics, optimization, graph and network theory, stochastic and computer models all offer complementary points of view. In addition to these model-driven approaches, data-driven approaches are also of course essential. Over the last few years, all these mathematical approaches have been applied in various and critical medical fields such as oncology, neurosciences, epidemiology, microbiology, etc.

This introductory chapter presents the main tools and concepts on which the rest of the thesis will be based. The first three sections follow the classical multiscale kinetic theory approach using as a running example the Vicsek model [321, 122, 140], on which most of the models studied in this thesis will be based. Section 1.2 focuses on particle systems. Section 1.3 explains how kinetic PDE models are derived when the number of particles grows to infinity. The so-called hydrodynamic limit of these kinetic models is developed in Section 1.4, which leads to the derivation of macroscopic (or fluid dynamics) PDE models. Finally the last Section 1.5 reviews some other classical swarming models and discusses recent applications in data science.

1.2 Individual Based Models

To begin with, this section reviews and introduces the particle systems which motivate this work. At this modelling level, sometimes referred as the *microscopic level*, the main objective is to introduce a proper mathematical formalisation of the interaction rules between the particles. The resulting models are referred as *Individual Based Models* (IBM).

From a mathematical point of view, a system of N particles is simply a Markov process (or a deterministic dynamical system) with values in a product space E^N. The state of a particle in the space E can be its position $E = \mathbb{R}^d$ in which case it will be usually denoted $\mathcal{X}_t^N = (X_t^1, \dots, X_t^N)_t$ where t is the time index. In kinetic theory the state space E is the phase space $E = \mathbb{R}^d \times \mathbb{R}^d$ in which case the state of the i-th particle is the couple (X_t^i, V_t^i) of its position and velocity. Such particle will be referred as a *kinetic particle*. One of the objectives of this work is to generalise this framework to more general state spaces endowed with a geometrical structure, for instance, by replacing the velocity by an element of a manifold. The following sections further elaborate on this idea and introduce the kinetic theory approach by taking as a running example the Vicsek model [321, 122, 140] which is the starting point of the models studied in this thesis.

1.2.1 Swarming models

Over the last twenty years, there has been a growing interest in both the mathematics and physics communities for theorizing the underlying principles of large animal societies. Among the most common examples of such systems, one can cite flocks of birds, fish schools, large herds of mammals or ant colonies. In all these systems, the individuals collectively produce large-scale coherent complex structures, called swarms, without any obvious exterior organizing principle such as a leader. Other examples can be found in the microscopic world (for instance colonies of bacteria or spermatozoa) or in human societies (for instance crowds phenomena or traffic flows). In all these systems, each individual can be roughly described as a kinetic particle (X_t^i, V_t^i) and the evolution over time of the system is typically modelled via Newton's laws (plus noise) $\mathrm{d}X_t^i = V_t^i \mathrm{d}t$ and $\mathrm{d}V_t^i = F(\mathcal{X}_t^N)\mathrm{d}t$, where F is a force or a sum of forces. This modelling perspective gives much freedom on the choice of the interaction mechanism itself (i.e. on the force F). From an analytical point of view, a fruitful idea is to look for minimal models, i.e. with interaction mechanisms taken as elementary as possible to exhibit a given collective behaviour. They are often based on the following assumptions.

1. **(Self-propulsion).** Active particles are said to be *self-propelled*, which means that they use their own energy to move. The force F does not need to be conservative and may for instance include a relaxation part towards a preferred moving speed.

2. **(Bounded vision).** The particles have a bounded, small, sensing region and interact only with the other particles which belong to this region. The easiest way to model this is to take an *observation kernel* $K : [0, +\infty) \to [0, +\infty)$ (also called *interaction* kernel) which vanishes at infinity, for instance $K(r) = \mathbb{1}_{[0,R]}(r)$ for a fixed interaction radius R, and to consider that the sensing region of a particle at position X_t^i depends on the map $x \mapsto K(|x - X_t^i|)$. A more elaborated point of view is the so-called three-zone model [65]. One may also consider non symmetric interaction kernels, for instance in order to model a cone of vision [90, 83, 84].

3. **(Randomness).** The individual based models in the present work are stochastic models. Randomness may be incorporated to model the environmental noise, the perception error of the agents or the uncertainty in general.

Then, the two following classical and elementary interaction rules are often assumed to give rise to collective dynamics.

1. **(Attraction-Repulsion).** A particle tends to avoid the other particles in its sensing region (for instance to avoid collisions) or on the contrary to move closer to the center of mass of its neighbours (in order to keep a coherent swarm).

2. **(Alignment).** A particle tends to align its direction of motion with the ones of the other particles in order to create a coherent motion. This is called a *flocking model* and this will be the main object of the present thesis.

These modelling assumptions have been used since the 80's in various contexts. Among the first works, one should cite the simulation of fish schools by Aoki [8] and the renowned *boids* model developed by Reynolds [285] which has been widely used for realistic computer graphics simulations in cinema or video games. Since then, there has been an intense research effort in the physics community to understand active particle systems, in particular based on the models introduced by Vicsek [321] and Couzin [92, 91]. A gallery of models can be found for instance in the reviews [322] or [4]. In addition to the Vicsek model discussed in the following sections within a mathematical kinetic theory perspective, other important swarming models in the mathematics literature will be reviewed in Section 1.5.1. Finally, in Section 1.5.2 we will discuss various so-called Swarm Intelligence algorithms which are based on the simulation of artificial particle systems with interaction mechanisms specifically designed to solve tough problems in data sciences.

1.2.2 The Vicsek model

In the 90's, Vicsek et al. [321] introduced a discrete-time "flocking algorithm", with an interaction mechanism based only on alignment, and the minimal assumption that the particles move at a fixed constant speed $c_0 > 0$. Despite its simplicity, the Vicsek model has quickly become one of the most prominent models in the active matter literature. Several works have numerically exhibited the emergence of complex patterns at the particle level; see for instance [80] where the emergence of high-density band-like structures on a compact spatial domain is studied.

From a mathematical point of view, since the speed of the particles is fixed, then the velocity of each particle is characterised by a unit vector which defines its direction of motion. The state of a particle (X_t^i, V_t^i) at any time t thus belongs to $E = \mathbb{R}^d \times \mathbb{S}^{d-1}$ where $\mathbb{S}^{d-1}$ denotes the unit sphere in dimension d. This seemingly small change, from a velocity in $\mathbb{R}^d$ to a direction of motion in the manifold $\mathbb{S}^{d-1}$, nevertheless leads to complex mathematical developments, as reviewed in the following. Moreover it paves the way to the development of a larger class of *geometrically enriched models* where the traditional velocity variable in kinetic theory now encompasses additional degrees of freedom or interaction specifications. A large part of this thesis is dedicated to the study of *body-oriented* particles, which model rigid bodies with an orientation defined by a rotation matrix in the manifold $\mathrm{SO}_3(\mathbb{R})$. Other examples can be found in the liquid crystal literature [13, 14] or in the modelling of the *nematic* alignment of bacteria [121] by un-oriented rod-like particles with a velocity which belongs the projective space $\mathbb{S}^{d-1}/\pm 1$.

In the seminal article of Vicsek et al. [322], the model introduced was a computational discrete-time model not well suited to mathematical analysis. A few years later, in the mathematics community, Degond and Motsch [122] thus introduced another version of the Vicsek model using a more classical continuous-time diffusion framework. This model will be discussed later. The basis of the present work is the following variant of the Vicsek model which has been introduced by Di Marco and Motsch [140] as an alternative to the diffusion framework. It is based on a Piecewise Deterministic Markov Process (PDMP) also known as a *run-and-tumble* process in the literature.

- To each agent $i \in \{1, \dots, N\}$ is attached an independent Poisson process with fixed intensity $\nu > 0$ and jump times $(T_n^i)_n$.
- Between two jump times, the evolution is deterministic: for all $i \in \{1, \dots, N\}$ and for all $t \in [T_n^i, T_{n+1}^i)$,

$$\mathrm{d}X_t^i = c_0 V_t^i \mathrm{d}t, \quad \mathrm{d}V_t^i = 0. \tag{1.1}$$

- At each jump time T_n^i, the agent labelled by $i \in \{1, \dots, N\}$ updates its orientation by taking a random perturbation of the average local orientation of its neighbours. Formally, the new orientation is obtained by drawing a random variable from a von Mises distribution

$$V_{T_n^i}^i \sim M_{\kappa(J_n^i)\,\mathbb{V}_n^i}, \tag{1.2}$$

where the parameters κ, J_n^i and $\mathbb{V}_n^i$ will be defined next. The von Mises distribution M_J with parameter $J \in \mathbb{R}^d$ is a probability distribution on the sphere $\mathbb{S}^{d-1}$ defined by its probability density function

$$M_J(v) := \frac{\exp(J \cdot v)}{\int_{\mathbb{S}^{d-1}} \exp(J \cdot v')\mathrm{d}v'}.$$

The von Mises distribution M_J is a spherical analog to the Gaussian distribution in a vector space [247, 246, 230]: it tends towards the Dirac delta distribution at the point $J/|J|$ as $|J| \to +\infty$ and towards the uniform distribution on $\mathbb{S}^{d-1}$ as $|J| \to 0$. In the present case, the parameter of the distribution is defined by a concentration parameter $\kappa : \mathbb{R}^d \to [0, +\infty)$ which sets the level of noise and the vectors J_n^i and $\mathbb{V}_n^i$ which define the average local direction of motion:

$$J_n^i := \lim_{t \to (T_n^i)^-} \frac{1}{N} \sum_{j=1}^{N} K\big(|X_t^i - X_t^j|\big) V_t^j \in \mathbb{R}^d, \quad \mathbb{V}_n^i := \frac{J_n^i}{|J_n^i|} \in \mathbb{S}^{d-1}, \tag{1.3}$$

where K is a given interaction kernel. Common choices for the concentration parameter κ are

$$\kappa(J) = \kappa_0 = \text{constant}, \quad \kappa(J) = \kappa_0 |J|.$$

A schematic representation of this process is depicted below.

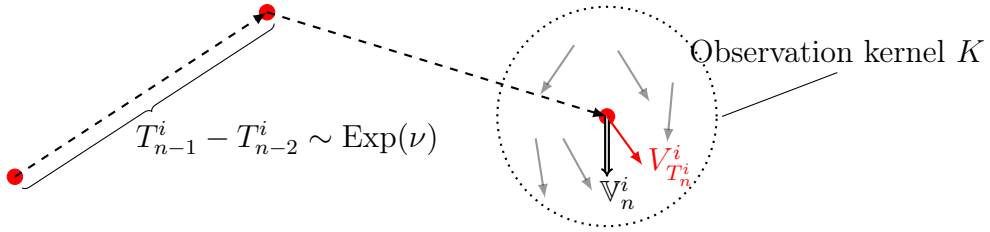

FIGURE 1.2: Alignment through a Piecewise Deterministic Markov Process. The dashed line depicts the trajectory of a particle (red points). At each jump time the new direction of motion $V_{T_n^i}^i$ is a random perturbation of the average direction of motion $\mathbb{V}_n^i$ within an observation kernel.

This simple interaction procedure will be the basis of most of the models studied in this thesis. Preceding the work of Di Marco and Motsch, the first mathematical formalisation of the original Vicsek model [321] based on a diffusion process was introduced by Degond and Motsch [122]. In this work, the N-particle process is defined by a set of $2N$ coupled Stratonovich Stochastic Differential Equations (SDE) :

$$\mathrm{d}X_t^i = c_0 V_t^i \mathrm{d}t, \tag{1.4a}$$

$$\mathrm{d}V_t^i = \nu\big(|J_t^i|\big)\mathsf{P}(V_t^i)\mathbb{V}_t^i \mathrm{d}t + \sqrt{2\sigma\big(|J_t^i|\big)}\mathsf{P}(V_t^i) \circ \mathrm{d}B_t^i, \tag{1.4b}$$

where $(B_t^i)_t$ are N independent Brownian motions in $\mathbb{R}^d$, $\mathsf{P}(v) := I_d - v \otimes v$ is the projection on the plane orthogonal to a unit vector v, the functions $\nu, \sigma : [0, +\infty) \to [0, +\infty)$ are respectively the intensity of the alignment and the strength of the diffusion and

$$J_t^i := \frac{1}{N}\sum_{j=1}^{N} K\big(|X_t^j - X_t^i|\big)V_t^j \in \mathbb{R}^d, \quad \mathbb{V}_t^i := \frac{J_t^i}{|J_t^i|} \in \mathbb{S}^{d-1}. \tag{1.5}$$

The drift term in equation (1.4b) is a relaxation force towards the local average velocity $\mathbb{V}_t^i$. The source of the noise comes from a Brownian motion. The Stratonovich framework and the projection operator $\mathsf{P}(V_t^i)$ ensure that V_t^i remains of norm one.

In the following, it will be shown that the scaling limits of the PDMP and diffusion variants of the Vicsek model, are, on many aspects, equivalent. However, the PDMP framework will lead to structurally simpler PDE models which justifies this modelling choice.

1.2.3 Mean-field particle systems

As N grows to infinity, the individual trajectories of the particles become intractable due to the high-dimension: for instance, in the Vicsek model, the N coupled trajectories $(X_t^1, V_t^1, \ldots, X_t^N, V_t^N)_t$ define a process in dimension $2Nd$. The system is therefore better understood using a statistical description inherited from the theory of Markov processes.

First of all, for a fixed finite value of N, the theory of Markov processes gives two ways to characterise globally the system. The first one is the law f_t^N of the particle system at any time t which is a probability measure on E^N. The second one is the N-particle generator $\mathcal{L}_N$. The two characterisations are linked by the linear Kolmogorov equations. The forward Kolmogorov equation is often called the *Liouville equation* in a kinetic theory context. The particle systems studied in this work are moreover said to be *exchangeable* which means that f_t^N is a symmetric probability measure (i.e. invariant by any permutation of its arguments). The exchangeability property assumes that all the particles are identical

and play an identical role. Thanks to a famous result due to De Finetti [136] and Hewitt and Savage, but used in a kinetic theory context since the work of Grünbaum [179], the law of an exchangeable particle system $\mathcal{X}_t^N = (X_t^1, \dots, X_t^N)$ on a state space E is essentially characterised by its empirical measure

$$\mu_{\mathcal{X}_t^N} := \frac{1}{N} \sum_{i=1}^{N} \delta_{X_t^i}, \tag{1.6}$$

where δ_x denotes the Dirac delta distribution at a point $x \in E$. Further technical details will be given in Chapter 3. Compared to the full particle system, the random empirical measure belongs to a space which does not depend on N, namely the space of probability measures on E as opposed to the product space E^N. Working with the empirical measure therefore transforms the study of N (finite-dimensional) processes into the study of only one process but which belongs to an infinite-dimensional space.

The empirical measure gives access to statistical averages of the form

$$\langle \mu_{\mathcal{X}_t^N}, \varphi \rangle := \int_E \varphi(x)\, \mu_{\mathcal{X}_t^N}(\mathrm{d}x) = \frac{1}{N} \sum_{i=1}^{N} \varphi(X_t^i),$$

where φ is a test function on the state space E. In the Vicsek model, the interactions are therefore fully described by the empirical measure since, for instance, (1.5) can be re-written as

$$J_t^i = \int_{\mathbb{R}^d \times \mathbb{S}^{d-1}} K(|x - X_t^i|) v\, \mu_{\mathcal{Z}_t^N}(\mathrm{d}x, \mathrm{d}v),$$

where $\mathcal{Z}_t^N = ((X_t^1, V_t^1), \dots (X_t^N, V_t^N))$. All the particle systems considered in this work will also be such that the interactions can be prescribed by the empirical measure. These particle systems are called *mean-field particle systems* (see Section 3.3 for a more formal definition). Notice that mean-field particle systems do not include binary "collisional" interactions as in classical collisional kinetic theory [324] (see also Section 10.2.4). In the next section, we will see how this statistical description behaves for mean-field systems when $N \to +\infty$.

1.3 Mesoscopic limit

As N grows to infinity, the empirical measure (1.6) defines a sequence of a random probability measures on E. The *mesoscopic description* of the N-particle system is given by the limit $N \to +\infty$ of this sequence (which will be assumed or shown to exist). This

limiting object thus describes the average statistical behaviour of the system for a large number of particles. As we shall see, studying its properties is both easier and more informative on the global behaviour of the system than tracking the individual information of the particles.

For the various mean-field models studied in the present work, we will either prove or assume that the following (weak) limit holds true:

$$\mu_{\mathcal{X}_t^N} \underset{N\to+\infty}{\longrightarrow} f_t, \tag{1.7}$$

for any $t > 0$ and where the limit $f_t \equiv f(t, x, v)$ is a *deterministic* solution of a PDE. For the different variants of the Vicsek model, this limit is the solution of a *nonlinear* kinetic PDE of the form

$$\partial_t f_t + c_0 v \cdot \nabla_x f_t = Q(f_t), \tag{1.8}$$

where $Q(f_t)$ is a nonlinear operator, usually called the *collision operator*. For the PDMP Vicsek model (1.1)-(1.2), the equation is the following nonlinear BGK-type equation [34]

$$\partial_t f_t + c_0 v \cdot \nabla_x f_t = \nu\big(\rho_{f_t} M_{\kappa(J_{K\star f_t})\mathbb{V}_{K\star f_t}} - f_t\big), \tag{1.9}$$

where $\rho_{f_t}(x) = \int_{\mathbb{S}^{d-1}} f_t(x, v)\mathrm{d}v$ and

$$J_{K\star f_t}(x) := \int_{\mathbb{R}^d\times\mathbb{S}^{d-1}} K\big(|x-y|\big) v\, f_t(y, v)\mathrm{d}y\mathrm{d}v, \quad \mathbb{V}_{K\star f_t}(x) := \frac{J_{K\star f_t}}{|J_{K\star f_t}|}. \tag{1.10}$$

For the diffusion model (1.4), this equation is replaced by a nonlinear Fokker-Planck equation

$$\partial_t f_t + c_0 v \cdot \nabla_x f_t = -\nu\big(|J_{K\star f_t}|\big)\nabla_v \cdot \big(\mathsf{P}(v)\mathbb{V}_{K\star f_t} f_t\big) + \sigma\big(|J_{K\star f_t}|\big)\Delta_v f_t, \tag{1.11}$$

where $\nabla_v\cdot$ and Δ_v denote respectively the divergence and Laplace-Beltrami operator on the manifold $\mathbb{S}^{d-1}$.

The kernels of the collision operators corresponding to the two variants, PDMP or diffusion process, can be shown to be the same. Moreover, these operators act on the x variable only through the convolution (in x) with K in (1.10). In some cases investigated in Chapter 4, it is possible to take simultaneously the limits $N \to +\infty$ and $K \to \delta_0$ (the interaction is said to be *moderate* [273, 221, 138]) in which case we simply write $J_{\delta_0\star f_t} \equiv J_{f_t}$. The interaction between the particles are then asymptotically purely local in space and Q becomes an operator which acts on the v variable only as it is classically assumed in kinetic

theory. We make this simplifying assumption in the subsequent examples.

The weak limit (1.7) is equivalent to a property called propagation of chaos which plays a major role in mathematical kinetic theory. It was used by Boltzmann and Maxwell before being mathematically rigorously formalised by Kac [223] and much developed by McKean [249] and Sznitman [307] for mean-field particle systems. This aspect will be discussed in great details in Part I and in particular in Chapter 3. For the time being, let us simply mention that it implies the following property: if the particles are initially independent, then at each later time $t > 0$, for each fixed number of $k \geq 1$ of particles, when $N \to +\infty$, any subset of k particles tends to k independent random variables with common law f_t. It means that despite the interactions, independence is still recovered for any finite group of particles. The solution f_t of the mesoscopic PDE (1.8) can therefore be understood as the law of an average particle (that is, the probability of finding a particle at a given state at a given time). It is thus often called the *particle distribution*. Note that the main difference with the N-particle distribution f_t^N is that f_t satisfies a nonlinear PDE in E whereas f_t^N satisfies the Kolmogorov equation which is a linear equation in E^N.

Thanks to this statistical description, the analytical (or numerical) study of the mesoscopic PDE can provide information on the long-time behaviour of the system. For the Vicsek model, the analytical study of the full kinetic PDEs (1.9) or (1.11) is still in progress and many questions are left open, in particular the long-time behaviour of the solutions. In a simpler spatially-homogeneous setting, where f_t solves the spatially homogeneous version of (1.8):

$$\partial_t f_t(v) = Q(f_t),$$

the long-time behaviour of the solution has been studied in particular in [160, 113] for different variants of the model. These results are based on the analysis of the equilibria of the collision operator Q, i.e. the functions f such that $Q(f) = 0$. The main result of [113] is a phase transition phenomenon which states that, depending on an explicit condition on the parameters ν and σ and the mass $\rho = \int f_t(v)\mathrm{d}v$, two kinds of asymptotic behaviours coexist: either

$$f_t \underset{t\to+\infty}{\longrightarrow} \rho, \quad \text{or} \quad f_t \underset{t\to+\infty}{\longrightarrow} \rho M_{\tilde{\kappa}\tilde{\mathbb{V}}}.$$

The first case corresponds to the convergence towards an asymptotic disordered isotropic equilibrium, which models a situation where the particles have a uniformly distributed orientation. The second case corresponds to the convergence towards an ordered flocking equilibrium where the particles move in average in the direction given by $\tilde{\mathbb{V}} \in \mathbb{S}^{d-1}$ with a concentration $\tilde{\kappa} > 0$ which are explicitly given by the parameters of the system. This result will be extended to the case of body-oriented particles in Chapter 7.

1.4 Macroscopic limit

The space and time scales at the mesoscopic level are the same as the ones of the particles at the microscopic level. For the PDMP Vicsek model it means that the interaction rate ν and the mean-free path of a particle set the time and space scale and therefore the typical size of the system. However, for biological systems, it is clear that the mean-free path of a particle should be much smaller than the size of the whole system. In order to capture this so-called macroscopic features of the system, one therefore needs to find an appropriate rescaling of the time and space scales. One choice is the hyperbolic scaling

$$\tilde{t} = \varepsilon t/t_0, \quad \tilde{x} = \varepsilon x/x_0,$$

where t, x are the microscopic time and space variables, t_0 and x_0 are the typical microscopic time and space units and $\varepsilon \ll 1$ is a scaling parameter. The resulting (dimensionless) variables $\tilde{t}$ and $\tilde{x}$ are the macroscopic time and space variables and the dimensionless speed is $\tilde{c}_0 = c_0 t_0/x_0$. Using these new variables, the rescaled distribution function

$$\tilde{f}^\varepsilon(\tilde{t}, \tilde{x}, v) := \left(\frac{x_0}{\varepsilon}\right)^d f\left(\frac{\tilde{t}t_0}{\varepsilon}, \frac{\tilde{x}x_0}{\varepsilon}, v\right),$$

satisfies, dropping the tilde for clarity,

$$\partial_t f^\varepsilon + c_0 v \cdot \nabla_x f^\varepsilon = \frac{1}{\varepsilon} Q(f^\varepsilon),$$

where we recall that the collision operator Q is given by (1.9) or (1.11) with $K = \delta_0$. For the Vicsek model, the formal limit $\varepsilon \to 0$ has been investigated in [122] for the Fokker-Planck model and in [140] for the BGK model. In both cases, the authors assume that

$$f^\varepsilon \underset{\varepsilon \to 0}{\longrightarrow} \rho M_{\kappa \mathbb{V}},$$

where $\rho \equiv \rho(t, x)$ and $\mathbb{V} \equiv \mathbb{V}(t, x)$ represent respectively the density of particles and average direction of motion at time t and position x. Then, it can be proved that $(\rho, \mathbb{V})$ are, also in both cases, the solutions of

$$\partial_t \rho + \nabla_x \cdot (c_1 \mathbb{V}) = 0 \tag{1.12}$$

$$(\partial_t + c_2 \mathbb{V} \cdot \nabla_x)\mathbb{V} + \lambda \mathsf{P}(\mathbb{V}) \nabla_x \log \rho = 0, \tag{1.13}$$

where c_1, c_2 and λ are explicit functions of κ and c_0. This formal derivation follows from the same arguments as the derivation of the compressible Euler equations from a kinetic PDE, as explained for instance in [108]. However, while the first equation (1.12) easily follows from the mass conservation, the second equation (1.13) is much more difficult to obtain due to the lack of conservation laws. In [122], Degond and Motsch introduced the concept of *Generalised Collision Invariant* (GCI) to cope with this difficulty and derived the equation (1.13). This methodology has been made rigorous in [214, 213] and has since then been applied to derive macroscopic models for a wide range of swarming models [114, 116, 121, 2, 140, 123]. As expected, the Equations (1.12) and (1.13) share similarities with the classical compressible Euler equations but with a new pressure term which involves the projection operator $\mathsf{P}(v) = I_d - v \otimes v$ in order to preserve the geometrical constraint $\mathbb{V} \in \mathbb{S}^{d-1}$. A numerical study of this model can be found in [263]. The macroscopic model associated to a body-orientation dynamics model derived using the same methodology in [114, 116] and in Chapter 7 will be studied in Chapter 8. It will be shown that more complex geometrical constraints lead to a novel class of explicit solutions characterised by a nontrivial topological structure.

1.5 Other collective dynamics models and applications

This section shortly reviews other related classical swarming models and introduces some recent applications of the mathematics of swarming to data science problems. This latter aspect will be further discussed in Chapter 6. Further examples can be found in the review article [76] on which this section is also based.

1.5.1 Classical models of swarming and self-organisation

The Vicsek model is only one of the several swarming models introduced in the past decades. For the sake of completeness, some important examples are discussed below. Note, however, that none of these models are geometrically enriched models like the Vicsek model.

Attraction-Repulsion.

One of the first deterministic mathematical swarming model is due to D'Orsogna et al. [99]. It is based on the combination of self-propulsion and an attraction-repulsion force. With

the mean-field scaling introduced in [68], the equations on the velocities in $\mathbb{R}^d$ are:

$$\frac{\mathrm{d}V_t^i}{\mathrm{d}t} = (\alpha - \beta|V_t^i|^2)V_t^i - \frac{1}{N}\nabla_{x^i}\sum_{j\neq i} U\big(|X_t^i - X_t^j|\big),$$

where $U(r) = -C_a\mathrm{e}^{-r/\ell_a} + C_r\mathrm{e}^{-r/\ell_r}$ is the Morse potential. The nonnegative constants α, β, C_a, ℓ_a, C_r, ℓ_r are respectively the self-propulsion and friction forces magnitudes, the strength of alignment, the typical alignment length, the strength of the repulsion and the typical repulsion length. Due to the propulsion and friction forces, each particle tends to adopt the fixed cruising speed $\sqrt{\alpha/\beta}$. Unlike the Vicsek model, the self-propulsion constraint is encoded as a "soft" constraint rather than as a "hard" geometrical constraint of the form $V_t^i \in \mathbb{S}^{d-1}$. The propagation of chaos property follows for instance from [40] and the limit PDE reads:

$$\partial_t f_t(x,v) + v\cdot\nabla_x f_t = -\nabla_v\cdot((\alpha - \beta|v|^2)vf_t) + (\nabla_x U \star \rho[f_t])\cdot\nabla_v f_t,$$

where $\rho[f_t](\mathrm{d}x) = \int_{\mathbb{R}^d} f_t(\mathrm{d}x,\mathrm{d}v)$. The analysis of the limit kinetic PDE and its macroscopic limit in [68] gives a rigorous theoretical explanation for the emergence of complex patterns such as rotating mills which were observed in numerical simulations only in [99].

Flocking.

Alternatively to the Vicsek model, Cucker and Smale [98] introduced a deterministic alignment mechanism for velocities in $\mathbb{R}^d$ given by:

$$\frac{\mathrm{d}V_t^i}{\mathrm{d}t} = \frac{1}{N}\sum_{j\neq i} K\big(|X_t^j - X_t^i|\big)(V_t^j - V_t^i),$$

where K is an observation kernel which is typically taken equal to $K(r) = (1+|r|^2)^{-\gamma/2}$, $\gamma > 0$. The main result is that if the observation kernel is large enough in the sense that $\int_0^{+\infty} K(r)\mathrm{d}r = +\infty$, then the particle system satisfies for all $i,j \in \{1,\dots,N\}$,

$$|V_t^i - V_\infty| \leq C_1\mathrm{e}^{-\lambda t}, \quad |X_t^i - X_t^j| \leq C_2,$$

for some constants $C_1, C_2, \lambda > 0$ and for an asymptotic velocity $V_\infty \in \mathbb{R}^d$. Note that since the momentum is preserved, $V_\infty = \frac{1}{N}\sum_{i=1}^N V_0^i$. There is an extensive literature on the deterministic Cucker-Smale model, see the reviews [65, 67, 4].

On the other hand, there are various ways to add a stochastic component to the

Cucker-Smale model. Maybe the most obvious way in this context, is to consider the diffusion model introduced in [185]:

$$\mathrm{d}V_t^i = \frac{1}{N}\sum_{j\neq i} K\big(|X_t^j - X_t^i|\big)(V_t^j - V_t^i) + \sigma \mathrm{d}B_t^i,$$

for N independent Brownian motions $(B_t^i)_t$. In this case, the propagation of chaos is proved in [40] using a so-called synchronous coupling method (see Chapter 3) or in [277] using martingale arguments. The difficulty here lies in the unboundedness of the kernel K. The limit Fokker-Planck equation reads:

$$\partial_t f_t(x,v) + v\cdot\nabla_x f_t = -\nabla_v\cdot(\xi[f_t]f_t) + \frac{\sigma^2}{2}\Delta_v f_t, \tag{1.14}$$

with

$$\xi[f_t](x,v) := \int_{\mathbb{R}^d\times\mathbb{R}^d} K(|x'-x|)(v'-v) f_t(\mathrm{d}x', \mathrm{d}v').$$

More refined models can also be considered to incorporate a self-propulsion force [17, 16], a non constant diffusion matrix, boundary conditions [83] or an anisotropic observation kernel (e.g. a cone of vision centered around the velocity of the particle) [84]. Macroscopic limits for various kinetic Cucker-Smale models have been obtained for instance in [46, 17, 228].

In [3], Ahn and Ha considered the Cucker-Smale model with a random environmental noise common to all the particles. In this case, the propagation of chaos does not hold in the usual sense. Given a realisation of the common noise, a *conditional* propagation of chaos property can be shown [87] by revisiting the classical arguments of Dobrushin [144] in the deterministic case. However the limit law f_t is not deterministic and satisfies a *stochastic* PDE which depends on the common noise (roughly speaking, it is the PDE (1.14) where the Laplacian is replaced by a Brownian motion). For the Cucker-Smale system, this type of result can be found in [85].

There exist many other Cucker-Smale models where the stochasticity is incorporated through a diffusive behaviour. For further examples, we refer the interested reader to the review [72] and the references therein. Lately, [165] proposed a stochastic Cucker-Smale model based on a PDMP mechanism.

The Kuramoto model

The Kuramoto model is the most classical model for synchronisation phenomena between populations of *oscillators*, which may be used to model a clapping crowd, a population

of fireflies or a system of neurons to cite a few examples. Despite its formal simplicity, the Kuramoto model exhibits a complex long-time behaviour which has motivated a vast literature, see for instance the reviews [1, 243], the articles [31, 32] and the references therein.

In the Kuramoto model, the particles are N *oscillators* defined by N angles $\Theta_t^N = (\theta_t^1, \dots, \theta_t^N) \in \mathbb{R}^N$ (defined modulo 2π so that they can actually be seen as elements of the circle) which satisfy the following system of SDEs:

$$\mathrm{d}\theta_t^i = \xi_i \mathrm{d}t - \frac{\lambda}{N} \sum_{j=1}^{N} \sin(\theta_t^i - \theta_t^j)\mathrm{d}t + \mathrm{d}B_t^i,$$

where $\lambda \in \mathbb{R}$ is a real parameter of the model and $(\xi_i)_{i\in\{1,\dots,N\}}$ are N i.i.d. random variables which model the natural frequency of the oscillators (also called the *disorder*). When a realisation of the natural frequency is chosen beforehand, then the model is said to be of *quenched* type and is equivalent to a spatially homogeneous Vicsek model in dimension 2. As a consequence, at least when $\xi_i = 0$ for all i, the propagation of chaos on any finite time interval easily follows (see McKean's Theorem in Chapter 3) and the limit Fokker-Planck equation admits as stationary solutions the family of von Mises distributions of the form $M_{\kappa e(\theta_0)}$ where $\kappa \geq 0$ is explicitly given, $\theta_0 \in \mathbb{R}$ is an arbitrary parameter and $e(\theta_0) := (\cos\theta_0, \sin\theta_0)^{\mathrm{T}}$. The trivial solution with $\kappa = 0$ is always a stationary solution but when $\lambda > 1$ there also exists a nontrivial solution with $\kappa > 0$ and the associated family of stationary solutions becomes *asymptotically stable*. This phase transition phenomenon and the long-time dynamics analysis of the solution of the Fokker-Planck equation can be found in [172, 113]. Recent works [32, 132] have studied, using a large deviation approach, the links between this phase transition phenomenon and the propagation of chaos property (see also Section 10.2.3). Earlier results in this direction can be found in [100, 103, 102].

1.5.2 Artificial particle systems in data sciences

Nowadays, the development of data sciences has pushed the development of ever more efficient algorithms. Typical tasks such as sampling or filtering are motivated by Monte Carlo problems and will be discussed in Chapter 6. For the sake of completeness, other important examples of particle methods in optimization and machine learning are discussed below, but will not be further addressed in this thesis (see however the last section of [76]). All these computational problems are challenging, in particular due to the curse of dimensionality, to the high computational cost of naive methods or to the difficulty of finding a satisfactory theoretical framework to prove the convergence of the algorithms.

To cope with these problems, various metaheuristic methods based on the simulation of systems of particles have been developed. Inspired by the biological models presented previously, the idea is to design *artificial* interaction mechanisms to be used to solve difficult numerical problems. The motivation is twofold: on the one hand, particle systems are easy to simulate and on the other hand, the mean-field theory gives a natural theoretical foundation for the convergence proof of the methods.

Particle based Monte Carlo methods

In the Bayesian analysis framework, a critical issue is the construction of *posterior distributions*. These probability distributions are most often not known in a closed form and may be difficult to evaluate (because they are obtained as the output of a computationally expensive code). As a consequence, a difficult but crucial task is the generation of i.i.d. random numbers $X^1, \dots, X^N$ distributed according to an arbitrary posterior distribution, usually denoted by π. Historically, this so-called *sampling problem* has been solved by the renowned Metropolis-Hastings algorithm [256, 255, 193] or its variants, see [289, 290, 288] for a review. Recently, new algorithms [54, 55, 134] have been proposed based on the idea of constructing *interacting* samples, that is, an artificial particle system $(X_t^1, \dots, X_t^N)_t$ such that asymptotically in N and in the time variable t,

$$\mathrm{Law}(X_t^1, \dots, X_t^N) \simeq \pi^{\otimes N}.$$

Chapter 6 will study such method based on a mean-field generalisation of the Metropolis-Hastings algorithm. The core idea of this method is to gain efficiency by dropping the independence between the samples. By introducing a well-chosen interaction mechanism, it is possible to prove that asymptotically in time and N, the independence is recovered thanks to a propagation of chaos property.

Other related works in this direction include [219, 220] which study scaling limits of the Metropolis-Hastings. Alternatively, the recent algorithm proposed and studied in [170, 142, 143] is based on the study of an interacting Langevin dynamics, which is an alternative to the Metropolis-Hastings algorithm based on a diffusion process. Finally, one may also consider non-static target distributions. This leads to so-called *filtering problems*. Recent work which study such particle methods within a mean-field framework include [129, 124]. See also [225, 96] for a survey on the more general so-called *Sequential Monte Carlo* methods and to the larger monographs [126, 127, 146, 125] for the theoretical foundations, in particular the links with mean-field theory.

Agent Based Optimization

Optimization problems are notoriously difficult in high dimensional spaces or for multimodal objective functions. In the 90's, Kennedy and Eberhart [229] introduced a class of optimization algorithms based on a the simulation of a swarm of interacting agents. The *Particle Swarm Optimization* (PSO) methods are inspired by biological concepts: each agent (or particle) follows a set of simple rules which is a mix between an individual exploration behaviour and a collective exploitation of the swarm knowledge in order to efficiently find and converge to the global minimum of the objective function. From an algorithmic point of view, the algorithm is appealing by its (relative) simplicity and its versatility as it does not requires expensive computations like the gradient of the objective function. In the last decades, many variants and practical implementations of the original PSO algorithm have been proposed and a full inventory of these so-called *Swarm Intelligence* (SI) methods would go beyond the present review.

Although these algorithms have proved their efficiency for notoriously difficult problems, their main drawback is their lack of theoretical mathematical foundations. Most of the SI methods are based on metaheuristic principles which can hardly be turned into rigorous convergence results, in particular when the number of agents involved becomes large. In reaction to this, there has been a growing interest for the convergence analysis of SI methods using the tools developed in the kinetic theory community for mean-field particle systems in physics or biology.

Following these ideas, a very simple though quite efficient method called *Consensus Based Optimization* (CBO) has recently been introduced by Pinneau et al. [281]. The analytical study of the long-time behaviour of the mean-field limit of this algorithm can be found in [64]. Partial rigorous results on the propagation of chaos property are available in [161]. Further developments on the CBO method can be found in [66]. A review and a comparison of recent SI methods, including the CBO method and the original PSO algorithm, can be found in [314, 315]. The recent article [177] gives a more unifying framework for the mean-field interpretation of PSO and CBO methods and introduces a mean-field variant of the original PSO algorithm which, unlike the algorithm in [281], is based on a kinetic system.

Overparametrized Neural Networks

Training neural networks can be understood as an optimization task. Whether the commonly used algorithms converge to the good optimum is in many cases still an open question. Recent independent works [251, 292, 302, 82] have shown that the training

process of neural networks possesses a natural mean-field interpretation which gives new insights towards a rigorous theoretical justification to this convergence problem.

More precisely, a (single hidden layer) neural network is characterised by a set of N parameters, interpreted as particles. During the training task, these parameters are adjusted to minimise a risk functional which associates a set of objects (e.g. images) to their known labels. The most common updating procedure for the parameters is the (noisy) Stochastic Gradient Descent (SGD) algorithm. The mean-field interpretation and long-time convergence of this algorithm can be found in the above-mentioned works.

Chapter 2

Scope of this work

This thesis is first motivated by the extension of the Vicsek model to an alignment model for rigid bodies. Following the kinetic theory approach, contributions are made to the derivation of PDE models from an individual based model and to the study of the associated kinetic and macroscopic models. At the particle level, the framework introduced is also adapted to the study of a swarm intelligence algorithm for sampling. For both aspects, this thesis also addresses the problem of the efficient simulation of mean-field particle systems.

2.1 The body-orientation dynamics model

2.1.1 Motivation and structure of $\mathrm{SO}_n(\mathbb{R})$

The main contributions of this thesis are related to the *body-orientation dynamics* model first introduced in [114] and [116]. It describes the evolution of a system of particles defined by their positions in the space $\mathbb{R}^3$ and their body-orientation modelled by a rotation matrix in $\mathrm{SO}_3(\mathbb{R})$ (that is, a rotation of the canonical basis denoted by (e_1, e_2, e_3), see Figure 2.1). The novelty of this model is to introduce an alignment (or coordination) mechanism for the body-orientations (or body-attitudes) which extends previous works where only the velocities of the particles were considered, as in the Vicsek model [322].

While the present work mostly focuses on theoretical aspects, it is motivated by the study of very diverse biological and physical systems. Hemelrijck, Hildenbrandt and Carrere [197, 196] have proposed an ethological model which takes into account the "aerodynamics of flight" to explain the emergence of self-organised flocks of birds. This model, which is more complex than the model studied in this thesis, is based on a traditional pitch-roll-yaw angles description of the internal structure of the birds. The

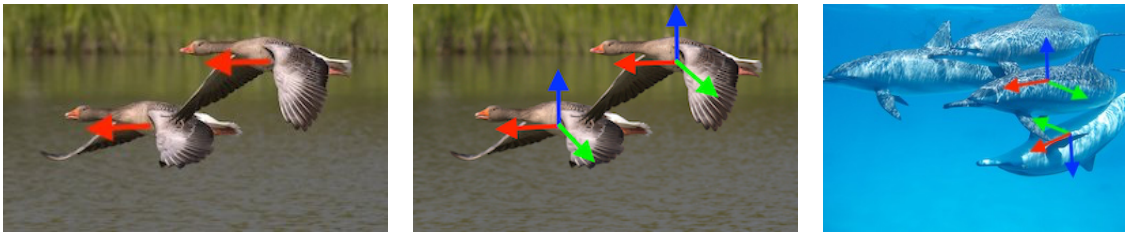

(A) (B) (C)

FIGURE 2.1: (A) The velocities of the two birds are aligned. (B) The body-orientations of the two birds are aligned. A body-orientation matrix in $\mathrm{SO}_3(\mathbb{R})$ is depicted by its three column vectors which form a direct orthonormal basis. The first column vector, depicted in red, is the direction of motion. (C) The velocities of the two dolphins are aligned but not their body-orientations. The additional degrees of freedom offered by the body-orientation framework allow one dolphin to swim upside-down.
Original pictures released under the Creative Commons CC0 licence by `pixabay.com`.

present work may offer a more intrinsic point of view by considering a dynamics on the manifold $\mathrm{SO}_3(\mathbb{R})$. In another context, the synchronisation and body-attitude coordination between spermatozoa has been shown [333] to play an important role in their motility and eventually on the fertility of sperm. These synchronisation effects are also believed to cause turbulence "whirlpool waves" observed in highly concentrated sperm [95] and other living fluids. Mathematical descriptions of these phenomena have focused on the Vicsek model and related continuum models [331, 94] but have not considered the influence of the shape of the spermatozoa. Finally, this work may also contribute to the design of bio-inspired swarming drones with applications for instance to the development of new efficient research strategies in a three-dimensional space [154].

In the mathematics literature, generalisations of the Cucker-Smale and Kuramoto models to body-oriented particles have been considered in [183] and are linked to the study of coordination models on matrix groups [184] or more generally on Lie groups [295]. Compared to the present work, all these models are deterministic models.

Before giving a formal definition of the model, let us first give a few elements on the structure of the space of rotation matrices in dimension n (we will mainly focus on the case $n = 3$). Throughout this work, $\mathrm{SO}_n(\mathbb{R})$ is seen as a (Riemaniann) submanifold of the Euclidean space formed by n-by-n square real matrices, denoted by $\mathcal{M}_n(\mathbb{R})$, endowed with the inner product

$$A \cdot B := \frac{1}{2}\mathrm{Tr}(A^{\mathrm{T}}B), \tag{2.1}$$

where Tr denotes the trace operator and A^{T} the transpose of the matrix $A \in \mathcal{M}_n(\mathbb{R})$. The

norm on $\mathcal{M}_n(\mathbb{R})$ associated to the inner product (2.1) will be denoted by $\|\cdot\|$. Moreover, since $\mathrm{SO}_n(\mathbb{R})$ has also a group structure, it is a Lie group.

Remark 2.1.1. The unusual scaling factor $1/2$ in the definition of the inner product (2.1) is chosen so that in dimension $n = 3$, the induced Riemaniann distance between a rotation matrix and the identity matrix is exactly equal to the angle of the rotation. Note that without this scaling factor, the matrix-norm induced by (2.1) is the classical Frobenius norm.

Since this group is compact and unimodular, there exists a unique normalised Haar measure on $\mathrm{SO}_n(\mathbb{R})$ which is simply denoted by $\mathrm{d}A$ and which is defined by the left and right invariance property:

$$\int_{\mathrm{SO}_n(\mathbb{R})} \varphi(AP)\mathrm{d}A = \int_{\mathrm{SO}_n(\mathbb{R})} \varphi(PA)\mathrm{d}A = \int_{\mathrm{SO}_n(\mathbb{R})} \varphi(A)\mathrm{d}A, \tag{2.2}$$

for all $P \in \mathrm{SO}_n(\mathbb{R})$ and for all measurable test function φ on $\mathrm{SO}_n(\mathbb{R})$.

2.1.2 Individual Based Model(s)

Let us consider $N \gg 1$ particles and let us denote their positions and body-orientations respectively by

$$\mathcal{X}_t^N := (X_t^1, \dots, X_t^N) \in (\mathbb{R}^3)^N, \quad \mathcal{A}_t^N := (A_t^1, \dots, A_t^N) \in \mathrm{SO}_3(\mathbb{R})^N.$$

The particles evolve according to the following Piecewise Deterministic Markov Process (PDMP) which extends the PDMP Vicsek model introduced in [141] and that was already detailed in Section 1.2.

- To each agent $i \in \{1, \dots, N\}$, it is attached an increasing sequence of random times (jump times) $T_1^i, T_2^i, \dots$ such that the intervals between two successive times are independent and follow an exponential law with constant parameter $\nu > 0$ (Poisson process). At each jump time T_n^i, the process $(X_t^i)_t$ is continuous and the process $(A_t^i)_t$ is right-continuous and has a discontinuity between its left and right states respectively denoted by $A^i_{T_n^{i,-}}$ and $A^i_{T_n^i}$.
- Between two jump times (T_n^i, T_{n+1}^i), the evolution is deterministic: the orientation of agent i does not change and it moves in straight line at speed $c_0 > 0$ in the direction of the first column vector of the body-orientation $A^i_{T_n^i} e_1$, i.e. for all $t \in [T_n^i, T_{n+1}^i)$, it holds that

$$X_t^i = X^i_{T_n^i} + c_0(t - T_n^i)A_t^i e_1, \;\; A_t^i = A^i_{T_n^i}. \tag{2.3}$$

- At T_n^i, the post-jump body-orientation $A^i_{T_n^i}$ is drawn from a von Mises distribution on $\mathrm{SO}_3(\mathbb{R})$:

$$A^i_{T_n^i} \sim M_{\mathbb{M}_n^i}. \tag{2.4}$$

Similarly to the von Mises distribution on the sphere, the von Mises distribution on $\mathrm{SO}_3(\mathbb{R})$ with parameter $\mathbb{M} \in \mathcal{M}_3(\mathbb{R})$ is defined by the probability density function:

$$M_{\mathbb{M}}(A) := \frac{\mathrm{e}^{\mathbb{M}\cdot A}}{\int_{\mathrm{SO}_3(\mathbb{R})} \mathrm{e}^{\mathbb{M}\cdot A'} \mathrm{d}A'}. \tag{2.5}$$

In the present case, the parameter matrix $\mathbb{M}_n^i$ is constructed by first computing the local flux defined at time $T_n^{i,-}$ by:

$$J_n^i := \frac{1}{N} \sum_{j=1}^{N} K\big(|X^i_{T_n^i} - X^j_{T_n^i}|\big) A^j_{T_n^{i,-}}, \tag{2.6}$$

having in mind that $A^j_{T_n^{i,-}} = A^j_{T_i^n}$ for $j \neq i$ and where K is an interaction kernel. The choice of the matrix $\mathbb{M}_n^i$ as a function of J_n^i defines different models. A natural choice when J_n^i is not singular, is to take

$$\mathbb{M}_n^i = \kappa \mathbb{A}_n^i, \tag{2.7}$$

where $\kappa > 0$ is a concentration parameter and $\mathbb{A}_n^i$ is the local average body-orientation defined as the projection of J_n^i on $\mathrm{SO}_3(\mathbb{R})$, that is the unique solution of the maximization problem:

$$\mathbb{A}_n^i := \mathrm{argmax}_{A \in \mathrm{SO}_3(\mathbb{R})}\, A \cdot J_n^i. \tag{2.8}$$

A less singular choice is simply $\mathbb{M}_n^i = J_n^i$ but in this case $\mathbb{M}_n^i$ does not necessarily belong to $\mathrm{SO}_3(\mathbb{R})$ and the shape of the associated von Mises distribution may become much more difficult to describe, as explained below (Figure 2.2).

The von Mises distribution on $\mathrm{SO}_3(\mathbb{R})$ is also known in the literature as the matrix Fisher distribution [230, 239]. The geometrical structure of $\mathrm{SO}_3(\mathbb{R})$ makes this distribution much more complex than its analog on the sphere. Similarly to a standard normal distribution in $\mathbb{R}$, the von Mises distribution on the sphere $\mathbb{S}^{d-1}$ is defined only by its center $\mathbb{V} \in \mathbb{S}^{d-1}$ and a nonnegative concentration parameter. Due to the additional degrees of freedom on $\mathrm{SO}_3(\mathbb{R})$, the matrix von Mises distribution cannot be so easily described. To give a brief overview of the possible shapes of the distribution, the first step is to decompose to parameter matrix $\mathbb{M}$ as $\mathbb{M} = PDQ$ where $P, Q \in \mathrm{SO}_3(\mathbb{R})$ and

D is a diagonal matrix whose elements are called the *singular values* of $\mathbb{M}$. Using this decomposition (which will be called *Special Singular Value Decomposition* in Chapter 7) and the invariance by translation of the Haar measure, one can reduce the problem to the study of the distribution M_D. Depending on the singular values, there is a whole range of possible shapes as illustrated on Figure 2.2.

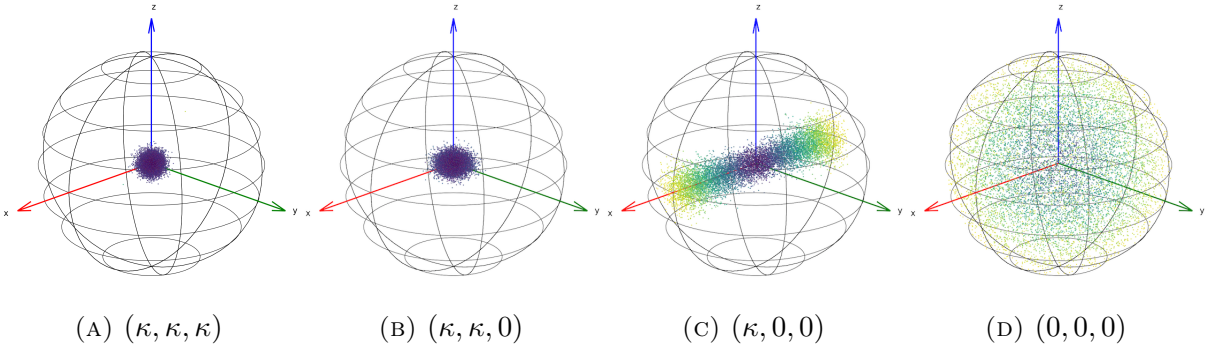

(A) (κ, κ, κ) (B) $(\kappa, \kappa, 0)$ (C) $(\kappa, 0, 0)$ (D) $(0, 0, 0)$

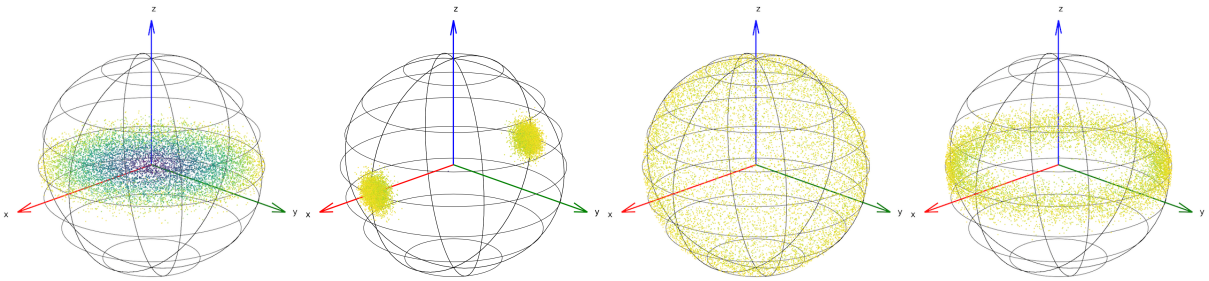

(E) $(\kappa, \kappa, -\kappa)$ (F) $(\kappa, -\kappa, -\kappa)$ (G) $(-\kappa, -\kappa, -\kappa)$ (H) $(0, 0, -\kappa)$

FIGURE 2.2: For various values of a triplet D of singular values with $\kappa = 40$, each figure shows 10^5 samples of the von Mises distribution M_D in a ball of radius π. The angle of the rotation is represented by the distance of the point to the center of the ball (and its color for better visualization). The axis of the rotation is the normalised vector associated to the point. The x, y and z axes are respectively depicted by red, green and blue arrows.

The simplest case happens when all the singular values are equal and nonnegative, that is, when the parameter is a nonnegative multiple of the identity matrix. In this case the von Mises distribution can be simply characterised by its center and a concentration parameter. By invariance by translation, this corresponds to the case (2.7) in the PDMP model. This is the model introduced in [114]. On the other hand, if $\mathbb{M}_n^i = J_n^i$, the post-jump distribution heavily depends on the singular values of J_n^i. The consequences of this choice are studied in [111] and Chapter 7.

It should be mentioned that at least when $\mathbb{M}_n^i$ is defined by (2.8), the N-particle process

could also be defined in a slightly more concise way using a system of N Poisson SDEs. However, in the following we will not use such representation and stick to the "algorithmic" definition of the system which has two main advantages: the first one is that it gives an explicit simulation procedure, the second one is that it does not raise wellposedness issues when J_n^i becomes singular.

In [114], a similar model is proposed where the PDMP is replaced by a diffusion process, defined by the system of $2N$ Stratonovich SDEs:

$$\left\{ \begin{array}{rcl} \mathrm{d}X_t^i &=& c_0 A_s^i e_1 \mathrm{d}t, \\ \mathrm{d}A_t^i &=& \mathsf{P}_{T_{A_t^i}} \circ \left(\nu \mathbb{M}_t^i \mathrm{d}t + \sqrt{2\sigma} \mathrm{d}B_t^i \right), \end{array} \right. \tag{2.9}$$

where $(B_t^i)_t$ are N independent Brownian motions on $\mathcal{M}_3(\mathbb{R})$, $\nu, \sigma > 0$ and P_{T_A} denotes the projection on the tangent plane to a rotation matrix $A \in \mathrm{SO}_3(\mathbb{R})$ (see Lemma 7.2.1). Finally, the body-orientation dynamics model (PDMP and diffusion versions) is written using quaternions instead of rotation matrices in [115, 116]. We will use the equivalence between quaternions and rotations in Chapter 7 and in Chapter 8 in a numerical context.

2.1.3 Kinetic model

Similarly to the Vicsek model, a propagation of chaos result can be proved when $N \to +\infty$ and leads to the study of the following BGK-type PDE for the particle distribution $f_t \equiv f_t(x, A)$ on the space $\mathbb{R}^3 \times \mathrm{SO}_3(\mathbb{R})$

$$\partial_t f_t + c_0 A e_1 \cdot \nabla_x f = \nu(\rho_{f_t} M_{\mathbb{M}[f_t]} - f_t). \tag{2.10}$$

A common framework for both the Vicsek model and the body-orientation model will be described in Chapter 4 (see also Section 2.2.1). The result is rigorous when the function $\mathbb{M}[f]$ is a smooth function of the flux

$$J_{K \star f_t}(x) := \iint_{\mathbb{R}^3 \times \mathrm{SO}_3(\mathbb{R})} K(x-y) A f_t(y, A) \mathrm{d}y \mathrm{d}A.$$

It does not include the case when

$$\mathbb{M}[f_t] = \mathrm{argmax}_{A \in \mathrm{SO}_3(\mathbb{R})} A \cdot J_{K \star f_t}, \tag{2.11}$$

which is not well-defined when J_{f_t} is singular. However, similarly to what has been proved in [50], it is expected that this happens with a probability which tends to 0 when $N \to +\infty$

on a short time interval and provided that the initial flux is not singular. This is not the main object of the present thesis and we will most of the time study the non singular model $\mathbb{M}[f_t] = J_{K\star f_t}$ or even

$$\mathbb{M}[f_t] = J_{f_t} = \int_{\mathrm{SO}_3(\mathbb{R})} Af(y, A)\mathrm{d}A, \tag{2.12}$$

when the interaction kernel $K = \delta_0$ is reduced to a Dirac delta. In this case, the well-posedness of the associated PDE model is also shown in [138] and Chapter 4.

In the spatially homogeneous case and analogously to the Vicsek model, the choice (2.12) leads to a phase transition phenomenon. In the present case, the equilibria of the BGK operator are of the form $f_{\mathrm{eq}} = \rho M_J$ where the matrix $J \in \mathcal{M}_3(\mathbb{R})$ is characterised by the equation

$$J = \rho \int_{\mathrm{SO}_3(\mathbb{R})} AM_J(A)\mathrm{d}A.$$

The solutions of this matrix equation as well as the long-time convergence of the solutions of the space-homogemeous BGK equation are completely characterised in [111] and Chapter 7. To obtain these results, the key element is the Special Singular Value Decomposition coupled with the group isomorphism between $\mathrm{SO}_3(\mathbb{R})$ and the space of unit quaternions where antipodal points are identified. This equivalence recasts the problem into a framework previously studied in the mathematical literature on liquid crystals [330].

Finally, when the dynamics is replaced by the diffusion process (2.9), the BGK equation is replaced by the Fokker-Planck equation

$$\partial_t f_t + c_0 Ae_1 \cdot \nabla_x f = -\nu \nabla_A \cdot (\mathbb{M}[f_t] f_t) + \sigma \Delta_A f_t. \tag{2.13}$$

The results of [111] have recently been extended to this case in [166].

2.1.4 Macroscopic model

Using a hyperbolic re-scaling, the kinetic PDE (2.10) becomes,

$$\partial_t f^\varepsilon + c_0 Ae_1 \cdot \nabla_x f^\varepsilon = \frac{1}{\varepsilon}\left(\rho_{f^\varepsilon} M_{\mathbb{M}[f^\varepsilon]} - f^\varepsilon\right) + \mathcal{O}(\varepsilon).$$

A macroscopic model was obtained in [116] by letting $\varepsilon \to 0$ following the Generalised Collision Invariants method introduced in [122]. Assuming that the limit is of the form

$$f^\varepsilon \underset{\varepsilon\to 0}{\longrightarrow} \rho M_{\kappa\mathbb{A}},$$

where $\rho \equiv \rho(t,x)$ and $\mathbb{A} \equiv \mathbb{A}(t,x) \in \mathrm{SO}_3(\mathbb{R})$ depend on t and x and where $\kappa > 0$ may depend on ρ, it is shown in [116] and in Chapter 7 that the couple $(\rho, \mathbb{A})$ satisfies (formally) the system:

$$\partial_t \rho + \nabla_x \cdot (c_1 \rho \Omega) = 0 \tag{2.14a}$$

$$(\partial_t + c_2(\Omega \cdot \nabla_x))\Omega + \mathsf{P}_{\Omega^\perp}(c_3 \nabla_x \log \rho + c_4 \mathbf{r}) = 0, \tag{2.14b}$$

$$(\partial_t + c_2(\Omega \cdot \nabla_x))u - u \cdot (c_3 \nabla_x \log \rho + c_4 \mathbf{r})\Omega + c_4 \delta v = 0, \tag{2.14c}$$

$$(\partial_t + c_2(\Omega \cdot \nabla_x))v - v \cdot (c_3 \nabla_x \log \rho + c_4 \mathbf{r})\Omega - c_4 \delta u = 0, \tag{2.14d}$$

where the rotation field $\mathbb{A}$ is written in terms of the basis vectors

$$\Omega = \mathbb{A}e_1, \quad u = \mathbb{A}e_2, \quad v = \mathbb{A}e_3.$$

This system is called the "Self-Organised Hydrodynamics for Body-orientation" (SOHB) model in [114]. The constants c_1, c_2, c_3, c_4 are explicit functions of κ and c_0. The vector field $\mathbf{r}(t,x) \in \mathbb{R}^3$ and the scalar field $\delta(t,x) \in \mathbb{R}$ are defined by

$$\begin{aligned} \mathbf{r} &:= (\nabla_x \cdot \Omega)\Omega + (\nabla_x \cdot u)u + (\nabla_x \cdot v)v, \\ \delta &:= [(\Omega \cdot \nabla_x)u] \cdot v + [(u \cdot \nabla_x)v] \cdot \Omega + [(v \cdot \nabla_x)\Omega] \cdot u. \end{aligned}$$

The operators $\mathbf{r}$ and δ makes the system (2.14) more complex than the analog macroscopic model (1.12)-(1.13) associated to the Vicsek model. In the body-orientation framework, there are additional degrees of freedom given by the two vectors (u, v) which are nonetheless subject to geometrical constraints. These constraints produce additional pressure terms involving $\mathbf{r}$ and δ. It will be shown in Chapter 8 that the interplay between the vectors Ω, u and v encoded in the operators $\mathbf{r}$ and δ create explicit solutions of the system (2.14). These solutions correspond to new self-organised phenomena in collective dynamics which are studied numerically in [106] and Chapter 8.

2.2 Systems of particles and applications

Part I of this thesis will be devoted to the study of stochastic particle systems initially motivated by the Vicsek and body-attitude coordination models. Three different aspects of particle systems will be discussed: their rigorous mean-field limit, their numerical simulation and their application to sampling problems.

2.2.1 Propagation of chaos and moderate interaction

The body-orientation dynamics model and the Vicsek model share many similarities. For the PDMP Vicsek model introduced in [140], a rigorous propagation of chaos result was missing. In Chapter 4 of this thesis, a common framework for a large class of piecewise deterministic geometrically enriched models which includes both models is introduced. The goal is to prove the propagation of chaos result which leads to various BGK-type equations (respectively (2.10) and (1.9) for the body-orientation and Vicsek models). As this topic is not new and many progress have been made in the last years, a short review on propagation of chaos is included in Chapter 3. It is based on the more extensive review article [76].

Although there already exist some methods to treat piecewise deterministic systems, there are two main contributions in this thesis. The first one is a new coupling method at the level of the trajectories for mean-field PDMP systems in the spirit of the renowned coupling method of Sznitman for diffusion processes [307]. This method shows a quantitative propagation of chaos property on any bounded time interval. This is a crucial element for the second contribution which is a moderate interaction result. As mentioned previously in this introduction, in moderately interacting particle systems, the interaction radius of the particles is scaled according to the total number of particles. As this number goes to infinity, a PDE with a purely local interaction term is obtained, which is a classical analytical setting to study kinetic equations. The concept of moderate interaction was introduced by Oelschläger [273] but the result in Chapter 4 is rather inspired by the work of Jourdain and Méléard [218] who use a more analytical approach at the PDE level.

2.2.2 Simulation of mean-field particle systems and applications

In parallel to the (rigorous or formal) derivation of PDE models, another more direct way to study particle systems is the numerical simulation of the Individual Based Model. The derivation of PDE models is not easy, often partially formal and the mathematical hypothesis and results are not always optimal. The direct simulation of the corresponding IBM is often the only way to check that a PDE model is relevant, by comparing its predictions to the output of the simulation of the IBM. Moreover, since swarming models can exhibit a wide range of complex unexpected phenomena, a single PDE model, which only describes a statistical behaviour, may not be able to capture all the complexity of the particle model. The fine study and tuning of the parameters of the particle simulations may help understanding which hypotheses should be made in order to derive the PDE model relevant to a specific phenomenon.

The simulation of particle systems is, at first sight, most often a relatively easy task which makes possible the design of versatile numerical codes, well suited to analyse the influence of the various modelling hypotheses. However, particle simulations are expensive. Especially when the number of particles is large (say more than 10^4), the computational cost may exceed the memory capability of a standard computer or become extremely time consuming. For mean-field particle systems, the naive cost is quadratic in the number of particles, which quickly becomes prohibitive. Many computational workarounds, often based on approximation procedures, have been developed in the past decades to cope with this difficulty. Some of them will be reviewed in Chapter 5. However, nowadays, the use of massively parallelised processors (GPU) opens the way to real-time large scale simulations which do not necessitate artificial numerical approximations. Thanks to the recent development of high-level user friendly interfaces for GPU computing [78], the `SiSyPHE` library [139] presented in Chapter 5 allows the efficient simulations of a wide range of classical swarming models within a common framework.

Two applications of these ideas are presented in this thesis. The first one is directly related to the body orientation model. In Chapter 8, the comparison between the particle simulations and the prediction of the macroscopic model both validates the kinetic theory approach and shows the existence of new unexpected phenomena. The second application is the design of efficient particle methods for sampling problems in Chapter 6.

2.2.3 A collective Monte Carlo method

Chapter 6 of the present thesis will present a new class of sampling algorithms based on the simulation of a system of interacting mean-field particles. This work generalises the classical Metropolis-Hastings algorithm whose basic form is recalled below.

In order to construct independent samples from an unknown distribution π, the Metropolis-Hastings is a sequential algorithm based on an accept-reject method: starting from an arbitrary state X, the idea is to construct a biased random-walk which is ergodic with respect to π. At each step, a random perturbation $Y \sim Q(\cdot|X)$ of the current state X is proposed using a random-walk kernel Q. Then, with a well-chosen probability, this new state may be accepted as the next state or rejected in which case the current state does not change. When the random walk kernel is symmetric, the classical choice for the acceptance probability is $\min(1, \pi(Y)/\pi(X))$ which means that the probability to accept a proposed state Y is all the more high than the acceptance ratio $\pi(Y)/\pi(X)$ is large. Under very mild assumptions, this biased random walk is shown to be ergodic with respect to π [253, 137, 289].

This simple procedure is generalised in [86] and Chapter 6 to a population of N particles $\mathcal{X}^N = (X^1, \dots, X^N)$ by allowing the random-walk kernel to depend on the full state of the system. For instance, one can propose for each particle $i \in \{1, \dots, N\}$, a new state:

$$Y^i \sim K \star \mu_{\mathcal{X}^N}, \tag{2.15}$$

where K is an interaction kernel, $\mu_{\mathcal{X}^N}$ the empirical measure of the system and $\star$ denotes the convolution product. In this case, the law of the proposition can be understood as a mixture of all the classical random-walk Metropolis-Hastings proposal laws associated to the N particles. Then each proposed state Y^i needs to be *individually* accepted or rejected depending on the generalised acceptance ratio

$$\frac{\pi(Y^i) K \star \mu_{\mathcal{X}_t^N}(X^i)}{\pi(X^i) K \star \mu_{\mathcal{X}_t^N}(Y^i)}. \tag{2.16}$$

This defines a Markov chain which is, in general, not ergodic with respect to $\pi^{\otimes N}$ but which satisfies the propagation of chaos property. As a consequence, the N particles asymptotically behave as N independent Markov chains. Using a mesoscopic PDE description, these Markov chains can then be shown to be ergodic with respect to π. This generalised procedure is as versatile as the classical Metropolis-Hastings algorithm. The convergence can be proved under mild assumptions, it can be easily adapted to various settings and only requires to evaluate π (and not its gradient, for instance). However, it will be shown in Chapter 6 that by taking advantage of the full knowledge of the N particles, the convergence speed is greatly improved. Moreover, there is much freedom in the choice of the interaction mechanism (here encoded in the choice of the proposition (2.15)) which can be adapted to various situations. As explained in the previous section, the additional computational cost due to the convolution operations in (2.16) may seem prohibitive but are easily handled using a GPU implementation.

2.3 Organisation of the thesis

This thesis is divided into two main parts which follow the natural progression from the microscopic scale to the macroscopic scale.

The first part is devoted to an analytical and numerical study of mean-field particle systems from a probabilistic point of view. The central question is the propagation of chaos property for various swarming models and its applications to sampling problems.

- Chapter 3 is an introductory chapter which reviews old and recent material on the mathematics of propagation of chaos. This chapter as well as most of the review material presented throughout the thesis are based on the review article [76].
- Chapter 4 proves the propagation of chaos and a so-called moderate interaction property for a large class of geometrically enriched particle systems which encompasses the Vicsek model and the body-orientation dynamics model. It is based on the article [138].
- Chapter 5 presents the main features of the `SiSyPHE` library [139] developed for the GPU simulation of large-scale mean-field interacting particle systems.
- Chapter 6 presents a new sampling algorithm based on the simulation of a swarm of particles as well as its convergence analysis. It is based on the article [86].

The second part of this thesis is devoted to the study of PDE models for the body-orientation dynamics model.

- Chapter 7 is devoted to the spatially homogeneous kinetic model associated to the body-orientation dynamics model. An appropriate choice of the target matrix leads to phase transition phenomena. The macroscopic limit of this model is also presented. It is based on the article [111].
- Chapter 8 is a numerical study of the macrosocopic model associated to the body-orientation dynamics model. A new class of explicit solutions is shown and studied using a direct simulation of the particle system. It is based on the article [106].
- Chapter 9 presents a derivation of the generalisation of the macroscopic model associated to the body-orientation dynamics model to an arbitrary dimension. It is based on the article [110].

Finally the concluding Chapter 10 is devoted to the future perspectives of this work.

2.4 Contribution statement

The results presented in this thesis are based on the following articles and preprints (sorted in chronological order) that I authored or co-authored.

- The article [138] (Chapter 4) is my own work. The original idea was initially proposed by Amic Frouvelle and the first version of the manuscript was substantially improved following the advice of Sara Merino-Aceituno, Pierre Degond and Amic Frouvelle.

- The article [111] (Chapter 7) is a collaboration with Pierre Degond, Amic Frouvelle and Sara Merino-Aceituno who proposed and conceptualized the study of the BGK model associated to the body-orientation dynamics. The methodology, investigations and the proofs were done in collaboration with Amic Frouvelle and Pierre Degond. I wrote a first version of the manuscript later improved by Sara Merino-Aceituno and Pierre Degond.

- The article [86] (Chapter 6) is a collaboration with Grégoire Clarté and Jean Feydy. The original idea and design of the algorithm are initially due to Grégoire Clarté and myself (equal contribution). I carried out the analytical study and designed the methodology of the proofs. The numerical code was written by Jean Feydy. The three authors equally contributed to the design and analysis of the numerical experiments, the development of the variants of the original algorithm as well as the writing of the manuscript.

- The article [106] (Chapter 8) is a collaboration with Pierre Degond and Mingye Na. The conceptualization and original idea is due to Pierre Degond. Pierre Degond and myself equally contributed to the analytical study of the solutions and the writing of the manuscript. A first version of the code was written by Mingye Na but I re-wrote a more efficient GPU code used for the simulations presented in the article.

- The Python library [139] (Chapter 5) is my own work.

- The review article [76] (Chapter 3) is a collaboration with Louis-Pierre Chaintron. We equally contributed to the choice of the content, to the organisation of the article and preliminary drafts, and to the original ideas presented. The writing of the final manuscript is mostly due to myself.

- The article [110] (Chapter 9) is a collaboration with Pierre Degond and Amic Frouvelle. The derivation of the model in arbitrary dimension was initially written by myself following a methodology designed by the three authors (equal contribution). The generalised framework using representation theory as well as the writing of the manuscript is due to Pierre Degond.

Notations and conventions

For the convenience of the reader, the main notations which are used throughout the thesis are gathered below.

Sets

$C(I, E)$	The set of continuous functions from a time interval $I = [0, T]$ to a set E, endowed with the uniform topology.
$C_b(E)$, $C_b^k(E)$	Respectively the set of real-valued bounded continuous functions and the set of functions with $k \geq 1$ bounded continuous derivatives on a set E.
$\mathcal{D}_n(\mathbb{R})$	The space of n-dimensional square diagonal matrices.
$D(I, E)$	The space of functions which are right continuous and have left limit everywhere from a time interval $I = [0, T]$ to a set E, endowed with the Skorokhod $J1$ topology. This is the space of the so-called *càdlàg* functions. This space is also called the *Skorokhod space* or the *path space*.
$\mathbb{H}$	The group of unit quaternions.
$L^p(E)$ or $L^p_\mu(E)$	The set of measurable functions φ defined almost everywhere on a measured space (E, μ) such that the $\lvert\varphi\rvert^p$ is integrable for $p \geq 1$. When $p = +\infty$, this is the set of functions with a bounded essential supremum. We do not specify the dependency in μ when no confusion is possible.
$\mathcal{M}_n(\mathbb{R})$	The set of n-dimensional square real matrices.
$\mathcal{M}(E)$	The set of signed measures on a measurable space E.
$\mathcal{M}^+(E)$	The set of positive measures on a measurable space E.
$\mathcal{P}(E)$	The set of probability measures on a space E.
$\mathcal{P}^{\mathrm{ac}}(E)$	The set of absolutely continuous probability measures on a space E. The measure and its associated probability density function are written indifferently $\mu(\mathrm{d}x) \equiv \mu(x)\mathrm{d}x$.

$\mathcal{P}_p(E)$	The set of probability measures with bounded moment of order $p \geq 1$ on a space E.
$\widehat{\mathcal{P}}_N(E)$	The set of empirical measures of size N over a set E, that is measures of the form $\mu = \frac{1}{N}\sum_{i=1}^N \delta_{x^i}$, where $x^i \in E$.
$\mathbb{R}_+$	The set $[0, +\infty)$.
$\mathfrak{S}_N$	The permutation group of the set $\{1, \dots, N\}$.
$\mathbb{S}^{d-1}$	The sphere of dimension $d-1$.

Generic elements and operations

$\mathcal{A}(\theta, \mathbf{n})$	The rotation of angle $\theta \in [0, \pi]$ around the axis $\mathbf{n} \in \mathbb{S}^2$.
C	A generic nonnegative constant, the value of which may change from line to line.
$C(a_1, \dots a_n)$	A generic nonnegative constant which depends on some fixed parameters denoted by $a_1, \dots, a_n$. Its value may change from line to line.
$\mathrm{diag}(x)$	The d-dimensional diagonal matrix whose diagonal coefficients $x_1, \dots, x_d$ are the components of the d-dimensional vector x.
$\nabla \cdot V$	The divergence of a vector field $V : \mathbb{R}^d \to \mathbb{R}^d$ or of a matrix field $V : \mathbb{R}^d \to \mathcal{M}_d(\mathbb{R})$, respectively defined by $\nabla \cdot V = \sum_{i=1}^d \partial_{x_i} V_i$ or componentwise by $(\nabla \cdot V)_i = \sum_{j=1}^d \partial_{x_j} V_{ij}$.
$A \cdot B$ and $\|A\|$	The inner product of two matrices $A, B \in \mathcal{M}_d(\mathbb{R})$ defined by $A \cdot B := \frac{1}{2}\sum_{i=1}^d \sum_{j=1}^d A_{ij} B_{ij}$ and the associated norm $\|A\| := \sqrt{A \cdot A}$.
$(e_1, e_2, \dots, e_n)$	The canonical basis of $\mathbb{R}^n$.
$\nabla^2 V$ or Hess$V$	The Hessian matrix of a scalar field $V : \mathbb{R}^d \to \mathbb{R}$ defined componentwise by $(\nabla^2 V)_{ij} = \partial^2_{x_i, x_j} V$.
I_d	The d-dimensional identity matrix.
Id	The identity operator on a vector space.
$\langle x, y \rangle$ or $x \cdot y$	The Euclidean inner product of two vectors $x, y \in \mathbb{R}^d$ defined by $\langle x, y \rangle \equiv x \cdot y := \sum_{i=1}^d x^i y^i$. One notation or the other may be preferred for typographical reasons in certain cases.
M_{ij}	The (i, j) (respectively row and column indexes) component of a matrix M.

$[\mathbf{w}]_\times$	For a vector $\mathbf{w} = (w_1, w_2, w_3)^{\mathrm{T}} \in \mathbb{R}^3$, the antisymmetric matrix $[\mathbf{w}]_\times := \begin{pmatrix} 0 & -w_3 & w_2 \\ w_3 & 0 & -w_1 \\ -w_2 & w_1 & 0 \end{pmatrix}$.
$\mathsf{P}(u)$ or $\mathsf{P}_{u^\perp}$	The projection matrix $\mathsf{P}(u) \equiv \mathsf{P}_{u^\perp} := I_d - \frac{u \otimes u}{\lvert u \rvert^2}$ on the plane orthogonal to a vector $u \in \mathbb{R}^d$.
$\mathsf{P}_{T_{\mathbb{A}}}$	The projection on the tangent plane to the point $\mathbb{A} \in \mathrm{SO}_3(\mathbb{R})$ defined by $\mathsf{P}_{T_{\mathbb{A}}} J = \frac{J\mathbb{A}^{\mathrm{T}} - \mathbb{A}J^{\mathrm{T}}}{2}\,\mathbb{A}$.
$\varphi \in C_b(E)$	A generic test function on E.
$\varphi_N \in C_b(E^N)$	A generic test function on the product space E^N.
$\Phi \in C_b(\mathcal{P}(E))$	A generic test function on the set of probability measures on E.
$u \otimes v$, $\mu \otimes \nu$ or $\varphi \otimes \psi$	Respectively, the matrix tensor product of two vectors $u, v \in \mathbb{R}^d$ defined componentwise by $(u \otimes v)_{ij} = u_i v_j$; the product measure on $E \times F$ of two measures μ, ν respectively on E and F; the product function on $E \times F$ defined by $(\varphi \otimes \psi)(x, y) = \varphi(x)\psi(y)$ for two real-valued function φ, ψ respectively on E and F.
$\mathrm{Tr}\, M$	The trace of the matrix M.
M^{T}	The transpose of the matrix M.
$\mathbf{x}^N = (x^1, \ldots, x^N)$	A generic element of a product space E^N. The components are indexed with a superscript.
$\mathbf{x}^{M,N} = (x^1, \ldots, x^M)$	The M-dimensional vector in E^M constructed by taking the M first components of $\mathbf{x}^N$.
$x = (x_1, \ldots, x_d)^{\mathrm{T}}$ and $\lvert x \rvert$	A generic element of a d-dimensional space and its norm. The coordinates are indexed with a subscript. The norm of x denoted by $\lvert x \rvert$ is the Euclidean norm.

Probability and measures

$K \star \mu$	The convolution of a function $K : E \times F \to G$ with a measure μ on F defined as the function $K \star \mu : x \in E \mapsto \int_F K(x, y)\mu(\mathrm{d}y) \in G$. When $E = F = G = \mathbb{R}^d$ and $K : \mathbb{R}^d \to \mathbb{R}^d$, we write $K \star \mu(x) = \int_{\mathbb{R}^d} K(x - y)\mu(\mathrm{d}y)$.
δ_x	The Dirac measure at the point x.

$\mu_{\mathbf{x}^N}$	The empirical measure defined by $\mu_{\mathbf{x}^N} = \frac{1}{N}\sum_{i=1}^N \delta_{x^i}$ where $\mathbf{x}^N = (x^1, \ldots, x^N)$.
$\mathbb{E}_\mu[\varphi]$	Alternative expression for $\langle \mu, \varphi \rangle$ when μ is a probability measure. When $\mu = \mathbb{P}$ on $(\Omega, \mathscr{F}, (\mathscr{F}_t)_t, \mathbb{P})$, the expectation is simply denoted by $\mathbb{E}$.
$H[\nu\|\mu]$	The relative entropy (or Kullback-Leibler divergence) between two measures μ, ν defined by $H[\nu\|\mu] := \int \frac{\mathrm{d}\nu}{\mathrm{d}\mu} \log\left(\frac{\mathrm{d}\nu}{\mathrm{d}\mu}\right) \mathrm{d}\mu$.
$\langle \mu, \varphi \rangle$ or $\langle \varphi \rangle_\mu$	The integral of a measurable function φ with respect to a measure μ.
$\mathrm{Law}(X)$	The law of a random variable X as an element of $\mathcal{P}(E)$ where X takes its value in the space E.
$(\Omega, \mathscr{F}, (\mathscr{F}_t)_t, \mathbb{P})$	A filtered probability space. Unless otherwise stated, all the random variables are defined on this set. The expectation is denoted by $\mathbb{E}$.
$\sigma(X^1, X^2, \ldots)$	The σ-algebra generated by the random variables $X^1, X^2, \ldots$.
$T_\# \mu$	The pushforward of the measure μ on a set E by the measurable map $T : E \to F$. This is a measure on the set F defined by $T_\#\mu(\mathscr{A}) = \mu(T^{-1}(\mathscr{A}))$ for any measurable set $\mathscr{A}$ of F.
$\|\cdot\|_{\mathrm{TV}}$	The Total Variation (TV) norm for measures.
W_p	The Wasserstein-p distance between probability measures.
$X \sim \mu$	It means that the law of the random variable X is μ.
$(\mathsf{X}_t)_t$ or $(\mathsf{Z}_t)_t$	The canonical process on the path space $D(I, E)$ defined by $\mathsf{X}_t(\omega) = \omega(t)$.
$(\mathbf{X}_t^N)_t$ or $(\mathbf{Z}_t^N)_t$	The canonical process on the product space $D(I, E)^N$ with components $\mathbf{X}_t^N = (\mathsf{X}_t^1, \ldots, \mathsf{X}_t^N)$.

Systems of particles and operators

E	The state space of the particles, assumed to be at least a Polish space.
f_t^N	The N-particle distribution in $\mathcal{P}(E^N)$ at time $t \geq 0$.
$f_t^{k,N}$	The k-th marginal of f_t^N.
f_I^N	The N-particle distribution on the path space in $\mathcal{P}(D(I, E^N))$ or $\mathcal{P}(C(I, E^N))$ for a time interval $I = [0, T]$. We identify $D(I, E^N) \simeq D(I, E)^N$.
f_t	The limit law in $\mathcal{P}(E)$ at time $t \geq 0$.
f_I	The limit law on the path space in $\mathcal{P}(D(I, E))$ or $\mathcal{P}(C(I, E))$.
F_t^N	The law of the empirical process in $\mathcal{P}(\mathcal{P}(E))$ at time $t \geq 0$.
F_I^N	The strong pathwise law of the empirical process in $\mathcal{P}(\mathcal{P}(D(I, E)))$ on the time interval $I = [0, T]$.
$\mathcal{L}_N$	The N-particle generator acting on (a subset of) $C_b(E^N)$.

$L \diamond_i \varphi_N$ The action of an operator L on (a subset of) $C_b(E)$ against the i-th variable of a function φ_N in $C_b(E^N)$, defined as the function in (a subset of) $C_b(E^N)$ $L \diamond_i \varphi_N : (x^1, \dots, x^N) \mapsto L[x \mapsto \varphi_N(x^1, \dots, x^{i-1}, x, x^{i+1}, \dots, x^N)](x^i)$. The definition readily extends to the case of an operator $L^{(2)}$ acting on $C_b(E^2)$ and two indexes $i < j$ in which case we write $L^{(2)} \diamond_{ij} \varphi_N$.

$\hat{\mu}_t^N$ An alternative lighter notation for the empirical measure of a system of particles when no confusion is possible.

$(\mathcal{X}_t^N)_t$ The N-particle process, with components $\mathcal{X}_t^N = (X_t^{1,N}, \dots, X_t^{N,N}) \in E^N$. Often we write $X_t^{i,N} \equiv X_t^i$ and $(\mathcal{X}_t^N)_t \equiv \mathcal{X}_{[0,T]}^N$.

$(\mathcal{Z}_t^N)_t$ An alternative notation for the N-particle process with $\mathcal{Z}_t^N = (Z_t^{1,N}, \dots, Z_t^{N,N})$. Often used for kinetic systems where $Z_t^i = (X_t^i, V_t^i)$ with X_t^i the position and V_t^i the velocity (or the body-orientation) of the i-th particle.

Acronyms and abbreviations

CMC	Collective Monte-Carlo (Chapter 6)
FS	Flocking State (Section 8.3)
GCI	Generalised Collision Invariant (Equation (7.42))
GS	Generalised topological Solution (Section 8.3)
GOP	Global Order Parameter (Section 8.5.1)
HW	Helical Wave (Section 8.3)
IBM	Individual Based Model
KIDS	Kernelised Importance-by-Deconvolution Sampling (Section 6.5.4)
MCMC	Markov Chain Monte Carlo
MO	Milling Orbit (Section 8.3)
MoKA	Mixture of Kernels Adaptive CMC (Section 6.5.3)
ODE	Ordinary Differential Equation
PDE	Partial Differential Equation
PMC	Population Monte Carlo [54]
PDMP	Piecewise Deterministic Markov Process
PMH	Parallel Metropolis-Hastings (Section 6.5.1)
RP, RPZ, RPX	Roll Polarization (Equation (8.36))
SMC	Sequential Monte Carlo [128]
SSVD	Special Singular Value Decomposition (Definition 7.2.7)
SOHB	Self-Organised Hydrodynamics for the Body-orientation (Section 2.1.4)

Part I

Systems of particles and propagation of chaos

Chapter 3

A review of models, methods and applications

The content of this chapter is based on the following review article written in collaboration with Louis-Pierre Chaintron

[76] L.-P. Chaintron and A. Diez. "Propagation of chaos: a review of models, methods and applications". *arXiv preprint: arXiv:2106.14812* (2021).

While the mathematical study of the propagation of chaos property traces back to Kac [223] and McKean [249], it has recently enjoyed some kind of revewal due to its importance in the study of collective dynamics models. The goal of the present work is to give a short overview of the recent advances on the subject in a unified modelling framework.

3.1 Introduction

When Boltzmann published his most famous article [44] one century and a half ago, the study of large systems of interacting particles was entirely motivated by the microscopic modelling of thermodynamic systems. Although it was far from being an accepted idea at that time, Boltzmann postulated that since a macroscopic volume of gas contains a myriad of elementary particles, it is both hopeless and needless to keep track of each particle and one should rather seek a statistical description. He thus derived the equation that now bears his name and which gives the time evolution of the continuum probability distribution (in the phase space) of a typical particle. With the H-theorem, he also extended and justified the pioneering works of Maxwell and Clausius for equilibrium thermodynamic

systems, paving the way alongside Gibbs for a consistent kinetic theory of gases. The Boltzmann equation is derived from first principles under a crucial assumption, called *molecular chaos*. This assumption was already known from Maxwell and is often called the *Stosszahlansatz* since Ehrenfest. Informally, it translates the idea that, despite the multitude of interactions, two particles taken at random should be statistically independent when the total number of particles grows to infinity. It is not so clear how the appearance of probability theory should be interpreted in this context. In the following years, the Stosszahlansatz and its consequences (the H-theorem) were the object of a fierce debate among physicists as they seem to break the microscopic reversibility. Beyond the scientific debate, it has raised metaphysical and philosophical questions about the profound nature of time and randomness [74, 88].

The rigorous justification of the work of Boltzmann and the status of molecular chaos became true mathematical questions when Hilbert addressed them in his Sixth Problem at the Paris International Congress of Mathematicians in 1900. Quoting Hilbert, the problem which motivates the present work is to *"[develop] mathematically the limiting processes [...] which lead from the atomistic view to the laws of motion of continua"*. Our starting point will be the seminal article of Kac [223]. More than half a century after Hilbert, Kac gave the first rigorous mathematical definition of chaos and introduced the idea that for time-evolving systems, chaos should be propagated in time, a property therefore called the *propagation of chaos*. Kac was still motivated by the mathematical justification of the classical collisional kinetic theory of Boltzmann for which he developed a simplified probabilistic model. Soon after Kac, McKean [250] introduced a class of diffusion models which were not originally part of Boltzmann theory but which satisfy Kac's propagation of chaos property. In the classical kinetic theory of Boltzmann, the problem is the derivation of continuum models starting from deterministic, Newtonian, systems of particles. In comparison, the fundamental contribution of Kac and McKean is to have shown that the classical equations of kinetic theory also have a natural stochastic interpretation. This philosophical shift is addressed in the enlightening introduction of Kac [224] written for the centenary of the Boltzmann equation.

Kac and McKean introduced a new mathematical formalism, gave many insights on the stochastic modelling in kinetic theory and proved the two building block theorems (see Theorem 3.4.2 in this Chapter). Their works have stimulated the development of a rich and still active *mathematical kinetic theory*. Keeping strong connections with the original theory of Boltzmann, some fundamental questions raised several decades ago have been answered only recently (see for instance [38, 168, 257]). On the other hand, systems of interacting particles are ubiquitous in many applications now and over the last two decades,

the tools and concepts developed in kinetic theory have somehow escaped the realm of pure statistical physics. As explained in the introduction of this thesis, some recent new domains of applications include mathematical biology and social sciences [21, 22, 266, 265, 109, 4, 322], data sciences and optimization [125, 126, 127, 281, 314, 177, 66, 251, 292, 302, 82, 104] or mean-field game theory [57, 56, 62, 63]. Compared to the models in statistical physics, many aspects should be reconsidered. To cite a few examples: the basic conservation laws (of momentum, energy...) do not always hold for biological systems and may be replaced by other types of constraints (optimization constraints, geometrical constraints...); the intrinsic randomness (or uncertainty) of the models in applied sciences is often a crucial modelling assumption; the complexity of the interaction mechanisms entails new analytical tools, etc. These differences have motivated many new techniques, new insights on the question of propagation of chaos and, in the end, new results.

There are already classical review articles on propagation of chaos in the literature which focus on different aspects. The famous course of Sznitman at Saint-Flour [307] studies many of the most important historical probabilistic models. The probabilistic methods are explained in details in the book [308] (in particular in the courses of Méléard [252] and Pulvirenti [282]). More recently, the review of Jabin and Wang [207] focuses on McKean mean-field systems and PDE applications. By its nature, the notion of chaos lies in the interplay between probability theory and Partial Differential Equations. Both analytic and probabilistic methods are discussed in this chapter. We also refer to the article by Hauray and Mischler [194] which is to our knowledge, the most complete reference on Kac's chaos (without propagation of chaos). For deterministic systems which will not be considered here, we refer to the very thorough reviews [205, 173].

3.2 Systems of particles, Kac's chaos and propagation of chaos

3.2.1 Markovian framework

Throughout this work, a particle system is defined as a Markov process $(\mathcal{X}_t^N)_{t\in I}$ with values in E^N where E is a Polish space, N is the number of particles and $I = [0, T]$, $T \in (0, +\infty]$ is a time interval. Throughout this chapter, we use the notation $\mathcal{X}_t^N = (X_t^{1,N}, \dots, X_t^{N,N})$ for the particle system and we write $X_t^i \equiv X_t^{i,N}$ without the N superscript for the i-th particle when no confusion is possible.

From the theory of Markov processes the probability distribution of the particle system

at time t denoted by $f_t^N \in \mathcal{P}(E^N)$ satisfies the (weak) *Liouville equation* (sometimes also called the *master equation*):

$$\forall \varphi_N \in \mathrm{Dom}(\mathcal{L}_N), \quad \frac{\mathrm{d}}{\mathrm{d}t}\langle f_t^N, \varphi_N \rangle = \langle f_t^N, \mathcal{L}_N \varphi_N \rangle, \tag{3.1}$$

where $\mathcal{L}_N$ is the infinitesimal generator of the particle system acting on a (dense) subset of test functions $\mathrm{Dom}(\mathcal{L}_N) \subset C_b(E^N)$. In stochastic analysis, the (more general) pathwise law $f_{[0,T]}^N \in \mathcal{P}(D([0,T], E^N))$ is sometimes preferred and is characterised as the solution of a martingale problem. Namely, $f_{[0,T]}^N$ is the unique probability distribution on the Skorokhod space of càdlàg functions $D([0,T], E^N)$ such that for any test function $\varphi_N \in \mathrm{Dom}(\mathcal{L}_N)$, the process defined by:

$$M_t^{\varphi_N} := \varphi_N(\mathbf{X}_t^N) - \varphi_N(\mathbf{X}_0^N) - \int_0^t \mathcal{L}_N \varphi_N(\mathbf{X}_s^N) \mathrm{d}s,$$

is a $f_{[0,T]}^N$-martingale. In this definition, the process $(\mathbf{X}_t^N)_{t \geq 0}$ denotes the canonical process on $D([0,T], E^N)$ defined for any $\omega \in D([0,T], E^N)$ and any $t \geq 0$ by $\mathbf{X}_t^N(\omega) = \omega(t)$.

3.2.2 Exchangeable particle systems

The particle system is assumed to be *exchangeable* in the sense that f_t^N (resp. its pathwise version $f_{[0,T]}^N$) is a symmetric probability distribution on E^N (resp. on the path space $D([0,T], E)^N \simeq D([0,T], E^N)$). This assumption is crucial for the rest of the theory. The structure of the space of symmetric probability measures has been much studied in the literature (not in relation with particle systems) and it will be useful to first review some of the key elements of the theory. Below we distinguish the case $N < +\infty$ considered up to now and the case $N = +\infty$ which will be useful later.

Finite particle systems

Given a symmetric probability distribution $f^N \in \mathcal{P}_{\mathrm{sym}}(E^N)$ and for any $k \leq N$, there exists a unique k-th marginal distribution denoted by $f^{k,N}$ on E^k defined by:

$$\forall \varphi_k \in C_b(E^k), \quad \langle f^{k,N}, \varphi_k \rangle = \langle f^N, \varphi_k \otimes 1^{\otimes(N-k)} \rangle.$$

The distribution $f^{k,N} \in \mathcal{P}_{\mathrm{sym}}(E^k)$ is itself a symmetric probability measure and the N-th marginal is of course the measure f^N itself. However, keeping in mind that the final goal is to take $N \to +\infty$, one can consider for any fixed $k \in \mathbb{N}$ the limit of $f^{k,N}$ in $\mathcal{P}(E^k)$,

which is not possible for f^N directly since it belongs to a space which depends on N. In a dynamic framework, when f_t^N solves the Liouville equation (3.1), for each given $k \in \mathbb{N}$, a natural idea is to derive an equation for the k-th marginal distribution by considering a test function in (3.1) of the form $\varphi_N = \varphi_k \otimes 1^{\otimes(N-k)}$ with $\varphi_k \in C_b(E^k)$. As the marginals are not independent, this leads to a hierarchy of equation called the BBGKY hierarchy, see for instance [28] and the references therein regarding the BBGKY hierarchy for mean-field models.

Alternatively to the marginal distributions and with a more probabilistic point of view, a system $\mathcal{X}^N = (X^1, \dots, X^N) \in E^N$ of f^N-distributed random variables is equivalently described by its (random) empirical measure

$$\mu_{\mathcal{X}^N} = \frac{1}{N} \sum_{i=1}^{N} \delta_{X^i} \in \mathcal{P}(E), \tag{3.2}$$

as this measure contains all the statistical information up to the particle numbering (a quantitative version is stated in the Lemma 3.2.2 below). One can immediately see the advantage of such representation: it is possible to work with only one element which belongs to the fixed space $\mathcal{P}(E)$, in contrast to $f^N \in \mathcal{P}(E^N)$ or to the N marginal distributions.

Remark 3.2.1. To be completely rigorous, one should work in the quotient space $E^N/\mathfrak{S}_N$, whose elements $\bar{\mathbf{x}}^N$ gather all the permutations of the vector $\mathbf{x}^N \in E^N$. There is the one to one mapping:

$$\boldsymbol{\mu}_N : E^N/\mathfrak{S}_N \to \widehat{\mathcal{P}}_N(E), \quad \bar{\mathbf{x}}^N \mapsto \mu_{\mathbf{x}^N}, \tag{3.3}$$

where $\widehat{\mathcal{P}}_N(E)$ denotes the space of empirical measures of size N on E. Note that the two sets $C_b(E^N/\mathfrak{S}_N)$ and $C_b(\widehat{\mathcal{P}}_N(E))$ are naturally identified by taking the composition with this map. Moreover, since all the measures considered are symmetric, integration on $E^N/\mathfrak{S}_N$ is equivalent to integration on E^N. This is why, with a slight abuse, the test functions always belong to $C_b(E^N)$.

Since $\mu_{\mathcal{X}^N} \in \widehat{\mathcal{P}}_N(E) \subset \mathcal{P}(E)$ is a random element, a somehow unfortunate complication arises for the space of observables $C_b(\mathcal{P}(E))$: in this framework, test functions are continuous bounded functions on (a subset of) the set of probability measures (endowed with the weak topology). This is clearly more difficult to handle than usual test functions on E^N or E^k.

From the point of view of measure theory, studying the empirical measure (3.2) means that the law f^N is seen through its push-forward by the map (3.3) (seen as a map

$E^N \to \mathcal{P}(E)$), defined by:

$$F^N := (\boldsymbol{\mu}_N)_\# f^N \in \mathcal{P}(\mathcal{P}(E)).$$

The following lemma shows that F^N is enough to characterise f^N, at least when N is large.

Lemma 3.2.2 (Approximation rate of marginals)**.** *For $k \leq N$, let the* moment measure *$F^{k,N} \in \mathcal{P}(E^k)$ be defined by:*

$$\forall \varphi_k \in C_b(E^k), \quad \langle F^{k,N}, \varphi_k \rangle = \int_{\mathcal{P}(E)} \langle \nu^{\otimes k}, \varphi \rangle F^N(\mathrm{d}\nu).$$

Then as $N \to +\infty$, it holds that:

$$\left\| f^{k,N} - F^{k,N} \right\|_{\mathrm{TV}} \leq 2\frac{k(k-1)}{N}. \tag{3.4}$$

Coming back to the probabilistic point of view, F^N is the law of the random measure $\mu_{\mathcal{X}^N}$ where $\mathcal{X}^N \sim f^N$. The moment measures can thus be written

$$F^{k,N} = \mathbb{E}\big[\mu_{\mathcal{X}^N}^{\otimes k}\big],$$

where this expression is understood in the weak sense, for all $\varphi_k \in C_b(E^k)$,

$$\langle F^{k,N}, \varphi_k \rangle = \big\langle \mathbb{E}\big[\mu_{\mathcal{X}^N}^{\otimes k}\big], \varphi_k \big\rangle = \mathbb{E}\big[\big\langle \mu_{\mathcal{X}^N}^{\otimes k}, \varphi_k \big\rangle\big].$$

This (elementary) lemma is known at least since [179] where it was used to prove a propagation of chaos result (see [258, 257]). This lemma can also be seen as a finite system version of the de Finetti theorem, see [136, Theorem 13].

Infinite particle systems and random measures

Extending the previous theory to $N = +\infty$, an infinite system of particles can be described either by the infinite sequence of marginal distributions $(f^k)_k$ or by the sequence of random empirical measures associated to any k sub-system of particles. However, compared to the finite case, the relation between the two is more subtle, it is the object of famous theorems due to de Finetti, Hewitt and Savage. Let us first cite a few preliminary results.

Given an infinite system of exchangeable particles $(\overline{X}^i)_{i\geq 1}$, important measurable events are given by two particular σ-algebras.

Definition 3.2.3 (Symmetric and asymptotic σ-algebras)**.** Let $C_{\mathrm{sym}}(E^N)$ denote the set of symmetric continuous $\mathbb{R}$-valued functions on E^N which are invariant under permutations of their arguments.

- The σ-algebra of *exchangeable* events (i.e. events which do not depend on any finite permutation of the $\overline{X}^i$) is defined by:

$$\mathcal{S}_\infty := \bigcap_{k\geq 1} \sigma\Big(\sigma\big(\varphi_k(\overline{X}^1,\ldots,\overline{X}^k), \varphi_k \in C_{\mathrm{sym}}(E^k)\big), \overline{X}^{k+1}, \overline{X}^{k+2}, \ldots\Big),$$

  where we recall that $\sigma(X^1, X^2, \ldots)$ is the σ-algebra generated by the random variables $X^1, X^2, \ldots$.

- The *asymptotic* σ-algebra (whose events do not depend on any finite number of the $\overline{X}^i$) is defined by:

$$\mathcal{A}_\infty := \bigcap_{k\geq 1} \sigma\big(\overline{X}^{k+1}, \overline{X}^{k+2}, \ldots\big).$$

The fundamental result for exchangeable systems is the following proposition.

Proposition 3.2.4 ([241])**.** *For exchangeable systems, the following equality holds*

$$\mathcal{S}_\infty = \mathcal{A}_\infty.$$

Corollary 3.2.5 (Hewitt-Savage 0-1 law)**.** *In the special case where the $\overline{X}^i$ are i.i.d. variables (and then automatically exchangeable), then any event in the σ-algebra $\mathcal{S}_\infty$ or in the σ-algebra $\mathcal{A}_\infty$ has measure 0 or 1. This is known as the Kolmogorov 0-1 law for $\mathcal{A}_\infty$ and the Hewitt-Savage 0-1 law for $\mathcal{S}_\infty$.*

Then, since we have to deal with sequences of random (empirical) measures, a few topological results on the space $\mathcal{P}(\mathcal{P}(E))$ are needed; this motivate the following results. A thorough discussion of the theory of random measures can be found in [101]. The most important notion in this context is the notion of moment measure defined below.

Definition 3.2.6 (Moment measures)**.** For $k \in \mathbb{N}$, the k-th moment measure of a measure $\pi \in \mathcal{P}(\mathcal{P}(E))$ is defined by:

$$\pi^k := \int_{\mathcal{P}(E)} \nu^{\otimes k} \pi(\mathrm{d}\nu) = \mathbb{E}_{\nu\sim\pi}\big[\nu^{\otimes k}\big] \in \mathcal{P}(E^k).$$

This definition is understood in the weak sense, so that $\langle \pi^k, \varphi_k\rangle = \mathbb{E}_{\nu\sim\pi}\langle \nu^{\otimes k}, \varphi_k\rangle$ for any φ_k in $C_b(E^k)$.

The moment measures are essential because they give useful characterisations of the convergence and the tightness in $\mathcal{P}(\mathcal{P}(E))$.

Lemma 3.2.7. *The following results hold true.*

(1) A sequence $(\pi_N)_N$ of random measures in $\mathcal{P}(\mathcal{P}(E))$ converges weakly towards $\pi \in \mathcal{P}(\mathcal{P}(E))$ if and only if

$$\forall k \geq 1, \quad \pi_N^k \underset{N\to+\infty}{\longrightarrow} \pi^k,$$

where the convergence is the weak convergence in $\mathcal{P}(E^k)$.

(2) The tightness of a sequence $(\pi_N)_N$ in $\mathcal{P}(\mathcal{P}(E))$ is equivalent to the tightness of the sequence $(\pi_N^1)_N$ in $\mathcal{P}(E)$.

Finally, the following theorem summarises the main results due to de Finetti, Hewitt and Savage.

Theorem 3.2.8. *Let $\pi \in \mathcal{P}(\mathcal{P}(E))$. Then there exists a sequence $(\overline{X}^i)_{i\geq 1}$ of E-valued exchangeable random variables such that the following properties hold.*

(1) For any $k \geq 1$, $(\overline{X}^1, \ldots, \overline{X}^k)$ has joint distribution π^k.

(2) The weak limit

$$\mu = \lim_{k\to+\infty} \frac{1}{k} \sum_{i=1}^{k} \delta_{\overline{X}^i} \in \mathcal{P}(E),$$

exists almost surely and μ is π-distributed.

(3) The random measure μ is $\mathcal{S}_\infty$-measurable, and conditionally on $\mathcal{S}_\infty$ the random variables $\overline{X}^i$ are independent and μ-distributed.

Conversely, if $(f^N)_N$ is an infinite sequence of symmetric probability measures on E^N, $N \in \mathbb{N}$, which satisfy the compatibility relation for all $j \leq k$,

$$\forall \varphi_j \in C_b(E^j), \quad \langle f^k, \varphi_j \otimes 1^{\otimes(k-j)} \rangle = \langle f^j, \varphi_j \rangle, \tag{3.5}$$

then there exists a unique $\pi \in \mathcal{P}(\mathcal{P}(E))$ such that for all N:

$$f^N = \pi^N := \int_{\mathcal{P}(E)} \nu^{\otimes N} \pi(\mathrm{d}\nu).$$

The first part of the theorem is due to de Finetti and can be found in [101, Theorem 11.2.1]. It states that infinite exchangeable systems are *conditionally* independent.

The question of chaos and propagation of chaos deals with the case when the "conditional" can be removed, i.e. when $\mathcal{S}_\infty$ is trivial. The second part of the theorem is due to Hewitt and Savage and can be found in [194, Theorem 5.1] with much more details and alternative quantitative versions. Note that when $f^N = f^{\otimes N}$ for a given f, then $\pi = \delta_f$ and this corresponds to the case when $\mathcal{S}_\infty$ is trivial in the first part.

3.2.3 Chaos and propagation of chaos

The mathematical notions of chaos and propagation of chaos, as defined below, have been introduced by Kac [223].

Definition 3.2.9 (Kac's chaos)**.** Let $f \in \mathcal{P}(E)$. A sequence $(f^N)_{N\geq 1}$ of symmetric probability measures on E^N is said to be *f-chaotic* when for any $k \in \mathbb{N}$ and any function $\varphi_k \in C_b(E^k)$,

$$\lim_{N\to+\infty} \langle f^N, \varphi_k \otimes 1^{\otimes N-k} \rangle = \langle f^{\otimes k}, \varphi_k \rangle.$$

It means that for all $k \in \mathbb{N}$, the k-th marginal satisfies $f^{k,N} \to f^{\otimes k}$ for the weak topology.

From now on, the initial distribution $f_0^N \in \mathcal{P}(E^N)$ of the various particle systems considered is always assumed to be f_0-chaotic for a given $f_0 \in \mathcal{P}(E)$. The goal is to prove that this initial chaoticity assumption is *propagated* at later times as in the following definition.

Definition 3.2.10 (Pointwise and pathwise propgation of chaos)**.** Let $f_0^N \in \mathcal{P}(E^N)$ be the initial f_0-chaotic distribution of $\mathcal{X}_0^N$ at time $t = 0$.

- *Pointwise propagation of chaos* holds towards a flow of measures $(f_t)_t \in C(I, \mathcal{P}(E))$ when the law $f_t^N \in \mathcal{P}(E^N)$ of $\mathcal{X}_t^N$ is f_t-chaotic for every time $t \in I$.
- *Pathwise propagation of chaos* holds towards a distribution $f_I \in \mathcal{P}(D(I, E))$ on the path space when the law $f_I^N \in \mathcal{P}\big(D(I, E)^N\big)$ of the process $\mathcal{X}_I^N$ (seen as a random element in $D(I, E)^N$) is f_I-chaotic.

The propagation of chaos property (pointwise or pathwise) describes the limit behaviour of the particle system when the number of particles grows to infinity. It implies that any subsystem (of fixed size) of the N-particle system asymptotically behaves as a system of i.i.d processes with common law f_t (note that the particles are always identically distributed by the exchangeability assumption). This translates the physical idea that for large systems, the correlations between two (or more) given particles which are due to the interactions become negligible. By looking at the whole system, only an averaged

behaviour can be observed instead of the detailed correlated trajectories of each particle. Thus, when propagation of chaos holds true, the central question becomes the description of the limit law f_t which will be defined as the solution of a nonlinear PDE or of a nonlinear martingale problem. The following characterization of the notion of chaos is very helpful to precise the notion of average behaviour and to construct the limit law.

Lemma 3.2.11. *Each of the following assertions is equivalent to Kac's chaos.*

(i) There exists $k \geq 2$ such that $f^{k,N}$ converges weakly towards $f^{\otimes k}$.

(ii) The random empirical measure

$$\mu_{\mathcal{X}^N} := \frac{1}{N} \sum_{i=1}^{N} \delta_{X^i},$$

converges in law towards the deterministic measure f, where for any $N \in \mathbb{N}$, $\mathcal{X}^N = (X^1, \ldots, X^N) \sim f^N$.

This lemma is not surprising owing to the results outlined in Section 3.2.2. An elementary proof can be found in [307].

3.3 Mean-field particle systems

All the particle systems discussed in this thesis belong the class of mean-field models. These models are defined by a N-particle generator $\mathcal{L}_N$ acting on N-particle test functions $\varphi_N \in C_b(E^N)$ which is of the form

$$\mathcal{L}_N \varphi_N(\mathbf{x}^N) = \sum_{i=1}^{N} L_{\mu_{\mathbf{x}^N}} \diamond_i \varphi_N(\mathbf{x}^N), \tag{3.6}$$

where $\mathbf{x}^N = (x^1, \ldots, x^N) \in E^N$ and given a probability measure $\mu \in \mathcal{P}(E)$, L_μ is the generator of a Markov process on E with domain $\mathcal{F}$ which will be either a diffusion or a jump process. We recall that $\mu_{\mathbf{x}^N} = \frac{1}{N} \sum_{i=1}^{N} \delta_{x^i}$ denotes the empirical measure. The notation $L \diamond_i \varphi_N$ denotes the function:

$$L \diamond_i \varphi_N : (x^1, \ldots, x^N) \in E^N \mapsto L[x \mapsto \varphi_N(x^1, \ldots, x^{i-1}, x, x^{i+1}, \ldots, x^N)](x^i) \in \mathbb{R}.$$

The limit behaviour when $N \to +\infty$ is commonly called a *mean-field limit* which, in this thesis, is in most cases a propagation of chaos result. The limit law will satisfy the

following weak nonlinear PDE

$$\forall \varphi \in \mathcal{F}, \quad \frac{\mathrm{d}}{\mathrm{d}t}\langle f_t, \varphi \rangle = \langle f_t, L_{f_t}\varphi \rangle. \tag{3.7}$$

There are other particle models which are not of mean-field type, in particular the Boltzmann models, also discussed in [76]. They will only be discussed in the present thesis as a perspective in Section 10.2.4.

McKean-Vlasov diffusion

When the generator L_μ in (3.6) is the generator of a diffusion process, the particle system is the solution the following system of SDEs

$$\forall i \in \{1, \dots, N\}, \quad \mathrm{d}X_t^{i,N} = b\big(X_t^{i,N}, \mu_{\mathcal{X}_t^N}\big)\mathrm{d}t + \sigma\big(X_t^{i,N}, \mu_{\mathcal{X}_t}\big)\mathrm{d}B_t^i, \tag{3.8}$$

for $i \in \{1, \dots, N\}$ where $(B_t^i)_t$ are N independent Brownian motions and the drift function b and diffusion matrix σ are of the form

$$b : \mathbb{R}^d \times \mathcal{P}(\mathbb{R}^d) \to \mathbb{R}^d, \quad \sigma : \mathbb{R}^d \times \mathcal{P}(\mathbb{R}^d) \to \mathcal{M}_d(\mathbb{R}).$$

The mean-field limit $N \to +\infty$ is given by the nonlinear Fokker-Planck equation

$$\partial_t f_t(x) = -\nabla_x \cdot \{b(x, f_t) f_t\} + \frac{1}{2}\sum_{i,j=1}^{d} \partial_{x_i}\partial_{x_j}\{a_{ij}(x, f_t) f_t\}, \tag{3.9}$$

where $a(x, \mu) := \sigma(x, \mu)\sigma(x, \mu)^{\mathrm{T}}$. This is the law of the *nonlinear McKean-Vlasov process* $(\overline{X}_t)_t$ which solves the following *nonlinear* SDE:

$$\mathrm{d}\overline{X}_t = b\big(\overline{X}_t, f_t\big)\mathrm{d}t + \sigma\big(\overline{X}_t, f_t\big)\mathrm{d}B_t. \tag{3.10}$$

where B_t is a Brownian motion and $f_t = \mathrm{Law}(\overline{X}_t)$. The wellposedness of (3.10) is proved under Lipschitz assumptions on b and σ in various settings in [250, Section 3], [307, Theorem 1.1], [252, Theorem 2.2] or [61, Theorem 1.7]. The denomination *nonlinear* (or more precisely, *nonlinear in the sense of McKean*) refers to the fact that the SDE (3.10) depends on the law f_t of the process that it defines.

Mean-field jump process

The N-particle process is defined by a generator of the form (3.6) where given $\mu \in \mathcal{P}(E)$, L_μ is the generator of a jump process of the form

$$L_\mu \varphi(x) = \lambda(x, \mu) \int_E \{\varphi(y) - \varphi(x)\} P_\mu(x, \mathrm{d}y).$$

It describes a system of N jump processes, driven by N independent Poisson processes with jump rate

$$\lambda : E \times \mathcal{P}(E) \to \mathbb{R}_+, \ (x, \mu) \mapsto \lambda(x, \mu).$$

The law of a particle after a jump is given by the jump measure:

$$P : E \times \mathcal{P}(E) \to \mathcal{P}(E), \ (x, \mu) \mapsto P_\mu(x, \mathrm{d}y).$$

Once again, at the particle level, both the jump rate and the post-jump distribution may depend on the whole system through the empirical measure.

One expects that in the limit $N \to +\infty$, the law f_t of a particle will satisfy the evolution equation (3.7) which, in this case, reads:

$$\frac{\mathrm{d}}{\mathrm{d}t}\langle f_t, \varphi \rangle = \iint_{E \times E} \lambda(x, f_t)\{\varphi(y) - \varphi(x)\} P_{f_t}(x, \mathrm{d}y) f_t(\mathrm{d}x), \tag{3.11}$$

for all $\varphi \in C_b(E)$. Note that one can easily add a piecewise deterministic component to this process by prescribing a deterministic flow between the jumps. Two important cases are given in the following examples.

Example 3.3.1 (BGK type model)**.** In kinetic theory the state space is $E = \mathbb{R}^d \times \mathbb{R}^d$ and the N particles are given by $Z_t^i = (X_t^i, V_t^i)$ with X_t^i the position and V_t^i the velocity of particle i at time t. Without external force, it is natural to expect that the particles evolve deterministically and continuously between two jumps as

$$\mathrm{d}X_t^i = V_t^i \mathrm{d}t, \quad \mathrm{d}V_t^i = 0.$$

Moreover, the post-jump distribution and the jump rate often do not depend specifically on the pre-jump velocity of the jumping particle but only on its position and on the distribution of particles. Thus we take:

$$P_\mu((x, v), \mathrm{d}x', \mathrm{d}v') = \delta_x(\mathrm{d}x') \otimes \mathscr{M}_{\mu,x}(v')\mathrm{d}v',$$

where given $\mu \in \mathcal{P}(E)$ and $x \in \mathbb{R}^d$, $\mathscr{M}_{\mu,x}$ is a probability density function. In this case, Equation (3.7) becomes:

$$\frac{\mathrm{d}}{\mathrm{d}t}\langle f_t, \varphi\rangle = \langle f_t, v \cdot \nabla_x \varphi\rangle + \iint_{\mathbb{R}^d \times \mathbb{R}^d} \lambda(x, f_t)\{\varphi(x, v') - \varphi(x, v)\}\mathscr{M}_{f_t,x}(v')\mathrm{d}v' f_t(\mathrm{d}x, \mathrm{d}v),$$

and its strong form reads:

$$\partial_t f_t(x, v) + v \cdot \nabla_x f_t(x, v) = \lambda(x, f_t)\Big(\rho_{f_t}(x)\mathscr{M}_{f_t,x}(v) - f_t(x, v)\Big),$$

where the spatial density of the particles at time t is defined by $\rho_{f_t}(x) := \int_{\mathbb{R}^d} f_t(x, v)\mathrm{d}v$. When $\mathscr{M}_{f_t,x}$ is the Maxwellian distribution

$$\mathscr{M}_{f_t,x}(v) = \frac{\rho_f}{(2\pi T)^{d/2}} \exp\left(\frac{|v - u|^2}{2T}\right),$$

with $(\rho_f u, \rho_f |u|^2 + \rho_f T) = \int_{\mathbb{R}^d}(v, |v|^2) f_t(x, v)\mathrm{d}v$, then this equation is called the Bhatnagar-Gross-Krook (BGK) equation [34]. It is used in mathematical physics as a simplified model of rarefied gas dynamics (for a detailed account of the subject, we refer the interested reader to the reviews [108] and [324] or to the book [75]).

It is sometimes useful to distinguish a class of mean-field jump models that we call *parametric models* which are defined by a jump measure of the form

$$P_\mu(x, \mathrm{d}y) = \Big(\psi(x, \mu, \cdot)_\# \nu\Big)(\mathrm{d}y),$$

where $\nu \in \mathcal{P}(\Theta)$ is a probability measure on a fixed parameter space Θ and

$$\psi : E \times \mathcal{P}(E) \times \Theta \to E.$$

In this case, for all test function $\varphi \in C_b(E)$,

$$\int_E \varphi(y) P_\mu(x, \mathrm{d}y) = \int_\Theta \varphi\big(\psi(x, \mu, \theta)\big)\nu(\mathrm{d}\theta).$$

One of the main advantages is that the N-particle process associated to a parametric model admits a natural SDE representation using the formalism of Poisson random measures.

Example 3.3.2 (SDE representation for parametric models)**.** Let us assume for all $\theta \in \Theta$, the function $\psi(\cdot, \cdot, \theta) : E \times \mathcal{P}(E) \to E$ is Lipschitz for the distance on E and the Wasserstein - 1 distance on $\mathcal{P}(E)$, with a Lipschitz constant $L(\theta) > 0$ and a

function $L \in L^1_\nu(\Theta)$. This (classical) hypothesis will ensure the wellposedness of the SDE representations of both the particle system and its nonlinear limit, see [5, Section 3.1] and [175, Theorem 1.2 and Theorem 2.1]. To each particle $i \in \{1, \dots, N\}$ is attached an independent Poisson random measure $\mathcal{N}^i(\mathrm{d}s, \mathrm{d}u, \mathrm{d}\theta)$ on $[0, +\infty) \times [0, +\infty) \times \Theta$ with intensity measure $\mathrm{d}s \otimes \mathrm{d}u \otimes \nu(\mathrm{d}\theta)$ where $\mathrm{d}t$ and $\mathrm{d}u$ denote the Lebesgue measure. The N independent random measures $\mathcal{N}^i$ play a comparable role to the N independent Brownian motions which define a McKean-Vlasov diffusion in (3.8). In the present case, the mean-field jump N-particle process is the solution of the following system of SDEs driven by the measures $\mathcal{N}^i$

$$X^i_t = X^i_0 + \int_0^t a(X^i_s)\mathrm{d}s + \int_0^t \int_0^{+\infty} \int_\Theta \left\{ \psi\Big(X^i_{s^-}, \mu_{\mathcal{X}^N_{s^-}}, \theta\Big) - X^i_{s^-} \right\} \mathbb{1}_{\left(0, \lambda\left(X^i_{s^-}, \mu_{\mathcal{X}^N_{s^-}}\right)\right]}(u)\, \mathcal{N}^i(\mathrm{d}s, \mathrm{d}u, \mathrm{d}\theta). \tag{3.12}$$

This is for instance a common modelling framework for many models of interacting neurons [5, 163, 105]. Similarly to the McKean-Vlasov case, the mean-field limit can be obtained by simply replacing in this equation the empirical measure by the limit law.

3.4 Proving propagation of chaos

Since the seminal work of McKean [250], later extended by Sznitman [307], a very popular method of proving propagation of chaos for mean-field systems is the so-called synchronous coupling method (Section 3.4.1). Over the last years, some alternative coupling methods have been proposed to handle either weaker regularity or to get uniform in time estimates under mild physically relevant assumptions (Section 3.4.2). Alternatively to these SDE techniques, the empirical process can be studied using stochastic compactness methods [306, 176], leading to (non quantitative) results valid for mixed jump-diffusion models (Section 3.4.3). A more analytical point of view on the empirical measure process, originally due to Grünbaum [179], has been recently developed by [258, 257] (Section 3.4.4). Finally, recent works focus on large deviation techniques, in particular the derivation of entropy bound from Girsanov transform [208, 235]. This allows interactions with a very weak regularity or with a very general form (Section 3.4.5).

3.4.1 McKean's theorem and the synchronous coupling method

When a trajectorial description of the particle system is available, the coupling method initiated by McKean [250] and Sznitman [307] consists in comparing the trajectories of the particle system with the trajectories of a system of N i.i.d processes with common law f_t.

Definition 3.4.1 (Chaos by coupling the trajectories)**.** Let be given a final time $T \in (0, \infty]$, a distance d_E on E and $p \in \mathbb{N}$. Propagation of chaos holds by coupling the trajectories when for all $N \in \mathbb{N}$ there exist

- a system of particles $(\mathcal{X}_t^N)_t$ with law $f_t^N \in \mathcal{P}(E^N)$ at time $t \leq T$,
- a system of *independent* processes $\big(\overline{\mathcal{X}}_t^N\big)_t$ with law $f_t^{\otimes N} \in \mathcal{P}(E^N)$ at time $t \leq T$,
- a number $\varepsilon(N,T) > 0$ such that $\varepsilon(N,T) \underset{N\to+\infty}{\longrightarrow} 0$,

such that (pathwise case)

$$\frac{1}{N}\sum_{i=1}^{N} \mathbb{E}\left[\sup_{t\leq T} d_E\big(X_t^i, \overline{X}_t^i\big)^p\right] \leq \varepsilon(N,T), \tag{3.13}$$

or (pointwise case)

$$\frac{1}{N}\sum_{i=1}^{N} \sup_{t\leq T} \mathbb{E}\big[d_E\big(X_t^i, \overline{X}_t^i\big)^p\big] \leq \varepsilon(N,T). \tag{3.14}$$

Note that (3.13) implies (3.14). The bound (3.14) implies:

$$\sup_{t\leq T} W_p\big(f_t^N, f_t^{\otimes N}\big) \leq \varepsilon(N,T) \underset{N\to+\infty}{\longrightarrow} 0,$$

where W_p denotes the Wasserstein-p distance on $\mathcal{P}(E^N)$ defined for $\mu, \nu \in E^N$ by:

$$W_p(\mu,\nu) := \inf_{\pi\in\Pi(\mu,\nu)} \left(\frac{1}{N}\sum_{i=1}^{N} \int_{E^N\times E^N} |x^i - y^j|^p \pi(\mathrm{d}\mathbf{x}^N, \mathrm{d}\mathbf{y}^N)\right)^{1/p},$$

and $\Pi(\mu,\nu)$ is the set of all probability measures on $E^N \times E^N$ with marginals μ and ν. It implies the propagation of chaos in the sense of Definition 3.2.10 since the topology induced by the Wasserstein distance is stronger than the topology of the weak convergence of probability measures (for more details on the use of the Wasserstein distance in this context, see for instance [194, 328, 326] or [76] and the references therein).

The following fundamental theorem originally due to McKean proves such coupling bound for the diffusion process (3.8).

Theorem 3.4.2 (McKean)**.** *Let the drift and diffusion coefficients in* (3.8) *be defined by*

$$\forall x \in \mathbb{R}^d, \forall \mu \in \mathcal{P}(\mathbb{R}^d), \quad b(x,\mu) := \tilde{b}\big(x, K_1 \star \mu(x)\big), \quad \sigma(x,\mu) = \tilde{\sigma}\big(x, K_2 \star \mu(x)\big), \quad (3.15)$$

where $K_1 : \mathbb{R}^d \times \mathbb{R}^d \to \mathbb{R}^m$, $K_2 : \mathbb{R}^d \times \mathbb{R}^d \to \mathbb{R}^n$, $\tilde{b} : \mathbb{R}^d \times \mathbb{R}^m \to \mathbb{R}^d$ *and* $\tilde{\sigma} : \mathbb{R}^d \times \mathbb{R}^n \to \mathcal{M}_d(\mathbb{R})$ *are globally Lipschitz and* K_1, K_2 *are bounded. Then pathwise chaos by coupling in the sense of Definition 3.4.1 holds for any* $T > 0$, $p = 2$, *with the synchronous coupling*

$$X_t^{i,N} = X_0^i + \int_0^t \tilde{b}\big(X_s^{i,N}, K_1 \star \mu_{\mathcal{X}_s^N}\big(X_s^{i,N}\big)\big)\mathrm{d}s + \int_0^t \tilde{\sigma}\big(X_s^{i,N}, K_2 \star \mu_{\mathcal{X}_s^N}\big(X_s^{i,N}\big)\big)\mathrm{d}B_s^i, \quad (3.16)$$

and

$$\overline{X}_t^{i,N} = X_0^i + \int_0^t \tilde{b}\big(\overline{X}_s^{i,N}, K_1 \star f_s\big(\overline{X}_s^{i,N}\big)\big)\mathrm{d}s + \int_0^t \tilde{\sigma}\big(\overline{X}_s^{i,N}, K_2 \star f_s\big(\overline{X}_s^{i,N}\big)\big)\mathrm{d}B_s^i. \quad (3.17)$$

The name "synchronous" comes from the fact that the Brownian motion $(B_t^i)_t$ *in* (3.16) *and* (3.17) *is the same for the two processes. More precisely, the trajectories satisfy:*

$$\frac{1}{N}\sum_{i=1}^N \mathbb{E}\left[\sup_{t\le T}\left|X_t^i - \overline{X}_t^i\right|^2\right] \le \varepsilon(N,T),$$

where the convergence rate is given by

$$\varepsilon(N,T) = \frac{c_1(b,\sigma,T)}{N}\mathrm{e}^{c_2(b,\sigma,T)T}, \quad (3.18)$$

for some absolute constants $C, \tilde{C}, C_{\mathrm{BDG}} > 0$ *not depending on* N, T,

$$c_1(b,\sigma,T) := CT\Big(T\|K_1\|_\infty^2\|\tilde{b}\|_{\mathrm{Lip}}^2 + C_{\mathrm{BDG}}\|K_2\|_\infty^2\|\tilde{\sigma}\|_{\mathrm{Lip}}^2\Big), \quad (3.19)$$

and

$$c_2(b,\sigma,T) := \tilde{C}\Big(T\big(1+\|K_1\|_{\mathrm{Lip}}^2\big)\|\tilde{b}\|_{\mathrm{Lip}}^2 + C_{\mathrm{BDG}}\big(1+\|K_2\|_{\mathrm{Lip}}^2\big)\|\tilde{\sigma}\|_{\mathrm{Lip}}^2\Big). \quad (3.20)$$

As the synchronous coupling idea will be at the basis of the propagation of chaos result in Chapter 4, we present two proofs of this result. The first one is the original proof due to McKean [250]. The second one is due to Sznitman [307]. Sznitman's proof is a slightly shorter and more general version of McKean's proof. We chose to include McKean's original argument for three reasons. First it gives an interesting and somehow unusual probabilistic point of view on the interplay between exchangeability and independence (see

Section 3.2.2). This is an underlying idea for all the models presented in this review which is made very explicit in McKean's proof. Secondly, although the computations in both proofs are very much comparable, McKean's proof is philosophically an existence result while Sznitman's proof is based on the wellposedness result stated in [307, Theorem 1.1]. Finally, it seems that McKean's proof has been somehow forgotten in the community or is sometimes confused with Sznitman's proof which in turn has become incredibly popular. McKean's argument was first published in [249] and then re-published in [250]. Both references are not easy to find nowadays and it is probably the source of the confusion between the two proofs.

Proof (McKean). The originality of this proof is that the nonlinear process is not introduced initially. It appears as the limit of a Cauchy sequence of coupled systems of particles with increasing size. Let $(B_t^i)_t$, $i \geq 1$ be an infinite collection of independent Brownian motions and for $N \in \mathbb{N}$ we recall the notation

$$\mathcal{X}_t^N = \big(X_t^{1,N}, \dots, X_t^{N,N}\big) \in (\mathbb{R}^d)^N,$$

where $(X_t^{i,N})_t$ solves (3.16). The idea is to prove that the sequence (in N) of processes $(X_t^{1,N})_t$ is a Cauchy sequence in $L^2\big(\Omega, C([0,T],\mathbb{R}^d)\big)$ and then to identify the limit as the solution of (3.17). The proof is split into several steps.

Step 1. *Cauchy estimate*

Let $M > N$ and let us consider the coupled particle systems $\mathcal{X}^N$ and $\mathcal{X}^M$ where the N first particles in $\mathcal{X}^M$ have the same initial condition as $X^{1,N}, \dots, X^{N,N}$ and are driven by the same Brownian motions $B^1, \dots B^N$. Using (3.16) and the Burkholder-Davis-Gundy inequality it holds that for a constant $C_{\mathrm{BDG}} > 0$,

$$\begin{aligned}\mathbb{E}\Big[\sup_{t\leq T}\big|X_t^{1,M} - X_t^{1,N}\big|^2\Big] \leq 2T\int_0^T \mathbb{E}\Big|b\Big(X_t^{1,M}, \mu_{\mathcal{X}_t^M}\Big) - b\Big(X_t^{1,N}, \mu_{\mathcal{X}_t^N}\Big)\Big|^2 \mathrm{d}t \\ + 2C_{\mathrm{BDG}}\int_0^T \mathbb{E}\Big|\sigma\Big(X_t^{1,M}, \mu_{\mathcal{X}_t^M}\Big) - \sigma\Big(X_t^{1,N}, \mu_{\mathcal{X}_t^N}\Big)\Big|^2 \mathrm{d}t. \quad (3.21)\end{aligned}$$

For the first term on the right-hand side of (3.21), we write:

$$\begin{aligned}\mathbb{E}\Big|b\Big(X_t^{1,M}, \mu_{\mathcal{X}_t^M}\Big) - b\Big(X_t^{1,N}, \mu_{\mathcal{X}_t^N}\Big)\Big|^2 \leq 2\mathbb{E}\Big|b\Big(X_t^{1,M}, \mu_{\mathcal{X}_t^M}\Big) - b\Big(X_t^{1,M}, \mu_{\mathcal{X}_t^{N,M}}\Big)\Big|^2 \\ + 2\mathbb{E}\Big|b\Big(X_t^{1,M}, \mu_{\mathcal{X}_t^{N,M}}\Big) - b\Big(X_t^{1,N}, \mu_{\mathcal{X}_t^N}\Big)\Big|^2, \quad (3.22)\end{aligned}$$

where $\mathcal{X}_t^{N,M} = \big(X_t^{1,M}, \dots, X_t^{N,M}\big) \in (\mathbb{R}^d)^N$. Each of the two terms on the right-hand side of (3.22) is controlled using (3.15), the Lipschitz assumptions and the fact that the $X^{j,M}$ are identically distributed. For the first term, expanding the square gives:

$$\begin{aligned}
&\mathbb{E}\Big|b\Big(X_t^{1,M}, \mu_{\mathcal{X}_t^M}\Big) - b\Big(X_t^{1,M}, \mu_{\mathcal{X}_t^{N,M}}\Big)\Big|^2 \\
&\leq \|\tilde{b}\|_{\mathrm{Lip}}^2\, \mathbb{E}\Big|\frac{1}{M}\sum_{j=1}^{M} K_1\Big(X_t^{1,M}, X_t^{j,M}\Big) - \frac{1}{N}\sum_{j=1}^{N} K_1\Big(X_t^{1,M}, X_t^{j,M}\Big)\Big|^2 \\
&\leq \|\tilde{b}\|_{\mathrm{Lip}}^2 \left(\frac{1}{M} + \frac{1}{N} - 2\frac{N}{MN}\right)\mathbb{E}\Big|K_1\Big(X_t^{1,M}, X_t^{2,M}\Big)\Big|^2 \\
&\quad + \|\tilde{b}\|_{\mathrm{Lip}}^2 \left(\frac{M-1}{M} + \frac{N-1}{N} - 2\frac{M(N-1)}{MN}\right)\times \\
&\qquad\qquad \times \mathbb{E}\Big[K_1\Big(X_t^{1,M}, X_t^{2,M}\Big)\cdot K_1\Big(X_t^{1,M}, X_t^{3,M}\Big)\Big] \\
&\leq 2\left(\frac{1}{N} - \frac{1}{M}\right)\|K_1\|_\infty^2 \|\tilde{b}\|_{\mathrm{Lip}}^2.
\end{aligned}$$

For the second term, the Lipschitz assumptions leads to:

$$\begin{aligned}
&\mathbb{E}\Big|b\Big(X_t^{1,M}, \mu_{\mathcal{X}_t^{N,M}}\Big) - b\Big(X_t^{1,N}, \mu_{\mathcal{X}_t^{N}}\Big)\Big|^2 \\
&\quad \leq 2\|\tilde{b}\|_{\mathrm{Lip}}^2\, \mathbb{E}\Big[\big|X_t^{1,N} - X_t^{1,M}\big|^2 \\
&\qquad\qquad + \Big|\frac{1}{N}\sum_{j=1}^{N} K_1\Big(X_t^{1,M}, X_t^{j,M}\Big) - \frac{1}{N}\sum_{j=1}^{N} K_1\Big(X_t^{1,N}, X_t^{j,N}\Big)\Big|^2\Big] \\
&\quad \leq 2\left(1 + 2\|K_1\|_{\mathrm{Lip}}^2\right)\|\tilde{b}\|_{\mathrm{Lip}}^2\, \mathbb{E}\big|X_t^{1,N} - X_t^{1,M}\big|^2.
\end{aligned}$$

The same estimates hold for the diffusion term on the right-hand side of (3.21) with σ instead of b and K_2 instead of K_1. Gathering everything thus leads to:

$$\mathbb{E}\Big[\sup_{t\leq T}\big|X_t^{1,M} - X_t^{1,N}\big|^2\Big] \leq \left(\frac{1}{N} - \frac{1}{M}\right)c_1(b,\sigma,T) + c_2(b,\sigma,T)\int_0^T \mathbb{E}\big|X_t^{1,N} - X_t^{1,M}\big|^2 \mathrm{d}t$$

where c_1 and c_2 are defined by (3.19) and (3.20). Using (a generalisation of) Gronwall lemma, it follows that:

$$\mathbb{E}\Big[\sup_{t\leq T}\big|X_t^{1,M} - X_t^{1,N}\big|^2\Big] \leq \left(\frac{1}{N} - \frac{1}{M}\right)c_1(b,\sigma,T)\mathrm{e}^{c_2(b,\sigma,T)T}. \tag{3.23}$$

Step 2. *Cauchy limit and exchangeability*

The previous estimate implies that the sequence of random variables $(X^{1,N})_N$ is a Cauchy sequence in $L^2(\Omega, C([0,T],\mathbb{R}^d))$. Since this space is complete, this sequence has a limit denoted by $\overline{X}^1 \equiv (\overline{X}^1_t)_t$. Applying the same reasoning for any $k \in \mathbb{N}$, there exists an infinite collection of processes $\overline{X}^k$, defined for each $k \geq 1$ as the limit of $(X^{k,N})_N$. These processes are identically distributed and their common law depends only on $(X^i_0)_{i\geq 1}$ and $(B^i)_{i\geq 1}$ which are independent random variables. Moreover, knowing (X^1_0, B^1) and for any measurable set $\mathscr{B}$, any event of the type $\{\overline{X}^1 \in \mathscr{B}\}$ belongs to the σ-algebra of exchangeable events generated by the random variables $(X^i_0)_{i\geq 2}$ and $(B^i)_{i\geq 2}$. Since these random variables are i.i.d, Hewitt-Savage 0-1 law states that this σ-algebra is actually trivial. It follows that $\overline{X}^1$ is a functional of X^1_0 and B^1 only. The same reasoning applies for each $\overline{X}^k$ and hence the processes $\overline{X}^k$ are also independent.

Step 3. *Identification of the limit*

At this point, propagation of chaos is already proved and it only remains to identify the law of the $\overline{X}^k_t$ as the law of the solution of (3.17). To do so, McKean defines for $i \in \{1,\dots,N\}$ the processes

$$\widetilde{X}^{i,N}_t = X^i_0 + \int_0^t b\Big(\overline{X}^i_s, \mu_{\overline{\mathcal{X}}^N_s}\Big)\mathrm{d}s + \int_0^t \sigma\Big(\overline{X}^i_s, \mu_{\overline{\mathcal{X}}^N_s}\Big)\mathrm{d}B^i_s,$$

where $\overline{\mathcal{X}}^N_t = (\overline{X}^1_t, \dots, \overline{X}^N_t)$. From the independence of the processes and by the strong law of large numbers, the right hand side converges almost surely as $N \to +\infty$ towards the right hand side of (3.17) with f_s being the law of $\overline{X}^i_s$ (which is the same for all i). Moreover, direct Lipschitz estimates lead to

$$\mathbb{E}\Big[\sup_{t\leq T}\big|\widetilde{X}^i_t - X^i_t\big|^2\Big] \leq \frac{C}{N},$$

where C is a constant which depends only on T, $\|K_1\|_{\mathrm{Lip}}$, $\|K_2\|_{\mathrm{Lip}}$. By uniqueness of the limit, it follows that $\overline{X}^i_t$ satisfies (3.17). Moreover, the bound (3.18) is obtained by taking the limit $M \to +\infty$ in (3.23). □

The following famous proof is due to Sznitman [307] in the case where σ is constant and with $p = 1$ in Definition 3.4.1. The following (direct) adaptation to the model of Theorem 3.4.2 can be found in [221, Proposition 2.3].

Proof (Sznitman). With a more direct approach, the strategy is to introduce both the particle system and its (known) limit given respectively by (3.16) and (3.17) and to estimate directly the discrepancy between the two processes. Using the Burkholder-Davis-Gundy

inequality, it holds that for a constant $C_{\mathrm{BDG}} > 0$,

$$\mathbb{E}\left[\sup_{t\le T}\left|\overline{X}_t^i - X_t^i\right|^2\right] \le 2T\int_0^T \mathbb{E}\Big|b\big(\overline{X}_t^i, f_t\big) - b\Big(X_t^i, \mu_{\mathcal{X}_t^N}\Big)\Big|^2 \mathrm{d}t \\ + 2C_{\mathrm{BDG}}\int_0^T \mathbb{E}\Big|\sigma\big(\overline{X}_t^i, f_t\big) - \sigma\Big(X_t^i, \mu_{\mathcal{X}_t^N}\Big)\Big|^2 \mathrm{d}t. \quad (3.24)$$

The drift term on the right-hand side of (3.24) is split into two terms as follows:

$$\mathbb{E}\Big|b\big(\overline{X}_t^i, f_t\big) - b\Big(X_t^i, \mu_{\mathcal{X}_t^N}\Big)\Big|^2 \le 2\mathbb{E}\Big|b\big(\overline{X}_t^i, f_t\big) - b\Big(\overline{X}_t^i, \mu_{\overline{\mathcal{X}}_t^N}\Big)\Big|^2 \\ + 2\mathbb{E}\Big|b\Big(\overline{X}_t^i, \mu_{\overline{\mathcal{X}}_t^N}\Big) - b\Big(X_t^i, \mu_{\mathcal{X}_t^N}\Big)\Big|^2. \quad (3.25)$$

For the first term on the right-hand side of (3.25), the assumption (3.15) and the Lipschitz assumptions give:

$$\mathbb{E}\Big|b\big(\overline{X}_t^i, f_t\big) - b\Big(\overline{X}_t^i, \mu_{\overline{\mathcal{X}}_t^N}\Big)\Big|^2 \le \|\tilde{b}\|_{\mathrm{Lip}}^2\,\mathbb{E}\Big|K_1 \star f_t(\overline{X}_t^i) - \frac{1}{N}\sum_{j=1}^N K_1(\overline{X}_t^i, \overline{X}_t^j)\Big|^2 \\ = \frac{\|\tilde{b}\|_{\mathrm{Lip}}^2}{N^2}\,\mathbb{E}\Big|\sum_{j=1}^N \Big\{K_1 \star f_t(\overline{X}_t^i) - K_1(\overline{X}_t^i, \overline{X}_t^j)\Big\}\Big|^2.$$

Expanding the square, it leads to:

$$\mathbb{E}\Big|b\big(\overline{X}_t^i, f_t\big) - b\Big(\overline{X}_t^i, \mu_{\overline{\mathcal{X}}_t^N}\Big)\Big|^2 \le \frac{4\|\tilde{b}\|_{\mathrm{Lip}}^2\|K_1\|_\infty^2}{N} \\ + \frac{\|\tilde{b}\|_{\mathrm{Lip}}^2}{N^2}\sum_{k\neq\ell}\mathbb{E}\big[\big(K_1 \star f_t(\overline{X}_t^i) - K_1(\overline{X}_t^i, \overline{X}_t^k)\big)\cdot\big(K_1 \star f_t(\overline{X}_t^i) - K_1(\overline{X}_t^i, \overline{X}_t^\ell)\big)\big].$$

When $k \neq \ell$, using the fact that $\overline{X}^k$ and $\overline{X}^\ell$ are independent gives:

$$\mathbb{E}\big[\big(K_1 \star f_t(\overline{X}_t^i) - K_1(\overline{X}_t^i, \overline{X}_t^k)\big)\cdot\big(K_1 \star f_t(\overline{X}_t^i) - K_1(\overline{X}_t^i, \overline{X}_t^\ell)\big)\big] = 0,$$

In conclusion,

$$\mathbb{E}\Big|b\big(\overline{X}_t^i, f_t\big) - b\Big(\overline{X}_t^i, \mu_{\overline{\mathcal{X}}_t^N}\Big)\Big|^2 \le \frac{4\|\tilde{b}\|_{\mathrm{Lip}}^2\|K_1\|_\infty^2}{N}. \quad (3.26)$$

For the second-term on the right-hand side of (3.25), the Lipschitz assumptions give:

$$\mathbb{E}\Big|b\Big(\overline{X}_t^i, \mu_{\overline{\mathcal{X}}_t^N}\Big) - b\Big(X_t^i, \mu_{\mathcal{X}_t^N}\Big)\Big|^2 \le C\|\tilde{b}\|_{\mathrm{Lip}}^2\big(1 + \|K_1\|_{\mathrm{Lip}}^2\big)\mathbb{E}\big|\overline{X}_t^i - X_t^i\big|^2. \quad (3.27)$$

The same estimates hold when b and K_1 are replaced by σ and K_2. Gathering everything leads to:

$$\begin{aligned}\mathbb{E}\left[\sup_{t\leq T}\left|\overline{X}_t^i - X_t^i\right|^2\right] &\leq \frac{1}{N}c_1(b,\sigma,T) + c_2(b,\sigma,T)\int_0^T \mathbb{E}\left|\overline{X}_t^i - X_t^i\right|^2 \mathrm{d}t \\ &\leq \frac{1}{N}c_1(b,\sigma,T) + c_2(b,\sigma,T)\int_0^T \mathbb{E}\left[\sup_{s\leq t}\left|\overline{X}_s^i - X_s^i\right|^2\right]\mathrm{d}t.\end{aligned}$$

The conclusion follows by Gronwall lemma. □

McKean's theorem can be directly generalised to more general, yet Lipschitz, settings, see for instance [5] where the authors consider a mixed jump-diffusion process with more general coefficients. A similar result with a more elementary method will also be presented in Chapter 4 for a PDMP process.

There are mainly two directions to improve the result of McKean's theorem: the first one is to consider weaker than globally Lipschitz interactions, the second one is to prove that the result holds uniformly in time. For the former, there are at least two general approaches. In [40] the authors prove that one can consider only locally Lipschitz interaction functions (3.15) with polynomial growth provided that high moment estimates can be proved. See also [153] for a similar result for PDMPs. A second approach is a cut-off approach in order to approximate singular or purely local systems. When the size of the cutoff is scaled with N, this kind of result is called *moderate interaction* following the terminology introduced by Oelschläger [273] and improved in [221]. A large part of Chapter 4 will be devoted to the question of moderate interaction for geometrically enriched PDMP systems. Regarding the question of uniform in time propagation of chaos using the synchronous coupling method, the main reference is the seminal work of Malrieu [245] which deals with gradient diffusion systems, that is when σ is constant and b is of the form $b(x,\mu) = -\nabla V(x) - \nabla W \star \mu(x)$ where V, W are two potentials which satisfy (strong) convexity assumptions. This model is linked to the study of the granular media equation [27, 26, 70, 71, 41] and has been widely studied in the last two decades as a prototypical model where uniform in time propagation of chaos may or may not hold due to phase transition phenomena. On this subject, see the recent works [133, 132] and the references therein, as well as the next section.

3.4.2 Other coupling methods

The uniform in time version of McKean's theorem can also be proved by considering other coupling techniques than the synchronous coupling. A recent and fruitful idea is the

reflection coupling originally developed in [151, 152]. Instead of taking the same Brownian motion in the two processes (3.16) and (3.17), the idea is to consider that one Brownian motion is a reflection of the other with respect to a well chosen hyperplane. Using Itō's formula, this change will add a new correction term which can be used to control the final Gronwall estimate. This idea has been put into practise in [150] which extends the work of [245] by weakening the regularity and convexity hypotheses. Finally, the two recent works [294] and [130] are based on a classical result in gradient flow theory to prove uniform in time propagation of chaos and convergence to equilibrium results for gradient systems. The article [294] shows that this approach actually provides a unifying and more analytical framework for all coupling methods.

3.4.3 Stochastic compactness methods

Compactness methods are based on the empirical measure characterisation given by Lemma 3.2.11. It reduces the problem to the convergence in law of a sequence of random probability measures, that is the convergence of a sequence of laws which belong to $\mathcal{P}(\mathcal{P}(E))$. This space does not depend on N but it is in turn much more delicate to handle than E. The stochastic analysis approach is based on the adaptation of the classical martingale arguments [217] to this extended setting. The first works in this direction trace back to Tanaka [309] and Sznitman [305] for questions related to the Boltzmann equation. The case of mean-field jump and diffusion processes is treated in particular in [176, 252]. The main arguments are summarised below.

(1) In stochastic analysis, a particle is seen as a random process, i.e. a random element of the Skorokhod space $D([0,T],E)$. The empirical measure $\mu_{\mathcal{X}^N_{[0,T]}}$ of a particle system $\mathcal{X}^N_{[0,T]} \in D([0,T],E)^N$ is therefore a random element of $\mathcal{P}(D([0,T],E))$ and its law will be denoted by $F^N_{[0,T]} \in \mathcal{P}(\mathcal{P}(D([0,T],E)))$.

(2) The key element of the proof is the tightness of the sequence $(F^N_{[0,T]})_N$ although it usually follows from the adaptation of classical tightness criteria.

(3) Prokhorov theorem then ensures the existence of a limit point $\pi \in \mathcal{P}(\mathcal{P}(D([0,T],E)))$. The π-distributed limit points are then shown to satisfy a limit martingale problem. This is the stochastic analog of a nonlinear PDE (it is actually more general).

(4) The conclusion follows by proving the uniqueness of the limit martingale problem (this implies that π is a Dirac delta at this point).

Note that an alternative, weaker, point of view is to see the empirical measure as a measure-valued process, that is a random element of $D([0,T],\mathcal{P}(E))$. The previous line of arguments remains the same but the convergence holds in the space $\mathcal{P}(D([0,T],\mathcal{P}(E)))$. This result is usually called a *functional law of large numbers* in this context. An example will be presented in the last section of Chapter 4. Finally an even weaker point of view is the pointwise version: at each time t, the law of the empirical measure belongs to $\mathcal{P}(\mathcal{P}(E))$ and this defines a curve with values in $\mathcal{P}(\mathcal{P}(E))$, that is an element of $C([0,T],\mathcal{P}(\mathcal{P}(E)))$. The recent article [69] is based on this point of view and a gradient-flow characterisation of McKean-Vlasov gradient systems.

3.4.4 Semi-group approach

In a series of recent works [258, 257], Mischler, Mouhot and Wennberg introduced a novel very general approach based on the fine study of the generator of the empirical measure process. This approach is inspired by the seminal work of Grünbaum [179]. This is also a pointwise approach which takes as a starting point the law $F_t^N \in \mathcal{P}(\mathcal{P}(E))$ of the empirical measure at each time $t \in [0,T]$. The idea is to compare F_t^N with the law $\overline{F}_t^N$ of the process $\overline{S}_t(\mu_{\mathcal{X}_0^N})$ where $(\overline{S}_t)_t$ is the nonlinear solution semi-group associated to the limit PDE and $\mu_{\mathcal{X}_0^N}$ is the initial random empirical measure of N i.i.d. f_0-distributed random variables. This law is expected to be close to the true solution $f_t = \overline{S}_t(f_0)$ using stability estimates on the limit PDE and Lemma 3.2.2. Taking a test function $\Phi \in C_b(\mathcal{P}(E))$, the two laws F_t^N and $\overline{F}_t^N$ define two dual semi-groups $\widehat{T}_{N,t}$ and $T_{\infty,t}$ acting on $C_b(\mathcal{P}(E))$ by

$$\begin{aligned}
\langle F_t^N, \Phi\rangle &= \int_{E^N} \widehat{T}_{N,t}\Phi(\mu_{\mathbf{x}^N}) f_0^{\otimes N}\big(\mathrm{d}\mathbf{x}^N\big),\\
\langle \overline{F}_t^N, \Phi\rangle &= \int_{E^N} T_{\infty,t}\Phi(\mu_{\mathbf{x}^N}) f_0^{\otimes N}\big(\mathrm{d}\mathbf{x}^N\big) := \int_{E^N} \Phi\big(\overline{S}_t\big(\mu_{\mathbf{x}^N}\big)\big) f_0^{\otimes N}\big(\mathrm{d}\mathbf{x}^N\big).
\end{aligned}$$

The goal is to prove the convergence of the semi-groups $\widehat{T}_{N,t} \to T_{\infty,t}$. In a classical setting, the convergence of a sequence of semi-groups acting on a set of test functions over a Banach space is solved by Trotter [316] by proving the convergence of the generators. While a notion of generator associated to $\widehat{T}_{N,t}$ can be easily defined, it is not the case for $T_{\infty,t}$ because $\mathcal{P}(E)$ is only a metric space and not a Banach space. The rigorous definition of this generator is one of the main contributions of [258, 257] and it is based in particular on a notion of differentiability on the space of probability measures. The main abstract theorems [258, Theorem 2.1] and [257, Theorem 3.1] can be applied to a wide range of particle systems by reducing the problem to the proof of a detailed set

of abstract assumptions which ensure (among other things) the well-posedness of the generator associated to $T_{\infty,t}$.

In parallel to the work of [257, 258], various similar in spirit semi-group approaches have also recently been developed in particular in the mean-field game community. All these approaches use at some point a tailored notion of differentiability in the space of measures. For recent developments, see for instance [81, 79, 131] and the references therein.

3.4.5 Large deviation methods and entropy bounds

Kac's chaos can be seen as a kind of weak law of large numbers, as it implies the weak convergence:

$$\langle \mu_{\mathcal{X}^N}, \varphi \rangle - \mathbb{E}_{\mathcal{X}^N}\left[\varphi\big(X^{1,N}\big)\right] \underset{N\to+\infty}{\longrightarrow} 0.$$

The main difference with the classical law of large numbers is that the random variables $\mathcal{X}^N$ are only exchangeable and not independent. When a strong law of large numbers holds, it is natural to look at the fluctuations of $\langle \mu_{\mathcal{X}^N}, \varphi \rangle$ by establishing some weak central limit theorem. Nonetheless, one can look at this issue the other way round, trying to deduce some weak law of large numbers from a fluctuation result. Indeed, the usual central limit theorem implies a weak version of the law of large numbers, although the latter is classically proven using quite different tools. In the seminal article [23], the authors improve earlier results from [234] and [43] on Large Deviation Principles (LDP) for Gibbs measure and obtain as a byproduct a pathwise propagation of chaos result for McKean-Vlasov diffusion processes. While this result is very abstract and the assumptions are not easy to check in practise, it also introduces a fruitful idea which is the link between the notion of relative entropy, as defined below, and the propagation of chaos. In [23], the relative entropy between the N-particle distribution and its tensorized limit appears as a kind of rate functional.

Definition 3.4.3 (Entropy, Fisher information)**.** Let $\mathscr{E}$ be a Polish space. Given two probability measures $\mu, \nu \in \mathcal{P}(\mathscr{E})$ (or more generally two measures), the relative entropy and Fisher information are respectively defined by

$$H(\nu|\mu) := \int_{\mathscr{E}} \frac{\mathrm{d}\nu}{\mathrm{d}\mu} \log\left(\frac{\mathrm{d}\nu}{\mathrm{d}\mu}\right) \mathrm{d}\mu, \quad I(\nu|\mu) := \int_{\mathscr{E}} \left|\nabla \log\left(\frac{\mathrm{d}\nu}{\mathrm{d}\mu}\right)\right|^2 \mathrm{d}\mu,$$

where $\mathrm{d}\nu/\mathrm{d}\mu$ is the Radon-Nikodym derivative. When the two measures are mutually singular, by convention, the relative entropy and Fisher information are set to $+\infty$.

In the subsequent article [24], a strengthened result is obtained thanks to the following

lemma which links entropy bound and Kac's chaos in Total Variation norm. It is a direct consequence of the Pinsker inequality and the Csiszar inequality [97].

Lemma 3.4.4. *Let $\mathscr{E}$ be a Polish space and let $f^N \in \mathcal{P}(\mathscr{E}^N)$ and $f \in \mathcal{P}(\mathscr{E})$. For every nonnegative integer $k(N) \leq N$, it holds that*

$$\frac{1}{2}\big\|f^{k(N),N} - f^{\otimes k(N)}\big\|_{\mathrm{TV}}^2 \leq H\big(f^{k(N),N}\big|f^{\otimes k(N)}\big) \leq \frac{k(N)}{N} H\big(f^N|f^{\otimes N}\big),$$

where $\|\cdot\|_{\mathrm{TV}}$ is the Total Variation norm (which induces a topology stronger than the topology of the weak convergence of probability measures).

Thanks to this lemma, one can see that a bound on $H(f^N|f^{\otimes N})$ implies Kac's chaos. For the McKean-Vlasov diffusion (3.8), the following lemma gives a way to bound the relative entropy between the N-particle distribution and its mean-field limit. The first pathwise inequality is a consequence of Girsanov theorem [227, Chapter 3, Theorem 5.1]. The second one can be formally obtained by direct computations.

Lemma 3.4.5 (Pathwise and pointwise entropy bounds)**.** *Let $T > 0$ and $I = [0,T]$. For $N \in \mathbb{N}$, let $f_I^N \in \mathcal{P}(C([0,T],(\mathbb{R}^d)^N))$ be the law of the McKean-Vlasov diffusion $(\mathcal{X}_t^N)_t$ defined by (3.8) with $b : \mathbb{R}^d \times \mathcal{P}(\mathbb{R}^d) \to \mathbb{R}^d$ and $\sigma = I_d$, and let $f_t^N \in \mathcal{P}((\mathbb{R}^d)^N)$ its time marginal at time $t \in [0,T]$. Let $f_I \in \mathcal{P}(D([0,T],\mathbb{R}^d))$ be the pathiwse law of the limit nonlinear McKean-Vlasov diffusion (3.10) and let $f_t \in \mathcal{P}(\mathbb{R}^d)$ be its time marginal at time $t \in [0,T]$.*

- *For any $k \leq N$ it holds that*

$$H\big(f_I^{k,N}|f_I^{\otimes k}\big) \leq \frac{k}{2}\mathbb{E}\bigg[\int_0^T \big|b\big(X_t^1, \mu_{\mathcal{X}_t^N}\big) - b(X_t^1, f_t)\big|^2 \mathrm{d}t\bigg]. \tag{3.28}$$

- *For every $\alpha > 0$ it holds that*

$$\frac{\mathrm{d}}{\mathrm{d}t} H\big(f_t^N|f_t^{\otimes N}\big) \leq \frac{\alpha - 1}{2} I\big(f_t^N|f_t^{\otimes N}\big) + \frac{N}{2\alpha}\mathbb{E}\Big[\big|b\big(X_t^1, \mu_{\mathcal{X}_t^N}\big) - b(X_t^1, f_t)\big|^2\Big]. \tag{3.29}$$

This lemma shows that the relative entropy is actually bounded by observables of the particle system without any particular regularity assumption on the drift b. These ideas are exploited in particular in [208, 180] and [235, 209] respectively for McKean-Vlasov systems with low regularity and with a very general and abstract interaction coefficient b. Following these works, recent articles have further deepened these relative entropy methods and successfully applied them to models with singular interactions. For recent developments, see for instance [48, 236, 311] and the references therein.

Chapter 4

Propagation of chaos and moderate interaction for a piecewise deterministic system of geometrically enriched particles

The content of this chapter is based on the following article

[138] A. Diez. "Propagation of chaos and moderate interaction for a piecewise deterministic system of geometrically enriched particles". *Electron. J. Probab.* 25 (2020).

While the main application of this work will be the system of body-oriented particles described in the introduction, the framework introduced encompasses much more general geometrically-enriched systems such as the Vicsek model [140, 321].

4.1 Introduction

The goal of this chapter is to prove a rigorous convergence result from a large class of geometrically enriched PDMP particle models towards purely local BGK equations. The prototypical model is the PDMP Vicsek model defined in Section 1.2.2 of the introduction of this thesis. Unlike the version of the model introduced in [140], we will consider in this chapter the choice $\kappa(J) = |J|$ so that, with the notations of the introduction,

$$\kappa(J_n^i)\mathbb{V}_n^i = J_n^i. \tag{4.1}$$

From a modelling point of view, in this *non-normalised* model, when a jump occurs, the bigger the norm of the flux, the more peaked the von Mises distribution is and therefore the new orientation of the agent is (expectedly) closer to the local normalised average orientation. From a mathematical point of view, the *normalised* version of the model, which is studied in [140], is more singular, as the normalised average orientation is not defined when the flux (1.3) is equal to zero. On the contrary, with the present choice (4.1), if the flux vanishes, then the agent will simply draw a new orientation uniformly on the sphere. It has also been shown in [113] that complex behaviours and in particular phase transitions only appear in models with a non-normalised flux. Without this singularity problem, the aim of this chapter is to prove the well-posedness of the BGK PDE (1.9) and to rigorously justify its derivation from the IBM by taking the limit (in a certain sense) when N tends to infinity and $K \to \delta_0$.

In order to also encompass the body-orientation model defined in Section 2.1.2 of the introduction, one will actually consider more general geometrically enriched PDMP models where the orientation of the agents is an element of an abstract compact Riemannian manifold $\mathscr{M}$: the choice $\mathscr{M} = \mathbb{S}^{d-1}$ gives the Vicsek model and the choice $\mathscr{M} = \mathrm{SO}_3(\mathbb{R})$ gives the body-orientation dynamics model.

The strategy followed in this chapter is two-fold. First, the coupling method described in Section 3.4.1 of the previous chapter is extended to the piecewise deterministic setting: a quantitative propagation of chaos property is proved for a geometrically enriched system of PDMPs where particles interact with their neighbours within a fixed interaction kernel. Then, following the approach of [221] the goal will be to prove a moderate interaction property. As explained in the introduction of this thesis (Section 1.3), it states that under an appropriate rescaling of the size of the neighbourhood of the agents with respect to the total number of agents, the interaction can be made purely local, which means that we can take $K = \delta_0$ in the BGK equation (1.9). This rescaling is achieved by taking in the IBM an observation kernel of the form:

$$K^N(|x|) = \frac{1}{\varepsilon_N^d} K_0\left(\frac{|x|}{\varepsilon_N}\right)$$

where K_0 is a fixed observation kernel and $\varepsilon_N \to 0$ slowly enough. This result will follow from the explicit bound in N obtained in the proof of the propagation of chaos and from classical compactness arguments to pass to the limit inside the BGK equation "with kernel interaction" when $K^N \to \delta_0$. This will require to prove *ad hoc* regularity properties on the solution of the BGK equation in the geometrically enriched specific setting considered (in particular various properties related to equicontinuity and stability under translations of

the sequence of solutions associated to the sequence of kernels).

The terminology "moderate interaction" comes from [273] where propagation of chaos and moderate interaction properties are proved using a different approach, based on martingale arguments. As explained in [221], in the model studied by Oelschläger, the random part is given by a constant diffusion matrix which does not depend on the current state of the system (i.e. of the empirical measure of the agents). This is not the case in most models of collective dynamics and in particular in the models studied in the present chapter. However, in a space homogeneous setting, we give an alternative proof of the propagation of chaos property based on martingale arguments. Let us also mention that martingales techniques have also recently been used in [165] to prove propagation of chaos for a PDMP Cucker-Smale model.

The organisation of the chapter is as follows. The first section introduces the general geometrical framework which encompasses the PDMP Vicsek model and its extensions (Section 4.2.1). In this framework, the IBM and its kinetic version are defined and studied respectively in Section 4.2.3 and Section 4.2.4. The main results are stated in Section 4.2.5, in particular Theorem 4.2.13 (propagation of chaos) and Theorem 4.2.15 (moderate interaction). Section 4.3 is devoted to the proof of the former. The latter is proved in Section 4.4 together with regularity results for the solution of the BGK equation. Finally, Section 4.5 presents an alternative approach based on martingale techniques for a spatially homogeneous model.

4.2 Abstract framework and main results

4.2.1 Assumptions and definitions

From now on we will use the following functional set up.

1. Let $(\mathscr{M}, g)$ be a compact finite dimensional Riemannian manifold. The Riemannian distance induced by g is denoted by d. On the product space $\mathbb{R}^d \times \mathscr{M}$ we take the metric
$$\tilde{d}\big((x_1, m_1), (x_2, m_2)\big) := |x_1 - x_2| + d(m_1, m_2)$$
and we write for short $\tilde{d} \equiv d$ when there is no possible confusion. The volume form associated to g is assumed to be normalised and will be denoted by $\mathrm{d}m$ (i.e. $\int_{\mathscr{M}} \mathrm{d}m = 1$). We will also assume that $\mathscr{M}$ is isometrically embedded in a Euclidean space E where the inner product is denoted by $\cdot$ and the norm by $|\cdot|$. This embedding

is never a loss of generality thanks to Nash's embedding theorem [267]. We will also assume without loss of generality that for all $m \in \mathscr{M}$, $|m| \leq 1$.

2. Let $\Phi : \mathscr{M} \to \mathbb{R}^d$ be a *velocity map* which is a continuous and λ-Lipschitz map for a given constant $\lambda \geq 0$.

3. Let K be a smooth observation kernel on $\mathbb{R}^d$, that is to say a radial smooth bounded Lipschitz function which tends to zero at infinity (typically a smoothened version of the indicator of a ball centred at the origin) such that $K \geq 0$ and $\int_{\mathbb{R}^d} K(x)\mathrm{d}x = 1$. Since K is radial, in order to alleviate the notations, we write indifferently $K(x) \equiv K(|x|)$.

4. Let M_J be an *interaction law*, defined for any parameter $J \in E$ as a probability density function on $\mathscr{M}$ which satisfies the following assumptions.

   Assumption 4.2.1 (Locally bounded)**.** *There exists a function $\alpha = \alpha(a)$ such that for any $a > 0$ and any $J \in E$ with $|J| \leq a$, it holds that*

   $$\|M_J\|_{L^\infty(\mathscr{M})} \leq \alpha(a). \tag{4.2}$$

   Assumption 4.2.2 (Locally Lipschitz)**.** *There exists a function $L = L(a)$ such that for any $a > 0$ and any $J \in E$ with $|J| \leq a$, it holds that*

   $$|M_J(m_1) - M_J(m_2)| \leq L(a)d(m_1, m_2). \tag{4.3}$$

   Assumption 4.2.3 (Flux Lipschitz)**.** *There exists a function $\theta = \theta(a)$ such that for any $a > 0$ and any $J, J' \in E$ with $|J|, |J'| \leq a$, it holds that*

   $$\|M_J - M_{J'}\|_{L^\infty(\mathscr{M})} \leq \theta(a)|J - J'|. \tag{4.4}$$

Remark 4.2.4. The Lipschitz regularity assumptions (for the interaction kernel and for the interaction law) are classical for mean-field type results (see [307]). The present work essentially focuses on the extension of classical results and techniques to the PDMP framework with geometrical constraints and the question of lower regularity, as outlined in Chapter 3, will not be addressed.

In order to define interaction rules between the agents we now define two objects: the *flux* of a measure which will be a way of constructing an average orientation from a distribution of orientations and the *observation measure*, the purpose of which will be to define the local average orientation around a point in the physical space $\mathbb{R}^d$.

- The *flux* of a positive measure $\mu \in \mathcal{M}_+(\mathscr{M})$ on $\mathscr{M}$ is defined by

$$J_\mu := \int_{\mathscr{M}} m \, \mu(\mathrm{d}m) \in E. \tag{4.5}$$

  The interaction law relative to a positive measure $\mu \in \mathcal{M}_+(\mathscr{M})$ is defined as the probability density function M_{J_μ} on $\mathscr{M}$ and will be denoted only by M_μ in the following.

- Given a probability measure p on $\mathbb{R}^d \times \mathscr{M}$, we define the *observation measure* by taking the convolution product of p with the observation kernel K: its purpose is to define the local orientation with respect to p around a point $x \in \mathbb{R}^d$. In particular p can be either the empirical measure of a system of processes given by an IBM or the solution of a BGK equation in a kinetic model.

  Definition 4.2.5 (Observation measure)**.** Let $p \in \mathcal{P}(\mathbb{R}^d \times \mathscr{M})$ and $x \in \mathbb{R}^d$. The observation measure $K \star p(x) \in \mathcal{M}_+(\mathscr{M})$ is defined by

$$\forall \varphi \in C_b(\mathscr{M}), \;\; \langle K \star p(x), \varphi \rangle := \iint_{\mathbb{R}^d \times \mathscr{M}} K(x-y)\varphi(m)p(\mathrm{d}y, \mathrm{d}m).$$

  Note that $K \star p : x \in \mathbb{R}^d \mapsto K \star p(x) \in \mathcal{M}_+(\mathscr{M})$ defines a smooth map for the total variation topology on $\mathcal{M}_+(\mathscr{M})$. The flux and interaction law will be denoted in this case:

$$J_{K\star p(x)} \equiv J_{K\star p}(x) \;\; \text{and} \;\; M_{K\star p(x)}(m) \equiv M_{K\star p}[x](m). \tag{4.6}$$

  If p is a probability density function in $L^\infty(\mathbb{R}^d \times \mathscr{M})$, then the previous definition makes sense in the degenerate case $K = \delta_0$, and we define

$$\forall \varphi \in C_b(\mathscr{M}), \;\; \langle p(x,\cdot), \varphi \rangle := \int_{\mathscr{M}} \varphi(m)p(x,m)\mathrm{d}m.$$

  The flux and interaction law will be denoted in this case:

$$J_{p(x,\cdot)} \equiv J_p(x) \;\; \text{and} \;\; M_{p(x,\cdot)}(m) \equiv M_p[x](m).$$

To conclude this section, we point out that the assumptions on the interaction law can be reinterpreted as regularity bounds in the space of probability measures when the interaction law comes from a measure on $\mathscr{M}$. In particular, since

$$W_1(M_\mu, M_\nu) \leq \|M_\mu - M_\nu\|_{\mathrm{TV}} = \|M_\mu - M_\nu\|_{L^1(\mathscr{M})} \leq \|M_\mu - M_\nu\|_{L^\infty(\mathscr{M})},$$

the flux-Lipschitz bound (4.4) implies that for $p_1, p_2 \in \mathcal{P}^{\mathrm{ac}}(\mathbb{R}^d \times \mathscr{M})$ and $x, x' \in \mathbb{R}^d$:

$$W_1(M_{K\star p_1}[x], M_{K\star p_2}[x']) \leq C\theta\big(\|K\|_{L^\infty}\big)\|K\|_{\mathrm{Lip}}\big(|x-x'| + W_1(p_1,p_2)\big), \tag{4.7}$$

where W_1 denotes the Wasserstein-1 distance on $\mathcal{P}(\mathbb{R}^d \times \mathscr{M})$ or $\mathcal{P}(\mathscr{M})$ indifferently.

4.2.2 Application to the Vicsek and body-orientation models

This general setting encompasses the two following examples derived from the Vicsek model.

- In the d-dimensional continuous Vicsek model described in the introduction of this chapter, the Riemannian manifold is taken to be equal to the sphere $\mathbb{S}^{d-1}$, viewed as a submanifold of $\mathbb{R}^d$ endowed with its canonical Euclidean structure. The velocity map Φ is then the canonical injection $\mathbb{S}^{d-1} \hookrightarrow \mathbb{R}^d$.
- In the three dimensional Body-Orientation model studied in [111] described in the introduction of this thesis, the Riemannian manifold is taken to be equal to $\mathrm{SO}_3(\mathbb{R})$ viewed as a submanifold of $\mathcal{M}_3(\mathbb{R})$ endowed with the inner product $A \cdot B := \frac{1}{2}\operatorname{Tr}(A^{\mathrm{T}}B)$. The velocity map is the projection $A \in \mathrm{SO}_3(\mathbb{R}) \mapsto Ae_1 \in \mathbb{R}^3$ where e_1 is a fixed vector (the first vector of a reference frame).

In both cases, in the previous works [140, 111], the interaction between the agents is given by a von Mises distribution. This family of probability laws has first been introduced for circular statistics on the circle and on the sphere [246]. It can be extended to a family of probability distributions on $\mathrm{SO}_3(\mathbb{R})$ (it is then sometimes referred as the von Mises–Fisher matrix distribution [247, 239]) and more generally to a family of probability distributions on any compact embedded manifold. This defines an interaction law which satisfies the Assumptions 4.2.1, 4.2.2, 4.2.3 as shown in the following proposition.

Proposition 4.2.6. *Let us define for $J \in E$ the von Mises distribution M_J on $\mathscr{M}$ by:*

$$M_J(m) := \frac{\mathrm{e}^{J\cdot m}}{\mathcal{Z}} \tag{4.8}$$

where $\mathcal{Z}$ is a normalisation constant. This defines an interaction law which satisfies Assumptions 4.2.1, 4.2.2, 4.2.3 with regularity constants

$$\alpha(a) = \mathrm{e}^{2a}, \;\; L(a) = a\mathrm{e}^{2a} \;\; \textit{and} \;\; \theta(a) = \mathrm{e}^{2a} + \mathrm{e}^{4a}.$$

Proof. Let $a > 0$ and $J, J' \in E$ be such that $|J|, |J'| \leq a$.

1. For any $m \in \mathscr{M}$ it holds that $|J \cdot m| \leq a$ so since the exponential function on $\mathbb{R}$ is non decreasing it holds that:

$$\mathrm{e}^{J\cdot m} \leq \mathrm{e}^{a} \text{ and } \mathcal{Z} := \int_{\mathscr{M}} \mathrm{e}^{J\cdot m'} \mathrm{d}m' \geq \mathrm{e}^{-a}.$$

From which we deduce that

$$\|M_J\|_{L^\infty(\mathscr{M})} \leq \mathrm{e}^{2a} =: \alpha(a). \tag{4.9}$$

2. Let $m_1, m_2 \in \mathscr{M}$. Using the mean-value inequality on the compact segment $[\mathrm{e}^{-a}, \mathrm{e}^{a}]$ and the fact that $\mathscr{M}$ is isometrically embedded into E, we obtain that:

$$|M_J(m_1) - M_J(m_2)| \leq \mathrm{e}^{2a}|J \cdot m_1 - J \cdot m_2| \leq a\mathrm{e}^{2a} d(m_1, m_2) =: L(a) d(m_1, m_2).$$

3. Let $m \in \mathscr{M}$. It holds that:

$$|M_J(m) - M_{J'}(m)| \leq \frac{1}{\mathcal{Z}}|\mathrm{e}^{J\cdot m} - \mathrm{e}^{J'\cdot m}| + \frac{\mathrm{e}^{J'\cdot m}}{\mathcal{Z}\mathcal{Z}'}|\mathcal{Z} - \mathcal{Z}'|$$

where

$$\mathcal{Z} := \int_{\mathscr{M}} \mathrm{e}^{J\cdot m} \mathrm{d}m \text{ and } \mathcal{Z}' = \int_{\mathscr{M}} \mathrm{e}^{J'\cdot m} \mathrm{d}m.$$

Using again the mean-value inequality and the bound (4.9), we obtain:

$$|M_J(m) - M_{J'}(m)| \leq (\mathrm{e}^{2a} + \mathrm{e}^{4a})|J - J'| =: \theta(a)|J - J'|.$$

□

As described in the introduction, for the Vicsek and Body-orientation cases, an agent interacts with its neighbours by sampling a new orientation from a von Mises distribution, the parameter of which reflects the local average orientation of the other agents. Two cases have to be considered depending on how "local" the interaction is.

1. The first case corresponds to the interaction at the level of the IBM: the density of the agents is given by a probability measure μ on $\mathbb{R}^d \times \mathscr{M}$ (typically the empirical distribution of the agents) and the interaction law for an agent at position $x \in \mathbb{R}^d$ is the von Mises distribution (4.8) with parameter J equal to the flux of the observation

measure $K \star \mu(x)$, namely

$$M_J \equiv M_{J_{K\star\mu}(x)} \equiv M_{K\star\mu}[x].$$

In this case, the regularity constants in Assumptions 4.2.1, 4.2.2, 4.2.3 are functions of $\|K\|_{L^\infty}$ since $|J_{K\star\mu}(x)| \leq \|K\|_{L^\infty}$.

2. The second case corresponds to the interaction at the kinetic level when we let $K \to \delta_0$: the density of agents is given by a probability density function f (typically the solution of a BGK equation) which we assume to be bounded in the L^∞ norm by a constant $a > 0$. The interaction law at position $x \in \mathbb{R}^d$ is then the von Mises distribution (4.8) with parameter J equal to the flux of the purely local observation measure $f(x, \cdot)$:

$$M_J \equiv M_{J_{f(x,\cdot)}} \equiv M_f[x].$$

4.2.3 Individual Based Model

In the abstract framework described in Subsection 4.2.1, the main focus of this article will be the study of the following IBM which is a direct generalisation of the PDMP Vicsek model [140].

An agent $i \in \{1, \dots, N\}$ is described at time t by a couple $Z_t^{i,N} = (X_t^{i,N}, m_t^{i,N}) \in \mathbb{R}^d \times \mathscr{M}$ of position and orientation. The evolution of the trajectories are given by the following Piecewise Deterministic Markov Process (PDMP) :

- Let $(S_n)_n$ be a sequence of independent holding times which follow an exponential law of parameter N (their expectation is $1/N$). The jump times are denoted by $T_n := S_1 + \ \dots + S_n$. We set $S_0 = T_0 = 0$.

- Let $(I_n)_n$ a sequence of independent indexes which follow a uniform law on $\{1, \dots, N\}$.

- Between two jump times on $[T_n, T_{n+1})$, the system evolves deterministically:

$$\forall t \in [T_n, T_{n+1}),\ \forall i \in \{1, \dots, N\},\quad \left\{ \begin{array}{rcl} X_t^{i,N} & = & X_{T_n}^{i,N} + (t - T_n)\Phi\big(m_t^{i,N}\big) \\ m_t^{i,N} & = & m_{T_n}^{i,N} \end{array} \right. . \quad (4.10)$$

- At T_{n+1} a jump occurs for the agent I_n which draws a new orientation according to the interaction law:

$$m_{T_{n+1}}^{I_n,N} \sim M_{K\star\hat{\mu}^N_{T_{n+1}^-}}\Big[X_{T_{n+1}^-}^{I_n,N}\Big], \quad (4.11)$$

where in order to keep lighter notations, the empirical measure at time t is denoted in this chapter by

$$\hat{\mu}_t^N := \frac{1}{N}\sum_{i=1}^{N} \delta_{(X_t^{i,N}, m_t^{i,N})},$$

and

$$Z_{T_{n+1}^-}^{i,N} = \left(X_{T_{n+1}^-}^{i,N}, m_{T_{n+1}^-}^{i,N}\right) := \left(X_{T_n}^{i,N} + S_{n+1}\Phi\big(m_{T_n}^{i,N}\big), m_{T_n}^{i,N}\right) \in \mathbb{R}^d \times \mathscr{M}.$$

Remark 4.2.7. Owing to [47, Chapter 8, Section 1.3], this definition is equivalent to the one in the introduction where each agent has an internal Poisson process.

4.2.4 Kinetic model: the BGK equation. Well-posedness results.

The kinetic model associated to the IBM described in Subsection 4.2.3 is given by the following BGK equation (see Theorem 4.2.13 below for more details on how the IBM is related to the kinetic model):

$$\partial_t f + \Phi(m)\cdot\nabla_x f = \rho_f M_{K\star f}[x] - f \tag{4.12}$$

where $f = f_t(\mathrm{d}x, \mathrm{d}m)$ is a time dependent probability measure on $\mathbb{R}^d \times \mathscr{M}$ and $\rho_{f_t}(\mathrm{d}x)$ is the first marginal of f_t, i.e. $\rho_{f_t}(\mathrm{d}x) := \int_{\mathscr{M}} f_t(\mathrm{d}x, \mathrm{d}m)$. For the sake of clarity, in the following we will write:

$$G_{f_t}^K(\mathrm{d}x, \mathrm{d}m) \equiv \rho_{f_t}(\mathrm{d}x) M_{K\star f_t}[x](m)\mathrm{d}m.$$

When f_t has a density, i.e. $f_t \in \mathcal{P}^{\mathrm{ac}}(\mathbb{R}^d \times \mathscr{M})$, we will write with a slight abuse of notations:

$$G_{f_t}^K(x, m) \equiv \rho_{f_t}(x) M_{K\star f_t}[x](m)$$

which is a probability density function on $\mathbb{R}^d \times \mathscr{M}$.

Lemma 4.2.8. *Let $f, g \in \mathcal{P}^{\mathrm{ac}}(\mathbb{R}^d \times \mathscr{M})$, then it holds that*

$$\|G_f^K - G_g^K\|_{L^1(\mathbb{R}^d\times\mathscr{M})} \leq \Big(\alpha\big(\|K\|_{L^\infty}\big) + \|K\|_{L^\infty}\theta\big(\|K\|_{L^\infty}\big)\Big)\|f - g\|_{L^1(\mathbb{R}^d\times\mathscr{M})} \tag{4.13}$$

Proof. Since the G_f^K and G_g^K are a product of two quantities, the L^1 norm of the difference

can be split into two parts:

$$\iint_{\mathbb{R}^d\times\mathscr{M}} |G_f^K - G_g^K|(x,m)\,\mathrm{d}x\mathrm{d}m = \iint_{\mathbb{R}^d\times\mathscr{M}} |\rho_f(x)M_{K\star f}[x](m) - \rho_g(x)M_{K\star g}[x](m)|\mathrm{d}x\mathrm{d}m$$
$$\leq \iint_{\mathbb{R}^d\times\mathscr{M}} |\rho_f(x) - \rho_g(x)|M_{K\star f}[x](m)\mathrm{d}x\mathrm{d}m$$
$$+ \iint_{\mathbb{R}^d\times\mathscr{M}} \rho_g(x)|M_{K\star f}[x](m) - M_{K\star g}[x](m)|\mathrm{d}x\mathrm{d}m.$$

Since for all $x \in \mathbb{R}^d$, $|J_{K\star f}(x)| \leq \|K\|_{L^\infty}$, the first integral on the right-hand side can be bounded by

$$\alpha(\|K\|_{L^\infty}) \iint_{\mathbb{R}^d\times\mathscr{M}} |\rho_f - \rho_g|\mathrm{d}x\mathrm{d}m$$

using Assumption 4.2.1. For the second integral on the right-hand side, using (4.4), it holds that:

$$\iint_{\mathbb{R}^d\times\mathscr{M}} \rho_g(x)|M_{K\star f}[x](m) - M_{K\star g}[x](m)|\mathrm{d}x\mathrm{d}m$$
$$\leq \theta(\|K\|_{L^\infty}) \iint_{\mathbb{R}^d\times\mathscr{M}} \rho_g(x)|J_{K\star f}(x) - J_{K\star g}(x)|\mathrm{d}x\mathrm{d}m$$
$$= \theta(\|K\|_{L^\infty}) \int_{\mathbb{R}^d} \rho_g(x)|J_{K\star f}(x) - J_{K\star g}(x)|\mathrm{d}x$$

where we have used that $\int_{\mathscr{M}} \mathrm{d}m = 1$. Then, we note that $|m| \leq 1$ so the previous bound gives:

$$\iint_{\mathbb{R}^d\times\mathscr{M}} \rho_g(x)|M_{K\star f}[x](m) - M_{K\star g}[x](m)|\mathrm{d}x\mathrm{d}m$$
$$\leq \theta(\|K\|_{L^\infty}) \iint_{\mathbb{R}^d\times\mathscr{M}} \rho_g(x)|K\star f(x,m) - K\star g(x,m)|\mathrm{d}x\mathrm{d}m.$$

By Definition 4.2.5 of the observation measure, we obtain:

$$\iint_{\mathbb{R}^d\times\mathscr{M}} \rho_g(x)|M_{K\star f}[x](m) - M_{K\star g}[x](m)|\mathrm{d}x\mathrm{d}m$$
$$\leq \theta(\|K\|_{L^\infty}) \iint_{\mathbb{R}^d\times\mathscr{M}} \rho_g(x)K(x-y)|f(y,m) - g(y,m)|\mathrm{d}x\mathrm{d}y\mathrm{d}m.$$

To conclude, we use the fact that g is a probability measure so that the last integral on the right-hand side can be bounded by $\|K\|_{L^\infty}\|f-g\|_{L^1(\mathbb{R}^d\times\mathscr{M})}$. The result follows. □

A mild-solution to (4.12) is defined as an element $f \in C\big([0,T], \mathcal{P}(\mathbb{R}^d\times\mathscr{M})\big)$ which

satisfies for all $\varphi \in C_b(\mathbb{R}^d \times \mathscr{M})$:

$$\langle f_t, \varphi \rangle = \mathrm{e}^{-t} \langle \mathsf{T}_t f_0, \varphi \rangle + \int_0^t \mathrm{e}^{-(t-s)} \langle \mathsf{T}_{t-s} G_{f_s}^K, \varphi \rangle \, \mathrm{d}s, \tag{4.14}$$

where T_t is the free-transport operator:

$$\langle \mathsf{T}_t \mu, \varphi \rangle := \iint_{\mathbb{R}^d \times \mathscr{M}} \varphi(x + t\Phi(m), m) \mu(\mathrm{d}x, \mathrm{d}m). \tag{4.15}$$

Similarly, in the degenerate case $K = \delta_0$, we consider

$$\partial_t f + (\Phi(m) \cdot \nabla_x) f = \rho_f M_f[x] - f \tag{4.16}$$

where $f = f_t(x, m)$ is a time dependent probability density in $L^\infty(\mathbb{R}^d \times \mathscr{M})$ and $\rho_{f_t}(\mathrm{d}x)$ is the first marginal of f_t. For the sake of clarity, in the following we will write:

$$G_{f_t}(\mathrm{d}x, \mathrm{d}m) \equiv \rho_{f_t}(\mathrm{d}x) M_{f_t}[x](\mathrm{d}m).$$

Lemma 4.2.9. *Let $a > 0$ and let $f, g \in L^\infty \cap \mathcal{P}^{\mathrm{ac}}(\mathbb{R}^d \times \mathscr{M})$ be two probability density functions such that $\|f\|_{L^\infty}, \|g\|_{L^\infty} \leq a$. Then*

$$\|G_f - G_g\|_{L^\infty(\mathbb{R}^d \times \mathscr{M})} \leq (\alpha(a) + a\theta(a)) \|f - g\|_{L^\infty(\mathbb{R}^d \times \mathscr{M})} \tag{4.17}$$

and

$$\|G_f - G_g\|_{L^1(\mathbb{R}^d \times \mathscr{M})} \leq (\alpha(a) + a\theta(a)) \|f - g\|_{L^1(\mathbb{R}^d \times \mathscr{M})} \tag{4.18}$$

Proof. The result follows as before from (4.2) and (4.4) by noticing that for all $x \in \mathbb{R}^d$, $|J_f(x)| \leq a$ and $|J_f(x) - J_g(x)| \leq \|f - g\|_{L^\infty}$. □

The well-posedness of (4.12) and (4.16) is given by the two following propositions. They are based on Duhamel's formula and on a fixed point argument.

Proposition 4.2.10 (Well-posedness of (4.12))**.** *For all $f_0 \in \mathcal{P}^{\mathrm{ac}}(\mathbb{R}^d \times \mathscr{M})$ and all $T > 0$, there exists a unique solution of (4.12) in $C\big([0,T], \mathcal{P}^{\mathrm{ac}}(\mathbb{R}^d \times \mathscr{M})\big)$ with initial condition f_0. Moreover if $t \mapsto f_t^1$ and $t \mapsto f_t^2$ are two solutions of (4.12) with respective initial conditions $f_0^1 \in \mathcal{P}^{\mathrm{ac}}(\mathbb{R}^d \times \mathscr{M})$ and $f_0^2 \in \mathcal{P}^{\mathrm{ac}}(\mathbb{R}^d \times \mathscr{M})$ then*

$$\sup_{t \in [0,T]} \|f_t^1 - f_t^2\|_{L^1(\mathbb{R}^d \times \mathscr{M})} \leq \|f_0^1 - f_0^2\|_{L^1(\mathbb{R}^d \times \mathscr{M})} \mathrm{e}^{\left(\alpha\left(\|K\|_{L^\infty}\right) + \|K\|_{L^\infty} \theta\left(\|K\|_{L^\infty}\right)\right) T}.$$

Proof. Let $f_0 \in \mathcal{P}^{\mathrm{ac}}(\mathbb{R}^d \times \mathscr{M})$ and $T > 0$ and let us define the map:

$$\mathcal{T} : C\big([0,T], \mathcal{P}^{\mathrm{ac}}(\mathbb{R}^d \times \mathscr{M})\big) \to C\big([0,T], \mathcal{P}^{\mathrm{ac}}(\mathbb{R}^d \times \mathscr{M})\big)$$

by

$$\mathcal{T}(g)(t,x,m) := \mathrm{e}^{-t} f_0(x - t\Phi(m), m) + \int_0^t \mathrm{e}^{-(t-s)} G^K_{g_s}\big(x - (t-s)\Phi(m), m\big)\mathrm{d}s.$$

We prove that $\mathcal{T}$ is a contraction. Let $g^1, g^2 \in C\big([0,T], \mathcal{P}^{\mathrm{ac}}(\mathbb{R}^d \times \mathscr{M})\big)$. One has:

$$\iint_{\mathbb{R}^d \times \mathscr{M}} |\mathcal{T}(g^1) - \mathcal{T}(g^2)|(t,x,m)\,\mathrm{d}x\mathrm{d}m \le \int_0^t \mathrm{e}^{-(t-s)} \iint_{\mathbb{R}^d \times \mathscr{M}} |G^K_{g^1_s} - G^K_{g^2_s}|(x,m)\,\mathrm{d}x\mathrm{d}m\,\mathrm{d}s.$$

The Lipschitz bound (4.13) leads to:

$$\sup_{t\in[0,T]} \|\mathcal{T}(g^1)(t) - \mathcal{T}(g^2)(t)\|_{L^1} \le \Big(\alpha\big(\|K\|_{L^\infty}\big) + \|K\|_{L^\infty}\theta\big(\|K\|_{L^\infty}\big)\Big) \int_0^t \sup_{u\in[0,s]} \|g^1_u - g^2_u\|_{L^1}\,\mathrm{d}s,$$

which proves that an iteration of $\mathcal{T}$ is a contraction and therefore $\mathcal{T}$ has a unique fixed point. This fixed point is a (mild) solution of (4.12). The stability estimate follows similarly by Gronwall lemma. □

Remark 4.2.11. The well-posedness result Proposition 4.2.10 is stated in an absolutely continuous framework (i.e. for probability density functions rather than probability measures) and a solution is defined as a fixed point of the map $\mathcal{T}$. The associated probability measure (i.e $f_t(x,m)\mathrm{d}x\mathrm{d}m$) is a mild solution of (4.12) as defined by (4.14). However, it should be possible to adapt this proof to give the well-posedness in $C\big([0,T], \mathcal{P}(\mathbb{R}^d \times \mathscr{M})\big)$ where $\mathcal{P}(\mathbb{R}^d \times \mathscr{M})$ is endowed with the total variation norm (which is the L^1 norm for probability density functions). The result is then similar to the one obtained in [260, Proposition 2] (by probabilistic coupling arguments) or in [53] (by Duhamel's formula and a fixed point argument). In the following, only the absolutely continuous framework will be considered.

For the well-posedness of (4.16), we consider the space $L^\infty \cap \mathcal{P}^{\mathrm{ac}}(\mathbb{R}^d \times \mathscr{M})$ which is a closed subspace of $L^\infty \cap L^1(\mathbb{R}^d \times \mathscr{M})$ and therefore complete for the norm $\|\cdot\|_{L^\infty} + \|\cdot\|_{L^1}$ which will be denoted for short by $\|\cdot\|_{L^1\cap L^\infty}$.

Proposition 4.2.12 (Well-posedness of (4.16))**.** *Let $f_0 \in L^\infty \cap \mathcal{P}^{\mathrm{ac}}(\mathbb{R}^d \times \mathscr{M})$ such that $\|f_0\|_{L^\infty} < a$ for a given $a > 0$. Then there exists a time $T > 0$ and a unique solution of (4.16) in $C\big([0,T], L^\infty \cap \mathcal{P}^{\mathrm{ac}}(\mathbb{R}^d \times \mathscr{M})\big)$ with initial condition f_0. Moreover if $t \mapsto f^1_t$*

and $t \mapsto f_t^2$ *are two solutions of* (4.16) *with respective initial conditions* f_0^1 *and* f_0^2 *such that* $\|f_0^1\|_{L^\infty}, \|f_0^2\|_{L^\infty} < a$ *for the same* $a > 0$ *then*

$$\sup_{t\in[0,T]} \|f_t^1 - f_t^2\|_{L^1\cap L^\infty} \leq \|f_0^1 - f_0^2\|_{L^1\cap L^\infty} \mathrm{e}^{c(T)}$$

where $c(T)$ *is a constant which depends only on* T*.*

Proof. Let $f_0 \in L^\infty \cap \mathcal{P}^{\mathrm{ac}}(\mathbb{R}^d \times \mathscr{M})$. Let $a > 0$ such that $\|f_0\|_{L^\infty} < a$. Let B_a the ball of radius a in $C\Big([0,T], L^\infty \cap \mathcal{P}^{\mathrm{ac}}(\mathbb{R}^d \times \mathscr{M})\Big)$ where $T > 0$ will be specified later and for the norm $\|h\| = \sup_{t\in[0,T]} \|h(t)\|_{L^\infty}$. We consider the map:

$$\mathcal{T} : B_a \to B_a$$

defined by:

$$\mathcal{T}(g)(t,x,m) := \mathrm{e}^{-t} f_0(x - t\Phi(m), m) + \int_0^t \mathrm{e}^{-(t-s)} G_{g_s}\big(x - (t-s)\Phi(m), m\big)\mathrm{d}s.$$

Using the bound (4.2), one has for $g \in B_a$:

$$|\mathcal{T}(g)(t,x,m)| \leq \mathrm{e}^{-t}\|f_0\|_{L^\infty} + (1 - \mathrm{e}^{-t})a\alpha(a)$$

and the map $\mathcal{T}$ is therefore well defined for $T > 0$ small enough to ensure that for all $t \in [0,T]$:

$$\mathrm{e}^{-t}\|f_0\|_{L^\infty} + (1 - \mathrm{e}^{-t})a\alpha(a) \leq a.$$

Namely $\mathcal{T}$ is well defined for

$$T \leq \log\left(\frac{a\alpha(a) - a}{a\alpha(a) - \|f_0\|_{L^\infty}}\right)$$

where we can assume without loss of generality that $\alpha(a) \geq 1$. We prove that $\mathcal{T}$ is a contraction. Let $g^1, g^2 \in B_a$. One has:

$$|\mathcal{T}(g^1) - \mathcal{T}(g^2)|(t,x,m) \leq \int_0^t \mathrm{e}^{-(t-s)} \big|G_{g_s^1} - G_{g_s^2}\big|\big(x - (t-s)\Phi(m), m\big)\mathrm{d}s.$$

Using the Lipschitz bounds (4.17) and (4.18) one has:

$$\sup_{t\in[0,T]} \|\mathcal{T}(g^1)(t) - \mathcal{T}(g^2)(t)\|_{L^\infty} \leq (\alpha(a) + a\theta(a)) \int_0^t \|g_s^1 - g_s^2\|_{L^\infty}\mathrm{d}s,$$

and

$$\sup_{t\in[0,T]} \|\mathcal{T}(g^1)(t) - \mathcal{T}(g^2)(t)\|_{L^1} \leq (\alpha(a) + a\theta(a)) \int_0^t \|g_s^1 - g_s^2\|_{L^1} \mathrm{d}s,$$

and therefore, an iteration of $\mathcal{T}$ is a contraction and therefore $\mathcal{T}$ has a unique fixed point which is a solution of (4.16). The stability estimate follows similarly by Gronwall lemma. □

4.2.5 Main results

Let $Z_t^{i,N} = (X_t^{i,N}, m_t^{i,N}) \in \mathbb{R}^d \times \mathscr{M}$, $i \in \{1, \dots, N\}$ be a system of PDMP defined by the IBM described in Subsection 4.2.3.

Theorem 4.2.13 (Propagation of chaos)**.** *Let $f_0 \in \mathcal{P}^{\mathrm{ac}}(\mathbb{R}^d \times \mathscr{M})$. Let f_t be the solution of (4.12) at time $t > 0$ with initial condition f_0. Assume that initially the agents are independent and identically distributed with respect to the law f_0.*

1. *For all $t > 0$, it holds that:*

$$\mathbb{E}[W_1(\hat{\mu}_t^N, f_t)] \underset{N\to+\infty}{\longrightarrow} 0 \tag{4.19}$$

where

$$\hat{\mu}_t^N := \frac{1}{N} \sum_{i=1}^N \delta_{(X_t^{i,N}, m_t^{i,N})}.$$

2. *Let $f_t^{1,N} \in \mathcal{P}(\mathbb{R}^d \times \mathscr{M})$ be the law at time $t > 0$ of any agent. Then for all $t > 0$ it holds that:*

$$W_1(f_t^{1,N}, f_t) \leq C \frac{\mathrm{e}^{\left(2\lambda + \frac{\sigma(K)}{N}\right)t} \sqrt{\|K\|_{L^\infty}}}{\|K\|_{\mathrm{Lip}} \sqrt{N}} \exp\left(t\sigma(K)\mathrm{e}^{\frac{\sigma(K)}{N}}\right), \tag{4.20}$$

where $C > 0$ is a constant which depends only on $\mathscr{M}$ and d and

$$\sigma(K) := 2\theta\big(\|K\|_{L^\infty}\big)\|K\|_{\mathrm{Lip}}.$$

The convergence result (4.19) and [307, Proposition 2.2] imply the f_t-chaoticity in the sense of Definition 3.2.10 of the law (in $\mathcal{P}((\mathbb{R}^d \times \mathscr{M})^N)$) of the system $(Z_t^{i,N})_t$, $i \in \{1, \dots, N\}$ as stated in the following corollary.

Corollary 4.2.14. *Let $k \in \mathbb{N}$ and let $f_t^{k,N}$ denote the law of any k agents of the system $(Z_t^{i,N})_t$, $i \in \{1, \dots, N\}$ at time t. Assume that initially the agents are independent and*

identically distributed with respect to the law f_0. Then for every k-tuple of bounded continuous functions $\phi_1, \dots \phi_k$ on $\mathbb{R}^d \times \mathscr{M}$ it holds that:

$$\int_{(\mathbb{R}^d \times \mathscr{M})^k} \phi_1(x_1, m_1) \dots \phi_k(x_k, m_k) f_t^{k,N}(\mathrm{d}x_1, \mathrm{d}m_1, \dots, \mathrm{d}x_k, \mathrm{d}m_k)$$
$$\underset{N \to +\infty}{\longrightarrow} \left(\int_{\mathbb{R}^d \times \mathscr{M}} \phi_1(x, m) f_t(x, m) \mathrm{d}x \mathrm{d}m \right) \times \dots \times \left(\int_{\mathbb{R}^d \times \mathscr{M}} \phi_k(x, m) f_t(x, m) \mathrm{d}x \mathrm{d}m \right)$$

where f_t is the solution of (4.12) at time $t > 0$ with initial condition f_0.

The bound (4.20) is similar to the bound obtained in [221, Proposition 2.3] for the classical McKean-Vlasov system. Moreover it is explicit in terms of the norm of K. In particular, it is possible to take a kernel which depends on the number of agents N. In the following, we will consider a sequence of kernels:

$$K^N(x) := \frac{1}{\varepsilon_N^d} K\left(\frac{x}{\varepsilon_N}\right),$$

where $\varepsilon_N \to 0$ and K is a smooth observation kernel. Without loss of generality, we can assume that the infinite and Lipschitz norms of K are equal to 1. In particular the sequence $(K^N)_N$ is an approximation of the unity (meaning that $K^N \to \delta_0$ as $N \to +\infty$) and the bound (4.20) is still relevant provided that $\varepsilon_N \to 0$ slowly enough. This type of interaction is called *moderate* following the terminology of [221, 273]. Based on this explicit bound and on regularity results for the sequence of solutions associated to the sequence of kernels (see in particular Lemma 4.4.1), we will prove the following theorem.

Theorem 4.2.15 (Moderate interaction)**.** *Let $a > 0$ and $T > 0$ such that (4.16) is well posed on $C([0,T], B_a)$ where B_a is the ball of radius $a > 0$ in $L^\infty \cap \mathcal{P}^{\mathrm{ac}}(\mathbb{R}^d \times \mathscr{M})$. Let $f_0 \in B_a$. Let us define the sequence of rescaled interaction kernels:*

$$K^N(x) := \frac{1}{\varepsilon_N^d} K\left(\frac{x}{\varepsilon_N}\right)$$

where $\varepsilon_N \to 0$ slowly enough so that:

$$\frac{\exp\left(2T\theta(\varepsilon_N^{-d})\varepsilon_N^{-(d+1)}\right)}{\sqrt{N}} \underset{N \to +\infty}{\longrightarrow} 0. \tag{4.21}$$

Let $f_t^{1,N}$ be the law at time $t < T$ of any agent defined by the PDMP (4.10), (4.11)

with the interaction kernel K^N. Then it holds that:

$$f_t^{1,N} \underset{N\to+\infty}{\longrightarrow} f_t,$$

where f_t is the solution of (4.16) *at time $t < T$ and where the convergence is the weak convergence of measures.*

Remark 4.2.16. In the Vicsek and Body-orientation cases, one has $\theta(\varepsilon_N^{-d}) = \mathrm{e}^{c/\varepsilon_N^{-d}}$. In order to fulfill Hypothesis (4.21), we have to take $\varepsilon_N \sim \log\log(N)^{-1/d}$. From a physical point of view, this is not a satisfactory order of magnitude even for very large values of N. Moreover ε_N decays much slower than $N^{-\alpha}$ with $\alpha \in (0,1)$ which is the result obtained in [273] in a much simpler setting with constant diffusion. Similarly as in [221], the estimate obtained here should therefore be understood as a purely theoretical result needed to obtain rigorously the purely local BGK equation and is not claimed to be optimal.

Remark 4.2.17. Both theorems rely on the fact that, despite its nonlinearity, the interaction is regular enough (Lipschitz assumptions) to prove the well-posedness of the kinetic PDEs. As mentioned in the introduction we could also consider another version of this model where the flux is "normalised" which consists in taking instead of a flux $J \in E$ its projection on the manifold $\mathscr{M}$. This case is much more singular and is left for future work. See however the approach of [50, 160, 169] for well-posedness results on the "normalised" Vicsek model.

4.3 Propagation of chaos (proof of Theorem 4.2.13)

This section is devoted to the proof of Theorem 4.2.13. It is based on a coupling argument as in [307]. More precisely we define N independent so-called McKean processes such that their common law satisfies (4.12) (also known as McKean-Vlasov processes or Distribution Dependent processes in the literature for diffusion models [152, 318, 329, 259] and in Section 3.3). We then use a coupling between each one of the N particles described in Subsection 4.2.3 with each one of the N McKean processes to control the expectation of the distance between their paths over time. To obtain this control, firstly, we couple the time of the jumps between the processes and secondly, we use an optimal coupling between the laws of the new orientations of the particle processes and the McKean processes to control the expectation of the distance between the two paths at a jump. At each jump time, the expectation of the distance between a particle process and its associated McKean

process is bounded by the sum of the average distance between each pair of particle and McKean processes just after the previous jump and an error term which tends to zero when N tends to $+\infty$. The control of the expectation of the distance between their paths over time then follows from a discrete Gronwall type inequality.

Proof (of Theorem 4.2.13). We first define N independent copies of a so-called McKean process $\overline{Z}_t$ with which the processes on the agents will be coupled.

Step 1. *McKean processes and coupling*

The McKean process is the PDMP defined by:

- a homogeneous Poisson process of rate 1, with holding times $(\overline{S}_n)_n$ and jumping times
$$\overline{T}_n := \overline{S}_1 + \ldots + \overline{S}_n,$$
- the deterministic flow $\phi_t : \mathbb{R}^d \times \mathscr{M} \to \mathbb{R}^d \times \mathscr{M}$ for $t \geq 0$:
$$\phi_t(x, m) = (x - t\Phi(m), m),$$
- the transition probability at time $\overline{T}_n$:
$$Q_{\overline{T}_n}(x, m) := \delta_x \otimes M_{K \star f_{\overline{T}_n^-}}[x],$$
where $f_{\overline{T}_n^-} := \mathsf{T}_{\overline{S}_n} f_{\overline{T}_{n-1}} = f_{\overline{T}_{n-1}} \circ \phi_{\overline{S}_n}$ and f_t is the solution at time t of (4.12).

The well definition of the McKean process follows from the wellposedness of (4.12) (Proposition 4.2.10) as in [307, Theorem 1.1]. It is defined in such a way that its law satisfies (4.12).

For $i \in \{1, \ldots, N\}$ let $(\overline{Z}_t^i)_t$ be an independent copy of the McKean process. The positions and orientation components are denoted by $\overline{Z}_t^i = (\overline{X}_t^i, \overline{m}_t^i)$. Let us define the holding times $(S_n)_n$ and jumping times $(T_n)_n$ resulting from merging the Poisson processes associated to the N independent copies of the McKean process. It defines a homogeneous Poisson process of rate N [47, Section 8.1.3]. In particular, the holding times S_n are independent and follow an exponential law of parameter N (their expectation is $1/N$). Let us also define $(I_n)_n$ the sequence of indexes in $\{1, \ldots, N\}$ such that the process I_n is responsible for the n-th jump. The I_n form a sequence of i.i.d. uniform random variables on $\{1, \ldots, N\}$.

Let us define a system of N PDMP $(Z_t^i)_t$, $i \in \{1, \ldots, N\}$, on $\mathbb{R}^d \times \mathscr{M}$, with components denoted by $Z_t^i = (X_t^i, m_t^i)$, as follows.

- Initially for all $i \in \{1, \dots, \}$, $\overline{Z}_0^i = Z_0^i$.
- The jump times (T_n) and the indexes (I_n) are given above.
- The processes follow the deterministic flow ϕ between two jump times.
- At time T_n, the new orientation $m_{T_n}^{I_n}$ of $Z_{T_n}^{I_n}$ is defined by:

$$m_{T_n}^{I_n} := s\left(\overline{m}_{T_n}^{I_n}\right),$$

where $\overline{m}_{T_n}^{I_n}$ is the orientation of $\overline{Z}_{T_n}^{I_n}$ at time T_n and $s : \mathscr{M} \to \mathscr{M}$ is a Borel map such that:

$$s_{\#} M_{K \star f_{T_n^-}} \left[\overline{X}_{T_n^-}^{I_n}\right] = M_{K \star \hat{\mu}_{T_n^-}} \left[X_{T_n^-}^{I_n}\right]$$

and s is an optimal transport map between the two distributions. In particular it implies that the random variable $m_{T_n}^{I_n}$ is distributed according to $M_{K \star \hat{\mu}_{T_n^-}} \left[X_{T_n^-}^{I_n}\right]$ (conditionally to $\mathcal{F}_{T_n^-}$) and

$$\mathbb{E}\left[d\left(m_{T_n}^{I_n}, \overline{m}_{T_n}^{I_n}\right) \middle| \mathcal{F}_{T_n^-}\right] = W_1\left(M_{K \star f_{T_n^-}} \left[\overline{X}_{T_n^-}^{I_n}\right], M_{K \star \hat{\mu}_{T_n^-}} \left[X_{T_n^-}^{I_n}\right]\right) \tag{4.22}$$

where the σ-algebra $\mathcal{F}_{T_n^-}$ is defined below.

The existence of such optimal transport map is given by [77] or [158, Theorem 1] (Monge problem, see [328] or [77]) and unicity can be recovered under additional assumptions which will not be needed here.

Remark 4.3.1. In [116, Section 3.3] an explicit transport map is introduced: in the $\mathrm{SO}_3(\mathbb{R})$-framework a transport map from a von Mises distribution of parameter $\mathbb{A}_1 \in \mathrm{SO}_3(\mathbb{R})$ to a von Mises of parameter $\mathbb{A}_2 \in \mathrm{SO}_3(\mathbb{R})$ is given by

$$A \mapsto \mathbb{A}_1^{\mathrm{T}} A \mathbb{A}_2.$$

We define the following filtrations:

$$\mathcal{G}_n := \sigma(S_1, \dots, S_n),$$

$$\mathcal{F}_t := \sigma\Big(Z_s^i, \overline{Z}_s^i \,|\, 0 \le s \le t,\, i \in \{1, \dots, N\}\Big),$$

and we will write:

$$\mathcal{F}_{T_n^-} := \mathcal{F}_{T_{n-1}} \vee \sigma(S_n) \vee \sigma(I_n).$$

In particular,

$$\mathcal{G}_n \subset \mathcal{F}_{T_n^-}.$$

Step 2. *Control of the jumps*

In this step, we bound the expectation of the distance between the processes at the jump time T_n, knowing the system at time T_{n-1} and the holding time S_n. By definition of the processes, the couples of position and orientation

$$Z_{T_n}^{I_n} = (X_{T_n}^{I_n}, m_{T_n}^{I_n}) \text{ and } \overline{Z}_{T_n}^{I_n} = (\overline{X}_{T_n}^{I_n}, \overline{m}_{T_n}^{I_n})$$

of the particle I_n and its associated McKean process satisfy:

$$\begin{aligned}\mathbb{E}\left[d\Big(Z_{T_n}^{I_n}, \overline{Z}_{T_n}^{I_n}\Big)\Big|\mathcal{F}_{T_n^-}\right] &\leq \big|X_{T_n^-}^{I_n} - \overline{X}_{T_n^-}^{I_n}\big| + W_1\Big(M_{K\star\hat{\mu}_{T_n^-}^N}\big[X_{T_n^-}^{I_n}\big], M_{K\star f_{T_n^-}}\big[\overline{X}_{T_n^-}^{I_n}\big]\Big) \\ &\leq (1+\lambda S_n) d\Big(Z_{T_{n-1}}^{I_n}, \overline{Z}_{T_{n-1}}^{I_n}\Big) + W_1\Big(M_{K\star\hat{\mu}_{T_n^-}^N}\big[X_{T_n^-}^{I_n}\big], M_{K\star f_{T_n^-}}\big[\overline{X}_{T_n^-}^{I_n}\big]\Big)\end{aligned} \tag{4.23}$$

where we used (4.22) in the first inequality and the fact that the flow is λ-Lipschitz in the second inequality.

The last W_1-distance is split into three parts.

$$\begin{aligned}&W_1\Big(M_{K\star\hat{\mu}_{T_n^-}^N}\big[X_{T_n^-}^{I_n}\big], M_{K\star f_{T_n^-}}\big[\overline{X}_{T_n^-}^{I_n}\big]\Big) \\ &\qquad\leq W_1\Big(M_{K\star\hat{\mu}_{T_n^-}^N}\big[X_{T_n^-}^{I_n}\big], M_{K\star\hat{\mu}_{T_n^-}^N}\big[\overline{X}_{T_n^-}^{I_n}\big]\Big) \\ &\qquad\qquad + W_1\Big(M_{K\star\hat{\mu}_{T_n^-}^N}\big[\overline{X}_{T_n^-}^{I_n}\big], M_{K\star\overline{\mu}_{T_n^-}^N}\big[\overline{X}_{T_n^-}^{I_n}\big]\Big) \\ &\qquad\qquad\qquad + W_1\Big(M_{K\star\overline{\mu}_{T_n^-}^N}\big[\overline{X}_{T_n^-}^{I_n}\big], M_{K\star f_{T_n^-}}\big[\overline{X}_{T_n^-}^{I_n}\big]\Big)\end{aligned} \tag{4.24}$$

Where $\overline{\mu}_t^N$ is the empirical measure of the nonlinear processes:

$$\overline{\mu}_t^N := \frac{1}{N}\sum_{i=1}^N \delta_{\overline{Z}_t^i}.$$

For the first term on the right-hand side of (4.24), we use (4.7) and the fact that the dynamics is deterministic on the time interval $[T_{n-1}, T_n)$, this leads to the following

estimate:

$$W_1\Big(M_{K\star\hat{\mu}^N_{T_n^-}}\big[X^{I_n}_{T_n^-}\big], M_{K\star\hat{\mu}^N_{T_n^-}}\big[\overline{X}^{I_n}_{T_n^-}\big]\Big) \le \theta\big(\|K\|_{L^\infty}\big)\|K\|_{\mathrm{Lip}}\big|X^{I_n}_{T_n^-} - \overline{X}^{I_n}_{T_n^-}\big|$$
$$\le \theta\big(\|K\|_{L^\infty}\big)\|K\|_{\mathrm{Lip}}(1+\lambda S_n)d\Big(Z^{I_n}_{T_{n-1}}, \overline{Z}^{I_n}_{T_{n-1}}\Big).$$

Similarly for the second term on the right-hand side of (4.24):

$$W_1\Big(M_{K\star\hat{\mu}^N_{T_n^-}}\big[\overline{X}^{I_n}_{T_n^-}\big], M_{K\star\overline{\mu}^N_{T_n^-}}\big[\overline{X}^{I_n}_{T_n^-}\big]\Big) \le \theta\big(\|K\|_{L^\infty}\big)\|K\|_{\mathrm{Lip}}W_1(\hat{\mu}^N_{T_n^-}, \overline{\mu}^N_{T_n^-})$$
$$\le \theta\big(\|K\|_{L^\infty}\big)\|K\|_{\mathrm{Lip}}\frac{1}{N}\sum_{i=1}^N d\Big(Z^i_{T_n^-}, \overline{Z}^i_{T_n^-}\Big)$$
$$\le \theta\big(\|K\|_{L^\infty}\big)\|K\|_{\mathrm{Lip}}(1+\lambda S_n)\frac{1}{N}\sum_{i=1}^N d\Big(Z^i_{T_{n-1}}, \overline{Z}^i_{T_{n-1}}\Big).$$

The third term on the right-hand side of (4.24) does not involve the processes Z^i_t and will be considered as an *error term*. Using (4.4), it holds that

$$W_1\Big(M_{K\star\overline{\mu}^N_{T_n^-}}\big[\overline{X}^{I_n}_{T_n^-}\big], M_{K\star f_{T_n^-}}\big[\overline{X}^{I_n}_{T_n^-}\big]\Big) \le \theta\big(\|K\|_{L^\infty}\big)\Big|J_{K\star\overline{\mu}^N_{T_n^-}}\big(\overline{X}^{I_n}_{T_n^-}\big) - J_{K\star f_{T_n^-}}\big(\overline{X}^{I_n}_{T_n^-}\big)\Big|$$
$$=: \theta\big(\|K\|_{L^\infty}\big)e^{I_n}_{T_n^-}.$$

In addition, for all $i \neq I_n$, it holds that

$$\mathbb{E}\Big[d\Big(Z^i_{T_n}, \overline{Z}^i_{T_n}\Big)\Big|\mathcal{F}_{T_n^-}\Big] \le (1+\lambda S_n)d\Big(Z^i_{T_{n-1}}, \overline{Z}^i_{T_{n-1}}\Big).$$

Gathering everything and from (4.23) it leads to

$$\mathbb{E}[Y_{T_n}|\mathcal{F}_{T_n^-}] \le (1+\lambda S_n)Y_{T_{n-1}}$$
$$+\theta\big(\|K\|_{L^\infty}\big)\|K\|_{\mathrm{Lip}}(1+\lambda S_n)d\Big(Z^{I_n}_{T_{n-1}}, \overline{Z}^{I_n}_{T_{n-1}}\Big)$$
$$+\theta\big(\|K\|_{L^\infty}\big)\|K\|_{\mathrm{Lip}}(1+\lambda S_n)\frac{1}{N}\sum_{i=1}^N d\Big(Z^i_{T_{n-1}}, \overline{Z}^i_{T_{n-1}}\Big) + \theta\big(\|K\|_{L^\infty}\big)e^{I_n}_{T_n^-}$$

where

$$Y_t := \sum_{i=1}^N d\Big(Z^i_t, \overline{Z}^i_t\Big).$$

Taking the conditional expectation with respect to $\mathcal{G}_n$ gives:

$$\mathbb{E}[Y_{T_n}|\mathcal{G}_n] \leq (1+\lambda S_n)\mathbb{E}[Y_{T_{n-1}}|\mathcal{G}_{n-1}] + (1+\lambda S_n)\frac{\sigma(K)}{N}\mathbb{E}[Y_{T_{n-1}}|\mathcal{G}_{n-1}] \\ + \theta\big(\|K\|_{L^\infty}\big)\mathbb{E}\Big[e^{I_n}_{T_n^-}\Big|\mathcal{G}_n\Big], \quad (4.25)$$

where we have used that S_n is $\mathcal{G}_n$-measurable and the independence relations : $I_n \perp \mathcal{F}_{T_{n-1}}$, $I_n \perp \mathcal{G}_n$ and $I_n \sim \mathcal{U}(1,\dots,N)$ which imply that

$$\mathbb{E}\left[d\left(Z^{I_n}_{T_{n-1}}, \overline{Z}^{I_n}_{T_{n-1}}\right)\Big|\mathcal{G}_n\right] = \frac{1}{N}\mathbb{E}\left[Y_{T_{n-1}}|\mathcal{G}_n\right],$$

and since $\mathcal{G}_n = \mathcal{G}_{n-1} \vee \sigma(S_n)$ and $S_n \perp \mathcal{F}_{T_{n-1}}$ the tower property [332, Section 9.7.(i)] implies,

$$\mathbb{E}\left[Y_{T_{n-1}}|\mathcal{G}_n\right] = \mathbb{E}\left[Y_{T_{n-1}}|\mathcal{G}_{n-1}\right].$$

Step 3. *Control of the error term*

We are now looking for a uniform bound on the error term which depends only on N. Recall that,

$$e^{I_n}_{T_n^-} = \left|\frac{1}{N}\sum_{j=1}^N K\left(\overline{X}^{I_n}_{T_n^-} - \overline{X}^j_{T_n^-}\right)\overline{m}^j_{T_n^-} - \iint_{\mathbb{R}^d\times\mathscr{M}} K\left(\overline{X}^{I_n}_{T_n^-} - x\right) m f_{T_n^-}(x,m)\mathrm{d}x\mathrm{d}m\right|.$$

Let us define:

$$b\left(\overline{Z}^i_{T_n^-}, \overline{Z}^j_{T_n^-}\right) := K\left(\overline{X}^i_{T_n^-} - \overline{X}^j_{T_n^-}\right)\overline{m}^j_{T_n^-} - \iint_{\mathbb{R}^d\times\mathscr{M}} K\left(\overline{X}^i_{T_n^-} - x\right) m f_{T_n^-}(x,m)\mathrm{d}x\mathrm{d}m.$$

These quantities are uniformly bounded:

$$\left|b\left(\overline{Z}^i_{T_n^-}, \overline{Z}^j_{T_n^-}\right)\right| \leq C\|K\|_{L^\infty}$$

and satisfy (by pairwise independence of the McKean processes):

$$\mathbb{E}\left[b\left(\overline{Z}^i_{T_n^-}, \overline{Z}^j_{T_n^-}\right)\Big|\overline{Z}^i_{T_n^-}\right] = 0. \quad (4.26)$$

The Cauchy-Schwarz inequality implies

$$\begin{aligned}\mathbb{E}\Big[e^{I_n}_{T_n^-}\Big|\mathcal{G}_n\Big]^2 &= \mathbb{E}\left[\left|\frac{1}{N}\sum_{j=1}^{N} b\left(\overline{Z}^{I_n}_{T_n^-},\overline{Z}^{j}_{T_n^-}\right)\right|\Big|\mathcal{G}_n\right]^2\\ &\leq \mathbb{E}\left[\frac{1}{N^2}\left(\sum_{j=1}^{N} b\left(\overline{Z}^{I_n}_{T_n^-},\overline{Z}^{j}_{T_n^-}\right)\right)^2\Big|\mathcal{G}_n\right]\\ &= \frac{1}{N^2}\sum_{j,k=1}^{N}\mathbb{E}\left[b\left(\overline{Z}^{I_n}_{T_n^-},\overline{Z}^{j}_{T_n^-}\right)b\left(\overline{Z}^{I_n}_{T_n^-},\overline{Z}^{k}_{T_n^-}\right)\Big|\mathcal{G}_n\right].\end{aligned}$$

And because of the centering property (4.26) and the pairwise independence, if $I_n \neq j$ and $I_n \neq k$:

$$\begin{aligned}\mathbb{E}\left[b\left(\overline{Z}^{I_n}_{T_n^-},\overline{Z}^{j}_{T_n^-}\right)b\left(\overline{Z}^{I_n}_{T_n^-},\overline{Z}^{k}_{T_n^-}\right)\Big|\mathcal{G}_n\right] &= \mathbb{E}\left[b\left(\overline{Z}^{I_n}_{T_n^-},\overline{Z}^{j}_{T_n^-}\right)\mathbb{E}\left[b\left(\overline{Z}^{I_n}_{T_n^-},\overline{Z}^{k}_{T_n^-}\right)\Big|\overline{Z}^{I_n}_{T_n^-},\overline{Z}^{j}_{T_n^-}\right]\Big|\mathcal{G}_n\right]\\ &= 0,\end{aligned}$$

which implies that there are only $\mathcal{O}(N)$ non-zero terms in the sum. Since these terms are uniformly bounded, we deduce:

$$\mathbb{E}\Big[e^{I_n}_{T_n^-}\Big|\mathcal{G}_n\Big] \leq C\sqrt{\frac{\|K\|_{L^\infty}}{N}}. \tag{4.27}$$

Remark 4.3.2. Note that in the second step we use only the bound (4.7) which is weaker than the assumption (4.4). The assumption (4.4) is only crucial in this proof to obtain the control of the error term in $1/\sqrt{N}$. However, a similar conclusion could be reached by applying more general quantitative results on the convergence in Wasserstein distance of the empirical measures of i.i.d random variables towards their common law, see for example [162]. This approach would require the adaptation of the existing results to our geometrical framework and we therefore choose to assume (4.4) and use the more straightforward computation presented in step 3 as in [307] and since it corresponds to the models [111, 140].

Step 4. *Gronwall lemma*

From the (4.25) and (4.27) we conclude that for all $n \geq 1$,

$$\mathbb{E}[Y_{T_n}|\mathcal{G}_n] \leq (1+\lambda S_n)\left(1+\frac{\sigma(K)}{N}\right)\mathbb{E}[Y_{T_{n-1}}|\mathcal{G}_{n-1}] + C\frac{\theta\big(\|K\|_{L^\infty}\big)\sqrt{\|K\|_{L^\infty}}}{\sqrt{N}} \tag{4.28}$$

and $Y_0 = 0$. This is a discrete Gronwall-type inequality and using the inequality $1+x \leq \mathrm{e}^x$,

it can be seen by induction that for all $n \geq 1$:

$$\mathbb{E}[Y_{T_n}|\mathcal{G}_n] \leq C\frac{\theta\big(\|K\|_{L^\infty}\big)\sqrt{\|K\|_{L^\infty}}}{\sqrt{N}} \sum_{k=0}^{n-1} \mathrm{e}^{\frac{\sigma(K)}{N}k+\big(\lambda+\frac{\sigma(K)}{N}\big)(T_n-T_{n-k})}. \tag{4.29}$$

Step 5. *Conclusion : bound at time $t > 0$*

In order to bound $\mathbb{E}[Y_t]$, we first look for a bound on $\mathbb{E}[Y_{T_{N_t}}]$ where

$$N_t = \sup\{n \in \mathbb{N},\ T_n \leq t\}.$$

The random variable N_t has a Poisson distribution of parameter Nt [47, Chapter 8.1.2] and in particular $\mathbb{P}(N_t = n) = \frac{(Nt)^n}{n!}\mathrm{e}^{-Nt}$. Since everything is deterministic on $[T_{N_t}, t)$, we will then use the fact that:

$$\mathbb{E}[Y_t] \leq (1 + \lambda t)\mathbb{E}[Y_{T_{N_t}}]. \tag{4.30}$$

Using the relation (4.29), we first have:

$$\begin{aligned}
\mathbb{E}[Y_{T_n}\mathbb{1}_{N_t=n}] &= \mathbb{E}\Big[\mathbb{E}\left[Y_{T_n}\mathbb{1}_{N_t=n}\middle|\mathcal{G}_{n+1}\right]\Big] \\
&= \mathbb{E}\Big[\mathbb{1}_{N_t=n}\mathbb{E}\left[Y_{T_n}\middle|\mathcal{G}_{n+1}\right]\Big] \\
&= \mathbb{E}\Big[\mathbb{1}_{N_t=n}\mathbb{E}\left[Y_{T_n}\middle|\mathcal{G}_{n}\right]\Big] \\
&\leq C\frac{\theta\big(\|K\|_{L^\infty}\big)\sqrt{\|K\|_{L^\infty}}}{\sqrt{N}}\mathbb{E}\left[\sum_{k=0}^{n-1}\mathrm{e}^{\frac{\sigma(K)}{N}k+\big(\lambda+\frac{\sigma(K)}{N}\big)t}\mathbb{1}_{N_t=n}\right] \\
&\leq C\frac{\theta\big(\|K\|_{L^\infty}\big)\sqrt{\|K\|_{L^\infty}}}{\sqrt{N}}\mathrm{e}^{\big(\lambda+\frac{\sigma(K)}{N}\big)t}\frac{\mathrm{e}^{\frac{\sigma(K)n}{N}}}{\mathrm{e}^{\frac{\sigma(K)}{N}}-1}\mathbb{P}(N_t = n)
\end{aligned}$$

And therefore,

$$\begin{aligned}
\mathbb{E}\left[Y_{T_{N_t}}\right] &= \sum_{n=0}^{\infty}\mathbb{E}[Y_{T_n}\mathbb{1}_{N_t=n}] \\
&\leq C\frac{\theta\big(\|K\|_{L^\infty}\big)\sqrt{\|K\|_{L^\infty}}}{\sqrt{N}}\frac{\mathrm{e}^{\big(\lambda+\frac{\sigma(K)}{N}\big)t}}{\mathrm{e}^{\frac{\sigma(K)}{N}}-1}\sum_{n=0}^{\infty}\mathrm{e}^{\frac{\sigma(K)}{N}n}\mathbb{P}(N_t = n) \\
&\leq C\frac{\theta\big(\|K\|_{L^\infty}\big)\sqrt{\|K\|_{L^\infty}}}{\sqrt{N}}\frac{\mathrm{e}^{\big(\lambda+\frac{\sigma(K)}{N}\big)t}}{\mathrm{e}^{\frac{\sigma(K)}{N}}-1}\exp\left(Nt\left(\mathrm{e}^{\frac{\sigma(K)}{N}}-1\right)\right).
\end{aligned}$$

Finally, from this last expression and expression (4.30) we conclude that

$$\frac{1}{N}\mathbb{E}[Y_t] \leq (1+\lambda t)\frac{1}{N}\mathbb{E}\left[Y_{T_{N_t}}\right] \\ \leq C\frac{\theta\big(\|K\|_{L^\infty}\big)\sqrt{\|K\|_{L^\infty}}}{\sqrt{N}}\frac{\mathrm{e}^{\left(2\lambda+\frac{\sigma(K)}{N}\right)t}}{N\left(\mathrm{e}^{\frac{\sigma(K)}{N}}-1\right)}\exp\left(Nt\left(\mathrm{e}^{\frac{\sigma(K)}{N}}-1\right)\right) \quad (4.31)$$

where we have used the fact that $1+\lambda t \leq \mathrm{e}^{\lambda t}$. To prove the first point of Theorem 4.2.13 we notice that

$$\mathbb{E}[W_1(\hat{\mu}_t^N, f_t)] \leq \mathbb{E}[W_1(\hat{\mu}_t^N, \overline{\mu}_t^N)] + \mathbb{E}[W_1(\overline{\mu}_t^N, f_t)] \\ \leq \frac{1}{N}\mathbb{E}[Y_t] + \mathbb{E}[W_1(\overline{\mu}_t^N, f_t)]$$

where the bound between the two empirical measures is a consequence of the Kantorovich dual formulation of the Wasserstein distance. Since $\mathbb{E}[W_1(\overline{\mu}_t^N, f_t)] \to 0$ as $N \to +\infty$ by independence of the McKean processes, the result follows from (4.31).

The second point of Theorem 4.2.13 follows from the definition of the Wasserstein distance which implies that

$$W_1(f_t^{1,N}, f_t) \leq \frac{1}{N}\mathbb{E}[Y_t].$$

The final bound is obtained from the right-hand side of (4.31) and the fact that for all $x \geq 0$, $x \leq \mathrm{e}^x - 1 \leq x\mathrm{e}^x$. □

Remark 4.3.3. The above proof is based on the same classical coupling arguments of [307] but in a PDMP framework and using an "algorithmic" definition of the process. This type of proof is rather elementary and allows an explicit control of the error. In the context of jump processes, another natural approach would be to re-write the IBM as a system of N stochastic differential equations with respect to N independent Poisson measures. Without a specific geometrical structure as in this chapter, a very comprehensive reference which proves propagation of chaos in this context is [5].

4.4 Moderate interaction (proof of Theorem 4.2.15)

This section is devoted to the proof of Theorem 4.2.15. We follow the approach of [221]. Given a sequence of kernels $(K^N)_N$, the goal is to apply Ascoli-Arzelà's theorem to show the convergence in $C([0,T], B_a)$ of a subsequence of the sequence of solutions of (4.12) associated to $(K^N)_N$ towards the unique solution of (4.16). To do so, we will first need

to prove some properties on the associate sequence of solutions of (4.12) (Lemma 4.4.1) and in particular an equicontinuity property. We will then prove a compactness result (Lemma 4.4.3) which is an adaptation of the classical Riesz-Fréchet-Kolmogorov to our geometrical context and which will be needed to prove the compactness of the sequence at a fixed time (pointwise compactness, Lemma 4.4.4). The proof of Theorem 4.2.15 can be found in Section 4.4.3.

4.4.1 First estimates

From now, we fix $a > 0$ and $T > 0$ such that (4.16) is wellposed on $C([0,T], B_a)$ where B_a is the ball of radius $a > 0$ in $L^\infty \cap \mathcal{P}^{\mathrm{ac}}(\mathbb{R}^d \times \mathscr{M})$. A key remark is that, if $g \in B_a$ then for all $N \in \mathbb{N}$ and all $x \in \mathbb{R}^d$,

$$|J_{K^N \star g}(x)| \leq \iint_{\mathbb{R}^d \times \mathscr{M}} K^N(x-y)|g(y,m)|\mathrm{d}y\mathrm{d}m \leq a,$$

since the integral of K^N is equal to 1 and where we have used that $\int_{\mathscr{M}} \mathrm{d}m = 1$. As a consequence, the solution f^N of (4.12) with kernel K^N and initial condition f_0 belongs to $C([0,T], B_a)$ as it can be seen by rewriting the proof of Proposition 4.2.12 for the interaction law with kernel K^N.

Lemma 4.4.1. *The sequence $(f^N)_N \in C([0,T], B_a)$ satisfies the following properties.*

(i) (space-translation stability) Let $h \in \mathbb{R}^d$, then

$$\sup_{t\in[0,T]} \|\tau_{(h,id)} f_t^N - f_t^N\|_{L^1(\mathbb{R}^d\times\mathscr{M})} \leq C(a,T)\|\tau_{(h,id)} f_0 - f_0\|_{L^1(\mathbb{R}^d\times\mathscr{M})}, \tag{4.32}$$

where the translation operator τ is defined for a measurable function g on $\mathbb{R}^d \times \mathscr{M}$, $h \in \mathbb{R}^d$ and $\psi \in C(\mathscr{M}, \mathscr{M})$ by $(\tau_{(h,\psi)} g)(x,m) := g(x+h, \psi(m))$.

(ii) (tightness) There exists $\beta > 0$ such that for $R > 0$ sufficiently big, then

$$\sup_{t\in[0,T]} \iint_{\{|x|\geq R\}\times\mathscr{M}} f_t^N(x,m)\mathrm{d}x\mathrm{d}m \leq C(T) \iint_{\{|x|\geq R-\beta T\}\times\mathscr{M}} f_0(x,m)\mathrm{d}x\mathrm{d}m. \tag{4.33}$$

(iii) (equicontinuity) Let $t \in [0,T)$ and $h > 0$ sufficiently small, then

$$\|f_{t+h}^N - f_t^N\|_{L^1(\mathbb{R}^d\times\mathscr{M})} \leq C(a,T)\Big(\|\mathsf{T}_h f_0 - f_0\|_{L^1(\mathbb{R}^d\times\mathscr{M})} + \varepsilon(h)\Big), \tag{4.34}$$

where $\varepsilon(h) \to 0$ uniformly in h and T_h is the free-transport operator defined by (4.15).

Proof. Recall that f^N is given by Duhamel's formula:

$$f_t^N(x,m) = \mathrm{e}^{-t} f_0(x - t\Phi(m), m) + \int_0^t \mathrm{e}^{-(t-s)} \rho_{f_s^N}(x - (t-s)\Phi(m)) M_{K^N \star f_s^N}[x - (t-s)\Phi(m)](m)\,\mathrm{d}s.$$

Or equivalently:

$$f_t^N = \mathrm{e}^{-t}\mathsf{T}_t f_0 + \int_0^t \mathrm{e}^{-(t-s)}\,\mathsf{T}_{t-s} G^K_{f_s^N}\,\mathrm{d}s,$$

where

$$G_f^K(x,m) := \rho_f(x) M_{K^N \star f}[x](m).$$

(i) Since $\tau_{(h,id)}\mathsf{T}_t = \mathsf{T}_t \tau_{(h,id)}$ and $\tau_{(h,id)} G_f^K = G^K_{\tau_{(h,id)} f}$, the conclusion follows from the stability estimate obtained by Duhamel formula by using the Lipschitz bound (4.18)

$$\|G_f^K - G_g^K\|_{L^1(\mathbb{R}^d \times \mathscr{M})} \leq (\alpha(a) + a\theta(a))\|f - g\|_{L^1(\mathbb{R}^d \times \mathscr{M})}$$

and Gronwall's lemma.

(ii) For a given $R > 0$

$$\iint_{\{|x| \geq R\} \times \mathscr{M}} f_t^N(x,m)\mathrm{d}x\mathrm{d}m = \mathrm{e}^{-t} \iint_{\{|x| \geq R\} \times \mathscr{M}} f_0(x - t\Phi(m), m)\mathrm{d}x\mathrm{d}m + \int_0^t \mathrm{e}^{-(t-s)} \iint_{\{|x| \geq R\} \times \mathscr{M}} G^K_{f_s^N}(x - (t-s)\Phi(m), m)\mathrm{d}x\mathrm{d}m\,\mathrm{d}s.$$

We define for $0 \leq s \leq t$ and for $R > 0$ sufficiently big:

$$\mathcal{I}_R^N(s) := \iint_{\{|x| \geq R - \beta(t-s)\} \times \mathscr{M}} f_s^N(x,m)\mathrm{d}x\mathrm{d}m$$

where $\beta > 0$ is such that $|\Phi(m)| \leq \beta$ for all $m \in \mathscr{M}$. For fixed $m \in \mathscr{M}$ and $s \in [0,t]$, with the change of variables $x \mapsto x - (t-s)\Phi(m)$, it holds that:

$$\begin{aligned}\int_{|x| \geq R} G^K_{f_s^N}(x - (t-s)\Phi(m), m)\mathrm{d}x &= \int_{|x + (t-s)\Phi(m)| \geq R} \rho_{f_s^N}(x) M_{K^N \star f_s^N}[x](m)\mathrm{d}x \\ &\leq \int_{|x| \geq R - \beta(t-s)} \rho_{f_s^N}(x) M_{K^N \star f_s^N}[x](m)\mathrm{d}x,\end{aligned}$$

where the last inequality comes from the fact that $\{x,\ |x + (t-s)\Phi(m)| \geq R\} \subset \{x,\ |x| \geq R - \beta(t-s)\}$. Integrating this expression on $\mathscr{M}$ and using the fact that

$M_{K^N \star f_s^N}[x]$ is a probability density function, we obtain:

$$\iint_{\{|x|\geq R\}\times\mathscr{M}} G^K_{f_s^N}(x-(t-s)\Phi(m),m)\mathrm{d}x \leq \mathcal{I}_R^N(s).$$

Then, since $\mathrm{e}^{-t}\leq 1$, it holds that

$$\mathcal{I}_R^N(t) \leq \mathcal{I}_R^N(0) + \int_0^t \mathcal{I}_R^N(s)\mathrm{e}^s \mathrm{d}s$$

from which we can conclude using Gronwall lemma that:

$$\begin{aligned}\mathcal{I}_R^N(t) = \iint_{\{|x|\geq R\}\times\mathscr{M}} f_t^N(x,m)\mathrm{d}x\mathrm{d}m &\leq C(t)\iint_{\{|x|\geq R-\beta t\}\times\mathscr{M}} f_0(x,m)\mathrm{d}x\mathrm{d}m \\ &\leq C(t)\mathcal{I}_R^N(0).\end{aligned}$$

(iii) We have:

$$\begin{aligned}\|f_{t+h}^N - f_t^N\|_{L^1(\mathbb{R}^d\times\mathscr{M})} \leq \mathrm{e}^{-t}\|\mathsf{T}_h f_0 - f_0\|_{L^1(\mathbb{R}^d\times\mathscr{M})} \\ + \int_0^t \mathrm{e}^{-(t-s)}\|\mathsf{T}_h G^K_{f_s^N} - G^K_{f_s^N}\|_{L^1(\mathbb{R}^d\times\mathscr{M})} + \varepsilon(|h|)\end{aligned}$$

where $\varepsilon(|h|)\to 0$ and depends only on a and T (it comes from the terms $\mathrm{e}^{-(t+h)}$ instead of e^{-t} and the integral between t and $t+h$). Then it holds that

$$\begin{aligned}&\|\mathsf{T}_h G^K_{f_s^N} - G^K_{f_s^N}\|_{L^1(\mathbb{R}^d\times\mathscr{M})} \\ &\quad= \iint_{\mathbb{R}^d\times\mathscr{M}} \Big| \int_{\mathscr{M}} f_s^N\left(x-h\Phi(m),m'\right) M_{K^N\star f_s^N}\left[x-h\Phi(m)\right](m) \\ &\qquad\qquad - f_s^N(x,m') M_{K^N\star f_s^N}[x](m)\mathrm{d}m'\Big|\mathrm{d}x\mathrm{d}m \\ &\quad\leq \int_{\mathscr{M}}\Big\{\iint_{\mathbb{R}^d\times\mathscr{M}} \Big| f_s^N\left(x-h\Phi(m),m'\right) M_{K^N\star f_s^N}\left[x-h\Phi(m)\right](m) \\ &\qquad\qquad - f_s^N(x,m') M_{K^N\star f_s^N}[x](m)\Big|\mathrm{d}m'\mathrm{d}x\Big\}\mathrm{d}m\end{aligned}$$

And it holds that for a given $m \in \mathscr{M}$:

$$\begin{aligned}
&\iint_{\mathbb{R}^d\times\mathscr{M}} \Big| f_s^N\left(x - h\Phi(m), m'\right) M_{K^N \star f_s^N}\left[x - h\Phi(m)\right](m) \\
&\qquad\qquad - f_s^N(x, m') M_{K^N \star f_s^N}\left[x\right](m) \Big| \mathrm{d}m' \mathrm{d}x \\
&\leq \alpha(a) \left\| (\tau_{(-h\Phi(m),id)} f_s^N) - f_s^N \right\|_{L^1(\mathbb{R}^d\times\mathscr{M})} \\
&\quad + Ca\theta(a) \iint_{\mathbb{R}^d\times\mathscr{M}} \iint_{\mathbb{R}^d\times\mathscr{M}} K^N(y) \big| f_s^N(x - h\Phi(m) - y, m'') \\
&\qquad\qquad - f_s^N(x - y, m'') \big| |m''| \mathrm{d}y \mathrm{d}m'' \mathrm{d}x \mathrm{d}m'.
\end{aligned}$$

Since $|m''| \leq 1$ and $\int_{\mathscr{M}} \mathrm{d}m' = 1$, by switching the integrals in x and in y (Fubini's theorem), with the change of variable $x' = x - y$ and since the integral of K^N is equal to 1, it holds that:

$$\begin{aligned}
&\iint_{\mathbb{R}^d\times\mathscr{M}} \iint_{\mathbb{R}^d\times\mathscr{M}} K^N(y) \left| f_s^N(x - h\Phi(m) - y, m'') - f_s^N(x - y, m'') \right| |m''| \mathrm{d}y \mathrm{d}m'' \mathrm{d}x \mathrm{d}m' \\
&\qquad\qquad \leq \left\| \tau_{(-h\Phi(m),id)} f_s^N - f_s^N \right\|_{L^1(\mathbb{R}^d\times\mathscr{M})}.
\end{aligned}$$

Gathering everything and using the space-translation stability property, we obtain:

$$\|\mathsf{T}_h G^K_{f_s^N} - G^K_{f_s^N}\|_{L^1(\mathbb{R}^d\times\mathscr{M})} \leq c(a,T) \int_{\mathscr{M}} \|\tau_{(-h\Phi(m),id)} f_0 - f_0\|_{L^1(\mathbb{R}^d\times\mathscr{M})} \mathrm{d}m,$$

where $c(a,T) > 0$ is a constant which depends only on a, $T > 0$ and $\mathscr{M}$. This last term vanishes uniformly on h by the dominated convergence theorem and the continuity of the shift operator in L^1 (as it can be seen by approximation by smooth functions [12, p.79]).

□

Remark 4.4.2. These properties can be understood at the level of the processes $\overline{Z}_t$. In particular, we can deduce some of them from [260]:

- Since $\tau_{(h,id)}$ commutes with all the operators, the space-translation stability follows from the stability result [260, Theorem 3].
- For the equicontinuity, since everything is Markovian, we can consider the two nonlinear processes starting from f_0 and f_h. Their laws at time t are respectively f_t

and f_{t+h}. The stability result [260, Theorem 3] shows that:

$$\|f_{t+h} - f_t\|_{\mathrm{TV}} \leq C(a,T)\|f_h - f_0\|_{\mathrm{TV}}.$$

To conclude, it is enough to write:

$$\|f_h - f_0\|_{\mathrm{TV}} \leq \|\mathsf{T}_h f_0 - f_0\|_{\mathrm{TV}} + \|f_h - \mathsf{T}_h f_0\|_{\mathrm{TV}}$$

and to notice that:

$$\|f_h - \mathsf{T}_h f_0\|_{\mathrm{TV}} \leq \mathbb{P}(\text{there is a jump on } [0,h]) = \mathcal{O}(h).$$

4.4.2 A compactness result

We first state a compactness lemma, which is the analog of the Riesz-Fréchet-Kolmogorov theorem in a Riemannian setting. The proof can be found in Appendix 4.A. The ideas of the proof come from [195, Chapter 2]. When ω and Ω are two open sets in a metric space, we write $\omega \subset\subset \Omega$ when $\omega \subset \Omega$, $\overline{\omega} \subset \Omega$ and $\overline{\omega}$ is compact where $\overline{\omega}$ is the closure of ω in the ambiant metric space.

Lemma 4.4.3. *Let $\mathcal{F} \subset L^1(\mathbb{R}^d \times \mathscr{M})$ be a bounded subset which satisfies the following properties.*

1. *For all $\varepsilon > 0$, there exists $R > 0$ such that:*

$$\forall f \in \mathcal{F}, \iint_{\{|x| \geq R\} \times \mathscr{M}} f(x,m)\mathrm{d}x\mathrm{d}m < \varepsilon.$$

2. *For all $\varepsilon > 0$ and for all $\omega \subset\subset \Omega \subset \mathscr{M}$ open sets, there exists $\eta > 0$ such that for any smooth function $\phi : \omega \to \Omega$ which satisfies*

$$\forall m \in \omega, \ \ d(\phi(m), m) < \eta,$$

and for all $h \in \mathbb{R}^d$ such that $|h| < \eta$, it holds that:

$$\forall f \in \mathcal{F}, \iint_{\mathbb{R}^d \times \omega} |f(x+h, \phi(m)) - f(x,m)|\mathrm{d}x\mathrm{d}m < \varepsilon.$$

Then $\mathcal{F}$ is relatively sequentially compact in $L^1(\mathbb{R}^d \times \mathscr{M})$.

Using this lemma, it can be shown that for every $t \in [0,T]$, the sequence $(f_t^N)_N$ is compact in $L^1(\mathbb{R}^d \times \mathscr{M})$.

Lemma 4.4.4 (Pointwise compactness)**.** *Let $t \in [0,T]$ be a given time. Then the sequence $(f_t^N)_N$ of solutions of (4.12) associated to the sequence of kernels $(K^N)_N$ is compact in $L^1(\mathbb{R}^d \times \mathscr{M})$.*

Proof. To prove this result, we will show that the family $(f_t^N)_N$ satisfies the conditions to apply Lemma 4.4.3. Firstly we see that the family is bounded in L^1 : for all $N \in \mathbb{N}$, $\|f_t^N\|_{L^1(\mathbb{R}^d \times \mathscr{M})} = 1$. Secondly thanks to the tightness result (4.33) the family satisfies the first point of Lemma 4.4.3. Finally we are left with proving that the family satisfies the second point in Lemma 4.4.3. The conclusion is then a direct consequence of Lemma 4.4.3. The rest of this proof is devoted to showing that the family $(f_t^N)_N$ satisfies condition 2 of Lemma 4.4.3.

Let $h \in \mathbb{R}^d$, $\omega \subset\subset \Omega \subset \mathscr{M}$ open sets and $\psi : \omega \to \Omega$ a continuous function. Recall the Duhamel's formula:

$$f_t^N = \mathrm{e}^{-t}\mathsf{T}_t f_0 + \int_0^t \mathrm{e}^{-(t-s)}\, \mathsf{T}_{t-s} G^K_{f_s^N}\, \mathrm{d}s$$

where the free-transport operator T_t is defined by (4.15) and the (h,ψ)-translation is defined by:

$$\tau_{(h,\psi)} f(x,m) := f(x+h, \psi(m)).$$

To show that the family $(f_t^N)_N$ fulfills condition 2 in Lemma 4.4.3, we have to bound:

$$\begin{aligned}
\|\tau_{(h,\psi)} f_t^N - f_t^N\|_{L^1(\mathbb{R}^d\times\omega)} \leq\, & \mathrm{e}^{-t}\|\tau_{(h,\psi)}\mathsf{T}_t f_0 - \mathsf{T}_t f_0\|_{L^1(\mathbb{R}^d\times\omega)} \\
& + \int_0^t \mathrm{e}^{-(t-s)}\|\tau_{(h,\psi)}\mathsf{T}_{t-s} G^K_{f_s^N} - \mathsf{T}_{t-s} G^K_{f_s^N}\|_{L^1(\mathbb{R}^d\times\omega)}\, \mathrm{d}s \\
\leq\, & \mathrm{e}^{-t}\|\tau_{(h,\psi)} f_0 - f_0\|_{L^1(\mathbb{R}^d\times\omega)} \\
& + \mathrm{e}^{-t}\|\tau_{(h,\psi)}\mathsf{T}_t f_0 - \mathsf{T}_t \tau_{(h,\psi)} f_0\|_{L^1(\mathbb{R}^d\times\omega)} \\
& + \int_0^t \mathrm{e}^{-(t-s)}\|\tau_{(h,\psi)} G^K_{f_s^N} - G^K_{f_s^N}\|_{L^1(\mathbb{R}^d\times\omega)}\, \mathrm{d}s \\
& + \int_0^t \mathrm{e}^{-(t-s)}\|\tau_{(h,\psi)}\mathsf{T}_{t-s} G^K_{f_s^N} - \mathsf{T}_{t-s}\tau_{(h,\psi)} G^K_{f_s^N}\|_{L^1(\mathbb{R}^d\times\omega)}\, \mathrm{d}s \\
& =: I_1 + I_2 + I_3 + I_4
\end{aligned} \tag{4.35}$$

where we have used that the free-transport operator is an L^1-isometry. We now bound each of the four terms in the right hand side.

- (**Term** I_1) For smooth compactly supported f_0, it follows by the dominated convergence theorem that:

$$\|\tau_{(h,\psi)}f_0 - f_0\|_{L^1(\mathbb{R}^d\times\omega)} \to 0$$

when $h \to 0$ and $\psi \to id$ (for the uniform convergence topology on $\mathscr{M}$). This limit still holds for any $f_0 \in L^1(\mathbb{R}^d \times \omega)$ by density in the L^1 norm of smooth compactly supported functions and the fact that the translation operator is an isometry.

- (**Term** I_2) By similar arguments,

$$\begin{aligned}
&\|\tau_{(h,\psi)}\mathsf{T}_t f_0 - \mathsf{T}_t\tau_{(h,\psi)}f_0\|_{L^1(\mathbb{R}^d\times\omega)} \\
&\qquad = \iint_{\mathbb{R}^d\times\omega} \left|\mathsf{T}_t f_0(x+h,\psi(m)) - (\tau_{(h,\psi)}f_0)(x - t\Phi(m),m)\right| \mathrm{d}x\mathrm{d}m \\
&\qquad = \iint_{\mathbb{R}^d\times\omega} \left|f_0\left(x+h-t\Phi\big(\psi(m)\big),\psi(m)\right) - f_0\left(x+h-t\Phi(m),\psi(m)\right)\right| \mathrm{d}x\mathrm{d}m \\
&\qquad = \iint_{\mathbb{R}^d\times\omega} \left|f_0\left(x - t\left(\Phi\big(\psi(m)\big) - \Phi(m)\right),\psi(m)\right) - f_0(x,\psi(m))\right| \mathrm{d}x\mathrm{d}m
\end{aligned}$$

converges to 0 as $h \to 0$ and $\psi \to id$ since Φ is Lipschitz.

- (**Term** I_3) We write the third term as:

$$
\begin{aligned}
&\|\tau_{(h,\psi)}G^K_{f^N_s} - G^K_{f^N_s}\|_{L^1(\mathbb{R}^d\times\omega)}\\
&= \iint_{\mathbb{R}^d\times\omega}\Big|\int_{\mathscr{M}} f^N_s(x+h,m')M_{K^N\star f^N_s}[x+h]\big(\psi(m)\big)\\
&\qquad\qquad - f^N_s(x,m')M_{K^N\star f^N_s}[x](m)\mathrm{d}m'\Big|\mathrm{d}x\mathrm{d}m\\
&\leq \int_{\mathscr{M}}\iint_{\mathbb{R}^d\times\omega}|f^N_s(x+h,m') - f^N_s(x,m')|M_{K^N\star f^N_s}[x+h]\big(\psi(m)\big)\mathrm{d}x\mathrm{d}m\mathrm{d}m'\\
&\quad + \int_{\mathscr{M}}\iint_{\mathbb{R}^d\times\omega} f^N_s(x,m')\left|M_{K^N\star f^N_s}[x+h]\big(\psi(m)\big) - M_{K^N\star f^N_s}[x](m)\right|\mathrm{d}x\mathrm{d}m\mathrm{d}m'\\
&\leq \alpha(a)\|\tau_{(h,id)}f^N_s - f^N_s\|_{L^1(\mathbb{R}^d\times\mathscr{M})}\\
&\quad + \int_{\mathscr{M}}\iint_{\mathbb{R}^d\times\omega} f^N_s(x,m')\left|M_{K^N\star f^N_s}[x+h]\big(\psi(m)\big) - M_{K^N\star f^N_s}[x]\big(\psi(m)\big)\right|\mathrm{d}x\mathrm{d}m\mathrm{d}m'\\
&\quad + \int_{\mathscr{M}}\iint_{\mathbb{R}^d\times\omega} f^N_s(x,m')\left|M_{K^N\star f^N_s}[x]\big(\psi(m)\big) - M_{K^N\star f^N_s}[x](m)\right|\mathrm{d}x\mathrm{d}m\mathrm{d}m'\\
&\leq \alpha(a)\|\tau_{(h,id)}f^N_s - f^N_s\|_{L^1(\mathbb{R}^d\times\mathscr{M})}\\
&\quad + a\int_{\mathbb{R}^d}\left\|M_{K^N\star f^N_s}[x+h] - M_{K^N\star f^N_s}[x]\right\|_{L^\infty(\mathscr{M})}\mathrm{d}x\\
&\quad + L(a)\sup_{m\in\omega} d(\psi(m),m)
\end{aligned}
$$

where we have used the fact that for all $N\in\mathbb{N}$ and all $t\in[0,T]$, $\|f^N_t\|_{L^\infty(\mathbb{R}^d\times\mathscr{M})}\leq a$ where $a>0$ is fixed (see beginning of Subsection 4.4.1). Using the bound (4.4), Fubini's theorem and the fact that the integral of K^N is equal to 1, it holds that

$$
\begin{aligned}
&\int_{\mathbb{R}^d}\left\|M_{K^N\star f^N_s}[x+h] - M_{K^N\star f^N_s}[x]\right\|_{L^\infty(\mathscr{M})}\mathrm{d}x\\
&\qquad\leq \theta(a)\int_{\mathbb{R}^d}\iint_{\mathbb{R}^d\times\mathscr{M}} K^N(y)|f^N_s(x+h-y,m) - f^N_s(x-y,m)|\mathrm{d}y\mathrm{d}m\mathrm{d}x\\
&\qquad= \theta(a)\|\tau_{(h,id)}f^N_s - f^N_s\|_{L^1(\mathbb{R}^d\times\mathscr{M})}
\end{aligned}
$$

Finally we conclude the following estimate:

$$\|\tau_{(h,\psi)}G^K_{f^N_s} - G^K_{f^N_s}\|_{L^1(\mathbb{R}^d\times\omega)} \leq (\alpha(a)+a\theta(a))\|\tau_{(h,id)}f^N_s - f^N_s\|_{L^1(\mathbb{R}^d\times\mathscr{M})} + L(a)\sup_{m\in\omega} d(\psi(m),m).$$

Using the space-translation stability (4.32) we deduce that this term goes to zero when $h\to 0$ and $\psi\to id$ (for the uniform convergence topology on $\mathscr{M}$).

- (**Term** I_4) We bound the fourth term:

$$\begin{aligned}
&\|\tau_{(h,\psi)}\mathsf{T}_{t-s}G^K_{f^N_s} - \mathsf{T}_{t-s}\tau_{(h,\psi)}G^K_{f^N_s}\|_{L^1(\mathbb{R}^d\times\omega)}\\
&\quad= \iint_{\mathbb{R}^d\times\omega}\left|G^K_{f^N_s}\left(x-(t-s)\left(\Phi\big(\psi(m)\big)-\Phi(m)\right),\psi(m)\right) - G^K_{f^N_s}(x,\psi(m))\right|\mathrm{d}x\mathrm{d}m\\
&\quad\leq \iint_{\mathbb{R}^d\times\omega}\int_{\mathscr{M}}\Big|f^N_s\left(x-(t-s)\left(\Phi\big(\psi(m)\big)-\Phi(m)\right),m'\right)\\
&\qquad\qquad\times M_{K^N\star f^N_s}[x-(t-s)\left(\Phi\left(\psi(m)\right)-\Phi(m)\right)]\big(\psi(m)\big)\\
&\qquad\qquad - f^N_s(x,m')M_{K^N\star f^N_s}[x]\big(\psi(m)\big)\Big|\mathrm{d}m'\mathrm{d}x\mathrm{d}m\\
&\quad\leq \big(\alpha(a)+a\theta(a)\big)\int_\omega \left\|\tau_{(-(t-s)(\Phi(\psi(m))-\Phi(m)),id)}f^N_s - f^N_s\right\|_{L^1(\mathbb{R}^d\times\mathscr{M})}\mathrm{d}m
\end{aligned}$$

Using the space-translation stability and the fact that Φ is Lipschitz, we conclude that this term goes to zero when $h\to 0$ and $\psi\to id$.

Finally, gathering the analysis of these four terms, we conclude that the right-hand side in expression (4.35) converges to 0 when $h\to 0$ and $\psi\to id$. Therefore the family $(f^N_t)_N$ fulfills condition 2 in Lemma 4.4.3, as we wanted to show. □

Remark 4.4.5. This result is similar to the compact injection $W^{1,1}(M)\hookrightarrow L^1(M)$ where M is compact Riemannian manifold (this follows from Rellich-Kondrakov injection theorem [195, Theorem 2.9] which is a consequence of Riesz-Fréchet-Kolmogorov theorem, as Lemma 4.4.3). We can apply directly this result under stronger assumptions on f_0 : if f_0 is compactly supported then it can be seen as a function on $\mathbb{T}^d\times\mathscr{M}$ where $\mathbb{T}^d$ is a sufficiently big d-dimensional torus. The tightness result (4.33) proves that f^N_t can also be seen as a function on $\mathbb{T}^d\times\mathscr{M}$. The space-translation stability (4.32) and the Lipschitz bound (4.3) on the interaction law ensure that if $f_0\in W^{1,1}(\mathbb{T}^d\times\mathscr{M})$ then $(f^N_t)_N$ is bounded in $W^{1,1}(\mathbb{T}^d\times\mathscr{M})$ hence compact in $L^1(\mathbb{T}^d\times\mathscr{M})$.

4.4.3 Proof of Theorem 4.2.15

Proof (of Theorem 4.2.15). Under hypothesis (4.21), it holds that

$$\frac{\sigma(K^N)}{N} \underset{N\to+\infty}{\longrightarrow} 0$$

and the right-hand side of (4.20) (at time T) goes to 0 as $N \to +\infty$:

$$\frac{\varepsilon_N^{d/2+1} \mathrm{e}^{T\frac{\sigma(K^N)}{N}}}{\sqrt{N}} \exp\left(T\theta(\varepsilon_N^{-d})\varepsilon_N^{-(d+1)}\mathrm{e}^{\frac{\sigma(K^N)}{N}}\right) \to 0,$$

where we can assume without loss of generality that $\|K\|_{L^\infty} = \|K\|_{\mathrm{Lip}} = 1$ which implies

$$\|K^N\|_{L^\infty} = \varepsilon_N^{-d} \text{ and } \|K^N\|_{\mathrm{Lip}} = \varepsilon^{-(d+1)}.$$

The propagation of chaos result (Theorem 4.2.13) therefore ensures that under Hypothesis (4.21),

$$W^1(f_t^{1,N}, f_t^N) \underset{N\to+\infty}{\longrightarrow} 0,$$

where f_t^N is the solution of (4.12) with kernel K^N. The Wasserstein-1 convergence implies the weak convergence of measures. It then remains to prove that

$$\|f_t^N - f_t\|_{L^1(\mathbb{R}^d\times\mathscr{M})} \to 0,$$

since it also implies the weak convergence of f_t^N towards f_t as measures. The equicontinuity property (4.34) and Lemma 4.4.4 are the two hypotheses of Ascoli's theorem [49, Theorem 4.25]. Therefore, we can extract a subsequence of $(f^N)_N$ which converges in $C([0,T], L^1(\mathbb{R}^d \times \mathscr{M}))$ towards $f \in C([0,T], L^1(\mathbb{R}^d \times \mathscr{M}))$. Note that since the sequence is also bounded in $L^\infty(\mathbb{R}^d \times \mathscr{M})$, we also have $f_t \in B_a$ for every $t \in [0,T]$. It remains to prove that the limit f_t is uniquely defined as the solution of (4.16). Thanks to Duhamel's formula. to do so, it is enough to prove that

$$\|G^K_{f_t^N} - G_{f_t}\|_{L^1(\mathbb{R}^d\times\mathscr{M})} \to 0$$

uniformly in t. This follows from:

$$\begin{aligned}\|G^K_{f_t^N} - G_{f_t}\|_{L^1(\mathbb{R}^d\times\mathscr{M}} &\leq \alpha(a)\|f_t^N - f_t\|_{L^1(\mathbb{R}^d\times\mathscr{M})} \\ &\quad + a\int_{\mathbb{R}^d}\left\|M_{K^N\star f_t^N}[x] - M_{K^N\star f_t}[x]\right\|_{L^\infty(\mathscr{M})}\mathrm{d}x \\ &\quad + a\int_{\mathbb{R}^d}\left\|M_{K^N\star f_t}[x] - M_{f_t}[x]\right\|_{L^\infty(\mathscr{M})}\mathrm{d}x \\ &\leq \big(\alpha(a) + a\theta(a)\big)\sup_{t\in[0,T]}\|f_t^N - f_t\|_{L^1(\mathbb{R}^d\times\mathscr{M})} \\ &\quad + a\theta(a)\int_{\mathscr{M}}\|K^N\star f_t(\cdot,m) - f_t(\cdot,m)\|_{L^1(\mathbb{R}^d)}\mathrm{d}m\end{aligned}$$

and the last term in the right hand side goes to zero by the dominated convergence theorem, uniformly in t by Ascoli's theorem. □

Remark 4.4.6. If f_0 is compactly supported, then

$$W_1(f_t^N, f_t) \leq C\|f_t^N - f_t\|_{L^1(\mathbb{R}^d\times\mathscr{M})}$$

and the convergence of $f_t^{1,N}$ towards f_t actually holds in Wasserstein-1 distance.

4.5 An alternative approach in the spatially homogeneous case

This section is an adaptation of the proof of the mean-field limit of the isotropic 4-wave kinetic equation with bounded jump kernel which can be found in [254, Section 4.3]. A more general result is also proved in [76].

The aim of this section is to write the solution of the space homogeneous BGK equation:

$$\partial_t\nu_t = M_{\nu_t} - \nu_t =: Q_{\mathrm{BGK}}(\nu_t),$$

as the mean-field limit of a system of interacting particles. Without loss of generality we will look for a solution is in $\mathcal{P}(\mathscr{M})$ (and not only $\mathcal{M}_+(\mathscr{M})$) since the total mass is preserved by the equation. In the following, we will say that a $\mathcal{P}(\mathscr{M})$-valued process $(\nu_t)_t$ is a weak solution of the space homogeneous BGK equation when it is continuous almost everywhere in time and satisfies for almost every $t \in \mathbb{R}_+$:

$$\forall\varphi \in C_b(\mathscr{M}), \quad \langle\nu_t,\varphi\rangle = \langle\nu_0,\varphi\rangle + \int_0^t Q^\star_{\mathrm{BGK}}\varphi(\nu_s)\,\mathrm{d}s,$$

where for $\varphi \in C_b(\mathscr{M})$ and $\nu \in \mathcal{P}(\mathscr{M})$,

$$Q^\star_{\mathrm{BGK}}\varphi(\nu) := \int_{\mathscr{M}}\int_{\mathscr{M}} \{\varphi(m') - \varphi(m)\} M_\nu(m')\mathrm{d}m'\nu(\mathrm{d}m). \tag{4.36}$$

Notice that:

$$Q^\star_{\mathrm{BGK}}\varphi(\nu) = \langle Q_{\mathrm{BGK}}(\nu), \varphi\rangle.$$

The proof of the well-posedness of such weak formulation can be found in [233, Theorem 6.1]. In the following a *test function* is a continuous bounded function. Notice that since $\mathscr{M}$ is compact, a continuous function on $\mathscr{M}$ is automatically bounded.

4.5.1 Individual Based Model

Consider the N-particle $(m_t^{1,N}, \dots, m_t^{N,N}) \in \mathscr{M}^N$ dynamics defined by the following jump process:

1. Let $(T_n)_n$ be an increasing sequence of jump times such that the increments are independent and follow an exponential law of parameter N.

2. At each jump time T_n, choose a particle $i \in \{1, \dots N\}$ uniformly among the N particles and draw the new body-orientation $m^{i,N}_{T_n^+}$ after the jump according to the law $M_{\hat{\mu}^N_{T_n^-}}$ where the empirical measure $\hat{\mu}^N_t$ is defined by

$$\hat{\mu}^N_t := \frac{1}{N}\sum_{i=1}^N \delta_{m_t^{i,N}}.$$

This defines a continuous time Markov process $(m_t^{1,N}, \dots, m_t^{N,N})_t \in \mathscr{M}^N$ with generator:

$$\begin{aligned}&\mathcal{L}_N\varphi(m_1, \dots, m_N)\\ &\qquad := \sum_{i=1}^N \int_{\mathscr{M}} \big(\varphi(m_1, \dots, m_i', \dots, m_N) - \varphi(m_1, \dots, m_i, \dots, m_N)\big) M_{\mu_{\mathbf{m}^N}}(m_i')\,\mathrm{d}m_i',\end{aligned}$$

where

$$\mu_{\mathbf{m}^N} = \frac{1}{N}\sum_{i=1}^N \delta_{m_i}.$$

4.5.2 A process on measures

Equivalently, we define a $\widehat{\mathcal{P}}_N(\mathscr{M}) \subset \mathcal{P}(\mathscr{M})$-valued Markov process with generator:

$$\mathcal{G}_N\phi(\nu) := N \int_{\mathscr{M}} \int_{\mathscr{M}} \left(\phi\left(\nu - \frac{1}{N}\delta_m + \frac{1}{N}\delta_{m'}\right) - \phi(\nu) \right) M_\nu(m')\mathrm{d}m'\nu(\mathrm{d}m),$$

where $\phi : \mathcal{P}(\mathscr{M}) \to \mathbb{R}$ is a test function and

$$\widehat{\mathcal{P}}_N(\mathscr{M}) := \left\{ \frac{1}{N}\sum_{i=1}^N \delta_{m_i},\ (m_1, \dots, m_N) \in \mathscr{M}^N \right\} \subset \mathcal{P}(\mathscr{M})$$

is the set of empirical measures of size N.

Lemma 4.5.1 (Links between the IBM and the measure-valued process)**.** *Let $(m_0^{i,N})_i \in \mathscr{M}^N$ an initial state and*

$$\hat{\mu}_0^N := \frac{1}{N}\sum_{i=1}^N \delta_{m_0^{i,N}}.$$

It holds that:

(i) the law of any of the $m_t^{i,N}$ is equal to $\mathbb{E}_{\hat{\mu}_0^N}\left[\hat{\mu}_t^N\right] \in \mathcal{P}(\mathscr{M})$,

(ii) for all $t \in \mathbb{R}_+$,

$$\mathbb{E}_{\hat{\mu}_0^N}\left[\hat{\mu}_t^N\right] = \mathbb{E}_{\hat{\mu}_0^N}\left[\nu_t^N\right],$$

where ν_t^N is the $\widehat{\mathcal{P}}_N(\mathscr{M})$-valued Markov process with generator $\mathcal{G}_N$ and initial state $\hat{\mu}_0^N$.

Proof. The first point is proved for example in [323, Section 1.4]. To prove the second point let $\varphi : \mathscr{M} \to \mathbb{R}$ be a test function and

$$\phi : \mathcal{P}(\mathscr{M}) \to \mathbb{R},\ \ \nu \mapsto \langle \nu, \varphi \rangle.$$

A direct calculation shows that:

$$\lim_{t\to 0} \frac{\mathbb{E}_{\hat{\mu}_0^N}\left[\phi(\widehat{\mu}_t^N)\right] - \phi(\hat{\mu}_0^N)}{t} = \mathcal{G}_N\phi(\hat{\mu}_0^N).$$

This proves that $\mathbb{E}_{\hat{\mu}_0^N}\left[\phi(\widehat{\mu}_t^N)\right]$ and $\mathbb{E}_{\hat{\mu}_0^N}\left[\phi(\nu_t^N)\right]$ satisfy the Kolmogorov equations with same initial condition. In conclusion, for all test function φ on $\mathscr{M}$:

$$\left\langle \mathbb{E}_{\hat{\mu}_0^N}\left[\hat{\mu}_t^N\right], \varphi \right\rangle = \left\langle \mathbb{E}_{\hat{\mu}_0^N}\left[\nu_t^N\right], \varphi \right\rangle.$$

□

Proposition 4.5.2. *Let $\phi : \mathcal{P}(\mathscr{M}) \to \mathbb{R}$ be a test function and ν_t^N the Markov process with generator $\mathcal{G}_N$. It holds that*

$$M_t^{N,\phi} := \phi(\nu_t^N) - \phi(\nu_0^N) - \int_0^t \mathcal{G}_N \phi(\nu_s^N)\,\mathrm{d}s \tag{4.37}$$

and

$$N_t^{N,\phi} := \left(M_t^{N,\phi}\right)^2 - N\int_0^t \iint_{\mathscr{M}\times\mathscr{M}} \left\{\phi\left(\nu_s^N - \frac{1}{N}\delta_m + \frac{1}{N}\delta_{m'}\right) - \phi(\nu_s^N)\right\}^2 \times M_{\nu_s^N}(m')\mathrm{d}m'\nu_s^N(\mathrm{d}m). \tag{4.38}$$

are two martingales.

Proof. These two results are a direct consequence of [231, Lemma 5.1]. □

4.5.3 Mean-field limit

Theorem 4.5.3. *Let $\nu_0^N \in \widehat{\mathcal{P}}_N(\mathscr{M})$ be an initial state for the process $(\nu_t^N)_t$ with generator $\mathcal{G}_N$. Assume that, as $N \to +\infty$,*

$$\forall \varphi \in C_b(\mathscr{M}),\ \ \langle \nu_0^N, \varphi\rangle \longrightarrow \langle \nu_0, \varphi\rangle.$$

Then, as $N \to +\infty$, the sequence $(\nu_t^N)_t$ converges weakly in $\mathcal{D}\big([0,\infty), \mathcal{P}(\mathscr{M})\big)$ towards $(\nu_t)_t$ the deterministic weak solution of the space homogeneous BGK equation with initial condition ν_0, where $\mathcal{D}\big([0,\infty), \mathcal{P}(\mathscr{M})\big)$ is the Skorokhod space of càdlàg functions from $[0,\infty)$ to $\mathcal{P}(\mathscr{M})$.

Proof. The proof is split into several steps.

Step 1. *The sequence of the laws of the processes $(\nu_t^N)_t$ is tight in $\mathcal{P}\big(\mathcal{D}([0,\infty), \mathcal{P}(\mathscr{M}))\big)$.*

Thanks to Jakubowski's criterion [211, Theorem 4.6], it is enough to prove that for all test functions $\varphi : \mathscr{M} \to \mathbb{R}$, the sequence of the laws of the processes $\big(\langle \nu_t^N, \varphi\rangle\big)_t$ is tight in $\mathcal{P}\big(\mathcal{D}([0,\infty), \mathbb{R})\big)$ (see [254, Lemma 4.23]). This last point is a consequence of the following martingale estimate, for $s \le t$:

$$\mathbb{E}\Big[\sup_{s\le r\le t} |M_r^{N,\phi} - M_s^{N,\phi}|^2\Big] \le \frac{4\|\varphi\|_\infty^2}{N}(t-s),$$

where

$$\phi : \mathcal{P}(\mathscr{M}) \to \mathbb{R},\ \ \nu \mapsto \langle \nu, \varphi\rangle.$$

The tightness of the laws of the processes $\left(\langle \nu_t^N, \varphi \rangle\right)_t$ then follows from the martingale estimates and Aldous criterion [210, Theorem VI.4.5].

Finally, by Prokhorov theorem, there exists $(\nu_t)_t \in \mathcal{D}([0,\infty), \mathcal{P}(\mathscr{M}))$ and we can extract a subsequence, still denoted by $(\nu_t^N)_t$, such that

$$(\nu_t^N)_t \longrightarrow (\nu_t)_t,$$

when $N \to \infty$ for the weak-convergence of measures.

Step 2. *The weak limit $(\nu_t)_t$ is continuous in time a.e. and the convergence is uniform in time.*

For any $\varphi \in C_b(\mathscr{M})$, we have for almost every $t \in \mathbb{R}_+$:

$$|\langle \nu_t^N, \varphi \rangle - \langle \nu_{t^-}^N, \varphi \rangle| \leq \frac{2\|\varphi\|_{L^\infty}}{N},$$

since there is almost surely at most one jump at a given time $t \in \mathbb{R}_+$. This proves that $(\nu_t)_t$ is continuous in time a.e.. As a consequence, we obtain by the continuity mapping theorem in the Skorokhod space (see [254, Lemma 4.26]), that for almost every $t \in \mathbb{R}_+$:

$$\sup_{s \leq t} |\langle \nu_s^N - \nu_s, \varphi \rangle| \to 0.$$

Step 3. *Passing to the limit.*

Let $\varphi \in C_b(\mathscr{M})$ and $\phi : \mathcal{P}(\mathscr{M}) \to \mathbb{R}$ defined by:

$$\phi(\nu) := \langle \nu, \varphi \rangle.$$

We want to pass to the limit in the representation formula (4.37).

- We have made the assumption that

$$\langle \nu_0^N, \varphi \rangle \to \langle \nu_0, \varphi \rangle. \tag{4.39}$$

- The martingale estimate (4.38) and Doob's inequality ensure that

$$\mathbb{E}\left[\sup_{s \leq t} |M_s^{N,\phi}|^2\right] \leq 4\mathbb{E}[(M_t^{N,\phi})^2] \leq \frac{16\|\varphi\|_\infty^2 t}{N} \to 0. \tag{4.40}$$

- We have for all $s \leq t$:

$$\iint_{\mathscr{M}\times\mathscr{M}} \{\varphi(m') - \varphi(m)\} M_{\nu_s^N}(m') \mathrm{d}m' \nu_s^N(\mathrm{d}m) = \int_{\mathscr{M}} \varphi(m') M_{\nu_s^N}(m') \mathrm{d}m' - \langle \nu_s^N, \varphi \rangle.$$

For the second term in the right-hand side we have proved in step 2 that:

$$\sup_{s\leq t} |\langle \nu_s^N - \nu_s, \varphi \rangle| \to 0.$$

For the first term in the right-hand side, we use the compactness of $\mathscr{M}$ and the flux-Lipschitz assumption (4.4) to bound:

$$\left| \int_{\mathscr{M}} \varphi(m') M_{\nu_s^N}(m') \mathrm{d}m' - \int_{\mathscr{M}} \varphi(m') M_{\nu_s}(m') \mathrm{d}m' \right| \leq C \|\varphi\|_{L^\infty} |J_{\nu_s^N} - J_{\nu_s}|,$$

where $C > 0$ is a constant. Using the uniform convergence proved in step 2 with the coordinates functions in the Euclidean space E (which are continuous and bounded), we deduce that:

$$\sup_{s\leq t} |J_{\nu_s^N} - J_{\nu_s}| \to 0.$$

Finally, it holds that:

$$\int_0^t \mathcal{G}_N \phi\left(\nu_s^N\right) \, \mathrm{d}s \longrightarrow \int_0^t Q_{\mathrm{BGK}}^\star \varphi(\nu_s) \, \mathrm{d}s. \tag{4.41}$$

Conclusion. Reporting (4.39), (4.40) and (4.41) in the representation formula (4.37), we obtain that the weak limit $(\nu_t)_t$ is deterministic and satisfies weakly the space homogeneous BGK equation with initial condition $\nu_0 \in \mathcal{P}(\mathscr{M})$:

$$\forall \varphi \in C_b(\mathscr{M}), \quad \langle \nu_t, \varphi \rangle = \langle \nu_0, \varphi \rangle + \int_0^t Q_{\mathrm{BGK}}^\star \varphi(\nu_s) \, \mathrm{d}s,$$

where the operator $Q_{\mathrm{BGK}}^\star$ is defined by (4.36). Since the limit is unique, the whole sequence $(\nu_t^N)_t$ actually converges to $(\nu_t)_t$. □

Corollary 4.5.4 (Convergence of the law of the IBM)**.** *Let $(\nu_t)_t$ the weak solution of the space homogeneous equation with initial condition $\nu_0 \in \mathcal{P}(\mathscr{M})$. Assume that, as $N \to +\infty$,*

$$\hat{\mu}_0^N \longrightarrow \nu_0,$$

for the weak convergence of measures. Then, for almost every $t \in \mathbb{R}_+$, it holds that,

as $N \to +\infty$,

$$\mathbb{E}_{\hat{\mu}_0^N}\left[\hat{\mu}_t^N\right] \longrightarrow \nu_t.$$

Proof. Thanks to lemma 4.5.1, we know that the law of any particle of the IBM at time $t \in \mathbb{R}_+$ is $\mathbb{E}_{\hat{\mu}_0^N}\left[\hat{\mu}_t^N\right]$ and that this law is equal (in $\mathcal{P}(\mathscr{M})$) to $\mathbb{E}_{\hat{\mu}_0^N}\left[\nu_t^N\right]$. The conclusion is therefore a consequence of Theorem 4.5.3 and [156, Theorem III.7.8]. □

4.6 Conclusion

We have proved a propagation of chaos property for a Piecewise Deterministic system of agents in a geometrically enriched context. The proof of this property was based on a coupling argument similar to the classical argument [307] for McKean-Vlasov systems. We have also proved that the under a moderate interaction assumption, as in [221], the interaction between the agents can be made purely local, in the sense that the size of the neighbourhood decreases with the number of agents. The resulting kinetic equation is a BGK equation which has been studied in [111]. Finally, an alternative approach based on martingale arguments can be carried out in the spatially homogeneous case.

Appendix

4.A Proof of Lemma 4.4.3

We are going to prove that there exists a Cauchy sequence in $\mathcal{F}$.

By compactness, $\mathscr{M}$ can be covered by finitely many open sets Ω_α and we can take a finite atlas $(\Omega_\alpha, \varphi_\alpha, \eta_\alpha)_\alpha$ with $\varphi_\alpha : \Omega_\alpha \to \varphi_\alpha(\Omega_\alpha) \subset \mathbb{R}^p$ where p is the dimension of $\mathscr{M}$ and η_α is an adapted partition of the unity. For all α, on the compact set $\operatorname{Supp}\eta_\alpha \subset \Omega_\alpha$, the metric tensor is bounded in the system of coordinates corresponding to the chart $(\Omega_\alpha, \varphi_\alpha)$ which implies that there exists a constant $C > 1$ such that for all α and all $x \in \operatorname{Supp}\eta_\alpha$,

$$\frac{1}{C} \leq \sqrt{|g|_x} \leq C, \tag{4.42}$$

where $|g|$ denotes the determinant of the matrix, the elements of which are the components of g in the chart $(\Omega_\alpha, \varphi_\alpha)$.

For a given α, we are going to prove that the set

$$\mathcal{F}_\alpha := \{(x,v) \mapsto \eta_\alpha(\varphi_\alpha^{-1}(v)) f(x, \varphi_\alpha^{-1}(v)), \;\; f \in \mathcal{F}\}$$

is relatively compact in $L^1(\mathbb{R}^d \times \varphi_\alpha(\Omega_\alpha))$. It is a consequence of Riesz-Fréchet-Kolmogorov theorem [49, Corollary 4.27]. Let $\varepsilon > 0$ and $R > 0$, $\eta > 0$ as in the hypothesis.

- The set $\mathcal{F}_\alpha$ is bounded: for all $f \in \mathcal{F}$, it holds that

$$\begin{aligned}\int_{\mathbb{R}^d \times \varphi_\alpha(\Omega_\alpha)} \eta(\varphi_\alpha^{-1}(v)) f(x, \varphi_\alpha^{-1}(v)) \mathrm{d}x\mathrm{d}v &\leq C \int_{\mathbb{R}^d \times \varphi_\alpha(\Omega_\alpha)} (\eta_\alpha f(x,\cdot)\sqrt{|g|}) \circ \varphi_\alpha^{-1} \mathrm{d}v\mathrm{d}x \\ &\leq C \iint_{\mathbb{R}^d \times \mathscr{M}} f(x,m) \mathrm{d}x\mathrm{d}m.\end{aligned}$$

- The tightness is given by a similar argument and the first hypothesis.

- Let $\omega \subset\subset \varphi_\alpha(\Omega_\alpha)$ and let δ be the distance between ω and the boundary of $\varphi_\alpha(\Omega_\alpha)$.

Let $(h,u) \in \mathbb{R}^d \times \mathbb{R}^p$ such that $|h| < \eta$ and $|u| < \min(\eta', \eta'')$ where η' and η'' will be defined later. It holds that:

$$\begin{aligned}
&\iint_{\mathbb{R}^d \times \omega} |\eta_\alpha(\varphi_\alpha^{-1}(v+u)) f(x+h, \varphi_\alpha^{-1}(v+u)) - \eta_\alpha(\varphi_\alpha^{-1}(v)) f(x, \varphi_\alpha^{-1}(v)| \mathrm{d}x\mathrm{d}v \\
&\quad \leq \iint_{\mathbb{R}^d \times \omega} |\eta_\alpha(\varphi_\alpha^{-1}(v)) f(x+h, \varphi_\alpha^{-1}(v+u)) - \eta_\alpha(\varphi_\alpha^{-1}(v)) f(x, \varphi_\alpha^{-1}(v)| \mathrm{d}x\mathrm{d}v \\
&\qquad + \iint_{\mathbb{R}^d \times \omega} |\eta_\alpha(\varphi_\alpha^{-1}(v+u)) - \eta_\alpha(\varphi_\alpha^{-1}(v))||f|(x+h, \varphi_\alpha^{-1}(v+u)) \mathrm{d}x\mathrm{d}v.
\end{aligned}$$

For the second term on the right-hand side:

$$\iint_{\mathbb{R}^d \times \omega} |\eta_\alpha(\varphi_\alpha^{-1}(v+u)) - \eta_\alpha(\varphi_\alpha^{-1}(v))||f|(x+h, \varphi_\alpha^{-1}(v+u)) \mathrm{d}x\mathrm{d}v \leq \varepsilon$$

for $|u| < \eta'$ where η' is smaller than $\delta/2$ and than the ε-modulus of uniform continuity of $\eta_\alpha \circ \varphi_\alpha^{-1}$ on the compact set constructed by enlarging ω by $\delta/2$. For the first term on the right hand side:

$$\begin{aligned}
&\iint_{\mathbb{R}^d \times \omega} |\eta_\alpha(\varphi_\alpha^{-1}(v)) f(x+h, \varphi_\alpha^{-1}(v+u)) - \eta_\alpha(\varphi_\alpha^{-1}(v)) f(x, \varphi_\alpha^{-1}(v)| \mathrm{d}x\mathrm{d}v \\
&\leq C \iint_{\mathbb{R}^d \times \omega} |\eta_\alpha(\varphi_\alpha^{-1}(v)) f(x+h, \varphi_\alpha^{-1}(v+u)) - \eta_\alpha(\varphi_\alpha^{-1}(v)) f(x, \varphi_\alpha^{-1}(v)| \\
&\qquad\qquad \times \sqrt{|g|} \circ \varphi_\alpha^{-1}(v) \mathrm{d}x\mathrm{d}v \\
&\leq \iint_{\mathbb{R}^d \times \varphi_\alpha^{-1}(\omega)} |f(x+h, \phi(m)) - f(x,m)| \mathrm{d}x\mathrm{d}m
\end{aligned}$$

where for $m \in \varphi_\alpha^{-1}(\omega)$,

$$\phi(m) := \varphi_\alpha^{-1}(\varphi_\alpha(m) + u) \in \Omega_\alpha$$

satisfies

$$d(\phi(m), m) \leq \eta$$

for $|u| \leq \eta''$ where η'' is smaller than $\delta/2$ and than the η-modulus of uniform continuity of φ_α^{-1} on the compact set constructed by enlarging ω by $\delta/2$. Finally, for $|h| < \eta$ and $|u| < \min(\eta', \eta'')$,

$$\iint_{\mathbb{R}^d \times \varphi_\alpha(\Omega_\alpha)} |\eta_\alpha(\varphi_\alpha^{-1}(v+u)) f(x+h, \varphi_\alpha^{-1}(v+u)) - \eta_\alpha(\varphi_\alpha^{-1}(v)) f(x, \varphi_\alpha^{-1}(v)| \mathrm{d}x\mathrm{d}v \leq 2\varepsilon.$$

Therefore we can apply Riesz-Fréchet-Kolmogorov theorem which shows that $\mathcal{F}_\alpha$ is relatively compact in $L^1(\mathbb{R}^d \times \varphi_\alpha(\Omega_\alpha))$. As a consequence, there exists a Cauchy sequence in $\mathcal{F}_\alpha$.

Now consider a sequence $(f_n)_n$ in $\mathcal{F}$. We can extract a subsequence still denoted by $(f_n)_n$ such that for all α, the sequence $(\eta_\alpha f_n \circ \varphi_\alpha^{-1})_n$ is a Cauchy sequence in $L^1(\mathbb{R}^d \times \varphi_\alpha(\Omega_\alpha))$. Inequality (4.42) implies that for any α, the sequence $(\eta_\alpha f_n)_n$ is a Cauchy sequence in the space $L^1(\mathbb{R}^d \times \Omega_\alpha)$. Then, for any $n, m \in \mathbb{N}$, since:

$$\|f_n - f_m\|_{L^1(\mathbb{R}^d \times \mathscr{M})} \leq \sum_\alpha \|\eta_\alpha f_n - \eta_\alpha f_m\|_{L^1(\mathbb{R}^d \times \Omega_\alpha)},$$

we conclude that $(f_n)_n$ is a Cauchy sequence in $L^1(\mathbb{R}^d \times \mathscr{M})$ and thus converges since the space $L^1(\mathbb{R}^d \times \mathscr{M})$ is complete.

Chapter 5

The SiSyPHE library

This chapter summarises the main objectives and methods of the SiSyPHE library

[139] A. Diez. "SiSyPHE: A Python package for the Simulation of Systems of interacting mean-field Particles with High Efficiency". *Journal of Open Source Software* 6.65 (2021), p. 3653.

This library was initially designed for the particle simulations presented in Chapter 8. The documentation and source code can be found on the website

`https://sisyphe.readthedocs.io/`

5.1 Simulating mean-field particle systems

This chapter is concerned with the numerical simulation of large mean-field systems, that is, McKean-Vlasov diffusion models or mean-field PDMP models as described in Section 3.3. The difficulty of this task essentially comes from the naive high computational cost when the number of particle is large. Particle simulations are, however, of primary interest, first because it provides an experimental counterpart in parallel to the theoretical analysis and secondly because the direct simulation of particle systems is at the core of Swarm Intelligence algorithms as explained in Section 1.5.2.

In order to simulate the time-continuous models in Section 3.3, the first step is to discretize the time. This is relatively classical for diffusive Stochastic Differential Equations [232] although the numerical schemes may require an adaptation when the dynamics lies on a manifold [280]. For PDMP models, deterministic schemes can be used for the deterministic part. For the jump part, since the jumps are exponentially distributed (with parameter λ), a simple procedure is the following: first choose a sufficiently small

time-step Δt, then for each particle and at each time step $k\Delta t$, draw an independent uniformly distributed random variable U_k^i on $[0,1]$ and then a post-jump state for the particles i such that $U_k^i \leq 1 - \mathrm{e}^{\lambda \Delta t}$, where $\lambda > 0$ is the jump rate (note that λ does not need to be constant). In this procedure, the most difficult and computationally-demanding step is the computation of the mean-field forces or of the post-jump state at each iteration. For a mean-field particle system $\mathcal{X}_t^N = (X_t^1, \dots, X_t^N)$, this leads, at each time-step $k\Delta t$, to N computations of the form

$$F_{k\Delta t}^i = \frac{1}{N} \sum_{i=1}^{N} b(X_{k\Delta t}^i, X_{k\Delta t}^j), \tag{5.1}$$

for $i \in \{1, \dots, N\}$, where b is a given function. For collective dynamics models, the function b is typically of the form

$$b(x,y) = K(|x-y|)\tilde{b}(y),$$

for another one-variable function $\tilde{b}$ and where K is an interaction kernel which specifies, depending on the distance between the states x, y, whether the particles will interact or not. For the body-orientation model, in the sampling step (2.4), the computation of the flux (2.6) corresponds to the case

$$b\big((x,A),(x',A')\big) = K(|x-x'|)A', \tag{5.2}$$

where $x, x' \in \mathbb{R}^3$ and $A, A' \in \mathrm{SO}_3(\mathbb{R})$.

Since N operations are needed to compute the sum (5.1) and that this computation has to be made for each of the N particles (or a fraction of N) at each time step, the total cost for the simulation of the system scales as $\mathcal{O}(N^2 T)$ where T is the total number of time-steps. This cost may become prohibitive when N is large. The simplest implementation with two nested loops in N may be a solution when implemented using low-level languages such as Fortran or C++ but at the price of a higher global coding effort. High level languages which support array programming allow more versatility but suffer from weaker performances and strong memory bounds. For instance a natural idea would be to pre-compute the matrix $\big(b(X_t^i, X_t^j)\big)_{i,j}$, called in this context the *kernel matrix*, and then simply sum its columns. When b is given by (5.2), this operation can also be understood as a matrix-vector product between the matrix $(K(X_t^i - X_t^j))_{i,j}$ and the vector $(\tilde{b}(X_t^j))_j$. However, when N becomes larger than 10^4, this $N \times N$ matrix would probably not fit into the memory of a standard computer.

In order to cope with this prohibitive quadratic cost, several computational and implementation methods have been proposed over the past decades. Popular and successful methods include the ones described below. Historically, most of them have been developed for the simulation of the N-body problem in celestial mechanics, in plasma physics and for molecular dynamics simulations. More recently, the same problem arose independently in machine learning.

1. **(Short-range interactions).** As explained in the introduction of this thesis, most models in collective dynamics are based on short-range interactions, meaning that each particle interacts only with its close neighbours. As a result, a majority of pairwise interactions are actually zero or negligible and an important computation time could be saved by simply dropping these terms out. It does require however to find an appropriate data structure which can efficiently store the list of neighbours for each particle. The basic idea is to use a uniform grid partition of the physical space with a mesh equal to the interaction radius of the particles. Each particle thus interacts at most with the particles in 3^d neighbouring cells. This is the original idea due to Verlet in the 60's for early molecular dynamic simulations [319]. In practise, the implementation is often rather based on the so-called *cell list* method (or *linked list*) [200, Section 8.4.2] developed later. This latter method uses only two lists, one of length N and the other of length the number of cells. The procedure to retrieve the neighbours of each particle is intrinsically sequential but it can nevertheless be easily parallelised for better performance. This simple idea leads to a drastically reduced computational time, in particular when a particle has typically only a few neighbours. This is a basic method presented in most Molecular Dynamics textbooks [240, Appendix A], [164, Appendix F]. Moreover, note that when the interaction kernel is compactly supported or for collisional processes [300], this method is exact.

2. **(Super particles).** On the opposite, when particles are subject to long-range interactions, far away particles can be grouped together into one heavier *super-particle* located at their center of mass. For instance, in celestial mechanics, the gravitational force exerted by a far-away galaxy is very naturally approximated by the force exerted by only one heavy entity rather than the sum of the gravitational forces exerted by its constituents. Once again, the practical implementation of this idea requires an adequate data structure to evaluate, for each particle, how the other particles should be grouped together. Classical implementations are based on an adaptive grid partition of the spatial domain using local meshes adapted to the local density of particles. The actual data is encoded in a tree-like structure (called

quadtree in dimension 2 and *octree* in dimension 3). A first historical implementation is due to Appel [9] although the most renowned algorithm is due to Barnes and Hut [18]. Finally, this method can be improved by considering directly interactions between super-particles. This is called the *Fast Multipole Method* introduced by Rokhlin and Greengard [291, 37].

3. **(Kernel methods).** The so-called kernel methods are commonly used in machine learning and rely on linear algebra routines to approximate the kernel matrix and reduce the memory usage. See for instance [334] and the references therein.

4. **(Random Batch Method).** The recent Random Batch Method introduced in [215] is based on a stochastic approximation of the true particle system where only interactions between randomly sampled subsets (called *batches*) of the particle system are computed. This method has recently been used in many contexts reviewed in the article [216] which discusses applications in molecular dynamics, data science problems, collective and quantum dynamics simulations.

Despite all these old and recent computational techniques, the simulation of many-particle systems remains limited by the hardware performances. In the celestial mechanics applications reported by Appel [9] and Barnes and Hut [18] in the 80's, the hours-long simulations could handle about 10^4 particles. The seminal work of Verlet [319] simulates less than a thousand particles subject to the Lennard-Jones potential. A similar system was considered previously in [284] where, to obtain better performances, it is reported that "for the most time consuming part, the program was written in machine language". Much better performances can of course be achieved on modern computers for much larger systems even with a naive brute force computation. In the last decade, the development and popularization of massively parallel Graphics Processing Units (GPU) represents a new big step forward. However, although GPUs coupled with the computational methods discussed above can drastically reduce the computation time by several orders of magnitude, it comes at the price of a much intense coding effort. Fortunately, the `KeOps` library recently developed by Charlier et al. [78] provides an end-user high-level solution for many kernel operations. While the library was originally mostly intended to solve machine learning and shape analysis problems, its core functionalities can also be directly applied to the simulation of mean-field particle systems. In practise, the `KeOps` library gives a transparent interface to efficiently compute sums like (5.1) using a GPU but within a traditional Python code based on the `PyTorch` library [275]. The fundamental idea is to use a symbolic definition of the kernel matrix, (i.e. given by a mathematical formula) which is

well adapted to the parallel architecture of GPU chips while keeping a low memory usage. An extensive literature review of classical methods which motivates the use of `KeOps` as well as a precise technical description of the library can be found in J. Feydy's PhD thesis [159].

The `SiSyPHE` library benefits from both these hardware and software improvements and is a direct application of these methods to the efficient simulation of particles systems in collective dynamics. Since most of the coding effort to achieve high-performance is (almost) directly provided by the `KeOps` library, it became possible to extend our original code initially developed for the simulation of the body-orientation dynamics to a versatile and centralized Python library for a large class of swarming models.

Remark 5.1.1. It should be emphasized that the contribution of this work is *not* on the high-performance computational methods which are due to the authors of the `KeOps` [78] and `PyTorch` [275] libraries and more generally to the CUDA ecosystem developed by Nvidia. The `SiSyPHE` library was initially only motivated by the simulation of body-oriented particle systems. However, it has been extended to a versatile and unified library for many other collective dynamics models, following the observation that despite the growing number of individual based models in the applied mathematics literature, very few open source efficient codes are available. Moreover, the use of GPUs does not seem to be a widely spread idea in the collective dynamics community despite the easy but enormous gain in efficiency. The `SiSyPHE` library has therefore also been developed to contribute to the dissemination of the method introduced in [78] in the machine learning community to this new research area.

5.2 Usage and benchmarks

5.2.1 Features

The swarming models presented in the introduction share many common features and may have several variants which lead to very different behaviours. In order to facilitate model comparisons, the `SiSyPHE` library provides a versatile interface where all these aspects are pre-implemented. The core element is the computation of fluxes of the form (2.6) where the body-orientation may be replaced by another custom state variable, typically the velocity, as in the Vicsek model. Various functions of the flux such as the ones presented in [113] can also be used. Moreover, the interaction kernel K can have various shapes, for instance to take into account the angle of vision of the agents as in [90] or because it derives from classical interaction potentials [99]. All these features are already pre-computed

operations called `targets` in the documentation of `SiSyPHE`. Then, several interaction mechanisms, called `models`, can be chosen which includes all the variants of the Vicsek model (diffusion model [122], synchronous [321, 80] and asynchronous jumps [140] models and body-orientation models [114]), other classical swarming models such as the D'Orsogna model [99] as well as a toy-model of tumor growth [264]. While most of these models are not new and although there already exist efficient implementations for a few of them [262], the `SiSyPHE` library provides a centralized, uniform and open-source interface better suited to model comparison and ambitious numerical experiments. Moreover, the computational improvement offered by the `KeOps` library speeds up traditional methods by one to three orders of magnitude.

5.2.2 Usage

The `SiSyPHE` library can be easily installed through `PyPi` and used on the free GPUs provided by Google Colaboratory (`https://colab.research.google.com/`). As an example, the following code snippet shows a typical simulation procedure for the Vicsek model.

LISTING 5.1: Example

```
import math
import torch
import sisyphe.models as models
from sisyphe.display import save

"""Simulation parameters"""

N = 100000      #Number of particles
L = 100.        #Size of the square domain
dt = .01        #Time step
nu = 5.         #Drift coefficient
sigma = 1.      #Diffusion coefficient
R = 1.          #Interaction radius
c = R           #Speed

"""Sample the initial conditions"""

# The type of the initial condition will determine the floating point precision.
dtype = torch.cuda.FloatTensor
```

```
# Replace by the following line for double precision tensors.
# dtype = torch.cuda.DoubleTensor

pos = L*torch.rand((N,2)).type(dtype)          #Initial positions
vel = torch.randn(N,2).type(dtype)
vel = vel/torch.norm(vel,dim=1).reshape((N,1)) #Initial velocities

"""Choose a variant and create a model"""

variant = {"name" : "normalised", "parameters" : {}}

simu = models.Vicsek(
    pos = pos,
    vel = vel,
    v = R,
    sigma = sigma,
    nu = nu,
    interaction_radius = R,
    box_size = L,
    dt = dt,
    variant = variant
    boundary_conditions = "periodic",
    block_sparse_reduction = True,
    number_of_cells = 42**2)

"""Run the simulation and save the positions and velocities every 0.01 time
    unit."""

T = 10,    #Total simulation time
frames = np.arange(0,T,0.01)
data = save(simu, frames, ["pos", "vel"], [])
```

5.2.3 Benchmarks

The `SiSyPHE` library can be equally used on a CPU or a GPU although much better performances are obtained with GPUs. The table below shows a comparison of the performance for the simulation of the Vicsek model during 10 units of time with the

parameters shown above and for the following configurations.

- The Fortran implementation due to Sébastien Motsch [262] using the Verlet list method with double precision float numbers, run on the NextGen compute cluster at Imperial College London.
- The CPU version of `SiSyPHE` with double precision tensors (float64) and the blocksparse-reduction method (BSR, see below), run on an Intel MacBook Pro (2GHz Intel Core i5 processor with 8GB of memory).
- The GPU version of `SiSyPHE` with single precision tensors (float32) with and without the blocksparse-reduction method (BSR), run on a GPU cluster at Imperial College London using an Nvidia GTX 2080 Ti GPU chip.
- The GPU version of `SiSyPHE` with double precision tensors (float64) with and without the blocksparse-reduction method (BSR), run on a GPU cluster at Imperial College London using an Nvidia GTX 2080 Ti GPU chip.

The *block-sparse reduction method* (BSR) implemented in `SiSyPHE` is based on the same idea as the classical Verlet cell list method [319, 200] to speed up the computation of short-range interactions. However, the traditional implementation is not well suited to the `KeOps` framework and needs a preliminary specific "vectorization" procedure.

For each value of N (the number of particles), three values of R (the interaction radius) are tested which correspond to a dilute regime, a moderate regime and a dense mean-field regime. When the particles are uniformly scattered in the box, the average number of neighbours in the three regimes is respectively ~ 3, ~ 30 and ~ 300. The regime has a strong effect on the efficiency of the Verlet list and blocksparse reduction methods. The worst computation times are written in *italic* and the best ones in **bold**.

		`Fortran`	`SiSyPHE64 CPU BSR`	`SiSyPHE32 GPU`	`SiSyPHE32 GPU BSR`	`SiSyPHE64 GPU`	`SiSyPHE64 GPU BSR`
$N = 10^4$	$R = 1$	19s	*26s*	**2.1s**	3.3s	13s	3.6s
	$R = 3$	*59s*	29s		3.4s		3.9s
	$R = 10$	*494s*	69s		3.4s		7.9s
$N = 10^5$	$R = 0.3$	309s	323s	29s	**4.3s**	973s	9.3s
	$R = 1$	*1522s*	384s		**4.5s**		11s
	$R = 3$	*3286s*	796s		**4.9s**		28s
$N = 10^6$	$R = 0.1$	*>12h*	6711s	2738s	**22s**	*>12h*	120s
	$R = 0.3$	*>12h*	6992s		**23s**		135s
	$R = 1$	*>12h*	9245s		**26s**		194s

The GPU implementation is at least 5 times faster in the dilute regime and outperform the other methods by three orders of magnitude in the mean-field regime with large values of N. Without the block-sparse reduction method, the GPU implementation does suffer from the quadratic complexity. The block-sparse reduction method is less sensitive to the density of particles than the traditional Verlet cell list method. It comes at the price of a higher memory cost but allows to run large scale simulations even on a CPU. On a CPU, the performances are not critically affected by the precision of the floating-point format so only simulations with double precision tensors are shown.

5.3 Examples

The original problem for which the `SiSyPHE` library was developed is the study of the body-orientation model in a macroscopic scaling presented in Chapter 8. The two following examples present open questions raised by the numerical simulations for two other models.

5.3.1 Band formation in the Vicsek model

The classical Vicsek model in a square periodic domain is known to produce band-like structures in a very dilute regime. However, it is not clear that the simulations reported in [80] can be explained by the kinetic theory approach as the system is so dilute that each particle interacts with less than ten other particles at most. When the density increases, no bands are observed and the system converges towards a very stable uniform flock which is consistent with the mathematical analysis conducted in [122, 112, 160]. However, band-like structures are recovered in a mean-field regime when the interaction is *non-normalised*, that is with the choice $\kappa(J) = |J|$ or $\kappa(J) = |J|/(1 + |J|)$ instead of $\kappa =$ constant in (1.5). This choice is known to create a phase transition phenomena [113] in the spatially-homogeneous case.

The snapshots below (Figure 5.3.1) show the formation of a high-density travelling band in the diffusion model (1.4) starting from a uniformly disordered state. The simulation time is less than 30 minutes with $N = 10^6$ particles in a mean-field regime where all the particles have at least a few hundreds of neighbours (i.e. about 0.05 seconds per time iteration).

There is to the best of our knowledge, no mathematical analytical result known to explain this self-organised behaviour.

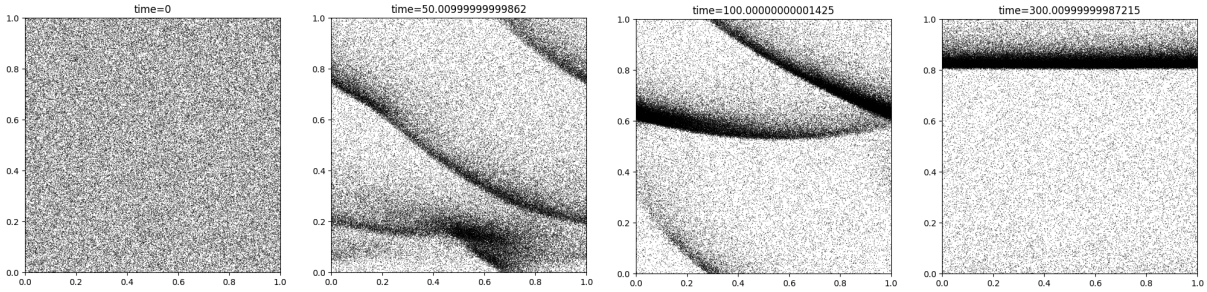

FIGURE 5.3.1: Four snapshots of the system at times $t = 0$, $t = 50$, $t = 100$ and $t = 300$. The parameters of the simulation are $N = 10^6$, $\nu = 3$, $\sigma = 1$, $R = 0.01$, $c_0 = 0.1$ and the time step is $\Delta t = 0.01$.

5.3.2 Volume exclusion model

A simple agent-based model of tumor growth has been proposed in [264]. The agents model spherical cells which interact by repulsing each other at short distance: their motion is given by the system of ODEs

$$\frac{\mathrm{d}X_t^i}{\mathrm{d}t} = -\frac{\alpha}{R_i}\sum_{j=1}^{N} K(X_t^i - X_t^j)\left(1 - \frac{|X_t^i - X_t^j|^2}{(R_i + R_j)^2}\right)(X_t^i - X_t^j), \tag{5.3}$$

where R_i is the repulsion radius of particle $i \in \{1, \dots, N\}$ and K is an overlapping kernel such that $K(X_t^i - X_t^j) = 1$ if $|X_t^i - X_t^j| < R_i + R_j$ and $K(X_t^i - X_t^j) = 0$ otherwise. This interaction derives from the logarithmic potential defined by $U(s) = -\log(s) + s - 1$ for $s < 1$ and $U(s) = 0$ otherwise. As a consequence, the energy functional of this system defined by $\mathcal{E} = -\frac{1}{2}\sum_{i,j} U\left(\frac{|X_t^i - X_t^j|^2}{(R_i+R_j)^2}\right)(R_i + R_j)^2$ is decaying. This observation suggests a numerical scheme with an adaptive time-step defined in [264] with a quadratic cost in N. Only small-scale simulations with a few hundreds of particles and a fixed repulsion radius for all the cells are shown in [264]. The `SiSyPHE` library allows more ambitious simulations with thousands of particles and various repulsion radii. Starting from a densely packed initial condition, the following snapshot (Figure 5.3.2) shows the final state of the system.

We observe a clusterization phenomenon depending on the radii of the particles (the black parts are composed of particles with a very small radius). There is to the best of our knowledge no mathematical analytical result available to explain this phenomenon.

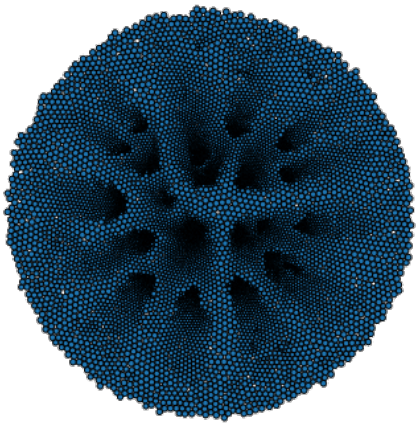

FIGURE 5.3.2: Final state of the system with $N = 10^4$ particles starting from an initial random densely packed state. The repulsion radii of the particles are uniformly sampled between 0.1 and 1. The system (5.3) is discretized using the very demanding adaptive scheme introduced in [264] which ensures the decay of the energy. The simulation time is about five minutes.

Chapter 6

Collective Monte Carlo methods

The content of this chapter is based on the following article co-authored with G. Clarté and J. Feydy

[86] G. Clarté, A. Diez, and J. Feydy. "Collective Proposal Distributions for Nonlinear MCMC samplers: Mean-Field Theory and Fast Implementation". *arXiv preprint: arXiv:1909.08988* (2021).

This chapter presents a new sampling algorithm which is a mean-field generalisation of the Metropolis-Hastings algorithm. The theoretical analysis of the algorithm follows from the techniques developed in Chapter 4 and entropy methods at the mesoscopic level. Numerical experiments implemented using the `KeOps` library [78] are also shown.

6.1 Introduction

6.1.1 Background

Monte Carlo methods are designed to estimate the expectation of an observable φ under a probability measure π. They approximate the quantity of interest by an estimator of the form

$$\frac{1}{N}\sum_{i=1}^{N}\varphi(X_i),$$

where X_i are independent and identically distributed (i.i.d.) random variables with law π. The law of large numbers ensures the convergence as $N \to +\infty$ of this estimator. For complex cases, a now classical procedure consists in constructing a Markov chain $(X_i)_i$ with stationary distribution π. Ergodic theory results then ensure that the estimator above

still converges, even though the X_i are not independent from each other. The Metropolis-Hastings algorithm [256, 255, 193] provides a simple construction for such a Markov chain that only requires to evaluate π up to a multiplicative constant. The constructed chain is a random walk biased by an accept-reject step outlined in the introduction of this thesis in Section 2.2.3. Its convergence properties have been thoroughly studied, for example in [253, 137].

This well-known procedure has become a building block for more advanced samplers, that are designed to overcome the known flaws of the Metropolis-Hastings algorithm: slow convergence, bad mixing properties for multimodal distributions *etc.* Such extensions include for instance the Wang and Landau algorithm [45], regional MCMC algorithms [93], or non Markovian (adaptive) versions [187, 186, 11, 10] where the next proposed state depends on the whole history of the process. The more recent PDMP samplers [157, 317] provide an alternative to the discrete-time accept-reject scheme, replacing it by a continuous-time non reversible Markov process with random jumps. Finally, more complex algorithms are based on the evaluation of the gradient of π, see for instance the Metropolis-adjusted Langevin [33] and the Hamiltonian Monte Carlo algorithms [147]. All these methods can be seen as "linear" as the next position of a single chain only depends on its current position.

A non-Markovian alternative to Metropolis-Hastings like methods is given by Importance Sampling algorithms. By drawing i.i.d. samples from an auxiliary distribution q, which is usually simple and called the importance distribution, an estimator can be built using the following identity:

$$\int \varphi(x)\pi(x)\mathrm{d}x = \int \frac{\pi(x)}{q(x)}\varphi(x)q(x)\mathrm{d}x \simeq \frac{1}{n}\sum_{i=1}^{n} w_i\varphi(X_i),$$

where the X_i are i.i.d. with law q and the $w_i \propto \pi(X_i)/q(X_i)$, are called the *importance weights*. The choice of q is critical, as bad choices can lead to a degeneracy of the importance weights. Iterative methods have been developed to sequentially update the choice of the importance distribution, and to update the X_i now interpreted as particles that evolve along iterations. Among these algorithms, we can cite the Sequential Importance Sampling algorithm [174], the Population Monte Carlo (PMC) methods [145, 54, 55] or the recent Safe Adaptive Importance Sampling (SAIS) algorithm [134]. This paradigm is in particular well-suited to the study of filtering problems [174], leading to the development of Sequential Monte Carlo (SMC) methods [128, 146]. A review of population-based algorithms and of the SMC method can be found in [212].

The SMC methodology has recently been used to design and study *nonlinear* MCMC algorithms [7]. This framework can be seen as a generalisation of some non-Markovian extensions of the Metropolis-Hastings algorithm (such as the "resampling from the past" procedure [187, 11]) but also allows the use of a wider range of algorithmic techniques. Examples are given in [7, 6] and are often based on the simulation of auxiliary chains. In the present article, we show that an alternative procedure based on the simulation of a swarm of *interacting* particles can also be used to approximate a nonlinear Markov chain. This provides a multi-particle generalisation of the Metropolis-Hastings procedure. Moreover, the various mean-field analysis techniques reviewed in Chapter 3 give a natural theoretical framework for the convergence analysis of particle methods.

6.1.2 Objective and methods

Let π be a target measure on $E \subset \mathbb{R}^d$, known up to a multiplicative constant and which is assumed to have a density with respect to the Lebesgue measure. We recall that $\mathcal{P}(E)$ denotes the set of probability measures on E. The goal of the present chapter is to build a *nonlinear* Markov chain $(\overline{X}_t)_t$ on E that samples π efficiently. Given a sample $\overline{X}_t$ at iteration t, we draw $\overline{X}_{t+1}$ according to

$$\overline{X}_{t+1} \sim K_{\mu_t}(\overline{X}_t, \mathrm{d}y) \ ,$$

where the *transition kernel* is defined by:

$$K_{\mu_t}(x, \mathrm{d}y) := \underbrace{h(\alpha_{\mu_t}(x,y))\Theta_{\mu_t}(\mathrm{d}y|x)}_{\text{accept}} + \underbrace{\Big[1 - \int_{z\in E} h(\alpha_{\mu_t}(x,z))\Theta_{\mu_t}(\mathrm{d}z|x)\Big]\delta_x(\mathrm{d}y)}_{\text{reject}} \qquad (6.1)$$

and where for $t \in \mathbb{N}$, $\mu_t \in \mathcal{P}(E)$ is the law of $\overline{X}_t$. In the discrete setting, this method is implemented by Algorithm 1, detailed below. It relies on the following quantities:

- The **proposal distribution**, a map

$$\Theta : E \times \mathcal{P}(E) \longrightarrow \mathcal{P}_0^{\mathrm{ac}}(E),$$

  where $\mathcal{P}_0^{\mathrm{ac}}(E)$ the subset of non-vanishing absolutely continuous probability measures. For $x \in E$ and $\mu \in \mathcal{P}(E)$, its associated proposal probability density function is denoted by:

$$\Theta(x,\mu)(y)\mathrm{d}y \equiv \Theta_\mu(y|x)\mathrm{d}y.$$

Intuitively, the probability distribution $\Theta(x, \mu)$ can be understood as an approximation of the target π that our method uses to *propose* new samples y in a neighborhood of a point x, relying on the information that is provided by a probability measure μ. In (6.1), μ is the law of the chain at the previous iteration. In the following μ will be the empirical distribution associated with a system of particles. To ensure a fast convergence of our method, both in terms of computation time and number of iterations, the distribution $\Theta(x, \mu)$ should be both easy to sample from and close to the target distribution π. In practice, the choice of a good proposal Θ depends on the assumptions that can be made on the distribution π. We will present several examples in Section 6.5. A simple example to keep in mind and which will be detailed in Section 6.5.2 is

$$\Theta_\mu(y|x) = K \star \mu(y), \tag{6.2}$$

where K is a random-walk kernel.

- For $\mu \in \mathcal{P}(E)$ and $x, y \in E$, the **acceptance ratio** is defined by:

$$\alpha_\mu(x, y) := \frac{\Theta_\mu(x|y)\pi(y)}{\Theta_\mu(y|x)\pi(x)}.$$

This quantity expresses the relative appeals of the transition $x \to y$ for the "model" density $\Theta_\mu(\mathrm{d}y|x)$ and the ground truth target $\pi(\mathrm{d}y)$, as in classical Metropolis-Hastings methods. Noticeably the denominator is never null because of the non-vanishing assumption on Θ. Crucially, it can be computed even when the law of π is only known up to a multiplicative constant and allows our method to account for mis-matches between the proposal Θ and the distribution to sample π. Note that in practice, for the sake of numerical stability, the acceptance ratio is often manipulated through its logarithm:

$$\underbrace{\log \alpha_\mu(x, y)}_{\text{"correction"}} := \underbrace{\big[\log \pi(y) - \log \pi(x)\big]}_{\text{appeal of } x \to y \text{ for } \pi} - \underbrace{\big[\log \Theta_\mu(y|x) - \log \Theta_\mu(x|y)\big]}_{\text{appeal of } x \to y \text{ for } \Theta_\mu}.$$

In the following, we will assume that π is bounded away from zero so that the acceptance ratio is always well-defined.

- The **acceptance function** is a non-decreasing Lipschitz map of the form $h : [0, +\infty) \to [0, 1]$ which satisfies

$$\forall u \in [0, \infty), \quad uh(1/u) = h(u). \tag{6.3}$$

A typical example is $h(u) = \min(1, u)$. As detailed in Algorithm 1, we combine the acceptance ratio $\alpha_\mu(x, y)$ and the acceptance function h to reject proposed samples y that are much more appealing for $\Theta_\mu(\cdot|x)$ than they are for π. This necessary correction ensures that our method samples the target π instead of the simpler proposal distribution. On the other hand, it can also slow down the method if the proposed samples y keep being rejected. Efficient proposal distributions should keep the acceptance ratio high enough to ensure good mixing properties.

Non-linearity. By analogy with McKean-Vlasov diffusion processes (see Section 3.3), we say that the transition kernel is nonlinear due to its dependency on the law of the chain that it generates. When the proposal distribution does not depend on μ_t, the kernel is *linear* and we obtain the general form of the classical Metropolis-Hastings kernel.

Interest of the method. The main interest of the method appears for complex distributions, that is multimodal distributions. From an MCMC point of view, the use of a non-linear sampler removes the mixing problem which is one of the main drawbacks of the Metropolis-Hastings algorithm. For nonlinear samplers, exponential convergence is ensured as soon as the distribution carries weight in every mode, without having to explore and exit each of the modes. On the contrary, the Metropolis-Hastings algorithms may remain stuck in a single mode even with long runs. Nonlinear methods allow to learn efficiently the relative weight of the distribution modes, which is unavailable even for several independent runs of Metropolis-Hastings algorithm with different initialisations, that is the most direct parallel version of Metropolis-Hastings. The numerical experiments will confirm that nonlinear methods perform better for both exploration and convergence.

Contributions. We follow [7] and split our analysis into two steps:

1. We show that our non-linear kernel admits π as a stationary distribution and study its asymptotic properties.

2. We present a practical implementation based on the simulation of a system of interacting particles that enables the simulation of this kernel for different choices of the proposal distribution.

Input: An initial population of particles $(X_0^1, \dots, X_0^N) \in E^N$, a maximum time $T \in \mathbb{N}$, a proposal distribution Θ and an acceptance function h

Output: A sample $\big(X_t^i\big)_{1 \leq i \leq N;\ 1 \leq t \leq T}$

for $t = 0$ **to** $T - 1$ **do**
  for $i = 1$ **to** N **do**
    (Proposal) Draw $Y_t^i \sim \Theta_{\hat{\mu}_t^N}(\,\cdot\,|X_t^i)$ a proposal for the new state of particle i;
    (Acceptation) Compute $\alpha_{\hat{\mu}_t^N}(X_t^i, Y_t^i) = \frac{\Theta_{\hat{\mu}_t^N}(X_t^i|Y_t^i)\pi(Y_t^i)}{\Theta_{\hat{\mu}_t^N}(Y_t^i|X_t^i)\pi(X_t^i)}$;
    Draw $U_t^i \sim \mathcal{U}([0,1])$;
    if $U_t^i \leq h\big(\alpha_{\hat{\mu}_t^N}(X_t^i, Y_t^i)\big)$ **then**
      Set $X_{t+1}^i = Y_t^i$; `// Accept, probability` $h(\alpha_{\hat{\mu}_t^N}(X_t^i, Y_t^i))$.
    else
      Set $X_{t+1}^i = X_t^i$; `// Reject, likely if` $\alpha_{\hat{\mu}_t^N}(X_t^i, Y_t^i) \simeq 0$.
    end
  end
end

Algorithm 1: Collective Monte Carlo (CMC)

Analytical study. Starting from an initial distribution $\mu_0 \in \mathcal{P}(E)$, the law μ_t of the nonlinear chain at the t-th iteration satisfies

$$\mu_{t+1} = \mathcal{T}[\mu_t]$$

where $\mathcal{T} : \mathcal{P}(E) \to \mathcal{P}(E)$ is the *transition operator* defined by duality in the space of measures by:

$$\langle \mathcal{T}[\mu], \varphi \rangle := \int_E \varphi(x) \mathcal{T}[\mu](\mathrm{d}x) = \iint_{E \times E} \varphi(y) K_\mu(x, \mathrm{d}y) \mu(\mathrm{d}x), \tag{6.4}$$

for any continuous bounded test function $\varphi \in C_b(E)$. Thanks to the *detailed balance condition* (also called *micro-reversibility* in the context of statistical mechanics [310]), for all $x, y \in E$ and $\mu \in \mathcal{P}(E)$:

$$\pi(x)\Theta_\mu(y|x)h(\alpha_\mu(x,y)) = \pi(y)\Theta_\mu(x|y)h(\alpha_\mu(y,x)), \tag{6.5}$$

the transition operator can be rewritten:

$$\mathcal{T}[\mu](\mathrm{d}x) = \mu(\mathrm{d}x) + \int_E \pi(x) W_\mu(x \to y) \left(\frac{\mu(\mathrm{d}y)}{\pi(y)} \mathrm{d}x - \frac{\mu(\mathrm{d}x)}{\pi(x)} \mathrm{d}y \right),$$

with $W_\mu(x \to y) := \Theta_\mu(y|x) h(\alpha_\mu(x, y))$, from which it can be easily seen that $\mathcal{T}[\pi] = \pi$.

We are going to develop an analytical framework in which the convergence of the sequence of iterations of the transition operator can be analysed. Using entropy methods, we prove the exponential convergence towards π for a large class of proposal distributions. We show that in an asymptotic regime to be detailed, the rate of convergence depends only on how close from the target is the initial condition. As a byproduct, in the linear Metropolis-Hastings case, we obtain, with a completely different technique, a convergence result similar to the one obtained in [137].

Efficient implementation. It is not possible in general to sample directly $\overline{X}_t$ from a nonlinear kernel because the law μ_t is not available. However, owing to the results in Chapter 3, a natural idea is to rely on a mean-field particle method to approximate such samples. Starting from a swarm of N particles $X_t^1, \ldots, X_t^N \in E$ at the iteration t, we construct the next iteration by sampling independently for $i \in \{1, \ldots, N\}$:

$$X_{t+1}^i \sim K_{\hat{\mu}_t^N}(X_t^i, \mathrm{d}y),$$

where, in order to keep lighter notations, the empirical measure is denoted by

$$\hat{\mu}_t^N := \frac{1}{N} \sum_{i=1}^N \delta_{X_t^i} \in \mathcal{P}(E).$$

This (random) measure is used as a proxy of the distribution μ_t. Following the classical propagation of chaos methodology, we show that as N goes to infinity and for each $t \in \mathbb{N}$, the empirical measure $\hat{\mu}_t^N$ converges towards a deterministic limit which is the t-th iterate of the nonlinear operator $\mathcal{T}$ starting from μ_0. Moreover, Lemma 3.2.11 shows that the N particles are asymptotically, in N, independent thus forming an approximation of a system of N independent nonlinear Markov chains with transition kernel (6.1).

A drawback of this approach is its high computational cost, that may scale in $\mathcal{O}(N^2)$ or $\mathcal{O}(N^3)$ for some choices of the proposal Θ. To overcome this difficulty and similarly to what has been proposed in Chapter 5, we propose an implementation based on GPU, more precisely on the techniques developed in the `KeOps` library [78] by the third author.

Outline. Section 6.2 is devoted to the convergence analysis of Algorithm 1 for a general class of proposal distributions. The mean-field limit and the long-time asymptotic properties are studied respectively in Section 6.3 and Section 6.4. Several variants of the main algorithm are presented in Section 6.5. The GPU implementation of the different algorithms is detailed in Section 6.6. Applications to various problems are presented in Section 6.7. In the appendix, we present the complementary proofs (Appendix 6.A) as well as variations on the results of the chapter (Appendix 6.B). We also add some complementary remarks on the links between our method and other classical methods (Appendix 6.C).

Throughout this chapter, we assume that π satisfies the following assumption.

Assumption 6.1.1. *The support of π, denoted by E, is a compact subset of $\mathbb{R}^d$. The target distribution π is Lipschitz continuous and π does not vanish on E :*

$$m_0 := \inf_E \pi > 0 \quad \textit{and} \quad M_0 := \sup_E \pi < +\infty.$$

6.2 Main results

Algorithm 1 gives a trajectorial approximation of the nonlinear Markov chain $(\overline{X}_t)_t$ with law $(\mu_t)_t$ defined by the transition kernel (6.1). In this section, we prove the convergence of this algorithm under general assumptions on the proposal distribution Θ described below. The proof of our main result is split into two steps each summarised in a theorem, first the mean-field limit when $N \to +\infty$ (Section 6.3) and then the long-time convergence towards π (Section 6.4).

6.2.1 Assumptions

For our theoretical results, we will need the following assumptions. The first three following assumptions are needed to prove the many-particle limit in Section 6.3.

Assumption 6.2.1 (Boundedness)**.** *There exist two constants $\kappa_-, \kappa_+ > 0$ such that for all $\mu \in \mathcal{P}(E)$ and for all $x, y \in E$:*

$$\kappa_- \leq \Theta_\mu(y|x) \leq \kappa_+.$$

Assumption 6.2.2 (L^∞ Lipschitz)**.** *The map $\Theta : E \times \mathcal{P}(E) \to \mathcal{P}_0^{\mathrm{ac}}(E)$ is globally Lipschitz for the L^∞-norm on E: there exists a constant $L > 0$ such that for all $x, y, x', y' \in E$ and*

for all $(\mu, \nu) \in \mathcal{P}(E)^2$ *:*

$$\left|\Theta_\mu(y|x) - \Theta_\nu(y'|x')\right| \leq L\Big(W_1(\mu,\nu) + |x - x'| + |y - y'|\Big).$$

Assumption 6.2.3 (W_1 non-expansive)**.** *The map* $\Theta : E \times \mathcal{P}(E) \to \mathcal{P}_0^{\mathrm{ac}}(E)$ *is non-expansive for the Wasserstein-1 distance: for all* $x, x' \in E$ *and for all* $(\mu, \nu) \in \mathcal{P}(E)^2$*,*

$$W_1\Big(\Theta_\mu(\mathrm{d}y|x), \Theta_\nu(\mathrm{d}y|x')\Big) \leq W_1(\mu,\nu) + |x - x'|.$$

All the proposal distributions presented in Section 6.5 are based on a convolution product with one or many fixed kernels. The smoothness and boundedness properties of the proposal distribution (Assumptions 6.2.1, 6.2.2, 6.2.3) are thus inherited from the properties of these kernels.

The next two assumptions are needed to prove the long-time convergence property in Section 6.4.

Assumption 6.2.4. *There exists* $\eta \in (0, 1)$ *such that*

$$\forall u \in [0, +\infty), \quad h(u) \leq \eta.$$

Remark 6.2.5. Assumption 6.2.4 is satisfied for instance for $h(u) = \eta \min(1, u)$. We make this assumption mostly for technical reasons in order to obtain in an easy manner an explicit convergence rate in Theorem 6.4.2. However, using compactness arguments, we can prove that the convergence of $(\mu_t)_t$ towards π still holds without this assumption (see Corollary 6.B.6).

The next assumption ensures that the proposal distribution is not too "far" from π.

Assumption 6.2.6 (Monotonicity)**.** *The proposal distribution* Θ *satisfies the following monotonicity property: there exists a non decreasing function*

$$c^- : [0, 1] \to (0, 1],$$

such that for all $\mu \in \mathcal{P}_0^{\mathrm{ac}}(E)$*,*

$$\inf_{(x,y)\in E^2} \frac{\Theta_\mu(y|x)}{\pi(y)} \geq c^-\left(\inf_{x\in E} \frac{\mu(x)}{\pi(x)}\right).$$

Remark 6.2.7. Note that under Assumptions 6.1.1 and 6.2.1, Assumption 6.2.6 is always satisfied with a constant function $c^- \equiv \kappa_-/M_0$. Sharper results can be obtained in specific

cases. Moreover, note that Assumptions 6.2.1, 6.2.2 and 6.2.3 are not necessary to prove Theorem 6.4.2.

Remark 6.2.8. The monotonicity Assumption 6.2.6 is satisfied for all the "convolution based" methods such as (6.2) outlined in the introduction and Algorithm 3 which will be introduced later, since for $m > 0$, it holds that:

$$[\forall y \in E, \quad m\pi(y) \leq \mu(y)] \quad \Longrightarrow \quad [\forall y \in E, \quad mK \star \pi(y) \leq K \star \mu(y)],$$

and therefore, if the left-hand side condition holds, dividing by $\pi(y)$ yields:

$$\forall y \in E, \quad \frac{K \star \mu(y)}{\pi(y)} \geq m \frac{K \star \pi(y)}{\pi(y)}.$$

On the right-hand side of the last inequality the ratio $K \star \pi(y)/\pi(y)$ depends only on π and is bounded from below, at least for small interaction kernels K, since $K \star \pi$ converges uniformly towards π as $K \to \delta_0$. In the degenerate case $K = \delta_0$, we obtain $c^-(m) = m$ for all $m > 0$ (see Remark 6.4.4).

6.2.2 Main result

The following theorem is our main convergence result.

Theorem 6.2.9. *Let $\hat{\mu}_t^N = \frac{1}{N}\sum_{i=1}^N \delta_{X_t^i}$ be the random empirical distribution of the particle system constructed at the t-th iteration of Algorithm 1 with an i.i.d. $\mu_0 \in \mathcal{P}_0^{\mathrm{ac}}(E)$ distributed initial condition. Under Assumptions 6.2.1, 6.2.2, 6.2.3, 6.2.4 and 6.2.6, there exist $C_1, C_2, C_3 > 0$ and $\lambda \in (0,1)$ which depend only on μ_0, π and E such that for all $t \in \mathbb{N}$,*

$$\mathbb{E}W_1(\hat{\mu}_t^N, \pi) \leq C_1 \beta(N) \mathrm{e}^{tC_2} + C_3(1-\lambda)^{t/2},$$

where

$$\beta(N) := \begin{cases} CN^{-1/2} & \text{if } d = 1 \\ CN^{-1/2}\log(N) & \text{if } d = 2 \\ CN^{-1/d} & \text{if } d > 2 \end{cases}, \tag{6.6}$$

and $C > 0$ is a constant which depends only on E and π. In particular $\beta(N) \to 0$ as $N \to +\infty$.

Proof. This result is deduced from Theorem 6.3.1 and 6.4.2, as it is a direct consequence

of the triangle inequality

$$\mathbb{E}W_1(\hat{\mu}_t^N, \pi) \leq \mathbb{E}W_1(\hat{\mu}_t^N, \mu_t) + \mathbb{E}W_1(\mu_t, \pi),$$

and the convergence results (6.8) and (6.11). In order to bound the second term on the right-hand side, we recall that on the compact set E, the total variation norm controls the Wasserstein-1 distance [328, Theorem 6.15]. □

By the Kantorovich characterisation of the Wasserstein distance [328, Remark 6.5], this result ensures the convergence in expectation of any Lipschitz observable (and by density of any continuous observable) in the double limit $N \to +\infty$ and $t \to +\infty$ provided that $\beta(N)\mathrm{e}^{C_2 t} \to 0$. These results and in particular the link between N and t are mostly of theoretical nature and often suboptimal; in practice higher convergence rates may be obtained (see Section 6.7).

Moreover, although Theorem 6.2.9 states a geometric convergence result for the nonlinear samplers which is similar to classical convergence results for the classical (linear) Metropolis-Hastings algorithm, the behaviours of nonlinear and linear samplers can be very different in practise, nonlinear samplers being much more efficient. In addition to the experiments shown in Section 6.7, Remark 6.4.4 gives a theoretical result obtained as a consequence of Theorem 6.2.9 which illustrates this difference.

6.3 Mean field approximation

In this section, we show that the system of particles defined by Algorithm 1 satisfies the propagation of chaos property and that the limiting law at each iteration is the law of the nonlinear Markov chain with transition kernel satisfying (6.1). From now on, we assume that the proposal distribution Θ satisfies Assumptions 6.2.1, 6.2.2 and 6.2.3 (see also the discussion in Remark 6.A.4 for alternative assumptions).

The main result of this section is the following theorem.

Theorem 6.3.1 (Coupling bound)**.** *Let Θ be a proposal distribution which satisfies Assumptions 6.2.1, 6.2.2 and 6.2.3. Let $t \in \mathbb{N}$. There exist a system of N i.i.d. nonlinear Markov chains $(\overline{X}_t^i)_t$, $i \in \{1, \dots, N\}$, defined by the transition kernel* (6.1) *and a system of N particles $(X_t^i)_t$, $i \in \{1, \dots, N\}$, which is equal in law to the N-particle system constructed by Algorithm 1, such that*

$$\forall i \in \{1, \dots, N\}, \quad \mathbb{E}|\overline{X}_t^i - X_t^i| \leq \beta(N)\mathrm{e}^{tC_\Theta}, \tag{6.7}$$

where $C_\Theta > 0$ is a constant which depends only on π and Θ and where $\beta(N)$ is defined by (6.6)

The proof of Theorem 6.3.1 is based on coupling arguments inspired by [307] and adapted from [138] (see Chapter 4). It can be found in Appendix 6.A. This coupling estimate classically implies the following properties (see [307] and Lemma 3.2.11).

Corollary 6.3.2 (Mean-field limit and propagation of chaos)**.** *Let Θ be a proposal distribution which satisfies Assumptions 6.2.1, 6.2.2 and 6.2.3. Let $(X_0^i)_{i\in\{1,\dots,N\}}$ be N i.i.d. random variables with common law $\mu_0 \in \mathcal{P}(E)$ (*chaoticity assumption*). Let $t \in \mathbb{N}$ and let $(X_t^i)_{i\in\{1,\dots,N\}}$ be the N particles constructed at the t-th iteration of Algorithm 1. Let $\mu_t = \mathcal{T}^{(t)}[\mu_0]$ be the t-th iterate of the transition operator* (6.4) *starting from μ_0, that is μ_t is the law of the nonlinear Markov chain defined by the transition kernel* (6.1) *at iteration t. Then the following properties hold true.*

1. *The (random) empirical measure $\hat{\mu}_t^N = \frac{1}{N}\sum_{i=1}^N \delta_{X_t^i}$ satisfies*

$$\mathbb{E}W_1(\hat{\mu}_t^N, \mu_t) \leq C_1 \beta(N) \mathrm{e}^{tC_2}, \tag{6.8}$$

   where $C_1, C_2 > 0$ are two absolute constants and $\beta(N)$ is defined by (6.6)*.*

2. *The (random) empirical measure $\hat{\mu}_t^N = \frac{1}{N}\sum_{i=1}^N \delta_{X_t^i}$ converges in law towards the deterministic limit :*

$$\hat{\mu}_t^N \underset{N\to+\infty}{\longrightarrow} \mu_t.$$

   We recall that $\mathcal{P}(E)$ is endowed with the topology of the weak convergence, i.e. convergence against bounded continuous test functions. The convergence in law of a random measure is the weak convergence in the space $\mathcal{P}(\mathcal{P}(E))$, which means that for all test function $\Phi \in C_b(\mathcal{P}(E))$, $\mathbb{E}[\Phi(\hat{\mu}_t^N)] \to \Phi(\mu_t)$.

3. *For every ℓ-tuple of continuous bounded functions $\varphi_1, \dots \varphi_\ell$ on E, it holds that:*

$$\int_{E^\ell} \varphi_1(x_1)\dots\varphi_\ell(x_\ell)\mu_t^{\ell,N}(\mathrm{d}x_1,\dots,\mathrm{d}x_\ell) \underset{N\to+\infty}{\longrightarrow} \prod_{k=1}^{\ell}\langle \mu_t, \varphi_k\rangle, \tag{6.9}$$

   where $\mu_t^{\ell,N}$ is the joint law at time t of any subset of ℓ particles constructed by Algorithm 1 at iteration t.

Proof. The first property follows from the triangle inequality

$$\mathbb{E}W_1(\hat{\mu}_t^N, \mu_t) \leq \mathbb{E}W_1(\hat{\mu}_t^N, \overline{\mu}_t^N) + \mathbb{E}W_1(\overline{\mu}_t^N, \mu_t),$$

where $\overline{\mu}_t^N = \frac{1}{N}\sum_{i=1}^N \delta_{\overline{X}_t^i}$ is the empirical measure of the N nonlinear Markov chains constructed in Theorem 6.3.1. The first term on the right-hand side is bounded by (6.7) by definition of the Wasserstein distance and the exchangeability of the processes. The second term on the right-hand side is bounded by $\beta(N)$ by [162, Theorem 1]. The second property is a classical consequence of (6.7), see [194, Section 1]. The third property is equivalent to the second property by [307, Proposition 2.2] (see Lemma 3.2.11). □

The property (6.9) corresponds to the original formulation of the propagation of chaos (Definition 3.2.10). From our perspective, it justifies the use of Algorithm 1 and ensures that as the number of particles grows to infinity and despite the interactions between the particles, we asymptotically recover an i.i.d. sample. The final MCMC approximation of the expectation of an observable $\varphi \in C_b(E)$ is thus given at the t-th iteration by:

$$\int_E \varphi(x)\pi(\mathrm{d}x) \simeq \frac{1}{N}\sum_{i=1}^N \varphi(X_t^i).$$

Remark 6.3.3. In [220], the authors prove the propagation of chaos towards a continuous-time (nonlinear) diffusion process for a classical random walk Metropolis-Hastings algorithm in the product space E^N where the trajectory of each of the N dimensions is interpreted as a particle, where the target distribution $\pi^{\otimes N}$ is tensorized and under a specific scaling limit in N for the time and the size of the random-walk kernel. In this algorithm, each move is globally accepted or rejected for the N particles whereas in Algorithm 1, the acceptance step is individualized for each particle. One consequence is that, unlike the algorithm in [220], for a fixed number N of particles, $\pi^{\otimes N}$ is in general *not* a stationary distribution of the particle system defined by Algorithm 1.

6.4 Long-time Asymptotics

In this section, we prove that π is the unique stationary measure of the nonlinear Markov chain defined by the transition kernel (6.1) and we give a quantitative long-time convergence result.

6.4.1 Main result

Let $(\mu_t)_{t\in\mathbb{N}}$ be the sequence of laws of the nonlinear Markov chain defined by the transition kernel (6.1). It satisfies the recurrence relation

$$\mu_{t+1} = \mathcal{T}[\mu_t], \tag{6.10}$$

where we recall that given $\mu \in \mathcal{P}(E)$, the transition operator $\mathcal{T}$ is defined by:

$$\mathcal{T}[\mu](\mathrm{d}x) = \mu(\mathrm{d}x) + \int_E \pi(x) W_\mu(x \to y)\left(\frac{\mu(\mathrm{d}y)}{\pi(y)}\mathrm{d}x - \frac{\mu(\mathrm{d}x)}{\pi(x)}\mathrm{d}y\right),$$

and

$$W_\mu(x \to y) := \Theta_\mu(y|x) h(\alpha_\mu(x,y)).$$

Note that if the initial condition has a density with respect to the Lebesgue measure, then μ_t has also a density with respect to the Lebesgue measure. In the following we make this assumption and we write with a slight abuse of notations $\mu_t(x)\mathrm{d}x \equiv \mu_t(\mathrm{d}x)$ for this density. The following elementary lemma shows that the ratio μ_t/π is controlled by the initial condition.

Lemma 6.4.1. *For any $t \in \mathbb{N}$, let $\mu_t \in \mathcal{P}_0^{\mathrm{ac}}(E)$ be given by the recurrence relation* (6.10) *with initial condition $\mu_0 \in \mathcal{P}_0^{\mathrm{ac}}(E)$. Then*

$$\inf_{x\in E} \frac{\mu_t(x)}{\pi(x)} \geq \inf_{x\in E} \frac{\mu_0(x)}{\pi(x)}, \quad \sup_{x\in E} \frac{\mu_t(x)}{\pi(x)} \leq \sup_{x\in E} \frac{\mu_0(x)}{\pi(x)}.$$

Proof. Since $W_\mu(x \to y) \geq 0$ and $\int_E W_\mu(x \to y)\mathrm{d}y \leq 1$, this comes directly from the relation

$$\frac{\mathcal{T}[\mu](x)}{\pi(x)} = \left(1 - \int_E W_\mu(x \to y)\mathrm{d}y\right)\frac{\mu(x)}{\pi(x)} + \int_E W_\mu(x \to y)\frac{\mu(y)}{\pi(y)}\mathrm{d}y,$$

for all $\mu \in \mathcal{P}_0^{\mathrm{ac}}(E)$ and $x \in E$. □

The main result of this section is the following convergence result which is a direct consequence of the results presented in the following sections and discussed below.

Theorem 6.4.2. *Let Θ be a proposal distribution which satisfies Assumption 6.2.6 and h be an acceptance function which satisfies Assumption 6.2.4. Then there exist two (explicit) constants $C > 0$ and $\lambda \in (0,1)$ which depend only on μ_0, π and E such that*

$$\|\mu_t - \pi\|_{\mathrm{TV}} \leq C(1-\lambda)^{t/2} \tag{6.11}$$

Proof. Using the fact that the Total Variation norm is equal to the L^1 norm of the probability density functions and the Cauchy-Schwarz inequality, it holds that

$$\|\mu_t - \pi\|_{\mathrm{TV}} = \int_E |\mu_t(x) - \pi(x)| \mathrm{d}x = \int_E \sqrt{\pi}\sqrt{\pi} \left| \frac{\mu_t(x)}{\pi(x)} - 1 \right| \mathrm{d}x \leq \sqrt{2\mathcal{H}[\mu_t|\pi]},$$

where $\mathcal{H}[\mu_t|\pi]$ is the relative entropy defined by (6.14) associated to the function $\phi : s \mapsto \frac{1}{2}(s-1)^2$. The conclusion follows from Proposition 6.4.7 which provides a bound on this quantity. □

Remark 6.4.3. The last inequality between the TV norm and the square root of the relative entropy is a simple form of a Csiszár-Kullback-Pinsker inequality, see [222, Appendix A] and [42].

Remark 6.4.4 (Convergence rate of nonlinear samplers). In this proof, the convergence rate λ is obtained by a crude estimate of the infimum of the jump rate $W_{f_t}(x \to y)$. We do not claim that this rate is optimal. In the degenerate case $\Theta_\mu(y|x) = \mu(y)$, the best rate obtained is equal to $h(1)$ by taking an initial condition arbitrarily close to π (see Remark 6.2.8). In Remark 6.5.1, it is shown that these proposal distributions can be obtained as the limit when $\sigma \to 0$ of the proposal distributions $\Theta_\mu(y|x) = K_\sigma \star \mu(y)$ where K_σ is a random-walk kernel with variance σ^2. These proposal distributions are the simplest nonlinear analog of the random-walk Metropolis-Hastings algorithm with kernel K_σ (the proposal distribution in this case is $K_\sigma \star \delta_x(y)$). However in the nonlinear case, the convergence rate tends to a constant nonnegative value when $\sigma \to 0$ while in the random-walk Metropolis-Hastings case the convergence rate tends to 0 (see Theorem 6.B.7).

In the linear case, that is when $\mathcal{T}$ is the linear transition operator of the classical random walk Metropolis-Hastings algorithm, the convergence of the sequence of iterates of $\mathcal{T}$ is studied in particular in [253] and more recently in [137] using analytical spectral methods. It is not possible to follow this strategy in the nonlinear case. In order to motivate our strategy, let us notice that the recurrence relation (6.10) can be interpreted as the explicit Euler discretization scheme

$$\frac{\mu_{t+1} - \mu_t}{\Delta t} = \mathcal{T}[\mu_t] - \mu_t, \tag{6.12}$$

of the nonlinear partial differential equation

$$\partial_t f_t = \mathcal{T}[f_t] - f_t \tag{6.13}$$

with a constant time-step $\Delta t = 1$. The PDE (6.13) has a remarkable entropic structure

which is detailed in Appendix 6.B and which allows to prove that $f_t \to \pi$ as $t \to +\infty$. Entropy methods are by now a classical tool to study the long-time properties of both linear and nonlinear PDEs, see [222, 297]. The proof of Theorem 6.4.2 is based on the adaptation of these ideas to the present discrete-time setting. A more detailed discussion of the links between (6.12) and (6.13) can be found in Appendix 6.B.3. Entropy methods have been used previously in a similar context in [219] to prove the long-time convergence of a process obtained as the scaling limit of a particle-based Metropolis-Hastings algorithm [220] which, unlike the present case, is a continuous-time (nonlinear) diffusion process (see Remark 6.3.3).

6.4.2 Entropy and dissipation

For a given convex function $\phi : [0, +\infty) \to [0, +\infty)$ such that $\phi(1) = 0$, the (generalised) relative entropy $\mathcal{H}[\mu|\pi]$ and dissipation $\mathcal{D}[\mu|\pi]$ of a probability density $\mu \in \mathcal{P}^{\mathrm{ac}}(E)$ with respect to π are defined respectively by

$$\mathcal{H}[\mu|\pi] := \int_E \pi(x)\phi\left(\frac{\mu(x)}{\pi(x)}\right)\mathrm{d}x, \quad \mathcal{D}[\mu|\pi] := -\int_E \phi'\left(\frac{\mu(x)}{\pi(x)}\right)\big(\mathcal{T}[\mu](x) - \mu(x)\big)\mathrm{d}x. \quad (6.14)$$

Using the detailed balance property

$$\pi(x)W_\mu(x \to y) = \pi(y)W_\mu(y \to x),$$

for all $x, y \in E$ and $\mu \in \mathcal{P}^{\mathrm{ac}}(E)$, it holds that

$$\mathcal{D}[\mu|\pi] = \frac{1}{2}\iint_{E\times E} \pi(x)W_\mu(x \to y)\left(\frac{\mu(y)}{\pi(y)} - \frac{\mu(x)}{\pi(x)}\right)\left(\phi'\left(\frac{\mu(y)}{\pi(y)}\right) - \phi'\left(\frac{\mu(x)}{\pi(x)}\right)\right)\mathrm{d}x\mathrm{d}y,$$

and thus $\mathcal{D}[\mu|\pi] \geq 0$ by convexity of ϕ.

In the following, we focus on the case $\phi(s) = \frac{1}{2}(s-1)^2$ for which we can prove the following crucial lemma. Note also that in this case the relative entropy is equal to a weighted L^2 norm and thus dominates the Total Variation norm between probability density functions.

Lemma 6.4.5. *Let $\phi(s) = \frac{1}{2}(s-1)^2$, then the sequence $(\mathcal{H}[\mu_t|\pi])_{t\in\mathbb{N}}$ is non-increasing.*

Proof. In this case,

$$\mathcal{H}[\mu|\pi] = \frac{1}{2}\int_E \pi(x)\left|\frac{\mu(x)}{\pi(x)} - 1\right|^2 \mathrm{d}x = \frac{1}{4}\iint_{E\times E} \pi(x)\pi(y)\left|\frac{\mu(x)}{\pi(x)} - \frac{\mu(y)}{\pi(y)}\right|^2 \mathrm{d}\mathrm{d}y, \quad (6.15)$$

and

$$\mathcal{D}[\mu|\pi] = \frac{1}{2}\iint_{E\times E} \pi(x) W_\mu(x \to y)\left|\frac{\mu(y)}{\pi(y)} - \frac{\mu(x)}{\pi(x)}\right|^2. \tag{6.16}$$

Moreover, since $\phi(s) = \frac{1}{2}(s-1)^2$ is a polynomial of order 2, the exact Taylor expansion

$$\phi(v) = \phi(u) + \phi'(u)(v-u) + \frac{1}{2}\phi''(u)(v-u)^2,$$

yields

$$\mathcal{H}[\mu_{t+1}|\pi] - \mathcal{H}[\mu_t|\pi] = -\mathcal{D}[\mu_t|\pi] + \frac{1}{2}\int_E \pi(x)\left|\frac{\mu_{t+1}(x)}{\pi(x)} - \frac{\mu_t(x)}{\pi(x)}\right|^2 \mathrm{d}x. \tag{6.17}$$

Using that $\mu_{t+1} = \mathcal{T}[\mu_t]$ and the definition of $\mathcal{T}$, it holds that

$$\int_E \pi(x)\left|\frac{\mu_{t+1}(x)}{\pi(x)} - \frac{\mu_t(x)}{\pi(x)}\right|^2 \mathrm{d}x = \int_E \pi(x)\left|\int_E W_{\mu_t}(x \to y)\left(\frac{\mu_t(y)}{\pi(y)} - \frac{\mu_t(x)}{\pi(x)}\right)\mathrm{d}y\right|^2 \mathrm{d}x.$$

By the Cauchy-Schwarz inequality, we get

$$\begin{aligned}\int_E \pi(x)\left|\frac{\mu_{t+1}(x)}{\pi(x)} - \frac{\mu_t(x)}{\pi(x)}\right|^2 \mathrm{d}x \\ \leq \iint_{E\times E} \pi(x) W_{\mu_t}(x \to y)\left|\frac{\mu_t(y)}{\pi(y)} - \frac{\mu_t(x)}{\pi(x)}\right|^2 \int_E W_{\mu_t}(x \to z)\mathrm{d}z\mathrm{d}x\mathrm{d}y.\end{aligned}$$

Reporting into (6.17) and using (6.16) yields

$$\begin{aligned}&\mathcal{H}[\mu_{t+1}|\pi] - \mathcal{H}[\mu_t|\pi] \\ &\quad\leq -\frac{1}{2}\iint_{E\times E} \pi(x) W_{\mu_t}(x \to y)\left(1 - \int_E W_{\mu_t}(x \to z)\mathrm{d}z\right)\left|\frac{\mu_t(y)}{\pi(y)} - \frac{\mu_t(x)}{\pi(x)}\right|^2 \mathrm{d}x\mathrm{d}y.\end{aligned} \tag{6.18}$$

Since $W_{\mu_t}(x \to y) \geq 0$ and $\int_E W_{\mu_t}(x \to z)\mathrm{d}z \leq 1$, the right-hand side is non negative which concludes the proof. □

6.4.3 Exponential decay of the entropy

Under the Assumptions 6.2.4 and 6.2.6, it is possible to improve the result of Lemma 6.4.5 and to prove a quantitative exponential decay result. Since the entropy is given by (6.15),

owing to (6.18), the goal is to bound from below by a multiple of $\pi(y)$ the quantity

$$W_{\mu_t}(x \to y)\left(1 - \int_E W_{\mu_t}(x \to z)\mathrm{d}z\right),$$

for all $x, y \in E$ and uniformly in t. This bound will be obtained as a consequence of Assumptions 6.2.4 and 6.2.6. First, Assumption 6.2.6 gives the following lower bound.

Lemma 6.4.6. *Let $h : [0, +\infty) \to [0, 1]$ be a continuous non-decreasing acceptance function which satisfies the relation (6.3). Let Θ be a proposal distribution which satisfies Assumption 6.2.6. Then for all $\mu \in \mathcal{P}_0^{\mathrm{ac}}(E)$ and all $x, y \in E$,*

$$W_\mu(x \to y) \geq \lambda(\mu)\pi(y), \quad \lambda(\mu) := c^-\left(\inf_{x \in E} \frac{\mu(x)}{\pi(x)}\right) h(1) \in (0, 1].$$

As a consequence, using the fact that c^- is non decreasing and Lemma 6.4.1, for any $t \in \mathbb{N}$, it holds that

$$W_{\mu_t}(x \to y) \geq \lambda_0\pi(y), \quad \lambda_0 := c^-\left(\inf_{x \in E} \frac{\mu_0(x)}{\pi(x)}\right) h(1).$$

Proof. Let us first prove that for any bounded interval $[a, b]$ with $a > 0$, it holds that

$$\inf_{(x,y) \in [a,b]^2} yh\left(\frac{x}{y}\right) = ah(1).$$

Since h is continuous non-decreasing, for each $y \in [a, b]$, the function $x \in [a, b] \mapsto yh(x/y)$ has a minimum in $x = a$. This shows that the minimum on the function $(x, y) \in [a, b]^2 \mapsto yh(x/y)$ is attained on the segment $\{(a, y), y \in [a, b]\}$. Since $yh(a/y) = ah(y/a)$, the same reasoning shows that this minimum is attained when $y = a$. The conclusion follows. Then, using Assumption 6.2.6 and applying this result with $a = c^-\left(\inf_{x \in E} \frac{\mu(x)}{\pi(x)}\right)$ yields

$$\begin{aligned} W_\mu(x \to y) = \Theta_\mu(y|x)h(\alpha_\mu(x, y)) &= \frac{\Theta_\mu(y|x)}{\pi(y)} h\left(\frac{\Theta_\mu(x|y)\pi(y)}{\pi(x)\Theta_\mu(y|x)}\right)\pi(y) \\ &\geq c^-\left(\inf_{x \in E} \frac{\mu(x)}{\pi(x)}\right) h(1)\pi(y). \end{aligned}$$

□

We are now ready to prove that in this case, the relative entropy converges exponentially fast towards zero.

Proposition 6.4.7. *Under Assumption 6.2.4 and Assumption 6.2.6, there exists a constant*

$\lambda \in (0,1)$ *such that for all* $t \in \mathbb{N}$,

$$\mathcal{H}[\mu_t|\pi] \leq (1-\lambda)^t \mathcal{H}[\mu_0|\pi].$$

Proof. From the relation (6.18) and using the assumptions on h and Θ, it holds that

$$\mathcal{H}[\mu_{t+1}|\pi] - \mathcal{H}[\mu_t|\pi] \leq -2\lambda_0(1-\eta)\mathcal{H}[\mu_t|\pi].$$

Moreover by definition of λ_0, it holds that $\lambda_0 \leq \eta$ and thus $\lambda := 2\lambda_0(1-\eta) < 1$. We deduce that

$$\mathcal{H}[\mu_{t+1}|\pi] \leq (1-\lambda)\mathcal{H}[\mu_t|\pi],$$

and the conclusion follows. □

6.5 Some Collective Proposal Distributions

The proposal distribution can be fairly general and so far, we have not detailed how to choose it. Several choices of proposal distributions are gathered in this section.

This proposal should use the maximum of information coming from the value of the target π, in order to increase the fitness of Θ_μ to the true distribution. However, the proposal must also allow for some exploration of the parameter space. Here, we only intend to present some of the possible proposals, each one having pros and cons, both on the theoretical and practical sides. Note also that a proposal distribution can always be constructed as a mixture of other proposal distributions.

In view of Theorem 6.3.2, we can see each of the proposal distributions presented in this section either as a specific choice of nonlinear kernel (6.1) with its associated nonlinear process or as its particle approximation given by Algorithm 1. From this second perspective the proposal distribution can be seen as a specific interaction mechanism between the particles. More specifically, it depicts a specific procedure which can be interpreted as "information sharing" between the particles: given the positions of *all* the N particles at a given time, we aim at constructing the best interaction mechanism which will favour a specific aspect such as acceptance, convergence speed, exploration etc. By analogy with systems of swarming particles which exchange local information (here, the local value of the target distribution) to produce global patterns (here, a globally well distributed sample), we call this class of proposal distributions *collective*. The class of methods introduced will be referred as Collective Monte Carlo methods (CMC). On the contrary, the nonlinear kernels introduced in [6] do not belong to this class as explained

in Appendix 6.C.1. For each proposal we give an implementation which, starting from population of particles $(X^1, \dots, X^N) \in E^N$, returns a proposal Y.

Although our theoretical results (Theorem 6.3.2 and Theorem 6.4.2) are general enough to encompass almost all of the proposal distributions described here (see Section 6.2.1), the validity and numerical efficiency of each of them will be assessed in Section 6.7 on various examples of target distributions.

6.5.1 Metropolis-Hastings Proposal (PMH)

Proposal distribution. The classical Metropolis-Hastings algorithm fits into our formalism, with

$$\Theta_\mu(\mathrm{d}y|x) = q(y|x)\mathrm{d}y,$$

where q is a fixed random walk kernel which does not depend on μ.

Particle implementation. In this case, Algorithm 1 reduces to the simulation of N independent Metropolis-Hastings chains in parallel.

6.5.2 Convolution Kernel Proposal (Vanilla CMC)

Proposal distribution. As already outlined in the introduction, a first and simple collective proposal distribution is given by the convolution:

$$\Theta_\mu(\mathrm{d}y|x) = K \star \mu(y)\mathrm{d}y := \left(\int_E K(y-z)\mu(\mathrm{d}z) \right) \mathrm{d}y,$$

where K is a fixed *interaction kernel*, that is a (smooth) radial function which tends to zero at infinity. Typical examples are $K(x) = \mathcal{N}(0, \sigma^2 I_d)$ and $K(x) = \frac{1}{|B_\sigma(0)|} 1_{B_\sigma(0)}(x)$, where $\sigma > 0$ is fixed and $B_\sigma(0)$ denotes the ball of radius $\sigma > 0$ centred at 0 in $\mathbb{R}^d$. Note that the proposal distribution does not depend on the starting point x. It may happen that the proposed state falls outside E. In this case it will be rejected since π is equal to zero outside E. One can therefore take equivalently $\Theta_\mu(\mathrm{d}y|x) \propto K \star \mu(y)\mathbb{1}_E(y)\mathrm{d}y$. The same remark holds for the other collective proposal distributions below.

Particle implementation. At each time step t, each particle i samples uniformly another particle j and then draw a proposal $Y_t^i \sim K(X_t^j, \mathrm{d}y)$ which can be seen as a "mutation" of X_t^j. This "resampling with mutation" procedure is somehow similar to a (genetic) Wright-Fisher model (see for instance [155] for a review of genetic models). Since

a "mutation" may or may not be accepted, it can be described as a *biased Wright-Fisher model*.

The collective aspect is twofold: first the proposal distribution allows large scale move on all the domain filled by the N particles; then during the acceptance step, for a particle at position X and a proposal at Y the acceptance ratio can be understood as a measure of discrepancy between the target ratio $\frac{\pi(Y)}{\pi(X)}$ and the observed ratio $\frac{K\star\hat{\mu}^N(Y)}{K\star\hat{\mu}^N(X)}$ between the (average) number of particles around Y and the (average) number of particles around X. In the linear Metropolis-Hastings case with a symmetric random-walk kernel, the acceptance ratio only takes into account the target ratio. As a consequence, the acceptance probability of a proposal state depends not only on how "good" it is when looking at the values of π but also on how many particles are (or are not) already around this proposal sate compared to the present state (and therefore on how accepting the proposal would improve the current global state of the system).

Remark 6.5.1 (Moderate interaction, part 1). When $\sigma \to 0$ we obtain the degenerate proposal distribution $\Theta_\mu(\mathrm{d}y|x) = \mu(\mathrm{d}y)$ (which does not satisfy the assumption $\Theta_\mu(\mathrm{d}y|x) \in \mathcal{P}_0^{\mathrm{ac}}(E)$ in general). It would not make sense to take this proposal distribution at the particle level in Theorem 6.3.1. However, it makes sense to consider the case $\Theta_\mu(y|x) = \mu(y)\mathrm{d}y$ in the nonlinear kernel (6.1) where $\mu \in \mathcal{P}_0^{\mathrm{ac}}(E)$. This degenerate proposal distribution still satisfies the assumptions of Theorem 6.4.2 and could lead to a better rate of convergence (see Remark 6.4.4). It is thus worth mentioning that this degenerate proposal distribution can also be obtained as the many-particle limit of a system of particles under an additional *moderate interaction* assumption [273, 221, 138]. See Remark 6.A.3 for additional details.

Draw uniformly $j \in \{1, \dots, N\}$;
Draw $e \sim K$;
Set $Y = X^j + e$;

Algorithm 2: Proposal through Convolution Kernel

6.5.3 Markovian Mixture of Kernels Proposal (MoKA)

Proposal distribution. A limitation of the Convolution Kernel Algorithm 2 is the fixed size of the interaction kernel. A remedy is given by the following collective proposal distribution which is a convolution with a mixture of kernels (with different sizes) with (potentially) nonlinear mixture weights:

$$\Theta_\mu(\mathrm{d}y|x) = \sum_{p=1}^{P} \alpha_p(\mu) K_p \star \mu(y)\mathrm{d}y,$$

A possible choice for the weights is to take a solution of the following minimisation problem:

$$\min_{\alpha \in S^p} \int_E \phi \left(\frac{\sum_p \alpha_p K_p \star \mu(x)}{\pi(x)} \right) \mu(\mathrm{d}x), \tag{6.19}$$

where S_p denotes the p-simplex and where ϕ is convex non-negative such that $\phi(1) = 0$. Typically $\phi(s) = s \log s - s + 1$. In this case, when $\mu = \pi$ it corresponds to minimising the Kullback-Leibler divergence of the mixture proposal relative to π. In our experiments, we found that optimising the quantity $\int_E |\sum_p \alpha_p K_p \star \mu(x) - \pi(x)| \mu(\mathrm{d}x)$ leads to similar, slightly better results. Moreover, this choice is also numerically more stable so we chose to implement this version, that we call Markovian Mixture of Kernels (MoKA-Markov).

Another choice for the weights, which is *non-Markovian*, is to take α_p proportional to the geometric mean of the acceptance ratio of the particles which have chosen the kernel p at the previous iteration. This method will be referred as Mixture of Kernels Adaptive CMC (MoKA). It shares similarities with the D-kernel algorithm of [145] and the arguments developed by the authors suggest that the two versions (Markovian and MoKA) may be asymptotically equivalent. The proof is left for future work.

Particle implementation. Same as in Algorithm 2 but with an additional step to choose a "mutation kernel" at each proposal step. The computation of the weights of the mixture can be done in a fully Markovian way at the beginning of each iteration before the proposal step or, in MoKA, are computed at the end of the iteration and used at the next iteration.

In Section 6.7 we will show that this algorithm can favour initial exploration if the particles are initially in an area of low potential.

Compute the weights $\alpha_1, \ldots, \alpha_P$ using (6.19);
Draw $p \in \{1, \ldots P\}$ with probability $(\alpha_1, \ldots, \alpha_P)$;
Draw uniformly $j \in \{1, \ldots, N\}$;
Draw $e \sim K_p$;
Set $Y = X^j + e$;

Algorithm 3: Markovian Mixture of Kernels proposal generation

6.5.4 Kernelised Importance-by-Deconvolution Sampling (KIDS)

Proposal distribution. Algorithms based on a simple convolution operator such as Algorithms 2 and 3 keep a "blind" resampling step. In order to improve the convergence speed of such algorithms one may want to favour the selection of "good" states. For a

fixed interaction kernel K, one can choose a proposal distribution of the form:

$$\Theta_\mu(y|x) = K \star \nu_\mu(y),$$

where ν_μ solves the following deconvolution problem with an absolute continuity constraint:

$$\nu_\mu = \text{argmin}_{\nu \ll \mu} \int_E \log\left(\frac{K \star \nu(x)}{\pi(x)}\right) K \star \nu(x) \mathrm{d}x. \tag{6.20}$$

That is, we are looking for a weight function $w \geq 0$ which satisfies the constraint

$$\int_E w(x)\mu(dx) = 1$$

and such that the measure defined by $\nu_\mu(A) = \int_A w(x)\mu(\mathrm{d}x)$ minimises the KL divergence above. The function w is the Radon-Nikodym derivative of ν with respect to μ. In other words the proposal distribution focuses on the parts of the support of μ which are "closer" to π.

Remark 6.5.2. Although this proposal distribution performs well in practise, we did not manage to prove the regularity Assumptions 6.2.2 and 6.2.3.

Particle implementation. In the case of an empirical measure $\hat{\mu}^N = \frac{1}{N}\delta_{X^i}$, the Radon-Nikodym weight function w can simply be seen as a vector of N weights $(w_1, \ldots, w_N) \in [0,1]^N$ such that $\sum_i w^i = 1$ and the measure $\nu_{\hat{\mu}^N}$ is thus a weighted empirical measure:

$$\nu_{\hat{\mu}^N} := \sum_{i=1}^N w_i \delta_{X^i}. \tag{6.21}$$

The deconvolution procedure gives more weight to the set of particles that are already "well distributed" according to π. These particles are thus more often chosen in the Wright-Fisher resampling step (see Algorithm 2).

Note that although the weighted empirical measure proposal (6.21) is very reminiscent of an Importance Sampling procedure, the computation of the weights here follows from a completely different idea.

In practice we solve the deconvolution problem using the Richardson-Lucy algorithm [286, 244] (also known as the Expectation Maximisation algorithm). See for instance [268, Section 5.3.2] where it is proved that the iterative algorithm below converges towards a minimiser of the Kullback-Leibler divergence (6.20) in the case of an empirical measure μ. Note that the computation of the weights (Richardson-Lucy loop) can be done

before the resampling step.

Set $w_i^{(0)} = 1$ for all $i \in \{1, \dots, N\}$;
for $s = 0$ *to* $S - 1$ **do**
  For all $i \in \{1, \dots, N\}$, update the weight by:
  $w_i^{(s+1)} = w_i^{(s)} \sum_{j=1}^{N} \frac{\pi(X_t^j) K(X_t^i - X_t^j)}{\sum_{k=1}^{N} w_k^{(s)} K(X_t^j - X_t^k)}$;
end
Set $w_i = w_i^{(S)}$ for all $i \in \{1, \dots, N\}$;
Normalize the weights $(w_1, \dots, w_N)$;
Draw $j \in \{1, \dots, N\}$ with probability w_j;
Draw $e \sim K$;
Set $Y = X^j + e$;

Algorithm 4: Kernel Importance-by-Deconvolution Sampling proposal generation

6.5.5 Bhatnagar-Gross-Krook sampling (BGK)

Proposal distribution. In Algorithms 2, 3 and 4, the proposal distribution is based on a (mixture of) symmetric kernels: this symmetry property is reflected in the proposal distribution and might not well represent the local properties of the target distribution. In dimension $d \geq 2$, we can adopt a different strategy by sampling proposals from a multivariate Gaussian distribution with a covariance matrix that is computed locally. An example is given by the following proposal distribution:

$$\Theta_\mu(\mathrm{d}y|x) = \left(\int_E G_{\widehat{\Sigma}_\mu(z)}(\widehat{m}_\mu(z) - y) \mu(\mathrm{d}z) \right) \mathrm{d}y,$$

where

$$\widehat{m}_\mu(z) = \frac{1}{\int_E K(z - z') \mu(\mathrm{d}z')} \int_E K(z - z') z' \mu(\mathrm{d}z'), \tag{6.22}$$

and

$$\widehat{\Sigma}_\mu(z) = \frac{1}{\int_E K(z - z') \mu(\mathrm{d}z')} \int_E K(z - z')(z' - \widehat{m}_\mu(z))(z' - \widehat{m}_\mu(z))^{\mathrm{T}} \mu(\mathrm{d}z'), \tag{6.23}$$

and where K is a fixed interaction kernel. This proposal distribution and the associated transition operator are reminiscent of a Bhatnagar-Gross-Krook (BGK) type operator [34].

In the particular case of $K(x, y) \equiv 1$, we have a more simple algorithm which can be interpreted as a Markovian version of the Adaptive Metropolis-Hastings algorithm introduced by [187]. However such algorithm does not benefit from the appealing properties of local samplers. Indeed, when the target distribution is multimodal, we can take more

advantageously as interaction kernel $K(x) \propto \mathbb{1}_{|x|<\sigma}$, where the threshold σ allows the proposal to be adapted to the local mode. Note that moving across the modes is still possible thanks to the choice of another particle at the first step (see proposal algorithm below). The main issue is the choice of σ that must be higher than the size of the modes but smaller than the distance between the modes.

Particle implementation. Each particle, say X_t^i samples another particle, say X_t^j. Then we compute the local mean and covariance around X_t^j and we draw a proposal Y_t^i for X_t^i according to a Normal law with the locally computed parameters. As before it may be cheaper to compute and store all the local means and covariances before the resampling loop.

Draw $j \in \{1 \dots, N\}$ uniformly;
Compute $\kappa = \sum_i K(X_t^i, X_t^j)$;
Compute the local mean $\widehat{m}_{X^j} = \frac{1}{\kappa} \sum_i K(X_t^i, X_t^j) X_t^i$;
Compute the local covariance $\widehat{\Sigma}_{X^j} = \frac{1}{\kappa} \sum_i K(X_t^i, X_t^j)(X^i - \widehat{m}_{X^j})(X^i - \widehat{m}_{X^j})^{\mathrm{T}}$;
Draw $Y \sim \mathcal{N}(\widehat{m}_{X^j}, \widehat{\Sigma}_{X^j})$;

Algorithm 5: BGK proposal generation

6.6 GPU implementation

The particle system defined by Algorithm 1 is of mean-field type and similarly to the other particle systems presented in this work, the major bottleneck is the computation of off-grid convolutions of the form:

$$a_i = \sum_{j=1}^{N} K(X_t^i, X_t^j)\, b_j, \tag{6.24}$$

which appear in the evaluation of kernel densities on in the computation of the importance weights in the Richardson-Lucy loop (Algorithm 4). As explained in Section 5.1, many methods are available in the literature to cope with the apparent prohibitive quadratic complexity of the algorithm. The simplest and most efficient implementation that we are aware of is based on the recent GPU routines which have been developed to tackle computations in the mould of (6.24) with maximum efficiency. These methods can be accessed through the `KeOps` extension for `PyTorch` [276] developed by Feydy et al. [78, 159].

These recent modern software and hardware improvements fully legitimates the use of collective algorithms based on the real-time simulation of large populations of *interacting* samples: as shown in the examples in Section 6.7, the Collective Monte Carlo methods presented in this Chapter advantageously trade computation time (in t) for computational cost (in N). As detailed in our documentation (`https://www.kernel-operations.io/monaco`), all the tests are run on a single gaming GPU, the Nvidia GeForce RTX 2080 Ti. With 10^4 to 10^6 particles handled at any given time, our simulations run in a handful of seconds at most without requiring approximation procedures.

6.7 Numerical experiments

We now run experiments on several target distributions in low and moderately large dimension. We always clip distributions on the unit (hyper)-cube $[0,1]^d$. We compare our method with the Safe Adaptive Importance sampling (SAIS) from [134], which is one of the state-of-the-art importance sampling based methods (see Section 6.C.2). We also include as baseline a parallel implementation of Metropolis-Hastings (PMH) with a number of parallel runs that is equal to the number of particles in our method. For all the methods we chose a poor initialisation with N particles independently distributed according to $X_0^i = (0.9, \dots, 0.9)^{\mathrm{T}} + 0.1 U_0^i$ where $U_0^i \sim \mathcal{U}([0,1]^d)$.

Among the variants of our method, we show results for vanilla CMC, MoKA-CMC, MoKA-Markov-CMC and MoKA-KIDS-CMC. Please note that we do not include the BGK and KIDS samplers in these experiments: although we believe that the ideas behind these methods are interesting enough to justify their presentation, we observe that they generally do not perform as well as the other CMC variants and leave them aside for the sake of clarity.

We compare the results in term of *energy distance* [287] between a true sample generated by rejection and the population of particles at each step. As baseline, we show the average energy distance between two i.i.d. exact samples of size N, and a 90% prediction interval for this quantity. For two independent samples X and Y of size n and m respectively, the energy distance is defined as:

$$\mathcal{E}(X,Y) = \frac{2}{nm}\sum_{i,j}|X_i - Y_j| - \frac{1}{n^2}\sum_{i,j}|X_i - X_j| - \frac{1}{m^2}|Y_i - Y_j|,$$

where $|\cdot|$ denotes the standard Euclidean norm.

Our code and its documentation are available online at `http://www.kernel-operations.`

`io/monaco/` or on the GitHub page of J. Feydy.

All our experiments can be run on Google Colaboratory (`colab.research.google.com`) with a GPU within a few seconds to a few minutes, depending on the method and number of independent runs. We note that MoKA-KIDS is a slightly heavier method, as it relies on the Richardson-Lucy iterations to optimise the deconvolution weights. We also note that unlike our Markovian methods, the memory cost of SAIS significantly increases with the number of iterations as particles are constantly added to the system – to the best of our knowledge, no procedure has yet been proposed to remove particles with time. Moreover, this algorithm also suffers from a naive high computational cost. Efficient implementations are introduced by the authors such as the batch sampler proposed in [134]. We did not implement these methods but rather relied on our fast GPU implementation which is also well-adapted to SAIS and thanks to which the computation time is not a problem. Experiments in non-Euclidean spaces such a the Poincaré hyperbolic plane and the group of 3D rotation matrices are available online in our documentation.

6.7.1 Banana shaped distribution

Our first target is inspired by the *Banana* example from [134], that is made up of three Gaussian bells with variance 0.2 and of a banana-shaped distribution. We represent a typical run of our method and the level sets of the distribution in Figure 6.7.1.

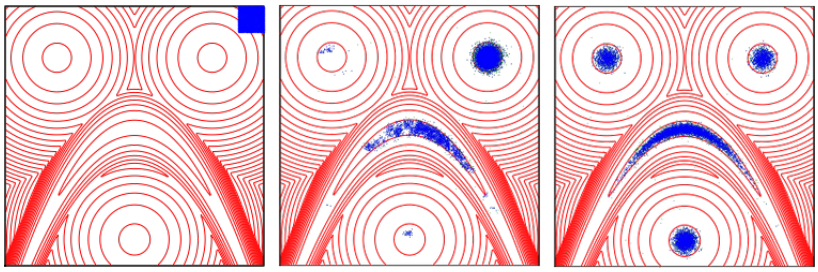

FIGURE 6.7.1: Banana-shaped distribution. Level sets (red) and particles (blue) from left to right at iterations 0, 10 and 50 of the MoKA-Markov sampler.

This distribution is renowned for being difficult to sample from, especially because of its geometry. Our proposals are uniform proposals in balls of various diameters depending on the method, that is not adapted to the distribution. We increase the difficulty of the problem with a starting particle swarm that is situated outside the modes of our target.

We run each method for 80 iterations with $N = 10^4$ particles. To promote the discovery of all modes, we run each method with an *exploration proposal*: a large Gaussian sample with standard deviation 0.30 that is selected with probability 0.01 and complements the

adaptive CMC, PMH or SAIS proposal (that is selected with probability 0.99). To generate perturbations, the vanilla CMC, PMH and SAIS methods rely on a uniform proposal on a ball of radius 0.10. The other methods are based on kernel selection and rely on uniform proposals on balls of four different radii: 0.01, 0.03, 0.10 and 0.30.

In Figure 6.7.2, we present the energy distance through iterations for each of our methods. All the methods except PMH reach the minimal distance, that is the average distance between two exact iid samples from the target. SAIS seems to be initially the fastest method, but its convergence speed decreases along the iterations and it reaches a lower final distance compared to our methods. CMC is the slower of our methods, because the kernel is not adapted in size, while the other methods are comparable with each other. The straight line for Vanilla CMC tends to confirm the exponential speed of the convergence that is proved in Section 6.4. The variance of the Energy Distance is given in Table 6.7.1. SAIS seems to have a high variance, as we observed that in some of the runs, the algorithm could not explore all the modes — we excluded these runs from the Energy distance plot — while CMC and MoKAs have lower variances.

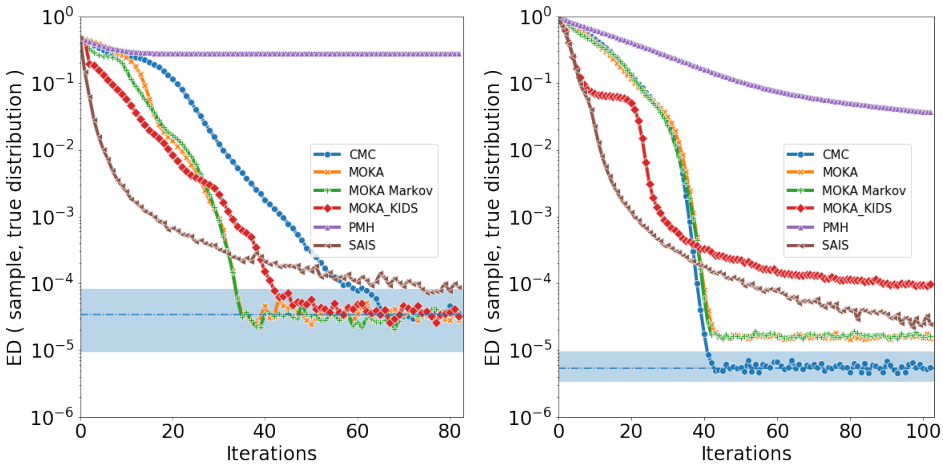

FIGURE 6.7.2: Mean energy distance to a true sample on 10 repetitions of the algorithm for the Banana-shaped distribution (left) and the eight-dimensional example (right). The dotted line represents the mean distance between two iid exact samples of size N from the target, computed over 100 independent realisations. The coloured area is the corresponding 90% prediction interval.

In Figure 6.7.3 we present a more in-depth analysis of the simulations. The acceptance rate of the vanilla CMC sampler is close to the one of PMH, but adaptive methods perform significantly better. This suggests that the proposal distribution that is created through our *advanced* methods is indeed closer to the target distribution, which should reflect positively on the variance of estimators. Although both MoKAs methods have a very similar behaviour in terms of convergence speed, we note that they select very different

weights. We believe that this is related to the L^1-like energy that is optimized in our MoKA-Markov implementation, and expect other criteria to exhibit different behaviours. Finally, we note that SAIS presents a large variance (unlike our method which produces consistent results across the runs). To remain fair with a method that can sometimes fail to converge, we only show 10 of the best among 50 runs for this algorithm.

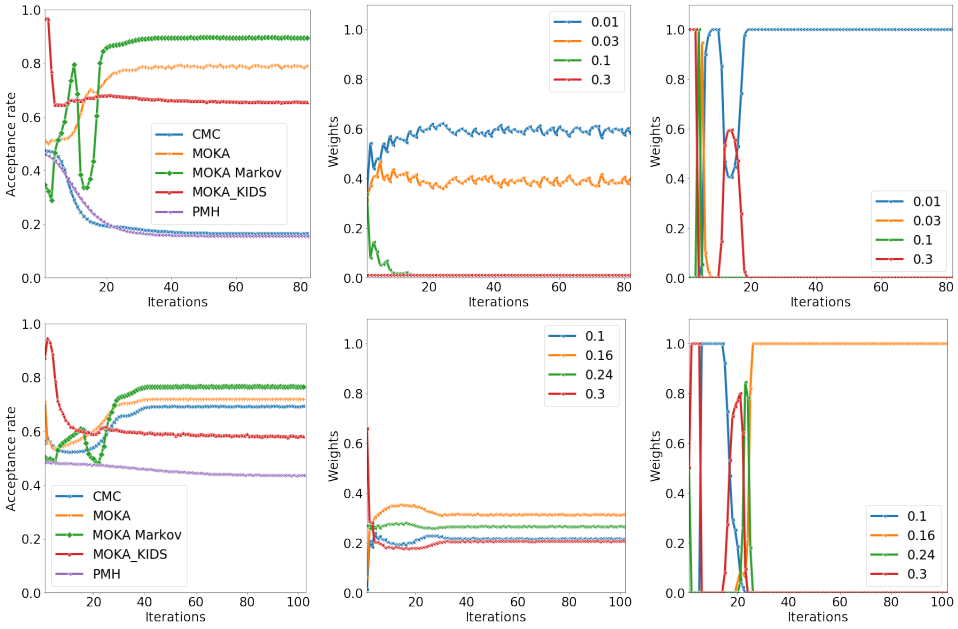

FIGURE 6.7.3: Convergence analysis for the Banana-shaped distribution (top row) and the 8-dimensional Gaussian mixture (bottom row). From left to right: acceptance rate, evolution of weights in MoKA and in MoKA-Markov.

6.7.2 Moderately large dimension

Our second target is constituted of two Gaussian distributions in dimension 8, with mean $(1/2 - 1/4\sqrt{8}, 1/2 + 1/4\sqrt{8}, \ldots, 1/2 + 1/4\sqrt{8})^{\mathrm{T}}$ and $(1/2 + 1/4\sqrt{8}, 1/2 - 1/4\sqrt{8}, \ldots, 1/2 - 1/4\sqrt{8})^{\mathrm{T}}$, and the same variance: $\sqrt{0.05}/2$. This example is inspired from the classical example introduced in [55, 134].

As the dimension increases, we also increase the number of particles to $N = 10^5$. We do not include an exploration proposal. We use vanilla CMC, PMH and SAIS with a single uniform proposal on a ball of radius 0.20, while the other methods based on kernel selection are given four different radii: 0.10, 0.16, 0.24 and 0.30. Due to the curse of dimensionality, the volumes of the balls that are induced by these radii are relatively smaller than in the previous experiment in dimension 2: this should reduce the exploration efficiency. We also slightly increase the number of iterations to 100.

In Figure 6.7.2 (right), we present the evolution of the Energy Distance. In this example, only CMC seems to reach the smallest possible distance. MoKA-KIDS first converges quickly towards a plateau as it visits the first mode, before finding the second one. The dimension of the problem may explain the relative failure of the adaptive methods, as they rely on the proximity of particles that are more isolated from each other in higher dimensional scenarios. As before (see Figure 6.7.3) MoKA-Markov and MoKA do not seem to converge to the same limit: MoKA chooses a mixture of kernels while our sparsity-inducing MoKA-Markov energy promotes the use of a single kernel during each *phase* of the convergence. In this example, we remark that SAIS seems more stable than in the previous experiment.

	CMC	MoKA	MoKA-Markov	MoKA-KIDS	PMH	SAIS
Banana-shaped	2.41e-05	2.25e-05	**1.91e-05**	2.04e-05	6.75e-04	6,07e-02
Gaussian	**1.74e-06**	2.32e-06	1.75e-06	5.29e-06	3.24e-04	1.03e-05

TABLE 6.7.1: Variance of the Energy distance at the last iteration for the targets.

6.8 Conclusion

Nonlinear MCMC samplers are appealing. They generalise more traditional methods and overcome many of their flaws. Getting back to the historical development of mathematical kinetic theory, we can advantageously simulate nonlinear Markov processes using systems of interacting particles. This versatility enables the development of a wide variety of algorithms that can tackle difficult sampling problems while remaining in a traditional Markovian framework. Although the implementation may, at first sight, seem computationally demanding, we have shown that modern GPU hardware can now enable the use of interacting particles for Monte Carlo sampling at scale.

Alongside its variants, the CMC algorithm can be implemented efficiently and leads to striking reductions in global convergence times. It relies on pairwise interactions to best leverage the information that is present in any given sample swarm, and thus make the most of each evaluation of the target distribution. CMC avoids the mixing issues of classical "one particle" methods such as Metropolis-Hastings, with a notable improvement of the convergence and mixing speed. In particular when dealing with multimodal distributions, where the relative weight of each mode is difficult to estimate. In practice, we thus expect that the benefits of this improved "sample efficiency" will outweigh the (small) computational overhead of our method for most applications.

We note that the present contribution shares similarities with some well-known and

recent nonlinear samplers, that are often based on non-Markovian importance sampling techniques. In the future, the joint development of Markovian and non-Markovian methods is likely to benefit both approaches: we may for instance improve the importance weights in SAIS-like methods as in the KIDS algorithm, or construct better proposal distributions in CMC which incorporate knowledge of (part of) the past. The theoretical study of such hybrid methods would however be challenging and require the development of new analytical tools.

Finally, one may think of extending the theoretical framework introduced here to other MCMC samplers, such as *nonlinear* PDMP samplers or *nonlinear* Langevin dynamics. This could open new problems in nonlinear analysis and statistics, both on the theoretical and computational sides.

Appendix

6.A Proof of Theorem 6.3.1

Let us start with the following lemma.

Lemma 6.A.1. *Let Θ be a proposal distribution which satisfies Assumptions 6.2.1, 6.2.2 and 6.2.3. Then the map*

$$\alpha : \mathcal{P}(E) \times E^2 \to \mathbb{R},\ (\mu, x, y) \mapsto \alpha_\mu(x, y) := \frac{\Theta_\mu(x|y)\pi(y)}{\Theta_\mu(y|x)\pi(x)},$$

is Lipschitz in the Wasserstein-1 distance, in the sense that there exists a constant $L_\Theta > 0$ (which depends also on π) such that for all $\mu, \nu \in \mathcal{P}(E)$ and $x, x', y, y' \in E$, it holds that:

$$|\alpha_\mu(x, y) - \alpha_\nu(x', y')| \leq L_\Theta\big(W_1(\mu, \nu) + |x - x'| + |y - y'|\big).$$

Proof. By the triangle inequality, it holds that:

$$|\alpha_\mu(x, y) - \alpha_\nu(x', y')| \leq \frac{\pi(y)}{\pi(x)}\left|\frac{\Theta_\mu(x|y)}{\Theta_\mu(y|x)} - \frac{\Theta_\nu(x'|y')}{\Theta_\nu(y'|x')}\right| + \frac{\Theta_\nu(x'|y')}{\Theta_\nu(y'|x')}\left|\frac{\pi(y)}{\pi(x)} - \frac{\pi(y')}{\pi(x')}\right|.$$

We bound each of the two terms on the right-hand side:

$$\begin{aligned}\frac{\pi(y)}{\pi(x)}\left|\frac{\Theta_\mu(x|y)}{\Theta_\mu(y|x)} - \frac{\Theta_\nu(x'|y')}{\Theta_\nu(y'|x')}\right| &\leq \frac{\pi(y)}{\pi(x)\Theta_\mu(y|x)}|\Theta_\mu(x|y) - \Theta_\nu(x'|y')| \\ &\quad + \frac{\pi(y)\Theta_\nu(x'|y')}{\pi(x)\Theta_\mu(x|y)\Theta_\mu(x'|y')}|\Theta_\mu(y|x) - \Theta_\nu(y'|x')| \\ &\leq \frac{LM_0}{m_0\kappa_-}\left(1 + \frac{\kappa_+}{\kappa_-}\right)\Big(W_1(\mu, \nu) + |x - x'| + |y - y'|\Big).\end{aligned}$$

and

$$\begin{aligned}\frac{\Theta_\nu(x'|y')}{\Theta_\nu(y'|x')}\left|\frac{\pi(y)}{\pi(x)}-\frac{\pi(y')}{\pi(x')}\right| &\leq \frac{\Theta_\nu(x'|y')}{\pi(x)\Theta_\nu(y'|x')}|\pi(y)-\pi(y')| \\ &\quad + \frac{\Theta_\nu(x'|y')\pi(y')}{\Theta_\nu(y'|x')\pi(x)\pi(x')}|\pi(x)-\pi(x')| \\ &\leq \frac{\|\pi\|_{\mathrm{Lip}}\kappa_+}{m_0\kappa_-}\left(|y-y'|+\frac{M_0}{m_0}|x-x'|\right),\end{aligned}$$

where $\|\pi\|_{\mathrm{Lip}}$ denotes the Lipschitz norm of π. Gathering everything gives the result with

$$L_\Theta = \frac{M_0}{m_0}\left(\frac{L}{\kappa_-}\left(1+\frac{\kappa_+}{\kappa_-}\right)+\frac{\|\pi\|_{\mathrm{Lip}}\kappa_+}{m_0\kappa_-}\right).$$

□

Proof (of Theorem 6.3.1). The strategy of the proof of Theorem 6.3.2 will be based on coupling arguments inspired by [307, 221], adapted from [138] and already presented in Chapter 4. We start by the following trajectorial representation of the nonlinear Markov chain $(\overline{X}_t)_t$ defined by the transition kernel (6.1).

Definition 6.A.2 (Nonlinear process)**.** Let $\overline{X}_0 \sim \mu_0$ be an initial state where $\mu_0 \in \mathcal{P}(E)$. The state $\overline{X}_t$ at time $t \in \mathbb{N}$, $t \geq 1$, is constructed from $\overline{X}_{t-1}$ and the law of $\overline{X}_{t-1}$ denoted by $\mu_{t-1} \in \mathcal{P}(E)$ as follows.

1. Take a proposal a random variable $\overline{Y}_t \sim \Theta_{\mu_{t-1}}(\cdot|\overline{X}_{t-1})$
2. Compute the ratio

$$\alpha_{\mu_{t-1}}(\overline{X}_{t-1},\overline{Y}_t) := \frac{\Theta_{\mu_{t-1}}(\overline{X}_{t-1}|\overline{Y}_t)\pi(\overline{Y}_t)}{\Theta_{\mu_{t-1}}(\overline{Y}_t|\overline{X}_{t-1})\pi(\overline{X}_{t-1})}.$$

3. Take $\overline{U}_t \sim \mathcal{U}([0,1])$ and if $\overline{U}_t \leq h\big(\alpha_{\mu_{t-1}}(\overline{X}_{t-1},\overline{Y}_t)\big)$, then accept the proposal, else reject it:

$$\overline{X}_t = \overline{X}_{t-1}\mathbb{1}_{\overline{U}_t \geq h(\alpha_{\mu_{t-1}}(\overline{X}_{t-1},\overline{Y}_t))} + \overline{Y}_t\mathbb{1}_{\overline{U}_t \leq h(\alpha_{\mu_{t-1}}(\overline{X}_{t-1},\overline{Y}_t))}.$$

From now on we consider N independent copies $(\overline{X}^i_t)_t$, $i \in \{1,\dots,N\}$, of the nonlinear process defined by Definition 6.A.2. We then construct a coupled particle process $(X^i_t)_t$ such that for all $i \in \{1,\dots,N\}$, initially $X^i_0 = \overline{X}^i_0 \sim \mu_0$ and for each time $t \in \mathbb{N}$ we take:

1. the same jump decision random variables $U^i_t = \overline{U}^i_t \sim \mathcal{U}([0,1])$,

2. optimal proposals of the form $Y_t^i = s(\overline{Y}_t^i)$ where s is an optimal transport map between $\Theta_{\mu_{t-1}}(\cdot|\overline{X}_{t-1}^i)$ and $\Theta_{\hat{\mu}_{t-1}^N}(\cdot|X_{t-1}^i)$. Since these two probability measures are absolutely continuous with respect to the Lebesgue measure, the existence of such optimal transport map (Monge problem) is proved for instance in [77] or [51]. By definition, the pathwise error between the proposals can thus be controlled by

$$\begin{aligned}\mathbb{E}\big[|Y_t^i - \overline{Y}_t^i|\big|\mathcal{F}_{t-1}\big] &= W_1\Big(\Theta_{\hat{\mu}_{t-1}^N}(\cdot|X_{t-1}^i), \Theta_{\mu_{t-1}}(\cdot|\overline{X}_{t-1}^i)\Big)\\ &\le W_1\Big(\Theta_{\hat{\mu}_{t-1}^N}(\cdot|X_{t-1}^i), \Theta_{\bar{\mu}_{t-1}^N}(\cdot|\overline{X}_{t-1}^i)\Big)\\ &\quad + W_1\Big(\Theta_{\bar{\mu}_{t-1}^N}(\cdot|\overline{X}_{t-1}^i), \Theta_{\mu_{t-1}}(\cdot|\overline{X}_{t-1}^i)\Big)\end{aligned}$$

where $\bar{\mu}_t^N = \frac{1}{N}\sum_{i=1}^N \delta_{\overline{X}_t^i}$ and $\mathcal{F}_t$ is the σ-algebra generated by the processes up to time $t \in \mathbb{N}$. We conclude that:

$$\mathbb{E}\big[|Y_t^i - \overline{Y}_t^i|\big|\mathcal{F}_{t-1}\big] \le W_1(\hat{\mu}_{t-1}^N, \bar{\mu}_{t-1}^N) + |X_{t-1}^i - \overline{X}_{t-1}^i| + e_t^N \tag{6.25}$$

where the error term e_t^N only depends on (the laws of) the N independent nonlinear processes $(\overline{X}_t^i)_t$:

$$e_t^N := W_1(\bar{\mu}_{t-1}^N, \mu_{t-1}).$$

Let $t \in \mathbb{N}$, $t \ge 1$. It holds that:

$$\begin{aligned}\mathbb{E}\big[|X_t^i - \overline{X}_t^i|\big|\mathcal{F}_{t-1}\big] &= \mathbb{E}\big[|Y_t^i - \overline{Y}_t^i|\mathbb{1}_{U_t^i \le \min(h_t^i, \overline{h}_t^i)}\big|\mathcal{F}_{t-1}\big]\\ &\quad + |X_{t-1}^i - \overline{X}_{t-1}^i|\mathbb{P}\big(U_t^i \ge \max(h_t^i, \overline{h}_t^i)\big|\mathcal{F}_{t-1}\big)\\ &\quad + \mathbb{E}\big[|X_t^i - \overline{Y}_t^i|\mathbb{1}_{h_t^i \le U_t^i \le \overline{h}_t^i}\big|\mathcal{F}_{t-1}\big]\\ &\quad + \mathbb{E}\big[|Y_t^i - \overline{X}_t^i|\mathbb{1}_{\overline{h}_t^i \le U_t^i \le h_t^i}\big|\mathcal{F}_{t-1}\big]\end{aligned}$$

where we write for short:

$$h_t^i \equiv h\big(\alpha_{\hat{\mu}_t^N}(X_t^i, Y_t^i)\big) \quad \text{and} \quad \overline{h}_t^i \equiv h\big(\alpha_{\mu_t}(\overline{X}_t^i, \overline{Y}_t^i)\big).$$

we deduce that:

$$\begin{aligned}\mathbb{E}\big[|X_t^i - \overline{X}_t^i|\big|\mathcal{F}_{t-1}\big] &\le W_1(\hat{\mu}_{t-1}^N, \bar{\mu}_{t-1}^N) + 2|X_{t-1}^i - \overline{X}_{t-1}^i|\\ &\quad + 2M_0(\mathbb{P}(h_t^i \le U_t^i \le \overline{h}_t^i\big|\mathcal{F}_{t-1}) + \mathbb{P}(\overline{h}_t^i \le U_t^i \le h_t^i\big|\mathcal{F}_{t-1})) + e_t^N\end{aligned} \tag{6.26}$$

The last two probabilities are bounded by $\mathbb{E}\big[|h_t^i - \overline{h}_t^i| \big| \mathcal{F}_{t-1}\big]$. Assuming that h is L_h-Lipschitz for a constant $L_h > 0$, it holds that:

$$|h_t^i - \overline{h}_t^i| \leq L_h \Big| \alpha_{\hat{\mu}_{t-1}}(X_{t-1}^i, Y_t^i) - \alpha_{\mu_{t-1}}(\overline{X}_{t-1}^i, \overline{Y}_t^i) \Big|.$$

Let $\bar{\mu}_t^N$ be the empirical measure of the N nonlinear Markov processes $\overline{X}_t^i$ at time t. It holds that:

$$\begin{aligned} |h_t^i - \overline{h}_t^i| \leq L_h \Big| \alpha_{\hat{\mu}_{t-1}}(X_{t-1}^i, Y_t^i) - \alpha_{\bar{\mu}_{t-1}}(\overline{X}_{t-1}^i, \overline{Y}_t^i) \Big| \\ + L_h \Big| \alpha_{\bar{\mu}_{t-1}}(\overline{X}_{t-1}^i, \overline{Y}_t^i) - \alpha_{\mu_{t-1}}(\overline{X}_{t-1}^i, \overline{Y}_t^i) \Big| \end{aligned}$$

Using Lemma 6.A.1 we get:

$$|h_t^i - \overline{h}_t^i| \leq C_\Theta \left(W_1(\hat{\mu}_{t-1}^N, \bar{\mu}_{t-1}^N) + |X_{t-1}^i - \overline{X}_{t-1}^i| + |Y_t^i - \overline{Y}_t^i| + e_t^N \right),$$

with $C_\Theta := L_h L_\Theta$. Therefore:

$$\mathbb{E}\big[|X_t^i - \overline{X}_t^i| \big| \mathcal{F}_{t-1}\big] \leq (1 + C_\Theta) \left(|X_{t-1}^i - \overline{X}_{t-1}^i| + W_1(\hat{\mu}_{t-1}^N + \bar{\mu}_{t-1}^N) \right) + (1 + 2C_\Theta) e_t^N.$$

Let us define:

$$S_t := \frac{1}{N} \sum_{i=1}^N |X_t^i - \overline{X}_t^i|.$$

Summing the previous expression for i from 1 to N and dividing by N gives the following estimate for S_t:

$$\mathbb{E}[S_t | \mathcal{F}_{t-1}] \leq 2 \left(1 + C_\Theta\right) S_{t-1} + (1 + 2C_\Theta) e_t^N \tag{6.27}$$

where we have used the fact that

$$W_1(\hat{\mu}_{t-1}^N, \bar{\mu}_{t-1}^N) \leq S_t.$$

Taking the expectation in (6.27), we deduce that:

$$\mathbb{E}[S_t] \leq (1 + C_\Theta) \, \mathbb{E}[S_{t-1}] + C_\Theta \mathbb{E}[e_t^N] \tag{6.28}$$

where the value of the constant C_Θ has been updated by $C_\Theta \leftarrow 1 + 2C_\Theta$.

The error term can be controlled uniformly on t using [62, Theorem 5.8] or [162]. In

particular, since π is a smooth probability density function on a compact set, it has finite moments of all orders and therefore it follows from [162, Theorem 1] that:

$$\forall t \in \mathbb{N},\ \mathbb{E}[e_t^N] \leq \beta(N) \tag{6.29}$$

where $\beta(N)$ is defined by (6.6).

One can easily prove by induction that:

$$\mathbb{E}[S_t] \leq C_\Theta \beta(N) \sum_{s=0}^{t-1} e^{C_\Theta s} \leq \beta(N) \frac{C_\Theta}{\mathrm{e}^{C_\Theta} - 1} \mathrm{e}^{tC_\Theta} \tag{6.30}$$

By symmetry of the processes, all the quantities $\mathbb{E}[|X_t^i - \overline{X}_t^i|]$ are equal and their common value is $\mathbb{E}[S_t]$. The result follows. □

Remark 6.A.3 (Moderate interaction, part 2). The result of Theorem 6.3.1 provides an explicit convergence rate in terms of N. Similarly to what has been presented in Chapter 4, this could be used to understand more precisely the moderate interaction assumption mentioned in Remark 6.5.1. In the case $\Theta_\mu(\mathrm{d}y|x) = K \star \mu(y)\mathrm{d}y$, one can take at the particle level (*i.e* in Algorithm 1) an interaction kernel $K \equiv K^N$ which depends on N and such that its size $\sigma_N \to 0$ as $N \to +\infty$ (and thus $K^N \to \delta_0$). As a consequence the constant $C_\Theta \equiv C_\Theta^N$ in Theorem 6.3.1 would depend on N. Since we have a precise control on $\beta(N)$ we can choose σ_N such that the following convergence still holds:

$$\beta(N)\mathrm{e}^{tC_\Theta^N} \underset{N\to+\infty}{\longrightarrow} 0.$$

In particular, σ_N should not converges to zero too fast, justifying the moderate interaction terminology introduced in [273]. In the limit $N \to +\infty$ we then obtain that the emprirical measure $\hat{\mu}_t^N$ converges towards the t-th iterate of the transition operator (6.4) with the degenerate choice of proposal distribution $\Theta_f(\mathrm{d}y|x) = f(y)\mathrm{d}y$ which makes sense as soon as $f \in \mathcal{P}_0^{\mathrm{ac}}(E)$. We refer the reader to [221] and [138] for two examples of propagation of chaos results under a moderate interaction assumption. Note that this result is mainly of theoretical interest as it does not give sharp estimates on how slow σ_N should decrease to zero.

Remark 6.A.4 (About the assumptions). In order to prove a propagation of chaos property, it is usually assumed that the parameters of the problem are Lipschitz [307, 252]. This corresponds to the two Lipschitz assumptions 6.2.2 and 6.2.3. Propagation of chaos in non-Lipschitz settings is a more difficult problem as explained in Chapter 3.

Assumption 6.1.1 and Assumption 6.2.1 should be understood as technical assumptions. In the proof of Theorem 6.3.2, we use the fact that the acceptance ratio is Lipschitz (Lemma 6.A.1) which follows directly from Assumptions 6.1.1, 6.2.1 and 6.2.2. However, we could relax the compactness assumption 6.1.1 and keep the same Lipschitz property by replacing Assumptions 6.1.1, 6.2.1 and 6.2.2 by the following assumption.

Assumption 6.A.5. *The target distribution π does not vanish on E and the map*

$$\mathcal{P}(E) \times E^2 \to \mathbb{R}, \quad (\mu, x, y) \mapsto g_\mu(y|x) := \frac{\Theta_\mu(y|x)}{\pi(y)}$$

satisfies the two following properties.

- ***(Boundedness).*** *There exist two constants $\kappa_- > 0$ and $\kappa_+ > 0$ such that*

$$\forall (x, y) \in E^2, \quad \kappa_- \leq g(y|x) \leq \kappa_+.$$

- ***(Lipschitz).*** *There exists a constant $L > 0$ such that*

$$\forall (\mu, x, y), (\nu, x', y') \in \mathcal{P}(E) \times E^2,$$
$$|g_\mu(y|x) - g_\nu(y'|x')| \leq \Big(W_1(\mu, \nu) + |x - x'| + |y - y'| \Big).$$

In practice, this would necessitate a precise control of the tails of π and of the proposal distribution. It seems easier for us to check the compactness and boundedness Assumptions 6.1.1, 6.2.1 and 6.2.2 (possibly up to truncating the support of π and replacing it by a compact set).

6.B Continuous time version

As mentioned in Section 6.4, entropy methods are widely used in a continuous-time context, in particular for the long-time analysis of nonlinear PDEs [222]. In this section, we define a continuous-time version of Algorithm 1, we show that the mean-field limit towards the solution of a nonlinear PDE and we prove the exponential long-time convergence of its solution towards π. This last step also motivates the discrete-time analysis in Section 6.4. Finally, the application of these ideas to the classical linear Metropolis-Hastings case leads (formally) to a convergence result obtained earlier in [137] with other techniques (Section 6.B.4).

6.B.1 Continuous-time particle system

The N-particle system constructed by Algorithm 1 is a standard Markov chain which can be turned into a continuous-time Markov process by subordinating it to a Poisson process, as explained in [47, Chapter 8, Definition 2.2]. Namely, let $(N_t)_{t\geq 0}$ be a Poisson process independent of all the other random variables and with constant parameter equal to 1. The continuous-time particle system is defined at time $t \geq 0$ by $\tilde{X}_t^i := X_{N_t}^i$ for $i \in \{1, \dots, N\}$, where $X_{N_t}^i$ is the i-th particle constructed by Algorithm 1 at iteration N_t. For notational simplicity, in the remaining of this section, we drop the tilde notation and simply write $X_t^i \equiv \tilde{X}_t^i$ with $t \in [0, +\infty)$.

The first step is the mean-field limit analog of Theorem 6.3.1 and is also very close to Theorem 4.2.13 in Chapter 4.

Theorem 6.B.1. *Let the particles $X_0^i \sim f_0$ be initially i.i.d. with common law $f_0 \in \mathcal{P}_0^{\mathrm{ac}}(E)$. Under the assumptions of Theorem 6.3.1, the (random) continuous-time empirical measure $\hat{\mu}_t^N = \frac{1}{N}\sum_{i=1}^N \delta_{X_t^i}$ at any time $t \geq 0$ satisfies*

$$\mathbb{E}W_1(\hat{\mu}_t^N, f_t) \leq C_1 \beta(N) \mathrm{e}^{tC_2},$$

where $C_1, C_2 > 0$ are two absolute constants, $\beta(N)$ is defined by (6.6) and f_t is the solution of the nonlinear PDE

$$\partial_t f_t = \mathcal{T}[f_t] - f_t, \tag{6.31}$$

with initial condition f_0.

Proof. It is enough to prove the analog of (6.7) in the time continuous framework. The end of the proof will then follows similarly as in Corollary 6.3.2. The nonlinear process $(\overline{X}_t)_t$ with law f_t is defined as follows.

1. Let $(T_n)_{n\in\mathbb{N}}$ the increasing sequence of jump times of the Poisson process $(N_t)_t$ with $T_0 = 0$ and initially $\overline{X}_0 \sim f_0$.
2. Between two jump times, at any $t \in [T_n, T_{n+1})$, $\overline{X}_t = \overline{X}_{T_n}$.
3. At each jump time T_n, we sample a proposal random variable $\overline{Y}_{T_n} \sim \Theta_{f_{T_n}}(\cdot|\overline{X}_{T_n})$ and accept or reject it as in Definition 6.A.2.

Then we construct two coupled systems of N independent nonlinear processes $(\overline{X}_t^i)_t$ and N particles as in the proof of Theorem 6.3.1. We define similarly $S_t := \frac{1}{N}\sum_{i=1}^N \mathbb{E}|X_t^i - \overline{X}_t^i|$. As in the discrete time case (6.27), at any jump time T_n, it holds that

$$\mathbb{E}[S_{T_n}|\mathcal{F}_{T_n^-}] \leq 2\,(1 + C_\Theta)\, S_{T_{n-1}} + C_\Theta \beta(N).$$

Taking the conditional expectation with respect to $\mathcal{G}_n = \sigma(T_1, T_2 - T_1, \dots, T_n - T_{n-1})$, we obtain:

$$\mathbb{E}[S_{T_n}|\mathcal{G}_n] \leq 2\,(1 + C_\Theta)\,\mathbb{E}[S_{T_{n-1}}|\mathcal{G}_{n-1}] + C_\Theta \beta(N).$$

And thus, for all $n \in \mathbb{N}$,

$$\mathbb{E}[S_{T_n}|\mathcal{G}_n] \leq \beta(N)\frac{C_\Theta}{\mathrm{e}^{C_\Theta} - 1}\mathrm{e}^{C_\Theta n}.$$

Since N_t follows a Poisson law with parameter t, it holds that:

$$\begin{aligned}
\mathbb{E}[S_{T_n}\mathbb{1}_{N_t=n}] &= \mathbb{E}[\mathbb{E}[S_{T_n}\mathbb{1}_{N_t=n}|\mathcal{G}_{n+1}]] \\
&= \mathbb{E}[\mathbb{1}_{N_t=n}\mathbb{E}[S_{T_n}|\mathcal{G}_n]] \\
&\leq \beta(N)\frac{C_\Theta}{\mathrm{e}^{C_\Theta} - 1}\mathrm{e}^{C_\Theta n}\mathbb{P}(N_t = n),
\end{aligned}$$

where the second inequality comes from the fact that the event $\{N_t = n\}$ is $\mathcal{G}_{n+1}$ measurable and the fact that S_{T_n} is independent from $T_{n+1} - T_n$. As a consequence, since $S_t = S_{T_{N_t}}$ and $\mathbb{P}(N_t = n) = \mathrm{e}^{-t}t^n/n!$, we conclude that:

$$\mathbb{E}[S_t] = \mathbb{E}[S_{T_{N_t}}] = \sum_{n=0}^{+\infty}\mathbb{E}[S_{T_n}\mathbb{1}_{N_t=n}] \leq \beta(N)\frac{C_\Theta}{\mathrm{e}^{C_\Theta} - 1}\exp(t(\mathrm{e}^{C_\Theta} - 1)).$$

□

6.B.2 Convergence of the nonlinear process

The analog of Theorem 6.4.2 in the continuous-time setting is the following theorem.

Theorem 6.B.2 (Convergence of the Nonlinear Process)**.** *Let Θ a proposal distribution which satisfies Assumption 6.2.6. Let $f_0 \in \mathcal{P}_0^{\mathrm{ac}}(E)$ and let f_t be the solution at time $t \in [0, +\infty)$ of the nonlinear PDE* (6.31)*. Then for all $t \geq 0$, it holds that:*

$$\|f_t - \pi\|_{\mathrm{TV}} \leq C_0\mathrm{e}^{-\lambda t},$$

where $C_0 > 0$ depends only on f_0 and π and where

$$\lambda := c^- \left(\inf_x \frac{f_0(x)}{\pi(x)}\right) h(1) > 0. \tag{6.32}$$

Note that in the continuous-time case, Assumption 6.2.4 is not required.

We recall that given a convex function $\phi : [0, +\infty) \to [0, +\infty)$ such that $\phi(1) = 0$, the relative entropy $\mathcal{H}[f|\pi]$ and dissipation $\mathcal{D}[f|\pi]$ of a probability density $f \in \mathcal{P}^{\mathrm{ac}}(E)$ with

respect to π are defined respectively by

$$\mathcal{H}[f|\pi] := \int_E \pi(x)\phi\left(\frac{f(x)}{\pi(x)}\right)\mathrm{d}x, \quad \mathcal{D}[f|\pi] := -\int_E \phi'\left(\frac{f(x)}{\pi(x)}\right)\big(\mathcal{T}[f](x) - f(x)\big)\mathrm{d}x.$$

In the continuous time framework when f_t solves (6.31), the entropy and dissipation are simply linked by the relation

$$\frac{\mathrm{d}}{\mathrm{d}t}\mathcal{H}[f_t|\pi] = -\mathcal{D}[f_t|\pi] \leq 0, \tag{6.33}$$

and therefore we conclude immediately that the entropy is non increasing (which is Lemma 6.4.5 in the discrete setting). A consequence of this fact is an alternative proof of Lemma 6.4.1.

Lemma 6.B.3. *Let f_t be the solution of the integro-differential equation* (6.31) *with initial condition $f_0 \in \mathcal{P}_0^{\mathrm{ac}}(E)$. Then*

$$\inf_{x\in E}\frac{f_t(x)}{\pi(x)} \geq \inf_{x\in E}\frac{f_0(x)}{\pi(x)}, \quad \sup_{x\in E}\frac{f_t(x)}{\pi(x)} \leq \sup_{x\in E}\frac{f_0(x)}{\pi(x)}.$$

Proof. Let us denote

$$m := \inf_{x\in E}\frac{f_0(x)}{\pi(x)} \quad \text{and} \quad M := \sup_{x\in E}\frac{f_0(x)}{\pi(x)}.$$

Let us take $\phi : [0, +\infty) \to [0, +\infty)$ a convex function such that $\phi \equiv 0$ on the segment $[m, M]$ and $\phi > 0$ elsewhere. Note that since f_0 and π are both probability densities, it holds that $m < 1$ and $M > 1$ and thus $\phi(1) = 0$. The entropy-dissipation relation (6.33) gives:

$$\frac{\mathrm{d}}{\mathrm{d}t}\mathcal{H}[f_t|\pi] \leq 0$$

and therefore for all $t \geq 0$,

$$\mathcal{H}[f_t|\pi] \leq \mathcal{H}[f_0|\pi] = 0$$

by definition of ϕ. As a consequence and since $\phi \geq 0$ and $\pi > 0$ on E, it holds that for all $t \geq 0$ and all $x \in E$,

$$\phi\left(\frac{f_t(x)}{\pi(x)}\right) = 0,$$

which implies that

$$\forall x \in E, \quad m \leq \frac{f_t(x)}{\pi(x)} \leq M.$$

□

In order to prove Theorem 6.B.2, we follow the classical steps which are detailed for instance in [222, Section 1.3] and can be applied to various linear and nonlinear jump and diffusion processes.

1. Compute the dissipation $\mathcal{D}[f_t|\pi] = -\frac{\mathrm{d}}{\mathrm{d}t}\mathcal{H}[f_t|\pi]$.

2. Prove that the dissipation can be bounded from below by a multiple of the entropy: for a constant $\lambda > 0$,
$$\mathcal{D}[f_t|\pi] \geq \lambda \mathcal{H}[f_t|\pi].$$

3. Apply Gronwall lemma to the relation $\frac{\mathrm{d}}{\mathrm{d}t}\mathcal{H}[f_t|\pi] \leq \lambda \mathcal{H}[f_t|\pi]$ to obtain the exponential decay of the entropy:
$$\mathcal{H}[f_t|\pi] \leq \mathcal{H}_0 \mathrm{e}^{-\lambda t}.$$

4. Show that the entropy controls the TV distance and conclude that for some constants $c, C_0 > 0$:
$$\|f_t - \pi\|_{\mathrm{TV}} \leq c\mathcal{H}[f_t|\pi] \leq C_0 \mathrm{e}^{-\lambda t}.$$

Proof (of Theorem 6.B.2). Let $\phi(s) = \frac{1}{2}(s-1)^2$. Most of the computations are the same as in the discrete-time case. From the entropy-dissipation relation (6.33), Lemma 6.B.3 and Lemma 6.4.6, it follows that

$$\begin{aligned}\frac{\mathrm{d}}{\mathrm{d}t}\mathcal{H}[f_t|\pi] &= -\mathcal{D}[f_t|\pi] \\ &\leq -\frac{c^-(m)h(1)}{2}\iint_{E\times E}\pi(x)\pi(y)\left|\frac{f_t(x)}{\pi(x)} - \frac{f_t(y)}{\pi(y)}\right|^2 \mathrm{d}x\mathrm{d}y = -2c^-(m)h(1)\mathcal{H}[f_t|\pi],\end{aligned}$$

where $m := \inf_{x\in E} f_0(x)/\pi(x)$. Using Gronwall's inequality we then deduce that:

$$\mathcal{H}[f_t|\pi] \leq \mathcal{H}[f_0|\pi]\mathrm{e}^{-2c^-(m)h(1)t}.$$

The conclusion follows from the Cauchy-Schwarz inequality by writing

$$\|f_t - \pi\|_{\mathrm{TV}} = \int_E |f_t(x) - \pi(x)|\mathrm{d}x = \int_E \sqrt{\pi}\sqrt{\pi}\left|\frac{f_t(x)}{\pi(x)} - 1\right|\mathrm{d}x \leq \sqrt{2\mathcal{H}[f_t|\pi]},$$

where we have used the fact that the TV norm is equal to the L^1 norm of the probability density functions. □

Remark 6.B.4. Another natural choice for ϕ would be $\phi(s) = s\log s - s + 1$. The relative entropy is in this case equal to the Kullback-Leibler divergence. However, the dissipation term becomes in this case:

$$\mathcal{D}[f_t|\pi] = \frac{1}{2}\iint_{E\times E} W_{f_t}(x \to y)\pi(x)\left(\frac{f_t(x)}{\pi(x)} - \frac{f_t(y)}{\pi(y)}\right) \times \left(\log\left(\frac{f_t(x)}{\pi(x)}\right) - \log\left(\frac{f_t(y)}{\pi(y)}\right)\right)\mathrm{d}x\mathrm{d}y,$$

and it is not clear that it can be bounded from below by the relative entropy. Note that this dissipation functional is very similar to the one obtained in the study of the Boltzmann equation (in this context, the Kullback-Leibler divergence is also called the Boltzmann entropy). The long-time asymptotics of this equation is a long-standing problem and the specific question of whether the dissipation controls the entropy is the object of a famous conjecture by Cercignani [135, 325]. In our case, we know that the Kullback-Leibler divergence is decreasing with time but all this suggests that its exponential decay could be harder to obtain or could hold only in specific cases.

Putting together Theorem 6.B.1 and Theorem 6.B.2 leads to the following corollary which is the continuous-time analog of Theorem 6.2.9.

Corollary 6.B.5. *Under the assumptions of Theorem 6.B.1 and Theorem 6.B.2, for any $t > 0$ and $N > 1$ it holds that*

$$\mathbb{E}[W_1(\hat{\mu}_t^N, \pi)] \leq C_1\beta(N)\mathrm{e}^{C_2 t} + C_3\mathrm{e}^{-\lambda t},$$

where $\beta(N)$ is given by (6.6)*, $\lambda > 0$ is given by* (6.32) *and $C_1, C_2, C_3 > 0$ are absolute constants.*

Proof. By the triangle inequality, it holds that

$$\mathbb{E}[W_1(\hat{\mu}_t^N, \pi)] \leq \mathbb{E}[W_1(\hat{\mu}_t^N, f_t)] + \mathbb{E}[W_1(f_t, \pi)].$$

The first term on the right-hand side is bounded by $C_1\beta(N)\mathrm{e}^{C_2 t}$ by Theorem 6.B.1. For the second term on the right-hand side, we first note that on the compact set E, the total variation norm controls the Wasserstein-1 distance [328, Theorem 6.15]. The conclusion therefore follows from Theorem 6.B.2. □

6.B.3 Links between the discrete- and continuous-time versions

The discrete-time counterpart of the entropy-dissipation relation (6.33) is the relation (6.17). The difference $\mathcal{H}[\mu_{t+1}|\pi] - \mathcal{H}[\mu_t|\pi]$ is the discrete analog of a time derivation. The main difference with the continuous-time entropy-dissipation relation is the additional non negative term on the right-hand side of (6.17). The role of the technical Assumption 6.2.4 is to ensure that this non negative term remains smaller than the dissipation in order to close the argument as in the continuous-time case. Since this term does not appear in the continuous-time setting, Assumption 6.2.4 is not required to prove Theorem 6.B.2.

Assumption 6.2.4 is actually better understood when the discrete-time relation (6.10) is seen as an explicit Euler discretization scheme (6.12) of the nonlinear PDE (6.31). More precisely, the numerical scheme (6.12) can be re-written

$$\mu_{t+1} = \mu_t + \Delta t Q[\mu_t], \tag{6.34}$$

where

$$Q[\mu](\mathrm{d}x) := \int_E \pi(x) W_\mu(x \to y) \left(\frac{\mu(\mathrm{d}y)}{\pi(y)} \mathrm{d}x - \frac{\mu(\mathrm{d}x)}{\pi(x)} \mathrm{d}y \right).$$

Note that $\mathcal{T}[\mu] = \mu + Q[\mu]$. In order to check that this numerical scheme preserves the continuous-time entropy-dissipation relation (6.33), let us write for a general function the second-order Taylor expansion:

$$\mathcal{H}[\mu_{t+1}|\pi] \simeq \mathcal{H}[\mu_t|\pi] - \Delta t \mathcal{D}[\mu_t|\pi] + \frac{\Delta t^2}{2} \int_E \pi(x) \phi'' \left(\frac{\mu_t(x)}{\pi(x)} \right) \left| \frac{Q[\mu_t](x)}{\pi(x)} \right|^2 \mathrm{d}x.$$

Since ϕ is a convex function, the second-order term of the Taylor expansion is non negative but it is dominated by the non positive first-order term (equal to minus the dissipation) for Δt small enough. For this reason, the explicit Euler discretization scheme does not unconditionally preserve the entropy structure of the continuous-time PDE. Since $W_\mu(x \to y) = \Theta_\mu(y|x) h(\alpha_\mu(x,y))$, the operator $Q[\mu]$ is proportional to h and it is equivalent to assume $\Delta t < 1$ or $h < 1$. With the notations of Section 6.4.3, the time-step is $\Delta t \equiv \eta$ and Assumption 6.2.4 can therefore be interpreted as a "numerical" condition to preserve the entropy structure of the discrete scheme. We did not manage to prove the exponential convergence of the discrete scheme when $\Delta t \equiv \eta = 1$. However, it is still possible to prove the convergence of the discrete scheme without rate and for a weaker topology using Theorem 6.B.2 and a compactness argument.

Corollary 6.B.6 (Convergence of the discrete scheme)**.** *Let $(\mu_t)_{t\in\mathbb{N}}$ be the sequence of probability laws defined by the recurrence relation* (6.10) *(i.e. by the discrete scheme* (6.34)

with $\Delta t = 1$). Let $\mu_0 \in \mathcal{P}_0^{\mathrm{ac}}(E)$ be the initial condition and let Θ satisfy Assumption 6.2.6. Then it holds that $\mu_t \to \pi$ as $t \to +\infty$ for the weak convergence of probability measures.

Proof. The sequence $(\mu_t)_{t\in\mathbb{N}}$ is tight because E is compact so it admits a converging subsequence. The limit of any converging subsequence is a fixed point of the operator $\mathcal{T}$. Since the convergence result stated in Theorem 6.B.2 does not depend on the initial condition in $\mathcal{P}_0^{\mathrm{ac}}(E)$, it implies that π is the unique fixed point of the operator $\mathcal{T}$ in $\mathcal{P}_0^{\mathrm{ac}}(E)$ and therefore, all the converging subsequences of $(\mu_t)_t$ converges towards π, which implies the convergence of the whole sequence. □

6.B.4 The Metropolis-Hastings case

The following theorem revisits the main result of [137] regarding the convergence rate of the Metropolis-Hastings algorithm, here formally proved with the entropy techniques introduced in Section 6.B.2 and in the continuous-time setting for simplicity.

Theorem 6.B.7 (Formal)**.** *Let us consider the linear case outlined in Section 6.5.1 with $q(y|x) = K_\sigma(x-y)$, where K_σ is a fixed symmetric random walk kernel of size $\sigma > 0$ (typically a Gaussian kernel with standard deviation σ). Assume that, as $\sigma \to 0$, the random-walk kernel K_σ satisfies for any smooth function $\varphi \in C^\infty(\mathbb{R}^d)$:*

$$\int_E \varphi(x) K_\sigma(x) \mathrm{d}x = \varphi(0) + \frac{1}{2}\sigma^2 \Delta\varphi(0) + o(\sigma^2). \tag{6.35}$$

Assume that π and E are such that the following Poincaré inequality holds:

$$\int_E u(x)^2 \pi(x)\mathrm{d}x - \left(\int_E u(x)\pi(x)\mathrm{d}x\right)^2 \leq \frac{1}{\lambda_P}\int_E |\nabla u|^2(x)\pi(x)\mathrm{d}x \tag{6.36}$$

for all functions u in the weighted Sobolev space $H^1_\pi(E)$ and for a constant $\lambda_P > 0$. Then, as $\sigma \to 0$, it holds that:

$$\|f_t - \pi\|_{\mathrm{TV}} \leq C_0 \mathrm{e}^{-\frac{1}{2}\sigma^2(\lambda_P + o(1))t},$$

for a constant $C_0 > 0$ which depends only on f_0 and π.

Proof. The formal Taylor expansion (6.35) as $\sigma \to 0$ applied to (6.33) leads to

$$\mathcal{D}_\phi[f_t|\pi] = \frac{\sigma^2}{2}\int_E \pi(x)\phi''\left(\frac{f_t(x)}{\pi(x)}\right)\left|\nabla_x\left(\frac{f_t}{\pi}\right)\right|^2 \mathrm{d}x + o(\sigma^2). \tag{6.37}$$

Taking $\phi(s) = \frac{1}{2}(s-1)^2$ gives:

$$\mathcal{D}_\phi[f_t|\pi] = \frac{\sigma^2}{2}\int_E \pi \left|\nabla\left(\frac{f_t}{\pi}\right)\right|^2 \mathrm{d}x + o(\sigma^2).$$

Using the Poincaré inequality with the function $u = f_t/\pi$, we obtain:

$$\mathcal{D}_\phi[f_t|\pi] \geq \frac{\sigma^2\lambda_P}{2}\left(\int_E \left(\frac{f_t}{\pi}\right)^2 \pi \mathrm{d}x - 1\right) + o(\sigma^2) = \sigma^2\lambda_P \mathcal{H}_\phi[f_t|\pi] + o(\sigma^2).$$

From the entropy-dissipation relation (6.33) and Gronwall lemma, we deduce that

$$\mathcal{H}_\phi[f_t|\pi] \leq C_0 \mathrm{e}^{-\sigma^2(\lambda_P + o(1))t}.$$

The conclusion follows from the Cauchy-Schwarz inequality as in the proof of Theorem 6.B.2. □

A similar result has been obtained rigorously in [137] using linear spectral theory. In particular, the fact that a Poincaré inequality holds depends on the regularity of the boundary of E. In our case, the argument could be made rigorous by studying in details the wellposedness of (6.31) in Sobolev spaces. The argument could also lead to a more detailed analysis of the convergence rate of the Metropolis-Hastings algorithm in other metrics. In particular, the same formal argument holds when we take $\phi(s) = s\log(s) - s + 1$ in (6.37). In this case, the relative entropy is the Kullback-Leibler divergence and its time derivative is controlled by the following dissipation:

$$\mathcal{D}_\phi[f_t|\pi] = \frac{\sigma^2}{2}\int_E \pi \left|\nabla\sqrt{\frac{f_t}{\pi}}\right|^2 \mathrm{d}x + o(\sigma^2).$$

In order to apply Gronwall lemma and obtain the exponential decay of the Kullback-Leibler divergence, we need the following convex Sobolev inequality:

$$\int_E u(x)^2 \log\left(\frac{u(x)^2}{\|u\|^2_{L^2_\pi}}\right)\pi(x)\mathrm{d}x \leq \frac{1}{\lambda_S}\int_E |\nabla u(x)|^2 \pi(x)\mathrm{d}x,$$

for all $u \in H^1_\pi$ and for a constant $\lambda_S > 0$. The conclusion follows by applying this inequality to $u = \sqrt{f_t/\pi}$ and as before from Gronwall lemma and from the classical Csiszár-Kullback-Pinsker inequality [222, Theorem A.2] which shows that the Total Variation norm is controlled by the Kullback-Leibler divergence. When the above convex Sobolev inequilty

holds, then the Poincaré inequality (6.36) also holds with $\lambda_P \geq 2\lambda_S$. More details on convex Sobolev inequalities can be found in [19] or[222, Section 2.2]. Their application to the rigorous computation of (optimal) convergence rates for the Metropolis-Hastings algorithm is left for future work.

6.C Related Works

6.C.1 Another Nonlinear MCMC sampler

A nonlinear kernel which does not fit into the "collective proposal" category has been introduced in [7] and is defined by:

$$K_\mu(x, \mathrm{d}y) = (1-\varepsilon)K^{MH}(x, \mathrm{d}y) + \varepsilon Q_\mu(x, \mathrm{d}y),$$

where K^{MH} is the Metropolis-Hastings kernel and

$$Q_\mu(x, \mathrm{d}y) = \left(1 - \int_E \alpha(x,u)\mu(\mathrm{d}u)\right)\delta_x(\mathrm{d}y) + \alpha_\eta(x,y)\mu(\mathrm{d}y).$$

The function α is defined by: $\alpha_\eta(x,y) = \eta(x)\pi(y)/(\eta(y)\pi(x))$, that is, $\alpha_\eta(x,y)$ is the Metropolis ratio associated to *another* distribution $\eta \in \mathcal{P}_0^{\mathrm{ac}}(E)$. In [7], the authors investigated the case $\eta = \pi^{\tilde{\alpha}}$ for $\tilde{\alpha} \in (0,1)$. This kernel satisfies:

$$\iint_{E\times E} \phi(y) K_\eta(x, \mathrm{d}y)\pi(\mathrm{d}x) = \int_E \phi(y)\pi(\mathrm{d}y).$$

The sampling procedure is therefore quite different as it requires an auxiliary chain to build samples from η first in order to construct a sample from the desired nonlinear kernel. More precisely, the authors propose the following iterative procedure to construct a couple of Markov chains (X_t, Y_t):

$$(X_{t+1}, Y_{t+1}) \sim \Big((1-\varepsilon)K^{MH}(X_t, \mathrm{d}x_{t+1}) + \varepsilon Q_{\hat{\mu}_t^Y}(X_t, \mathrm{d}x_{t+1})\Big)P(Y_t, \mathrm{d}y_{t+1}),$$

where P is a (linear) Markov transition kernel with invariant distribution η and $(Y_t)_t$ is a Markov chain with transition kernel P. The empirical measure of this chain is denoted by:

$$\hat{\mu}_t^Y = \frac{1}{t+1}\sum_{s=0}^{t} \delta_{Y_s}.$$

The final MCMC approximation of an observable φ is given in this case by:

$$\int_E \varphi(x)\pi(\mathrm{d}x) \simeq \frac{1}{t+1}\sum_{s=0}^{t}\varphi(X_s). \tag{6.38}$$

In this empirical sum, the successive iterations of the single chain $(X_t)_t$ are used. In the collective proposal framework introduced in Section 6.2, the algorithm produces N (asymptotically) independent copies of a nonlinear chain $(X_t^i)_t$, $i \in \{1, \dots, N\}$ and we have at our disposal a *sequence* of MCMC approximations of the form:

$$\int_E \varphi(x)\pi(\mathrm{d}x) \simeq \frac{1}{N}\sum_{i=1}^{N}\varphi(X_t^i), \tag{6.39}$$

as $t \to +\infty$. We can therefore interpret the sum (6.38) as a *time average* and the sum (6.39) as an *ensemble average*.

6.C.2 Links with Importance Sampling Based Methods

Even though CMC does not use importance weights, it shares some similarities with importance sampling methods, in particular SMC [128] and PMC methods [54]. As SMC relies on tempering schemes, we will mainly focus on PMC.

According to [54], in PMC methods, without the importance correction, a regular acceptance step — as in Metropolis-Hastings — for each mutation would lead to a simple parallel implementation of N Metropolis-Hastings algorithm. Under the same parallel, we can compare the mutation step in PMC with the proposal step of CMC.

In the first implementation of PMC, at each mutation step, each particle X_t^i is updated independently from the others, according to a kernel $q_{it}(\cdot)$ (that can depend on t and i), the new particle X_{t+1}^i is then associated with a weight proportional to the ratio $\pi(X_{t+1}^i)/q_{it}(X_{t+1}^i)$. In PMC, a mutation therefore occurs according to q_{it}, that is only depends on the position of the ancestor particle. In CMC, the mutation occurs according to $\Theta_{\hat{\mu}_t^N}(\cdot \mid X_t^i)$, the update thus depends on the position of all the particles as Θ depends on the empirical measure of the system $\hat{\mu}_t^N$. This additional dependency is particularly emphasized in the case of Algorithm 2. This corresponds to the Rao-Blackwellised version of PMC, in which we integrate over the position of all the particles.

Recently, [134] also proposed to Rao-Blackwellise the mutation kernel in PMC while keeping an importance sampling framework. The resulting algorithm is non-Markovian and does not conserve the number of particles. At each iteration a batch of particles

is added to the system according to the previous estimation of the target density. The number of particles N grows with the number of iterations. Once a particle is added, its position does not change, only its weight is updated along the iterations. A particle X_{N+1} is added according to $q_N = \sum_i w_i K_N(\cdot \mid X_i)$, where K_N is a kernel whose bandwidth typically decreases with N and where (w_i) is a vector of normalised importance weights. The weight of X_{N+1} is initially proportional to the standard importance weight associated to q_N and is then updated at each iteration by re-normalisation as new particles are added to the system. The weight of the added particle depends on all the other particles already present in the system from the first iteration. This method shares some similarities with ours, an important difference being that an old particle cannot be improved through time and a "bad" particle will indefinitely remain in the system at the same place, while its weight decreases through time, eventually increasing the computation cost.

Importance sampling based methods output unbiased estimators. For CMC, as stated before, except for the Metropolis-Hastings proposal, each one of the methods previously described is biased. Indeed, for a fixed number N of particles, the algorithm does not converge to the target distribution. For a large number of particles, the algorithm provides however a good approximation of the target density, according to Theorem 6.2.9. In addition, as a byproduct, we can re-use this approximation to provide an *unbiased* estimator by simply using the (sequence of) collective proposal distributions as importance distributions in any importance sampling based sampler.

Part II

Partial Differential Equation models of body-attitude coordination

Chapter 7

Phase transitions in the spatially homogeneous kinetic model and macroscopic limit

The content of the present chapter is based on the following article co-authored with P. Degond, A. Frouvelle and S. Merino-Aceituno

[111] P. Degond, A. Diez, A. Frouvelle, and S. Merino-Aceituno. "Phase Transitions and Macroscopic Limits in a BGK Model of Body-Attitude Coordination". *J. Nonlinear Sci.* 30.6 (2020), pp. 2671–2736.

7.1 Introduction and main results

This chapter studies the long-time behaviour of the solution of the spatially homogeneous version of the body-orientation dynamics kinetic model (2.10) with $\nu = 1$ and $\mathbb{M}$ given by (2.12), that is the equation

$$\partial_t f = \rho M_{J_f} - f, \quad J_f(t) := \int_{\mathrm{SO}_3(\mathbb{R})} A f(t, A) \mathrm{d}A, \tag{7.1}$$

where the function $f(t, A)$ only depends on the body-orientation variable and the time.

In this spatially homogeneous setting, the local density of agents previously denoted by ρ_f does not depend on f in the sense that an initial density $\rho_{f_0} \in (0, +\infty)$ associated to the initial condition f_0 is preserved by the dynamics:

$$\forall t \in \mathbb{R}_+, \quad \rho_f(t) = \rho_{f_0},$$

as it can be seen by integrating the equation over $\mathrm{SO}_3(\mathbb{R})$. In all this chapter, we therefore take $\rho \in (0, +\infty)$ as a fixed parameter of the problem and the initial condition f_0 such that $\int_{\mathrm{SO}_3(\mathbb{R})} f_0 = \rho$. Note also that the well-posedness of (7.1) directly follows from Duhamel's formula:

$$f(t) = \mathrm{e}^{-t} f_0 + \rho \int_0^t \mathrm{e}^{-(t-s)} M_{J_f(s)} \mathrm{d}s,$$

since J_f is given as the solution of the following differential equation on $\mathcal{M}_3(\mathbb{R})$:

$$\frac{\mathrm{d}}{\mathrm{d}t} J_f = \rho \langle A \rangle_{M_{J_f}} - J_f, \quad J_f(t=0) = J_{f_0},$$

as it can be seen by multiplying (7.1) by A and integrating over $\mathrm{SO}_3(\mathbb{R})$.

The main results of this chapter are (informally) summarised in the following theorem which states a phase transition phenomenon: there exist critical values of ρ which determine the existence of various families of equilibria and the long-time convergence properties.

Theorem 7.1.1. *Let f be a solution of (7.1) for a fixed density of agents $\rho \in (0, +\infty)$.*

1. *The equilibria f^{eq} of the spatially homogeneous BGK model are either the uniform equilibrium $f^{\mathrm{eq}} = \rho$ or of the form $f^{\mathrm{eq}} = \rho M_{\alpha \mathbb{A}}$ or $f^{\mathrm{eq}} = \rho M_{\alpha\, p \otimes q}$ where $\mathbb{A} \in \mathrm{SO}_3(\mathbb{R})$, and $p, q \in \mathbb{S}^2$ are arbitrary parameters and $\alpha \equiv \alpha(\rho) \in \mathbb{R}$ is a parameter which depends on ρ through a compatibility equation to be defined later (see Section 7.3 and Equations (7.15) and (7.16)).*

2. *Depending on the density of agents $\rho \in \mathbb{R}_+$, the only stable equilibria are either the uniform equilibrium $f^{\mathrm{eq}} = \rho$ or the equilibria of the form $f^{\mathrm{eq}} = \rho M_{\alpha \mathbb{A}}$ where $\mathbb{A} \in \mathrm{SO}_3(\mathbb{R})$ and where $\alpha \in (0, +\infty)$ depends on ρ through a compatibility equation to be defined later.*

The first point of this theorem is detailed in Section 7.3 (see in particular Theorem 7.3.4 and Corollary 7.3.17). The second point is detailed in Section 7.4 (see in particular Theorem 7.4.2).

The analogous phase transition problem for the spatially homogeneous kinetic Vicsek model has been completely treated by [113] in the Fokker-Planck case (1.11). In comparison, the BGK operator is simpler and, in the present body-orientation framework, it leads to a complete and explicit characterisation of the behaviour of the solution. Moreover, the techniques and results in this chapter have recently been used to treat the body-orientation Fokker-Planck case in [166]. The main difference with the Vicsek model is the more complex geometrical structure inherent to body-orientation models which requires specific tools and techniques. In this chapter, it will be shown that the body-attitude coordination

model shares structural properties with nematic alignment models of polymers, studied in a completely different context to model liquid crystals [189, 330, 335, 14, 13]. These two worlds will be formally linked through the isomorphism between $\mathrm{SO}_3(\mathbb{R})$ and the group of unit quaternions detailed in Section 7.3.2 and Appendix 7.A. It will lead to the first point of Theorem 7.1.1 (the complete description of the equilibria in Section 7.3). The key argument is a result due to [330] which studies generalisations of traditional liquid crystals models to higher dimensions and in particular gives a classification of the equilibria of the Smoluchowski equation for rigid, rod-like polymers. Following this work, in the present case, one of our results is the existence of a class of equilibria which cannot be interpreted as equilibria around a mean-body orientation. These equilibria were not known in the previous works on the body-orientation dynamics [114, 116].

The stability of the different equilibria are studied in Section 7.4.3. We will show that our model has an underlying gradient-flow structure which will allow us to determine the asymptotic behaviour of the system after a reduction to an ODE in $\mathbb{R}^3$. This is a specificity of the BGK model which does not hold for the other models of body-attitude coordination [114, 116] based on a Fokker-Planck operator. This specificity allows us to use different and simpler techniques. In particular, we will prove that the equilibria which cannot be interpreted as equilibria around a mean body-orientation are always unstable, which tends to justify the analysis carried out in [114] for a model where only equilibria around a mean body-orientation were considered.

Finally in Section 7.5 we will formally derive the macroscopic models associated to the non-spatially homogeneous equation (4.16) for the stable equilibria. This is a simple extension of the work of [119] to the case of a density-dependent concentration parameter.

This chapter is organised as follows. The first Section 7.2 gathers preliminary technical results on the space $\mathrm{SO}_3(\mathbb{R})$ that are used throughout this chapter and the following ones. The starting point of the present study is the computation of the equilibria of the BGK operator in Section 7.3. Then, in Section 7.4, we will describe the asymptotic behaviour of the system and in particular which equilibria are attained, leading to a self-organised dynamics or not. This will be based on a specific underlying gradient-flow structure of the BGK equation. Finally, macroscopic models for the stable equilibria are derived in Section 7.5.

7.2 Preliminaries: calculus in $\mathrm{SO}_n(\mathbb{R})$

This paragraph collects the main properties of the Riemannian manifold $\mathrm{SO}_n(\mathbb{R})$ and other technical results which are used in this Chapter and the subsequent ones. In this section the dimension is denoted by $n \geq 3$ but we will mainly consider the case $n = 3$ in the following.

7.2.1 Tangent spaces

We start with a characterisation of the tangent spaces of the manifold $\mathrm{SO}_n(\mathbb{R})$ endowed with the Euclidean structure given by (2.1).

Lemma 7.2.1. *The following properties hold true.*

- *The sets $\mathcal{S}_n(\mathbb{R})$ and $\mathcal{A}_n(\mathbb{R})$ of symmetric and antisymmetric matrices are orthogonal for the dot product (2.1) and $\mathcal{M}_n(\mathbb{R}) = \mathcal{S}_n(\mathbb{R}) \oplus \mathcal{A}_n(\mathbb{R})$.*

- *For $\mathbb{A} \in \mathrm{SO}_n(\mathbb{R})$, the tangent space to $\mathrm{SO}_n(\mathbb{R})$ at $\mathbb{A}$ is denoted by $T_{\mathbb{A}}$ and is characterised as follows:*

$$T_{\mathbb{A}} = \{P\mathbb{A}, \mid P \in \mathcal{A}_n(\mathbb{R})\}.$$

  The orthogonal projection (with respect to the inner product (2.1)) of $J \in \mathcal{M}_n(\mathbb{R})$ onto $T_{\mathbb{A}}$ is given by

$$\mathsf{P}_{T_{\mathbb{A}}} J = \frac{J\mathbb{A}^{\mathrm{T}} - \mathbb{A}J^{\mathrm{T}}}{2}\,\mathbb{A}.$$

  Likewise, the orthogonal complement $T_{\mathbb{A}}^{\perp}$ is given by

$$T_{\mathbb{A}}^{\perp} = \{S\mathbb{A} \mid S \in \mathcal{S}_n(\mathbb{R})\},$$

  and the orthogonal projection of J onto $T_{\mathbb{A}}^{\perp}$ is

$$\mathsf{P}_{T_{\mathbb{A}}^{\perp}} J = \frac{J\mathbb{A}^{\mathrm{T}} + \mathbb{A}J^{\mathrm{T}}}{2}\,\mathbb{A}.$$

7.2.2 Changes of variable and applications

We will often need to compute integrals over $\mathrm{SO}_n(\mathbb{R})$. As a consequence of the left and right invariance of the Haar measure, for any $P \in \mathrm{SO}_n(\mathbb{R})$, the maps $A \mapsto PA$ and $A \mapsto AP$ are two changes of variable with unit Jacobian. Based on this observation, we will very often use the following changes of variable.

Definition 7.2.2 (Useful changes of variable)**.** Let us define the following matrices:

- For $i \neq j \in \{1, \dots, n\}$, $D^{ij} \in \mathrm{SO}_n(\mathbb{R})$ is the diagonal matrix such that all its coefficients are equal to 1 except at positions i and j where they are equal to -1.
- For $i \neq j \in \{1, \dots, n\}$, $P^{ij} \in \mathrm{SO}_n(\mathbb{R})$ is the matrix such that $P^{ij}_{ii} = P^{ij}_{jj} = 0$, $P^{ij}_{kk} = 1$ for $k \neq i, j$, $P^{ij}_{ij} = 1$ and $P^{ij}_{ji} = -1$. The other coefficients are equal to 0.

Then we define the following changes of variable with unit Jacobian:

- $A' = D^{ij}A$ multiplies the rows i and j by -1. Everything else remains unchanged.
- $A' = AD^{ij}$ multiplies the columns i and j by -1. Everything else remains unchanged.
- $A' = D^{ij}AD^{ij}$ multiplies the elements (k, i), (k, j) and (i, k), (j, k) by -1 for $k \neq i, j$. Everything else remains unchanged
- $A' = P^{ij}A$ multiplies row i by -1 and permutes the rows i and j.
- $A' = P^{ij}A(P^{ij})^{\mathrm{T}}$ exchanges the diagonal coefficients (i, i) and (j, j) (and involves other changes).

The two following lemmas are important applications of these results.

Lemma 7.2.3. *Let $D \in \mathcal{M}_n(\mathbb{R})$ be a diagonal matrix and M_D the von Mises distribution with parameter D, then the average*

$$\langle A \rangle_{M_D} := \int_{\mathrm{SO}_n(\mathbb{R})} A M_D(A) \mathrm{d}A$$

is a diagonal matrix.

Proof. Let $k \neq \ell$ and $m \neq k, \ell$. The change of variable $A \mapsto D^{km}AD^{km}$ gives:

$$\int_{\mathrm{SO}_n(\mathbb{R})} a_{k\ell} \, \mathrm{e}^{D \cdot A} \, \mathrm{d}A = -\int_{\mathrm{SO}_n(\mathbb{R})} a_{k\ell} \, \mathrm{e}^{D \cdot A} \, \mathrm{d}A = 0,$$

where we have used that $D^{k,m}DD^{k,m} = D$. □

Lemma 7.2.4. *For any $n \geq 3$ and any $J \in \mathcal{M}_n(\mathbb{R})$,*

$$\int_{\mathrm{SO}_n(\mathbb{R})} (J \cdot A) A \, \mathrm{d}A = \frac{1}{2n} J.$$

Lemma 7.2.5. *Let $n \geq 3$, $n \neq 4$. Let $g : \mathrm{SO}_n(\mathbb{R}) \to \mathbb{R}$ such that for all $A, P \in \mathrm{SO}_n(\mathbb{R})$, $g(A) = g(A^{\mathrm{T}}) = g(PAP^{\mathrm{T}})$. For all $J \in \mathcal{M}_n(\mathbb{R})$ we have:*

$$\int_{\mathrm{SO}_n(\mathbb{R})} (J \cdot A) A \, g(A) \, \mathrm{d}A = a \, \mathrm{Tr}(J) I_n + bJ + cJ^{\mathrm{T}},$$

for given $a, b, c \in \mathbb{R}$ depending on g and on the dimension, the expressions of which can be found in the proof.

The proof of these lemmas and other technical results about $\mathrm{SO}_3(\mathbb{R})$ and $\mathrm{SO}_n(\mathbb{R})$ are postponed to Appendix 7.B.

7.2.3 Volume forms in $\mathrm{SO}_3(\mathbb{R})$

When an explicit calculation will be needed, we will use one of the two following parametrisations of $\mathrm{SO}_3(\mathbb{R})$ which give two explicit expressions of the normalised Haar measure in dimension 3.

- To a matrix $A \in \mathrm{SO}_3(\mathbb{R})$ there is an associated angle $\theta \in [0, \pi]$ and a vector $\mathbf{n} \in \mathbb{S}^2$ such that A is the rotation of angle θ around the axis $\mathbf{n}$. Rodrigues' formula gives a representation of A knowing θ and $\mathbf{n} = (n_1, n_2, n_3)$:

$$A = \mathcal{A}(\theta, \mathbf{n}) = I_3 + \sin\theta [\mathbf{n}]_\times + (1 - \cos\theta)[\mathbf{n}]_\times^2 = \exp(\theta[\mathbf{n}]_\times), \tag{7.2}$$

  where

$$[\mathbf{n}]_\times := \begin{pmatrix} 0 & -n_3 & n_2 \\ n_3 & 0 & -n_1 \\ -n_2 & n_1 & 0 \end{pmatrix}. \tag{7.3}$$

  Note that it holds that

$$[\mathbf{n}]_\times^2 = \mathbf{n} \otimes \mathbf{n} - I_3.$$

  If $f(\mathcal{A}(\theta, \mathbf{n})) = \bar{f}(\theta, \mathbf{n})$ the volume form of $\mathrm{SO}_3(\mathbb{R})$ is given by:

$$\int_{\mathrm{SO}_3(\mathbb{R})} f(A) \, \mathrm{d}A = \frac{2}{\pi} \int_0^\pi \sin^2(\theta/2) \int_{\mathbb{S}^2} \bar{f}(\theta, \mathbf{n}) \, \mathrm{d}\mathbf{n} \, \mathrm{d}\theta.$$

  The sphere $\mathbb{S}^2$ can be parametrised with the following usual system of coordinates at

any point $\mathbf{n} = (n_1, n_2, n_3)^{\mathrm{T}}$:

$$\begin{cases} n_1 &= \sin\psi\cos\varphi, \\ n_2 &= \sin\psi\sin\varphi, \\ n_3 &= \cos\psi, \end{cases}$$

where $\psi \in [0, \pi]$ and $\varphi \in [0, 2\pi]$. The volume form for the sphere is then given by:

$$\mathrm{d}\mathbf{n} = \frac{1}{4\pi}\sin\psi \mathrm{d}\psi\mathrm{d}\varphi.$$

- We have the following one to one map :

$$\Psi : \left| \begin{array}{rcl} \mathrm{SO}_2(\mathbb{R}) \times \mathbb{S}^2 & \longrightarrow & \mathrm{SO}_3(\mathbb{R}) \\ (A, p) & \longmapsto & M(p)A^a \end{array} \right. \tag{7.4}$$

where

$$A^a := \begin{pmatrix} A & 0 \\ 0 & 1 \end{pmatrix} \in \mathrm{SO}_3(\mathbb{R}),$$

and for $p = (\sin\phi_1\ \sin\phi_2, \cos\phi_1\ \sin\phi_2, \cos\phi_2)^{\mathrm{T}}$ in spherical coordinates $\phi_1 \in [0, 2\pi]$ and $\phi_2 \in [0, \pi]$, we define:

$$M(p) := \begin{pmatrix} \cos\phi_1 & \sin\phi_1\ \cos\phi_2 & \sin\phi_1\ \sin\phi_2 \\ -\sin\phi_1 & \cos\phi_1\ \cos\phi_2 & \cos\phi_1\ \sin\phi_2 \\ 0 & -\sin\phi_2 & \cos\phi_2 \end{pmatrix} \in \mathrm{SO}_3(\mathbb{R}).$$

The matrix A^a performs an arbitrary rotation of the first 2 coordinates and the matrix $M(p) \in \mathrm{SO}_3(\mathbb{R})$ maps the vector e_3 to $p \in \mathbb{S}^2$. A matrix $A \in \mathrm{SO}_3(\mathbb{R})$ can thus be written as the product:

$$\begin{pmatrix} \cos\phi_1 & \sin\phi_1\ \cos\phi_2 & \sin\phi_1\ \sin\phi_2 \\ -\sin\phi_1 & \cos\phi_1\ \cos\phi_2 & \cos\phi_1\ \sin\phi_2 \\ 0 & -\sin\phi_2 & \cos\phi_2 \end{pmatrix} \begin{pmatrix} \cos\theta & \sin\theta & 0 \\ -\sin\theta & \cos\theta & 0 \\ 0 & 0 & 1 \end{pmatrix}$$

where $\phi_1, \theta \in [0, 2\pi]$ and $\phi_2 \in [0, \pi]$. With this parametrisation:

$$\int_{\mathrm{SO}_3(\mathbb{R})} f(A)\mathrm{d}A = \frac{1}{2\pi}\int_0^{2\pi}\int_{\mathbb{S}^2} f\left(M(p)\begin{pmatrix} \cos\theta & \sin\theta & 0 \\ -\sin\theta & \cos\theta & 0 \\ 0 & 0 & 1 \end{pmatrix}\right)\mathrm{d}\theta\,\mathrm{d}p, \tag{7.5}$$

and the volume form on the sphere is given by:

$$\mathrm{d}p = \frac{1}{4\pi} \sin\phi_2 \, \mathrm{d}\phi_1 \, \mathrm{d}\phi_2.$$

This parametrisation can be extended in any dimension and comes from the Lie groups quotient:

$$\frac{\mathrm{SO}_n(\mathbb{R})}{\mathrm{SO}_{n-1}(\mathbb{R})} \cong \mathbb{S}^{n-1}.$$

7.2.4 Singular Value Decomposition (SVD)

We recall the following classical result proved for instance in [283, Section 1.9].

Proposition 7.2.6 (Singular Value Decomposition, SVD)**.** *Any matrix $M \in \mathcal{M}_n(\mathbb{R})$ can be written:*

$$M = PDQ$$

where $P, Q \in \mathcal{O}_n(\mathbb{R})$ are orthogonal matrices and D is diagonal with nonnegative coefficients listed in decreasing order.

In order to use the properties of the Haar measure, we will need the matrices P and Q to belong to $\mathrm{SO}_3(\mathbb{R})$ (not only $\mathcal{O}_3(\mathbb{R})$). We therefore define another decomposition, called the Special Singular Value Decomposition (SSVD) in the following.

Definition 7.2.7 (SSVD in $\mathrm{SO}_3(\mathbb{R})$)**.** A *Special Singular Value Decomposition* (SSVD) of a matrix $M \in \mathcal{M}_3(\mathbb{R})$ is a decomposition of the form

$$M = PDQ$$

where $P, Q \in \mathrm{SO}_3(\mathbb{R})$ and $D = \mathrm{diag}(d_1, d_2, d_3)$ with

$$d_1 \geq d_2 \geq |d_3|.$$

We recall that $\mathrm{diag} : \mathbb{R}^3 \to \mathcal{M}_3(\mathbb{R})$ denotes the map which transforms a vector $x = (x_1, x_2, x_3)^{\mathrm{T}}$ into a diagonal matrix D with component $D_{ii} = x_i$. The existence of a SSVD follows from Proposition 7.2.6. Starting from a SVD

$$M = P'D'Q',$$

the SSVD can be constructed as follows.

- If $\det M > 0$, either $P', Q' \in \mathrm{SO}_3(\mathbb{R})$ and the SVD is a SSVD or P', Q' have both negative determinant and in this case we can take

$$P = P'\tilde{D}, \quad Q = \tilde{D}Q' \quad \text{and} \quad D = D'$$

  where $\tilde{D} = \mathrm{diag}(1, 1, -1)$.

- If $\det M < 0$, either $P' \in \mathrm{SO}_3(\mathbb{R})$ or $Q' \in \mathrm{SO}_3(\mathbb{R})$ (only one of them). Assume without loss of generality that $Q' \in \mathrm{SO}_3(\mathbb{R})$. Then we can take:

$$P = P'\tilde{D}, \quad D = \tilde{D}D \quad \text{and} \quad Q = Q'.$$

- If $\det M = 0$, then the last coefficient of D' is equal to 0 so $\tilde{D}D' = D'$ and $D'\tilde{D} = D'$. We can take $D = D'$. If $P' \notin \mathrm{SO}_3(\mathbb{R})$ we can take $P = P'\tilde{D}$ and if $Q' \notin \mathrm{SO}_3(\mathbb{R})$ we can take $Q = \tilde{D}Q'$.

Remark 7.2.8. As for the polar decomposition and the standard SVD, the matrix D is always unique. However the matrices P and Q may not be unique.

The subset $\mathscr{D} \subset \mathcal{M}_3(\mathbb{R})$ of the diagonal matrices which are the diagonal part of a SSVD is the cone delimited by the image by the isomorphism diag of the three planes $\{d_1 = d_2\}$, $\{d_2 = d_3\}$ and $\{d_2 = -d_3\}$ in $\mathbb{R}^3$ and depicted in Figure 7.3.2 :

$$D = \mathrm{diag}(d_1, d_2, d_3) \in \mathscr{D} \text{ if and only if } d_1 \geq d_2 \geq |d_3|. \tag{7.6}$$

In other words, the existence of a SSVD shows that any matrix is in the orbit of a diagonal matrix $D \in \mathscr{D}$ for the action of $\mathrm{SO}_3(\mathbb{R}) \times \mathrm{SO}_3(\mathbb{R})$, where for a matrix $M \in \mathcal{M}_3(\mathbb{R})$, the *orbit* $\mathrm{Orb}(M) \subset \mathcal{M}_3(\mathbb{R})$ is defined by:

$$\mathrm{Orb}(M) := \{PMQ, \ \ P, Q \in \mathrm{SO}_3(\mathbb{R})\}. \tag{7.7}$$

In many cases, we will use this property to reduce a problem on $\mathcal{M}_3(\mathbb{R})$ to a simpler problem on $\mathscr{D}$.

7.3 Equilibria of the BGK operator

In this section we determine the equilibria for the BGK operator:

$$Q_{\mathrm{BGK}}(f) := \rho M_{J_f} - f, \tag{7.8}$$

that is to say the distributions f such that $Q_{\mathrm{BGK}}(f) = 0$. In Section 7.3.1 we characterise these equilibria (Theorem 7.3.4) and show that for them to exist, compatibility equations must be fulfilled. These compatibility equations depend on the density ρ. Therefore, for different values of the density ρ, there exist different equilibria. These will be determined in Section 7.3.2 by studying the compatibility equations. A full description of the equilibria of the BGK operator is finally given in Corollary 7.3.17.

7.3.1 Characterisation of the equilibria and compatibility equations

The main result of this section is Theorem 7.3.4 which gives all the equilibria of the BGK operator (7.8). Before stating and proving it, we will need the following lemma which is the analog of Lemma 4.4 in [114]. The proof of this lemma is an application of the results presented in Section 7.2.

Lemma 7.3.1 (Consistency relations)**.** *The following holds:*

(i) There exists a function $c_1 = c_1(\alpha)$ defined for all $\alpha \in \mathbb{R}$ such that for all $\mathbb{A} \in \mathrm{SO}_3(\mathbb{R})$,

$$\langle A \rangle_{M_{\alpha\mathbb{A}}} = c_1(\alpha)\mathbb{A}. \tag{7.9}$$

The function c_1 can be explicitly written $c_1(\alpha) = \frac{1}{3}\big\{(2\cos\theta + 1)\big\}_\alpha$ where $\{\cdot\}_\alpha$ denotes the mean with respect to the probability density

$$\theta \in [0,\pi] \longmapsto \frac{\sin^2(\theta/2)\mathrm{e}^{\alpha\cos\theta}}{\int_0^\pi \sin^2(\theta'/2)\mathrm{e}^{\alpha\cos\theta'}\,\mathrm{d}\theta'}. \tag{7.10}$$

(ii) Consider the set $\mathscr{B} \subset \mathcal{M}_3(\mathbb{R})$ defined by:

$$\mathscr{B} := \left\{ B = P \begin{pmatrix} 1 & & \\ & 0 & \\ & & 0 \end{pmatrix} Q, \quad P, Q \in \mathrm{SO}_3(\mathbb{R}) \right\} = \{p \otimes q, \;\; p, q \in \mathbb{S}^2\}.$$

There exists a function $c_2 = c_2(\alpha)$ defined for all $\alpha \in \mathbb{R}$ such that for all $B \in \mathscr{B}$,

$$\langle A \rangle_{M_{\alpha B}} = c_2(\alpha)B. \tag{7.11}$$

The function c_2 can be explicitly written: $c_2(\alpha) = [\cos\phi]_\alpha$, where $[\cdot]_\alpha$ denotes the

mean with respect to the probability density

$$\varphi \in [0,\pi] \longmapsto \frac{\sin\varphi\, \mathrm{e}^{\frac{\alpha}{2}\cos\varphi}}{\int_0^\pi \sin\varphi'\, \mathrm{e}^{\frac{\alpha}{2}\cos\varphi'}\, \mathrm{d}\varphi'}. \tag{7.12}$$

Remark 7.3.2. The relevance of the set $\mathscr{B}$ will become apparent in Proposition 7.3.12.

Proof. (i) Using the left invariance of the Haar measure, it is enough to prove the result for $\mathbb{A} = I_3$, since

$$\langle A\rangle_{M_{\alpha\mathbb{A}}} = \frac{\int_{\mathrm{SO}_3(\mathbb{R})} A\mathrm{e}^{\alpha A\cdot\mathbb{A}}\,\mathrm{d}A}{\int_{\mathrm{SO}_3(\mathbb{R})} \mathrm{e}^{\alpha\mathbb{A}\cdot A}\,\mathrm{d}A} = \mathbb{A}\frac{\int_{\mathrm{SO}_3(\mathbb{R})} \mathbb{A}^{\mathrm{T}}A\mathrm{e}^{\alpha\mathbb{A}^{\mathrm{T}}A\cdot I_3}\,\mathrm{d}A}{\int_{\mathrm{SO}_3(\mathbb{R})} \mathrm{e}^{\alpha\mathbb{A}^{\mathrm{T}}A\cdot I_3}\,\mathrm{d}A} = \mathbb{A}\langle A\rangle_{M_{\alpha I_3}}.$$

When $\mathbb{A} = I_3$, Lemma 7.2.3 first ensures that $\langle A\rangle_{M_{\alpha I_3}}$ is diagonal, then the change of variable $A' = P^{12}A(P^{12})^{\mathrm{T}}$ (see Definition 7.2.2) shows that:

$$\langle a_{11}\rangle_{M_{\alpha I_3}} = \langle a_{22}\rangle_{M_{\alpha I_3}}.$$

Proceeding analogously with the other coefficients we have that $\langle A\rangle_{M_{\alpha I_3}}$ is proportional to I_3, i.e. there exists $c_1 = c_1(\alpha) \in \mathbb{R}$ such that

$$c_1(\alpha) I_3 = \langle A\rangle_{\alpha I_3}. \tag{7.13}$$

The parametrisation of $\mathrm{SO}_3(\mathbb{R})$ using Rodrigues' formula (7.2) then gives the explicit expression of c_1 by taking the trace in Equation (7.13) and using that for $A = \mathcal{A}(\theta, \mathbf{n})$, $\mathrm{Tr}(A) = 2\cos\theta + 1$.

(ii) As before, using the left and right invariance of the Haar measure it is enough to prove the result for $B = \mathrm{diag}(1,0,0)$. Now if $D = \mathrm{diag}(a,b,-b)$ for $a, b \in \mathbb{R}$, then the change of variable $A \mapsto P^{23}A(P^{23})^{\mathrm{T}}$ followed by the change of variable $A \mapsto D^{23}A$ (see Definition 7.2.2) show that

$$\int_{\mathrm{SO}_3(\mathbb{R})} a_{22}\mathrm{e}^{D\cdot A}\,\mathrm{d}A = -\int_{\mathrm{SO}_3(\mathbb{R})} a_{33}\mathrm{e}^{D\cdot A}\,\mathrm{d}A,$$

which proves with lemma 7.2.3 that $\langle A\rangle_{M_D}$ is diagonal of the form $\mathrm{diag}(\tilde{a}, \tilde{b}, -\tilde{b})$ for $\tilde{a}, \tilde{b} \in \mathbb{R}$. Similarly, if $D = \mathrm{diag}(a,b,b)$ then $\langle A\rangle_{M_D}$ is of the form $\mathrm{diag}(\tilde{a}, \tilde{b}, \tilde{b})$. These two results prove that $\langle A\rangle_{M_{\alpha B}}$ is proportional to B, i.e. there exists $c_2 = c_2(\alpha) \in \mathbb{R}$ such that (7.11) holds. The parametrisation of $\mathrm{SO}_3(\mathbb{R})$ coming from the isomorphism (7.4) then gives the explicit expression of c_2 by taking $B = \mathrm{diag}(1,0,0)$

in Equation (7.11). First, using the change of variable $A \mapsto P^{13}A(P^{13})^{\mathrm{T}}$ it holds that,

$$c_2(\alpha) = \frac{1}{Z}\int_{\mathrm{SO}_3(\mathbb{R})} a_{11}\mathrm{e}^{\frac{\alpha}{2}a_{11}}\,\mathrm{d}A = \frac{1}{Z}\int_{\mathrm{SO}_3(\mathbb{R})} a_{33}\mathrm{e}^{\frac{\alpha}{2}a_{33}}\,\mathrm{d}A$$

where

$$Z = \int_{\mathrm{SO}_3(\mathbb{R})} \mathrm{e}^{\frac{\alpha}{2}a_{11}}\,\mathrm{d}A = \int_{\mathrm{SO}_3(\mathbb{R})} \mathrm{e}^{\frac{\alpha}{2}a_{33}}\,\mathrm{d}A.$$

Then, using the parametrisation (7.5), it follows that:

$$c_2(\alpha) = \frac{\int_0^\pi \cos\varphi \sin\varphi \mathrm{e}^{\frac{\alpha}{2}\cos\varphi}\,\mathrm{d}\varphi}{\int_0^\pi \sin\varphi \mathrm{e}^{\frac{\alpha}{2}\cos\varphi}\,\mathrm{d}\varphi}.$$

□

Remark 7.3.3. We could alternatively use one of the two parametrisations of $\mathrm{SO}_3(\mathbb{R})$ given in Section 7.2.3 or the quaternion formulation to prove that $\langle A\rangle_{\alpha I_3}$ and $\langle A\rangle_{\alpha B}$ are proportional to I_3 and B. However, the proof that we have just presented here holds in any dimension (the value of the constants $c_1(\alpha)$ and $c_2(\alpha)$ depends on the dimension but not the form of the matrices) whereas the volume forms and the quaternion formulation strongly depend on the dimension $n = 3$.

We can now state the main result of this section.

Theorem 7.3.4 (Equilibria for the homogeneous Body-Orientation BGK equation)**.** *Let $\rho \in \mathbb{R}_+$ be a given density. The equilibria of the spatially homogeneous BGK equation* (7.1) *are the distributions of the form $f = \rho M_J$ where $J \in \mathcal{M}_3(\mathbb{R})$ is a solution of the matrix compatibility equation:*

$$J = \rho\langle A\rangle_{M_J}. \tag{7.14}$$

The solutions of the compatibility equation (7.14) *are:*

1. *the matrix $J = 0$,*
2. *the matrices of the form $J = \alpha\mathbb{A}$ with $\mathbb{A} \in \mathrm{SO}_3(\mathbb{R})$ and where $\alpha \in \mathbb{R}$ satisfies the scalar compatibility equation*
$$\alpha = \rho c_1(\alpha), \tag{7.15}$$
3. *the matrices of the form $J = \alpha B$ where $B \in \mathscr{B}$ and where $\alpha \in \mathbb{R}$ satisfies the scalar compatibility equation*
$$\alpha = \rho c_2(\alpha), \tag{7.16}$$

where the set $\mathscr{B}$ and the functions c_1 and c_2 are defined in Lemma 7.3.1.

Remark 7.3.5. Notice that the existence of a non-zero solution for the scalar compatibility equations (7.15) and (7.16) is not guaranteed for all values of $\rho > 0$. The existence of non-zero solutions for these equations will be explored in Section 7.3.2. They will determine the existence of equilibria for Equation (7.1) for a given value of ρ (Corollary 7.3.17).

Remark 7.3.6. The fact that these matrices are solutions of the matrix compatibility equation (7.14) follows directly from the consistency relations (7.9) and (7.11) as it will be shown in the proof of Theorem 7.3.4. The main difficulty of the proof is therefore the necessary condition: we will prove that a solution of the matrix compatibility equation (7.14) is necessarily of one of the forms listed in Theorem 7.3.4.

Remark 7.3.7 (Physical interpretation of the equilibria). The first two types of equilibria can be interpreted as statistical descriptions of respectively a disordered state (case $J = 0$) or an ordered (or flocking) state where a physical average body-orientation $\mathbb{A} \in \mathrm{SO}_3(\mathbb{R})$ can be identified and where α plays the role of a concentration parameter around the "mean" value $\mathbb{A}$. Note that α depends on ρ. In the following, it will be shown that the flocking equilibrium is stable when the density ρ is sufficiently large. Moreover, the concentration parameter α will be larger for larger values of the density (after a certain threshold of the density). The third type of equilibria is specific to the body-orientation model and can be physically understood as the statistical description of a system composed of two groups of agents moving in the same direction but where one group is oriented upside-down with respect to the other (see Figure 2.1c). The diagonal element $\mathrm{diag}(1, 0, 0) \in \mathscr{B}$ can indeed be obtained as the arithmetic average of the body-orientations $\mathrm{diag}(1, 1, 1) \in \mathrm{SO}_3(\mathbb{R})$ and $\mathrm{diag}(1, -1, -1) \in \mathrm{SO}_3(\mathbb{R})$. It corresponds to the case of two agents moving in the e_1 direction and where the body-orientation of an agent can be obtained from the other by a rotation of angle π around the e_1 axis. As it can be expected, equilibria of this type will be shown to be always unstable.

The proof of this theorem will use the two following propositions. The first one and its corollary (Proposition 7.3.8 and Corollary 7.3.9) show that the compatibility equation (7.14) can be reduced to a compatibility equation on diagonal matrices (Equation (7.17)) using the notion of orbit (7.7). The second one (Proposition 7.3.12) provides a necessary condition for a diagonal matrix to be a solution of (7.17). The proof of Proposition 7.3.12 is deferred to the next section.

Proposition 7.3.8 (Orbital reduction)**.** *The following equivalence holds: $J \in \mathcal{M}_3(\mathbb{R})$ is a solution of the matrix compatibility equation* (7.14) *if and only if for all $J' \in \mathrm{Orb}(J)$, J' is a solution of the matrix compatibility equation* (7.14)*.*

Proof. This is a consequence of the left and right invariance of the Haar measure which ensures that for any $J \in \mathcal{M}_3(\mathbb{R})$ and any $P, Q \in \mathrm{SO}_3(\mathbb{R})$, $\langle PAQ \rangle_{M_J} = \langle A \rangle_{M_{PJQ}}$. □

Since the diagonal part of the SSVD of a matrix J is in the orbit of J, we obtain the following corollary:

Corollary 7.3.9 (Reduction to diagonal matrices)**.** *Let $J \in \mathcal{M}_3(\mathbb{R})$ with SSVD given by $J = PDQ$. The following equivalence holds: J is a solution of* (7.14) *if and only if D is a solution of* (7.14)*.*

We will therefore consider only the following problem in dimension 3: find all the diagonal matrices $D \in \mathcal{M}_3(\mathbb{R})$ such that

$$\begin{cases} D = \rho \langle A \rangle_{M_D} \\ D \in \mathscr{D}, \end{cases} \tag{7.17}$$

where the set $\mathscr{D}$ is the subset of diagonal matrices which are the diagonal part of a SSVD and is defined by (7.6). Notice that Equation (7.17) is just Equation (7.14) restricted to the set $\mathscr{D}$.

Remark 7.3.10. The diagonal part $D \in \mathcal{M}_3(\mathbb{R})$ of a SSVD of a matrix $J \in \mathcal{M}_3(\mathbb{R})$ is unique so the problems (7.14) and (7.17) are equivalent. Notice that there might be other diagonal matrices in $\mathrm{Orb}(J)$ (take for example J diagonal which does not satisfy the conditions (7.6)). However the diagonal part of any SSVD of these matrices is D : the diagonal part of the SSVD characterises the orbit of a matrix. In the following, we will find all the diagonal solutions of (7.14) (i.e. the solutions of (7.17) without the restriction $D \in \mathscr{D}$) and then only consider the ones which belong to $\mathscr{D}$. For instance we will see that there are solutions of (7.14) of the form $\mathrm{diag}(0, -\alpha, 0)$ where $\alpha > 0$. The diagonal part of their SSVD is $\mathrm{diag}(\alpha, 0, 0)$ and is a solution of (7.17).

Remark 7.3.11. A diagonal solution D of the matrix compatibility equation (7.14) verifies that D/ρ belongs to the set:

$$\Omega = \Big\{ D = \mathrm{diag}(d_1, d_2, d_3),\ \ \exists\ f \in \mathcal{P}(\mathrm{SO}_3(\mathbb{R})),\ \ J_f = D \Big\} \subset \mathcal{D}_3(\mathbb{R}),$$

where $\mathcal{P}(\mathrm{SO}_3(\mathbb{R}))$ is the set of probability measures on $\mathrm{SO}_3(\mathbb{R})$. The set $\mathrm{diag}^{-1}(\Omega) \subset \mathbb{R}^3$ is exactly the tetrahedron $\mathscr{T}$ defined as the convex hull of the points $(\pm 1, \pm 1, \pm 1)$ with an even number of minuses (which we will call *Horn's tetrahedron*). It is a consequence of Horn's theorem [201, Theorem 8] which states that $\mathscr{T}$ is exactly the set of vectors which

are the diagonal of an element of $\mathrm{SO}_3(\mathbb{R})$. It ensures that if f is a probability measure, we have by convexity of $\mathscr{T}$:

$$\int_{\mathrm{SO}_3(\mathbb{R})} f(A)A \,\mathrm{d}A \in \mathrm{diag}(\mathscr{T})$$

and therefore $\mathrm{diag}^{-1}(\Omega) \subset \mathscr{T}$. Conversely, taking the Dirac deltas δ_{I_3} and similarly for the other vertices of $\mathscr{T}$, we see that the four vertices of Horn's tetrahedron belong to $\mathrm{diag}^{-1}(\Omega)$. Since Ω is convex, we conclude that $\mathscr{T} \subset \mathrm{diag}^{-1}(\Omega)$.

The diagonal solutions of the matrix compatibility equation (7.14) satisfy the following necessary condition.

Proposition 7.3.12. *The diagonal solutions of the compatibility equation* (7.14) *are necessarily of one of the following the types :*

(a) $D = 0$.

(b) $D = \alpha \,\mathrm{diag}(\pm 1, \pm 1, \pm 1)$ *with an even number of minus signs and where* $\alpha \in \mathbb{R} \setminus \{0\}$.

If $\alpha \in (0, +\infty)$*, the diagonal part of the SSVD of these diagonal matrices is equal to* $D = \alpha I_3$.

If $\alpha \in (-\infty, 0)$*, the diagonal part of the SSVD of these diagonal matrices is equal to* $D = \alpha \,\mathrm{diag}(-1, -1, 1) = |\alpha| \,\mathrm{diag}(1, 1, -1)$.

(c) $D = \alpha \,\mathrm{diag}(\pm 1, 0, 0)$ *and the matrices obtained by permutation of the diagonal coefficients and where* $\alpha \in \mathbb{R} \setminus \{0\}$.

The diagonal part of the SSVD of these diagonal matrices is equal to $D = \mathrm{diag}(|\alpha|, 0, 0)$.

Section 7.3.2 will be devoted to the proof of this proposition, which is the main technical contribution of this section. We are now ready to prove Theorem 7.3.4.

Proof (of Theorem 7.3.4). An equilibrium of the BGK equation is of the form

$$f = \rho M_J,$$

where

$$J = J_f = \rho \langle A \rangle_{M_J}.$$

It is straightforward to check that $J = 0$ is a solution of (7.14). Now, let D a matrix of one the form described in Proposition 7.3.12 with a parameter $\alpha \in \mathbb{R}$. For instance, for a matrix of type *(c)* like $D = \alpha \,\mathrm{diag}(0, -1, 0)$, thanks to Lemma 7.3.1 we have:

$$D = \rho \langle A \rangle_{M_D} \iff D = \rho c_2(\alpha) \,\mathrm{diag}(0, -1, 0) \iff \alpha = \rho c_2(\alpha).$$

Similarly for the other diagonal matrices of type *(c)*, we prove that they are solution of the matrix compatibility equation (7.14) if and only if their parameter $\alpha \in \mathbb{R}$ is solution of the scalar compatibility equation (7.16). Analogously one can check that the diagonal matrices of type *(b)* are solutions of the matrix compatibility equation (7.14) if and only if their parameters $\alpha \in \mathbb{R}$ are solutions of the scalar compatibility equation (7.15). This yields all the diagonal solutions of (7.14). Now, the solutions of (7.14) are exactly the matrices $J \in \mathrm{Orb}(D)$ where D is a diagonal solution of (7.14) and the set $\mathrm{Orb}(D) \subset \mathcal{M}_3(\mathbb{R})$ is the orbit of D defined by (7.7). We conclude by noticing that if D is of type (b) then $\mathrm{Orb}(D) = \mathrm{SO}_3(\mathbb{R})$ and if D is of type (c) then $\mathrm{Orb}(D) = \mathscr{B}$. □

Remark 7.3.13. When applied to diagonal matrices, the last part of Theorem 7.3.4 states that the diagonal solutions of (7.14) are necessarily of one of the types (a), (b) or (c) defined in Proposition 7.3.12 and that, it holds that

1. the matrix 0 is always a solution of (7.14),
2. a matrix of type *(b)* is a solution of (7.14) if and only if its parameter $\alpha \in \mathbb{R} \setminus \{0\}$ satisfies (7.15),
3. a matrix of type *(c)* is a solution of (7.14) if and only if its parameter $\alpha \in \mathbb{R} \setminus \{0\}$ satisfies (7.16).

7.3.2 Proof of Proposition 7.3.12

The proof of Proposition 7.3.12 is based on two results. The first one has been proved in [330, Section 4] to study the nematic alignment of polymers in higher dimensional spaces:

Theorem 7.3.14 ([330])**.** *Let $n \geq 3$, $b \in \mathbb{R}_+$ and $\mathbf{s} = (s_1, s_2, \ldots, s_n) \in \mathbb{R}^n$ be a solution of the nonlinear system*

$$s_j = \langle m_j^2 \rangle_{g_{\mathbf{s},b}}, \quad j = 1, \ldots, n, \tag{7.18}$$

where the average is taken with respect to the probability density function on the sphere $\mathbb{S}^{n-1}$:

$$g_{\mathbf{s},b}(m_1, \ldots, m_n) := \frac{1}{Z} \exp\left(b \sum_{j=1}^{n} s_j m_j^2 \right), \tag{7.19}$$

where Z is the normalisation constant. Then the set $\{s_1, \ldots, s_n\}$ has at most two distinct elements (i.e. $\mathrm{Card}\{s_1, s_2, \ldots, s_n\} \leq 2$*).*

The second tool that we will use to prove Proposition 7.3.12 is the isomorphism between $\mathrm{SO}_3(\mathbb{R})$ and the space of unitary quaternions which transforms the compatibility equation (7.17) into the compatibility equation (7.18) studied in Theorem 7.3.14.

Proposition 7.3.15.

1. *There is an isomorphism between the group* $\mathrm{SO}_3(\mathbb{R})$ *and the quotient group* $\mathbb{H}/\pm 1$, *where* $\mathbb{H}$ *is the group of unit quaternions. Since* $\mathbb{H}$ *is homeomorphic to* $\mathbb{S}^3$, *there is an isomorphism* Φ *:*

$$\Phi : \mathbb{S}^3/\pm 1 \longrightarrow \mathrm{SO}_3(\mathbb{R}).$$

   Moreover Φ *is an isometry in the sense that it maps the volume form of* $\mathbb{S}^3/\pm 1$ *(defined as the image measure of the usual measure on* $\mathbb{S}^3$ *by the projection on the quotient space) to the volume form on* $\mathrm{SO}_3(\mathbb{R})$*: for any measurable function* f *on* $\mathrm{SO}_3(\mathbb{R})$,

$$\int_{\mathbb{S}^3/\pm 1} f\big(\Phi(q)\big)\,\mathrm{d}q = \int_{\mathrm{SO}_3(\mathbb{R})} f(A)\,\mathrm{d}A.$$

2. *There is a linear isomorphism between the vector space* $\mathcal{M}_3(\mathbb{R})$ *and the vector space* $\mathcal{S}_4^0(\mathbb{R})$ *of trace free symmetric matrices of dimension 4:*

$$\phi \ : \mathcal{M}_3(\mathbb{R}) \longrightarrow \mathcal{S}_4^0(\mathbb{R}),$$

   such that for all $J \in \mathcal{M}_3(\mathbb{R})$, *and* $q \in \mathbb{H}/\pm 1$,

$$\frac{1}{2} J \cdot \Phi(q) = q \cdot \phi(J) q.$$

   The dot product on the left-hand side is defined by Equation (2.1) *and the one on the right-hand side is the usual dot product in* $\mathbb{R}^4$.

3. *For all* $q \in \mathbb{H}/\pm 1$, *it holds that* $\phi\big(\Phi(q)\big) = q \otimes q - \frac{1}{4} I_4$.

4. *The isomorphism* ϕ *preserves the diagonal structure: if* $D = \mathrm{diag}(d_1, d_2, d_3)$ *then,*

$$\phi(D) = \frac{1}{4} \begin{pmatrix} d_1 + d_2 + d_3 & 0 & 0 & 0 \\ 0 & d_1 - d_2 - d_3 & 0 & 0 \\ 0 & 0 & -d_1 + d_2 - d_3 & \\ & 0 & 0 & -d_1 - d_2 + d_3 \end{pmatrix}$$

and if $Q = \mathrm{diag}(s_1, s_2, s_3, s_4)$ *with* $s_1 + s_2 + s_3 + s_4 = 0$*, then*

$$\phi^{-1}(Q) = 2 \begin{pmatrix} s_1 + s_2 & 0 & 0 \\ 0 & s_1 + s_3 & 0 \\ 0 & 0 & s_1 + s_4 \end{pmatrix}.$$

The proof of this proposition can be found in Appendix 7.A. We are now ready to prove Proposition 7.3.12.

Proof (of Proposition 7.3.12). Using the first and second points of Proposition 7.3.15, it holds that

$$\int_{\mathrm{SO}_3(\mathbb{R})} A \mathrm{e}^{A \cdot D} \, \mathrm{d}A = \int_{\mathbb{S}^3/\pm 1} \Phi(q) \mathrm{e}^{\Phi(q) \cdot D} \, \mathrm{d}q = \int_{\mathbb{S}^3/\pm 1} \Phi(q) \mathrm{e}^{2q \cdot \phi(D) q} \, \mathrm{d}q.$$

The compatibility equation (7.17) then becomes:

$$D = \frac{\rho}{Z} \int_{\mathbb{S}^3/\pm 1} \Phi(q) \mathrm{e}^{2q \cdot \phi(D) q} \, \mathrm{d}q.$$

Applying the isomorphism ϕ defined in Proposition 7.3.15 to this last equation, we can exchange ϕ and the integral by linearity and we obtain thanks to the third point of Proposition 7.3.15 :

$$\phi(D) = \frac{\rho}{Z} \int_{\mathbb{S}^3/\pm 1} \phi\big(\Phi(q)\big) \mathrm{e}^{2q \cdot \phi(D) q} \, \mathrm{d}q = \frac{\rho}{Z} \int_{\mathbb{S}^3/\pm 1} \left(q \otimes q - \frac{1}{4} I_4 \right) \mathrm{e}^{2q \cdot \phi(D) q} \, \mathrm{d}q.$$

Using the fourth point of Proposition 7.3.15, we then obtain the following equivalent problem: find all the trace-free diagonal matrices $Q = \mathrm{diag}(s_1, s_2, s_3, s_4)$ of dimension 4 such that

$$Q = \rho \frac{\int_{\mathbb{S}^3/\pm 1} \mathrm{e}^{\sum_{i=1}^4 2 s_i q_i^2} (q \otimes q - \frac{1}{4} I_4) \, \mathrm{d}q}{Z},$$

where Z is a normalisation constant:

$$Z := \int_{\mathbb{S}^3/\pm 1} \mathrm{e}^{\sum_{i=1}^4 2 s_i q_i^2} \, \mathrm{d}q.$$

Equivalently, defining for $i \in \{1, 2, 3, 4\}$:

$$s_i' := \frac{s_i}{\rho} + \frac{1}{4},$$

we want to solve the system of compatibility equations:

$$s'_i = \int_{\mathbb{S}^3/\pm 1} q_i^2 g_{\mathbf{s}',2\rho}(q)\,\mathrm{d}q, \quad i = 1,2,3,4, \tag{7.20}$$

where $\mathbf{s}' = (s'_1, s'_2, s'_3, s'_4)$ and $g_{\mathbf{s}',2\rho}$ is given by (7.19). Thanks to Theorem 7.3.14, we conclude that if $\mathbf{s}'$ is a solution of (7.20), then the coefficients s'_1, s'_2, s'_3, s'_4 can take at most two distinct values. So, the same result holds for the coefficients s_1, s_2, s_3, s_4. Now thanks to the fourth point of Proposition 7.3.15, we only have the following possibilities:

- if $s_1 = s_2 = s_3 = s_4 = 0$, then

$$D = \phi^{-1}(Q) = 0,$$

- if $s_1 = 3\alpha/4$ and $s_2 = s_3 = s_4 = -\alpha/4$ for $\alpha \in \mathbb{R}$, then

$$D = \phi^{-1}(Q) = \alpha I_3,$$

- if $s_2 = 3\alpha/4$ and $s_1 = s_3 = s_4 = -\alpha/4$ for $\alpha \in \mathbb{R}$, then

$$D = \phi^{-1}(Q) = \alpha \begin{pmatrix} 1 & 0 & 0 \\ 0 & -1 & 0 \\ 0 & 0 & -1 \end{pmatrix},$$

  and similarly by permuting the diagonal elements when $s_3 = 3\alpha/4$ and when the other elements are equal $s_1 = s_2 = s_4 = -\alpha/4$ or when $s_4 = 3\alpha/4$ and $s_1 = s_2 = s_3 = -\alpha/4$,

- if $s_1 = s_2 = \alpha/4$ and $s_3 = s_4 = -\alpha/4$ for $\alpha \in \mathbb{R}$, then

$$D = \phi^{-1}(Q) = \alpha \begin{pmatrix} 1 & 0 & 0 \\ 0 & 0 & 0 \\ 0 & 0 & 0 \end{pmatrix},$$

  and similarly by permuting the diagonal elements when $s_1 = s_3 = \alpha/4$ and when $s_2 = s_4 = -\alpha/4$ or $s_1 = s_4 = \alpha/4$ and $s_2 = s_3 = -\alpha/4$.

The computation of the SSVD for these matrices is an easy computation. This concludes the proof of Proposition 7.3.12. □

7.3.3 Determination of the equilibria for each density

In Theorem 7.3.4 we saw that the BGK operator can have three types of equilibria. The uniform equilibria $f = \rho$ (corresponding to $J = 0$) is always an equilibrium. However, the existence of the other two types of equilibria depends on Equations (7.15) and (7.16) having a solution for a given ρ. Therefore the existence of these types of equilibria will depend on the value of ρ. In this section we will determine the existing equilibria for each value of ρ. In particular, we will draw the phase diagram for ρ and α, that is to say the parametrised curves defined by Equations (7.15) and (7.16) in the plane (ρ, α) (see Figure 7.3.1). We first prove the following proposition.

Proposition 7.3.16. *Let* $\rho_c := 6$.

(i) The function $\alpha \mapsto \alpha/c_1(\alpha)$ *is well-defined on* $\mathbb{R}$*, its value at zero is* ρ_c*. Moreover, there exists* $\alpha^* > 0$ *such that this function is decreasing on* $(-\infty, \alpha^*]$ *and increasing on* $[\alpha^*, +\infty)$*. Defining* $\rho^* := \alpha^*/c_1(\alpha^*)$*, it holds that* $\rho^* < \rho_c$.

(ii) The function $\alpha \mapsto \alpha/c_2(\alpha)$ *is even. It is decreasing on* $(-\infty, 0)$*, increasing on* $(0, \infty)$ *and its value at zero is* ρ_c.

(iii) We have the following asymptotic behaviours:

$$\frac{\alpha}{c_1(\alpha)} \underset{\alpha\to+\infty}{\sim} \alpha + 1,$$

$$\frac{\alpha}{c_2(\alpha)} \underset{\alpha\to+\infty}{\sim} \alpha + 2.$$

Proof. The idea of the proof is taken from [330].

(i) Since

$$\frac{d}{d\theta}\Big\{ \sin^2(\theta/2)\sin\theta \Big\} = \sin^2(\theta/2)(1 + 2\cos\theta),$$

an integration by parts shows that:

$$\frac{\alpha}{c_1(\alpha)} = 3\frac{\int_0^\pi \sin^2(\theta/2)\mathrm{e}^{\alpha\cos\theta}\,\mathrm{d}\theta}{\int_0^\pi \sin^2(\theta/2)\sin^2\theta\mathrm{e}^{\alpha\cos\theta}\,\mathrm{d}\theta} = \frac{3}{\{\sin^2\theta\}_\alpha}.$$

It proves that α and $c_1(\alpha)$ have the same sign for all $\alpha \in \mathbb{R}$. Then we define function $m : \alpha \mapsto \{\sin^2\theta\}_\alpha = 3c_1(\alpha)/\alpha$ which satisfies the property:

$$m'(\alpha) = 0 \implies m''(\alpha) < 0,$$

since

$$m'(\alpha) = \{\sin^2\theta\cos\theta\}_\alpha - \{\sin^2\theta\}_\alpha\{\cos\theta\}_\alpha,$$

and

$$m''(\alpha) = -\operatorname{Var}_\alpha(\cos^2\theta) - 2\{\cos\theta\}_\alpha m'(\alpha),$$

where $\operatorname{Var}_\alpha$ is the variance for the probability density (7.10). This property implies that $\alpha/c_1(\alpha)$ has only one critical point which is a global minimum. This minimum is attained at a point $\alpha^* > 0$ as a simple computation shows that $m'(0) > 0$ and consequently $\rho^* < \rho_c$. A simple computation gives $m(0) = \frac{1}{2}$ so $\rho_c = 6$.

(ii) We have similarly:

$$\frac{\alpha}{c_2(\alpha)} = 4\frac{\int_0^\pi \sin\varphi \mathrm{e}^{\frac{\alpha}{2}\cos\varphi}\,\mathrm{d}\varphi}{\int_0^\pi \sin^3\varphi \mathrm{e}^{\frac{\alpha}{2}\cos\varphi}\,\mathrm{d}\varphi} = \frac{4}{[\sin^2\varphi]_\alpha}, \tag{7.21}$$

from which we can easily see that $\alpha \mapsto \alpha/c_2(\alpha)$ is even and has only one minimum attained at $\alpha = 0$. A simple computation shows that its value at 0 is $\rho_c = 6$.

(iii) The behaviour at infinity is obtained by Laplace's method: with the change of variable $s = 1 - \cos\theta$ on $[0, \pi]$, we get

$$\frac{\alpha}{c_1(\alpha)} = 3\frac{\mathrm{e}^\alpha \int_0^2 \mathrm{e}^{-\alpha s}\frac{s}{2\sqrt{1-(1-s)^2}}\,ds}{\mathrm{e}^\alpha \int_0^2 \mathrm{e}^{-\alpha s}\frac{s}{2}\sqrt{1-(1-s)^2}\,ds} \underset{\alpha\to+\infty}{\sim} \alpha + 1.$$

With the same method we have:

$$\frac{\alpha}{c_2(\alpha)} = 4\frac{\int_0^2 \mathrm{e}^{-\frac{\alpha}{2}s}\,ds}{\int_0^2 \mathrm{e}^{-\frac{\alpha}{2}s}(1-(1-s)^2)\,ds} \underset{\alpha\to+\infty}{\sim} \alpha + 2.$$

□

Thanks to Proposition 7.3.16 and Theorem 7.3.4 we can now fully describe the equilibria of the BGK operator. A graphical representation of this result is given by the phase diagram depicted in Figure 7.3.1 :

Corollary 7.3.17 (Equilibria of the BGK operator, depending on the density ρ)**.** *The set of equilibria of the BGK operator* (7.8) *depends on the value of ρ. In particular we need to distinguish three regions $\rho \in (0, \rho^*)$, $\rho \in (\rho^*, \rho_c)$ and $\rho > \rho_c$ where ρ^* and ρ_c are defined in Proposition 7.3.16. We have the following equilibria in each region:*

- *For $0 < \rho < \rho^*$, $\alpha = 0$ is the unique solution of Equations* (7.15) *and* (7.16) *and therefore the only equilibrium is the uniform equilibrium $f^{\mathrm{eq}} = \rho$.*

- *For $\rho = \rho^*$, in addition to the uniform equilibrium, there is a family of anisotropic equilibria given by $f^{\mathrm{eq}} = \rho^* M_{\alpha^* \mathbb{A}}$ where $\mathbb{A} \in \mathrm{SO}_3(\mathbb{R})$ and $\alpha^* = \rho^* c_1(\alpha^*)$.*

- *For $\rho^* < \rho < \rho_c$, the compatibility equation* (7.15) *has two solutions α_+ and α_- with $0 < \alpha_- < \alpha_+$ which give, in addition to the uniform equilibrium, two families of anisotropic equilibria : $f^{\mathrm{eq}} = \rho M_{\alpha_+ \mathbb{A}}$ and $f^{\mathrm{eq}} = \rho M_{\alpha_- \mathbb{A}}$ with $\mathbb{A} \in \mathrm{SO}_3(\mathbb{R})$.*

- *For $\rho = \rho_c$, we have $\alpha_- = 0$.*

- *For $\rho > \rho_c$, Equation* (7.15) *has two solutions $\alpha_3 < 0 < \alpha_1$ which give two families of anisotropic equilibria $f^{\mathrm{eq}} = \rho M_{\alpha_3 \mathbb{A}}$ and $f^{\mathrm{eq}} = \rho M_{\alpha_1 \mathbb{A}}$ with $\mathbb{A} \in \mathrm{SO}_3(\mathbb{R})$. Moreover, Equation* (7.16) *has two solutions $-\alpha_2 < 0 < \alpha_2$ which give another family of equilibria: $f^{\mathrm{eq}} = \rho M_{\alpha_2 B}$ where $B \in \mathscr{B}$. The uniform equilibrium is always an equilibrium.*

When an equilibrium is of the form $f^{\mathrm{eq}} = \rho M_{\alpha \mathbb{A}}$ with parameters $\alpha > 0$ and $\mathbb{A} \in \mathrm{SO}_3(\mathbb{R})$ then these parameters can respectively be interpreted as a concentration parameter and a mean body-orientation. They are analogous to the equilibria found in [113] in the Vicsek case. However, in $\mathrm{SO}_3(\mathbb{R})$, there exist other equilibria which are not of this form. We will see in Section 7.4 that these latter equilibria are always unstable.

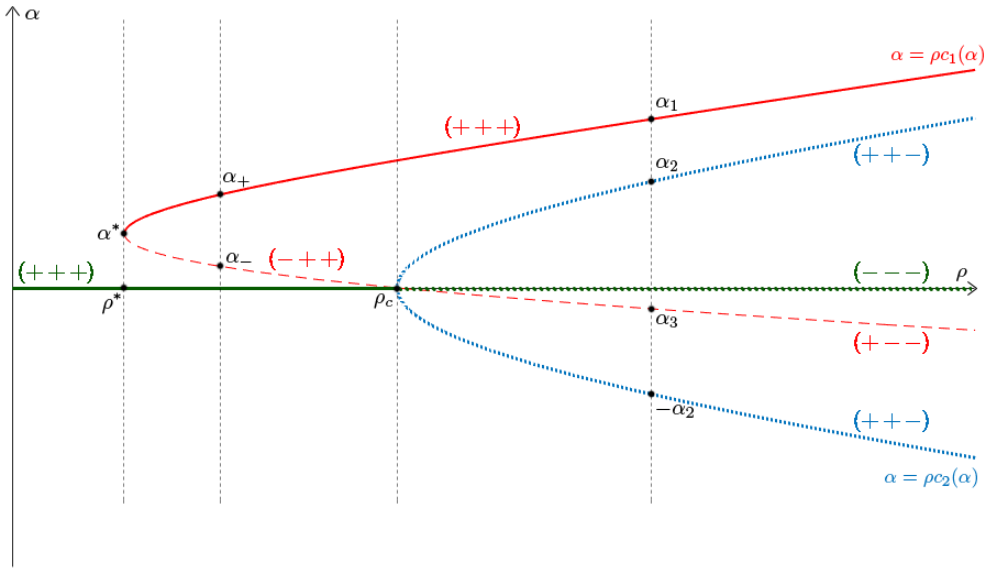

FIGURE 7.3.1: Phase diagram for the equilibria of the BGK operator (7.8). Depending on the density, there are one, two, three or four branches of equilibria (α_2 and $-\alpha_2$ give the same orbit). The uniform equilibrium $f^{\mathrm{eq}} = \rho$ is always an equilibrium (corresponding to $\alpha = 0$, depicted in green). The equilibria of the form $f^{\mathrm{eq}} = \rho M_{\alpha\mathbb{A}}$, $\mathbb{A} \in \mathrm{SO}_3(\mathbb{R})$ exist for $\rho > \rho^*$ and correspond to the two branches of the red curve $\alpha = \rho c_1(\alpha)$. Finally the equilibria of the form $f^{\mathrm{eq}} = \rho M_{\alpha B}$, $B \in \mathscr{B}$ exist for $\rho > \rho_c$ and correspond to the two branches of the blue curve $\alpha = \rho c_2(\alpha)$. The dotted and dashed lines correspond to unstable equilibria (as shown in Section 7.4). The signs are the signature of the Hessian matrix $\mathrm{Hess}\, V(D)$ defined in Section 7.4 taken at an equilibrium point. The elements α^*, ρ^* and ρ_c are defined in Proposition 7.3.16; the elements α_+, α_-, α_1, α_2 and α_3 are given in Corollary 7.3.17.

Finally the following picture (Figure 7.3.2) is a representation in the space $\mathbb{R}^3$ of the diagonal parts of the SSVDs of the solution of the matrix compatibility equation (7.14) when $\rho > \rho_c$. They all belong to the domain $\mathscr{D}$ defined by (7.6) and depicted in orange in Figure 7.3.2.

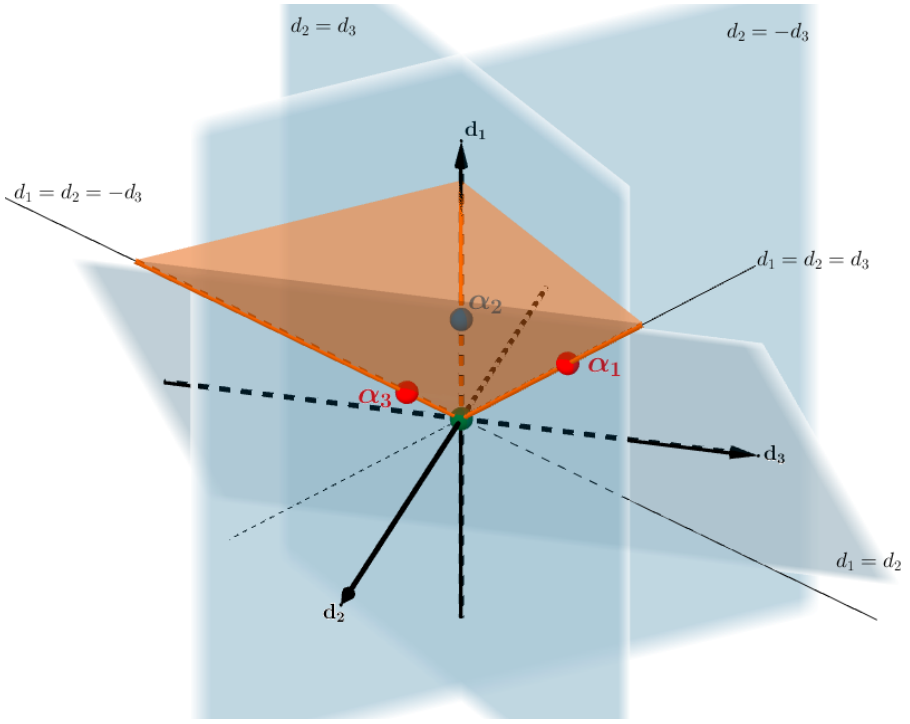

FIGURE 7.3.2: The 4 diagonal parts of the SSVDs of the diagonal equilibria seen as elements of the space $\mathbb{R}^3$ for $\rho > \rho_c$, as described in Corollary 7.3.17. The ones with non zero determinant are in red (type *(b)* in Proposition 7.3.12), the non-zero one with determinant equal to zero is in blue (type *(c)*) and the matrix 0 is in green. They all lie in the domain $\mathrm{diag}^{-1}(\mathscr{D})$ depicted in orange and delimited by the three blue planes $\{d_1 = d_2\}$, $\{d_2 = d_3\}$ and $\{d_2 = -d_3\}$.

7.4 Convergence to equilibria

7.4.1 Main result

Now that we know all the equilibria of the spatially homogeneous BGK equation (7.1) we proceed to investigate the asymptotic behaviour of $f(t, A)$ as $t \to +\infty$. This problem can be reduced to looking at the asymptotic behaviour of J_f since, if $J_f \to J_\infty \in \mathcal{M}_3(\mathbb{R})$, then $f(t)$ will converge as $t \to +\infty$ towards ρM_{J_∞} as it can be seen by writing Duhamel's formula for equation (7.1) :

$$f(t) = \mathrm{e}^{-t} f_0 + \rho \int_0^t \mathrm{e}^{-(t-s)} M_{J_f(s)} \, \mathrm{d}s. \tag{7.22}$$

The asymptotic behaviour of J_f is much simpler than the one of f since J_f is the solution of the following ODE

$$\frac{\mathrm{d}}{\mathrm{d}t} J_f = \rho \langle A \rangle_{M_{J_f}} - J_f, \quad J_f(t=0) = J_{f_0}, \tag{7.23}$$

as it can be seen by multiplying (7.1) by $A \in \mathrm{SO}_3(\mathbb{R})$ and integrating over $\mathrm{SO}_3(\mathbb{R})$. Since $J \in \mathcal{M}_3(\mathbb{R}) \mapsto M_J \in L^\infty(\mathrm{SO}_3(\mathbb{R}))$ is locally Lipschitz, the flow of Equation (7.23) is defined globally in time since the map $J \mapsto \rho\langle A \rangle_{M_J}$ is Lipschitz with bounded Lipschitz seminorm.

Notice that the solutions of the compatibility equation (7.14) are exactly the equilibria of the dynamical system (7.23). We therefore obtain the following proposition:

Proposition 7.4.1 (Equilibria of the BGK operator, equilibria of the ODE (7.23))**.** *A distribution $f^{\mathrm{eq}} = \rho M_J$ is an equilibrium of the BGK operator* (7.8) *if and only if $J \in \mathcal{M}_3(\mathbb{R})$ is an equilibrium of the dynamical system* (7.23)*.*

We will call stable/unstable an equilibrium of the BGK operator (7.8) such that the associated matrix $J \in \mathcal{M}_3(\mathbb{R})$ is a stable/unstable equilibrium of the ODE (7.23). This section is devoted to the proof of the following theorem:

Theorem 7.4.2 (Convergence towards equilibria)**.** *Let $\rho \in \mathbb{R}_+$ be such that $\rho \neq \rho^*$ and $\rho \neq \rho_c$ (as defined in Proposition 7.3.16). Let f_0 be an initial condition for* (7.1) *and let $J_{f_0} = PD_0Q$ be a SSVD. Let $f(t)$ be the solution at time $t \in \mathbb{R}_+$ of the spatially homogeneous BGK equation* (7.1) *with initial condition f_0. Let $D(t)$ be the solution at time $t \in \mathbb{R}_+$ of the ODE* (7.23) *with initial condition $D_0 \in \mathscr{D}$. It holds that:*

$$J_{f(t)} = PD(t)Q$$

is a SSVD and there exists a subset $\mathscr{N}_\rho \subset \mathbb{R}^3$ of zero Lebesgue measure such that, writing $\mathcal{N}_\rho := \mathrm{diag}(\mathscr{N}_\rho) \subset \mathcal{M}_3(\mathbb{R})$:

1. *if $D_0 \notin \mathcal{N}_\rho$, then $f(t)$ converges as $t \to \infty$ towards an equilibrium f^{eq} of the BGK operator* (7.8) *of the form $f^{\mathrm{eq}} = \rho M_{J^{\mathrm{eq}}}$, where $J^{\mathrm{eq}} \in \mathcal{M}_3(\mathbb{R})$ is of one of the forms described in Theorem 7.3.4. The convergence is locally exponentially fast in the sense that there exist constants $\delta, K, \mu > 0$ such that if $\|J_{f_0} - J^{\mathrm{eq}}\| \leq \delta$ then for all $t > 0$,*

$$\forall A \in \mathrm{SO}_3(\mathbb{R}), \ \ |f(t,A) - f^{\mathrm{eq}}(A)| \leq \mathrm{e}^{-\mu t}\Big(K\rho + |f_0(A) - f^{\mathrm{eq}}(A)|\Big).$$

2. *If $D_0 \notin \mathcal{N}_\rho$, we have the following asymptotic behaviours depending on the density ρ:*

(i) *if* $0 < \rho < \rho^*$, *then* $D(t) \to 0$ *as* $t \to +\infty$ *and, consequently,* $f^{\mathrm{eq}} = \rho$,

(ii) *if* $\rho^* < \rho < \rho_c$, *then* $D(t) \to 0$ *or* $D(t) \to \alpha_+ I_3$ *as* $t \to +\infty$ *and, consequently,* $f^{\mathrm{eq}} = \rho$ *or* $f^{\mathrm{eq}} = \rho M_{\alpha_+ \mathbb{A}}$ *respectively, where* $\alpha_+ > 0$ *is defined in Corollary 7.3.17 and* $\mathbb{A} := PQ \in \mathrm{SO}_3(\mathbb{R})$,

(iii) *if* $\rho > \rho_c$, *then* $D(t) \to \alpha_1 I_3$ *as* $t \to +\infty$ *and, consequently,* $f^{\mathrm{eq}} = \rho M_{\alpha_1 \mathbb{A}}$ *where* $\alpha_1 > 0$ *is defined in Corollary 7.3.17 and* $\mathbb{A} := PQ \in \mathrm{SO}_3(\mathbb{R})$.

Remark 7.4.3 (Phase transitions). Theorem 7.4.2 demonstrates a phase transition phenomenon triggered by the density of agents ρ : when $\rho < \rho^*$, the system is disordered (asymptotically in time) in the sense that $J_f \to 0$ and we therefore cannot define a mean body-attitude. When the density increases and exceeds the critical value ρ_c, the system is self-organised (asymptotically in time and for almost every initial data), in the sense that $J_f \to \alpha \mathbb{A}$ where $\alpha \in \mathbb{R}_+$ and $\mathbb{A} \in \mathrm{SO}_3(\mathbb{R})$ can be respectively interpreted as a concentration parameter and a mean body attitude. When $\rho^* < \rho < \rho_c$ the self-organised and disordered states are both asymptotically stable and the convergence towards one or the other state depends on the initial data. Such "transition region" also appears in the Vicsek model, as studied in [113], and gives rise to an hysteresis phenomenon.

Remark 7.4.4. Thanks to Horn's theorem [201], it can be checked that in the cases where D_0 is such that $D(t) \to \alpha I_3$ for $\alpha > 0$, then D_0 does not belong to the plane $\{d_2 = -d_3\}$ and the matrix PQ is indeed uniquely defined as $PQ = \mathsf{P}_{\mathrm{SO}_3(\mathbb{R})} J_{f_0}$.

The proof of this theorem can be found at the end of Section 7.4.3. It is based on a gradient flow structure for the flux J_f studied in Section 7.4.2. This structure ensures the convergence of J_f towards a matrix $J^{\mathrm{eq}} \in \mathcal{M}_3(\mathbb{R})$ as $t \to +\infty$ and consequently the convergence of $f(t)$ as $t \to +\infty$ towards an equilibrium. The stability of the equilibria determines which equilibrium can be attained. This question is addressed in Section 7.4.3.

7.4.2 A gradient-flow structure in $\mathbb{R}^3$

In this section we show that the ODE (7.23) can be reduced to a gradient-flow ODE in $\mathbb{R}^3$. We first show how (7.23) can be reduced to an ODE in $\mathbb{R}^3$, the equilibria of which are linked to the equilibria of (7.23) (and therefore of (7.1)). Then we show that this ODE in $\mathbb{R}^3$ has a gradient-flow structure which will allow us to conclude on the asymptotic behaviour of the solution of (7.1).

The ODE (7.23) is a matrix-valued nonlinear ODE (in dimension 9) but, as in the previous section (Proposition 7.3.8 and Corollary 7.3.9), we will use the left and right

invariance of the Haar measure and the SSVD to reduce the problem to a vector-valued nonlinear ODE in dimension 3, as explained in Proposition 7.4.5 and Corollary 7.4.7.

Proposition 7.4.5 (Reduction to a nonlinear ODE in dimension 3)**.** *Let $J_0 \in \mathcal{M}_3(\mathbb{R})$ be a given matrix and let $D_0 \in \mathrm{Orb}(J_0)$ be diagonal. Let $P, Q \in \mathrm{SO}_3(\mathbb{R})$ such that $J_0 = PD_0Q$. Let $J : [0, \infty) \to \mathcal{M}_3(\mathbb{R})$ be a C^1 curve in $\mathcal{M}_3(\mathbb{R})$ with $J(0) = J_0$. For all $t > 0$, let $D(t) \in \mathcal{M}_3(\mathbb{R})$ be the matrix such that $J(t) = PD(t)Q$. It holds that:*

(i) $J = J(t)$ is the solution of the ODE (7.23) with initial condition $J(t = 0) = J_0$ if and only if $D = D(t)$ is the solution of the same ODE (7.23) with initial condition $D(t = 0) = D_0$.

(ii) Moreover, if (i) holds, then the matrix $D(t) \in \mathcal{M}_3(\mathbb{R})$ is diagonal for all time.

Proof. (i) Using the left and right invariance of the Haar measure, we see that if the matrix $J(t) \in \mathcal{M}_3(\mathbb{R})$ is a solution of (7.23), then for any $P, Q \in \mathrm{SO}_3(\mathbb{R})$, $PJ(t)Q$ is also a solution (and conversely).

(ii) Since D_0 is diagonal, the fact that $D(t)$ is also diagonal is a consequence of Lemma 7.2.3 which states that $\langle A \rangle_{M_D}$ is diagonal when D is diagonal.

□

For any matrix J_0, such a diagonal matrix D_0 always exists: we can take the diagonal part of the SSVD of J_0. We therefore only have to study the following ODE for diagonal matrices. Since this vector space is isomorphic to $\mathbb{R}^3$ through the isomorphism $\mathrm{diag} : \mathbb{R}^3 \to \mathcal{M}_3(\mathbb{R})$, we obtain two equivalent ODEs:

$$\frac{\mathrm{d}}{\mathrm{d}t} D(t) = \rho \langle A \rangle_{M_{D(t)}} - D(t), \quad D(t = 0) = D_0, \tag{7.24a}$$

$$\frac{\mathrm{d}}{\mathrm{d}t} \widehat{D}(t) = \rho \, \mathrm{diag}^{-1} \left(\langle A \rangle_{M_{\mathrm{diag}(\widehat{D}(t))}} \right) - \widehat{D}(t), \quad \widehat{D}(t = 0) = \widehat{D}_0, \tag{7.24b}$$

where $\widehat{D}_0 = \mathrm{diag}^{-1}(D_0)$ and the following equivalence holds : $\widehat{D}(t) = \mathrm{diag}^{-1}(D(t))$ is the solution of (7.24b) if and only if $D(t) = \mathrm{diag}(\widehat{D}(t))$ is the solution of (7.24a).

Note that it is not clear that if $J_0 = PD_0Q$ is a SSVD, then $J(t) = PD(t)Q$ is a SSVD for all $t > 0$. The following proposition and corollary ensure that the SSVD is preserved by the dynamical system which will allow us to restrict the domain on which the ODE (7.24a) is posed.

Proposition 7.4.6 (Invariant manifolds)**.** *The following subsets of $\mathbb{R}^3$ are invariant manifolds of the dynamical system* (7.24b) *:*

- *the planes* $\left\{(d_1, d_2, d_3) \in \mathbb{R}^3,\ d_i + d_j = 0\right\}$ *for* $i \neq j \in \{1, 2, 3\}$,
- *the planes* $\left\{(d_1, d_2, d_3) \in \mathbb{R}^3,\ d_i - d_j = 0\right\}$ *for* $i \neq j \in \{1, 2, 3\}$,
- *the intersections of two of these planes and in particular the lines*

$$\mathbb{R}\begin{pmatrix}1\\1\\1\end{pmatrix}, \quad \mathbb{R}\begin{pmatrix}1\\0\\0\end{pmatrix}, \quad \mathbb{R}\begin{pmatrix}1\\1\\-1\end{pmatrix}\dots$$

Proof. For $i = 2$ and $j = 3$, the result has already been proved in the second point of Lemma 7.3.1. The other cases are similar. □

Corollary 7.4.7. *Let* $J_0 \in \mathcal{M}_3(\mathbb{R})$ *and* $J_0 = PD_0Q$ *be a SSVD with* $P, Q \in \mathrm{SO}_3(\mathbb{R})$ *and* $D_0 \in \mathcal{D}_3(\mathbb{R})$ *diagonal. Let* $J(t)$ *be the solution of the ODE* (7.23) *with initial condition* $J(t = 0) = J_0$. *Let* $D(t)$ *the solution of the ODE* (7.24a) *with initial condition* $D(t = 0) = D_0$. *Then the decomposition* $J(t) = PD(t)Q$ *is a SSVD for* $J(t)$.

Proof. The fact that $J(t) = PD(t)Q$ is a consequence of the first point of Proposition 7.4.5. The fact that it is a SSVD is a consequence of Proposition 7.4.6 which ensures that the conditions (7.6) remain true for all $t > 0$: $\mathscr{D}$ is stable in the sense that if $D_0 \in \mathscr{D}$, then $D(t) \in \mathscr{D}$ for all time $t > 0$. This follows from the fact that the image by the isomorphism diag of the invariant manifolds of (7.24b) described in Proposition 7.4.6 are invariant manifolds of the dynamical system (7.24a). These manifolds in $\mathcal{D}_3(\mathbb{R})$ form the boundary of the subset $\mathscr{D}$. □

In conclusion, the study of the asymptotic behaviour of $f(t)$ as $t \to +\infty$ can be reduced to the study of the asymptotic behaviour of the solutions of the ODE (7.24a) posed on the domain $\mathscr{D}$ (see Figure 7.3.2).

The following Proposition describes the equilibria of the dynamical system (7.24a) and is a consequence of the results of Section 7.3.

Proposition 7.4.8 (Equilibria of the dynamical system (7.24a))**.** *The equilibria of the dynamical system* (7.24a) *are, depending on the density* ρ *:*

- *the matrix* $D = 0$ *for any density* ρ,
- *the diagonal matrices of type (b) with parameters* α_+ *and* α_- *when* $\rho^* < \rho < \rho_c$,
- *the diagonal matrices of type (b) with parameters* α_1 *and* α_3 *and the diagonal matrices of type (c) with parameters* $\pm\alpha_2$ *when* $\rho > \rho_c$,

where the types (b) and (c) are defined in Proposition 7.3.12 and the elements α_+, α_-, α_1, α_2 and α_3 are defined in Corollary 7.3.17.

Proof. The equilibria of (7.24a) are the diagonal matrices D such that

$$\rho\langle A\rangle_{M_D} - D = 0,$$

which is exactly Equation (7.14) for the diagonal matrices. This equation has been solved in Theorem 7.3.4, Remark 7.3.13 and Corollary 7.3.17. □

Remark 7.4.9. As in the previous section, we have found all the diagonal equilibria of (7.24a). However, thanks to Corollary 7.4.7, only the ones which belong to $\mathscr{D}$ are needed.

The following proposition is a straightforward consequence of the previous results.

Proposition 7.4.10 (Equilibria of the BGK operator, equilibria of the ODE (7.24a))**.** *Let $J \in \mathcal{M}_3(\mathbb{R})$ with a SSVD given by $J = PDQ$. The following assertions are equivalent.*

(1) The distribution $f^{\mathrm{eq}} = \rho M_J$ is an equilibrium of the BGK operator (7.8)*.*

(2) The matrix D is an equilibrium of the dynamical system (7.24a) *on the domain $\mathscr{D}$.*

(3) The matrix D is of one of the forms:

- *$D = 0$, when $\rho < \rho^*$,*
- *$D = 0$ or $D = \alpha_- I_3$ or $D = \alpha_+ I_3$, when $\rho^* \leq \rho \leq \rho_c$,*
- *$D = 0$ or $D = \alpha_1 I_3$ or $D = \alpha_3 \operatorname{diag}(-1,-1,1)$ or $D = \alpha_2 \operatorname{diag}(1,0,0)$, when $\rho > \rho_c$,*

where ρ^*, ρ_c, α_-, α_+, α_1, α_2 and α_3 are defined in Proposition 7.3.16 and Corollary 7.3.17.

Lemma 7.4.11 (Gradient-flow structure)**.** *We define the partition function of a matrix $J \in \mathcal{M}_3(\mathbb{R})$:*

$$\mathcal{Z}(J) := \int_{\mathrm{SO}_3(\mathbb{R})} \mathrm{e}^{J\cdot A}\,\mathrm{d}A, \tag{7.25}$$

and the potentials $V(J)$ and $\widehat{V}(\widehat{D})$ respectively on $\mathscr{M}_3(\mathbb{R})$ and on $\mathbb{R}^3$:

$$V(J) := \frac{1}{2}\|J\|^2 - \rho \log \mathcal{Z}(J), \tag{7.26a}$$

$$\widehat{V}(\widehat{D}) := \frac{1}{2}|\widehat{D}|^2 - 2\rho \log \mathcal{Z}(\operatorname{diag}(\widehat{D})) \tag{7.26b}$$

where $\|\cdot\|$ *and* $|\cdot|$ *are respectively the norm on* $\mathcal{M}_3(\mathbb{R})$ *induced by the inner product* (2.1) *and the Euclidean norm on* $\mathbb{R}^3$*. Then we can rewrite equations* (7.24a) *and* (7.24b) *into a gradient flow structure as follows:*

$$\frac{\mathrm{d}}{\mathrm{d}t}D(t) = \rho\langle A\rangle_{M_{D(t)}} - D(t) = -\nabla V(D), \tag{7.27a}$$

$$\frac{\mathrm{d}}{\mathrm{d}t}\widehat{D}(t) = \rho\,\mathrm{diag}^{-1}\left(\langle A\rangle_{M_{\mathrm{diag}(\widehat{D}(t))}}\right) - \widehat{D}(t) = -\nabla\widehat{V}(\widehat{D}), \tag{7.27b}$$

where ∇ *is the gradient operator in* $\mathcal{M}_3(\mathbb{R})$ *endowed with the Riemaniann structure* (2.1) *or the gradient operator in* $\mathbb{R}^3$ *endowed with the usual Euclidean structure.*

Proof. The partition function satisfies that for all $J \in \mathcal{M}_3(\mathbb{R})$,

$$\nabla(\log\mathcal{Z})(J) = \langle A\rangle_{M_J},$$

since $\nabla(e^{J\cdot A}) = Ae^{J\cdot A}$. The result follows in $\mathcal{M}_3(\mathbb{R})$. The result in $\mathbb{R}^3$ follows from the fact that for any $w_1, w_2 \in \mathbb{R}^3$, it holds that:

$$w_1 \cdot w_2 = 2\,\mathrm{diag}(w_1)\cdot\mathrm{diag}(w_2)$$

where $\cdot$ denotes the dot product on $\mathbb{R}^3$ and on $\mathcal{M}_3(\mathbb{R})$ as defined in (2.1). □

Remark 7.4.12. This gradient-flow structure on J_f is specific to the BGK equation and does not hold for the Fokker-Planck operator (as shown in [113], the differential equation satisfied by J_f in the Vicsek case involves the spherical harmonics of degree 2 and higher of f; here the equation for J_f is closed).

Remark 7.4.13 (Free-energy). The following functional is a free-energy for both the spatially homogeneous BGK equation and the spatially homogeneous version of the Fokker-Planck equation (2.13) (though with a different dissipation term):

$$\mathcal{F}[f] := \int_{\mathrm{SO}_3(\mathbb{R})} f\log f - \frac{1}{2}|J_f|^2. \tag{7.28}$$

It satisfies in both cases:

$$\frac{\mathrm{d}}{\mathrm{d}t}\mathcal{F}[f] = -\mathcal{D}[f] \le 0,$$

where $\mathcal{D}[f]$ is the dissipation term which is equal for the BGK model to:

$$\mathcal{D}[f] = \int_{\mathrm{SO}_3(\mathbb{R})} (f - \rho M_{J_f})(\log f - \log(\rho M_{J_f})) \ge 0.$$

In the context of the Vicsek model, this free energy was the key to study the phase transition phenomena [113]. Moreover, in the Fokker-Planck case this dissipation inequality implies a gradient flow structure in the Wasserstein-2 distance which has been studied (in the Vicsek case) in [160]. Recently, it has been shown in [166] that this gradient-flow structure and the properties of the potential V introduced in the present work can be used to study the phase transition phenomena for a large class of Fokker-Planck models which includes the case of the body-orientation model. However, the BGK model has another underlying gradient-flow dynamics (studied in Section 7.4) on which the present study will be based, and we will therefore not use this free-energy in the present work.

As an application of the gradient-flow structure, we can prove that all the trajectories of (7.23) and (7.27a) are bounded: since the potential V in (7.26a) is decreasing along the trajectories, we can write for all $t > 0$

$$\frac{1}{2}\|J(t)\|^2 \leq V(J_0) + \rho \log \mathcal{Z}(J(t)).$$

Using the fact that $\mathrm{SO}_3(\mathbb{R})$ is compact with volume one, by the mean-value theorem applied to (7.25) there exists $\bar{A} \in \mathrm{SO}_3(\mathbb{R})$ such that $\mathcal{Z}(J(t)) \leq \mathrm{e}^{\bar{A}\cdot J(t)}$. Therefore, owing to the fact that $\|A\| \leq \sqrt{3/2}$ for all $A \in \mathrm{SO}_3(\mathbb{R})$, we obtain using the Cauchy-Schwarz inequality that $\log \mathcal{Z}(J(t)) \leq \sqrt{\frac{3}{2}}\|J(t)\|$. Then, by Young's inequality we get:

$$\frac{1}{4}\|J(t)\|^2 \leq V(J_0) + \frac{3}{2}\rho^2.$$

Moreover, since the potential V is analytic, a classical result by Łojasiewicz [190, 242] implies that the solution to (7.27a) and (7.23) will converge towards an equilibrium. The same holds for the system (7.27b).

When all the equilibria of the dynamical system (7.24a) are hyperbolic the convergence towards the stable equilibria is exponentially fast (see [198, Section 9.3] and the Hartman-Grobman theorem [278, Section 2.8]). The goal of the next section is to find which equilibria among the ones found in Section 7.3 are stable and to completely describe the asymptotic behaviour of the system depending on the initial condition and the local density ρ. We will see that phase transitions appear between ordered and disordered dynamics when the density ρ increases.

7.4.3 Stability of the equilibria and conclusion

Since the flow of (7.24b) is the image by the isomorphism diag^{-1} of the flow of (7.24a), an equilibrium D^{eq} of (7.24a) is stable (resp. unstable) if and only if $\mathrm{diag}^{-1}(D^{\mathrm{eq}})$ is a stable (resp. unstable) equilibria of (7.24b). The stability properties of the equilibria of (7.24b) are much simpler to study than the stability properties of the equilibria of (7.24a) since they are given by the signature of the Hessian matrix $\mathrm{Hess}\,\widehat{V}(\widehat{D}^{\mathrm{eq}}) \in \mathcal{S}_3(\mathbb{R})$ of the potential $\widehat{V}$ given in equation (7.26b) (the linearisation of ODE (7.24b) around an equilibrium $\widehat{D}^{\mathrm{eq}}$ is indeed $\frac{\mathrm{d}}{\mathrm{d}t}\widehat{H} = -\,\mathrm{Hess}\,\widehat{V}(\widehat{D}^{\mathrm{eq}})\widehat{H}$). In particular, an equilibrium $\widehat{D}^{\mathrm{eq}}$ is stable if and only if the signature of $\mathrm{Hess}\,\widehat{V}(\widehat{D}^{\mathrm{eq}})$ is $(+++)$.

Note that in the matrix framework (7.27a), the Hessian of the potential (7.26a) in the Euclidean space $\mathcal{M}_3(\mathbb{R})$ would be a rank 4 tensor. Here we are reduced to the computation of the signature of 3×3 symmetric matrices. For a diagonal matrix $D \in \mathcal{D}_3(\mathbb{R})$ and $\widehat{D} = \mathrm{diag}^{-1}(D)$ we will write with a slight abuse of notations:

$$\mathrm{Hess}\,V(D) \equiv \mathrm{Hess}\,\widehat{V}(\widehat{D}).$$

When $D \in \mathcal{D}_3(\mathbb{R})$ is an equilibrium of (7.24a) we call signature of the Hessian matrix $\mathrm{Hess}\,V(D)$ the signature of $\mathrm{Hess}\,\widehat{V}(\widehat{D})$ where $\widehat{D} = \mathrm{diag}^{-1}(D)$. A simple computation shows that the Hessian matrix $\mathrm{Hess}\,V(D)$ is given by :

$$\mathrm{Hess}\,V(D) = I_3 - \frac{1}{2}\rho\Gamma^D, \tag{7.29}$$

where $\Gamma^D = (\Gamma^D_{ij})_{i,j}$ with :

$$\Gamma^D_{ij} = \langle a_{ii}a_{jj}\rangle_{M_D} - \langle a_{ii}\rangle_{M_D}\langle a_{jj}\rangle_{M_D}.$$

The following theorem is an extension of Corollary 7.3.17 and gives a full description of the equilibria of the BGK operator with their stability.

Theorem 7.4.14 (Stability of the equilibria of the ODE (7.24a))**.**

- *For $0 < \rho < \rho^*$, the only equilibrium is $D = 0$. This equilibrium is stable.*
- *For $\rho^* < \rho < \rho_c$, the equilibrium $D = 0$ and the equilibria of type (b) with parameter α_+ are stable. The equilibria of type (b) with parameter α_- are unstable and the signature of the Hessian matrix is $(-++)$.*
- *For $\rho > \rho_c$, the stable equilibria are the equilibria of type (b) with parameter α_1. The other equilibria ($D = 0$, type (b) with parameter α_3 and type (c) with parameter*

$\pm\alpha_2$) *are unstable and the signatures of the Hessian matrix are respectively* $(---)$, $(+--)$ *and* $(++-)$.

The proof of Theorem 7.4.14 will be based on the following lemma which states an important orbital invariance principle for the signature of the Hessian matrix.

Lemma 7.4.15 (Orbital invariance of the signature)**.** *Let* G_D *and* G_P *the subgroups of* $\mathrm{SO}_3(\mathbb{R})$ *respectively generated by the matrices* D^{ij} *and* P^{ij} *defined in Definition 7.2.2. These subgroups act on* $\mathcal{D}_3(\mathbb{R})$ *respectively by left multiplication and by conjugation. Let* $D \in \mathcal{D}_3(\mathbb{R})$ *be a diagonal matrix. Then the signature of* $\operatorname{Hess} V(D)$ *is invariant by the action of* G_D *and* G_P *on* D.

Proof. Let us first introduce the map $\pi^{\mathrm{diag}} : \mathcal{M}_3(\mathbb{R}) \to \mathbb{R}^3, M \mapsto (M_{ii})_i$. Let $L \in G_D$ and $P \in G_P$. The map π^{diag} satisfies for all $M \in \mathcal{M}_3(\mathbb{R})$:

$$\pi^{\mathrm{diag}}(LM) = L\pi^{\mathrm{diag}}(M), \text{ and } \pi^{\mathrm{diag}}(PMP^{\mathrm{T}}) = R\pi^{\mathrm{diag}}(M) \tag{7.30}$$

where $R := P \odot P \in \mathcal{O}_3(\mathbb{R})$ is the Hadamard product (or element-wise product) of P with itself (that is R is the permutation matrix obtained by removing all the minuses in P). Let $\widehat{H} \in \mathbb{R}^3$ and $H := \operatorname{diag}(\widehat{H}) \in \mathcal{D}_3(\mathbb{R})$. From the expression (7.29) of the Hessian matrix $\operatorname{Hess} V(D) \equiv \operatorname{Hess} \widehat{V}(\widehat{D})$ it follows that:

$$\operatorname{Hess} V(D)\widehat{H} = \widehat{H} - \rho\left(\left\langle (A \cdot H)\pi^{\mathrm{diag}}(A)\right\rangle_{M_D} - \langle A \cdot H\rangle_{M_D}\langle \pi^{\mathrm{diag}}(A)\rangle_{M_D}\right).$$

Using the left and right invariance of the Haar measure and (7.30), we obtain:

$$\begin{aligned}\operatorname{Hess} V(LD)\widehat{H} &= \widehat{H} - \rho L\left(\left\langle (A \cdot L^{\mathrm{T}}H)\pi^{\mathrm{diag}}(A)\right\rangle_{M_D} - \langle A \cdot L^{\mathrm{T}}H\rangle_{M_D}\langle \pi^{\mathrm{diag}}(A)\rangle_{M_D}\right)\\ &= L \operatorname{Hess} V(D) \operatorname{diag}^{-1}(L^{\mathrm{T}}H)\end{aligned}$$

and therefore, since $\operatorname{diag}^{-1}(L^{\mathrm{T}}H) = L^{\mathrm{T}}\widehat{H}$, it follows that

$$\operatorname{Hess} V(LD) = L \operatorname{Hess} V(D) L^{\mathrm{T}}.$$

Similarly, using (7.30), we obtain

$$\operatorname{Hess} V(PDP^{\mathrm{T}})\widehat{H} = \widehat{H} - \rho R\left(\left\langle (A \cdot P^{\mathrm{T}}HP)\pi^{\mathrm{diag}}(A)\right\rangle_{M_D} - \langle A \cdot P^{\mathrm{T}}HP\rangle_{M_D}\langle \pi^{\mathrm{diag}}(A)\rangle_{M_D}\right)$$

and since $\mathrm{diag}^{-1}(P^{\mathrm{T}}HP) = R^{\mathrm{T}}\widehat{H}$, it follows that

$$\mathrm{Hess}\, V(PDP^{\mathrm{T}}) = R\,\mathrm{Hess}\, V(D)R^{\mathrm{T}}.$$

The conclusion follows from Sylvester's law of inertia ([238, Chapter 8 Theorem 1]). □

If $\widehat{D}$ is an equilibrium of (7.24b) then $\mathrm{diag}(\widehat{D})$ is of one type (a), (b) or (c) defined in Proposition 7.3.12. For the types (b) and (c), the diagonal matrix $\mathrm{diag}(\widehat{D})$ is therefore in the orbit of respectively αI_3 (by the action of G_D) or $\alpha\,\mathrm{diag}(1,0,0)$ (by the action of G_P) where α solves the associated compatibility equation. As a consequence of Lemma 7.4.15, one only needs to look at the signature of the Hessian matrix of $\widehat{V}$ taken in one of these two representatives. We are now ready to prove Theorem 7.4.14.

Proof (of Theorem 7.4.14). Thanks to lemma 7.4.15, we therefore do not have to compute the signatures of the Hessian matrix taken at all equilibria, it is enough to choose one matrix in each orbit: for the equilibria of type (b) (see Proposition 7.3.12) we will compute the signature of $\mathrm{Hess}\, V(\alpha I_3)$ where $\alpha = \rho c_1(\alpha)$ and for the equilibria of type (c) we will compute the signature of $\mathrm{Hess}\, V(\alpha\,\mathrm{diag}(1,0,0))$ where $\alpha = \rho c_2(\alpha)$. We first start with the case of the uniform equilibrium.

Case 1. Uniform equilibrium $D = 0$

For the uniform equilibrium $D = 0$, $\langle a_{ij}\rangle = 0$ for all (i,j). Moreover, by the change of variable $A' = D^{ik}A$ where $k \neq i,j$, we have when $i \neq j$:

$$\langle a_{ii}a_{jj}\rangle = -\langle a_{ii}a_{jj}\rangle = 0.$$

It proves that Γ is diagonal. Then with the changes of variables $A' = P^{ij}A$ or $A' = AP^{ij}$ it can be seen that all the 3^2 quantities $\langle a_{ij}^2\rangle$ are equal. Since their sum is equal to $n = 3$ we get that

$$\mathrm{Hess}\, V(0) = \left(1 - \frac{1}{2}\rho\langle a_{11}^2\rangle\right) I_3 = \left(1 - \frac{\rho}{\rho_c}\right) I_3,$$

where $\rho_c = 6$. In conclusion, the signature of $\mathrm{Hess}\, V(0)$ is $(+++)$ if $\rho < \rho_c$ and $(---)$ if $\rho > \rho_c$.

Case 2. Equilibria of type (b) : $D = \alpha I_3$

Let $D = \alpha I_3$ with $\alpha = \rho c_1(\alpha)$. We have $c_1(\alpha) = \langle a_{11}\rangle_{M_D} = \langle a_{22}\rangle_{M_D} = \langle a_{33}\rangle_{M_D}$ and a change of variable of the type $A' = P^{ij}A(P^{ij})^{\mathrm{T}}$ shows that all the $\langle a_{kk}a_{\ell\ell}\rangle_{M_D}$ are equal.

The Hessian matrix is therefore equal to :

$$\operatorname{Hess} V(\alpha I_3) = I_3 - \frac{1}{2}\rho \begin{pmatrix} \nu & \gamma & \gamma \\ \gamma & \nu & \gamma \\ \gamma & \gamma & \nu \end{pmatrix},$$

with $\nu = \langle a_{11}^2 \rangle_{M_D} - \langle a_{11} \rangle_{M_D}^2$ and $\gamma = \langle a_{11} a_{22} \rangle_{M_D} - \langle a_{11} \rangle_{M_D} \langle a_{22} \rangle_{M_D}$. The eigenvalues of $\operatorname{Hess} V(D)$ are :

- $1 - \frac{1}{2}\rho\nu - \rho\gamma$ of order 1 with eigenvector $(1,1,1)^{\mathrm{T}}$. But taking the derivative with respect to α of (7.9) with $\mathbb{A} = I_3$ we obtain the relation :

$$c_1'(\alpha) = \frac{1}{2}\langle a_{11}^2 \rangle_{M_D} + \langle a_{11} a_{22} \rangle_{M_D} - \frac{3}{2}\langle a_{11} \rangle_{M_D}^2 = \frac{1}{2}\nu + \gamma,$$

  and using $\rho = \alpha / c_1(\alpha)$ we can rewrite :

$$1 - \frac{1}{2}\rho\nu - \rho\gamma = 1 - \frac{\alpha c_1'(\alpha)}{c_1(\alpha)} = c_1(\alpha) \left(\frac{id}{c_1} \right)' (\alpha).$$

  Its sign is then given by Proposition 7.3.16 and the fact that $c_1(\alpha)$ has the same sign as α : $c_1(\alpha) \left(\frac{id}{c_1} \right)' (\alpha) > 0$ when $\alpha < 0$, $c_1(\alpha) \left(\frac{id}{c_1} \right)' (\alpha) < 0$ when $0 \leq \alpha < \alpha^*$ and $c_1(\alpha) \left(\frac{id}{c_1} \right)' (\alpha) > 0$ when $\alpha > \alpha^*$.

- $1 - \frac{1}{2}\rho\nu + \frac{1}{2}\rho\gamma$ of order 2 with eigenvectors $(1,-1,0)^{\mathrm{T}}$ and $(0,1,-1)^{\mathrm{T}}$. It can be rewritten as:

$$1 - \frac{1}{2}\rho\nu + \frac{1}{2}\rho\gamma = 1 - \frac{\alpha}{4c_1(\alpha)} \big\langle (a_{11} - a_{22})^2 \big\rangle_{M_D}.$$

  To determine this sign, we use the explicit volume form of $\mathrm{SO}_3(\mathbb{R})$ given by Rodrigues' formula (7.2) to see that :

$$\frac{\alpha}{4c_1(\alpha)} \Big\langle (a_{11} - a_{22})^2 \Big\rangle_{M_D} = \frac{\alpha}{5} \cdot \frac{\int_0^\pi \sin^2(\theta/2)(1-\cos\theta)^2 \mathrm{e}^{\alpha\cos\theta}\,\mathrm{d}\theta}{\int_0^\pi \sin^2(\theta/2)(1+2\cos\theta)\mathrm{e}^{\alpha\cos\theta}\,\mathrm{d}\theta}.$$

  Lemma 7.4.16. *The function*

$$f : x \longmapsto 1 - \frac{x}{5} \cdot \frac{\int_0^\pi \sin^2(\theta/2)(1-\cos\theta)^2 \mathrm{e}^{x\cos\theta}\,\mathrm{d}\theta}{\int_0^\pi \sin^2(\theta/2)(1+2\cos\theta)\mathrm{e}^{x\cos\theta}\,\mathrm{d}\theta},$$

  satisfies $f(0) = 0$, $f(x) \geq 0$ *if* $x \geq 0$ *and* $f(x) \leq 0$ *if* $x \leq 0$

Proof. The value of $f(0)$ is given by the expansion of exp. Note that :

$$\frac{\mathrm{d}}{\mathrm{d}\theta}\Big\{\sin^2(\theta/2)\sin\theta\Big\} = \sin^2(\theta/2)(1+2\cos\theta),$$

so that an integration by parts shows :

$$\int_0^\pi \sin^2(\theta/2)(1+2\cos\theta)\mathrm{e}^{x\cos\theta}\,\mathrm{d}\theta = x\int_0^\pi \sin^2(\theta/2)\sin^2(\theta)\mathrm{e}^{x\cos\theta}\mathrm{d}\theta.$$

We get that :

$$f(x) = 1 - \frac{1}{5}\frac{\int_0^\pi \sin^2(\theta/2)(1-\cos\theta)^2\mathrm{e}^{x\cos\theta}\,\mathrm{d}\theta}{\int_0^\pi \sin^2(\theta/2)\sin^2(\theta)\mathrm{e}^{x\cos\theta}\mathrm{d}\theta}.$$

We have :

$$f(x)\geq 0 \Longleftrightarrow \int_0^\pi \sin^2(\theta/2)\left(\frac{1}{5}(1-\cos\theta)^2 - \sin^2(\theta)\right)\mathrm{e}^{x\cos\theta}\,\mathrm{d}\theta \leq 0.$$

Linearizing $\sin^2(\theta/2)$ and expanding everything gives :

$$\sin^2(\theta/2)\left(\frac{1}{5}(1-\cos\theta)^2 - \sin^2(\theta)\right) = \frac{-1}{5}(3\cos\theta+2)(1-\cos\theta)^2,$$

so that :

$$f(x)\geq 0 \Longleftrightarrow \int_0^\pi (3\cos\theta+2)(1-\cos\theta)^2\mathrm{e}^{x\cos\theta}\,\mathrm{d}\theta \geq 0.$$

Now for $x\geq 0$, let $\theta_0 = \arccos(-2/3)$. We cut the integral at θ_0 and we get

$$\int_0^{\theta_0} (3\cos\theta+2)(1-\cos\theta)^2\mathrm{e}^{x\cos\theta}\,\mathrm{d}\theta \geq \mathrm{e}^{-\frac{2}{3}x}\int_0^{\theta_0}(3\cos\theta+2)(1-\cos\theta)^2\,\mathrm{d}\theta,$$

since the integrand is nonnegative and $x\geq 0$. Similarly when the integrand is nonpositive

$$\int_{\theta_0}^\pi (3\cos\theta+2)(1-\cos\theta)^2\mathrm{e}^{x\cos\theta}\,\mathrm{d}\theta \geq \mathrm{e}^{-\frac{2}{3}x}\int_{\theta_0}^{\pi}(3\cos\theta+2)(1-\cos\theta)^2\,\mathrm{d}\theta.$$

And finally :

$$\int_0^\pi (3\cos\theta+2)(1-\cos\theta)^2\mathrm{e}^{x\cos\theta}\,\mathrm{d}\theta \geq \mathrm{e}^{-\frac{2}{3}x}\int_0^{\pi}(3\cos\theta+2)(1-\cos\theta)^2\,\mathrm{d}\theta = 0.$$

We find similarly that $f(x)\leq 0$ when $x\leq 0$. □

And therefore, we can deduce the sign of the eigenvalue: $1-\frac{\alpha}{4c_1(\alpha)}\big\langle (a_{11}-a_{22})^2\big\rangle_{M_D} > 0$ when $\alpha > 0$ and $1-\frac{\alpha}{4c_1(\alpha)}\Big\langle (a_{11}-a_{22})^2\Big\rangle_{M_D} < 0$ when $\alpha < 0$.

Case 3. Equilibria of type (c) : $D = \alpha\,\mathrm{diag}(1,0,0)$

For $D = \alpha\,\mathrm{diag}(1,0,0)$ with $\alpha = \rho c_2(\alpha)$, using the parametrisation (7.5), it holds that :

$$\begin{aligned}\int_{\mathrm{SO}_3(\mathbb{R})} a_{22}\mathrm{e}^{\frac{\alpha}{2}a_{11}}\,\mathrm{d}A &= \int_{\mathrm{SO}_3(\mathbb{R})} a_{22}\mathrm{e}^{\frac{\alpha}{2}a_{33}}\,\mathrm{d}A \\ &= \frac{1}{8\pi^2}\int_{\theta=0}^{2\pi}\int_{\phi_2=0}^{\pi} \mathrm{e}^{\frac{\alpha}{2}\cos\phi_2}\sin\phi_2 \int_{\phi_1=0}^{2\pi}(-\sin\theta\sin\phi_1+\cos\theta\cos\phi_1\cos\phi_2)\mathrm{d}\phi_1\mathrm{d}\phi_2\mathrm{d}\theta \\ &= 0.\end{aligned}$$

where the first equality comes from the change of variable $A \mapsto P^{13}A(P^{13})^{\mathrm{T}}$. Similarly,

$$\langle a_{22}\rangle_{M_D} = \langle a_{33}\rangle_{M_D} = \langle a_{11}a_{22}\rangle_{M_D} = \langle a_{11}a_{33}\rangle_{M_D} = 0.$$

The Hessian matrix is therefore equal to :

$$I_3 - \frac{1}{2}\rho\begin{pmatrix} \langle a_{11}^2\rangle_{M_D} - \langle a_{11}\rangle_{M_D}^2 & 0 & 0 \\ 0 & \langle a_{22}^2\rangle_{M_D} & \langle a_{22}a_{33}\rangle_{M_D} \\ 0 & \langle a_{22}a_{33}\rangle_{M_D} & \langle a_{33}^2\rangle_{M_D} \end{pmatrix},$$

and since $\langle a_{22}^2\rangle_{M_D} = \langle a_{33}^2\rangle_{M_D}$ as it can be seen with the change of variable $A \mapsto P^{23}A(P^{23})^{\mathrm{T}}$, its eigenvalues are :

$$1 - \frac{1}{2}\rho\Big(\langle a_{11}^2\rangle_{M_D} - \langle a_{11}\rangle_{M_D}^2\Big),$$

with eigenvector $(1,0,0)^{\mathrm{T}}$,

$$1 - \frac{1}{2}\rho\Big(\langle a_{22}^2\rangle_{M_D} - \langle a_{22}a_{33}\rangle_{M_D}\Big),$$

with eigenvector $(0,1,-1)^{\mathrm{T}}$ and

$$1 - \frac{1}{2}\rho\Big(\langle a_{22}^2\rangle_{M_D} + \langle a_{22}a_{33}\rangle_{M_D}\Big),$$

with eigenvector $(0,1,1)^{\mathrm{T}}$. We have as before :

$$c_2'(\alpha) = \frac{1}{2}\Big(\langle a_{11}^2\rangle_{M_D} - \langle a_{11}\rangle_{M_D}^2\Big),$$

so the first eigenvalue can be rewritten

$$1-\frac{1}{2}\rho\Big(\langle a_{11}^2\rangle_{M_D}-\langle a_{11}\rangle_{M_D}^2\Big)=1-\frac{\alpha c_2'(\alpha)}{c_2(\alpha)}=c_2(\alpha)\left(\frac{id}{c_2}\right)'(\alpha)>0,$$

where we have used Proposition 7.3.16 to determine the sign. The two other eigenvalues are equal to:

$$1-\frac{1}{4}\rho\Big\langle(a_{22}\pm a_{33})^2\Big\rangle_{M_D}$$

Using the change of variable $A\mapsto P^{13}A(P^{13})^{\mathrm{T}}$ and the parametrisation (7.5), one can see that :

$$\begin{aligned}&\int_{\mathrm{SO}_3(\mathbb{R})}(a_{22}\pm a_{33})^2\mathrm{e}^{\frac{\alpha}{2}a_{11}}\,\mathrm{d}A=\int_{\mathrm{SO}_3(\mathbb{R})}(a_{22}\pm a_{11})^2\mathrm{e}^{\frac{\alpha}{2}a_{33}}\,\mathrm{d}A\\&=\frac{1}{8\pi^2}\int_{\theta=0}^{2\pi}\int_{\phi_1=0}^{2\pi}\cos^2(\phi_1\pm\theta)\int_{\phi_2=0}^{\pi}\sin\phi_2\,(1\pm\cos\phi_2)^2\mathrm{e}^{\frac{\alpha}{2}\cos\phi_2}\,\mathrm{d}\phi_2\,\mathrm{d}\phi_1\,\mathrm{d}\theta\end{aligned}$$

so that :

$$\Big\langle(a_{22}\pm a_{33})^2\Big\rangle_{M_D}=\frac{1}{2}\Big[(1\pm\cos\phi)^2\Big]_\alpha$$

where $[\cdot]_\alpha$ is defined in Proposition 7.3.1. Using the relation $\rho=\frac{\alpha}{c_2(\alpha)}=\frac{4}{[\sin^2\phi]_\alpha}$ (see Formula (7.21)), the two eigenvalues are equal to:

$$1-\frac{1}{2}\frac{\int_0^\pi\sin\phi(1\pm\cos\phi)^2\mathrm{e}^{\frac{\alpha}{2}\cos\phi}\,\mathrm{d}\phi}{\int_0^\pi\sin^3\phi\mathrm{e}^{\frac{\alpha}{2}\cos\phi}\,\mathrm{d}\phi}.$$

With the same technique used in the previous paragraph (Lemma 7.4.16) it is possible to show that the eigenvalue $1-\frac{1}{4}\rho\Big\langle(a_{22}-a_{33})^2\Big\rangle_{M_D}$ is nonpositive when $\alpha<0$ and nonnegative when $\alpha>0$. The contrary holds for the other eigenvalue (nonnegative when $\alpha<0$ and nonpositive when $\alpha>0$). Finally the signs of these two eigenvalues are always $(+-)$.

The conclusion of the proof follows from the study of the roots of Equations (7.15) and (7.16) provided by Corollary 7.3.17 and depicted in Figure 7.3.1. □

Remark 7.4.17. The above calculations are similar to the computation of the equilibria and their stability of

$$\Psi\ :D\in\mathrm{diag}(\mathscr{T})\mapsto\mathcal{F}[M_D]$$

where $\mathcal{F}$ is the free-energy (7.28). In particular, it can be shown that the equilibria of Ψ and their stability are the same as the ones described in Theorem 7.4.14. In particular,

since (7.28) is also a free energy in the Fokker-Planck case, this analysis shows the instability of equilibria of the Fokker-Planck of the form ρM_D when D is of one of the unstable equilibria of (7.24a) described in Theorem 7.4.14. This technique is similar to the one which was used in [335] in the case of 3D polymers. However, it does not provide global or local convergence of the solution of the Fokker-Planck equation towards an equilibrium. The problem has been recently tackled in [166] where a complete study of the phase transition phenomena in the body-orientation Fokker-Planck case can be found.

We can finally prove Theorem 7.4.2 :

Proof (of Theorem 7.4.2). Thanks to the Duhamel's formula (7.22), the asymptotic behaviour of $f(t)$ as $t \to +\infty$ is given by the asymptotic behaviour of $J_{f(t)}$. Thanks to Proposition 7.4.5 and Corollary 7.4.7, we only have to study the asymptotic behaviour of the solution of the ODE (7.24a) where the initial condition is the diagonal part of a SSVD of J_{f_0}. Since this equation has a gradient-flow structure (7.27a), by analyticity of the potential and boundedness of the trajectories, Łojasiewicz inequality [190, 242] implies that the solution $D(t)$ converges as $t \to +\infty$ towards an equilibrium D^{eq} and consequently $J_{f(t)} \to PD^{\mathrm{eq}}Q := J^{\mathrm{eq}}$. Moreover the equilibrium D^{eq} is a stable equilibrium provided that D_0 does not belong to the stable manifold of an unstable equilibrium. Since these manifolds have dimension at most 2, the union of these manifolds, called $\mathcal{N}_\rho$ is of zero measure and there is convergence towards a stable equilibrium for all $D_0 \notin \mathcal{N}_\rho$. In this case, since all the equilibria are hyperbolic, the Hartman-Grobman theorem [278, Section 2.8] ensures that the convergence is locally exponentially fast in the sense that there exist constants $\delta, \lambda, C > 0$ such that if $\|J_{f_0} - J^{\mathrm{eq}}\| \leq \delta$ then for all $t > 0$,

$$\|J_{f(t)} - J^{\mathrm{eq}}\| \leq C\mathrm{e}^{-\lambda t}. \tag{7.31}$$

Let $f^{\mathrm{eq}} = \rho M_{J^{\mathrm{eq}}}$. It follows from Duhamel's formula (7.22) that for all $A \in \mathrm{SO}_3(\mathbb{R})$:

$$|f(t,A) - f^{\mathrm{eq}}(A)| \leq \mathrm{e}^{-t}|f_0(A) - f^{\mathrm{eq}}(A)| + \rho\mathrm{e}^{-t}\int_0^t \mathrm{e}^s |M_{J_{f(s)}}(A) - M_{J^{\mathrm{eq}}}(A)|\mathrm{d}s. \tag{7.32}$$

Since $\mathrm{SO}_3(\mathbb{R})$ is compact and $J_{f(t)}$ is bounded uniformly in t, there exists a constant $L > 0$ such that for all $t > 0$, the following Lipschitz bound holds:

$$\forall A \in \mathrm{SO}_3(\mathbb{R}),\ \ |M_{J_{f(t)}}(A) - M_{J^{\mathrm{eq}}}(A)| \leq L\|J_{f(t)} - J^{\mathrm{eq}}\|. \tag{7.33}$$

Reporting (7.33) into (7.32) and using (7.31), the first point of Theorem 7.4.2 follows with constants $K = CL/|1-\lambda|$ and $\mu = \min(1,\lambda)$ when $\lambda \neq 1$ and $K = CL$ and $\mu = 1 - \varepsilon$ for

any $\varepsilon > 0$ when $\lambda = 1$.

The stability of the equilibria of the dynamical system (7.24a) is given in Theorem 7.4.14. Finally the conclusions of points 2.(ii) and 2.(iii) follow from the fact that the diagonal parts of the SSVD of the equilibria of type (b) with parameters α_+ and α_1 are respectively $\alpha_+ I_3$ and $\alpha_1 I_3$. □

Remark 7.4.18. The main advantage of the choice of the BGK operator clearly appears in this theorem: the infinite dimensional PDE can be reduced to a three-dimensional dynamical system for which there is a local and global convergence theory. In particular, we could push further the analysis and describe the zero-measure set $\mathscr{N}_\rho$. When $\rho \neq \rho^*$ and $\rho \neq \rho_c$, all the equilibria are hyperbolic and the set $\mathscr{N}_\rho$ is an intersection of stable manifolds of unstable equilibria [278, Section 2.7]. Using the stable manifold theorem, the proof of Theorem 7.4.14 and Proposition 7.4.6, it is possible to characterise precisely the behaviour of the system for each initial condition in $\mathscr{N}_\rho$. Some details are given in [111, Section 5.3]. In the critical case $\rho = \rho^*$ or $\rho = \rho_c$, the equilibria are not hyperbolic and the behaviour is ruled by the center manifold theory.

7.5 Macroscopic limit for the stable equilibria

7.5.1 Scaling of the spatially inhomogeneous BGK equation

We now go back to the spatially inhomogeneous model (2.10) (still with $c_0 = 1$, $\nu = 1$ and $\mathbb{M}[f] = J_f$). We want to investigate (at least formally) the hydrodynamic models derived from the BGK equation (2.10). To do so, as in [114] and Section 1.4, we introduce the scaling $t' = \varepsilon t$ and $x' = \varepsilon x$ for $\varepsilon > 0$ and we define $f^\varepsilon(t', x', A) := f(t, x, A)$. After this change of variables in (2.10) and dropping the primes, we see that f^ε satisfies the following equation:

$$\partial_t f^\varepsilon + (Ae_1 \cdot \nabla_x) f^\varepsilon = \frac{1}{\varepsilon} \left(\rho_{f^\varepsilon} M_{J_{f^\varepsilon}} - f^\varepsilon \right). \tag{7.34}$$

We want to investigate the macroscopic limit $\varepsilon \to 0$ with the assumption that f^ε converges towards a stable equilibrium. Thanks to the results of the last section, we will assume that $f^\varepsilon \to \rho M_{\alpha \mathbb{A}}$ where $\rho = \rho(t, x)$, $\alpha = \rho c_1(\alpha)$, $\alpha \in \mathbb{R}_+$ and $\mathbb{A} = \mathbb{A}(t, x) \in \mathcal{M}_3(\mathbb{R})$ (with a notion of convergence as strong as needed). Since the equilibrium is assumed to be stable there are two cases: either $\mathbb{A} \in \mathrm{SO}_3(\mathbb{R})$ (and therefore $\rho > \rho^*$) or $\mathbb{A} = 0$ that is to say f^ε is uniform in the body-orientation variable and converges towards $\rho = \rho(t, x)$ (and therefore $\rho < \rho_c$). For a given time $t \in \mathbb{R}_+$, we will say that $x \in \mathbb{R}^3$ belongs to a

disordered region when $\mathbb{A}(t,x) = 0$. Otherwise, when $\mathbb{A}(t,x) \in \mathrm{SO}_3(\mathbb{R})$, we will say that $x \in \mathbb{R}^3$ belongs to an ordered region.

The purpose of the two next sections is to write at least formally the hydrodynamic equations satisfied by $\rho \equiv \rho(t,x)$ and $\mathbb{A} \equiv \mathbb{A}(t,x)$. First notice that integrating (7.34) over $\mathrm{SO}_3(\mathbb{R})$ leads to the conservation law:

$$\partial_t \rho^\varepsilon + \nabla_x \cdot j[f^\varepsilon] = 0, \tag{7.35}$$

where $\rho^\varepsilon \equiv \rho_{f^\varepsilon}$ and

$$j[f^\varepsilon] := \int_{\mathrm{SO}_3(\mathbb{R})} A e_1 f^\varepsilon \, \mathrm{d}A \equiv J_{f^\varepsilon} e_1.$$

The macroscopic model then depends on the region considered.

1. In a disordered region, $j[f^\varepsilon] \to 0$ and assuming that the convergence is sufficiently strong, we get that $\partial_t \rho = 0$. To obtain more information we will look at the next order in the Chapman-Enskog expansion (Section 7.5.2).

2. In an ordered region, $j[f^\varepsilon] \to \alpha \mathbb{A} e_1$ where $\alpha = \rho c_1(\alpha)$ and therefore, assuming that the convergence is strong enough:

   $$\partial_t \rho + \nabla_x \cdot (\alpha \mathbb{A} e_1) = 0.$$

   However due to the lack of conserved quantities, we will need specific tools to write an equation satisfied by $\mathbb{A} = \mathbb{A}(t,x)$ in order to obtain a closed system of equations on $(\rho, \mathbb{A})$. This is the purpose of Section 7.5.3.

7.5.2 Diffusion model in a disordered region

We consider a region where f^ε converges as $\varepsilon \to 0$ to a density $\rho(t,x)$ uniform in the body-attitude variable. The following proposition gives the diffusion model obtained by looking at the next order in the Chapman-Enskog expansion.

Proposition 7.5.1 (Formal)**.** *In a disordered region, the density ρ^ε satisfies formally at first order the following diffusion equation:*

$$\partial_t \rho^\varepsilon = \varepsilon \nabla_x \cdot \begin{pmatrix} \frac{1}{3} \nabla_x \rho^\varepsilon \\ 1 - \frac{\rho^\varepsilon}{\rho_c} \end{pmatrix}, \quad \rho_c = 6. \tag{7.36}$$

Proof. We follow the same calculations as in [113] : we write $f^\varepsilon = \rho^\varepsilon + \varepsilon f_1^\varepsilon$ (where f_1^ε is defined by this relation) and notice that:

$$J_{f^\varepsilon} = \varepsilon J_{f_1^\varepsilon} \quad \text{and} \quad M_{J_{f^\varepsilon}}(A) = 1 + \varepsilon J_{f_1^\varepsilon} \cdot A + \mathcal{O}(\varepsilon^2).$$

Inserting this in (7.34), multiplying by A and integrating over $\mathrm{SO}_3(\mathbb{R})$ leads to:

$$J_{f_1^\varepsilon} = \rho^\varepsilon \int_{\mathrm{SO}_3(\mathbb{R})} (J_{f_1^\varepsilon} \cdot A) A \,\mathrm{d}A - \int_{\mathrm{SO}_3(\mathbb{R})} A e_1 \cdot \nabla_x \rho^\varepsilon A \,\mathrm{d}A + \mathcal{O}(\varepsilon). \tag{7.37}$$

Using Lemma 7.2.4, it holds that

$$\int_{\mathrm{SO}_3(\mathbb{R})} (J_{f_1^\varepsilon} \cdot A) A \,\mathrm{d}A = \frac{1}{6} J_{f_1^\varepsilon}. \tag{7.38}$$

To compute the second term, we note that $Ae_1 \cdot \nabla_x \rho^\varepsilon = 2A \cdot R_{\rho^\varepsilon}$ where R_{ρ^ε} is the matrix, the first column of which is equal to $\nabla_x \rho^\varepsilon$ and the others are equal to zero. Using Lemma 7.2.4 we obtain

$$\int_{\mathrm{SO}_3(\mathbb{R})} A e_1 \cdot \nabla_x \rho^\varepsilon A \,\mathrm{d}A = \frac{1}{3} R_{\rho^\varepsilon}. \tag{7.39}$$

By multiplying (7.37) by e_1, it follows from (7.38) and (7.39) that :

$$\left(1 - \frac{\rho^\varepsilon}{\rho_c}\right) J_{f_1^\varepsilon} e_1 = -\frac{1}{3} \nabla_x \rho^\varepsilon + \mathcal{O}(\varepsilon),$$

which gives the result by inserting this in (7.35). □

Remark 7.5.2. This analysis does not depend on the dimension. In $\mathrm{SO}_n(\mathbb{R})$ the same formal result holds:

$$\partial_t \rho^\varepsilon = \varepsilon \nabla_x \cdot \left(\frac{\frac{1}{n} \nabla_x \rho^\varepsilon}{1 - \frac{\rho^\varepsilon}{\rho_c}} \right), \quad \rho_c = 2n.$$

7.5.3 Self-organised hydrodynamics in an ordered region

In the following, for a given density $\rho \in \mathbb{R}_+$, $\alpha(\rho)$ denotes the maximal nonnegative root of $\alpha = \rho c_1(\alpha)$. We are going to prove the following theorem.

Theorem 7.5.3 (Formal)**.** *We suppose that $f^\varepsilon \to \rho(x,t) M_{J(t,x)}$ (as strongly as necessary) as $\varepsilon \to 0$ where $J(x,t) = \alpha(\rho(t,x)) \mathbb{A}(t,x)$ and $\mathbb{A}(t,x) \in \mathrm{SO}_3(\mathbb{R})$. Then ρ and $\mathbb{A}$ satisfy*

the following system of partial differential equations:

$$\partial_t \rho + \nabla_x \cdot (\rho c_1(\alpha(\rho)) \mathbb{A} e_1) = 0, \tag{7.40a}$$

$$\rho\big(\partial_t \mathbb{A} + \tilde{c}_2(\mathbb{A}e_1 \cdot \nabla_x)\mathbb{A}\big) + \tilde{c_3}[\mathbb{A}e_1 \times \nabla_x \rho]_\times \mathbb{A} + c_4 \rho[-\mathbf{r} \times \mathbb{A}e_1 + \delta \mathbb{A}e_1]_\times \mathbb{A} = 0. \tag{7.40b}$$

where $\tilde{c}_2$, $\tilde{c_3}$, c_4 are functions of ρ to be defined later and δ and $\mathbf{r}$ are the "divergence" and "rotational" operators defined in [114] : if $\mathbb{A}(x) = \exp([\mathbf{b}(x)]_\times)\mathbb{A}(x_0)$ with $\mathbf{b}$ smooth around the point x_0 and $\mathbf{b}(x_0) = 0$, then

$$\delta(x_0) := \nabla_x \cdot \mathbf{b}(x)|_{x=x_0}, \quad \mathbf{r}(x_0) := \nabla_x \times \mathbf{b}(x)|_{x=x_0}, \tag{7.41}$$

where $\nabla_x \times$ is the curl operator.

The first equation (7.40a) is the conservation law (7.35) and the goal is to obtain the equation (7.40b) for $\mathbb{A} = \mathbb{A}(t, x)$. However, here and contrary to the classical gas dynamics, the total momentum is not conserved:

$$\frac{\mathrm{d}}{\mathrm{d}t} \int_{\mathrm{SO}_3(\mathbb{R})} f A \, \mathrm{d}A \neq 0$$

and we therefore cannot deduce easily a closed system of equations. This lack of conserved quantities is specific to self-propelled particle models such as the Vicsek model. The main tool to tackle the problem will be the Generalised Collision Invariants (GCI) method introduced in [122] for the study of the hydrodynamic limit of the continuum Vicsek model. This method can be adapted to the present context as follows.

For a given $J \in \mathcal{M}_3(\mathbb{R})$, we define first the linear collision operator:

$$\mathcal{L}_J(f) = \rho_f M_J - f,$$

so that $Q_{\mathrm{BGK}}(f) = \mathcal{L}_{J_f}(f)$. If $J \in \mathcal{M}_3(\mathbb{R})$ is not singular (i.e. $\det J \neq 0$) then let $\mathbb{A} := \mathsf{P}_{\mathrm{SO}_3(\mathbb{R})}(J) \in \mathrm{SO}_3(\mathbb{R})$ be the projection of J on $\mathrm{SO}_3(\mathbb{R})$. Note that when $\det J > 0$ then $\mathbb{A}$ is simply the orthogonal part of the polar decomposition of J (see[116, Proposition 7]). The set of GCI associated to J is defined as:

$$\mathscr{C}_J := \left\{ \psi \ : \mathrm{SO}_3(\mathbb{R}) \to \mathbb{R}, \ \int_{\mathrm{SO}_3(\mathbb{R})} \mathcal{L}_J(f)\, \psi \, \mathrm{d}A = 0 \ \text{ for all } f \text{ such that } \mathsf{P}_{T_{\mathbb{A}}}(J_f) = 0 \right\}. \tag{7.42}$$

The goal is to obtain an explicit definition of the set $\mathscr{C}_J$. We first observe that the condition

$\psi \in \mathscr{C}_J$ is equivalent to:

$$\int_{\mathrm{SO}_3(\mathbb{R})} f(\langle\psi\rangle_{M_J} - \psi)\,\mathrm{d}A = 0 \quad \text{for all } f \text{ such that } \mathsf{P}_{T_{\mathbb{A}}}(J_f) = 0.$$

Therefore, following the ideas of the proof of [114, Proposition 4.3], we have:

$$\psi \in \mathscr{C}_J \iff \exists B \in T_{\mathbb{A}},\ \langle\psi\rangle_{M_J} - \psi(A) = B \cdot A,$$

that is to say:

$$\psi \in \mathscr{C}_J \iff \exists B \in T_{\mathbb{A}},\ \exists C \in \mathbb{R},\ \psi(A) = -B \cdot A + C,$$

or equivalently since $B \in T_{\mathbb{A}}$ means that there exists $P \in \mathcal{A}_3(\mathbb{R})$ such that $B = \mathbb{A}P$:

$$\mathscr{C}_J = \mathrm{Span}\left(1,\ \bigcup_{P\in\mathcal{A}_3(\mathbb{R})} \psi_P^{\mathbb{A}}\right),$$

where

$$\psi_P^{\mathbb{A}}(A) = -P \cdot (\mathbb{A}^{\mathrm{T}} A).$$

We are now ready to give formal proof of Theorem 7.5.3.

Proof (of Theorem 7.5.3). For any $P \in \mathcal{A}_3(\mathbb{R})$, by Definition (7.42) of the GCI, we get by multiplying the equation (7.34) by $\psi_P^{\mathbb{A}^\varepsilon}$:

$$\int_{\mathrm{SO}_3(\mathbb{R})} (\partial_t f^\varepsilon + Ae_1 \cdot \nabla_x f^\varepsilon) P \cdot ((\mathbb{A}^\varepsilon)^{\mathrm{T}} A)\,\mathrm{d}A = 0, \tag{7.43}$$

where $\mathbb{A}^\varepsilon = \mathsf{P}_{\mathrm{SO}_3(\mathbb{R})}(J_{f^\varepsilon})$. Note that if $f^\varepsilon \to \rho M_J$ with $\det(J) > 0$, we can also assume $\det(J_{f^\varepsilon}) > 0$ for ε sufficiently small and $\mathbb{A}^\varepsilon \in \mathrm{SO}_3(\mathbb{R})$ can be constructed using the polar decomposition as in [114].

Then, taking formally the limit $\varepsilon \to 0$ in (7.43) and since it is true for all $P \in \mathcal{A}_3(\mathbb{R})$, we obtain:

$$X := \int_{\mathrm{SO}_3(\mathbb{R})} \Big(\partial_t(\rho M_{\alpha\mathbb{A}}) + Ae_1 \cdot \nabla_x(\rho M_{\alpha\mathbb{A}})\Big)(\mathbb{A}^{\mathrm{T}} A - A^{\mathrm{T}}\mathbb{A})\,\mathrm{d}A = 0. \tag{7.44}$$

We have:

$$\begin{aligned}\partial_t(M_{\alpha\mathbb{A}}) &= \Big(\partial_t(\alpha\mathbb{A})\cdot A - \langle\partial_t(\alpha\mathbb{A})\cdot A\rangle_{M_{\alpha\mathbb{A}}}\Big)M_{\alpha\mathbb{A}}\\ &= \alpha'\partial_t\rho(A\cdot\mathbb{A} - \langle A\cdot\mathbb{A}\rangle_{M_{\alpha\mathbb{A}}})M_{\alpha\mathbb{A}} + \alpha\partial_t\mathbb{A}\cdot(A - \langle A\rangle_{M_{\alpha\mathbb{A}}})M_{\alpha\mathbb{A}},\end{aligned}$$

where α' denotes the derivative of $\rho\mapsto\alpha(\rho)$ with respect to ρ and similarly for $\partial_i(M_{\alpha\mathbb{A}})$. With this we compute the term:

$$\begin{aligned}(\partial_t + Ae_1\cdot\nabla_x)(\rho M_{\alpha\mathbb{A}}) = M_{\alpha\mathbb{A}}(A)\left(1+\rho\alpha'\left(A\cdot\mathbb{A} - \frac{3}{2}c_1(\alpha)\right)\right)(\partial_t + Ae_1\cdot\nabla_x)\rho\\ + M_{\alpha\mathbb{A}}(A)\rho\alpha A\cdot(\partial_t + Ae_1\cdot\nabla_x)\mathbb{A},\end{aligned}$$

where we have used that:

$$\langle A\cdot\mathbb{A}\rangle_{M_{\alpha\mathbb{A}}} = \frac{3}{2}c_1(\alpha),$$

and

$$\mathbb{A}\cdot(\partial_t + Ae_1\cdot\nabla_x)\mathbb{A} = 0.$$

Most of the terms that appear in X are computed in [114]. Precisely,

$$X = X_1 + X_2 + X_3 + X_4 + Y \tag{7.45}$$

where X_1, X_2, X_3 and X_4 are computed in [114] :

$$\begin{aligned}X_1 &:= \int_{\mathrm{SO}_3(\mathbb{R})}\partial_t\rho M_{\alpha\mathbb{A}}(A)(\mathbb{A}^{\mathrm{T}}A - A^{\mathrm{T}}\mathbb{A})\,\mathrm{d}A = 0,\\ X_2 &:= \int_{\mathrm{SO}_3(\mathbb{R})}\alpha\rho(A\cdot\partial_t\mathbb{A})M_{\alpha\mathbb{A}}(A)(\mathbb{A}^{\mathrm{T}}A - A^{\mathrm{T}}\mathbb{A})\,\mathrm{d}A = C_2\rho\alpha\mathbb{A}^{\mathrm{T}}\partial_t\mathbb{A},\\ X_3 &:= \int_{\mathrm{SO}_3(\mathbb{R})}Ae_1\cdot\nabla_x\rho M_{\alpha\mathbb{A}}(A)(\mathbb{A}^{\mathrm{T}}A - A^{\mathrm{T}}\mathbb{A})\,\mathrm{d}A = C_3[e_1\times\mathbb{A}^{\mathrm{T}}\nabla_x\rho]_\times,\\ X_4 &:= \int_{\mathrm{SO}_3(\mathbb{R})}\rho\alpha\big(A\cdot(Ae_1\cdot\nabla_x)\mathbb{A}\big)M_{\alpha\mathbb{A}}(A)(\mathbb{A}^{\mathrm{T}}A - A^{\mathrm{T}}\mathbb{A})\,\mathrm{d}A\\ &\qquad = \rho\alpha(C_4[Le_1]_\times + C_5[L^{\mathrm{T}}e_1 + \mathrm{Tr}(L)e_1]_\times),\end{aligned}$$

where the coefficients

$$C_2 = C_3 := \frac{2}{3}\{\sin^2\theta\}_\alpha,\quad C_4 := \frac{2}{15}\{\sin^2\theta(1+4\cos\theta)\}_\alpha,\quad C_5 := \frac{2}{15}\{\sin^2\theta(1-\cos\theta)\}_\alpha,$$

and the matrix

$$L := \mathbb{A}^{\mathrm{T}} \mathcal{D}_x(\mathbb{A}) \mathbb{A},$$

are the same as in [114]. The matrix $\mathcal{D}_x(\mathbb{A}) \in \mathcal{M}_3(\mathbb{R})$ is defined as the unique matrix such that for all $\mathbf{w} \in \mathbb{R}^3$, and smooth functions $\mathbb{A} : \mathbb{R}^3 \to \mathrm{SO}_3(\mathbb{R})$,

$$(\mathbf{w} \cdot \nabla_x)\mathbb{A} = [\mathcal{D}_x(\mathbb{A})\mathbf{w}]_\times \mathbb{A}$$

(see [114, Section 4.5]). Note that $C_3 = C_2$ since the noise and alignement parameters which were denoted by ν and d in [114] have been taken equal to 1 here. Note also that these coefficients are functions of ρ (through α only). The term Y is an additional term which appears here due to the presence of the parameter $\alpha = \alpha(\rho)$ which is a function of ρ. It depends also on the derivative α' of α :

$$Y \ := \rho\alpha' \int_{\mathrm{SO}_3(\mathbb{R})} (\mathbb{A}^{\mathrm{T}} A - A^{\mathrm{T}} \mathbb{A}) M_{\alpha\mathbb{A}}(A) \left(A \cdot \mathbb{A} - \frac{3}{2} c_1(\alpha) \right) (\partial_t + Ae_1 \cdot \nabla_x) \rho \, \mathrm{d}A.$$

All the terms that involve the time derivative of ρ are equal to zero since $\partial_t \rho$ does not depend on A and with the change of variable $A' = \mathbb{A} A^{\mathrm{T}} \mathbb{A}$ which has unit jacobian, it holds that $A' \cdot \mathbb{A} = A \cdot \mathbb{A}$ and therefore

$$\begin{aligned} \int_{\mathrm{SO}_3(\mathbb{R})} (\mathbb{A}^{\mathrm{T}} A - A^{\mathrm{T}} \mathbb{A}) M_{\alpha\mathbb{A}}(A) \left(A \cdot \mathbb{A} - \frac{3}{2} c_1(\alpha) \right) \mathrm{d}A \\ = - \int_{\mathrm{SO}_3(\mathbb{R})} (\mathbb{A}^{\mathrm{T}} A' - A' T \mathbb{A}) M_{\alpha\mathbb{A}}(A') \left(A' \cdot \mathbb{A} - \frac{3}{2} c_1(\alpha) \right) \mathrm{d}A' = 0. \end{aligned}$$

We thus have:

$$Y = Y_1 + Y_2,$$

where

$$Y_1 \ := \rho\alpha' \int_{\mathrm{SO}_3(\mathbb{R})} (A \cdot \mathbb{A})(Ae_1 \cdot \nabla_x) \rho \, (\mathbb{A}^{\mathrm{T}} A - A^{\mathrm{T}} \mathbb{A}) M_{\alpha\mathbb{A}}(A) \, \mathrm{d}A,$$

and

$$Y_2 \ := \frac{3}{2} c_1(\alpha) \rho\alpha' \int_{\mathrm{SO}_3(\mathbb{R})} (Ae_1 \cdot \nabla_x) \rho \, (\mathbb{A}^{\mathrm{T}} A - A^{\mathrm{T}} \mathbb{A}) M_{\alpha\mathbb{A}}(A) \, \mathrm{d}A.$$

With the change of variable $A \mapsto \mathbb{A}^{\mathrm{T}} A$ these terms become

$$Y_1 = \rho\alpha' \int_{\mathrm{SO}_3(\mathbb{R})} (\mathbb{A} B e_1 \cdot \nabla_x \rho)(B - B^{\mathrm{T}})(B \cdot I_3) M_{\alpha I_3}(B) \, \mathrm{d}B,$$

$$Y_2 := \frac{3}{2} c_1(\alpha)\rho\alpha' \int_{\mathrm{SO}_3(\mathbb{R})} (\mathbb{A}Be_1 \cdot \nabla_x \rho)(B - B^{\mathrm{T}}) M_{\alpha I_3}(B)\, \mathrm{d}B,$$

and they can be computed using the same techniques as in [114] or lemma 7.2.5 in the appendix. More precisely, we can write

$$\mathbb{A}Be_1 \cdot \nabla_x \rho = B \cdot R_{1,\rho},$$

where $R_{1,\rho}$ is the matrix, the first column of which is equal to $2\mathbb{A}^{\mathrm{T}}\nabla_x\rho$ and the others are all equal to zero. It satisfies:

$$\frac{R_{1,\rho} - R_{1,\rho}^{\mathrm{T}}}{2} = [e_1 \times \mathbb{A}^{\mathrm{T}}\nabla_x\rho]_\times.$$

By the change of variable $B \mapsto B^{\mathrm{T}}$, we have

$$\begin{aligned} Y_1 &= \rho\alpha' \int_{\mathrm{SO}_3(\mathbb{R})} (B \cdot R_{1,\rho})(B - B^{\mathrm{T}})(B \cdot I_3) M_{\alpha I_3}(B)\, \mathrm{d}B, \\ &= \rho\alpha' \int_{\mathrm{SO}_3(\mathbb{R})} A \cdot (R_{1,\rho} - R_{1,\rho}^{\mathrm{T}}) A (A \cdot I_3) M_{\alpha I_3}(A)\, \mathrm{d}A. \end{aligned}$$

This integral is of the form (7.46) where

$$g(A) := A \cdot I_3 M_{\alpha I_3}(A)$$

is invariant by transposition and conjugation and

$$J := R_{1,\rho} - R_{1,\rho}^{\mathrm{T}}$$

is an antisymmetric matrix. From (7.48) and (7.49) we get

$$Y_1 = \rho\alpha\mu(R_{1,\rho} - R_{1,\rho}^{\mathrm{T}})$$

with

$$\mu := \frac{1}{8} \int_{\mathrm{SO}_3(\mathbb{R})} (a_{21} - a_{12})^2 \,\mathrm{Tr}(A) M_{\alpha I_3}(A)\, \mathrm{d}A.$$

The first term Y_1 can therefore be written:

$$Y_1 = 2\mu\rho\alpha'[e_1 \times \mathbb{A}^{\mathrm{T}}\nabla_x\rho]_\times,$$

and using Rodrigues' formula (7.2) we obtain:

$$2\mu = \frac{1}{3}\Big\{ (1+2\cos\theta)\sin^2(\theta)\Big\}_\alpha$$

where $\{\cdot\}_\alpha$ has been defined in Proposition 7.3.1. Similarly the second term Y_2 can be written:

$$Y_2 = \frac{3}{2}c_1(\alpha)C_3\rho\alpha'[e_1 \times \mathbb{A}^{\mathrm{T}}\nabla_x\rho]_\times,$$

where the coefficient C_3 is the same as in [114] :

$$C_3 = \frac{2}{3}\{\sin^2\theta\}_\alpha = C_2.$$

Finally, we obtain:

$$Y = \rho\alpha'\left(\frac{3}{2}c_1(\alpha)C_3 + \frac{1}{3}\Big\{ (1+2\cos\theta)\sin^2(\theta)\Big\}_\alpha\right)[e_1 \times \mathbb{A}^{\mathrm{T}}\nabla_x\rho]_\times.$$

Putting all the terms together, we can conclude as in [114]. First we notice that:

$$\mathrm{Tr}(L) = \delta, \quad [\mathbb{A}L^{\mathrm{T}}e_1]_\times = [(\mathcal{D}_x(\mathbb{A}) - [\mathbf{r}]_\times)\mathbb{A}e_1]_\times, \quad [\mathbb{A}Le_1]_\times\mathbb{A} = \big(\mathbb{A}e_1\cdot\nabla_x\big)\mathbb{A}.$$

Therefore we obtain by multiplying (7.45) by $\mathbb{A}$ and dividing by αC_2 :

$$\rho(\partial_t\mathbb{A} + c_2(\mathbb{A}e_1\cdot\nabla_x)\mathbb{A}) + \tilde{c_3}[\mathbb{A}e_1\times\nabla_x\rho]_\times\mathbb{A} + c_4\rho[-\mathbf{r}\times\mathbb{A}e_1 + \delta\mathbb{A}e_1]_\times\mathbb{A} = 0,$$

where the coefficients

$$\tilde{c_2} := \frac{C_4+C_5}{C_2} = \frac{1}{5}\frac{\{\sin^2\theta(2+3\cos\theta)\}_\alpha}{\{\sin^2\theta\}_\alpha} \quad \text{and} \quad c_4 := \frac{C_5}{C_2} = \frac{1}{5}\frac{\{\sin^2\theta(1-\cos\theta)\}_\alpha}{\{\sin^2\theta\}_\alpha}$$

are respectively equal to the coefficients c_2 and c_4 in [114] and the coefficient c_3 in [114] (which is equal to 1) becomes:

$$\tilde{c_3} = \frac{1}{\alpha} + \frac{\rho\alpha'}{\alpha}\left(\frac{3}{2}c_1(\alpha) + \frac{1}{2}\frac{\Big\{(1+2\cos\theta)\sin^2\theta\Big\}_\alpha}{\{\sin^2\theta\}_\alpha}\right).$$

□

7.6 Conclusion and perspectives

In this chapter, we have presented an analysis at the kinetic level of the body-attitude coordination level. In the spatially homogeneous case, we have drawn a parallel between this Vicsek-type model and the models of nematic alignment of polymers. We then have deduced the equilibria of the system and have shown a phase transition phenomenon triggered by the density of agents. Thanks to a gradient-flow structure specific to the BGK equation we have been able to describe the asymptotic behaviour of the system. Finally, we have derived the macroscopic models (SOHB) in the spatially inhomogeneous case.

This model and its analysis raise many open questions. At the kinetic level, research perspectives include the following:

1. it would be interesting to quantify the time that takes a solution to reach the basin of attraction of a stable equilibria. This question has been addressed recently for the Kuramoto model in [261].

2. Our study relies on the dimension 3. The complete description of the equilibria of the BGK (or the Fokker-Planck) operator in any dimension and their stability is still an open question. Note however that the derivation of the macroscopic model in any dimension is investigated in Chapter 9.

3. The space-inhomogeneous case, not considered here, is much more difficult to tackle due to the transport operator which prevents the reduction to a gradient-flow (in finite dimension for the BGK operator and in infinite dimension for the Fokker-Planck operator). This situation is not specific to the body-orientation model presented here and the question is largely open even in the Vicsek case (see the conclusion of [113]). Numerical simulations of the individual-based model suggest that clusterisation phenomena appear: the space can be decomposed in large-density regions (the clusters) and low-density regions. Inside a cluster, flocking is observed which is consistent with the fact that it is the only stable equilibrium in large density regions. Between the clusters, a diffusive behaviour is observed, again it seems consistent with the analysis in the low-density (homogenous) case presented in this article. The dynamics of the clusters (which can be seen as a kind of free-boundary problem) remains an open problem.

Appendix

7.A Quaternions and rotations

This appendix is devoted to the proof of Proposition 7.3.15. We also give additional results about quaternions. The following lemma gives a link between quaternions and the theory of Q-tensors.

Lemma 7.A.1. *Let $\mathcal{S}_4^0(\mathbb{R})$ be the space of symmetric 4×4 trace free matrices. If $Q \in \mathcal{S}_4^0(\mathbb{R})$ has two eigenvalues with eigenspaces of dimensions 1 and 3, then Q can be written*

$$Q = \alpha\left(q \otimes q - \frac{1}{4}I_4\right),$$

for a given unit quaternion q seen as a vector of $\mathbb{R}^4$. A matrix of this form is called a uniaxial Q-tensor. When $\alpha = 1$ we will say that Q is a normalised uniaxial Q-tensor.

Proof. Let $Q \in \mathcal{S}_4^0(\mathbb{R})$ such that Q has two eigenvalues with eigenspaces of dimensions 1 and 3. By the spectral theorem, there exists $P \in \mathcal{O}_3(\mathbb{R})$ such that for a given $\alpha > 0$:

$$Q = \frac{\alpha}{4}P\,\mathrm{diag}(3,-1,-1,-1)P^{\mathrm{T}} = \alpha P\,\mathrm{diag}(1,0,0,0)P^{\mathrm{T}} - \frac{\alpha}{4}I_4,$$

and the result follows by taking q equals to the first column of P. □

Proof of Proposition 7.3.15. 1. The group isomorphism Φ is explicitly computed in [293]. In particular, let $q \in \mathbb{S}^3/\pm 1$. The matrix $A = \Phi(q)$ is defined for all purely imaginary quaternion $u \in \mathbb{H}$ by $A[u] = [quq^*]$ where $(u_1,u_2,u_3)^{\mathrm{T}} =: [u] \in \mathbb{R}^3$ is the vector associated to $u = u_1 i + u_2 j + u_3 k$. More explicitly, if $q = x + iy + zj + tk$, then

$$A = \begin{pmatrix} x^2+y^2-z^2-t^2 & 2(yz-xt) & 2(xz+yt) \\ 2(xt+yz) & x^2-y^2+z^2-t^2 & 2(zt-xy) \\ 2(yt-xz) & 2(xy+zt) & x^2-y^2-z^2+t^2 \end{pmatrix}.$$

Note that we have identified $q \in \mathbb{H}$ and its equivalence class in $\mathbb{S}^3/\pm 1$ and that Φ is well defined since only quadratic expressions are involved. The fact that this group isomorphism is an isometry follows from [116, Proposition A.3] and [114, Lemma 4.2].

2. The expression
$$J \cdot A = \frac{1}{2}\operatorname{Tr}(\Phi(q)^{\mathrm{T}} J)$$
is a quadratic form for q. We take Q the matrix associated to this quadratic form. For $J = (J_{ij})_{i,j}$, using the explicit form of $A = \Phi(q)$ with $q = x + yi + zj + tk$ we obtain:
$$Q = \frac{1}{4}\begin{pmatrix} J_{11}+J_{22}+J_{33} & J_{32}-J_{23} & J_{13}-J_{31} & J_{21}-J_{12} \\ J_{32}-J_{23} & J_{11}-J_{22}-J_{33} & J_{12}+J_{21} & J_{13}+J_{31} \\ J_{13}-J_{31} & J_{12}+J_{21} & -J_{11}+J_{22}-J_{33} & J_{23}+J_{32} \\ J_{21}-J_{12} & J_{13}+J_{31} & J_{23}+J_{32} & -J_{11}-J_{22}+J_{33} \end{pmatrix}.$$
This is an isomorphism since $\dim \mathcal{M}_3(\mathbb{R}) = \dim \mathcal{S}_4^0(\mathbb{R})$ and J can be obtained from Q similarly. Moreover, since the bilinear matrix associated to a quadratic form is uniquely defined, if $Q \in \mathcal{S}_4^0(\mathbb{R})$ is such that $\frac{1}{2}J \cdot \Phi(q) = q \cdot Qq$ for all $q \in \mathbb{S}^3/\pm 1$, then $Q = \phi(J)$.

3. To prove the third point, we note that a unit quaternion can be seen as a rotation in $\mathbb{R}^3$ in a more geometrical way ([116, Section 5.1]): for $\theta \in [0, \pi]$ and $\mathbf{n} = (n_1, n_2, n_3)^{\mathrm{T}} \in \mathbb{S}^2$, let us define the unit quaternion q by
$$q = \cos\frac{\theta}{2} + \sin\frac{\theta}{2}(n_1 i + n_2 j + n_3 k),$$
The unit quaternion q represents the rotation of angle $\theta \in [0, \pi]$ and axis $\mathbf{n} \in \mathbb{S}^2$ in the sense that if $\mathcal{A}(\theta, \mathbf{n}) \in \mathrm{SO}_3(\mathbb{R})$ denotes the matrix associated to the rotation of angle $\theta \in [0, \pi]$ around the axis $\mathbf{n} \in \mathbb{S}^2$ then $\Phi(q) = \mathcal{A}(\theta, \mathbf{n})$. Note that q and $-q$ represent the same rotation so $\Phi(q)$ is well defined by identifying q with its equivalence class in $\mathbb{S}^3/\pm 1$.

In $\mathbb{R}^3$ the composition of two rotations of respective angles and axis $(\theta, \mathbf{n}) \in [0, \pi] \times \mathbb{S}^2$ and $(\theta', \mathbf{n}') \in [0, \pi] \times \mathbb{S}^2$ is itself a rotation: we have $\mathcal{A}(\theta, \mathbf{n})\mathcal{A}(\theta', \mathbf{n}') = \mathcal{A}(\hat{\theta}, \hat{\mathbf{n}})$ where the angle $\hat{\theta} \in [0, \pi]$ is defined by
$$\cos\frac{\hat{\theta}}{2} = \cos\frac{\theta}{2}\cos\frac{\theta'}{2} - \mathbf{n} \cdot \mathbf{n}' \sin\frac{\theta}{2}\sin\frac{\theta'}{2}.$$
Note that $\cos(\hat{\theta}/2) = q \cdot \bar{q}'$ where q and q' are the associated unit quaternions seen as

vectors of dimension 4. In particular the dot product of two rotations matrices is

$$\mathcal{A}(\theta,\mathbf{n})\cdot\mathcal{A}(\theta',\mathbf{n}') = \frac{1}{2}\,\mathrm{Tr}\left(\mathcal{A}(\theta,\mathbf{n})\mathcal{A}(\theta',-\mathbf{n}')\right) = \frac{1}{2}(2\cos\tilde{\theta}+1)$$

where

$$\cos\frac{\tilde{\theta}}{2} = \cos\frac{\theta}{2}\cos\frac{\theta'}{2} + \mathbf{n}\cdot\mathbf{n}'\sin\frac{\theta}{2}\sin\frac{\theta'}{2}.$$

Besides, for the quaternions q and q' respectively associated to the rotations $\mathcal{A}(\theta,\mathbf{n})$ and $\mathcal{A}(\theta',\mathbf{n}')$, we have:

$$q'\cdot Qq' = (q\cdot q')^2 - \frac{1}{4} = \cos^2\frac{\tilde{\theta}}{2} - \frac{1}{4} = \frac{1}{4}(2\cos\tilde{\theta}+1),$$

where Q is the normalised uniaxial Q-tensor:

$$Q = q\otimes q - \frac{1}{4}I_4.$$

Finally $\frac{1}{2}\mathcal{A}(\theta,\mathbf{n})\cdot\mathcal{A}(\theta',\mathbf{n}') = q'\cdot Qq'$ and we obtain thanks to the previous point:

$$\phi\Big(\mathcal{A}(\theta,\mathbf{n})\Big) = Q,$$

that is to say: if $J\in\mathrm{SO}_3(\mathbb{R})$ then $\phi(J)$ is a normalised uniaxial Q-tensor.

4. If $D=\mathrm{diag}(d_1,d_2,d_3)$ then using the explicit form of ϕ given in the second point:

$$\phi(D) = \frac{1}{4}\begin{pmatrix} d_1+d_2+d_3 & & & \\ & d_1-d_2-d_3 & & \\ & & -d_1+d_2-d_3 & \\ & & & -d_1-d_2+d_3 \end{pmatrix},$$

and if $Q=\mathrm{diag}(s_1,s_2,s_3,s_4)$ with $s_1+s_2+s_3+s_4=0$ then

$$\phi^{-1}(Q) = 2\begin{pmatrix} s_1+s_2 & & \\ & s_1+s_3 & \\ & & s_1+s_4 \end{pmatrix}.$$

□

7.B More about $\mathrm{SO}_n(\mathbb{R})$

Lemma 7.B.1. *For all $n \geq 3$:*

$$\mathrm{Span}(\mathrm{SO}_n(\mathbb{R})) = \mathcal{M}_n(\mathbb{R}).$$

Proof. First we prove that the diagonal matrices form a subset of $\mathrm{Span}(\mathrm{SO}_n(\mathbb{R}))$: it is enough to show that

$$D := \begin{pmatrix} 1 & & & \\ & 0 & & \\ & & \ddots & \\ & & & 0 \end{pmatrix} \in \mathrm{Span}(\mathrm{SO}_n(\mathbb{R}))$$

(the other diagonal matrices with only one nonzero coefficient can be obtained in a similar way). When n is odd:

$$2D = I_n + \begin{pmatrix} 1 & & & \\ & -1 & & \\ & & \ddots & \\ & & & -1 \end{pmatrix}$$

and both matrices in the sum are in $\mathrm{SO}_n(\mathbb{R})$. When $n \geq 4$ is even,

$$\begin{pmatrix} 0_4 & \\ & I_{n-4} \end{pmatrix} = \frac{1}{2} I_n + \frac{1}{2} \begin{pmatrix} -I_4 & \\ & I_{n-4} \end{pmatrix} \in \mathrm{Span}(\mathrm{SO}_n(\mathbb{R})),$$

thus:

$$\begin{pmatrix} 1 & & & & & \\ & -1 & & & & \\ & & -1 & & & \\ & & & 1 & & \\ & & & & 0_{n-4} \end{pmatrix} = \begin{pmatrix} 1 & & & & & \\ & -1 & & & & \\ & & -1 & & & \\ & & & 1 & & \\ & & & & I_{n-4} \end{pmatrix} - \begin{pmatrix} 0_4 & \\ & I_{n-4} \end{pmatrix} \in \mathrm{Span}(\mathrm{SO}_n(\mathbb{R})),$$

and similarly:

$$4D = \begin{pmatrix} 1 & & & & \\ & 1 & & & \\ & & 1 & & \\ & & & 1 & \\ & & & & 0_{n-4} \end{pmatrix} + \begin{pmatrix} 1 & & & & \\ & -1 & & & \\ & & -1 & & \\ & & & 1 & \\ & & & & 0_{n-4} \end{pmatrix} + \begin{pmatrix} 1 & & & & \\ & 1 & & & \\ & & -1 & & \\ & & & -1 & \\ & & & & 0_{n-4} \end{pmatrix}$$
$$+ \begin{pmatrix} 1 & & & & \\ & -1 & & & \\ & & 1 & & \\ & & & -1 & \\ & & & & 0_{n-4} \end{pmatrix} \in \mathrm{Span}(\mathrm{SO}_n(\mathbb{R})).$$

The SSVD (Definition 7.2.7) gives the result for any matrix. □

Corollary 7.B.2. *For $n \geq 3$, a matrix that commutes with any matrix of $\mathrm{SO}_n(\mathbb{R})$ is of the form λI_n.*

We can now prove Lemma 7.2.4 and its generalisation Lemma 7.2.5.

Proof (of Lemma 7.2.4). The linear map $\Phi : \mathcal{M}_n(\mathbb{R}) \to \mathcal{M}_n(\mathbb{R})$ defined by

$$\Phi(J) := \int_{\mathrm{SO}_n(\mathbb{R})} (J \cdot A) A \, \mathrm{d}A,$$

satisfies for all $P \in \mathrm{SO}_n(\mathbb{R})$,

$$\Phi(P) = P\Phi(I_n) = \Phi(I_n)P,$$

which by Corollary 7.B.2 means that

$$\Phi(I_n) = \lambda I_n.$$

Therefore, $\Phi(P) = \lambda P$ for any $P \in \mathrm{SO}_n(\mathbb{R})$ and the same is true for any matrix $J \in \mathcal{M}_n(\mathbb{R})$ by Lemma 7.B.1. To compute λ, notice that for the matrix $e_i \otimes e_j$:

$$\frac{1}{2} \int_{\mathrm{SO}_n(\mathbb{R})} (e_i \cdot A e_j)^2 \, \mathrm{d}A = \lambda.$$

Summing this equality for all i, j gives:

$$\frac{n}{2} = \lambda n^2,$$

and $\lambda = 1/2n$. □

Proof (of Lemma 7.2.5). Let us define the linear map $\psi : \mathcal{M}_n(\mathbb{R}) \longrightarrow \mathcal{M}_n(\mathbb{R})$ by

$$\psi(J) := \int_{\mathrm{SO}_n(\mathbb{R})} (J \cdot A) A \, g(A) \, \mathrm{d}A. \tag{7.46}$$

1. We first note that ψ is self-adjoint for the dot product $A \cdot B = \frac{1}{2}\operatorname{Tr}(A^{\mathrm{T}}B)$: for any $K \in \mathcal{M}_n(\mathbb{R})$,

$$\psi(J) \cdot K = \int_{\mathrm{SO}_n(\mathbb{R})} (J \cdot A)(K \cdot A) \, g(A) \, \mathrm{d}A = J \cdot \psi(K).$$

2. We prove that $\mathrm{Span}(I_n)$ is a stable subspace for ψ : for any $P \in \mathrm{SO}_n(\mathbb{R})$ we have:

$$P\psi(I_n)P^{\mathrm{T}} = \int_{\mathrm{SO}_n(\mathbb{R})} (I_n \cdot A) PAP^{\mathrm{T}} \, g(A) \, \mathrm{d}A = \psi(I_n),$$

   and we conclude with Corollary 7.B.2 that $\psi(I_n) = \alpha I_n$ with:

$$\alpha = \frac{2}{n} I_n \cdot \psi(I_n) = \frac{1}{2n} \int_{\mathrm{SO}_n(\mathbb{R})} \operatorname{Tr}(A)^2 g(A) \, \mathrm{d}A.$$

3. Since ψ is a self-adjoint operator, the orthogonal subspace $\mathrm{Span}(I_n)^{\perp}$ is also a stable subspace. Moreover, using the change of variable $A \mapsto A^{\mathrm{T}}$, we see that $\psi(J^{\mathrm{T}}) = \psi(J)^{\mathrm{T}}$ and we have the decomposition:

$$\mathrm{Span}(I_n)^{\perp} = \mathcal{S}_n^0(\mathbb{R}) \overset{\perp}{\oplus} \mathcal{A}_n(\mathbb{R}),$$

   where $\mathcal{S}_n^0(\mathbb{R})$ and $\mathcal{A}_n(\mathbb{R})$ are respectively the subspace of trace free symmetric matrices and the subspace of antisymmetric matrices. They are both stable subspaces.

4. We prove now that $\psi : \mathcal{S}_n^0(\mathbb{R}) \to \mathcal{S}_n^0(\mathbb{R})$ is a uniform scaling. By the spectral theorem, every matrix $J \in \mathcal{S}_n^0(\mathbb{R})$ can be written

$$J = PDP^{\mathrm{T}},$$

where $P \in \mathrm{SO}_n(\mathbb{R})$ and D is diagonal. Since

$$\psi(PDP^{\mathrm{T}}) = P\psi(D)P^{\mathrm{T}},$$

it is enough to prove that there exists $\lambda \in \mathbb{R}$ such that for all diagonal matrices D, $\psi(D) = \lambda D$. For $D = \mathrm{diag}(d_1, \ldots, d_n)$, we have:

$$\psi(D) = \frac{1}{2}\sum_{k=1}^{n} d_k \int_{\mathrm{SO}_n(\mathbb{R})} a_{kk} A \, g(A) \, \mathrm{d}A.$$

Now, if $i \neq j$, let $D^{ik} \in \mathrm{SO}_n(\mathbb{R})$ be the diagonal matrix such that all the coefficients are equal to 1 except D^{ik}_{ii} and D^{ik}_{kk} which are equal to -1. Then the change of variable $A \mapsto D^{ik} A (D^{ik})^{\mathrm{T}}$ gives

$$\int_{\mathrm{SO}_n(\mathbb{R})} a_{kk} a_{ij} \, g(A) \, \mathrm{d}A = -\int_{\mathrm{SO}_n(\mathbb{R})} a_{kk} \, a_{ij} \, g(A) \, \mathrm{d}A = 0,$$

which proves that $\psi(D)$ is diagonal and the i-th coefficient of $\psi(D)$ is:

$$\psi(D)_{ii} = \frac{1}{2}\sum_{k=1}^{n} d_k \int_{\mathrm{SO}_n(\mathbb{R})} a_{kk} \, a_{ii} \, g(A) \, \mathrm{d}A.$$

Using the fact that $\mathrm{Tr}(D) = 0$ and that all the $\int_{\mathrm{SO}_n(\mathbb{R})} a_{ii} \, a_{kk} \, g(A) \, \mathrm{d}A$ are equal for $i \neq k$ (by using conjugation by the matrices P^{ij}, $i, j \neq k$, see Definition 7.2.2), we obtain:

$$\psi(D)_{ii} = \frac{1}{2} d_i \int_{\mathrm{SO}_n(\mathbb{R})} (a_{11}^2 - a_{11} \, a_{22}) \, g(A) \, \mathrm{d}A,$$

and we conclude that for all $J \in \mathcal{S}_n^0(\mathbb{R})$:

$$\psi(J) = \lambda J,$$

with

$$\lambda = \frac{1}{2} \int_{\mathrm{SO}_n(\mathbb{R})} (a_{11}^2 - a_{11} \, a_{22}) \, g(A) \, \mathrm{d}A = \frac{1}{4} \int_{\mathrm{SO}_n(\mathbb{R})} (a_{11} - a_{22})^2 \, g(A) \, \mathrm{d}A.$$

5. We prove similarly that $\psi \ : \mathcal{A}_n(\mathbb{R}) \to \mathcal{A}_n(\mathbb{R})$ is a uniform scaling. Every $J \in \mathcal{A}_n(\mathbb{R})$ can be written

$$J = PCP^{\mathrm{T}},$$

where

$$C = \begin{pmatrix} C_1 & & & & & & \\ & C_3 & & & & & \\ & & \ddots & & & & \\ & & & C_{2p-1} & & & \\ & & & & 0 & & \\ & & & & & \ddots & \\ & & & & & & 0 \end{pmatrix} \tag{7.47}$$

is a block diagonal matrix with blocks

$$C_i = \begin{pmatrix} 0 & -c_i \\ c_i & 0 \end{pmatrix}, \quad c_i \in \mathbb{R}^*, \quad i \in \{1, 3, 5, \ldots, 2p-1\}$$

so that,

$$\psi(J) = \psi(PCP^{\mathrm{T}}) = P\psi(C)P^{\mathrm{T}},$$

and

$$\psi(C) = \frac{1}{2}\sum_{k=1}^{p} c_{2k-1} \int_{\mathrm{SO}_n(\mathbb{R})} (a_{2k,2k-1} - a_{2k-1,2k})\, A\, g(A)\, \mathrm{d}A.$$

When $n \geq 3$, by using conjugation by the matrices $D^{2j-1,2j}$ for $j \in \{1, \ldots, \lfloor n/2 \rfloor\}$ (Definition 7.2.2) we can see that for each $k \in \{1, \ldots, p\}$, the matrix

$$M_k := \int_{\mathrm{SO}_n(\mathbb{R})} (a_{2k,2k-1} - a_{2k-1,2k})\, A\, g(A)\, \mathrm{d}A$$

is of the form (7.47). Moreover, when $n \geq 5$, by using conjugation by matrices $D^{2j-1,2\ell-1}$ for $j \neq \ell$, $j, \ell \in \{1, \ldots, \lfloor n/2 \rfloor\}$ and $j, \ell \neq k$, we can see that all the diagonal blocks of M_k are equal to zero except the one in position $2k-1$. When $n = 3$ there is only one block in position 1 so the result holds but when $n = 4$ such j and ℓ do not exist. In conclusion, when $n \neq 4$, $\psi(C)$ is of the form (7.47) and each diagonal block C'_{2k-1} of $\psi(C)$ is written

$$C'_{2k-1} = \mu_{2k-1} C_{2k-1}$$

with

$$\mu_{2k-1} := \int_{\mathrm{SO}_n(\mathbb{R})} (a_{2k,2k-1} - a_{2k-1,2k}) a_{2k,2k-1} g(A)\, \mathrm{d}A = \int_{\mathrm{SO}_n(\mathbb{R})} (a_{21} - a_{12}) a_{21} g(A)\, \mathrm{d}A,$$

where this equality follows by using conjugation by “block-permutation matrices":

$$Q^k := \begin{pmatrix} I_2 & & & & & & & & & & \\ & \ddots & & & & & & & & & \\ & & I_2 & & & & & & & & \\ & & & 0_2 & -I_2 & & & & & & \\ & & & I_2 & 0_2 & & & & & & \\ & & & & & I_2 & & & & & \\ & & & & & & \ddots & & & & \\ & & & & & & & I_2 & & & \\ & & & & & & & & 1 & & \\ & & & & & & & & & \ddots & \\ & & & & & & & & & & 1 \end{pmatrix},$$

where the first zero on the diagonal is in position $2k-1$. Therefore,

$$\psi(C) = \mu C, \tag{7.48}$$

with

$$\mu = \frac{1}{2}\int_{\mathrm{SO}_n(\mathbb{R})} (a_{21} - a_{12}) a_{21}\, g(A)\,\mathrm{d}A = \frac{1}{4}\int_{\mathrm{SO}_n(\mathbb{R})} (a_{21} - a_{12})^2\, g(A)\,\mathrm{d}A. \tag{7.49}$$

6. Finally, for $J \in \mathrm{Span}(I_n)^\perp$, writing

$$J = \frac{J + J^{\mathrm{T}}}{2} + \frac{J - J^{\mathrm{T}}}{2},$$

we have:

$$\psi(J) = \beta J + \gamma J^{\mathrm{T}},$$

with

$$\beta = \frac{1}{2}(\lambda + \mu) = \frac{1}{4}\int_{\mathrm{SO}_n(\mathbb{R})} \Big((a_{11}^2 - a_{11}\, a_{22}) + (a_{21} - a_{12}) a_{21} \Big)\, g(A)\,\mathrm{d}A,$$

and

$$\gamma = \frac{1}{2}(\lambda - \mu) = \frac{1}{4}\int_{\mathrm{SO}_n(\mathbb{R})} \Big((a_{11}^2 - a_{11}\, a_{22}) - (a_{21} - a_{12}) a_{21} \Big)\, g(A)\,\mathrm{d}A.$$

7. In conclusion, writing the decomposition

$$J = \frac{1}{n}\operatorname{Tr}(J) I_n + K,$$

where $K \in \operatorname{Span}(I_n)^{\perp}$, we obtain

$$\psi(J) = a \operatorname{Tr}(J) I_n + bJ + cJ^{\mathrm{T}},$$

with

$$a = \frac{\alpha - \beta - \gamma}{n},$$

and

$$b = \beta = \frac{1}{8}\int_{\mathrm{SO}_n(\mathbb{R})} \Big((a_{11} - a_{22})^2 + (a_{12} - a_{21})^2 \Big)\, g(A)\, \mathrm{d}A,$$

and

$$c = \gamma = \frac{1}{8}\int_{\mathrm{SO}_n(\mathbb{R})} \Big((a_{11} - a_{22})^2 - (a_{12} - a_{21})^2 \Big)\, g(A)\, \mathrm{d}A.$$

And there are of course many other ways to write the coefficients a, b and c.

□

Remark 7.B.3. In dimension 4, the result still holds for symmetric matrices. For general matrices, the result can be proved in particular cases, for instance when g is a function of the trace, by using an explicit parametrisation of $\mathrm{SO}_4(\mathbb{R})$ such as the 4-dimensional version of (7.4). An alternative more general approach will be presented in Chapter 9 (see Lemma 9.3.2).

Chapter 8

Bulk topological states in the macroscopic SOHB model

The present chapter is based on the following article co-authored with P. Degond and M. Na

[106] P. Degond, A. Diez, and M. Na. "Bulk topological states in a new collective dynamics model". *arXiv preprint: arXiv:2101.10864* (2021).

8.1 Introduction

This chapter is devoted to the macroscopic model (2.14) associated to the body-attitude coordination model outlined in the introduction. This model was first derived in [116] following the methodology of [122]. All the variants of the individual based models described in the introduction (Section 2.1.2) actually lead to structurally the same macroscopic model, called the "Self-Organised Hydrodynamics for Body-attitude coordination" (SOHB) model in [114]. The only difference between the different macroscopic models is the value of the coefficients c_i. When the IBM is a piecewise deterministic process, these coefficients can be computed explicitly as shown in the previous chapter and recalled in this chapter. For the alternative diffusion process (2.9), they depend on the solution of a differential equation which comes from the computation of the Generalised Collision Invariants. These differences are summarised in the review article [116] (see in particular [116, Proposition 11]). In the previous chapter, the model was derived in a slightly more general framework (starting from the PDMP IBM), where the concentration parameter depends on the spatial density of agents. In this case, the coefficients c_i also involve the derivatives of the function α defined in Section 7.5.3. In this chapter we focus on the simplest form of the coefficients which are obtained from the PDMP IBM (2.3), (2.4) when

the target body-orientation at each jump is given by (2.7).

In this chapter, we investigate the specificity of the SOHB model among the other collective dynamics models. In particular, we derive explicit solutions and numerically study the long-time behaviour of the system. To do so, we rely on an efficient direct simulation of the IBM in a macroscopic regime, namely

$$N \gg 1, \qquad \frac{R}{L} \sim \frac{c_0}{\nu\, L} \ll 1, \tag{8.1}$$

where N is the number of particles, R is the interaction radius, L is the typical macroscopic length, c_0 is the moving speed and ν is the interaction rate. On the analytical side, the derivation of the SOHB model starting from the IBM is only "formally rigorous". On the one hand, the mean-field limit cannot be guaranteed in all situations, on the other hand the derivation of the macroscopic model starting from the kinetic model is rigorous under appropriate, possibly strong, smoothness assumptions on the involved mathematical objects. However, despite this lack of a complete rigorous theoretical convergence framework, we have numerically checked in this chapter that there is a quantitative agreement between the SOHB model and the IBM in the regime (8.1). This legitimates the kinetic theory approach and enables a numerical study of the SOHB model. Using this approach, we have numerically explored several situations where the long-time behaviour of the system is characterised by a transition between the different classes of solutions derived. This is a first step towards a rigorous stability analysis of the SOHB model.

One of the guiding question of the present chapter is the topological structure of the solutions of the SOHB model. The internal geometrical properties of the particles indeed translate at the macroscopic level into topological properties of the solutions. It is not clear at this point whether these properties are linked to long-time stability. However, this is reminiscent of the notion of "topological states" introduced in the study of the quantum Hall effect and the design of so-called "topological insulators" [270, 269]. In collective dynamics, topological states have recently been derived under various geometrical configurations [299, 303, 304] in the Toner and Tu model [312], which is a continuum analog of the Vicsek model [321]. These states propagate on the boundary of the domain (they are thus called "edge states") and are characterised by an increased robustness against perturbations. By comparison, the topological states derived in this chapter propagate in the whole domain and are therefore called "bulk states". This comes from the fact that they are not induced by the geometry of the domain but rather by the internal geometry of the agents.

This chapter is organised as follows. In Section 8.2, we recall the SOHB model and

describe its specific features among other continuum collective dynamics models. Then explicit solutions of the macroscopic model are derived in Section 8.3 and are shown to exhibit non-trivial topology. They also serve as benchmarks to show that the IBM is an accurate approximation of the macroscopic model in Section 8.4. But after some time, the IBM departs from the special solutions of the macroscopic model and undergoes a topological phase transition. The study of these phase transitions require appropriate topological indicators which are developed in Section 8.5. Then, the topological phase transitions are analysed numerically in Section 8.6.2. A discussion and some open questions raised by these observations can be found in Section 8.7. Several appendices complete this chapter and include supplementary videos (Appendix 8.A), details on the numerical methods (Appendices 8.B and 8.C), proofs (Appendices 8.D and 8.E) and complementary experiments (Appendix 8.F).

8.2 The macroscopic body-alignment model

8.2.1 Description of the model

For the convenience of the reader, we recall below the macroscopic model outlined in the introduction of this thesis and derived in Section 7.5 of the previous chapter. The unknowns in the SOHB model are the particle density $\rho(t, \mathbf{x})$ and mean body-orientation $\mathbb{A}(t, \mathbf{x}) \in \mathrm{SO}_3(\mathbb{R})$ at time t and at a position denoted in this chapter by $\mathbf{x} = (x, y, z)^{\mathrm{T}} \in \mathbb{R}^3$. They satisfy the following set of equations:

$$\partial_t \rho + c_1 \nabla_{\mathbf{x}} \cdot (\rho \mathbb{A} e_1) = 0, \tag{8.2a}$$

$$\big(\partial_t + c_2 (\mathbb{A} e_1) \cdot \nabla_{\mathbf{x}}\big)\mathbb{A} + \big[(\mathbb{A} e_1) \times (c_3 \nabla_{\mathbf{x}} \log \rho + c_4 \mathbf{r}) + c_4 \delta \mathbb{A} e_1\big]_{\times} \mathbb{A} = 0. \tag{8.2b}$$

We recall that $\times$ denotes the cross product and we refer to formula (7.3) for the definition of $[\mathbf{w}]_{\times}$ when $\mathbf{w}$ is a vector in $\mathbb{R}^3$. The quantities $\mathbf{r}$ and δ have intrinsic expressions in terms of $\mathbb{A}$ (see (7.41)). However, in this chapter it will be more convenient to write the rotation field $\mathbb{A}$ in terms of the basis vectors

$$\Omega = \mathbb{A} e_1, \quad \mathbf{u} = \mathbb{A} e_2, \quad \mathbf{v} = \mathbb{A} e_3.$$

With these notations, the vector field $\mathbf{r}(t,\mathbf{x}) \in \mathbb{R}^3$ and the scalar field $\delta(t,\mathbf{x}) \in \mathbb{R}$ are given by

$$\mathbf{r} = (\nabla_{\mathbf{x}} \cdot \Omega)\,\Omega + (\nabla_{\mathbf{x}} \cdot \mathbf{u})\,\mathbf{u} + (\nabla_{\mathbf{x}} \cdot \mathbf{v})\,\mathbf{v}, \tag{8.3}$$

$$\delta = [(\Omega \cdot \nabla_{\mathbf{x}})\,\mathbf{u}] \cdot \mathbf{v} + [(\mathbf{u} \cdot \nabla_{\mathbf{x}})\mathbf{v}] \cdot \Omega + [(\mathbf{v} \cdot \nabla_{\mathbf{x}})\Omega] \cdot \mathbf{u}. \tag{8.4}$$

The macroscopic model (8.2) can also be equivalently rewritten as a set of four equations for the unknowns $(\rho, \Omega, \mathbf{u}, \mathbf{v})$

$$\partial_t \rho + \nabla_{\mathbf{x}} \cdot (c_1 \rho \Omega) = 0 \tag{8.5a}$$

$$(\partial_t + c_2(\Omega \cdot \nabla_{\mathbf{x}}))\Omega + \mathsf{P}_{\Omega^\perp}(c_3 \nabla_{\mathbf{x}} \log \rho + c_4 \mathbf{r}) = 0, \tag{8.5b}$$

$$(\partial_t + c_2(\Omega \cdot \nabla_{\mathbf{x}}))\mathbf{u} - \mathbf{u} \cdot (c_3 \nabla_{\mathbf{x}} \log \rho + c_4 \mathbf{r})\Omega + c_4 \delta \mathbf{v} = 0, \tag{8.5c}$$

$$(\partial_t + c_2(\Omega \cdot \nabla_{\mathbf{x}}))\mathbf{v} - \mathbf{v} \cdot (c_3 \nabla_{\mathbf{x}} \log \rho + c_4 \mathbf{r})\Omega - c_4 \delta \mathbf{u} = 0. \tag{8.5d}$$

The following lemma provides alternate expressions for δ.

Lemma 8.2.1. *We have*

$$\delta = -\big\{[(\mathbf{u} \cdot \nabla_{\mathbf{x}})\,\Omega] \cdot \mathbf{v} + [(\mathbf{v} \cdot \nabla_{\mathbf{x}})\mathbf{u}] \cdot \Omega + [(\Omega \cdot \nabla_{\mathbf{x}})\mathbf{v}] \cdot \mathbf{u}\big\} \tag{8.6}$$

$$= -\frac{1}{2}\big\{(\nabla_{\mathbf{x}} \times \Omega) \cdot \Omega + (\nabla_{\mathbf{x}} \times \mathbf{u}) \cdot \mathbf{u} + (\nabla_{\mathbf{x}} \times \mathbf{v}) \cdot \mathbf{v}\}. \tag{8.7}$$

Proof. Eq. (8.6) follows from inserting the formula

$$0 = \nabla_{\mathbf{x}}(\Omega \cdot \mathbf{u}) = (\Omega \cdot \nabla_{\mathbf{x}})\mathbf{u} + (\mathbf{u} \cdot \nabla_{\mathbf{x}})\Omega + \Omega \times (\nabla_{\mathbf{x}} \times \mathbf{u}) + \mathbf{u} \times (\nabla_{\mathbf{x}} \times \Omega),$$

and similar formulas after circular permutation of $\{\Omega, \mathbf{u}, \mathbf{v}\}$ into (8.4). Eq. (8.7) follows from taking the half sum of (8.4) and (8.6) and applying the formula

$$\nabla_{\mathbf{x}} \times \mathbf{v} = \nabla_{\mathbf{x}} \times (\Omega \times \mathbf{u}) = (\nabla_{\mathbf{x}} \cdot \mathbf{u})\,\Omega - (\nabla_{\mathbf{x}} \cdot \Omega)\,\mathbf{u} + (\mathbf{u} \cdot \nabla_{\mathbf{x}})\Omega - (\Omega \cdot \nabla_{\mathbf{x}})\mathbf{u},$$

and similar formulas after circular permutation of $\{\Omega, \mathbf{u}, \mathbf{v}\}$. □

The quantities c_1, c_2, c_3, c_4 are functions of κ and c_0 and have been computed in the previous chapter in the generalised case when κ is a function of ρ. In the present case, κ

is a fixed constant and the coefficients were known from [116]. They are given as follows.

$$\frac{c_1}{c_0} = \frac{2}{3}\left\langle \frac{1}{2} + \cos\theta \right\rangle_{\exp\left(\kappa\left(\frac{1}{2}+\cos\theta\right)\right)\,\sin^2\left(\frac{\theta}{2}\right)}, \tag{8.8}$$

$$\frac{c_2}{c_0} = \frac{1}{5}\left\langle 2 + 3\cos\theta \right\rangle_{\exp\left(\kappa\left(\frac{1}{2}+\cos\theta\right)\right)\,\sin^4\left(\frac{\theta}{2}\right)\,\cos^2\left(\frac{\theta}{2}\right)}, \tag{8.9}$$

$$\frac{c_3}{c_0} = \frac{1}{\kappa}, \tag{8.10}$$

$$\frac{c_4}{c_0} = \frac{1}{5}\left\langle 1 - \cos\theta \right\rangle_{\exp\left(\kappa\left(\frac{1}{2}+\cos\theta\right)\right)\,\sin^4\left(\frac{\theta}{2}\right)\,\cos^2\left(\frac{\theta}{2}\right)}, \tag{8.11}$$

where, for two functions f and g: $[0,\pi] \to \mathbb{R}$, we write

$$\langle f \rangle_g = \frac{\int_0^\pi f(\theta)\, g(\theta)\, \mathrm{d}\theta}{\int_0^\pi g(\theta)\, \mathrm{d}\theta}.$$

Fig. 8.2.1 provides a graphical representation of these functions.

Remark 8.2.2. In order to keep lighter notations, the coefficients of the model are still denoted by c_1, c_2, c_3, c_4 but compared to the coefficients derived in the last Chapter (Theorem 7.5.3), they are all normalised by c_0 (previously $c_0 = 1$), the tildes are dropped and the concentration parameter is constant (i.e. $\alpha(\rho) = \kappa$).

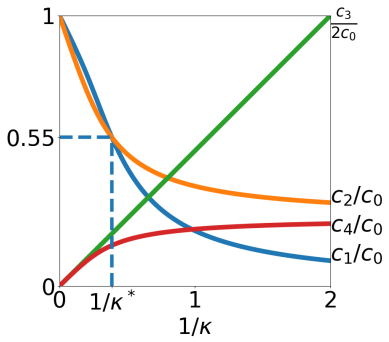

FIGURE 8.2.1: Dimensionless coefficients c_i/c_0 as functions of the inverse of concentration parameter $1/\kappa$. Blue curve c_1/c_0, orange curve c_2/c_0, green curve $c_3/2c_0$ and red curve c_4/c_0. At the crossover value $\kappa^* \simeq 2.58$, the sign of $c_2 - c_1$ changes (see Section 8.3.5).

8.2.2 Interpretation of the model

To better understand what the SOHB system (8.2) does, we re-write it as follows:

$$\partial_t \rho + c_1 \nabla_{\mathbf{x}} \cdot (\rho \Omega) = 0, \tag{8.12a}$$

$$D_t \mathbb{A} + [\mathbf{w}]_\times \mathbb{A} = 0, \tag{8.12b}$$

where the convective derivative D_t and the vector $\mathbf{w}$ are given by:

$$D_t = \partial_t + c_2 \Omega \cdot \nabla_{\mathbf{x}}, \tag{8.13}$$

$$\mathbf{w} = -\Omega \times \mathbf{F} + c_4 \delta \Omega, \quad \text{with} \quad \mathbf{F} = -c_3 \nabla_{\mathbf{x}} \log \rho - c_4 \mathbf{r}, \tag{8.14}$$

Eq. (8.12a) is the mass conservation equation of the fluid. The vector Ω gives the direction of the fluid motion. The fluid velocity deduced from (8.12a) is $c_1\Omega$. Since $c_1/c_0 \in [0, 1]$ as can be seen from Fig. 8.2.1, the fluid motion is oriented positively along Ω and its magnitude is smaller than the particles self-propulsion velocity c_0. This is because the average of vectors of identical norms has smaller norm. The quantity c_1/c_0 can be seen as an order parameter as in Chapter 7 but we will not dwell on this issue here.

Eq. (8.12b) provides the rate of change of $\mathbb{A}$ with time along the integral curves of the vector field $c_2\Omega$ as expressed by the convective derivative D_t. Note that this vector field is not the fluid velocity $c_1\Omega$ since $c_2 \neq c_1$. It can be interpreted as the propagation velocity of $\mathbb{A}$ when $\mathbf{w}$ is zero. Since $D_t\mathbb{A}$ is the derivative of an element of $\mathrm{SO}_3(\mathbb{R})$, it must lie in the tangent space to $\mathrm{SO}_3(\mathbb{R})$ at $\mathbb{A}$ which consists of all matrices of the form $\mathbb{W}\mathbb{A}$ with $\mathbb{W}$ antisymmetric (see Lemma 7.2.1). This structure is indeed satisfied by Eq. (8.12b) since, from the definition (7.3), the matrix $[\mathbf{w}]_\times$ is antisymmetric. It can be shown that the SOHB system is hyperbolic [117].

In fact, Eq. (8.12b) shows that the vector $\mathbf{w}$ is the instantaneous rotation vector of the frame $\mathbb{A}(t, \mathbf{X}(t))$, where $t \mapsto \mathbf{X}(t)$ is any solution of $\frac{\mathrm{d}\mathbf{X}}{\mathrm{d}t} = c_2\, \Omega(t, \mathbf{X}(t))$. Indeed, in the equivalent formulation Eq. (8.5), the equations on $(\Omega, \mathbf{u}, \mathbf{v})$ are of the form $D_t\mathbf{Z} = \mathbf{w} \times \mathbf{Z}$, with $\mathbf{Z} = \Omega$, $\mathbf{u}$, $\mathbf{v}$. This describes a rigid body rotation of the frame $\{\Omega, \mathbf{u}, \mathbf{v}\}$ with angular velocity $\mathbf{w}$. The rotation vector $\mathbf{w}$ has two components. The first one is $\Omega \times \mathbf{F}$ and tends to relax Ω towards $\mathbf{F}$. Due to its expression (8.14), the force $\mathbf{F}$ includes two contributions: that of the pressure gradient $-c_3\, \nabla_{\mathbf{x}} \log \rho$ and that of gradients of the body orientation through the vector $-c_4\, \mathbf{r}$. The second component of the rotation vector is $-c_4\delta\Omega$ and corresponds to a rotation of the body frame about the self propulsion direction Ω driven by gradients of the body orientation through the scalar $-c_4\, \delta$. The contributions of gradients of body orientation in the two components of the rotation vector are under the control of

the single coefficient c_4. Fig. 8.2.2 gives a graphical representation of the actions of these two infinitesimal rotations.

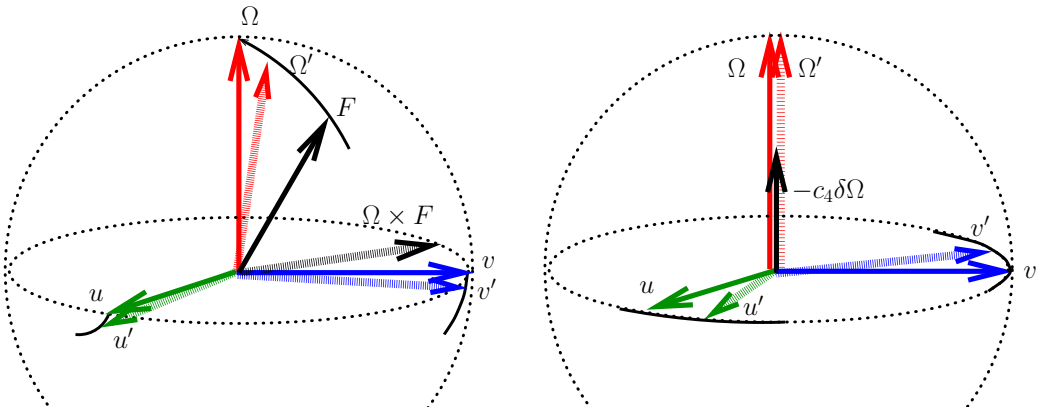

(A) Action of $\Omega \times \mathbf{F}$ (B) Action of $-c_4\delta\Omega$

FIGURE 8.2.2: Graphical representations of the two components of the infinitesimal rotation. $(\Omega, \mathbf{u}, \mathbf{v})$ denotes the position of the frame at time t while $(\Omega', \mathbf{u}', \mathbf{v}')$ is its position at time $t + \Delta t$ with $\Delta t \ll 1$. The frame at time t is denoted in plain colors (red for Ω, green for $\mathbf{u}$ and blue for $\mathbf{v}$) while that at time $t + \Delta t$ is in light colors. The motion of the vectors is indicated by a segment of circle in black color. (a) Action of $\Omega \times \mathbf{F}$: the vectors $\mathbf{F}$ and $\Omega \times \mathbf{F}$ are in plain and light black respectively. The vector $\mathbf{F}$ is shown with unit norm for the ease of the representation but could be of any norm in reality. The passage from $(\Omega, \mathbf{u}, \mathbf{v})$ to $(\Omega', \mathbf{u}', \mathbf{v}')$ is via an infinitesimal rotation of axis $\Omega \times \mathbf{F}$. (b) Action of δ: the vector $-c_4\delta\Omega$ is shown in black. The vectors Ω and Ω' are identical and collinear to $-c_4\delta\Omega$. The passage from $(\Omega, \mathbf{u}, \mathbf{v})$ to $(\Omega', \mathbf{u}', \mathbf{v}')$ is via an infinitesimal rotation of axis Ω.

8.2.3 Relation with other models

To better understand how the SOHB model (8.2) relates to other models, we re-write the equation for Ω as follows:

$$D_t\Omega = \mathsf{P}_{\Omega^\perp}\mathbf{F}, \tag{8.15}$$

where $\mathsf{P}_{\Omega^\perp}$ is the 3×3 projection matrix on the orthogonal plane to the vector Ω and is written $\mathsf{P}_{\Omega^\perp} = \mathrm{I}_3 - \Omega \otimes \Omega$ with $\otimes$ standing for the tensor (or outer) product. Eq. (8.15) bears similarities and differences with the momentum equation of isothermal compressible fluids. The latter is exactly recovered if the following three modifications are made:

1. the projection matrix $\mathsf{P}_{\Omega^\perp}$ is removed from (8.15) (i.e. it is replaced by I_3);
2. $c_2 = c_1$ in the convective derivative D_t (see (8.13));
3. $c_4 = 0$ in the expression of $\mathbf{F}$ (see (8.14)).

Indeed, under these three modifications, we get the following system for $(\rho, \mathbf{U})$ where $\mathbf{U} = c_1\Omega$ is the fluid velocity:

$$\partial_t \rho + \nabla_{\mathbf{x}} \cdot (\rho \mathbf{U}) = 0, \quad (\partial_t + \mathbf{U} \cdot \nabla_{\mathbf{x}})\mathbf{U} = -\Theta \nabla_{\mathbf{x}} \log \rho.$$

This is exactly the isothermal compressible Euler equations with the fluid temperature $\Theta = c_1 c_3$.

We now investigate what consequences follow from undoing the above three modifications, one by one.

1. Introducing the projection $\mathsf{P}_{\Omega^\perp}$ in (8.15) guarantees that the constraint $|\Omega| = 1$ is preserved in the course of time, if it is satisfied at time 0. Indeed, dotting Eq. (8.15) with Ω (and assuming that all functions are smooth) leads to $D_t|\Omega|^2 = 0$, which guarantees that $|\Omega|$ is constant along the integral curves of the vector field $c_2\Omega$. Thus, if $|\Omega| = 1$ at time $t = 0$, it will stay so at any time.

2. Having $c_2 \neq c_1$ is a signature of a loss of Galilean invariance. This is consistent with the fact that the microscopic system is not Galilean invariant as well, Indeed, there is a distinguished reference frame where the particle speed is c_0. Of course, this speed does not remain equal to c_0 in frames that translate at constant speed with respect to this frame.

   So far, with the introduction of $\mathsf{P}_{\Omega^\perp}$ and different constants $c_2 \neq c_1$ but still with $c_4 = 0$, the system for (ρ, Ω) is decoupled from the equations for $\mathbf{u}$ and $\mathbf{v}$ and is written (see Eqs. (8.12a), (8.15) with $\mathbf{F}$ given by (8.14) in which $c_4 = 0$):

$$\partial_t \rho + c_1 \nabla_{\mathbf{x}} \cdot (\rho\, \Omega) = 0, \tag{8.16a}$$

$$D_t \Omega + c_3\, \mathsf{P}_{\Omega^\perp} \nabla_{\mathbf{x}} \log \rho = 0. \tag{8.16b}$$

   This is nothing but the hydrodynamic limit (1.12), (1.13) of the Vicsek particle model outlined in the introduction of this thesis and known as "Self-organised Hydrodynamics (SOH)" as established in [122, 140]. This system has been shown to be hyperbolic [122] and to have local-in-time smooth solutions [120].

3. When $c_4 \neq 0$, in addition to the pressure gradient, a second component of the force $\mathbf{F}$ appears. This component depends on the full rotation matrix $\mathbb{A}$ through Ω, $\mathbf{u}$, $\mathbf{v}$ and their gradients (see Eq. (8.3)). It is thus truly specific of the body-orientation model.

8.3 Explicit solutions of the macroscopic model

In this section, we exhibit three different classes of global-in-time solutions of the SOHB model (8.12). They are special classes of a larger family of solutions which will also be introduced. All these solutions are characterised by uniform (i.e. independent of the spatial coordinate) fields ρ, $\mathbf{r}$ and δ. From now on we fix a wave-number (inverse of the length) $\xi \in \mathbb{R} \setminus \{0\}$ and define

$$\omega = \xi c_4, \qquad \lambda = c_2 + c_4. \tag{8.17}$$

We denote by $\mathbf{x} = (x, y, z)^{\mathrm{T}}$ the coordinates of a point $\mathbf{x} \in \mathbb{R}^3$ in the basis (e_1, e_2, e_3).

8.3.1 Flocking state

The flocking state (FS) is a trivial but important special solution of the SOHB model (8.12) where both the density and rotation fields are constant (i.e. independent of time) and uniform, for all $(t, \mathbf{x}) \in [0, \infty) \times \mathbb{R}^3$,

$$\rho(t, \mathbf{x}) \equiv \rho_0 = \text{constant}, \quad \mathbb{A}(t, \mathbf{x}) \equiv \mathbb{A}_0 = \text{constant}.$$

8.3.2 Milling orbits

We have the following

Lemma 8.3.1 (Milling solution)**.** *The pair $(\rho, \mathbb{A})$ consisting of a constant and uniform density $\rho(t, \mathbf{x}) = \rho_0 = $ constant and the following rotation field:*

$$\begin{aligned} \mathbb{A}(t, \mathbf{x}) &= \mathbb{A}_{\mathrm{mill}}(t, z) \\ &= \begin{pmatrix} \cos(\omega t) & \sin(\omega t)\cos(\xi z) & -\sin(\omega t)\sin(\xi z) \\ -\sin(\omega t) & \cos(\omega t)\cos(\xi z) & -\cos(\omega t)\sin(\xi z) \\ 0 & \sin(\xi z) & \cos(\xi z) \end{pmatrix} \qquad (8.18) \\ &= \mathcal{A}(-\omega t, e_3)\, \mathcal{A}(\xi z, e_1), \qquad (8.19) \end{aligned}$$

is a solution of the SOHB system (8.12)*, where ω and ξ are given by* (8.17)*. We recall that $\mathcal{A}(\theta, \mathbf{n})$ is the rotation of axis $\mathbf{n} \in \mathbb{S}^2$ and angle $\theta \in \mathbb{R}$ defined by* (7.2)*. This solution will be referred to as a* milling orbit (MO)*.*

The proof of this lemma is deferred to Section 8.D.

The MO is independent of x and y. Its initial condition is

$$\mathbb{A}_{\text{mill}}(0,z) = \mathcal{A}(\xi z, e_1) = \begin{pmatrix} 1 & 0 & 0 \\ 0 & \cos(\xi z) & -\sin(\xi z) \\ 0 & \sin(\xi z) & \cos(\xi z) \end{pmatrix}. \tag{8.20}$$

The initial direction of motion (the first column of $\mathbb{A}_{\text{mill}}(0,z)$) is independent of z and aligned along the x-direction, i.e. $\Omega(0,z) \equiv e_1$. As z varies, the body-orientation rotates uniformly about the x-direction with spatial angular frequency ξ. As the rotation vector is perpendicular to the direction of variation, (8.20) is called a *"perpendicular twist"*. As time evolves, the rotation field is obtained by multiplying on the left the initial perpendicular twist by the rotation $\mathcal{A}(-\omega t, e_3)$. This means that the whole body frame undergoes a uniform rotation about the z-axis with angular velocity $-\omega$. As a consequence, the direction of motion is again independent of z. It belongs to the plane orthogonal to z and undergoes a uniform rotation about the z-axis. Consequently, the fluid streamlines, which are the integral curves of $c_1\Omega$, are circles contained in planes orthogonal to z of radius $\frac{c_1}{\omega} = \frac{c_1}{c_4}\frac{1}{\xi}$ traversed in the negative direction if $\xi > 0$. These closed circular streamlines motivate the "milling" terminology. It can be checked that the MO satisfies:

$$\mathbf{r} = \xi\,(\sin(\omega t), \cos(\omega t), 0)^{\mathrm{T}}, \qquad \delta = 0.$$

As announced, $\mathbf{r}$ and δ are uniform but $\mathbf{r}$ depends on time. Actually, $\Omega \times \mathbf{r} = \xi e_3$ is independent of time. The MO is depicted in Fig. 8.3.1 and its dynamics is visualized in Video 2 (see Section 8.A).

Many examples of milling (also known as vortex) solutions have been observed in the collective dynamics literature as well as in biological systems [52, 91, 322]. On the modelling side, milling states have not been observed so far in alignment models without the inclusion of an additional process such as an attraction-repulsion force between the agents [68], a bounded cone of vision [90] or an anticipation mechanism [171]. The body-orientation framework is, to the best of our knowledge, a new situation in which milling can be observed with only alignment assumptions. Milling states can also be found in physical systems. A typical and important example is the motion of a charged particle in a uniform magnetic field, resulting in the formation of so-called cyclotron orbits. Once again, in the body-orientation framework, an external field is not needed and self-induced cyclotron orbits emerge only from the variations of the internal body-orientation. Here, the analog of the magnetic field would be $\Omega \times \mathbf{r}$ and the cyclotron frequency would be ω. Note that ω is under the control of coefficient c_4 which depends on the noise intensity $1/\kappa$.

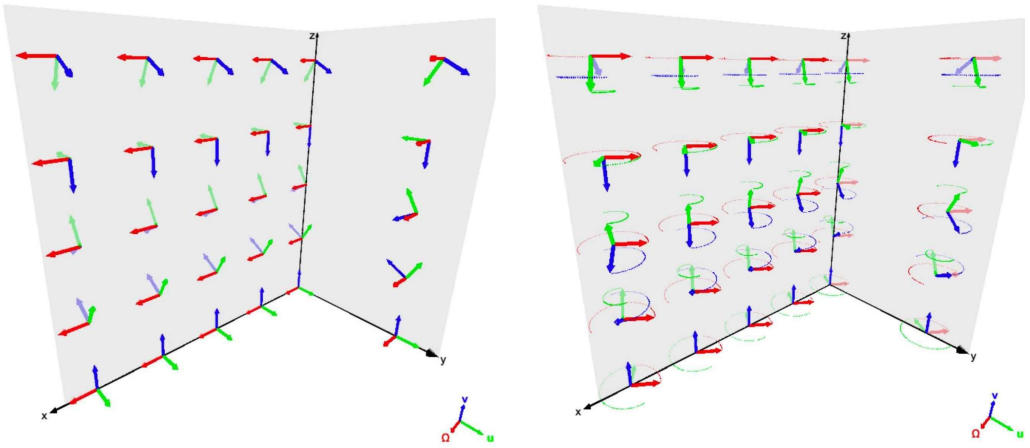

(A) $t = 0$ (B) $t > 0$

FIGURE 8.3.1: Graphical representation of the milling orbit (MO) at (a): initial time, and (b): time $t > 0$. The frame vectors Ω, $\mathbf{u}$ and $\mathbf{v}$ are represented at a certain number of points of the (O, x, y) and (O, y, z) planes. In (b), the rotation motion of the frame vectors is depicted by dotted circles of the color of the corresponding frame vector. The red dotted circle can be seen as a depiction of the fluid streamlines. See also Section 8.A, Video 2.

8.3.3 Helical traveling wave

We have the following

Lemma 8.3.2 (Helical wave solution)**.** *The pair* $(\rho, \mathbb{A})$ *consisting of a constant and uniform density* $\rho(t, \mathbf{x}) = \rho_0 = \text{constant}$ *and the following rotation field:*

$$\begin{aligned}
\mathbb{A}(t, \mathbf{x}) &= \mathbb{A}_{\text{htw}}(t, x) \\
&= \begin{pmatrix} 1 & 0 & 0 \\ 0 & \cos(\xi(x - \lambda t)) & -\sin(\xi(x - \lambda t)) \\ 0 & \sin(\xi(x - \lambda t)) & \cos(\xi(x - \lambda t)) \end{pmatrix} \qquad (8.21) \\
&= \mathcal{A}(\xi(x - \lambda t), e_1), \qquad (8.22)
\end{aligned}$$

is a solution of the SOHB system (8.12) *where* ξ *and* λ *are defined by* (8.17)*. This solution will be referred to as a* helical traveling wave (HW)*.*

The proof of this lemma is given in Section 8.D.2.

The HW is independent of y and z. Its initial condition is

$$\mathbb{A}_{\text{htw}}(0,x) = \mathcal{A}(\xi x, e_1) = \begin{pmatrix} 1 & 0 & 0 \\ 0 & \cos(\xi x) & -\sin(\xi x) \\ 0 & \sin(\xi x) & \cos(\xi x) \end{pmatrix}. \tag{8.23}$$

Here the self-propulsion direction is still independent of x and equal to e_1. Also, the body orientation still rotates uniformly about e_1 with spatial angular frequency ξ but when x is varied instead of z. This means that the body orientation is now twisted when varied along the propagation direction. So, this initial condition is called a *"parallel twist"*. In the HW, the self propulsion direction Ω remains constant in time and uniform in space. The initial twist is propagated in time in this direction at speed λ and gives rise to a traveling wave

$$\mathbb{A}_{\text{htw}}(t,x) = \mathbb{A}_{\text{htw}}(0, x - \lambda t).$$

Note that the traveling wave speed λ depends on the noise intensity $1/\kappa$ and is different from the fluid speed c_1. So, the frame carried by a given fluid element followed in its motion is not fixed but rotates in time. Since Ω does not change, the fluid streamlines are now straight lines parallel to e_1. So, as a fluid element moves, the ends of the frame vectors $\mathbf{u}$ and $\mathbf{v}$ follow a helical trajectory with axis e_1, hence the terminology "helical traveling waves" for these solutions. It can be checked that

$$\mathbf{r} = 0, \qquad \delta = \xi,$$

and again, $\mathbf{r}$ and δ are spatially uniform as announced. The HW is depicted graphically in Fig. 8.3.2. Its dynamics is visualized in Video 3 (see Section 8.A). The HW belongs to a larger class of solutions described in Section 8.D.2.

8.3.4 Generalised topological solutions

The three above described classes of solutions can be encompassed by a single family of generalised solutions as stated in the following lemma.

Lemma 8.3.3 (Generalised solutions)**.** *Let $\xi \in \mathbb{R}$ and $\theta \in [0,\pi]$ be two parameters. Let $\omega \in \mathbb{R}$ and $\tilde{\lambda} \in \mathbb{R}$ be defined by*

$$\omega = c_4 \xi, \quad \tilde{\lambda} = c_2 \cos\theta.$$

The pair $(\rho, \mathbb{A})$ consisting of a constant and uniform density $\rho(t,\mathbf{x}) = \rho_0 =$ constant and

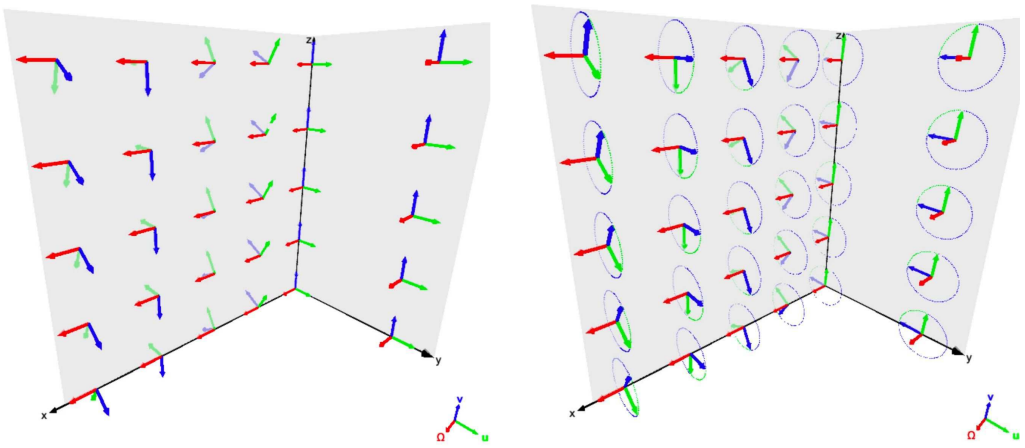

(A) $t = 0$ (B) $t > 0$

FIGURE 8.3.2: Graphical representation of the helical traveling wave (HW) at (a): initial time, and (b): time $t > 0$. See Fig. 8.3.1 for captions. See also Section 8.A, Video 3.

the following rotation field:

$$\mathbb{A}(t, \mathbf{x}) = \mathbb{A}_{\xi,\theta}(t, z) := \mathcal{A}(-\omega t, \mathbf{e}_3)\, \mathcal{A}\left(\theta - \frac{\pi}{2}, \mathbf{e}_2\right) \mathcal{A}(\xi(z - \tilde{\lambda}t), \mathbf{e}_1), \tag{8.24}$$

is a solution of the SOHB system (8.12). *We recall that* $\mathcal{A}(\theta, \mathbf{n})$ *is the rotation of axis* $\mathbf{n} \in \mathbb{S}^2$ *and angle* $\theta \in \mathbb{R}$. *This solution will be referred to as a Generalised topological Solution (GS).*

The proof of this lemma is deferred to the Appendix 8.D.3. Each of the three previous classes of solutions can be obtained for specific values of the parameters ξ and θ.

- When $\xi = 0$, the solution $\mathbb{A}_{0,\theta}$ is constant for any θ, which corresponds to a FS.
- When $\theta = \frac{\pi}{2}$ and $\xi \in \mathbb{R}$, then $\tilde{\lambda} = 0$ and the rotation with respect to the y-axis is equal to the identity: the solution $\mathbb{A}_{\xi,\pi/2}$ is therefore equal to the MO (8.19).
- When $\theta = 0$ and $\xi \in \mathbb{R}$ then $\tilde{\lambda} = c_2$ and the solution $\mathbb{A}_{\xi,0}$ is equal to

$$\mathbb{A}_{\xi,0} = \begin{pmatrix} 0 & -\sin(\xi(z - \lambda t)) & -\cos(\xi(z - \lambda t)) \\ 0 & \cos(\xi(z - \lambda t)) & -\sin(\xi(z - \lambda t)) \\ 1 & 0 & 0 \end{pmatrix}, \quad \lambda = c_2 + c_4,$$

which is an HW along the z-axis. The situation is analogous when $\theta = \pi$.

All these solutions have a non-zero gradient in the body-orientation variable which is always along the z-axis. This gradient is controlled by the parameter ξ. However, in the GS, the direction of motion Ω (or fluid velocity) is not necessarily parallel nor perpendicular to this gradient. Specifically, Ω has a constant polar angle equal to the parameter θ. The behaviour of the solution is then a combination of the two previously introduced phenomena: milling around the z-axis and a travelling wave of the body-orientation variable along the same axis. The applet accessible at `https://www.glowscript.org/#/user/AntoineDiez/folder/MyPrograms/program/BOfield` provides a graphical representation of the GS for arbitrary polar angles using `VPython` [296] and with the same conventions as in Fig. 8.3.1.

In the following, we will focus on each of these two elementary behaviours, i.e. the standard milling and helical travelling wave solutions, and in particular on their topological properties. The study of the full continuum of generalised solutions is left for future work. However, we will encounter GS obtained from a perturbed milling solution in Section 8.6.4.

8.3.5 Some properties of these special solutions

Clearly, in the definitions of the MO and HW, the choice of reference frame is unimportant. So, in the whole space $\mathbb{R}^3$, such solutions exist in association with any reference frame. In a square domain of side-length L with periodic boundary conditions, periodicity imposes some constraints on the direction of the reference frame. For simplicity, we will only consider the case where the reference frame has parallel axes to the sides of the square and ξ is linked to L by an integrality condition $L\,\xi = 2\pi\,n$, with $n \in \mathbb{Z} \setminus \{0\}$.

The study of the stability of the MO and the HW is left for future work. By contrast, the FS is linearly stable as the SOHB system is hyperbolic [117]. However, there is no guarantee that the FS at the level of the IBM is stable. Indeed, there are strong indications that the FS is not stable for the Vicsek model [80] for some parameter ranges and a similar trend is likely to occur here.

The existence of these solutions show that the inclusion of the full body orientation induces important changes in the dynamics of the particle positions and directions compared to the Vicsek model. To this end, we consider the corresponding macroscopic models, i.e. the SOH model (8.16) for the Vicsek model and the SOHB model (8.2) for the body-orientation dynamics. If we initialize the SOH model with uniform initial density ρ and mean direction Ω, inspection of (8.16) shows that the solution remains constant in time and thus corresponds to a flocking state of the Vicsek model. In the SOHB model, the three classes of solutions described in the previous sections (the FS, MO and HW) also have uniform initial density ρ and mean direction Ω. If the dynamics of the particle

positions and directions in the body orientation model was the same as in the Vicsek model, these three classes of solutions should have a constant mean direction Ω. However, it is not the case for the MO, where Ω changes with time and is subject to a planar rotation. This means that gradients of body attitude do have a non-trivial influence on the direction of motion of the particles and that the body orientation model does not reduce to a Vicsek model for the particle positions and directions.

There is another, more subtle, difference between the two models concerning the dynamics of Ω. It does not concern the MO and HW but we discuss it here in relation with the previous paragraph. Indeed, Fig. 8.2.1 reveals that the velocities c_1 and c_2 for the SOHB model crossover at a certain value κ^* of the concentration parameter. The coefficients c_1 and c_2 for the SOH model can be found in [140, Fig. A1(b)] and appear to satisfy $c_1 > c_2$ for the whole range of values of κ, i.e. do not exhibit any crossover. In particular, at large noise, the propagation velocity c_2 of Ω in the SOHB model is larger than the mass transport velocity c_1. This means that information (which triggers adjustments in Ω) propagates downstream the fluid by contrast to the Vicsek case where it propagates upstream. While the reason for this difference is unclear at this stage, we expect that it may induce large qualitative differences in the behaviour of the system in some cases. This point will be investigated in future work.

Numerical simulation of the SOHB will be subject to future work. Here, we will restrict ourselves to the MO and HW for which we have analytical formulas. In the next section, using these two special solutions, we verify that the SOHB model and the IBM are close in an appropriate parameter range.

8.4 From the IBM to the macroscopic model

In this section, we give some details on our numerical framework based on the direct simulation of the underlying IBM (2.3), (2.4), (2.7). Then, under the scaling (8.1), we show that the IBM converges towards the SOHB as expected by the theory.

8.4.1 Numerical simulations of the IBM

Unless otherwise specified, throughout this paper, a square box of side length L with periodic boundary conditions is used. As sensing kernel K, we use the indicator function of the ball centered at 0 and of radius R. Thus, an agent interacts with all its neighbors at a distance less than R (radius of interaction). Table 8.4.1 summarises the model parameters.

For the numerical simulations presented in this chapter, we have used the convenient

Parameter	Symbol
Number of particles	N
Computational box side length	L
Interaction radius	R
Particle speed	c_0
Concentration parameter	κ
Alignment frequency	ν

TABLE 8.4.1: Parameters of the IBM (2.3), (2.4).

framework offered by quaternions, already used in Chapter 7, and detailed in Section 8.B. Indeed, let us recall that there is a group isomorphism between $\mathrm{SO}_3(\mathbb{R})$ and $\mathbb{H}/\{\pm 1\}$, where $\mathbb{H}$ is the group of unit quaternions, and that it is possible to express the IBM (2.3), (2.4), (2.7) using this representation (see [116] and Section 8.B). Roughly speaking, body-alignment as described here is equivalent to nematic alignment of the corresponding quaternions (nematic alignment of a unit quaternions q to the mean direction $\bar{q}$ is unchanged if q is replaced by $-q$, as opposed to polar alignment where the result depends on the sign of q). This is because a given rotation can be represented by two opposite quaternions and thus, the outcome of the alignment process should not depend of the choice of this representative. The numerical algorithm is described in Section 8.C. Additionally, the quaternion framework also suggests to use order parameters derived from nematic alignment dynamics (such as in liquid crystal polymers). We shall use this analogy to define appropriate order parameters in Section 8.5.1.

All the simulations were written in Python using the `SiSyPHE` library [139] described in Chapter 5. The outcomes of the simulations were analysed and plotted using the `NumPy` [191] and `Matplotlib` [203] libraries. The 3D particle plots were produced using `VPython` [296]. All the particle simulations have been run on a GPU cluster at Imperial College London using an Nvidia GTX 2080 Ti GPU chip.

A typical outcome of the IBM is shown in Figure 8.4.1 (see also Section 8.A, Video 1) for a moderate number of particles ($N = 3000$). Throughout this paper, in the plots, we will represent each agent graphically by an elongated tetrahedron pointing in the direction of motion. The three large faces around the height will be painted in blue, green and magenta and the base will be in gold, as described in Fig. 8.4.1a. We notice that, starting from a uniformly random initial state (Fig. 8.4.1b), the system self-organizes in small clusters (Fig. 8.4.1c) and finally reaches a flocking equilibrium where all the agents have roughly the same body-orientation (Fig. 8.4.1d). The goal of this chapter is to show that

flocking is not necessarily the ultimate fate of the system, because it may be trapped in a so-called topologically protected state, i.e. in one of the solutions of the macroscopic model.

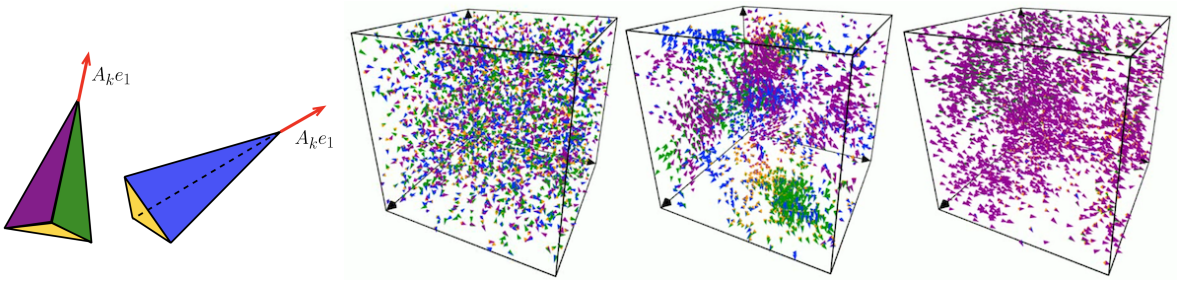

(A) Graphical representation of particles

(B) Time=0

(C) Time=4

(D) Time=40

FIGURE 8.4.1: (a) Graphical representation of particles and their body orientations as elongated tetrahedra pointing towards the self-propulsion direction with blue, magenta and green large faces and gold bases. (b,c,d) Snapshots of a typical output of the simulation at three different times (b) Time=0, (c) Time=4 and (d) Time=40. Parameters: $N = 3000$, $L = 1$, $R = 0.075$, $\kappa = 20$, $\nu = 5$, $c_0 = 0.2$. see also Section 8.A, Video 1.

8.4.2 The IBM converges to the macroscopic model as $N \to \infty$

In this section we use the MO and HW to demonstrate the quantitative agreement between the SOHB model (8.2) and the IBM (2.3), (2.4), (2.7) in the scaling (8.1). In the simulations below, we consider a periodic cube of side-length L and choose

$$R = 0.025, \quad \nu = 40, \quad c_0 = 1, \quad L = 1, \quad \xi = 2\,\pi, \tag{8.25}$$

so that $\frac{R}{L} = \frac{c_0}{\nu L} = 0.025 \ll 1$, ensuring that the scaling (8.1) is satisfied. Furthermore, we see that the choice of ξ is such that the twists in the MO or HW have exactly one period over the domain size.

Then, we numerically demonstrate that the solutions of the IBM converge to those of the macroscopic model in the limit $N \to \infty$ and investigate the behaviour of the IBM at moderately high values of N.

We sample N particles according to the initial condition (8.20) of the MO and simulate the IBM (2.3), (2.4), (2.7). We recall that the average direction $\Omega(t)$ of the exact MO (8.18) is spatially uniform at any time and undergoes a uniform rotation motion about the z-axis.

So, we will compare $\Omega(t)$ with the average direction $\overline{\Omega}(t)$ of all the particles of the IBM, where $\overline{\Omega}(t) = (\overline{\Omega}_1, \overline{\Omega}_2, \overline{\Omega}_3)^{\mathrm{T}}$ is defined by:

$$\overline{\Omega}(t) = \frac{\sum_{k=1}^{N} \Omega_t^k}{|\sum_{k=1}^{N} \Omega_t^k|},$$

(provided the denominator is not zero, and where we recall that $\Omega_k(t) = A_k(t)\, e_1$). To ease the comparison, we compute the azimuthal and polar angles of $\overline{\Omega}$ respectively defined by:

$$\bar{\varphi} := \arg(\overline{\Omega}_1 + i\overline{\Omega}_2) \in [0, 2\pi), \quad \bar{\theta} = \arccos(\overline{\Omega}_3) \in [0, \pi], \tag{8.26}$$

where $\arg(x + iy)$ stands for the argument of the complex number $x + iy$. We note that the corresponding angles φ and θ of $\Omega(t)$ are given by

$$\varphi(t) = -\omega\, t = -2\pi\, c_4(\kappa)\, t, \qquad \theta = \pi/2, \tag{8.27}$$

where we have used (8.17) and (8.25) to compute the value of ω.

Fig. 8.4.2a shows the azimuthal angle $\bar{\varphi}$ as a function of time over 5 units of time, for increasing particle numbers: $N = 5\,10^4$ (green curve), $N = 1.5\,10^5$ (orange curve) and $N = 1.5\,10^6$ (blue curve). Note that for very small values of N, the macroscopic model loses its relevance: below a few thousand particles we only observe a noisy behaviour, not shown in the figure. For the considered range of particle numbers, we notice that the angle $\bar{\varphi}$ decreases linearly with time, which shows that the behaviour of the IBM is consistent with the exact solution (8.27). However, quantitatively, we see that $|\mathrm{d}\bar{\varphi}/\mathrm{d}t|$ depends on the particle number and decreases with increasing particle number. We investigate this behaviour in more detail in Fig. 8.4.2b where the difference between the measured angular velocity $|\mathrm{d}\bar{\varphi}/\mathrm{d}t|$ and the theoretical prediction $2\pi c_4(\kappa)$ is plotted as a function of N. Each data point (blue dot) is an average of 10 independent simulations. This figure confirms that, as N increases, $|\mathrm{d}\bar{\varphi}/\mathrm{d}t|$ decreases and converges towards $2\pi c_4(\kappa)$. The inset in Fig. 8.4.2b shows the same data points in a log-log-scale with the associated regression line (orange solid line). We observe that the error between the measured and theoretical angular velocities behaves like $N^{-\alpha}$ with a measured exponent $\alpha \simeq 1.01$ which is close to the theoretical value $\alpha = 1$ derived in Section 8.E of the Supplementary Material.

8.4.3 Quantitative comparison between the models

In order to quantitatively confirm the agreement between the IBM and the macroscopic model, we fix a large number $N = 1.5\,10^6$ of particles and we run the IBM for different

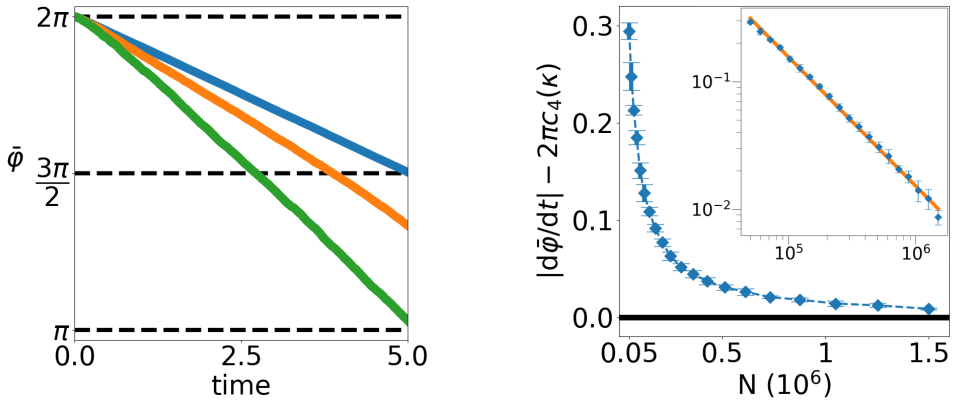

(A) (B)

FIGURE 8.4.2: (a) Time evolution of the angle $\bar{\varphi}$ for three values of N : $N = 0.05\,10^6$ (green curve), $N = 0.15\,10^6$ (orange curve) and $N = 1.5\,10^6$ (blue curve). (b) Difference between the measured angular velocity $|\mathrm{d}\bar{\varphi}/\mathrm{d}t|$ and the theoretical value $2\pi c_4(\kappa)$. Each data point (blue dot) is an average of 10 independent simulations with the error bar showing one standard deviation. Solid black horizontal line at 0 for convenience. Inset: same data in log-log scale and regression line (solid orange line). Parameters: $L = 1$, $\xi = 2\pi$, $R = 0.025$, $\nu = 40$, $c_0 = 1$, $\kappa = 10$.

values of the concentration parameter κ and for the two classes of special solutions, the MO and the HW. To compare the models, we compute the following macroscopic quantities:

- For the MO: starting from a sampling of the initial condition (8.20), we measure the angular velocity $|\mathrm{d}\bar{\varphi}/\mathrm{d}t|$ in a similar way as in the previous section. Given the parameter choice (8.25), the theoretical value of $|\mathrm{d}\varphi/\mathrm{d}t|$ predicted by (8.18) is $|\omega| = 2\pi c_4(\kappa)$ where the function c_4 is given by (8.11).

- For the HW, starting from a sampling of the initial condition (8.23), we measure the wave speed. To this aim, using (2.8), we compute the mean body-orientation $\mathbb{A}$ of the agents in a slice of size 10^{-3} along the x-axis (which is the global direction of motion) as a function of time. As predicted by (8.21) the coefficient $\mathbb{A}_{22}$ of the mean orientation is a periodic signal. The inverse of the period of this signal (obtained through a discrete Fourier transform) gives the traveling wave speed of the HW. The theoretical value predicted by (8.21) is given by $\lambda = c_2(\kappa) + c_4(\kappa)$ where the function c_2 is given by (8.9).

The output of these simulations is shown in Figs. 8.4.3a for the MO and 8.4.3b for the HW. They respectively display the angular velocity and traveling wave speed obtained by running the IBM for a discrete set of values of κ (big blue dots). By comparison, the black dotted curves show the theoretical values as functions of κ. For the parameters of Fig. 8.4.3,

the order of magnitude of the standard deviation of 10 independent simulations is 10^{-3}. The relative error between the average measured value and its theoretical prediction varies between 2% and 5% on the whole range of concentration parameters considered.

These figures show an excellent agreement between the prediction of the macroscopic SOHB model and the results obtained by running the IBM when the number of particles is large. This confirms that the SOHB model provides an excellent approximation of the IBM, at least during a certain period of time which is a function of the particle number. We will see below that fluctuations induced by the finite number of particles may eventually destabilize the MO and lead to a HW or a FS. As these solutions are associated with different topological structure, these transitions will be analysed as topological phase transitions in the forthcoming sections.

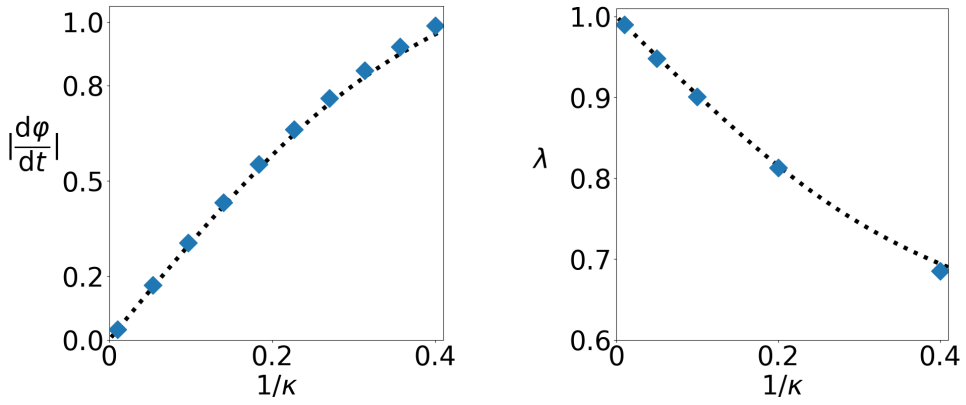

(A) (B)

FIGURE 8.4.3: (a) MO: angular velocity $|\mathrm{d}\varphi/\mathrm{d}t|$ as a function of $1/\kappa$. (b) HW: traveling wave speed λ as a function of $1/\kappa$. Measured values from the IBM at discrete values of κ (big blue dots) and theoretical prediction from the SOHB model (dotted black curve). Parameters: $N = 1.5\,10^6$, $L = 1$, $\xi = 2\pi$, $R = 0.025$, $\nu = 40$, $c_0 = 1$.

8.4.4 Topology

Both the MO and HW have non-trivial topology: inspecting the perpendicular twist (8.20) (see also Fig. 8.3.1a), we observe that the two-dimensional curve generated by the end of the vector $\mathbf{u}$ in the (y, z)-plane as one moves along the z-axis is a closed circle. A similar observation can be made on the parallel twist (8.23) (see Fig. 8.3.2a) as one moves along the x-axis. Both curves have therefore non-zero winding numbers about the origin. When the domain is $\mathbb{R}^3$, these winding numbers are $\pm\infty$ (where the sign corresponds to that of ξ) as these curves make an infinite number of turns. If the domain has finite extension L along the z-axis (in the MO case) or the x-axis (in the HW case) and, due to the periodic

boundary conditions, L is related to ξ by $L = n\,2\pi/\xi$ with $n \in \mathbb{Z} \setminus \{0\}$, then the winding numbers are equal to n. As observed on Formulas (8.18) and (8.21) (or on Figs 8.3.1b and 8.3.2b), this initial non-trivial topological structure is propagated in time.

When we initialize particles by sampling the initial conditions (8.20) or (8.23), we expect that the solution of the IBM remains an approximation of the MO (8.18) or HW (8.21) respectively as evidenced in Section 8.4.3. However, noise induced by both the inherent stochasticity of the IBM and finite particle number effects as explained in Section 8.4.2 may eventually destabilize the IBM. Then, in most cases, its solution is seen to transition towards an approximation of the FS after some time. This transition implies a change of the topology of the solution which, from initially non-trivial, becomes trivial, since the winding number of the FS is zero. One may wonder whether the evolution towards a FS is slower if the initial state has non-trivial topology and exhibits some kind of "topological protection" against noise-induced perturbations. To test this hypothesis quantitatively, we first need to develop appropriate indicators. This is done in the next section.

8.5 Order parameters and topological indicators

We will use two types of indicators. The first one is the global order parameter which will discriminate between the various types of organization of the system (disorder, MO or HW and FS). The second type of indicators are based on analysing the roll angle. They will enable a finer characterization of topological phase transitions.

8.5.1 Global order parameter

We first introduce the following scalar binary order parameter which measures the degree of alignment between two agents with body-orientations A, $\tilde{A} \in \mathrm{SO}_3(\mathbb{R})$:

$$\psi(A, \tilde{A}) := \frac{1}{2}\, A \cdot \tilde{A} + \frac{1}{4}. \tag{8.28}$$

In the quaternion framework (see Section 8.4.1 and 8.B for details), we have

$$\psi(A, \tilde{A}) = (q \cdot \tilde{q})^2, \tag{8.29}$$

where q and $\tilde{q}$ are two unit quaternions respectively associated to A and $\tilde{A}$, and $q \cdot \tilde{q}$ indicates the inner product of two quaternions. This expression makes it clear that $\psi(A, \tilde{A}) \in [0, 1]$. The square exponent in (8.29) indicates that $\psi(A, \tilde{A})$ measures the nematic alignment

of the two associated unit quaternions, as it should because two opposite quaternions represent the same rotation. We note that $\psi(A, \tilde{A}) = 1$ if and only if $\tilde{A} = A$. On the other hand, $\psi(A, \tilde{A}) = 0$ if and only if $A \cdot \tilde{A} = -1/2$, which corresponds to the two rotation axes being orthogonal and one rotation being an inversion about its axis.

The Global Order Parameter (GOP) of a system of N agents at time $t > 0$ is the average of all binary order parameters over all pairs of particles:

$$\mathrm{GOP}^N(t) = \frac{1}{N(N-1)} \sum_{k \neq \ell} \psi\big(A_t^k, A_t^\ell\big). \tag{8.30}$$

From (8.30) we have $\mathrm{GOP}^N(t) \in [0, 1]$. A small GOP^N indicates large disorder and a large one, strong alignment. This is a global measure of alignment, by contrast to a local one where ψ would be averaged over its neighbors only (and the result, averaged over all the particles). This global measure of alignment allows us to separate the MO and HW from the FS as shown below, which would not be possible with a local one.

The GOP (8.30) can also be defined at the continuum level. Since in the macroscopic limit the particles become independent and identically distributed over $\mathbb{R}^3 \times \mathrm{SO}_3(\mathbb{R})$, with common distribution $\rho M_{\kappa\mathbb{A}}$ where $(\rho, \mathbb{A})$ satisfies the SOHB system (8.2) and $M_{\kappa\mathbb{A}}$ is the von Mises distribution (2.5). Therefore, the GOP of a solution of the SOHB system $(\rho, \mathbb{A})$ is obtained as (8.30) where the sum is replaced by an integral, A_t^k is replaced by A distributed according to the measure $(\rho M_{\kappa\mathbb{A}})(t, \mathbf{x}, A)\,\mathrm{d}\mathbf{x}\,\mathrm{d}A$ and A_t^ℓ is replaced by $\tilde{A}$ distributed according to the same measure, but independently to A. Therefore,

$$\mathrm{GOP}(\rho, \mathbb{A}) := \iint_{(\mathbb{R}^3 \times \mathrm{SO}_3(\mathbb{R}))^2} \psi(A, \tilde{A})\, \rho(\mathbf{x})\, \rho(\tilde{\mathbf{x}})\, M_{\kappa\mathbb{A}(\mathbf{x})}(A)\, M_{\kappa\mathbb{A}(\tilde{\mathbf{x}})}(\tilde{A})\, \mathrm{d}\mathbf{x}\, \mathrm{d}\tilde{\mathbf{x}}\, \mathrm{d}A\, \mathrm{d}\tilde{A}.$$

Using Lemma 7.3.1, for any $\mathbb{A} \in \mathrm{SO}_3(\mathbb{R})$, we have

$$\int_{\mathrm{SO}_3(\mathbb{R})} A\, M_{\kappa\mathbb{A}}(A)\, \mathrm{d}A = \frac{c_1(\kappa)}{c_0}\, \mathbb{A}, \tag{8.31}$$

with $c_1(\kappa)/c_0$ defined by (8.8). Using (8.28), we obtain:

$$\mathrm{GOP}(\rho, \mathbb{A}) = \frac{1}{2} \left(\frac{c_1(\kappa)}{c_0} \right)^2 \int_{\mathbb{R}^3 \times \mathbb{R}^3} \mathbb{A}(\mathbf{x}) \cdot \mathbb{A}(\tilde{\mathbf{x}})\, \rho(\mathbf{x})\, \rho(\tilde{\mathbf{x}})\, \mathrm{d}\mathbf{x}\, \mathrm{d}\tilde{\mathbf{x}} + \frac{1}{4}. \tag{8.32}$$

From now on, we let ρ be the uniform distribution on a square box of side-length L. We can compute the GOP corresponding to each of the solutions defined in Section 8.3. For the MO (8.18), the HW (8.21) and the GS (8.24), for all time $t > 0$ and in both cases,

the GOP remains equal to:

$$\mathrm{GOP}_1 = \frac{1}{4}\left(\frac{c_1(\kappa)}{c_0}\right)^2 + \frac{1}{4}. \tag{8.33}$$

For the FS, $\mathbb{A}(\mathbf{x}) \equiv \mathbb{A} = \text{constant}$ and the GOP is equal to

$$\mathrm{GOP}_2 = \frac{3}{4}\left(\frac{c_1(\kappa)}{c_0}\right)^2 + \frac{1}{4}. \tag{8.34}$$

Note that the GOP:

$$\mathrm{GOP}_0 = \frac{1}{4},$$

corresponds to a disordered state of the IBM where the body-orientations of the particles are chosen independently and randomly uniformly (or equivalently to the SOHB case $\kappa \to 0$ in (8.33) and (8.34)). For the typical value $\kappa = 10$ used in our simulations, one can compute that:

$$\mathrm{GOP}_1 \simeq 0.45, \qquad \mathrm{GOP}_2 \simeq 0.85. \tag{8.35}$$

The GOP values between GOP_1 and GOP_2 can be reached by generalised HW as shown in Section 8.D.4.

8.5.2 Roll angle

Definition

Let $A = [\Omega, \mathbf{u}, \mathbf{v}] \in \mathrm{SO}_3(\mathbb{R})$ be a body-orientation. Let $\theta \in [0, \pi]$, $\varphi \in [0, 2\pi)$ be the spherical coordinates of Ω defined by (8.26) (omitting the bars). We let $\{\Omega, e_\theta, e_\varphi\}$ be the local orthonormal frame associated with the spherical coordinates (θ, φ) and we define $\mathbf{p}(\Omega) = e_\varphi$ and $\mathbf{q}(\Omega) = -e_\theta$. Then we define the rotation matrix

$$\mathsf{R}(\Omega) := [\Omega, \mathbf{p}(\Omega), \mathbf{q}(\Omega)] = \begin{pmatrix} \sin\theta\,\cos\varphi & -\sin\varphi & -\cos\theta\,\cos\varphi \\ \sin\theta\,\sin\varphi & \cos\varphi & -\cos\theta\,\sin\varphi \\ \cos\theta & 0 & \sin\theta \end{pmatrix}.$$

Since $\mathbf{u}$ and $\mathbf{v}$ belong to the plane spanned by $\mathbf{p}(\Omega)$ and $\mathbf{q}(\Omega)$, we let $\zeta \in [0, 2\pi)$ be the angle between $\mathbf{p}(\Omega)$ and $\mathbf{u}$. Then, it is an easy matter to show that $A = \mathsf{R}(\Omega)\,\mathcal{A}(\zeta, e_1)$. In aircraft navigation, θ, φ and ζ are respectively called the pitch, yaw and roll angles: the pitch and yaw control the aircraft direction with respect to the vertical and in the horizontal plane respectively, while the roll controls the plane attitude (see Fig. 8.5.1a).

These angles are related to the Euler angles. The construction of the roll angle ζ is summarised in Figure 8.5.1b. Pursuing the analogy with aircraft navigation, we see from Fig. 8.2.2 that $\mathbf{F}$ controls variations of pitch and yaw while δ controls variations of roll.

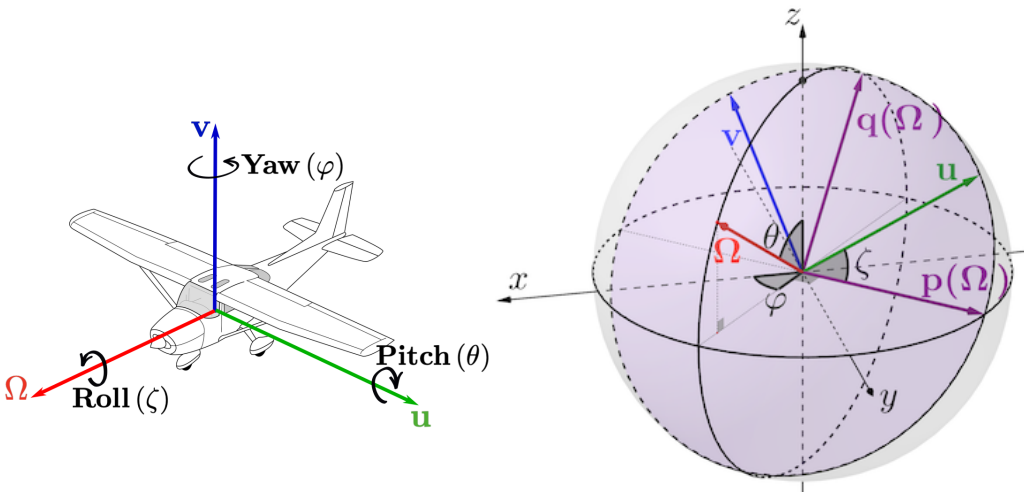

(A) (B)

FIGURE 8.5.1: (a) Pitch, yaw and roll angles of an aircraft with body orientation $[\Omega, \mathbf{u}, \mathbf{v}]$ (original picture released under the Creative Commons CC0 license by `https://pixabay.com`). (b) Construction of the roll angle of $A = [\Omega, \mathbf{u}, \mathbf{v}]$, where the vectors Ω, $\mathbf{u}$ and $\mathbf{v}$ are respectively in red, green and blue. The local frame is $(\Omega, \mathbf{p}(\Omega), \mathbf{q}(\Omega))$ where $\mathbf{p}(\Omega)$ and $\mathbf{q}(\Omega))$ and the plane generated by them are in purple. $\mathbf{u}$ and $\mathbf{v}$ belong to this plane. ζ is the angle between $\mathbf{p}(\Omega)$ and u.

As an example, we examine the pitch, yaw and roll of the three solutions of the SOHB model (8.2) described in Section 8.3.

1. FS: $\mathbb{A}$ is constant and uniform. Then, the pitch, yaw and roll are also constant and uniform.

2. MO: $\mathbb{A}$ is given by (8.18) (see Figs. 8.3.1). Using Eq. (8.19), we have $\mathsf{R}(\Omega) = \mathcal{A}(-\omega\, t, e_3)$ and the roll is given by $\zeta = \xi z$. The pitch and yaw are constant and uniform. The roll is constant in time and is also uniform on planes of constant z. The non-trivial topology of the MO results from the roll making a complete turn when z increases by the quantity $2\pi/\xi$.

3. HW: $\mathbb{A}$ is given by (8.21) (see Fig. 8.3.2). Then, we have $\mathsf{R}(\Omega) = \mathrm{I}_3$ and $\zeta = \xi\,(x - \lambda\, t)$. The pitch and yaw are constant and uniform while the roll is uniform on planes of constant x. It depends on x and time through the traveling phase $x - \lambda\, t$. Here, the non-trivial topology results from the roll making a complete turn when x increases by the quantity $2\pi/\xi$.

The goal of the next section is to see how we can recover the roll field from the simulation of a large particle system.

Roll polarization

As shown in the last section, the roll of the MO is uniform on planes of constant z. When simulating the MO by the IBM, we will use this property to compute an average roll on planes of constant z. To cope with the discreteness of the particles, we will rather consider slices comprised between two planes of constant z. If the distance Δz between the planes is chosen appropriately, we can access to both the average and the variance of the roll. They will be collected into one single vector, the Roll Polarization in planes of constant z or RPZ. A similar quantity characterises the HW, the Roll Polarization in planes of constant x or RPX. Below, we detail the construction of the RPZ. Obviously the procedure is the same (changing z into x) for the RPX.

We assume that the domain is a rectangular box of the form $\mathcal{D} := [0, L_x] \times [0, L_y] \times [0, L_z]$, and $L_z = n\,(2\pi/\xi)$ with $n \in \mathbb{Z} \setminus \{0\}$. The domain $\mathcal{D}$ is partitioned into M slices of fixed size across z, where M is a fixed integer. For $m \in \{1, \ldots, M\}$, the slice S_m is defined by:

$$S_m := [0, L_x] \times [0, L_y] \times \left[\frac{m-1}{M} L_z, \frac{m}{M} L_z\right].$$

Let us consider a system of N agents with positions and body-orientations (X^k, A^k), indexed by $k \in \{1, \ldots, N\}$. Each body orientation A^k has roll $\zeta^k \in [0, 2\pi)$. We define the discrete RPZ for Slice m, $\bar{\mathbf{u}}_m$, by

$$\bar{\mathbf{u}}_m := \frac{1}{N_m} \sum_{k \in I_m} (\cos \zeta^k, \sin \zeta^k)^{\mathrm{T}} \in \mathbb{R}^2, \tag{8.36}$$

where $I_m = \{k \in \{1, \ldots, N\}, X^k \in S_m\}$ and N_m is the cardinal of I_m. Note that the RPZ $\bar{\mathbf{u}}_m$ has norm smaller than one. The unit vector $\bar{\mathbf{u}}_m / |\bar{\mathbf{u}}_m|$ or equivalently, its angle with the vector $(1, 0)^{\mathrm{T}}$ gives the average roll in S_m. The euclidean norm $|\bar{\mathbf{u}}_m|$ is a measure of the variance of the set of roll angles $\{\zeta_k\}_{k \in I_m}$. If this variance is small, then $|\bar{\mathbf{u}}_m| \sim 1$, while if the variance is large, $|\bar{\mathbf{u}}_m| \ll 1$. When plotted in the plane $\mathbb{R}^2$, the set of RPZ $\{\bar{\mathbf{u}}_m\}_{m=1,\ldots,M}$ forms a discrete curve referred to as the RPZ-curve. It will be used to characterise the topological state of the particle system. A summary of this procedure is shown in Figure 8.5.2.

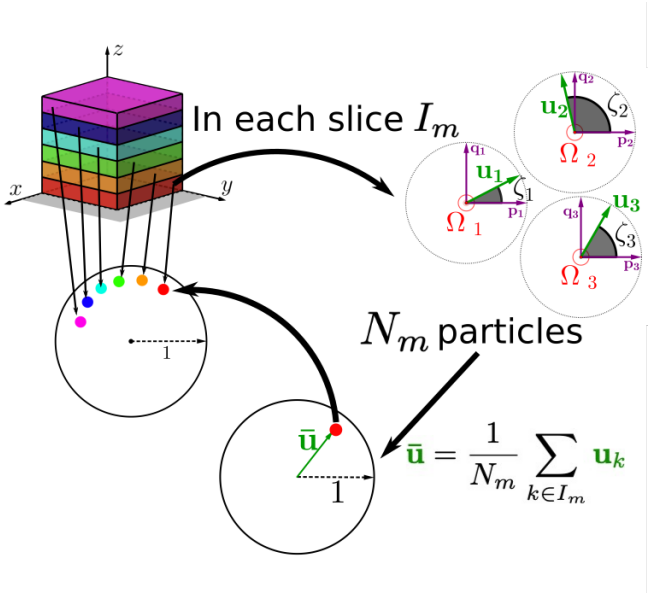

FIGURE 8.5.2: Construction of the RPZ and graphical representation. The spatial domain $\mathcal{D}$ is partitioned into M slices represented in different colors (top left). In each slice S_m, we have I_m particles with roll ζ_k each of them plotted in the particle's local plane spanned by $\mathbf{p}(\Omega_k)$, $\mathbf{q}(\Omega_k)$ (top right: we plot 3 particles in the slice S_1). Note that the local planes of different particles of the same slice may not coincide when imbedded in $\mathbb{R}^3$. For this given slice, the RPZ $\bar{\mathbf{u}}_m$ is computed and plotted in $\mathbb{R}^2$ (bottom right). The RPZ has norm smaller than 1 and belongs to the unit disk, whose boundary, the unit circle, is plotted for clarity. The RPZ of each slice is then plotted on a single figure in the same color as the slice it corresponds to (bottom left). This collection of points forms a discrete curve (here a fragment of a circle): the RPZ-curve.

Indicators of RPZ-curve morphology

The RPZ-curve is shown in Figure 8.5.3 (a) to (c), in the three following cases.

1. **Disordered state:** the particles are drawn independently uniformly randomly in the product space $\mathcal{D} \times \mathrm{SO}_3(\mathbb{R})$. For each m, the RPZ (8.36) is an average of uniformly distributed vectors on the circle and its norm is therefore close to 0. The RPZ-curve is thus reduced to the origin, as shown in Figure 8.5.3a;

2. **FS:** the positions of the particles are drawn independently uniformly in $\mathcal{D}$ and their body-orientations independently according to a von Mises distribution $M_{\kappa \mathbb{A}_0}$ with a fixed mean body orientation $\mathbb{A}_0 \in \mathrm{SO}_3(\mathbb{R})$. In this case, for all slices, the corresponding RPZ (8.36) is an average of identically distributed vectors on the circle whose distribution is peaked around the same point of the unit circle, and the peak is narrower as κ is larger. Therefore, the RPZ vectors (8.36) concentrate on a

point near the unit circle (Figure 8.5.3b). The RPZ-curve reduces to a single point different from the origin;

3. **MO:** the positions of the particles are drawn independently uniformly in $\mathcal{D}$. Then for a particle at position $\mathbf{x}$, its body-orientation is drawn independently according to a von Mises distribution $M_{\kappa\mathbb{A}_{\text{mill}}(0,z)}$ with $\mathbb{A}_{\text{mill}}(0,z)$ defined by (8.20) (with $\xi = 2\pi/L_z$). This time, the von Mises distribution is peaked around a point which depends on z. For each slice, the position of the RPZ (8.36) depends on m. Since $\mathbb{A}_{\text{mill}}(0,z)$ is L_z-periodic, the RPZ-curve is a discrete closed circle (Figure 8.5.3c). Note that the RPX-curve of a HW is similar.

From Figure 8.5.3, we realize that three quantities of interest can be extracted from the RPZ-curve:

1. the distance of its center of mass to the origin d_z:

$$d_z = \Big|\frac{1}{M}\sum_{m=1}^{M}\bar{\mathbf{u}}_m\Big|, \tag{8.37}$$

2. its mean distance to the origin $\bar{r}_z$:

$$\bar{r}_z = \frac{1}{M}\sum_{m=1}^{M}|\bar{\mathbf{u}}_m|, \tag{8.38}$$

3. its winding number about the origin w_z: for $m \in \{1,\dots,M\}$, let $\beta_m = \arg\big(\bar{\mathbf{u}}_{m,1} + i\bar{\mathbf{u}}_{m,2}\big) \in [0,2\pi)$ (with $\bar{\mathbf{u}}_m = (\bar{\mathbf{u}}_{m,1}, \bar{\mathbf{u}}_{m,2})^{\mathrm{T}}$) and $\delta\beta_{m+1/2} \in [-\pi,\pi)$ be such that $\delta\beta_{m+1/2} \equiv \beta_{m+1} - \beta_m$ modulo 2π, where we let $\beta_{M+1} = \beta_1$. Then:

$$w_z = \frac{1}{2\pi}\sum_{m=1}^{M}\delta\beta_{m+1/2},$$

(see e.g. [202, p. 176]).

The subscript z indicates that the slicing has been made across z. Similar quantities with an index 'x' will correspond to the slicing made across x. Fig. 8.5.3d provides a graphical illustration of the triple $(d_z, \bar{r}_z, w_z)$. For the examples given above, this triple has the

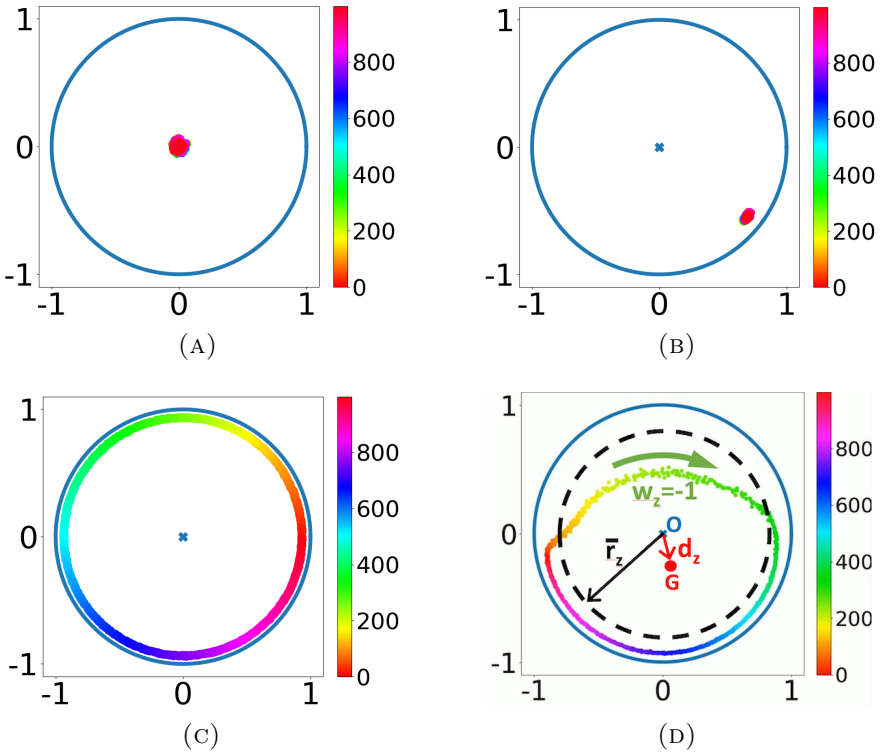

FIGURE 8.5.3: Examples of RPZ-curves: in each figure, the roll Polarization RPZ vectors corresponding to $M = 1000$ slices are plotted. The color bar to the right of each figure assigns a unique color to each slice. The same color is used to plot the corresponding RPZ. In each figure the unit circle and its center are represented in blue. (a) Disordered state: all RPZ concentrate near the origin. (b) FS: all RPZ concentrate on a point close to the unit circle. (c) MO (8.20): the RPZ-curve is a discrete circle centered at the origin and of radius close to unity. The total number of particles is $N = 1.5 \cdot 10^6$. Note that in Figs. (a) and (b), all RPZ are superimposed and only the last one (in magenta color) is visible. (d) Quantifiers of RPZ curve morphology: point G (in red) is the center-of-mass of the RPZ curve and d_z is its distance to the origin O (shown in blue). The mean radius $\bar{r}_z$ of the RPZ curve is illustrated by the circle in black broken line which has same radius. The winding number, which is the number of turns one makes following the spectrum of colors in the same order as in the color bar from bottom to top (the green arrow indicates the direction of progression along the RPZ curve) is $w_z = -1$ in this example.

following values:

$$\text{Disordered state:} \quad (d_z, \bar{r}_z, w_z) = (0, 0, \text{ND}), \text{ where ND stands for "undefined",} \tag{8.39}$$

$$\text{FS:} \quad (d_z, \bar{r}_z, w_z) \approx (1, 1, 0), \tag{8.40}$$

$$\text{MO:} \quad (d_z, \bar{r}_z, w_z) \approx (0, 1, w), \text{ with } w \neq 0. \tag{8.41}$$

We have a similar conclusion with $(d_x, \bar{r}_x, w_x)$ for a disordered state or an FS. For an

HW, we have $(d_x, \bar{r}_x, w_x) \approx (0, 1, w)$ with $w \neq 0$. Thus, monitoring either or both triples (according to the situation) will give us an indication of the state of the system in the course of time. In particular, non-trivial topological states are associated with non-zero winding numbers w_x or w_z. In practice, we will use the nonzero-rule algorithm to compute the winding numbers numerically [202, p. 176].

8.6 Topological phase transitions: are the MO and HW topologically protected?

As pointed out in Section 8.4.4, for the IBM, the MO and HW are only metastable: they typically persist for a finite time before degenerating into a FS. This is in stark contrast with the macroscopic model for which they persist for ever. The transition of a MO or HW to a FS implies a topological change. To analyse whether the MO or HW are more robust due to their non-trivial topological structure (i.e. are topologically protected), we will compare them with similar but topologically trivial initial conditions (Sections 8.6.1, 8.6.2 and 8.6.3). We also test their robustness against perturbed initial conditions and show that, in this case, MO may transition to GS (Section 8.6.4). In the Appendix 8.F, we investigate rarer events, where an MO does not transition directly to an FS but through a HW.

8.6.1 Initial conditions

In Section 8.6.2, we will compare the solutions of the IBM with different initial conditions using the perpendicular or parallel twists as building blocks. Some will have a non-trivial topology and the others, a trivial one. Specifically we define the following initial conditions.

Milling orbit

Let $\mathcal{D} = [0, L] \times [0, L] \times [0, 2L]$ be a rectangular domain with periodic boundary conditions and let $\xi = 2\pi/L$. We consider the following two initial conditions:

- **Double mill** initial condition MO1:

$$\mathbb{A}_{m,1}(0, z) = \mathcal{A}(\xi\, z, \mathbf{e}_1), \quad z \in [0, 2L], \tag{8.42}$$

  where we recall again that $\mathcal{A}(\theta, \mathbf{n})$ is the rotation of axis $\mathbf{n} \in \mathbb{S}^2$ and angle $\theta \in \mathbb{R}$ defined by (7.2). This initial condition has non-trivial topology: the curve generated

by the end of the vector $\mathbf{u}$ in the (y, z)-plane as z ranges in $[0, 2L]$ makes two complete turns around the origin in the same direction. Thus, this initial condition has winding number equal to 2.

- **Opposite mills** initial condition MO2:

$$\mathbb{A}_{m,2}(0, z) = \begin{cases} \mathcal{A}(\xi\, z, \mathbf{e}_1), & z \in [0, L], \\ \mathcal{A}(-\xi\, z, \mathbf{e}_1), & z \in [L, 2L]. \end{cases} \tag{8.43}$$

  This initial condition has trivial topology: starting from $z = 0$, the curve generated by the end of the vector $\mathbf{u}$ makes one complete turn around the origin in the counterclockwise direction until it reaches $z = L$ but then reverses its direction and makes a complete turn in the clockwise direction until it reaches $z = 2L$. Thus, this initial condition has winding number equal to 0 and has trivial topology.

- **Perturbed double mill** initial condition MO3:

$$\mathbb{A}_{m,3}(0, z) = \mathcal{A}(\xi\, z + \sqrt{\sigma} B_z, \mathbf{e}_1), \quad z \in [0, 2L], \tag{8.44}$$

  where $(B_z)_z$ is a given one-dimensional standard Brownian motion in the z variable and $\sigma > 0$ is a variance parameter which sets the size of the perturbation. The Brownian motion is subject to $B_0 = B_{2L} = 0$ (i.e. it is a Brownian bridge). Similarly to the initial condition MO1 (8.42), this initial condition has a nontrivial topology, in this case a winding number equal to 2.

Helical traveling wave

Let now $\mathcal{D} = [0, 2L] \times [0, L] \times [0, L]$. Compared to the previous case, the domain has size $2L$ in the x-direction instead of the z-direction. Let again $\xi = 2\pi/L$. We consider now the following two initial conditions:

- **Double helix** initial condition HW1:

$$\mathbb{A}_{h,1}(0, x) = \mathcal{A}(\xi\, x, \mathbf{e}_1), \quad x \in [0, 2L], \tag{8.45}$$

  This initial condition has non-trivial topology and has winding number equal to 2 by the same consideration as for initial condition MO1.

- **Opposite helices** initial condition HW2:

$$\mathbb{A}_{h,2}(0,x) = \begin{cases} \mathcal{A}(\xi\, x, \mathbf{e}_1), & x \in [0, L], \\ \mathcal{A}(-\xi\, x, \mathbf{e}_1), & x \in [L, 2L]. \end{cases} \tag{8.46}$$

  Again, by the same considerations as for MO2, this initial condition has trivial topology, i.e. winding number equal to 0.

8.6.2 Observation of topological phase transitions

We initialize the IBM by drawing N positions independently uniformly randomly in the spatial domain and N body-orientations independently from the von Mises distribution $M_{\mathbb{A}(0,\mathbf{x})}$ where $\mathbb{A}(0,\mathbf{x})$ is one of the initial conditions MO1 or MO2. Then, we run the IBM and record the various indicators introduced in Section 8.5 as functions of time. The results are plotted in Fig. 8.6.1, as plain blue lines for the solution issued from MO1 (the topologically non-trivial initial condition), and as broken orange lines for that issued from MO2 (the topologically trivial one). We proceed similarly for the two initial conditions HW1 and HW2 and display the results in Fig. 8.6.2. See also Videos 4 to 7 in Section 8.A supplementing Fig. 8.6.1 and Videos 8 to 11 supplementing Fig. 8.6.2.

Figs. 8.6.1a and 8.6.2a display the GOP. We observe that, for all initial conditions, the GOP has initial value GOP_1, which is consistent with the fact that the initial conditions are either MO or HW. Then, again, for all initial conditions, at large times, the GOP has final value GOP_2 which indicates that the final state is a FS. This is confirmed by the inspection of the second line of figures in Figs. 8.6.1 and 8.6.2 which provide the triplet of topological indicators $(d_z, \bar{r}_z, w_z)$ for MO solutions and $(d_x, \bar{r}_x, w_x)$ for HW solutions. Specifically, d_z and d_x are given in Figs. 8.6.1d and 8.6.2d respectively, $\bar{r}_z$ and $\bar{r}_x$ in Figs. 8.6.1e and 8.6.2e, and w_z and w_x in Figs. 8.6.1f and 8.6.2f. Initially both triplets corresponding to MO1 or HW1 solutions have value $(0, 1, 2)$ as they should (see (8.41)). Their final value is $(1, 1, 0)$ which indicates a FS (see (8.40)). The fact that the final state is a FS implies, for MO1 and HW1, first that the IBM has departed from the MO and HW exact solutions of the macroscopic model described in Sections 8.3.2 and 8.3.3, and second, that a topological phase transition has taken place, bringing the topologically non-trivial MO1 and HW1 to a topologically trivial FS. For the topologically trivial MO2 and HW2 initial conditions, no topological phase transition is needed to reach the FS. The differences in the initial topology of the solutions induce strong differences in the trajectories followed by the system.

For the topologically non-trivial initial conditions MO1 or HW1, the system remains

in the MO or HW state for some time; hence it follows the macroscopic solution during this phase. Indeed, the GOP displays an initial plateau at the value GOP_1, while the triplet of topological indicators stays at the value $(0, 1, 2)$, which characterize the MO or HW state. For MO1, this is also confirmed by the yaw $\bar{\varphi}$ (Fig. 8.6.1c, blue curve), which varies linearly in time and by the pitch $\bar{\theta}$ (Fig. 8.6.1b blue curve) which is constant in time, consistently with the MO solution of the macroscopic model (Section 8.3.2) (see also Fig. 8.4.2a for the linear variation of the yaw). The duration of this initial phase, also referred to as the persistence time, is significantly longer for HW1 than for MO1. In our experiments, the former can reach several hundred units of time and sometimes be infinite (up to our computational capacity). By contrast, the latter is random and of the order of ten units of time. After this initial plateau, the GOP decreases until it reaches a minimum at a time highlighted in Figs. 8.6.1, 8.6.2 and subsequent figures by a gray shaded zone, showing that the system passes through a state of maximal disorder. Around that time, $\bar{r}$ has a sharp drop which is another confirmation of an increased disorder. The topological transition precisely occurs at this time with a transition of the winding number from 2 to 0 through a short sequence of oscillations. However, $\bar{r}$ has not reached 0 and d has already started to increase, which suggests that disorder is not complete. At this time also, the linear variation of $\bar{\varphi}$ suddenly stops and $\bar{\varphi}$ remains constant afterward, while $\bar{\theta}$ shows a small oscillation and jump. For HW1, $\bar{\theta}$ and $\bar{\varphi}$ are initially plateauing with small oscillations. At the time when the system leaves the HW state (around $t \simeq 178$), we observe a sudden drop of $\bar{\varphi}$ from 2π to π which indicates that the system suddenly reverses its average direction of motion. The GOP starts to decrease significantly before this time so we can infer that during the time period between $t \simeq 125$ and $t \simeq 178$, even though the mean direction of motion $\bar{\Omega}$ remains constant, groups of particles of almost similar proportions are moving in opposite directions, which preserves the average direction of motion (and may explain the oscillations during the initial persistence phase). This is confirmed by Video 8 (see description in Section 8.A). Then, once this minimum is reached, the GOP increases quickly to finally reach the value GOP_2 of the FS. Likewise, $\bar{r}$ and d quickly reach the value 1 while the winding number stays at the value 0.

By contrast to the previous case, the system immediately leaves the topologically trivial initial conditions MO2 or HW2 as shown by the GOP immediately leaving the value GOP_1. For HW2 the GOP increases right after initialization and smoothly reaches the value GOP_2, at a much earlier time than HW1. The trend is different for MO2. In this case, the GOP first decreases. Then, after a minimum value, it increases again and smoothly reaches the value GOP_2 at a time similar to MO1. The initial decay of the GOP for the MO2 solution can be explained by the fact that the macroscopic direction Ω turns

in opposite directions for the two opposite mills, thus decreasing the global order. For HW2, the macroscopic direction stays constant and uniform. So, it is the same for the two opposite helices, giving rise to a larger GOP. The mean radii $\bar{r}_z$ and $\bar{r}_x$ stay constant it time, showing that the evolutions of MO2 and HW2 do not involve phases of larger disorder. The quantity d_x increases monotonically towards the value 1 while d_z is subject to some oscillations close to convergence. This is due to the fact that the RPZ or RPX curves stay arcs of circles with decreasing arc length for the RPX and with some arc length oscillations for the RPZ as displayed in Videos 7 and 11. Of course, the winding number stays constant equal to 0 as it should for topologically trivial solutions. In both the MO2 and HW2 cases, $\bar{\theta}$ and $\bar{\varphi}$ remain constant throughout the entire simulation. In the MO2 case, this is the consequence of the two counter-rotating mills which preserve the direction of motion on average. In the HW2 case, this is due to the fact that there is no variation of the direction of motion for HW solutions in general (see also Video 6 and Video 10). Again, we observe that the convergence towards the FS takes more time for HW2 than for MO2. This points towards a greater stability of the HW-type solutions compared to the MO ones.

8.6.3 Reproducibility

Since the IBM is a stochastic model, one may wonder whether Figs. 8.6.1 and 8.6.2 are representative of a typical solution. In Fig. 8.6.3, the GOP is plotted as a function of time for 20 independent simulations with MO1 initial conditions and the same parameters as in Fig. 8.6.1 (blue curves). The same features as in Fig. 8.6.1 are observed, namely: (i) an initial stable milling phase which lasts about 10 units of time; (ii) a decrease of the GOP between approximately 10 to 15 units of time; (iii) a subsequent increase of the GOP which reaches the value GOP_2 of the FS. A similar reproducibility of the results has been observed for the other initial conditions (MO2, HW1, HW2) (not shown).

8.6.4 Robustness against perturbations of the initial conditions

In this section, we study the robustness of the MO when the initial condition is randomly perturbed as described by the initial condition MO3 (8.44). Three typical outcomes for three different values of the perturbation size σ are shown in Fig. 8.6.4. For each value of σ, the temporal evolution of the four main indicators are shown: the GOP (Figs. 8.6.4a, 8.6.4e, 8.6.4i), the mean polar angle or pitch (Figs. 8.6.4b, 8.6.4f, 8.6.4j), the mean azimuthal angle or yaw (Figs. 8.6.4c, 8.6.4g, 8.6.4k) and the winding number along the z-axis (Figs. 8.6.4d, 8.6.4h, 8.6.4l). For small to moderate values (approximately $\sigma < 100$), the outcomes of the

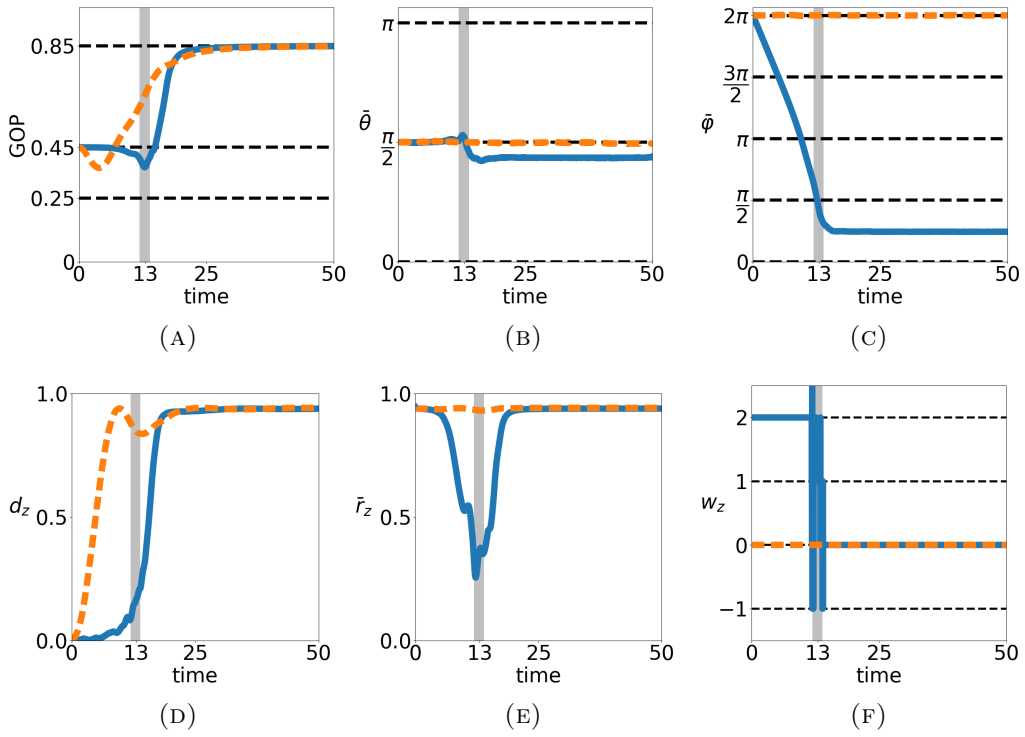

(A) (B) (C)

(D) (E) (F)

FIGURE 8.6.1: Examples of solutions of the IBM for initial conditions sampled from the double mill MO1 (plain blue curves) and the opposite mills MO2 (boken orange curves). The following indicators are plotted as functions of time: (a) Global Order Parameter (GOP) (see Eq. (8.30)). Horizontal lines at GOP values 0.25, 0.45 and 0.85 materialize the special values GOP_0, GOP_1 and GOP_2 respectively corresponding to totally disordered states, MO or HW, and FS (see Eqs. (8.33)-(8.35)). (b) Pitch angle $\bar{\theta}$ of the global particle average direction $\bar{\Omega}$ (see (8.26)). (c) Yaw $\bar{\varphi}$ of $\bar{\Omega}$. (d) Distance of center of mass of RPZ curve to the origin d_z (see (8.37)). (e) Mean distance of RPZ curve to the origin $\bar{r}_z$ (see (8.38)). (f) Winding number of RPZ curve w_z (see (8.37)). Gray shaded zones highlight a small region around the time of minimal GOP for the MO1 solution. Parameters: $N = 3\,10^6$, $R = 0.025$, $\kappa = 10$, $\nu = 40$, $c_0 = 1$, $L = 1$, $\xi = 2\pi$. See also Videos 4 to 7 in Section 8.A.

simulation are the same as in Fig. 8.6.1 and are not shown. However, they demonstrates the robustness of the topological solutions. When σ increases and crosses this threshold, the behaviour becomes different. Around this threshold (for $\sigma = 134$), in Fig. 8.6.4a, we observe that the GOP does not remain initially constant (contrary to the un-perturbed case shown in Fig. 8.6.1a) but immediately decreases, then increases and oscillates around the value GOP_1 before transitioning towards the value GOP_2 corresponding to a FS. In Figs. 8.6.4c and 8.6.4d, we observe that the MO is preserved during a comparable, slightly longer, time than in Figs. 8.6.1c and 8.6.1f (around 20 units of time) before degenerating into a FS.

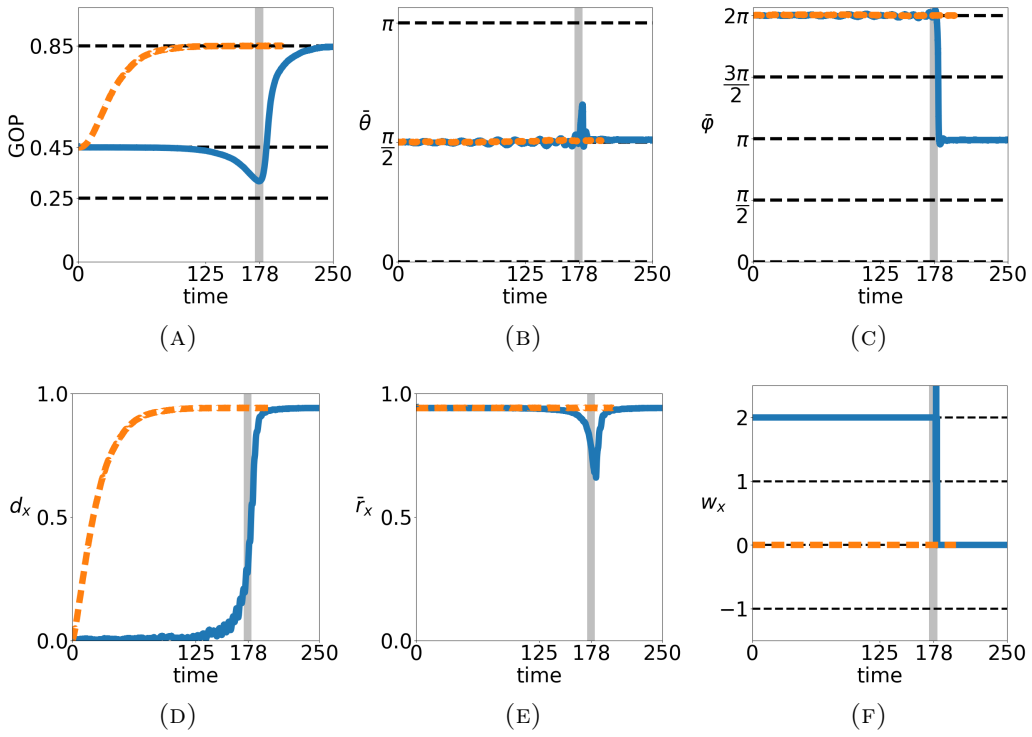

FIGURE 8.6.2: Examples of solutions of the IBM for initial conditions sampled from the double helix HW1 (plain blue curves) and the opposite helices HW2 (broken orange curves). The following indicators are plotted as functions of time: (a) Global Order Parameter (GOP). (b) Pitch angle $\bar{\theta}$ of $\bar{\Omega}$. (c) Yaw $\bar{\varphi}$ of $\bar{\Omega}$. (d) Distance of center of mass of RPX curve to the origin d_x. (e) Mean distance of RPX curve to the origin $\bar{r}_x$. (f) Winding number of RPX curve w_x. Gray shaded zones highlight a small region around the time of minimal GOP for the HW1 solution. The HW2 and HW1 solutions are computed during 200 and 250 units of time respectively. The two simulations have reached equilibrium by their final time. Parameters: $N = 3\,10^6$, $R = 0.025$, $\kappa = 10$, $\nu = 40$, $c_0 = 1$, $L = 1$, $\xi = 2\pi$. See caption of Fig. 8.6.1 for further indications. See also Videos 8 to 11 in Section 8.A.

Passed this threshold, when σ increases again and up to another threshold value around $\sigma \simeq 1000$, a new topological phase transition is observed from a MO with winding number 2 to a GS (8.24) with winding number 1. For $\sigma = 753$, the GOP shown in Fig. 8.6.4e initially strongly oscillates around the value GOP_1 before stabilizing, still around this value, which is in stark contrast with the previous experiments. The winding number shown in Fig. 8.6.4h reveals that this final steady behaviour is linked to a winding number equal to 1 after a transition around $t \simeq 12$. Consequently, a milling behaviour is observed in Fig. 8.6.4g for the mean azimuthal angle. This angle evolves linearly but with a slower speed, approximately divided by 2, after the transition, as expected since the winding number has dropped from 2 to 1. However, the final mean polar angle $\bar{\theta}$

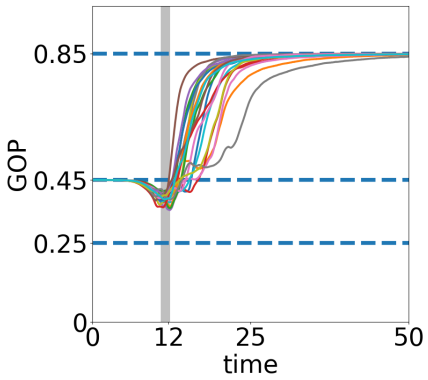

FIGURE 8.6.3: GOP as a function of time for 20 independent simulations of the transition from a MO to a FS starting from MO1. The parameters are the same as the ones on Figure 8.6.1.

shown in Fig. 8.6.4f is not equal to $\pi/2$. Since the gradient in body-orientation is along the z-axis, this indicates that the final state corresponds to a GS rather than a standard MO. This demonstrates that the family of generalised topological solutions enjoys some greater stability. The transition between MO and GS has not been observed when starting from a non-perturbed initial state. However, starting with perturbed initial conditions, the MO and GS with winding number 1 seem stable during several tens of units of time.

The transition between MO and GS with different winding numbers happens when the perturbation size is large enough and seems to be the typical behaviour: out of 6 independent simulations for values of σ evenly spread between 258 and 876, 5 simulations led to a MO or a GS with winding number 1 stable during more than 50 units of time. The other one led to a FS. We can think that the perturbation brings the system to a state closer to the MO with winding number 1, in particular due to the stochastic spatial inhomogeneities of the perturbation. On the particle simulations, we observe that the density of agents does not remain uniform, which creates different milling zones with possibly different milling speeds depending on the local gradient of body-orientations. The denser region then seems to attract the other particles before expanding into the full domain. The global direction of motion is not necessarily preserved during this process. In comparison, starting from an unperturbed MO with winding number 2, the density remains uniform and the system is globally subject to numerical errors which homogeneously degrade the topology up to the point that the system becomes closer to a FS. The situation is analogous when the size of the perturbation is too large as shown in Figs. 8.6.4i, 8.6.4k, 8.6.4l for $\sigma = 1000$: the MO is preserved during less than 5 units of time and after an immediate drop of the GOP, the system quickly reaches a FS.

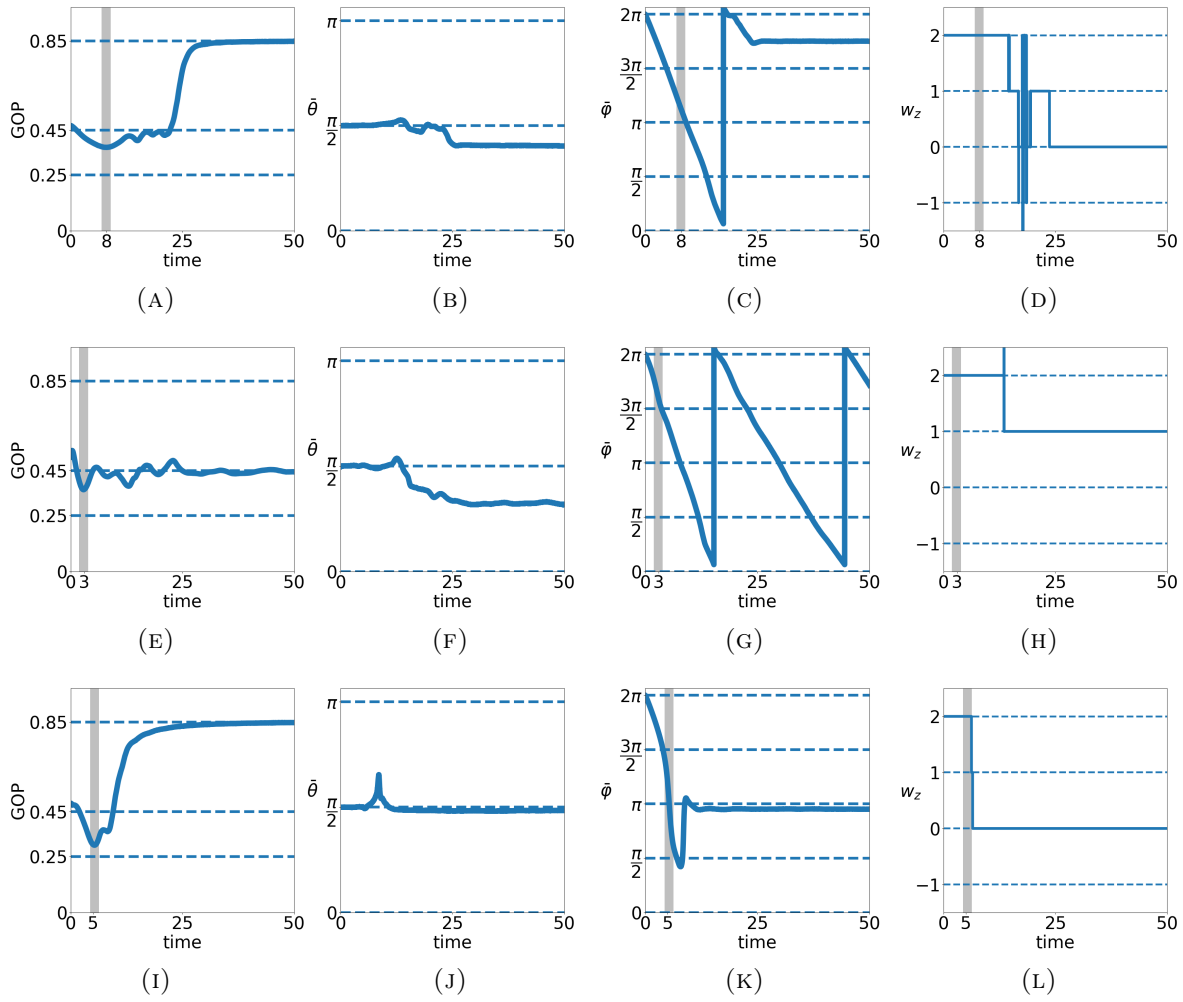

FIGURE 8.6.4: Different outcomes of the simulation of the IBM starting from perturbed initial MO. Only the four main indicators are shown: from left to right, the GOP, the mean polar angle (or pitch) $\bar{\theta}$, the mean azimuthal angle (or yaw) $\bar{\varphi}$ and the winding number w_z. (a)-(d) For $\sigma = 134$, the system stays a MO for a long time ($t \simeq 20$) but eventually converges to a FS; (e)-(h) for $\sigma = 753$, the system converges towards a generalised solution with a polar angle not equal to $\pi/2$ and a winding number equal to 1 along the z-axis; (i)-(l) for $\sigma = 1000$, the MO is quickly disrupted (at $t \simeq 5$) and converges almost immediately towards a FS. Parameters: $N = 3\,10^6$, $R = 0.025$, $\kappa = 10$, $\nu = 40$, $c_0 = 1$, $L = 1$, $\xi = 2\pi$.

8.6.5 Critique

The existence of a persistence time for the MO1 and HW1 solutions suggests that they enjoy some kind of topological protection against the noisy perturbations induced by the IBM and that MO2 and HW2 do not have such protection. However, since explicit solutions of the SOHB model for the initial conditions MO2 and HW2 are not available, it is not possible to assess the role of noise in the observed evolutions of the MO2 and

HW2 solutions. So, further investigations are needed to confirm that non-trivial topology actually provides increased robustness against perturbations. Moreover, the MO1 is robust against perturbed initial conditions. The MO and GS with winding number 1 seem to be much more more stable than with winding number 2.

8.7 Discussion and conclusion

At the particle level, the body-attitude coordination model involves new kinds of internal degrees of freedom involving geometrical constraints, here due to the manifold structure of $SO_3(\mathbb{R})$. At the macroscopic level, it leads to new types of self-organised phenomena. In particular, the macroscopic model has been shown to host special solutions with non-trivial topological structures. Corresponding solutions of the Individual Based Model have been computed and their non-trivial topological structure, shown to persist for a certain time before being destroyed by noise-induced fluctuations. Quantitative estimates of the agreement between the Individual Based Model and the macroscopic model have been given. This study provides one more evidence of the role of geometry and topology in the emergence of self-organised behaviour in active particle systems. The SOHB model presented in this chapter opens many new research directions. Some of them are listed below.

1. The stability of the MO (8.18), HW (8.21) and GS (8.24) solutions as well as those of the generalised HW solutions described in Section 8.D is an open problem. It would enable us to investigate the potential link between topological structure and stability.

2. Numerical simulations have been carried out in a periodic setting. Real systems though are confined by solid walls. To model the influence of confinement, it is necessary to explore wider classes of boundary conditions.

3. Most topological states in physical systems consist of linear perturbations of bulk states that propagate on the edges of the system (edge states). It would be interesting to determine whether linear perturbations of the MO or HW solutions could host such edge states.

4. Direct numerical simulations of the macroscopic model need to be developed to answer some of the questions raised by the study of topological protection (see Section 8.6.2).

5. It is desirable to develop more sophisticated topological indicators to gain better insight into the topological structure of the solutions.

6. The multiscale approach developed here could be extended to other geometrically structured systems involving e.g. a wider class of manifolds which would enlarge the applicability of the models.

Appendix

8.A List of supplementary videos

This chapter is supplemented by several videos which can be accessed by following this link: `https://figshare.com/projects/Bulk_topological_states_in_a_new_collective_dynamics_model/96491`. They are listed and described below.

Video 1. It supplements Fig. 8.4.1 of Section 8.4.1 and provides a visualization of the time evolution of the system considered in this figure.

Video 2. It supplements Fig. 8.3.1 of Section 8.3.2: it provides a visualization of the time evolution of a MO. Several frames $\mathbb{A} = (\Omega, \mathbf{u}, \mathbf{v}) \in \mathrm{SO}_3(\mathbb{R})$ are placed at various locations of space and evolve according to (8.18) (with arbitrary chosen parameters). The vectors Ω, $\mathbf{u}$ and $\mathbf{v}$ are displayed respectively in red, green and blue.

Video 3. It supplements Fig. 8.3.2 of Section 8.3.3: it provides a visualization of the time evolution of a HW. See caption of Video 2 for details on the graphical representation.

Video 4. It supplements Fig. 8.6.1 in Section 8.6.2. It shows the time-evolution of the particles for the initial condition MO1 (8.42). For clarity, only a sample of 5000 particles are shown. We refer to Fig. 8.4.1a for details on the representation of the body orientation using four-colored tetrahedra. We notice the ensemble rotation of the particle directions about the z axis until an instability disrupts the body orientation twist along the z axis (around time $t \approx 13$) and eventually drives the system to a FS.

Video 5. It supplements Fig. 8.6.1 in Section 8.6.2. It provides the time-evolution of the RPZ curve for the initial condition MO1 (8.42). The RPZ curve remains a circle until time $t \approx 8$ where its radius shrinks down. Then, the RPZ-curve shows a fairly chaotic dynamics during which the topology is lost. This happens around time $t \approx 13$ which is the first time when the RPZ-curve passes through the origin; at this time, the winding number is not defined. Then, the RPZ-curve slowly migrates towards the unit circle while shrinking to a single point which signals a FS. From time $t \approx 15$ on, it remains a single immobile point.

Video 6. It supplements Fig. 8.6.1 in Section 8.6.2. It shows the time-evolution of the particles for the initial condition MO2 (8.43). For clarity, only a sample of 5000 particles are shown (see Fig. 8.4.1a for details on the representation of the body orientation). We notice the counter-rotation of the particle directions about the z axis in the bottom and top halves of the domain, corresponding to the opposite mills. These two counter-rotations gradually dissolve while the solution approaches the FS.

Video 7. It supplements Fig. 8.6.1 in Section 8.6.2. It provides the time-evolution of the RPZ curve for the initial condition MO2 (8.43). The circle formed by the initial RPZ curve immediately opens. The opening width constantly increases, until the arc is reduced to a single point opposite to the opening point at time $t \approx 10$. Then there is a bounce and the arc forms again and increases in size until it reaches a maximum and decreases again. Several bounces are observed with decreasing amplitudes. These bounces result in the non-monotonous behaviour of the quantity d_z displayed on Fig. 8.6.1d.

Video 8. It supplements Fig. 8.6.2 in Section 8.6.2. It shows the time-evolution of the particles for the initial condition HW1 (8.45) (see Fig. 8.4.1a for details on the representation of the body orientation). For clarity, only a sample of 5000 particles are shown. Before time $t \simeq 125$, we observe a steady HW state. Then, after time $t \approx 125$, the particles show an undulating wave-like behaviour, with slowly increasing frequency and amplitude, which causes the decrease of the GOP. Around time $t \approx 178$, the particles are divided into two groups with pitch angles $\theta \simeq 0$ and $\theta \simeq \pi$, which suddenly reverses the global direction of motion. After time $t \approx 178$, the particles quickly adopt the same body-orientation. Shortly after time $t = 178$, the particles still have an undulating behaviour but it quickly fades away until a FS is reached.

Video 9. It supplements Fig. 8.6.2 in Section 8.6.2. It shows the time-evolution of the RPX-curve for the initial condition HW1. Unlike in the MO case, the RPX curve does not shrinks to the center of the circle before migrating to its limiting point. In this case, the limiting point near the unit circle towards which the RPX curve is converging attracts the RPX. During this transition, the circular shape of the RPX curve is preserved until it becomes a point.

Video 10. It supplements Fig. 8.6.2 in Section 8.6.2. It shows the time-evolution of the particles for the initial condition HW2 (8.46). For clarity, only a sample of 5000 particles are shown (see Fig. 8.4.1a for details on the representation of the body orientation). At the beginning, we see two opposite alternations of the three side colors of the tetrahedra (green-blue-magenta followed by green-magenta-blue), which signals a double parallel twist. Then, gradually, the green color is eaten up by the blue and magenta ones and only one

alternation of the blue and magenta colors remains. Then the color alternation shades away and gives room to a homogeneous color showing that the body orientations have stopped rolling and a FS is attained.

Video 11. It supplements Fig. 8.6.2 in Section 8.6.2. It provides the time-evolution of the RPX curve for the initial condition HW2 (8.46). The circle formed by the initial RPX curve immediately opens. The opening width constantly increases, although at a slower pace than for MO2 (see Video 7). Here, also contrasting with the MO2 case, the monotonous opening of the arc results in a monotonously increasing quantity d_x as shown in Fig. 8.6.2d.

Video 12. It supplements Fig. 8.F.1 in Section 8.F.1. It shows the time-evolution of the particles for a MO initial condition (8.42) in a rare case where it evolves into a HW. For clarity, only a sample of 5000 particles are shown (see Fig. 8.4.1a for details on the representation of the body orientation). It starts like Video 4 with the ensemble rotation of the particle directions about the z axis until an instability initiated at time $t \approx 10$ gradually disrupts this organization. However, the disruption does not drive the system to an FS, but rather to a HW as shown by the alternations of blue, green and magenta colors propagating along the particle orientations.

Video 13. It supplements Fig. 8.F.1 in Section 8.F.1. It provides the time-evolution of the RPZ curve for a MO initial condition (8.42) in a rare case where it evolves into a HW. The behaviour is essentially the same as in Video 5 except that the RPZ-curve shrinks to a single point far away from the unit circle. This shows that the end state of the RPZ-curve is closer to disorder than for a milling to flocking transition. Before that, the non-trivial topology across z is lost following a similar scenario as for the milling-to-flocking transition.

Video 14. It supplements Fig. 8.F.1 in Section 8.F.1. It provides the time-evolution of the RPX curve for a MO initial condition (8.42) in a rare case where it evolves into a HW. Initially, the RPX-curve is reduced to the origin, showing total disorder across the x direction. Then, after some chaotic transient, a closed curve enclosing the origin is formed. This curve initially stays close to the origin, still showing strong disorder. But gradually, the radius of the curve increases and approaches the unit circle. Thus, across x, the topology is initially undefined, but when it builds up, it shows its non-trivial character, the emerging RPX-curve having non-zero winding number about the origin.

Video 15. It supplements Fig. 8.F.2 in Section 8.F.2. It shows the time-evolution of the particles for a MO initial condition (8.42) in a rare case where it evolves into a FS through a transient HW. For clarity, only a sample of 5000 particles are shown (see Fig. 8.4.1a for details on the representation of the body orientation). The point of view is changed

from Video 12 to better visualize the transient HW moving along the diagonal, appearing around time $t \approx 16$. At the beginning we witness the ensemble rotation of the particles and its disruption by an instability. After some chaotic behaviour, the transient HW establishes as shown by the alternations of blue, green and magenta colors propagating along the diagonal. But after some time, the HW structure is disrupted again and the system eventually establishes a FS.

Video 16. It supplements Fig. 8.F.2 in Section 8.F.2. It provides the time-evolution of the RPZ curve for a MO initial condition (8.42) in a rare case where it evolves into a FS through a transient HW. The behaviour is essentially the same as in Video 5 except that the RPZ-curve undergoes a longer-lasting chaotic dynamics before shrinking to a point which migrates towards the unit circle.

8.B Quaternion framework

Despite its formal simplicity, the $\mathrm{SO}_3(\mathbb{R})$-framework used in the definition of the Individual Based Model is not well suited to numerical simulations due to the high computational cost required to store and manipulate rotation matrices. A more efficient representation of rotations in $\mathbb{R}^3$ is the quaternion representation already used in Chapter 7 in a different context. We recall that it is based on the group isomorphism

$$\begin{array}{rcl} \Phi : \mathbb{H}/\pm 1 & \longrightarrow & \mathrm{SO}_3(\mathbb{R}) \\ q & \longmapsto & \Phi(q) : \mathbf{w} \in \mathbb{R}^3 \mapsto \{q[\mathbf{w}]q^*\} \in \mathbb{R}^3, \end{array}$$

where the 3-dimensional vector $\mathbf{w} = (w_1, w_2, w_3)^{\mathrm{T}} \in \mathbb{R}^3$ is identified with the pure imaginary quaternion denoted by $[\mathbf{w}] = iw_1 + jw_2 + kw_3$ and q^* denotes the conjugate quaternion to q. Conversely, the pure imaginary quaternion $q = iq_1 + jq_2 + kq_3$ is identified with the 3-dimensional vector denoted by $\{q\} := (q_1, q_2, q_3)^{\mathrm{T}}$. Note that for any quaternion q and any vector $\mathbf{w} \in \mathbb{R}^3$, the quaternion $q[\mathbf{w}]q^*$ is a pure imaginary quaternion. The group of unit quaternions is denoted by $\mathbb{H}$ and is homeomorphic to the sphere $\mathbb{S}^3 \subset \mathbb{R}^4$.

We refer the reader to [116, Section 2] and [115, Appendix A] where details about the equivalence between the two representations can be found. Note that [115] studies a model in a full quaternion framework. The main difference with the $\mathrm{SO}_3(\mathbb{R})$-framework is the computation of the flux (2.6). In the quaternion framework, the flux is defined as the local average of the normalised uniaxial Q-tensors associated to the body-orientations of the particles (See Lemma 7.A.1). This is a symmetric matrix of dimension 4 and the quaternion version of the projection of the flux on $\mathrm{SO}_3(\mathbb{R})$ is a normalised eigenvector of

this matrix associated to the maximal eigenvalue.

Table 8.B.1 below summarises how the different objects can be computed in either of the two representations.

	Matrix	Quaternion
Orientation	$A \in \mathrm{SO}_3(\mathbb{R})$	$q \in \mathbb{H}/\pm 1$ such that $\Phi(q) = A$
Flux	$J_t^k = \sum_j K(\lvert X_t^k - X_t^j \rvert) A_t^j$	$Q_t^k = \sum_j K(\lvert X_t^k - X_t^j \rvert)\,(q_t^j \otimes q_t^j - 1/4\mathrm{I}_4)$
Mean orientation	$\mathbb{A} = \arg\max\{A \mapsto A \cdot J\}$	$\bar{q} \in \mathbb{H}$ eigenvector associated to the largest eigenvalue of Q
Von Mises distribution	$M_{\kappa\mathbb{A}}(A) = \dfrac{\exp(\kappa \mathbb{A} \cdot A)}{\mathcal{Z}}$	$M_{\kappa\bar{q}}(q) = \dfrac{\exp(2\kappa(\bar{q} \cdot q)^2)}{\mathcal{Z}}$

TABLE 8.B.1: Matrix *vs* quaternion formulation

8.C Numerical methods

The IBM (2.3), (2.4) has been discretized within the quaternion framework using the time-discrete Algorithm 6 below (in pseudo-code using a naive implementation). This algorithm shows one iteration of the algorithm during which the positions $X_n^k \in \mathbb{R}^3$ and orientations $q_n^k \in \mathbb{H}$ for $k \in \{1, \dots, N\}$ are updated into X_{n+1}^k and q_{n+1}^k respectively. Note that the source code used for the simulations in this chapter can be found on the `SiSyPHE` GitHub page `https://github.com/antoinediez/Sisyphe`.

The Poisson process is discretized with a time step Δt during which the indices of the jumping agents are recorded. In the simulations Δt has to be chosen small enough so that the event that an agent jumps twice or more during a time interval of size Δt is negligible. In all the simulations, we take Δt such that $\nu\,\Delta t = 10^{-2}$.

The orientations of a subset of agents is updated at each time step by drawing random quaternions from a von Mises distribution with prescribed mean orientation. Note that a quaternion $q \sim M_{\kappa\bar{q}}$ for a given $\bar{q}$ can be obtained as $q = \bar{q}r$ where $r \in \mathbb{H}$ is sampled from a von Mises distribution with mean orientation 1 (see [116, Proposition 9]). We use an efficient rejection algorithm to sample von Mises distributions which is due to [230].

All the simulations in this paper take place in a periodic box of size $L = (L_x, L_y, L_z)$. The observation kernel K is the indicator of the ball centered at 0 and of radius $R > 0$.

Input: The set of positions $(X_n^1, \dots, X_n^N) \in (\mathbb{R}^3)^N$ and orientations $(q_n^1, \dots, q_n^N) \in \mathbb{H}^N$ at iteration n and the parameters in Table 8.4.1.

Output: The positions and orientations at iteration $n+1$

for $k = 1$ **to** N **do**

  Set $X_{n+1}^k = X_n^k + c_0 \{q_n^k[e_1](q_n^k)^*\} \Delta t$; `// Update the position`

  Draw r^k uniformly in $[0,1]$;

  if $r^k > \exp(-\nu \Delta t)$ **then**

    Set $\overline{Q}_n^k = \frac{1}{N} \sum_{j=1}^N K(|X_n^k - X_n^j|) \, (q_n^j \otimes q_n^j - \frac{1}{4} I_4)$. ; `// Average Q-tensor`

    Compute one unit vector $\overline{q}_n^k$ of Q_n^k of maximal eigenvalue ;

    Draw $q_{n+1}^k \sim M_{\kappa \overline{q}_n^n}$; `// Draw a new orientation`

  else

    Set $q_{n+1}^k = q_n^k$; `// Do not update the orientation`

  end

end

Algorithm 6: Iteration $n \to n+1$ of the time-discrete algorithm

The six parameters of the simulations are summarised in Table 8.4.1.

8.D MO, HW, GS and generalised HW solutions

In this section, we provide proofs of Lemmas 8.3.1, 8.3.2 and 8.3.3. The prototypical helical traveling wave (HW) presented in Lemma 8.3.2 belongs to a more general class of solutions called generalised HW solutions described in Section 8.D.2 below.

8.D.1 Proof of Lemma 8.3.1

Starting from the initial condition (8.20), we are looking for solutions of (8.2b) of the form

$$\mathbb{A}(t, \mathbf{x}) = \begin{pmatrix} \cos(\omega t) & u_1(t,z) & v_1(t,z) \\ -\sin(\omega t) & u_2(t,z) & v_2(t,z) \\ 0 & u_3(t,z) & v_3(t,z) \end{pmatrix},$$

where $\omega \in \mathbb{R}$ is an angular velocity which will be related to the parameters of the problem later and where the basis vectors $\mathbf{u} = (u_1, u_2, u_3)^{\mathrm{T}}$ and $\mathbf{v} = (v_1, v_2, v_3)^{\mathrm{T}}$ depend only on the z variable and time. In this situation, Equation (8.2a) is trivially satisfied which means that the system stays homogeneous in space. Solutions of this form have to satisfy three

geometrical constraints which ensure that $\mathbb{A} \in \mathrm{SO}_3(\mathbb{R})$. The first two ones are $\Omega \times \mathbf{u} = \mathbf{v}$ and $\mathbf{v} \times \Omega = \mathbf{u}$, which lead to

$$\mathbb{A}(t, \mathbf{x}) = \begin{pmatrix} \cos(\omega t) & \sin(\omega t) v_3(t,z) & -\sin(\omega t) u_3(t,z) \\ -\sin(\omega t) & \cos(\omega t) v_3(t,z) & -\cos(\omega t) u_3(t,z) \\ 0 & u_3(t,z) & v_3(t,z) \end{pmatrix}. \tag{8.47}$$

The third one is a normalization constraint:

$$\forall t > 0, \quad \forall z \in \mathbb{R}, \qquad u_3(t,z)^2 + v_3(t,z)^2 = 1. \tag{8.48}$$

Using (8.48), we define a function $\alpha \equiv \alpha(t,z)$ such that

$$u_3(t,z) = \sin(\alpha(t,z)), \qquad v_3(t,z) = \cos(\alpha(t,z)).$$

A direct computation shows that for $\mathbb{A}$ of the form (8.47), we have

$$\mathbf{r} = (\partial_z u_3)\, \mathbf{u} + (\partial_z v_3)\, \mathbf{v}, \qquad \delta = 0.$$

Therefore, Eq. (8.2b) can be rewritten more concisely into:

$$\partial_t \mathbb{A} + c_4 \, [\Omega \times \mathbf{r}]_\times \mathbb{A} = 0, \tag{8.49}$$

where we recall Eq. (7.3) for the definition of $[\,]_\times$. A direct computation shows that

$$\Omega \times \mathbf{r} = (v_3\, \partial_z u_3 - u_3\, \partial_z v_3)\, \mathbf{e}_3 = (\partial_z \alpha)\, \mathbf{e}_3. \tag{8.50}$$

Inserting this in (8.49) implies that $u_3(t,z) \equiv u_3(z)$ and $v_3(t,z) \equiv v_3(z)$ are independent of time. We then observe that:

$$\mathbb{A}(t, \mathbf{x}) = \mathcal{A}(-\omega t, \mathbf{e}_3)\, \mathcal{A}(\alpha(z), \mathbf{e}_1), \tag{8.51}$$

where we recall Eq. (7.2) for the meaning of $\mathcal{A}$. Therefore, using (8.49) and (8.50), we obtain:

$$-\omega \, [\mathbf{e}_3]_\times \mathbb{A} + c_4 \, (\partial_z \alpha) \, [\mathbf{e}_3]_\times \mathbb{A} = 0,$$

from which we deduce that $\mathbb{A}$ satisfies (8.2b) if and only if α and ω satisfy:

$$c_4 \partial_z \alpha = \omega,$$

which implies

$$\alpha(z) = \frac{\omega}{c_4}\, z + \bar{\alpha}, \tag{8.52}$$

where $\bar{\alpha}$ is a constant, which can be interpreted as the phase at the origin $z = 0$. To recover Eq. (8.18), we just need to take $\bar{\alpha} = 0$ and define $\xi = \omega/c_4$. Eq. (8.19) follows from (8.51).

8.D.2 Generalised HW and proof of Lemma 8.3.2

Starting from the initial condition (8.23), we are looking for solutions of (8.2b) of the form

$$\mathbb{A}(t, \mathbf{x}) = \begin{pmatrix} 1 & 0 & 0 \\ 0 & \cos(\alpha(t,x)) & -\sin(\alpha(t,x)) \\ 0 & \sin(\alpha(t,x)) & \cos(\alpha(t,x)) \end{pmatrix},$$

for a real-valued function α of the t and x variables only. In this case, Ω is a constant vector and Equation (8.12a) is trivially satisfied. Moreover a direct computation shows that:

$$\mathbf{r} = 0, \qquad \delta = (\partial_x \alpha)(t, x).$$

As a consequence, Eq. (8.15) is trivially satisfied and straightforward computations show that Eq. (8.2b) reduces to

$$\partial_t \alpha + (c_2 + c_4)\, \partial_x \alpha = 0.$$

This last equation is a linear transport equation with velocity $c_2 + c_4$, the solutions of which are given by

$$\alpha(t, x) = \alpha_0(x - (c_2 + c_4)t) \tag{8.53}$$

for any initial condition $\alpha_0 \in L^1_{\mathrm{loc}}(\mathbb{R})$. In the case of (8.23), $\alpha_0(x) = \xi\, x$. However, we see that there are as many different solutions as functions in $L^1_{\mathrm{loc}}(\mathbb{R})$. Such general solutions are called "generalised HW".

8.D.3 Proof of Lemma 8.3.3

The three rotation matrices are given by

$$\mathcal{A}(-\omega t, \mathbf{e}_3) = \begin{pmatrix} \cos(\omega t) & \sin(\omega t) & 0 \\ -\sin(\omega t) & \cos(\omega t) & 0 \\ 0 & 0 & 1 \end{pmatrix},$$

$$\mathcal{A}(\theta-\pi/2,\mathbf{e}_2)=\begin{pmatrix}\sin\theta & 0 & -\cos\theta\\ 0 & 1 & 0\\ \cos\theta & 0 & \sin\theta\end{pmatrix},$$

$$\mathcal{A}(\xi(z-\tilde{\lambda}t),\mathbf{e}_1)=\begin{pmatrix}1 & 0 & 0\\ 0 & \cos(\xi(z-\tilde{\lambda}t)) & -\sin(\xi(z-\tilde{\lambda}t))\\ 0 & \sin(\xi(z-\tilde{\lambda}t)) & \cos(\xi(z-\tilde{\lambda}t))\end{pmatrix},$$

and a direct computation shows that the three column vectors Ω, $\mathbf{u}$ and $\mathbf{v}$ of the matrix $\mathbb{A}_{\xi,\theta}$ are given by

$$\Omega=\begin{pmatrix}\sin\theta\cos(\omega t)\\ -\sin\theta\sin(\omega t)\\ \cos\theta\end{pmatrix},$$

$$\mathbf{u}=\begin{pmatrix}-\cos\theta\sin(\xi(z-\tilde{\lambda}t))\cos(\omega t)+\cos(\xi(z-\tilde{\lambda}t))\sin(\omega t)\\ \cos\theta\sin(\xi(z-\tilde{\lambda}t))\sin(\omega t)+\cos(\xi(z-\tilde{\lambda}t))\cos(\omega t)\\ \sin\theta\sin(\xi(z-\tilde{\lambda}t))\end{pmatrix},$$

$$\mathbf{v}=\begin{pmatrix}-\cos\theta\cos(\xi(z-\tilde{\lambda}t))\cos(\omega t)-\sin(\xi(z-\tilde{\lambda}t))\sin(\omega t)\\ \cos\theta\cos(\xi(z-\tilde{\lambda}t))\sin(\omega t)-\sin(\xi(z-\tilde{\lambda}t))\cos(\omega t)\\ \sin\theta\cos(\xi(z-\tilde{\lambda}t))\end{pmatrix}.$$

Then we compute

$$\mathbf{r}=\xi\sin\theta\cos(\xi(z-\tilde{\lambda}t))\mathbf{u}-\xi\sin\theta\sin(\xi(z-\tilde{\lambda}t))\mathbf{u}=\xi\sin\theta(\sin(\omega t),\cos(\omega t),0)^{\mathrm{T}},$$
$$\delta=\cos\theta\partial_z\mathbf{u}\cdot\mathbf{v}+u_3\delta_z\mathbf{v}\cdot\Omega=\xi\cos\theta,$$

where we have used that $\partial_z\mathbf{u}=\xi\mathbf{v}$ and $\partial_z\mathbf{v}=-\xi\mathbf{u}$. It remains to check that Eq. (8.2b) holds true. We split this equation into three equations (8.5), one for each vector Ω, $\mathbf{u}$ and $\mathbf{v}$. The first equation on Ω reads

$$(\partial_t+c_2(\Omega\cdot\nabla_{\mathbf{x}}))\Omega+c_4\mathsf{P}_{\Omega^\perp}\mathbf{r}=0.$$

This equation holds true because

$$\partial_t\Omega=-\omega\begin{pmatrix}\sin\theta\sin(\omega t)\\ \sin\theta\cos(\omega t)\\ 0\end{pmatrix},\quad(\Omega\cdot\nabla_{\mathbf{x}})\Omega=0,\quad\mathsf{P}_{\Omega^\perp}\mathbf{r}=\xi\sin\theta\begin{pmatrix}\sin(\omega t)\\ \cos(\omega t)\\ 0\end{pmatrix},$$

and $\omega = c_4\xi$. The second equation on $\mathbf{u}$ reads

$$(\partial_t + c_2(\Omega \cdot \nabla_{\mathbf{x}}))\mathbf{u} - c_4(\mathbf{u} \cdot \mathbf{r})\Omega + c_4\delta\mathbf{v} = 0.$$

Because $\tilde{\lambda} = c_2 \cos\theta$, we have

$$\partial_t + c_2\Omega \cdot \nabla_{\mathbf{x}} = \partial_t + c_2 \cos\theta \partial_z = \partial_t + \tilde{\lambda}\partial_z \quad \text{and} \quad \partial_t + \tilde{\lambda}\partial_z(z - \tilde{\lambda}t) = 0.$$

Thus

$$(\partial_t + c_2(\Omega \cdot \nabla_{\mathbf{x}}))\mathbf{u} = \omega \begin{pmatrix} \cos\theta \sin(\xi(z - \tilde{\lambda}t)) \sin(\omega t) + \cos(\xi(z - \tilde{\lambda}t)) \cos(\omega t) \\ \cos\theta \sin(\xi(z - \tilde{\lambda}t)) \cos(\omega t) - \cos(\xi(z - \tilde{\lambda}t)) \sin(\omega t) \\ 0 \end{pmatrix},$$

and using $\omega = c_4\xi$, it can be checked that

$$(\partial_t + c_2(\Omega \cdot \nabla_{\mathbf{x}}))\mathbf{u} - c_4(\mathbf{u} \cdot \mathbf{r})\Omega = -c_4\xi \cos\theta \mathbf{v} = -c_4\delta\mathbf{v},$$

which yields the result. The equation on $\mathbf{v}$ is analogous.

8.D.4 GOP of the MO and generalised HW

The GOP (given by Eq. (8.32)) of the MO and HW do not depend on time and only depend on the function α defined respectively by (8.52) and (8.53). Using Eq. (8.32), we can compute that the GOP is equal to:

$$\text{GOP} = \frac{1}{2}\left(\frac{c_1(\kappa)}{c_0}\right)^2 \left(1 + 2\,|\langle \mathbf{u} \rangle|^2\right) + \frac{1}{4},$$

where $\langle \mathbf{u} \rangle$ denotes the spatial average of the vector $\mathbf{u}$ with respect to ρ (here the with respect to the uniform measure on the domain since ρ is constant and uniform). With the previous notations, we obtain

$$|\langle \mathbf{u} \rangle|^2 = \langle \cos\alpha \rangle^2 + \langle \sin\alpha \rangle^2,$$

For the generalised HW, depending on the choice of α, the GOP can take any value between GOP_1 and GOP_2, these two extreme values being attained respectively when $|\langle \mathbf{u} \rangle| = 0$ and $|\langle \mathbf{u} \rangle| = 1$.

8.E Convergence rate of $|\mathrm{d}\bar{\varphi}/\mathrm{d}t|$ as $N \to \infty$

The fact that the convergence rate of $|\mathrm{d}\bar{\varphi}/\mathrm{d}t|$ is close to N^{-1} agrees with previously documented observations in spherical statistics. Indeed, it has been shown in [298, Theorem 3(e)] that the estimation of the concentration parameter of a (spherical) von Mises distribution obtained from a crude averaging procedure from N independent samples produces a biased estimator with a (nonnegative) bias of order N^{-1} (see also [247, Section 10.3]). In the present case, a similar reasoning can be applied, which we now briefly develop. The key observation is that all the measured quantities are functions of empirical averages of the form (2.6). Under the chaos assumption, when N is large, the body-orientations of the particles behave as N independent samples with common law $M_{\kappa\mathbb{A}}$, where $\mathbb{A}$ solves the SOHB model (8.2) and $M_{\kappa\mathbb{A}}$ is defined by (2.5). In [114, Theorem 4.1], it has been shown that $c_4(\kappa)$ can actually be expressed as a function of a certain number p of averaged quantities

$$c_4(\kappa) = F\big(\langle g_1\rangle_{M_{\kappa\mathbb{A}}}, \dots, \langle g_p\rangle_{M_{\kappa\mathbb{A}}}\big),$$

where $g_i : \mathrm{SO}_3(\mathbb{R}) \to \mathcal{M}_3(\mathbb{R})$ and $F : \mathcal{M}_3(\mathbb{R})^p \to \mathbb{R}$ are smooth functions. The IBM simulation thus defines an estimator $\hat{\kappa}$ of the concentration parameter such that

$$c_4(\hat{\kappa}) = F(\hat{g}_1, \dots, \hat{g}_p),$$

where $\hat{g}_i$ is the average of g_i obtained by replacing $M_{\kappa\mathbb{A}}$ by the empirical measure of the N body-orientations of the particles. We can then measure the bias by taking the expectation of the Taylor expansion of the previous expression around the point $(\langle g_1\rangle_{M_{\kappa\mathbb{A}}}, \dots, \langle g_p\rangle_{M_{\kappa\mathbb{A}}})$

$$c_4(\hat{\kappa}) = c_4(\kappa) + \delta\hat{\mathbf{g}} \cdot \nabla F + (\delta\hat{\mathbf{g}})^{\mathrm{T}}(\mathrm{Hess}\, F)\delta\hat{\mathbf{g}} + R,$$

where $\delta\hat{\mathbf{g}} = (\hat{g}_1, \dots, \hat{g}_p)^{\mathrm{T}} - (\langle g_1\rangle_{M_{\kappa\mathbb{A}}}, \dots, \langle g_p\rangle_{M_{\kappa\mathbb{A}}})^{\mathrm{T}}$ and R is a remainder. The gradient ∇ and Hessian Hess are defined within the Euclidean framework given by (2.1). By the chaos hypothesis $\mathbb{E}[\delta\hat{\mathbf{g}}] = 0$ and by the central limit theorem, the term of order two behaves as N^{-1}. Since $\mathrm{SO}_3(\mathbb{R})$ is compact, higher order moments of $\delta\hat{\mathbf{g}}$ can be controlled by a classical argument based on Hoeffding's inequality [320, Lemma 5.5 and Theorem 5.29]. This ensures that $\mathbb{E}[R]$ is $\mathcal{O}(N^{-2})$. We therefore obtain a biased estimator:

$$\mathbb{E}[c_4(\hat{\kappa})] = c_4(\kappa) + \frac{a}{N} + \mathcal{O}(N^{-2}),$$

where $a \in \mathbb{R}$ depends on the derivatives of the considered functions and on the variance of the estimator (2.6) where the particles are replaced by independent identically distributed

samples with law $M_{\kappa\mathbb{A}}$. The fact that $a > 0$ can be empirically verified on Fig. 8.4.2b but has not been proved yet. For each N, the fluctuations around the average (biased) value can be monitored by computing the standard deviation of the 10 independent simulations. Fig. 8.E.1 shows this standard deviation as a function of N in a log-log-scale (blue dots). Although fluctuations remain significant with only 10 simulations per data point, by a standard linear regression (solid orange line) we obtain that the size of the standard deviation behaves as $N^{-\beta}$ with $\beta \simeq 0.54$. which is close to the value $\beta = 1/2$ which we expect from an application of the central limit theorem.

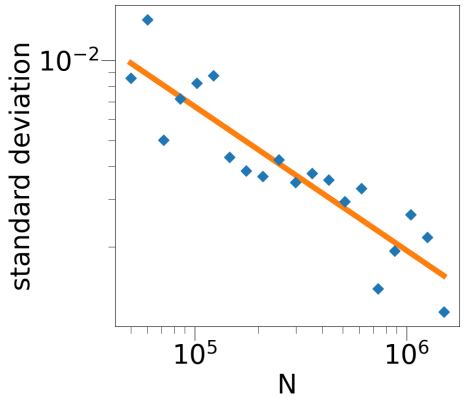

FIGURE 8.E.1: Standard deviation of the 10 independent simulations as a function of N (blue dots) and regression line (solid orange line) in log-log scale. Parameters: $L = 1$, $\xi = 2\pi$, $R = 0.025$, $\nu = 40$, $c_0 = 1$, $\kappa = 10$.

8.F Rare events

Although the scenario described in Section 8.6 is the most common one, the IBM sometimes leads to different, slightly more complex scenarios which are described in the present section. Now, the IBM is initialized by drawing N positions independently uniformly in the cubic domain $\mathcal{D} = [0, L] \times [0, L] \times [0, L]$ with periodic boundary conditions and N body-orientations independently from the von Mises distribution $M_{\mathbb{A}(0,\mathbf{x})}$ where $\mathbb{A}(0, \mathbf{x})$ is given by (8.20) with $\xi = 2\pi/L$ (winding number equal to 1).

8.F.1 From milling orbit to helical wave

Here, we report on the occurrence of transitions from a MO to a HW. Among twenty independent simulations, this transition occurred only once (the other cases being a transition from a MO to a FS). We run the IBM and record the time-evolution of a set of indicators as shown in Fig. 8.F.1 (see also supplementing videos 12 to 14 in Section 8.A).

As shown in Fig. 8.F.1a, the GOP does not converge towards GOP_2 characterizing the FS, but towards an intermediate value between GOP_1 (which characterizes MO or HW) and GOP_2. As explained in Section 8.D.4, such values of the GOP can be attained by a generalised helical wave solution (as can be observed in Video 12). The pitch $\bar{\theta}$ (Fig. 8.F.1b) and yaw $\bar{\varphi}$ (Fig. 8.F.1c) behave like in the milling-to-flocking transition (see Figs. 8.6.1b and 8.6.1c) except for small-amplitude, slow-frequency oscillations appearing after the topological transition time. This may be due to some competition between two attractors, the FS and the HW, which being alternately stronger and weaker, generate this oscillatory behaviour. Note that a transition to a HW cannot occur when the global direction of motion at the transition time is not one of the principal axes of the square domain since a HW along another direction is not compatible with the periodic boundary conditions (see Section 8.F.2). This is confirmed by the final values of $\bar{\varphi}$ and $\bar{\theta}$ (both equal to $\pi/2$) which correspond to a global direction of motion oriented along the y-axis (in what follows, in reference to (8.45) and to avoid confusion, we will still call that direction, the x direction).

The second and third lines of figures in Fig. 8.F.1 show the triplets of topological indicators $(d_z, \bar{r}_z, w_z)$ and $(d_x, \bar{r}_x, w_x)$ which materialize the MO and HW structures respectively. The mean distance of the RPZ-curve to the origin $\bar{r}_z$ (Figs. 8.F.1e) decreases, revealing an increase of the disorder. Simultaneously, the distance of its center of mass to the origin d_z increases (Figs. 8.F.1d) showing a transition trend to a FS. The winding number w_z (Fig. 8.F.1f) jumps from 1 to 0 at the time of maximal disorder. However, d_z and $\bar{r}_z$ do not reach zero, showing that complete disorder across z is not reached. Since the final state of the system is a generalised helical wave state (see Section 8.D.4), we do not necessarily expect that complete disorder will be reached along the z-direction. In the mean time, $\bar{r}_x$ starts from 0 (complete disorder) and increases up to a value close to unity, showing the build-up of a HW. The quantity d_x increases during some time but eventually decreases to 0 (not shown in the figure) as it should for a HW. Finally, the winding number w_x is undefined in the initial stage, as it should for complete disorder, but builds up to 1 at the time where the winding number w_z drops to 0. There is a transfer of non-trivial topology from an MO structure to a HW structure.

8.F.2 From milling to flocking via a helical wave state

In some rare cases an intermediate unstable HW can be observed. Note that due to the periodic setting, an HW cannot be stable for most of the global directions of motion. Although stable or unstable HW typically appear in one over twenty of our simulations, it

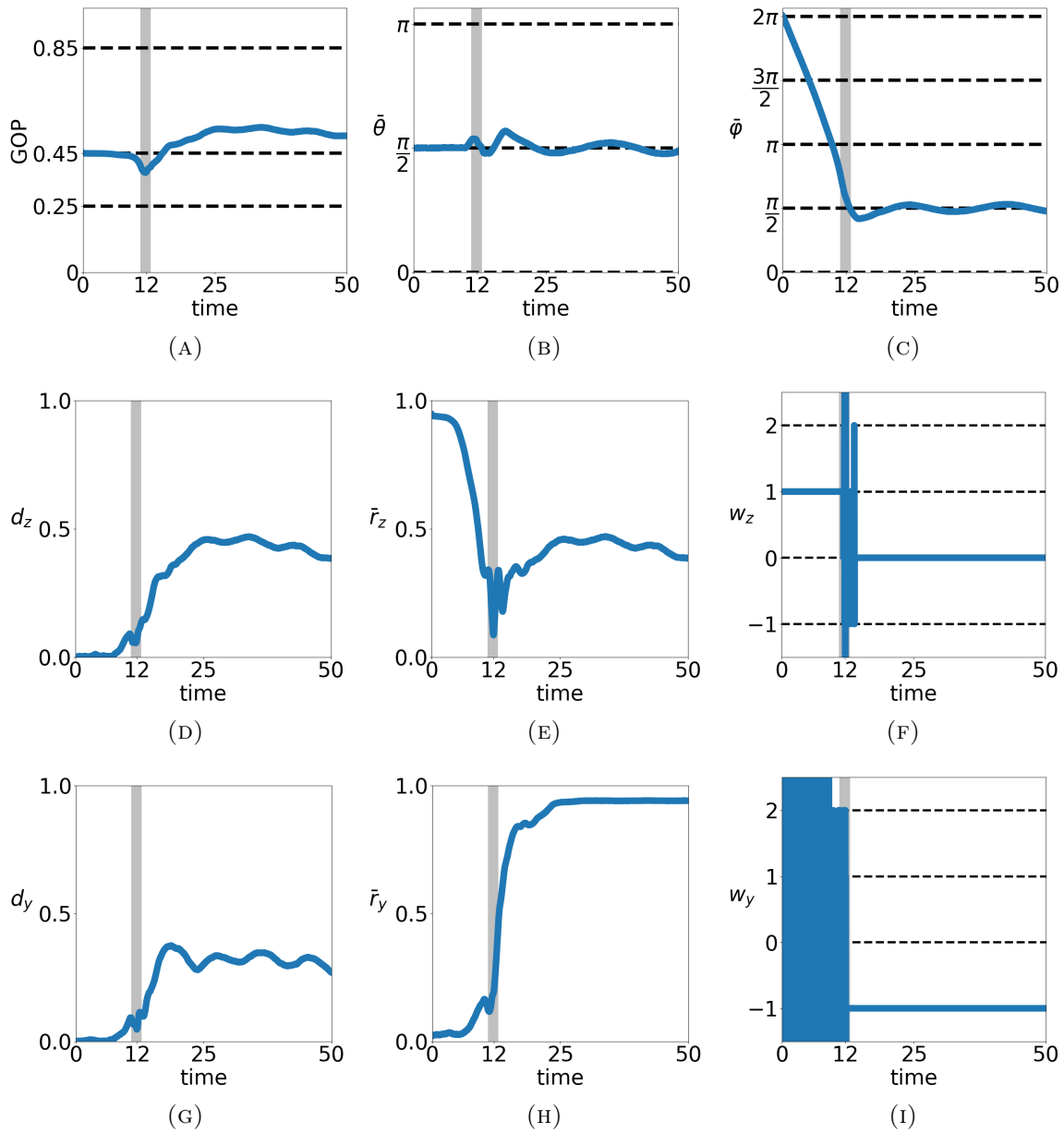

(A) (B) (C)

(D) (E) (F)

(G) (H) (I)

FIGURE 8.F.1: Transition from a MO to a HW: example of a solution of the IBM for an initial condition sampled from (8.42) in the rare case where it leads to a HW. The following indicators are plotted as functions of time: (a) GOP (b) Pitch $\bar{\theta}$ of $\bar{\Omega}$. (c) Yaw $\bar{\varphi}$ of $\bar{\Omega}$. (d) Distance of center of mass of RPZ curve to the origin d_z. (e) Mean distance of RPZ curve to the origin $\bar{r}_z$. (f) Winding number of RPZ curve w_z. (g) Distance of center of mass of RPX curve to the origin d_x. (h) Mean distance of RPX curve to the origin $\bar{r}_x$. (i) Winding number of RPX curve w_x. Gray shaded zones highlight a small region around the time of minimal GOP. Parameters: $N = 1.5 \cdot 10^6$, $R = 0.025$, $L = 1$, $D = 0.1$, $\nu = 40$, $c_0 = 1$. See caption of Fig. 8.6.1 for further indications. See also Videos 12 to 14 in Section 8.A.

should be kept in mind that the occurrence frequency also depends on the geometry of the domain and that this phenomena may be more frequent for other simulation settings. The procedure is the same as in the previous section. Fig. 8.F.2 shows the results (see also supplementing videos 15 and 16 in Section 8.A).

The transition stage between the MO and FS is significantly longer than in the previous situations. During that phase, the GOP (Fig. 8.F.2a) oscillates between the value Ψ_1 characterizing the MO and lower values, i.e. lower order. Likewise, there are significant variations of the pitch $\bar{\theta}$ (Fig. 8.F.2b) and yaw $\bar{\varphi}$ (Fig. 8.F.2c). As in the previous section, this could be explained by antagonist effects of different attractors (the MO and HW) and subsequent oscillations of the system between them. Video 15 reveals large scale band structures similar to a HW except that the global direction of motion is not one of the principal axes of the square domain. As, in most cases, this cannot be compatible with the periodic boundary conditions, such state cannot persist in time. The relatively long-time persistence of this stage could be explained in the present case by the fact that the global direction of motion seems to oscillate around the direction given by $\mathbf{e}_1 + \mathbf{e}_2$ (i.e. $\varphi = \pi/4$ and $\theta = \pi/2$) which is theoretically compatible with the periodic boundary conditions, provided the wave length ξ is changed from $2\pi/L$ to $\sqrt{2}\pi/L$. This state does not seem to be stable as shown by the large oscillations of $\bar{\varphi}$ and $\bar{\theta}$. The topological indicators $(d_z, \bar{r}_z, w_z)$ shown in the second line of figures of Fig. 8.F.2 also display large oscillations. The quantity $\bar{r}_z$ drops, and at the same time, d_z remains small, while the winding number w_z has strong oscillations, indicating a state of large disorder across z, which is consistent with the fact that the temporary HW order is organized in a different direction. However, we see that w_z has a calmer period between two series of oscillations. This calmer period corresponds to the interval of time during which the temporary HW order prevails. Eventually the triplet converges to the value $(1, 1, 0)$ characterizing the FS.

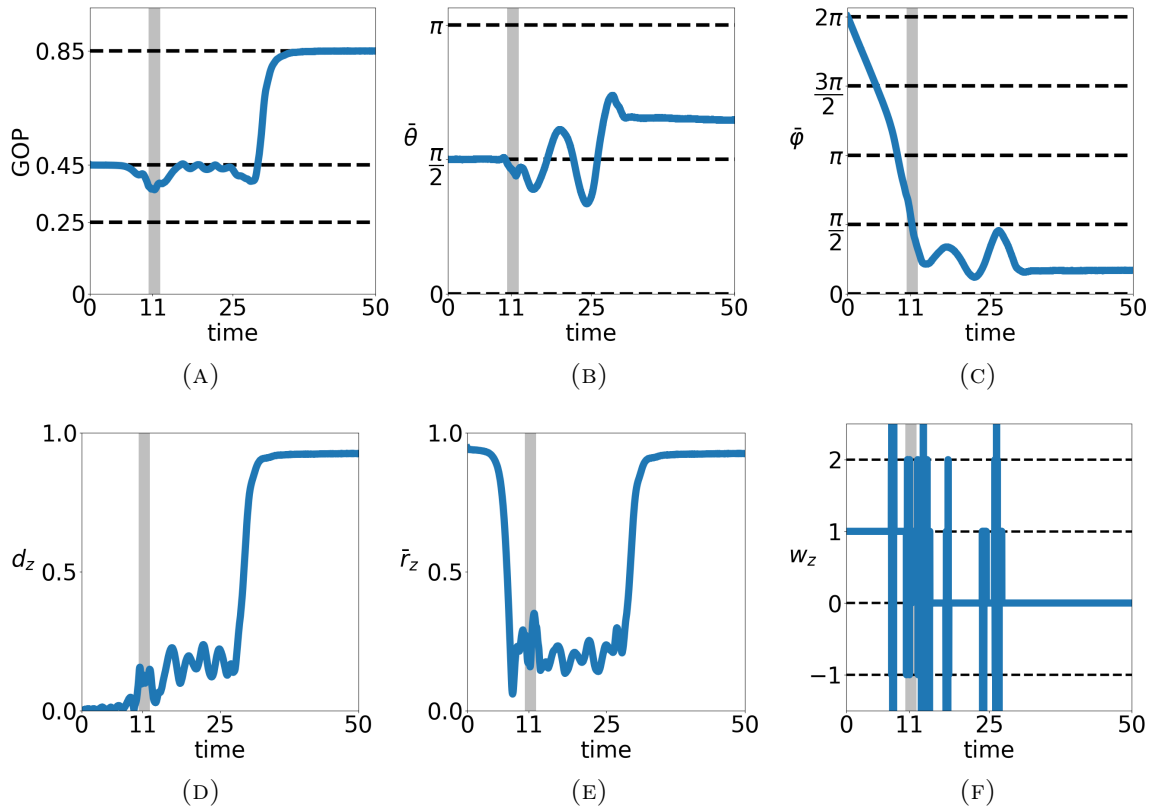

FIGURE 8.F.2: Transition from a MO to a FS via an unstable HW: example of a solution of the IBM for an initial condition sampled from (8.42) in the rare case where it leads to a FS through a transient HW. The following indicators are plotted as functions of time: (a) GOP (b) Pitch $\bar{\theta}$ of $\bar{\Omega}$. (c) Yaw $\bar{\varphi}$ of $\bar{\Omega}$. (d) Distance of center of mass of RPZ curve to the origin d_z. (e) Mean distance of RPZ curve to the origin $\bar{r}_z$. (f) Winding number of RPZ curve w_z. Gray shaded zones highlight a small region around the time of minimal GOP. Parameters: $N = 1.5 \cdot 10^6$, $R = 0.025$, $L = 1$, $D = 0.1$, $\nu = 40$, $c_0 = 1$. See caption of Fig. 8.6.1 for further indications. See also Videos 15 and 16 in Section 8.A.

Chapter 9

Body-attitude coordination in arbitrary dimension

The present chapter shortly summarises the main result of the following article co-authored with P. Degond and A. Frouvelle

[110] P. Degond, A. Diez, and A. Frouvelle. "Body-attitude coordination in arbitrary dimension". *arXiv preprint: arXiv:2111.05614* (2021).

9.1 Introduction

From a modelling perspective, the concept body-orientation is naturally defined in a three dimensional setting. However, from a purely mathematical perspective, there is no reason to restrict to the dimension three. The PDMP individual based model introduced in Section 2.1.2 with body-orientations in $\mathrm{SO}_3(\mathbb{R})$ can be straightforwardly extended in any dimension, with body-orientations in $\mathrm{SO}_n(\mathbb{R})$ (and positions in $\mathbb{R}^n$) for any $n \geq 3$. Similarly, the mean-field limit result presented in Chapter 4 does not depend on the dimension. However, this is not the case for the derivation of the macroscopic model in [114] recalled in Section 7.5. In order to obtain the fluid model (2.14), a specific parametrization of $\mathrm{SO}_3(\mathbb{R})$ is used, either based on Rodrigues formula (7.2) or a quaternion formulation [115]. In arbitrary dimension n, there is no such natural parametrization of $\mathrm{SO}_n(\mathbb{R})$. Writing a macrosocopic model for the n-dimensional model is therefore not a simple exercise. The present chapter introduces some tools and ideas to fulfill this task, based on representation theory [167, 188].

Beyond the purely mathematical game, there are at least two reasons to consider such generalisation. The first one is to obtain a more intrinsic formulation of the model

(including in dimension three) which does not depend on an arbitrary parametrization which may hide its underlying geometrical structure. The second reason is a more long-term perspective. Extending the result from $\mathrm{SO}_3(\mathbb{R})$ to $\mathrm{SO}_n(\mathbb{R})$ may be seen as a first step towards a generalisation to an arbitrary manifold or at least to a larger class of manifolds. Identifying what kind of geometrical properties lead to non-trivial effects in macroscopic models in collective dynamics is undoubtedly an important modelling question. In particular, although most (if not all) biologically related questions are bound to dimensions two or three, collective dynamics models are nowadays used in optimization and data sciences where understanding the "shape of data" in high-dimensional problems is a crucial issue. This chapter remains of course a modest contribution to this program but it may be considered as a first step to better understand high-dimensional collective dynamics effects.

9.2 Main result

The starting point is the re-scaled BGK equation in dimension n

$$\partial_t f^\varepsilon + (Ae_1 \cdot \nabla_x) f^\varepsilon = \frac{1}{\varepsilon}\big(\rho_{f^\varepsilon} M_{\mathbb{A}_{f^\varepsilon}} - f^\varepsilon\big), \tag{9.1}$$

with $\mathbb{A}_f = \mathbb{M}[f] \in \mathrm{SO}_n(\mathbb{R})$ is the projection of J_f on $\mathrm{SO}_n(\mathbb{R})$ given by (2.11) with $K = \delta_0$. The main result of this chapter is the following formal theorem.

Theorem 9.2.1 (formal)**.** *Let $n \in \mathbb{N}$, $n \geq 3$. We assume that* (9.1) *has a smooth solution f^ε which converges as $\varepsilon \to 0$ as smoothly as needed towards a smooth function f. Then,*

$$f = \rho M_{\mathbb{A}}, \tag{9.2}$$

where $\rho = \rho(t,x)$ and $\mathbb{A} = \mathbb{A}(t,x)$ are functions from $(0,\infty) \times \mathbb{R}^n$ to $(0,\infty)$ and $\mathrm{SO}_n(\mathbb{R})$ respectively which are solutions of the following system:

$$\partial_t \rho + \nabla_x \cdot (c_1 \rho \Omega_1) = 0, \tag{9.3}$$

$$\rho\big(\partial_t + c_2 \Omega_1 \cdot \nabla_x\big)\mathbb{A} = \mathbb{W}\mathbb{A}, \tag{9.4}$$

where

$$\mathbb{W} = F \wedge \Omega_1 - c_4 \rho \nabla_x \wedge \Omega_1, \tag{9.5}$$

$$F = -c_3 \nabla_x \rho - c_4 \rho \mathbf{r}, \tag{9.6}$$

$$\mathbf{r} = \sum_{k=1}^{n} (\nabla_x \cdot \Omega_k) \Omega_k, \tag{9.7}$$

with $\Omega_k = \mathbb{A} e_k$, $k = 1, \ldots, n$. *In Equation* (9.5), *we use the following notation: for two vectors* $X = (X_i)_{i=1,\ldots,n}$ *and* $Y = (Y_i)_{i=1,\ldots,n}$, $X \wedge Y$ *and* $\nabla_x \wedge X$ *denote the antisymmetric matrices:*

$$(X \wedge Y)_{ij} = X_i Y_j - X_j Y_i, \quad (\nabla_x \wedge X)_{ij} = \partial_{x_i} X_j - \partial_{x_j} X_i.$$

The constants c_i, $i = 1, \ldots, 4$ *are expressed as follows depending on the parity of the dimension. Let* $p \in \mathbb{N}$ *such that* $n = 2p$ *or* $n = 2p + 1$. *Then it holds that*

$$c_1 = \frac{1}{n} \frac{\displaystyle\int_{[0,2\pi]^p} C_n^{(1)} \exp\left(\kappa C_n^{(1)}\right) u_n d\tilde{\theta}_p}{\displaystyle\int_{[0,2\pi]^p} \exp\left(\kappa C_n^{(1)}\right) u_n \mathrm{d}\tilde{\theta}_p}, \tag{9.8}$$

$$c_2 = \frac{\displaystyle\int_{[0,2\pi]^p} \left(2C_n^{(3)} - nC_n^{(1)} C_n^{(2)} + (n^2 - 2) C_n^{(1)}\right) \exp\left(\kappa C_n^{(1)}\right) u_n \mathrm{d}\tilde{\theta}_p}{n(n-2)(n+2) \displaystyle\int_{[0,2\pi]^p} \left(1 - \frac{1}{n} C_n^{(2)}\right) \exp\left(\kappa C_n^{(1)}\right) u_n \mathrm{d}\tilde{\theta}_p}, \tag{9.9}$$

$$c_3 = \frac{1}{\kappa}, \tag{9.10}$$

$$c_4 = \frac{\displaystyle\int_{[0,2\pi]^p} \left(C_n^{(3)} - \frac{2}{n} C_n^{(1)} C_n^{(2)} + C_n^{(1)}\right) \exp\left(\kappa C_n^{(1)}\right) u_n \mathrm{d}\tilde{\theta}_p}{2(n-2)(n+2) \displaystyle\int_{[0,2\pi]^p} \left(1 - \frac{1}{n} C_n^{(2)}\right) \exp\left(\kappa C_n^{(1)}\right) u_n \mathrm{d}\tilde{\theta}_p}, \tag{9.11}$$

with the notation $\mathrm{d}\tilde{\theta}_p = \mathrm{d}\theta_1 \ldots \mathrm{d}\theta_p$, *where the probability density functions* u_n *are defined by* (9.15) *and* (9.16) *below and where for* $k \in \mathbb{Z}$, *the functions* $C_{2p}^{(k)}$ *and* $C_{2p+1}^{(k)}$: $\mathbb{R}^p \to \mathbb{R}$ *are defined by*

$$C_{2p}^{(k)}(\theta_1, \ldots, \theta_p) = 2(\cos k\theta_1 + \ldots + \cos k\theta_p), \tag{9.12}$$

$$C_{2p+1}^{(k)}(\theta_1, \ldots, \theta_p) = 2(\cos k\theta_1 + \ldots + \cos k\theta_p) + 1. \tag{9.13}$$

The coefficients in the theorem are computed using Weyl integration formula [301,

Theorems IX.9.4 & IX.9.5] recalled below.

Proposition 9.2.2 (Weyl integration formula)**.** *Let $n \in \mathbb{N}$, $n \geq 3$. Let $p \in \mathbb{N}$ such that $n = 2p$ or $n = 2p+1$. For any integrable class function f on $\mathrm{SO}_n(\mathbb{R})$ (i.e. such that it only depends on the conjugation class), it holds that*

$$\int_{\mathrm{SO}_n(\mathbb{R})} f(A)\,\mathrm{d}A = \frac{1}{(2\pi)^p} \int_{[0,2\pi]^p} f(R_{\theta_1 \dots \theta_p})\, u_n(\theta_1, \dots, \theta_p)\,\mathrm{d}\theta_1 \dots \mathrm{d}\theta_p, \tag{9.14}$$

where $u_n \colon \mathbb{R}^p \to \mathbb{R}$ are defined when $n = 2p$ or $n = 2p+1$ by

$$u_{2p}(\theta_1, \dots, \theta_p) = \frac{2^{(p-1)^2}}{p!} \prod_{1 \leq j < k \leq p} \big(\cos\theta_j - \cos\theta_k\big)^2, \tag{9.15}$$

$$u_{2p+1}(\theta_1, \dots, \theta_p) = \frac{2^{p(p-1)}}{p!} \prod_{1 \leq j < k \leq p} \big(\cos\theta_j - \cos\theta_k\big)^2 \prod_{j=1}^{p} \big(1 - \cos\theta_j\big), \tag{9.16}$$

and using the notations: for $\theta \in \mathbb{R}$,

$$R_\theta = \begin{pmatrix} \cos\theta & -\sin\theta \\ \sin\theta & \cos\theta \end{pmatrix},$$

and for $(\theta_1, \dots, \theta_p) \in \mathbb{R}^p$, $R_{\theta_1,\dots,\theta_p}$ denotes the following matrix defined by blocks:

- *in the case $n = 2p$, $p \geq 2$,*

$$R_{\theta_1,\dots,\theta_p} = \begin{pmatrix} R_{\theta_1} & & & 0 \\ & R_{\theta_2} & & \\ & & \ddots & \\ 0 & & & R_{\theta_p} \end{pmatrix} \in \mathrm{SO}_{2p}(\mathbb{R}), \tag{9.17}$$

- *in the case $n = 2p+1$, $p \geq 1$,*

$$R_{\theta_1,\dots,\theta_p} = \begin{pmatrix} R_{\theta_1} & & & 0 & 0 \\ & R_{\theta_2} & & & \vdots \\ & & \ddots & & \vdots \\ 0 & & & R_{\theta_p} & 0 \\ 0 & \dots & \dots & 0 & 1 \end{pmatrix} \in \mathrm{SO}_{2p+1}(\mathbb{R}). \tag{9.18}$$

There is an alternate expression of (9.4) which generalises (2.14) more directly but which first requires the introduction of additional notations. Suppose A, B and C are three smooth vector fields $\mathbb{R}^n \to \mathbb{R}^n$ and let us consider the following generalisation of (8.4)

$$\delta(A, B, C) := \big((A \cdot \nabla_x)B\big) \cdot C + \big((B \cdot \nabla_x)C\big) \cdot A + \big((C \cdot \nabla_x)A\big) \cdot B, \tag{9.19}$$

and for $\mathbb{A} = (\Omega_1, \dots, \Omega_n) \in \mathrm{SO}_n(\mathbb{R})$,

$$\Delta_{ijk} := \delta(\Omega_i, \Omega_j, \Omega_k). \tag{9.20}$$

It is easy to check that Δ_{ijk} is antisymmetric by permutations of the indices (i, j, k). Then, we define the following antisymmetric matrix field:

$$\Gamma = \sum_{k,\ell=1}^{n} \Delta_{1k\ell}\, \Omega_k \otimes \Omega_\ell, \tag{9.21}$$

where $\otimes$ denotes the tensor product of two vectors. The matrix Γ is just the matrix with entries $\Delta_{1k\ell}$ in the basis $(\Omega_1, \dots, \Omega_n)$. We note that

$$\Gamma\Omega_1 = \sum_{k,\ell=1}^{n} \Delta_{1k\ell}(\Omega_\ell \cdot \Omega_1)\Omega_k = \sum_{k=1}^{n} \Delta_{1k1}\Omega_k = 0, \tag{9.22}$$

by the antisymmetry of Δ_{ijk}. Finally, we define

$$\widetilde{\mathbb{W}} = F \wedge \Omega_1 + c_4\rho\Gamma. \tag{9.23}$$

Then, we have the following proposition (see [110, Appendix 10]).

Proposition 9.2.3. *Eq.* (9.4) *is equivalent to*

$$\rho\big(\partial_t + (c_2 - c_4)\,\Omega_1 \cdot \nabla_x\big)\mathbb{A} = \widetilde{\mathbb{W}}\mathbb{A}. \tag{9.24}$$

Finally, Equation (9.24) can be expanded into equations for the basis vectors Ω_j, which

is the direct generalisation of the 3D system (2.14). For $j = 2, \dots, n$, it holds that

$$\rho\big(\partial_t + (c_2 - c_4)\Omega_1 \cdot \nabla_x\big)\Omega_1 = -c_3 \mathsf{P}_{\Omega_1^\perp} \nabla_x \rho - c_4 \rho \sum_{k \neq 1} (\nabla_x \cdot \Omega_k)\Omega_k, \tag{9.25}$$

$$\rho\big(\partial_t + (c_2 - c_4)\Omega_1 \cdot \nabla_x\big)\Omega_j = \big(c_3(\Omega_j \cdot \nabla_x)\rho + c_4\rho(\nabla_x \cdot \Omega_j)\big)\Omega_1 - c_4\rho \sum_{k \neq 1,j} \delta(\Omega_1, \Omega_j, \Omega_k)\Omega_k, \tag{9.26}$$

where $\mathsf{P}_{\Omega_1^\perp} = \mathrm{Id} - \Omega_1 \otimes \Omega_1$ is the orthogonal projection onto $\Omega_1^\perp$.

Remark 9.2.4. In order to maintain light notations, the same notation is used for the coefficient c_2 but in dimension three it is not equal to the coefficient c_2 in (2.14). Namely, $c_2 \leftarrow c_2 - c_4$. The fact that (9.25) and (9.26) coincide with (2.14) in dimension three is checked in [110, Appendix 10].

9.3 A few elements of proof

The methodology of the proof of Theorem 9.2.1 is the same as the one exposed in Chapter 7 (Section 7.5) based on the notion of Generalised Collision Invariants [122]. The method reduces the problem to the computation of two integral operators, one linear and one bilinear, defined on spaces of matrices. In dimension n, these operators will be seen as maps between representations of $\mathrm{SO}_n(\mathbb{R})$.

9.3.1 Using the GCI: proof of Theorem 9.2.1

First, let us note that Equation (9.3) on ρ simply stems from the mass conservation and its derivation does not depend on the dimension. Then in order to derive the second Equation (9.4), let us extend the definition and computation of the set of GCI (Definition 7.42) in Section 7.5 to the n-dimensional case. Namely, for a given non singular matrix $J \in \mathcal{M}_n(\mathbb{R})$, the set of GCI is defined by

$$\mathscr{C}_J := \left\{ \psi \ : \mathrm{SO}_n(\mathbb{R}) \to \mathbb{R}, \ \int_{\mathrm{SO}_n(\mathbb{R})} (\rho_f M_J - f)\, \psi \, \mathrm{d}A = 0, \ \forall f \text{ such that } \mathsf{P}_{T_{\mathbb{A}}}(J_f) = 0 \right\}, \tag{9.27}$$

where $\mathbb{A} = \mathsf{P}_{\mathrm{SO_n}(\mathbb{R})} J$. Then it holds that

$$\mathscr{C}_J = \mathrm{Span}\left(1, \bigcup_{P \in \mathcal{A}_n(\mathbb{R})} \psi_P^{\mathbb{A}}\right), \quad \psi_P^{\mathbb{A}}(A) := -P \cdot (\mathbb{A}^{\mathrm{T}} A).$$

Multiplying (9.1) by the $\psi_P^{\mathbb{A}}(A)$ for any $P \in \mathcal{A}_n(\mathbb{R})$ and using Lemma 7.2.1 leads to the following relation when $\varepsilon \to 0$

$$X := \int_{\mathrm{SO}_n(\mathbb{R})} (\partial_t + Ae_1 \cdot \nabla_x)(\rho M_{\mathbb{A}}(A)) \mathsf{P}_{T_{\mathbb{A}}} A \, \mathrm{d}A = 0, \tag{9.28}$$

This is the n-dimensional analog of (7.44) except that for later convenience, here, we have multiplied the expression by $\mathbb{A}/2$ on the left and used Lemma 7.2.1. The quantity X is the sum of a linear part and a bilinear part, respectively:

$$X = X_\ell + X_b,$$

with

$$X_\ell := \int_{\mathrm{SO}_n(\mathbb{R})} \big[(\mathsf{P}_{T_{\mathbb{A}}} A)e_1 \cdot \nabla_x \rho + \kappa\rho \mathsf{P}_{T_{\mathbb{A}}} A \cdot \partial_t \mathbb{A}\big] \mathsf{P}_{T_{\mathbb{A}}} A \, M_{\kappa\mathbb{A}}(A) \, \mathrm{d}A, \tag{9.29}$$

$$X_b := \kappa\rho \int_{\mathrm{SO}_n(\mathbb{R})} \mathsf{P}_{T_{\mathbb{A}}} A \cdot \big((\mathsf{P}_{T_{\mathbb{A}}^\perp} A)e_1 \cdot \nabla_x\big) \mathbb{A} \, \mathsf{P}_{T_{\mathbb{A}}} A \, M_{\kappa\mathbb{A}}(A) \, \mathrm{d}A. \tag{9.30}$$

The following lemma shows that each of these quantities can be expressed in terms of two simple integral operators.

Lemma 9.3.1. *The quantity X_ℓ and X_b satisfy*

$$X_\ell = L(\mathbb{P})\mathbb{A}, \quad (X_b \mathbb{A}^{\mathrm{T}}) \cdot P = \kappa\rho \sum_{k,\ell=1}^{n} B_{k\ell}(\mathbb{T}_{\cdot\cdot k\ell}, P),$$

for any antisymmetric matrix $P \in \mathcal{A}_n(\mathbb{R})$ and where we have defined the following tensors

$$\mathbb{P} = \frac{1}{2}\big((\nabla_x \rho \otimes e_1)\, \mathbb{A}^{\mathrm{T}} - \mathbb{A}\, (\nabla_x \rho \otimes e_1)^{\mathrm{T}}\big) + \kappa\rho\, (\partial_t \mathbb{A})\, \mathbb{A}^{\mathrm{T}}, \tag{9.31}$$

$$\mathbb{T}_{ijk\ell} = \frac{1}{2}\big(\mathbb{A}_{k1}\, \mathbb{A}_{jm}\, \partial_{x_\ell} \mathbb{A}_{im} + \mathbb{A}_{\ell 1}\, \mathbb{A}_{jm}\, \partial_{x_k} \mathbb{A}_{im}\big), \tag{9.32}$$

and the linear and bilinear maps

$$L : \mathcal{A}_n \to \mathcal{A}_n, \quad P \mapsto L(P) := \int_{\mathrm{SO}_n(\mathbb{R})} (A \cdot P)\, \frac{A - A^{\mathrm{T}}}{2}\, M_{I_n}(A) \, \mathrm{d}A, \tag{9.33}$$

$$B : \mathcal{A}_n \times \mathcal{A}_n \to \mathcal{S}_n, \quad (P, Q) \mapsto B(P, Q) := \int_{\mathrm{SO}_n(\mathbb{R})} (A \cdot P)\, (A \cdot Q)\, \frac{A + A^{\mathrm{T}}}{2}\, M_{I_n}(A) \, \mathrm{d}A. \tag{9.34}$$

The main technical contribution of [110] is an explicit computation of the maps L and B, summarised in the following lemma. Once this result is proved, the derivation of (9.4) from the relation (9.28) follows from tedious but elementary computations summarised below and detailed in [110, Lemma 4.10].

Lemma 9.3.2. *For all antisymmetric matrices $P, Q \in \mathcal{A}_n(\mathbb{R})$, it holds that*

$$L(P) = C_2 P, \tag{9.35}$$

$$B(P,Q) = C_3 \mathrm{Tr}(PQ)\mathrm{Id} + C_4\Big(\frac{PQ+QP}{2} - \frac{1}{n}\mathrm{Tr}(PQ)\mathrm{Id}\Big), \tag{9.36}$$

with

$$C_2 = \frac{1}{n-1}\Big(1 - \big\langle \frac{\mathrm{Tr}\, A^2}{n}\big\rangle_{\exp(\kappa \mathrm{Tr} A)}\Big), \tag{9.37}$$

$$C_3 = \frac{1}{n-1}\Big\langle \Big(\frac{\mathrm{Tr} A^2}{n} - 1\Big)\frac{\mathrm{Tr} A}{n}\Big\rangle_{\exp(\kappa \mathrm{Tr} A)}, \tag{9.38}$$

$$C_4 = \frac{2n}{(n-1)(n-2)(n+2)}\Big\langle \frac{\mathrm{Tr} A^3}{n} - 2\frac{\mathrm{Tr} A}{n}\frac{\mathrm{Tr} A^2}{n} + \frac{\mathrm{Tr} A}{n}\Big\rangle_{\exp(\kappa \mathrm{Tr} A)}. \tag{9.39}$$

There are at least two proofs of this result. One is more elementary and rely on simple algebra using the changes of variables described in Definition 7.2.2. For instance, note that the first result (9.35) is a particular case of Lemma 7.2.5 proved using this method (for $n \neq 4$). For the second result (9.36), an elementary proof in three steps is outlined below.

1. Since, B takes its values in the space of symmetric matrices, the goal is to compute $B(P,Q)\cdot S$ for arbitrary $P, Q \in \mathcal{A}_n(\mathbb{R})$ and $S \in \mathcal{S}_n(\mathbb{R})$. An important property is the invariance by conjugation

$$\forall P_1, P_2 \in \mathcal{A}_n(\mathbb{R}), \quad \forall U \in \mathrm{SO}_n(\mathbb{R}), \quad B(UP_1U^T, UP_2U^T) = UB(P_1,P_2)U^T.$$

   Using this property and the spectral theorem, one can take for S a diagonal matrix.

2. By linearity, it remains to compute the quantities $B(\alpha_{ij}, \alpha_{k\ell})\cdot\sigma_m$ for $i,j,k,\ell,m \in \{1,\dots,n\}$, $i<j$, $k<\ell$ and where $\alpha_{ij} := e_i \wedge e_j$, $\sigma_m := e_m \otimes e_m$.

3. Using the invariance by conjugation again with the changes of variable described in Definition 7.2.2, it can be proved that, at least when n is large enough, it holds that $B(\alpha_{ij}, \alpha_{k\ell})\cdot\sigma_m = 0$ if $(i,j) \neq (k,\ell)$ and there exist $\lambda, \mu \in \mathbb{R}$ such that

$B(\alpha_{ij},\alpha_{ij})\cdot\sigma_i = B(\alpha_{ij},\alpha_{ij})\cdot\sigma_j = \lambda$ for all $i<j$ and $B(\alpha_{ij},\alpha_{ij})\cdot\sigma_m = \mu$ for all $i<j$ and $m\neq i,j$. The result then follows by a direct computation.

Similarly to the proof of Lemma 7.2.5, the third step is quite tedious, especially for small dimensions, and does not explicitly use the underlying algebraic structure of the problem. Another approach investigated in [110] and summarised in the next section is based on representation theory. This approach focuses more on the Lie group structure of $\mathrm{SO}_n(\mathbb{R})$ rather than on the fact that it is a matrix group. It may therefore be more easily generalised to other Lie groups. Once Lemma 9.3.2 is proved, the proof of the main Theorem 9.2.1 follows from direct computations.

Proof (of Theorem 9.2.1). First, we note that

$$(\nabla_x\rho\otimes e_1)\mathbb{A}^{\mathrm{T}} - \mathbb{A}(\nabla_x\rho\otimes e_1)^{\mathrm{T}} = \nabla_x\rho\wedge\Omega_1.$$

Thus Lemma 9.3.1 and Lemma 9.3.2 give

$$X_\ell = C_2\mathbb{P}\mathbb{A} = \kappa C_2(\rho\partial_t\mathbb{A} + c_3(\nabla_x\rho\wedge\Omega_1)\mathbb{A}).$$

Similarly, for the bilinear term, for all $P\in\mathcal{A}_n(\mathbb{R})$, it holds that

$$(X_b\mathbb{A}^{\mathrm{T}})\cdot P = \kappa\rho\Big[\Big(C_3-\frac{C_4}{n}\Big)\sum_{k=1}^n \mathrm{Tr}(\mathbb{T}_{\cdot\cdot kk}P) + \frac{C_4}{2}\sum_{k,\ell=1}^n \big(\mathbb{T}_{\cdot\cdot k\ell}P + P\mathbb{T}_{\cdot\cdot k\ell}\big)_{k\ell}\Big].$$

Using the definition of $\mathbb{T}_{ijk\ell}$ and the fact that it is anti-symmetric with respect to (i,j) and symmetric with respect to (k,ℓ), one can prove the following relations

$$\sum_{k=1}^n \mathrm{Tr}(\mathbb{T}_{\cdot\cdot kk}P) = -\big((\Omega_1\cdot\nabla_x)\mathbb{A}\mathbb{A}^{\mathrm{T}}\big)\cdot P$$
$$\sum_{k,\ell=1}^n \big(\mathbb{T}_{\cdot\cdot k\ell}P + P\mathbb{T}_{\cdot\cdot k\ell}\big)_{k\ell} = \frac{1}{2}(\mathbf{r}\wedge\Omega_1 + \nabla_x\wedge\Omega_1)\cdot P.$$

Finally, since $X_b\mathbb{A}^{\mathrm{T}}$ is antisymmetric and that the relation is valid for any $P\in\mathcal{A}_n(\mathbb{R})$, it follows that

$$X_b = \kappa C_2\rho\Big[c_2\,(\Omega_1\cdot\nabla_x)\mathbb{A} + c_4\,(\mathbf{r}\wedge\Omega_1+\nabla_x\wedge\Omega_1)\,\mathbb{A}\Big], \tag{9.40}$$

where

$$c_2 = -\frac{1}{C_2}\Big(C_3-\frac{C_4}{n}\Big), \qquad c_4 = \frac{C_4}{4C_2}, \tag{9.41}$$

which concludes the proof. □

9.3.2 Representation theory

Before giving the main steps of the proof of Lemma 9.3.2, let us recall below some of the key concepts of representation theory.

Definition 9.3.3 (Representation)**.** Let G be a Lie group. A real or complex representation of G of dimension n is a group morphism $G \to \mathrm{GL}(V)$ into the group of automorphisms of the vector space $V = \mathbb{R}^n$ or $\mathbb{C}^n$ respectively. Equivalently, a representation of G can be seen as a group action of G on V. Likewise, if $\mathfrak{g}$ is a Lie algebra, a representation of $\mathfrak{g}$ is a map of Lie algebras $\mathfrak{g} \to \mathfrak{gl}(V)$, where $\mathfrak{gl}(V)$ is the space of endomorphisms of V.

Example 9.3.4. The simplest representations are the following.

- **(Trivial representation).** This is the representation $\rho : G \to \mathrm{GL}(V), \quad g \mapsto \mathrm{id}_V$ where id_V is the identity operator.
- **(Standard representation).** When $G \subset \mathrm{GL}(V)$ is a matrix group, the standard representation is $\rho : G \to \mathrm{GL(V)}, \quad g \mapsto g$.

Definition 9.3.5 (Map of representations)**.** Let $\rho : G \to \mathrm{GL}(V)$ and $\rho' : G \to \mathrm{GL}(V')$ be two representations of a group G. A linear map $T : V \mapsto V'$ is said to be a *map of representations* when for all $g \in G$ it satisfies the commutation relation $\rho'(g) \circ T = T \circ \rho(g)$. The map T is also said to *intertwin* the representations. When there exists such map T which is an isomorphism, the two representations are said to be isomorphic. This definition extends similarly to the case of Lie algebra.

Definition 9.3.6 (Subrepresentation)**.** A *subrepresentation* $W \subset V$ of a representation V on G is a subspace of V stable by G, i.e. such that for all $g \in G$, $g(W) \subset W$. A representation V is said to be *irreducible* when $\{0\}$ and V are the only subrepresentations. This definition extends similarly to the case of Lie algebra.

In the cases considered here, any representation can be decomposed into the direct sum of irreducible representations [188, Section 4.4], making irreducible representations the building blocks of the theory. The reason why irreducible representations are so appealing is the so called Schur Lemma.

Lemma 9.3.7 (Schur Lemma)**.** *Let V and W be two irreducible* complex *representations of a group G and let T: $V \mapsto W$ be a map of representations. Then, there exists $C \in \mathbb{C}$ such that $T = C\,\mathrm{Id}$. Furthermore, $C = 0$ if the two representations are not isomorphic. If V and W are non-isomorphic* real *irreducible representations then $T = 0$.*

9.3.3 An alternative proof of (7.9)

As a first application of the theory, let us give an alternative proof of the first point of Lemma 7.3.1. By invariance by transposition, the goal is to prove that

$$\int_{\mathrm{SO}_n(\mathbb{R})} \big(\frac{A+A^{\mathrm{T}}}{2} - \frac{\mathrm{Tr}A}{n} I_n\big)\, M_{I_n}(A)\, \mathrm{d}A = 0.$$

Let us introduce the map $K : \mathcal{S}_n^0(\mathbb{R}) \to \mathbb{R}$ defined on the space $\mathcal{S}_n^0(\mathbb{R})$ of trace-free symmetric matrices by

$$K(S) := \int_{\mathrm{SO}_n(\mathbb{R})} (A \cdot S)\, M_{I_n}(A)\, \mathrm{d}A.$$

The goal is to prove that $K = 0$. Using the action of $\mathrm{SO}_n(\mathbb{R})$ on $\mathcal{S}_n^0(\mathbb{R})$ by conjugation and the properties of the Haar measure, the map K satisfies for all $U \in \mathrm{SO}_n(\mathbb{R})$ and all $S \in \mathcal{S}_n^0(\mathbb{R})$,

$$K(USU^{\mathrm{T}}) = K(S).$$

In other words, K is a map which intertwins the two representations $\mathcal{S}_n^0(\mathbb{R})$ and $\mathbb{R}$. The trivial representation $\mathbb{R}$ is always irreducible and it can be shown that $\mathcal{S}_n^0(\mathbb{R})$ is also irreducible [110, Lemma 7.1]. These two representations do not have the same dimension and therefore are not isomorphic. The conclusion follows by Schur lemma.

9.3.4 Proof of (9.35)

The proof of Lemma 9.3.2 is more difficult but it is based on the same idea: write the two operators as maps of representations, decompose the domain and codomain into the direct sum of irreducible representations and use Schur lemma on each pair of irreducible representations. However, this time, the starting point is not a map of representations of $\mathrm{SO}_n(\mathbb{R})$ but rather a map of representations of the complex Lie algebra $\mathfrak{so}_n(\mathbb{C})$. The representations of a Lie algebra often gives the representations of the Lie groups which share this Lie algebra. In our case, the irreducible representations of $\mathfrak{so}_n(\mathbb{C})$ lift into irreducible representations of $\mathrm{SO}_n(\mathbb{C})$ [167, Proposition 23.13 (iii)]. The complex irreducible representations of $\mathrm{SO}_n(\mathbb{C})$ and $\mathrm{SO}_n(\mathbb{R})$ are the same [167, §26.1, Section "Real groups"] and in most cases these complex representations are complexification of real ones which finally leads to real irreducible representations of $\mathrm{SO}_n(\mathbb{R})$.

The first step is therefore to extend the map L to the space of antisymmetric matrices

with complex entries:

$$\tilde{L} : \mathcal{A}_n(\mathbb{C}) \to \mathcal{A}_n(\mathbb{C}), \quad P + iQ \mapsto \tilde{L}(P + iQ) = L(P) + iL(Q).$$

The space $\mathcal{A}_n(\mathbb{C})$ is isomorphic to the space of exterior products $\Lambda^2(V)$ with $V = \mathbb{C}^n$ and where for $d \geq 2$ and $V = \mathbb{C}^n$,

$$\Lambda^d(V) := \text{Span}\left\{ v_1 \wedge \ldots \wedge v_d := \sum_{\sigma \in \mathfrak{S}_d} \varepsilon(\sigma) v_{\sigma(1)} \otimes \ldots \otimes v_{\sigma(d)} \,\middle|\, v_1, \ldots, v_d \in V \right\} \subset V^{\otimes d}, \tag{9.42}$$

In the case $n \neq 4$, the space $\Lambda^2(V)$ is an irreducible representation of $\mathfrak{so}_n(\mathbb{C})$ and consequently of $\mathrm{SO}_n(\mathbb{R})$ (for the action by conjugation). It is easy to check that the map $\tilde{L} : \Lambda^2(V) \to \Lambda^2(V)$ intertwins the two representations and thus by Schur lemma, it follows that $\tilde{L}(P + iQ) = C_2(P + iQ)$ for a constant $C_2 \in \mathbb{C}$. Taking $Q = 0$ and since $L(P)$ has real entries, we conclude that $C_2 \in \mathbb{R}$. Its expression follows by a direct computation.

The case $n = 4$ is more difficult because in this case $\Lambda^2(V)$ is not an irreducible representation of $\mathfrak{so}_4(\mathbb{C})$. It decomposes into the direct sum of two non-isomorphic irreducible representations of $\mathfrak{so}_4(\mathbb{C})$ using [167, Theorem 19.2 (ii)]:

$$\Lambda^2(V) = \Lambda_+ \oplus \Lambda_-, \tag{9.43}$$

both having dimension 3. Furthermore, as before, Λ_+ and Λ_- lift into complex irreducible representations of $\mathrm{SO}_4(\mathbb{C})$ and thus, of $\mathrm{SO}_4(\mathbb{R})$ [167, Proposition 23.13 (iii)]. The map $\tilde{L}$ can be decomposed by blocks using (9.43) on both its domain and codomain. Each block being a complex irreducible representation of $\mathrm{SO}_4(\mathbb{R})$, we can apply Schur lemma and conclude that any map between two blocks is equal to 0 if the blocks are not isomorphic and equal to $C\mathrm{Id}$ for some constant $C \in \mathbb{C}$ if the blocks are isomorphic. The pairs of isomorphic blocks are (Λ_+, Λ_+) and (Λ_-, Λ_-). It follows that there exist two constants C_2^+, $C_2^- \in \mathbb{C}$ such that

$$\tilde{L} = C_2^+ \, \mathcal{T}_+ + C_2^- \, \mathcal{T}_-, \tag{9.44}$$

where $C_2^+, C_2^- \in \mathbb{C}$ and $\mathcal{T}_\pm : \Lambda^2(V) \to \Lambda_\pm$ are the projections on the two subrepresentations. The rest of the proof consists in computing these operators and constants, and in particular it can be shown that $C_2^+ = C_2^-$ and $\mathcal{T}_+ + \mathcal{T}_- = \mathrm{Id}_{\Lambda^4(V)}$ which concludes the proof.

9.3.5 Elements of proof of (9.36)

The second point (9.36) is again more difficult. The complexification of the map B defines a symmetric bilinear map, denoted by $\breve{B}$: $\Lambda^2(V) \times \Lambda^2(V) \to \mathrm{Sym}^2(V)$ and given by

$$\breve{B}(P_1 + iQ_1, P_2 + iQ_2) = B(P_1, P_2) - B(Q_1, Q_2) + i(B(P_1, Q_2) + B(Q_1, P_2)),$$

for all P_1, P_2, Q_1, $Q_2 \in \mathcal{A}_n(\mathbb{R})$ and where

$$\mathrm{Sym}^d(V) := \mathrm{Span}\left\{ v_1 \circ \ldots \circ v_d := \sum_{\sigma \in \mathfrak{S}_d} v_{\sigma(1)} \otimes \ldots \otimes v_{\sigma(d)} \,\middle|\, v_1, \ldots, v_d \in V \right\} \subset V^{\otimes d}. \tag{9.45}$$

Due to the universal property of the symmetric product [167, Appendix B], $\breve{B}$ determines a unique linear map $\tilde{B}$: $\mathrm{Sym}^2(\Lambda^2(V)) \to \mathrm{Sym}^2(V)$ given for all $v_1, v_2, w_1, w_2 \in V$ by

$$\tilde{B}\big((v_1 \wedge v_2) \circ (w_1 \wedge w_2)\big) = \breve{B}(v_1 \wedge v_2, w_1 \wedge w_2).$$

Both $\mathrm{Sym}^2(\Lambda^2(V))$ and $\mathrm{Sym}^2(V)$ are complex representations of $\mathrm{SO}_n(\mathbb{R})$. Furthermore, the invariance properties of the Haar measure imply that $\tilde{B}$ intertwins the two representations. So, we are led to find the decompositions of $\mathrm{Sym}^2(\Lambda^2(V))$ and $\mathrm{Sym}^2(V)$ into irreducible representations of $\mathrm{SO}_n(\mathbb{R})$. As in the proof of (9.35), the starting point is the decomposition of $\mathrm{Sym}^2(V)$ into complex irreducible representations of $\mathfrak{so}_n(\mathbb{C})$. For the space $\mathrm{Sym}^2(\Lambda^2(V))$, things are more challenging and it needs to be first decomposed into irreducible representations of the Lie algebra $\mathfrak{sl}_n(\mathbb{C})$. This comes from the fact that the spaces of symmetric tensors (9.45) and exterior products (9.42) of V are irreducible representations of $\mathfrak{sl}_n(\mathbb{C})$. Irreducible representations of $\mathfrak{sl}_n(\mathbb{C})$ are not always irreducible representations of $\mathfrak{so}_n(\mathbb{C})$. However, their decomposition into irreducible representations of $\mathfrak{so}_n(\mathbb{C})$ can be obtained using a result called the *Weyl contraction* [167, Section 19.5]. The passage from $\mathfrak{so}_n(\mathbb{C})$ to $\mathrm{SO}_n(\mathbb{C})$ and $\mathrm{SO}_n(\mathbb{R})$ has been illustrated before. The full proof is detailed in [110, Appendix 9].

Conclusion

Chapter 10

Conclusion and perspectives

10.1 Conclusion

10.1.1 First part

The first part of this thesis was devoted to the study of many-particle systems with a probabilistic approach. Starting from a stochastic model, the fundamental concept of propagation of chaos gives an asymptotic description when the number of particles grows to infinity. This result can be understood as a kind of law of large numbers: by averaging out the numerous interactions between the particles, only a statistical deterministic behaviour is retained which reduces the initial high-dimensional complexity of the N-particle system to a single nonlinear PDE. This idea which traces back to the roots of statistical physics has been applied in the mathematical literature to various models and in particular in collective dynamics during the last two decades. Several techniques reviewed in Chapter 3 have been developed in various settings. In Chapter 4, a new method inspired by [218] has been described to treat the case of piecewise deterministic geometrically enriched models, including the classical Vicsek model and the body-orientation coordination model studied in the second part of the thesis. The two main contributions are a propagation of chaos result and moderate interaction property which legitimate the study of PDE models with purely local interactions. In addition to these rigorous convergence results, an efficient numerical framework for the simulation of mean-field particle systems has been exposed in Chapter 5. Thanks to recent hardware and software breakthroughs [78], the proposed implementation speeds up traditional methods by one to three orders of magnitude within a generalist and versatile Python library. This implementation was initially developed in parallel to the theoretical study of the body-attitude coordination model. It both confirms the results obtained analytically and offers an experimental tool to test new

conjectures for various collective dynamics models. Moreover, the efficient simulation of large systems of interacting particles has also been pushed by the recent development of particle methods in data sciences and optimization. Within this perspective a new sampling algorithm which generalizes the traditional Metropolis-Hastings algorithm to a population of interacting particles has been introduced and studied in Chapter 6. Both the analytical convergence properties obtained using the method developed in Chapter 4 and the GPU implementation which uses the same ideas as in Chapter 6 confirm its good performances.

10.1.2 Second part

The second part of this thesis was devoted to the study of PDE models of body-orientation coordination. The starting point was the kinetic PDE model obtained in Chapter 4 as the mean-field limit of an individual based model. In Chapter 7 it has been shown that, in a spatially homogeneous setting, the solution of this BGK equation has a complex behaviour due to a phase transition phenomenon. In order to obtain a complete characterisation and stability analysis of the different equilibria, new parallels have been drawn between the initial body-orientation framework and some recent results in the nematic alignment of high-dimensional polymers [330]. Then, using a framework developed in [122], a macroscopic fluid model has been obtained as a scaling limit of the kinetic PDE, this was an easy generalisation of the result obtained in [116]. Chapter 8 provides a theoretical and numerical analysis of this fluid model. The main result is the existence of three classes of explicit solutions which were not known in previous works and which are characterised by a topological structure. Numerical experiments have been designed to explore the links between this topological structure and the long-time stability and robustness of the solutions. It may open the way to the study of the interplay between geometrically enriched models in collective dynamics and a notion of topological protection. Finally, in Chapter 9, a derivation of the generalised macroscopic fluid model in arbitrary dimension is outlined using representation theory.

10.2 Perspectives

10.2.1 Topological protection in collective dynamics

A somehow unexpected finding of this work was the derivation of explicit solutions of the macroscopic fluid model. The existence of such solutions is a direct consequence of

the geometrical constraints inherent to $SO_3(\mathbb{R})$ as it can be seen by looking at the role of the two operators $\mathbf{r}$ and δ which are specific to this model. However, these solutions are also characterised by a nontrivial topological structure. The numerical experiments in Chapter 8 suggest that these solutions enjoy some kind of stability and robustness against noise. Although the setting is much different, this is reminiscent from the notion of topological protection developed in the physics community [269, 270]. Collective dynamics models associated to the Vicsek model have been shown to exhibit topological protected *edge* states when the motion is constrained in appropriate geometrical configurations [299, 303, 304]. In our setting, the solutions derived should better be called *bulk* states as they are not linked to boundary conditions and the topological properties are due to the internal geometry of the particles. Following this work, there are at least two perspectives. The first one is the study of the body-attitude coordination model with different boundary conditions and in domains with a more complex geometry in order to observe topological *edged* states. The second one is the analytical study of the stability of the solutions. This is a difficult because the functions are constrained on the manifold $SO_3(\mathbb{R})$ and further investigations are needed. In this direction, in a work in progress with Pierre Degond and Adam Walczak, we study a simpler extension of the Vicsek model which also produces topologically nontrivial states. This model is inspired by the swarmalator model [272, 271, 181, 182] which is a Vicsek model where each particle has an additional variable, called the phase, which creates an attraction-repulsion force between particles with different phases. This simpler model can be studied both analytically and numerically, in particular, using a direct scheme for the macroscopic model (which is not known for the body-attitude coordination model).

10.2.2 Full kinetic equations and hypocoercivity

In Chapter 7, the study is limited to the spatially homogeneous case and does not say anything about the long-time behaviour of the full kinetic equation with a transport term. Nevertheless, complex emerging phenomena do happen in a spatially in-homogeneous setting. The most renowned example is the spontaneous emergence of high-density travelling bands in the Vicsek model as reported in numerical simulations in Section 5.3.1. Unlike previous works in the physics community [80], these simulations are obtained in a mean-field regime in a framework where the propagation of chaos result applies. However to the best of our knowledge, an analytical explanation of this emergence from the limit kinetic equation still remains out of reach, despite some other numerical evidence at the kinetic level [178]. Similarly, it is not known whether these structures can be obtained

as solutions of a macroscopic model such as the one derived in [122]. Further numerical simulations at the particle level using the `SiSyPHE` library also suggest that other complex structures can emerge depending on the various non-local parameters. Finally, for some models such as the ant trail formation model introduced by [39], the spatial structure cannot be ignored and a rigorous analytical framework able to capture the full complexity of the model is still lacking.

In the kinetic theory community, it is well-known that spatially in-homogeneous equations are often not coercive, but rather, hypocoercive [327]. There is a vast literature on the subject, mostly for linear and linearized equations. In the present case, for the Vicsek and body-attitude coordination models, in addition to the nonlinearity, a major difficulty arises due to the geometrical constraints so that the long-time behaviour of these models at the kinetic level remains mostly an open, and active, question.

In a work in progress with Pierre Degond, Amic Frouvelle and Charles Elbar, we are studying the hypocoercivity properties of the multi-dimensional generalisation of another model introduced by [123]. In this model, which is an extension of the Vicsek model, the alignment interactions are not directly implemented on the velocity variable as in (1.4) but rather on an additional internal variable which is the curvature in dimension two and an antisymmetric matrix in higher dimension. This model is also motivated by physical considerations [73]. The spatially homogeneous version of this model still depends on two variables: the curvature and the velocity. The structure of this equation shares similarities with the spatially in-homogeneous kinetic Vlasov-Fokker-Planck equation where the couple position and velocity is replaced respectively by the couple velocity and curvature. However, compared to the Vicsek model, the geometrical complexity is delocalised to the velocity which plays the role of a position in a classical setting, which makes things much easier to study. Although it may seem quite far from the spatially in-homogeneous Vicsek model, we hope that the techniques and tools developed for this model may help for the future study of the Vicsek models and other models of collective dynamics in a spatially in-homogeneous setting.

10.2.3 Long-time behaviour and mean-field limit

Most of the results developed in Part II concern the long-time behaviour of PDE models. As these models are obtained as the limit of a particle system, it may be natural to wonder whether the propagation of chaos result holds uniformly in time or at least, how the long-time properties obtained for the PDE models really relate to the long-time behaviour of the particle system. In turns out that in many cases, propagation of chaos does not hold

uniformly in time and in certain cases, it can be shown that the two limits $N \to +\infty$ and $t \to +\infty$ do not commute, in particular when there is a phase transition as investigated in [132]. More precisely, the authors study a class of McKean-Vlasov systems on the torus which generalises the Kuramoto model. They introduce a diffusive rescaling of the particle distribution function with N fixed, namely

$$f_t^{\varepsilon,N}(\theta^1, \dots, \theta^N) := \varepsilon^{Nd} f_{\varepsilon^2 t}^N(\varepsilon\theta^1, \dots, \varepsilon\theta^N),$$

where $\varepsilon > 0$ is the scaling parameter. In the Kuramoto model framework, the distribution $f_t^{\varepsilon,N}$ is the law of a highly oscillating system with a frequency of order ε^{-1}. Using a gradient flow framework, one of the main results of the article [132, Corollary 1.27] is an explicit counter example which proves that for some chaotic initial conditions and in an appropriate convergence framework, the two limits $N \to +\infty$ and $\varepsilon \to 0$ exist but do not always commute. Consequently, the propagation of chaos cannot hold uniformly in time.

A similar result has been found and quantified in [32] for the Kuramoto model outlined in the introduction. With the same notations, if the propagation of chaos holds uniformly in time, then the empirical measure $\mu_{\Theta_t^N}$ necessarily converges towards a von Mises distribution $M_{\kappa e(\theta_0)}$ as $N, t \to +\infty$ for some parameters κ and θ_0. This is not always the case as shown by the large deviation principle proved in [32, Theorem 1.1]. When the particles are initially independent, the authors show that, given a time $T > 0$, there exist $\theta_0 \in \mathbb{R}$ and a sequence of processes $(W_t^{N,T})_{t\in[0,T]}$ which converges weakly to a standard Brownian motion as $N \to +\infty$ such that for all $\varepsilon > 0$:

$$\lim_{N\to+\infty} \mathbb{P}\left(\sup_{\tau\in[C(\lambda)/N,T]} \left\| \mu_{\Theta_{\tau N}^N} - M_{\kappa e\left(\theta_0 + D(\lambda) W_\tau^{N,T}\right)} \right\|_{H^{-1}} \leq \varepsilon \right) = 1,$$

where $C(\lambda), D(\lambda) > 0$ depend only on the parameter λ, the initial condition and ε. As a consequence, the propagation of chaos is *not* uniform in time and breaks down at times proportional to N.

For the body-orientation dynamics, including in the spatially-homogeneous setting, the long-time behaviour of the particle system is still not entirely known. It may be conjectured that at least for the spatially-homogeneous diffusion model, a result analog to the one in [32] holds, namely that the empirical measure behaves as a von Mises distribution with a random parameter which performs a Brownian motion on $\mathrm{SO}_3(\mathbb{R})$ around the average body-orientation solution of the macroscopic model.

10.2.4 Boltzmann interactions

As explained in Chapter 3, the models presented in this thesis are limited to mean-field interactions. This type of interaction is perhaps the simplest one and the general behaviour of mean-field models is relatively well-understood. However, from a modelling perspective, mean-field interactions can sometimes hardly be justified. In some cases, the interactions between the particles are better described by binary "collisional" instantaneous events which happen between two particles only. Going back to the classical kinetic theory of gas of Boltzmann, the classical example is the motion of N hard-spheres driven by the free-transport and elastic collisions. More recently, examples can be found in various modelling problems. For instance, in socio-economical models, an interaction between two individuals is an exchange of opinions [313, 119], of wealth [248, 89, 148] or may model the outcome of a one-versus-one game such as chess [149, 206]. These models are called *Boltzmann models* and further examples in collective dynamics will be given below.

To distinguish Boltzmann models from mean-field models, a general framework has been proposed in [76]. Similarly to (3.6), the motion of N particles is described by an infinitesimal generator $\mathcal{L}_N$ acting on N-particle test functions $\varphi_N \in C_b(E^N)$ of the form:

$$\mathcal{L}_N \varphi_N = \sum_{i=1}^{N} L^{(1)} \diamond_i \varphi_N + \frac{1}{N} \sum_{i<j} L^{(2)} \diamond_{ij} \varphi_N. \tag{10.1}$$

The operator $L^{(1)}$ acts on one-variable test functions and describes the individual flow of each particle and possibly the boundary conditions. The operator $L^{(2)}$ acts on two-variable test functions. We recall the notation for $i < j$:

$$L^{(2)} \diamond_{ij} \varphi_N : (z^1, \dots, z^N) \in E^N \mapsto L^{(2)}\big[(u,v) \mapsto \varphi_N(z^1, \dots, z^{i-1}, u, z^{i+1}, \dots, z^{j-1}, v, z^{j+1}, \dots, z^N)\big](z^i, z^j) \in \mathbb{R}.$$

The operator $L^{(2)}$ is typically of the form

$$L^{(2)}\varphi_2(z_1, z_2) = \lambda(z_1, z_2) \iint_{E\times E} \{\varphi_2(z_1', z_2') - \varphi_2(z_1, z_2)\} \Gamma^{(2)}(z_1, z_2, \mathrm{d}z_1', \mathrm{d}z_2'), \tag{10.2}$$

where

$$\Gamma^{(2)} : (z_1, z_2) \in E \times E \mapsto \Gamma^{(2)}(z_1, z_2, \mathrm{d}z_1', \mathrm{d}z_2') \in \mathcal{P}(E \times E),$$

is a given map which defines the post-collisional distribution of two colliding particles with

pre-collisional states (z_1, z_2) and

$$\lambda : (z_1, z_2) \in E \times E \mapsto \lambda(z_1, z_2) \in \mathbb{R}_+,$$

is a symmetric function which defines the (possibly non-homogeneous) collision rate between each pair of particles. In order to preserve the exchangeability between the particles, it is necessary to assume that $\Gamma^{(2)}$ satisfies for all $z_1, z_2 \in E$,

$$\Gamma^{(2)}(z_1, z_2, \mathrm{d}z_1', \mathrm{d}z_2') = \Gamma^{(2)}(z_2, z_1, \mathrm{d}z_2', \mathrm{d}z_1'). \tag{10.3}$$

When $N \to +\infty$, and similarly to mean-field particle systems, it is possible to prove under certain conditions that a propagation of chaos result holds towards a limit distribution f_t which, in this case, solves the following weak Boltzmann equation: for any test function $\varphi \in C_b(E)$,

$$\frac{\mathrm{d}}{\mathrm{d}t}\langle f_t, \varphi\rangle = \langle f_t, L^{(1)}\varphi\rangle + \langle f_t^{\otimes 2}, L^{(2)}(\varphi \otimes 1)\rangle,$$

or in a more symmetric form, using (10.3):

$$\begin{aligned}\frac{\mathrm{d}}{\mathrm{d}t}\langle f_t, \varphi\rangle &= \langle f_t, L^{(1)}\varphi\rangle \\ &+ \frac{1}{2}\int_{E^4} \lambda(z_1, z_2)\big\{\varphi(z_1') + \varphi(z_2') - \varphi(z_1) - \varphi(z_2)\big\}\Gamma^{(2)}(z_1, z_2, \mathrm{d}z_1', \mathrm{d}z_2')f_t(\mathrm{d}z_1)f_t(\mathrm{d}z_2).\end{aligned} \tag{10.4}$$

This property is in general more difficult to obtain than for mean-field particle systems. For the hard-sphere system this result is a renowned theorem due to Lanford [237] and recently improved in [168]. For stochastic systems in classical kinetic theory, fundamental results on the propagation of chaos and long-time properties of the solutions have been obtained in particular by Kac [223], Sznitman [305] and more recently Mischler and Mouhot [257]. For collective dynamics models, things are still quite open. A Boltzmann interaction version of the Vicsek model was introduced in the physics community by [29, 30]. In this alignment model, the post-collisional orientations of two colliding particles with pre-collisional orientations $v, v' \in \mathbb{S}^{d-1}$ are sampled from a distribution on the sphere centered around the mean orientation $(v + v')/|v + v'|$. The propagation of chaos property for this model is proved using a BBGKY hierarchy approach in [60, 59]. However, the complete description of the equilibria of the Boltzmann collision operator is still missing, see [58, 25] for some results in this direction. Recently, an extension of this alignment mechanism has been proposed in [199, 226] to model the swarming behaviour of myxobacteria. There are

two main reasons which make the analysis much difficult. The first one is the stochasticity: if the post-collisional orientations are exactly equal to the mean orientation, then the associated collision operator is completely studied in [118]. The second difficulty is, again, due to the geometrical constraints. Without these constraints the model has been widely studied in particular in the literature on evolution dynamics where it is sometimes called the infinitesimal model [20] and in other contexts in [274].

10.2.5 Metric and topological interactions

Ethological studies [15] suggest that in bird flocks, the individuals do not interact with all their neighbours within a given interaction radius but rather with a fixed number of neighbours, regardless of their distance. This is called a *topological interaction* mechanism. More formally, given a particle i, the influence of a particle j on i at time t depends on the rank $R_{ij} \in \{1, \dots, N\}$ of particle j defined such that particle j is the R_{ij}-th nearest neighbour of i:

$$R_{ij} := \#\big\{k \in \{1, \dots, N\},\ |X_t^i - X_t^k| < |X_t^i - X_t^j|\big\}.$$

In a mean-field framework, it is more natural to use the normalised rank defined by $r[\mu_{\mathcal{X}_t^N}](X_t^i, X_t^j) = R_{ij}/N$ where given $x, y, z \in \mathbb{R}^d$ and $\mu \in \mathcal{P}(\mathbb{R}^d)$,

$$r[\mu](x, y) := \big\langle \mu, \psi(x, y, \cdot)\big\rangle, \quad \psi(x, y, z) := \mathbb{1}_{[0,1)}\left(\frac{|x - z|}{|x - y|}\right). \tag{10.5}$$

All the swarming models previously described can be alternatively defined using *topological interactions* by replacing the metric observation kernel $K(|X_t^i - X_t^j|)$ by the rank-based observation kernel $K\big(r[\mu_{\mathcal{X}_t^N}](X_t^i, X_t^j)\big)$, where in this case $K : [0, 1] \to [0, +\infty)$ is a smooth given function. This change has two consequences: first the interaction is no longer symmetric and secondly, this adds a new source of nonlinearity (which is nevertheless of mean-field type). Using mean-field arguments, the propagation of chaos limit can be derived, at least formally. For the (deterministic) Cucker-Smale model, this is investigated in [192]. For Boltzmann interactions with a collision rate which depends on $K\big(r[\mu_{\mathcal{X}_t^N}](X_t^i, X_t^j)\big)$, several models are discussed in [35, 36] and a rigorous propagation of chaos result is proved in [107]. Apart from these works, topological interaction models have not been much studied in the mathematics literature and despite their biological interest, a detailed mathematical comparison between metric and topological models remains a largely open research path.

Bibliography

[1] J. A. Acebrón, L. L. Bonilla, C. J. Pérez Vicente, F. Ritort, and R. Spigler. "The Kuramoto model: A simple paradigm for synchronization phenomena". *Rev. Modern Phys.* 77.1 (2005), pp. 137–185.

[2] P. Aceves-Sanchez, M. Bostan, J.-A. Carrillo, and P. Degond. "Hydrodynamic limits for kinetic flocking models of Cucker-Smale type". *Math. Biosci. Eng.* 16 (2019), pp. 7883–7910.

[3] S. M. Ahn and S.-Y. Ha. "Stochastic flocking dynamics of the Cucker–Smale model with multiplicative white noises". *J. Math. Phys.* 51.10 (2010), p. 103301.

[4] G. Albi, N. Bellomo, L. Fermo, S.-Y. Ha, J. Kim, L. Pareschi, D. Poyato, and J. Soler. "Vehicular traffic, crowds, and swarms: From kinetic theory and multiscale methods to applications and research perspectives". *Math. Models Methods Appl. Sci.* 29.10 (2019), pp. 1901–2005.

[5] L. Andreis, P. Dai Pra, and M. Fischer. "McKean–Vlasov limit for interacting systems with simultaneous jumps". *Stoch. Anal. Appl.* 36.6 (2018), pp. 960–995.

[6] C. Andrieu, A. Jasra, A. Doucet, and P. Del Moral. "Non-linear Markov Chain Monte Carlo". *ESAIM: Proc.* 19 (2007), pp. 79–84.

[7] C. Andrieu, A. Jasra, A. Doucet, and P. Del Moral. "On nonlinear Markov Chain Monte Carlo". *Bernoulli* 17.3 (2011), pp. 987–1014.

[8] I. Aoki. "A simulation study on the schooling mechanism in fish". *Bull. Japan. Soc. Sci. Fish* 48 (1982), pp. 1081–1088.

[9] A. W. Appel. "An Efficient Program for Many-Body Simulation". *SIAM J. Sci. and Stat. Comput.* 6.1 (1985), pp. 85–103.

[10] Y. Atchadé, G. Fort, E. Moulines, and P. Priouret. "Adaptive Markov Chain Monte Carlo: Theory and Methods". In: *Bayesian Time Series Models*. Ed. by D. Barber, A. Taylan Cemgil, and S. Chiappa. Cambridge Univ. Press., 2011, pp. 32–51.

[11] Y. F. Atchadé and J. S. Rosenthal. "On adaptive Markov Chain Monte Carlo algorithms". *Bernoulli* 11.5 (2005), pp. 815–828.

[12] T. Aubin. *Nonlinear Analysis on Manifolds. Monge-Ampère Equations*. Grundlehren der mathematischen Wissenschaften 252. Springer New York, 1982.

[13] J. M. Ball. "Mathematics and liquid crystals". *Molecular Crystals and Liquid Crystals* 647.1 (2017), pp. 1–27. Publisher: Taylor & Francis.

[14] J. M. Ball and A. Majumdar. "Nematic liquid crystals: from Maier-Saupe to a continuum theory". *Molecular Crystals and Liquid Crystals* 525.1 (2010), pp. 1–11. Publisher: Taylor & Francis.

[15] M. Ballerini, N. Cabibbo, R. Candelier, A. Cavagna, E. Cisbani, I. Giardina, V. Lecomte, A. Orlandi, G. Parisi, A. Procaccini, M. Viale, and V. Zdravkovic. "Interaction ruling animal collective behavior depends on topological rather than metric distance: Evidence from a field study". *Proc. Natl. Acad. Sci. USA* 105.4 (2008), pp. 1232–1237.

[16] A. B. Barbaro, J. A. Canizo, J. A. Carrillo, and P. Degond. "Phase transitions in a kinetic flocking model of Cucker–Smale type". *Multiscale Model. Simul.* 14.3 (2016), pp. 1063–1088. Publisher: SIAM.

[17] A. B. Barbaro and P. Degond. "Phase transition and diffusion among socially interacting self-propelled agents". *Discrete Contin. Dyn. Syst. Ser. B* 19.3 (2014), pp. 1249–1278. Publisher: AIMS.

[18] J. Barnes and P. Hut. "A hierarchical O(N log N) force-calculation algorithm". *Nature* 324 (1986), pp. 446–449.

[19] J.-P. Bartier and J. Dolbeault. "Convex Sobolev inequalities and spectral gap". *C. R. Math. Acad. Sci. Paris* 342.5 (2006), pp. 307–312. Publisher: Elsevier.

[20] N. Barton, A. Etheridge, and A. Véber. "The infinitesimal model: Definition, derivation, and implications". *Theor. Popul. Biol.* 118 (2017), pp. 50–73.

[21] N. Bellomo, P. Degond, and E. Tadmor, eds. *Active Particles, Volume 1: Advances in Theory, Models, and Applications*. Modeling and Simulation in Science, Engineering and Technology. Springer International Publishing, 2017.

[22] N. Bellomo, P. Degond, and E. Tadmor, eds. *Active Particles, Volume 2: Advances in Theory, Models, and Applications*. Modeling and Simulation in Science, Engineering and Technology. Springer International Publishing, 2019.

[23] G. Ben Arous and M. Brunaud. “Methode de Laplace: étude variationnelle des fluctuations de diffusions de type “champ moyen"”. *Stochastics and Stochastics Reports* 31.1-4 (1990), pp. 79–144.

[24] G. Ben Arous and O. Zeitouni. “Increasing propagation of chaos for mean field models”. *Ann. Inst. Henri Poincaré Probab. Stat.* 35.1 (1999), pp. 85–102.

[25] E. Ben-Naim and P. L. Krapivsky. “Alignment of rods and partition of integers”. *Phys. Rev. E* 73.3 (2006), p. 031109.

[26] D. Benedetto, E. Caglioti, J. A. Carrillo, and M. Pulvirenti. “A Non-Maxwellian Steady Distribution for One-Dimensional Granular Media”. *J. Stat. Phys.* 91.5/6 (1998), pp. 979–990.

[27] D. Benedetto, E. Caglioti, and M. Pulvirenti. “A kinetic equation for granular media”. *ESAIM: Mathematical Modelling and Numerical Analysis* 31.5 (1997), pp. 615–641.

[28] L. Berlyand, R. Creese, P.-E. Jabin, and M. Potomkin. “Continuum Approximations to Systems of Correlated Interacting Particles”. *J. Stat. Phys.* 174.4 (2019), pp. 808–829.

[29] E. Bertin, M. Droz, and G. Grégoire. “Boltzmann and hydrodynamic description for self-propelled particles”. *Phys. Rev. E* 74.2 (2006), p. 022101.

[30] E. Bertin, M. Droz, and G. Grégoire. “Hydrodynamic equations for self-propelled particles: microscopic derivation and stability analysis”. *J. Phys. A* 42.44 (2009), p. 445001. Publisher: IOP Publishing.

[31] L. Bertini, G. Giacomin, and K. Pakdaman. “Dynamical Aspects of Mean Field Plane Rotators and the Kuramoto Model”. *J. Stat. Phys.* 138 (2009), pp. 270–290.

[32] L. Bertini, G. Giacomin, and C. Poquet. “Synchronization and random long time dynamics for mean-field plane rotators”. *Probab. Theory Related Fields* 160.3-4 (2014), pp. 593–653.

[33] J. Besag. “Comments on “Representations of knowledge in complex systems" by U. Grenander and MI Miller”. *J. R. Stat. Soc. Ser. B. Stat. Methodol.* 56 (1994), pp. 591–592.

[34] P. L. Bhatnagar, E. P. Gross, and M. Krook. “A model for collision processes in gases. I. Small amplitude processes in charged and neutral one-component systems”. *Phys. Rev.* 94.3 (1954), p. 511. Publisher: APS.

[35] A. Blanchet and P. Degond. "Topological Interactions in a Boltzmann-Type Framework". *J. Stat. Phys.* 163.1 (2016), pp. 41–60.

[36] A. Blanchet and P. Degond. "Kinetic Models for Topological Nearest-Neighbor Interactions". *J. Stat. Phys.* 169.5 (2017), pp. 929–950.

[37] G. Blelloch and G. Narlikar. "A Practical Comparison of N-Body Algorithms". In: *Parallel Algorithms*. Series in Discrete Mathematics and Theoretical Computer Science. American Mathematical Society, 1997.

[38] T. Bodineau, I. Gallagher, and L. Saint-Raymond. "The Brownian motion as the limit of a deterministic system of hard-spheres". *Invent. math.* 203.2 (2016), pp. 493–553.

[39] E. Boissard, P. Degond, and S. Motsch. "Trail formation based on directed pheromone deposition". *J. Math. Biol.* 66.6 (2013), pp. 1267–1301.

[40] F. Bolley, J. A. Cañizo, and J. A. Carrillo. "Stochastic mean-field limit: non-Lipschitz forces and swarming". *Math. Models Methods Appl. Sci.* 21.11 (2011), pp. 2179–2210. Publisher: World Scientific.

[41] F. Bolley, I. Gentil, and A. Guillin. "Uniform Convergence to Equilibrium for Granular Media". *Arch. Ration. Mech. Anal.* 208.2 (2013), pp. 429–445.

[42] F. Bolley and C. Villani. "Weighted Csiszár-Kullback-Pinsker inequalities and applications to transportation inequalities". *Ann. Fac. Sci. Toulouse Math. (6)* 14.3 (2005), pp. 331–352.

[43] E. Bolthausen. "Laplace approximations for sums of independent random vectors". *Probab. Theory Related Fields* 72.2 (1986), pp. 305–318.

[44] L. Boltzmann. "Weitere Studien über das Wärmegleichgewicht unter Gasmolekülen". *Sitzungsberichte der Akademie der Wissenschaften* 66 (1872), pp. 275–370. Translation: Further studies on the thermal equilibrium of gas molecules, in *Kinetic Theory 2*, 88–174, Ed. S.G. Brush, Pergamon, Oxford (1966).

[45] L. Bornn, P. E. Jacob, P. Del Moral, and A. Doucet. "An adaptive interacting Wang–Landau algorithm for automatic density exploration". *J. Comput. Graph. Statist.* 22.3 (2013), pp. 749–773. Publisher: Taylor & Francis Group.

[46] M. Bostan and J. A. Carrillo. "Fluid models with phase transition for kinetic equations in swarming". *Math. Models Methods Appl. Sci.* 30.10 (2020), pp. 2023–2065.

[47] P. Brémaud. *Markov Chains: Gibbs Fields, Monte Carlo Simulation, and Queues*. Texts in Applied Mathematics 31. Springer New York, 1999.

[48] D. Bresch, P.-E. Jabin, and Z. Wang. "On mean-field limits and quantitative estimates with a large class of singular kernels: Application to the Patlak–Keller–Segel model". *C. R. Math. Acad. Sci. Paris* 357.9 (2019), pp. 708–720.

[49] H. Brezis. *Functional Analysis, Sobolev Spaces and Partial Differential Equations*. Springer New York, 2011.

[50] M. Briant, A. Diez, and S. Merino-Aceituno. "Cauchy theory and mean-field limit for general Vicsek models in collective dynamics". *arXiv preprint: arXiv:2004.00883* (2021).

[51] L. Caffarelli, M. Feldman, and R. McCann. "Constructing optimal maps for Monge's transport problem as a limit of strictly convex costs". *J. Amer. Math. Soc.* 15.1 (2002), pp. 1–26.

[52] D. S. Calovi, U. Lopez, S. Ngo, C. Sire, H. Chaté, and G. Theraulaz. "Swarming, schooling, milling: phase diagram of a data-driven fish school model". *New J. Phys.* 16.1 (2014), p. 015026. Publisher: IOP Publishing.

[53] J. A. Cañizo and H. Yolda. "Asymptotic behaviour of neuron population models structured by elapsed-time". *Nonlinearity* 32 (2018).

[54] O. Cappé, A. Guillin, J. M. Marin, and C. P. Robert. "Population Monte Carlo". *J. Comput. Graph. Statist.* 13.4 (2004), pp. 907–929.

[55] O. Cappé, R. Douc, A. Guillin, J.-M. Marin, and C. P. Robert. "Adaptive importance sampling in general mixture classes". *Stat. Comput.* 18 (2008), pp. 447–459. Publisher: Springer.

[56] P. Cardaliaguet. "Notes on mean field games (from P.-L. Lions' lectures at Collège de France)". In: *Lecture given at Tor Vergata*. 2010, pp. 1–59.

[57] P. Cardaliaguet, F. Delarue, J.-M. Lasry, and P.-L. Lions. *The Master Equation and the Convergence Problem in Mean Field Games*. Annals of Mathematics Studies 201. Princeton University Press, 2019.

[58] E. Carlen, M. C. Carvalho, P. Degond, and B. Wennberg. "A Boltzmann model for rod alignment and schooling fish". *Nonlinearity* 28.6 (2015), pp. 1783–1803.

[59] E. Carlen, R. Chatelin, P. Degond, and B. Wennberg. "Kinetic hierarchy and propagation of chaos in biological swarm models". *Phys. D* 260 (2013), pp. 90–111.

[60] E. Carlen, P. Degond, and B. Wennberg. “Kinetic limits for pair-interaction driven master equations and biological swarm models”. *Math. Models Methods Appl. Sci.* 23.7 (2013), pp. 1339–1376.

[61] R. Carmona. *Lectures on BSDEs, Stochastic Control, and Stochastic Differential Games with Financial Applications*. SIAM, 2016.

[62] R. Carmona and F. Delarue. *Probabilistic Theory of Mean Field Games with Applications I, Mean Field FBSDEs, Control, and Games*. Probability Theory and Stochastic Modelling 83. Springer International Publishing, 2018.

[63] R. Carmona and F. Delarue. *Probabilistic Theory of Mean Field Games with Applications II, Mean Field Games with Common Noise and Master Equations*. Probability Theory and Stochastic Modelling 84. Springer International Publishing, 2018.

[64] J. A. Carrillo, Y.-P. Choi, C. Totzeck, and O. Tse. “An analytical framework for consensus-based global optimization method”. *Math. Models Methods Appl. Sci.* 28.06 (2018), pp. 1037–1066.

[65] J. A. Carrillo, M. Fornasier, G. Toscani, and F. Vecil. “Particle, kinetic, and hydrodynamic models of swarming”. In: *Mathematical Modeling of Collective Behavior in Socio-Economic and Life Sciences*. Ed. by G. Naldi, L. Pareschi, and G. Toscani. Birkhäuser Boston, 2010, pp. 297–336.

[66] J. A. Carrillo, S. Jin, L. Li, and Y. Zhu. “A consensus-based global optimization method for high dimensional machine learning problems”. *ESAIM Control Optim. Calc. Var.* 27 (2021), S5.

[67] J. A. Carrillo, Y.-P. Choi, and M. Hauray. “The derivation of swarming models: Mean-field limit and Wasserstein distances”. In: *Collective Dynamics from Bacteria to Crowds*. Ed. by A. Muntean and F. Toschi. CISM International Centre for Mechanical Sciences 553. Springer, Vienna, 2014, pp. 1–46.

[68] J. A. Carrillo, M. R. D’Orsogna, and V. Panferov. “Double milling in self-propelled swarms from kinetic theory”. *Kinet. Relat. Models* 2.2 (2009), pp. 363–378.

[69] J. A. Carrillo, M. Delgadino, and G. Pavliotis. “A λ-convexity based proof for the propagation of chaos for weakly interacting stochastic particles”. *J. Funct. Anal.* 279.10 (2020).

[70] J. A. Carrillo, R. J. McCann, and C. Villani. “Kinetic equilibration rates for granular media and related equations: entropy dissipation and mass transportation estimates”. *Rev. Mat. Iberoamericana* 19 (2003), pp. 971–1018.

[71] J. A. Carrillo, R. J. McCann, and C. Villani. "Contractions in the 2-Wasserstein Length Space and Thermalization of Granular Media". *Arch. Ration. Mech. Anal.* 17 (2006), pp. 217–263.

[72] P. Cattiaux, F. Delebecque, and L. Pédèches. "Stochastic Cucker–Smale models: Old and new". *Ann. Appl. Probab.* 28.5 (2018).

[73] A. Cavagna, L. Del Castello, I. Giardina, T. Grigera, A. Jelic, . Melillo, T. Mora, L. Parisi, E. Silvestri, M. Viale, and A. M. Walczak. "Flocking and Turning: a New Model for Self-organized Collective Motion". *J. Stat. Phys.* 158.3 (2015), pp. 601–627.

[74] C. Cercignani. *Ludwig Boltzmann, the Man Who Trusted Atoms*. Oxford University Press, 2006.

[75] C. Cercignani, R. Illner, and M. Pulvirenti. *The Mathematical Theory of Dilute Gases*. Applied Mathematical Sciences 106. Springer-Verlag New York, 1994.

[76] L.-P. Chaintron and A. Diez. "Propagation of chaos: a review of models, methods and applications". *arXiv preprint: arXiv:2106.14812* (2021).

[77] T. Champion and L. De Pascale. "The Monge problem in $\mathbb{R}^d$". *Duke Math. J.* 157.3 (2011), pp. 551–572.

[78] B. Charlier, J. Feydy, J. A. Glaunès, F.-D. Collin, and G. Durif. "Kernel Operations on the GPU, with Autodiff, without Memory Overflows". *J. Mach. Learn. Res.* 22.74 (2021), pp. 1–6.

[79] J.-F. Chassagneux, L. Szpruch, and A. Tse. "Weak quantitative propagation of chaos via differential calculus on the space of measures". *arXiv preprint arXiv:1901.02556* (2019).

[80] H. Chaté, F. Ginelli, G. Grégoire, and F. Raynaud. "Collective motion of self-propelled particles interacting without cohesion". *Phys. Rev. E* 77.4 (2008), p. 046113.

[81] P.-E. Chaudru de Raynal and N. Frikha. "From the backward Kolmogorov PDE on the Wasserstein space to propagation of chaos for McKean-Vlasov SDE's". *arXiv preprint arXiv:1907.01410* (2019).

[82] L. Chizat and F. Bach. "On the Global Convergence of Gradient Descent for Over-parameterized Models using Optimal Transport". In: *Advances in Neural Information Processing Systems 31 (NeurIPS 2018)*. Ed. by S. Bengio, H. Wallach, H. Larochelle, K. Grauman, N. Cesa-Bianchi, and R. Garnett. Montreal, Canada: Curran Associates, Inc., 2018, pp. 3040–3050.

[83] Y.-P. Choi and S. Salem. “Propagation of chaos for aggregation equations with no-flux boundary conditions and sharp sensing zones”. *Math. Models Methods Appl. Sci.* 28.02 (2018), pp. 223–258.

[84] Y.-P. Choi and S. Salem. “Collective behavior models with vision geometrical constraints: Truncated noises and propagation of chaos”. *J. Differential Equations* 266.9 (2019), pp. 6109–6148.

[85] Y.-P. Choi and S. Salem. “Cucker-Smale flocking particles with multiplicative noises: Stochastic mean-field limit and phase transition”. *Kinet. Relat. Models* 12.3 (2019), pp. 573–592.

[86] G. Clarté, A. Diez, and J. Feydy. “Collective Proposal Distributions for Nonlinear MCMC samplers: Mean-Field Theory and Fast Implementation”. *arXiv preprint: arXiv:1909.08988* (2021).

[87] M. Coghi and F. Flandoli. “Propagation of chaos for interacting particles subject to environmental noise”. *Ann. Appl. Probab.* 26.3 (2016).

[88] E. G. D. Cohen and W. Thirring, eds. *The Boltzmann Equation, Theory and Applications*. Acta Physica Austriaca Supplementum X. Springer Vienna, 1973. Proceedings of the International Symposium "100 Years Boltzmann Equation" in Vienna 4th-8th September 1972.

[89] R. Cortez and J. Fontbona. “Quantitative propagation of chaos for generalized Kac particle systems”. *Ann. Appl. Probab.* 26.2 (2016), pp. 892–916.

[90] A. Costanzo and C. Hemelrijk. “Spontaneous emergence of milling (vortex state) in a Vicsek-like model”. *J. Phys. D: Appl. Phys.* 51.13 (2018), p. 134004. Publisher: IOP Publishing.

[91] I. D. Couzin and N. R. Franks. “Self-organized lane formation and optimized traffic flow in army ants”. *Proc. Biol. Sci.* 270.1511 (2003), pp. 139–146. Publisher: The Royal Society.

[92] I. D. Couzin, J. Krause, R. James, G. D. Ruxton, and N. R. Franks. “Collective memory and spatial sorting in animal groups”. *Journal of theoretical biology* 218.1 (2002), pp. 1–12. Publisher: London, New York, Academic Press.

[93] R. V. Craiu, J. Rosenthal, and C. Yang. “Learn from thy neighbor: Parallel-chain and regional adaptive MCMC”. *J. Amer. Statist. Assoc.* 104.488 (2009), pp. 1454–1466. Publisher: Taylor & Francis.

[94] A. Creppy, F. Plouraboué, O. Praud, X. Druart, S. Cazin, H. Yu, and P. Degond. "Symmetry-breaking phase transitions in highly concentrated semen". *J. R. Soc. Interface* 13.123 (2016), p. 20160575. Publisher: The Royal Society.

[95] A. Creppy, O. Praud, X. Druart, P. L. Kohnke, and F. Plouraboué. "Turbulence of swarming sperm". *Phys. Rev. E* 92.3 (2015), p. 032722.

[96] D. Crisan and A. Doucet. "A survey of convergence results on particle filtering methods for practitioners". *IEEE Trans. Signal Process.* 50.3 (2002), pp. 736–746.

[97] I. Csiszár. "Sanov Property, Generalized I-Projection and a Conditional Limit Theorem". *Ann. Probab.* 12.3 (1984), pp. 768–793.

[98] F. Cucker and S. Smale. "On the mathematics of emergence". *Jpn. J. Math.* 2.1 (2007), pp. 197–227.

[99] M. R. D'Orsogna, Y. L. Chuang, A. L. Bertozzi, and L. S. Chayes. "Self-Propelled Particles with Soft-Core Interactions: Patterns, Stability, and Collapse". *Phys. Rev. Lett.* 96.10 (2006), p. 104302.

[100] P. Dai Pra and F. den Hollander. "McKean-Vlasov limit for interacting random processes in random media". *J. Stat. Phys.* 84 (1996), pp. 735–772.

[101] D. Dawson. "Measure-valued Markov processes". In: *École d'Été de Probabilités de Saint-Flour XXI-1991*. Ed. by P. Hennequin. Lecture Notes in Mathematics 1541. Springer Berlin Heidelberg, 1993.

[102] D. Dawson and J. Gärtner. "Large deviations from the McKean-Vlasov limit for weakly interacting diffusions". *Stochastics* 20.4 (1987).

[103] D. A. Dawson. "Critical dynamics and fluctuations for a mean-field model of cooperative behavior". *J. Stat. Phys.* 31.1 (1983), pp. 29–85.

[104] V. De Bortoli, A. Durmus, X. Fontaine, and U. Simsekli. "Quantitative Propagation of Chaos for SGD in Wide Neural Networks". *arXiv preprint: arXiv:2007.06352* (2020).

[105] A. De Masi, A. Galves, E. Löcherbach, and E. Presutti. "Hydrodynamic Limit for Interacting Neurons". *J. Stat. Phys.* 158.4 (2015), pp. 866–902.

[106] P. Degond, A. Diez, and M. Na. "Bulk topological states in a new collective dynamics model". *arXiv preprint: arXiv:2101.10864* (2021).

[107] P. Degond and M. Pulvirenti. "Propagation of chaos for topological interactions". *Ann. Appl. Probab.* 29.4 (2019).

[108] P. Degond. "Macroscopic limits of the Boltzmann equation: a review". In: *Modeling and Computational Methods for Kinetic Equations*. Ed. by P. Degond, L. Pareschi, and G. Russo. Springer, 2004, pp. 3–57.

[109] P. Degond. "Mathematical models of collective dynamics and self-organization". In: *Proceedings of the International Congress of Mathematicians ICM 2018*. Vol. 4. Rio de Janeiro, Brazil, 2018, pp. 3943–3964.

[110] P. Degond, A. Diez, and A. Frouvelle. "Body-attitude coordination in arbitrary dimension". *arXiv preprint: arXiv:2111.05614* (2021).

[111] P. Degond, A. Diez, A. Frouvelle, and S. Merino-Aceituno. "Phase Transitions and Macroscopic Limits in a BGK Model of Body-Attitude Coordination". *J. Nonlinear Sci.* 30.6 (2020), pp. 2671–2736.

[112] P. Degond, A. Frouvelle, and J.-G. Liu. "Macroscopic limits and phase transition in a system of self-propelled particles". *J. Nonlinear Sci.* 23.3 (2013), pp. 427–456. Publisher: Springer.

[113] P. Degond, A. Frouvelle, and J.-G. Liu. "Phase transitions, hysteresis, and hyperbolicity for self-organized alignment dynamics". *Arch. Ration. Mech. Anal.* 216.1 (2015), pp. 63–115. Publisher: Springer.

[114] P. Degond, A. Frouvelle, and S. Merino-Aceituno. "A new flocking model through body attitude coordination". *Math. Models Methods Appl. Sci.* 27.06 (2017), pp. 1005–1049.

[115] P. Degond, A. Frouvelle, S. Merino-Aceituno, and A. Trescases. "Quaternions in Collective Dynamics". *Multiscale Model. Simul.* 16.1 (2018), pp. 28–77.

[116] P. Degond, A. Frouvelle, S. Merino-Aceituno, and A. Trescases. "Alignment of Self-propelled Rigid Bodies: From Particle Systems to Macroscopic Equations". In: *Stochastic Dynamics Out of Equilibrium, Institut Henri Poincaré, Paris, France, 2017*. Ed. by G. Giacomin, S. Olla, E. Saada, H. Spohn, and G. Stoltz. Springer Proceedings in Mathematics & Statistics 282. Springer, Cham, 2019, pp. 28–66.

[117] P. Degond, A. Frouvelle, S. Merino-Aceituno, and A. Trescases. "Hyperbolicity of SOHB models". In preparation.

[118] P. Degond, A. Frouvelle, and G. Raoul. "Local Stability of Perfect Alignment for a Spatially Homogeneous Kinetic Model". *J. Stat. Phys.* 157.1 (2014), pp. 84–112.

[119] P. Degond, J.-G. Liu, S. Merino-Aceituno, and T. Tardiveau. "Continuum dynamics of the intention field under weakly cohesive social interaction". *Math. Models Methods Appl. Sci.* 27.01 (2017), pp. 159–182.

[120] P. Degond, J.-G. Liu, S. Motsch, and V. Panferov. "Hydrodynamic models of self-organized dynamics: derivation and existence theory". *Methods Appl. Anal.* 20 (2013), pp. 89–114.

[121] P. Degond and S. Merino-Aceituno. "Nematic alignment of self-propelled particles: From particle to macroscopic dynamics". *Math. Models Methods Appl. Sci.* 30.10 (2020), pp. 1935–1986.

[122] P. Degond and S. Motsch. "Continuum limit of self-driven particles with orientation interaction". *Math. Models Methods Appl. Sci.* 18.Suppl. (2008), pp. 1193–1215.

[123] P. Degond and S. Motsch. "A macroscopic model for a system of swarming agents using curvature control". *J. Stat. Phys.* 143.4 (2011), pp. 685–714. Publisher: Springer.

[124] P. Del Moral and J. Tugaut. "On the stability and the uniform propagation of chaos properties of Ensemble Kalman–Bucy filters". *Ann. Appl. Probab.* 28.2 (2018).

[125] P. Del Moral. "Measure-valued processes and interacting particle systems. Application to nonlinear filtering problems". *Ann. Appl. Probab.* 8 (1998), pp. 438–495.

[126] P. Del Moral. *Feynman-Kac Formulae, Genealogical and Interacting Particle Systems with Applications*. Probability and Its Applications. Springer-Verlag New York, 2004.

[127] P. Del Moral. *Mean field simulation for Monte Carlo integration*. Monographs on Statistics and Applied Probability 126. CRC Press, Taylor & Francis Group, 2013.

[128] P. Del Moral, A. Doucet, and A. Jasra. "Sequential Monte Carlo samplers". *J. R. Stat. Soc. Ser. B. Stat. Methodol.* 68.3 (2006), pp. 411–436. Publisher: Wiley Online Library.

[129] P. Del Moral, A. Kurtzmann, and J. Tugaut. "On the Stability and the Uniform Propagation of Chaos of a Class of Extended Ensemble Kalman-Bucy Filters". *SIAM J. Control Optim.* 55.1 (2017), pp. 119–155.

[130] P. Del Moral and J. Tugaut. "Uniform propagation of chaos and creation of chaos for a class of nonlinear diffusions". *Stoch. Anal. Appl.* 37.6 (2019), pp. 909–935.

[131] F. Delarue and A. Tse. “Uniform in time weak propagation of chaos on the torus”. *arXiv preprint: arXiv:2104.14973* (2021).

[132] M. G. Delgadino, R. S. Gvalani, and G. A. Pavliotis. “On the Diffusive-Mean Field Limit for Weakly Interacting Diffusions Exhibiting Phase Transitions”. *Arch. Ration. Mech. Anal.* (2021).

[133] M. G. Delgadino, R. S. Gvalani, G. A. Pavliotis, and S. A. Smith. “Phase transitions, logarithmic Sobolev inequalities, and uniform-in-time propagation of chaos for weakly interacting diffusions”. *arXiv preprint: arXiv:2112.06304* (2021).

[134] B. Delyon and F. Portier. “Safe and adaptive importance sampling: a mixture approach”. *arXiv preprint arXiv:1903.08507* (2020).

[135] L. Desvillettes, C. Mouhot, and C. Villani. “Celebrating Cercignani’s conjecture for the Boltzmann equation”. *Kinet. Relat. Models* 4.1 (2001), pp. 277–294.

[136] P. Diaconis and D. Freedman. “Finite Exchangeable Sequences”. *Ann. Probab.* 8.4 (1980), pp. 745–764.

[137] P. Diaconis, G. Lebeau, and L. Michel. “Geometric analysis for the Metropolis algorithm on Lipschitz domains”. *Invent. Math.* 185.2 (2011), pp. 239–281. Publisher: Springer.

[138] A. Diez. “Propagation of chaos and moderate interaction for a piecewise deterministic system of geometrically enriched particles”. *Electron. J. Probab.* 25 (2020).

[139] A. Diez. “SiSyPHE: A Python package for the Simulation of Systems of interacting mean-field Particles with High Efficiency”. *Journal of Open Source Software* 6.65 (2021), p. 3653.

[140] G. Dimarco and S. Motsch. “Self-alignment driven by jump processes: Macroscopic limit and numerical investigation”. *Math. Models Methods Appl. Sci.* 26.07 (2016), pp. 1385–1410.

[141] G. Dimarco and L. Pareschi. “Numerical methods for kinetic equations”. *Acta Numerica* 23 (2014), pp. 369–520.

[142] Z. Ding and Q. Li. “Ensemble Kalman inversion: mean-field limit and convergence analysis”. *Stat. Comput.* 31.1 (2021), p. 9.

[143] Z. Ding and Q. Li. “Ensemble Kalman Sampler: Mean-field Limit and Convergence Analysis”. *SIAM J. Math. Anal.* 53.2 (2021), pp. 1546–1578.

[144] R. L. Dobrushin. “Vlasov equations”. *Funct. Anal. Appl.* 13.2 (1979), pp. 115–123.

[145] R. Douc, A. Guillin, J.-M. Marin, and C. P. Robert. "Convergence of adaptive mixtures of importance sampling schemes". *The Annals of Statistics* 35.1 (2007), pp. 420–448. Publisher: The Institute of Mathematical Statistics.

[146] A. Doucet, N. Freitas, and N. Gordon, eds. *Sequential Monte Carlo Methods in Practice*. Information Science and Statistics. Springer-Verlag New York, 2001.

[147] S. Duane, A. D. Kennedy, B. J. Pendleton, and D. Roweth. "Hybrid Monte Carlo". *Phys. Lett. B* 195.2 (1987), pp. 216–222.

[148] B. Düring, N. Georgiou, S. Merino-Aceituno, and E. Scalas. "Continuum and thermodynamic limits for a simple random-exchange model". *arXiv preprint: arXiv:2003.00930* (2020).

[149] B. Düring, M. Torregrossa, and M.-T. Wolfram. "Boltzmann and Fokker–Planck Equations Modelling the Elo Rating System with Learning Effects". *J. Nonlinear Sci.* 29.3 (2019), pp. 1095–1128.

[150] A. Durmus, A. Eberle, A. Guillin, and R. Zimmer. "An elementary approach to uniform in time propagation of chaos". *Proc. Amer. Math. Soc.* (2020).

[151] A. Eberle. "Reflection couplings and contraction rates for diffusions". *Probab. Theory Related Fields* 166 (2016), pp. 851–886.

[152] A. Eberle, A. Guillin, and R. Zimmer. "Quantitative Harris-type theorems for diffusions and McKean-Vlasov processes". *Trans. Amer. Math. Soc.* 371 (2019), pp. 7135–7173.

[153] X. Erny. "Well-posedness and propagation of chaos for McKean-Vlasov equations with jumps and locally Lipschitz coefficients". *arXiv preprint: arXiv:2102.06472* (2021).

[154] G. Estrada-Rodriguez and H. Gimperlein. "Interacting Particles with Lévy Strategies: Limits of Transport Equations for Swarm Robotic Systems". *SIAM J. Appl. Math.* 80.1 (2020), pp. 476–498.

[155] A. Etheridge. *Some Mathematical Models from Population Genetics. École d'Été de Probabilités de Saint-Flour XXXIX-2009*. Lecture Notes in Mathematics 2012. Springer Berlin Heidelberg, 2011.

[156] S. N. Ethier and T. G. Kurtz. *Markov processes: characterization and convergence*. Wiley series in probability and mathematical statistics. New York: Wiley, 1986.

[157] P. Fearnhead, J. Bierkens, M. Pollock, G. O. Roberts, et al. "Piecewise deterministic Markov processes for continuous-time Monte Carlo". *Statist. Sci.* 33.3 (2018), pp. 386–412. Publisher: Institute of Mathematical Statistics.

[158] M. Feldman and R. J. McCann. "Monge's transport problem on a Riemannian manifold". *Trans. Amer. Math. Soc.* 354.4 (2001), pp. 1667–1697.

[159] J. Feydy. "Geometric data analysis, beyond convolutions". PhD Thesis. Université Paris-Saclay, 2020.

[160] A. Figalli, M.-J. Kang, and J. Morales. "Global Well-posedness of the Spatially Homogeneous Kolmogorov–Vicsek Model as a Gradient Flow". *Arch. Ration. Mech. Anal.* 227.3 (2018), pp. 869–896.

[161] M. Fornasier, H. Huang, L. Pareschi, and P. Sünnen. "Consensus-based optimization on hypersurfaces: Well-posedness and mean-field limit". *Math. Models Methods Appl. Sci.* 30.14 (2020), pp. 2725–2751.

[162] N. Fournier and A. Guillin. "On the rate of convergence in Wasserstein distance of the empirical measure". *Probab. Theory Related Fields* 162.3-4 (2015), pp. 707–738. Publisher: Springer.

[163] N. Fournier and E. Löcherbach. "On a toy model of interacting neurons". *Ann. Inst. Henri Poincaré Probab. Stat.* 52.4 (2016).

[164] D. Frenkel and B. Smit. *Understanding molecular simulation: from algorithms to applications*. 2nd ed. San Diego: Academic Press, 2002.

[165] M. Friesen and O. Kutoviy. "Stochastic Cucker-Smale flocking dynamics of jump-type". *Kinet. Relat. Models* 13.2 (2020), pp. 211–247.

[166] A. Frouvelle. "Body-attitude alignment: first order phase transition, link with rodlike polymers through quaternions, and stability". *arXiv preprint: arXiv:2011.14891* (2020).

[167] W. Fulton and J. Harris. *Representation theory: a first course*. Vol. 129. Springer Science & Business Media, 2013.

[168] I. Gallagher, L. Saint-Raymond, and B. Texier. "From Newton to Boltzmann: Hard Spheres and Short-Range Potentials". *Zur. Lect. Adv. Math.* 18 (2014).

[169] I. M. Gamba and M.-J. Kang. "Global Weak Solutions for Kolmogorov–Vicsek Type Equations with Orientational Interactions". *Arch. Ration. Mech. Anal.* 222.1 (2016), pp. 317–342.

[170] A. Garbuno-Inigo, F. Hoffmann, W. Li, and A. M. Stuart. "Interacting Langevin Diffusions: Gradient Structure and Ensemble Kalman Sampler". *SIAM J. Appl. Dyn. Syst.* 19.1 (2020), pp. 412–441.

[171] P. Gerlee, K. Tunstrøm, T. Lundh, and B. Wennberg. "Impact of anticipation in dynamical systems". *Phys. Rev. E* 96.6 (2017), p. 062413. Publisher: American Physical Society.

[172] G. Giacomin, K. Pakdaman, and X. Pellegrin. "Global attractor and asymptotic dynamics in the Kuramoto model for coupled noisy phase oscillators". *Nonlinearity* 25.5 (2012), pp. 1247–1273.

[173] F. Golse. "On the Dynamics of Large Particle Systems in the Mean Field Limit". *Lecture notes. arXiv:1301.5494* (2016), pp. 1–144. arXiv: 1301.5494.

[174] N. J. Gordon, D. J. Salmond, and A. F. Smith. "Novel approach to nonlinear/non-Gaussian Bayesian state estimation". In: *IEE proceedings F (radar and signal processing)*. Vol. 140. IET, 1993, pp. 107–113.

[175] C. Graham. "McKean-Vlasov Itō-Skorohod equations, and nonlinear diffusions with discrete jump sets". *Stochastic Process. Appl.* 40 (1992), pp. 69–82.

[176] C. Graham and S. Méléard. "Stochastic particle approximations for generalized Boltzmann models and convergence estimates". *Ann. Probab.* 25.1 (1997), pp. 115–132.

[177] S. Grassi and L. Pareschi. "From particle swarm optimization to consensus based optimization: stochastic modeling and mean-field limit". *arXiv preprint: arXiv:2012.05613* (2020).

[178] Q. Griette and S. Motsch. "Kinetic equations and self-organized band formations". In: *Active Particles, Volume 2*. Springer, 2019, pp. 173–199.

[179] F. A. Grünbaum. "Propagation of chaos for the Boltzmann equation". *Arch. Ration. Mech. Anal.* 42 (1971).

[180] A. Guillin, P. Le Bris, and P. Monmarché. "Uniform in time propagation of chaos for the 2D vortex model and other singular stochastic systems". *arXiv preprint: arXiv:2108.08675* (2021).

[181] S.-Y. Ha, J. Jung, J. Kim, J. Park, and X. Zhang. "Emergent behaviors of the swarmalator model for position-phase aggregation". *Math. Models Methods Appl. Sci.* 29.12 (2019), pp. 2225–2269.

[182] S.-Y. Ha, J. Jung, J. Kim, J. Park, and X. Zhang. "A mean-field limit of the particle swarmalator model". *Kinet. Relat. Models* 14.3 (2021), p. 429.

[183] S.-Y. Ha, D. Kim, J. Lee, and S. Eun Noh. "Emergent dynamics of an orientation flocking model for multi-agent system". *Discrete Contin. Dyn. Syst.* 40.4 (2020), pp. 2037–2060.

[184] S.-Y. Ha, D. Ko, and S. W. Ryoo. "Emergent Dynamics of a Generalized Lohe Model on Some Class of Lie Groups". *J. Stat. Phys.* 168.1 (2017), pp. 171–207.

[185] S.-Y. Ha, K. Lee, and D. Levy. "Emergence of time-asymptotic flocking in a stochastic Cucker-Smale system". *Commun. Math. Sci.* 7.2 (2009), pp. 453–469.

[186] H. Haario, E. Saksman, and J. Tamminen. "Adaptive proposal distribution for random walk Metropolis algorithm". *Comput. Statist.* 14.3 (1999), pp. 375–396. Publisher: Heidelberg: Physica-Verlag,[1992-.

[187] H. Haario, E. Saksman, and J. Tamminen. "An adaptive Metropolis algorithm". *Bernoulli* 7.2 (2001), pp. 223–242. Publisher: Bernoulli Society for Mathematical Statistics and Probability.

[188] B. C. Hall. *Lie Groups, Lie Algebras, and Representations: An Elementary Introduction*. Graduate Texts in Mathematics 222. Springer, Cham, 2015.

[189] J. Han, Y. Luo, W. Wang, P. Zhang, and Z. Zhang. "From microscopic theory to macroscopic theory: a systematic study on modeling for liquid crystals". *Arch. Ration. Mech. Anal.* 215.3 (2015), pp. 741–809. Publisher: Springer.

[190] A. Haraux. "Some applications of the Łojasiewicz gradient inequality". *Commun. Pure Appl. Anal.* 6 (2012), pp. 2417–2427.

[191] C. R. Harris, K. J. Millman, S. J. v. d. Walt, R. Gommers, P. Virtanen, D. Cournapeau, E. Wieser, J. Taylor, S. Berg, N. J. Smith, R. Kern, M. Picus, S. Hoyer, M. H. v. Kerkwijk, M. Brett, A. Haldane, J. F. d. Río, M. Wiebe, P. Peterson, P. Gérard-Marchant, K. Sheppard, T. Reddy, W. Weckesser, H. Abbasi, C. Gohlke, and T. E. Oliphant. "Array programming with NumPy". *Nature* 585.7825 (2020), pp. 357–362.

[192] J. Haskovec. "Flocking dynamics and mean-field limit in the Cucker–Smale-type model with topological interactions". *Phys. D* 261 (2013), pp. 42–51.

[193] W. K. Hastings. "Monte Carlo sampling methods using Markov chains and their applications". *Biometrika* 57.1 (1970), pp. 97–109.

[194] M. Hauray and S. Mischler. "On Kac's chaos and related problems". *J. Funct. Anal.* 266 (2014), pp. 6055–6157.

[195] E. Hebey. *Nonlinear analysis on manifolds: Sobolev spaces and inequalities*. Courant lecture notes 5. American Mathematical Soc., 2000.

[196] C. K. Hemelrijk, H. Hildenbrandt, J. Reinders, and E. J. Stamhuis. "Emergence of oblong school shape: models and empirical data of fish". *Ethology* 116.11 (2010), pp. 1099–1112. Publisher: Wiley Online Library.

[197] H. Hildenbrandt, C. Carere, and C. Hemelrijk. "Self-organized aerial displays of thousands of starlings: a model". *Behavioral Ecology* 21.6 (2010), pp. 1349–1359.

[198] M. W. Hirsch, S. Smale, and R. L. Devaney. *Differential equations, dynamical systems, and an introduction to chaos*. Academic press, 2012.

[199] S. Hittmeir, L. Kanzler, A. Manhart, and C. Schmeiser. "Kinetic modelling of colonies of myxobacteria". *Kinet. Relat. Models* 14.1 (2021), p. 1.

[200] R. W. Hockney and J. W. Eastwood. *Computer Simulation Using Particles*. CRC Press, 1988.

[201] A. Horn. "Doubly stochastic matrices and the diagonal of a rotation matrix". *Amer. J. Math.* 76.3 (1954), pp. 620–630.

[202] J. F. Hughes, A. van Dam, M. McGuire, D. F. Sklar, J. D. Foley, S. K. Feiner, and A. Kurt. *Computer Graphics: Principles and Practice*. 3rd Edition. Addison-Wesley Professional, 2013.

[203] J. D. Hunter. "Matplotlib: A 2D graphics environment". *Comput Sci Eng.* 9.3 (2007), pp. 90–95.

[204] C. J. Ingham and E. Jacob. "Swarming and complex pattern formation in Paenibacillus vortex studied by imaging and tracking cells". *BMC Microbiol.* 8.1 (2008), p. 36.

[205] P.-E. Jabin. "A review of the mean field limits for Vlasov equations". *Kinet. Relat. Models* 7 (2014), pp. 661–711.

[206] P.-E. Jabin and S. Junca. "A Continuous Model For Ratings". *SIAM J. Appl. Math.* 75.2 (2015), pp. 420–442.

[207] P.-E. Jabin and Z. Wang. "Mean Field Limit for Stochastic Particle Systems". In: *Active Particles, Volume 1 : Advances in Theory, Models, and Applications*. Ed. by N. Bellomo, P. Degond, and E. Tadmor. Modeling and Simulation in Science, Engineering and Technology. Birkhäuser Basel, 2017, pp. 379–402.

[208] P.-E. Jabin and Z. Wang. "Quantitative estimates of propagation of chaos for stochastic systems with $W^{-1,\infty}$ kernels". *Invent. Math.* 214 (2018), pp. 523–591.

[209] J.-F. Jabir. "Rate of propagation of chaos for diffusive stochastic particle systems via Girsanov transformation". *arXiv preprint arXiv:1907.09096* (2019).

[210] J. Jacod and A. N. Shiryaev. *Limit Theorems for Stochastic Processes*. Second edition. Grundlehren der mathematischen Wissenschaften 288. Springer Berlin Heidelberg, 2003.

[211] A. Jakubowski. "On the Skorokhod topology". *Ann. Inst. Henri Poincaré Probab. Stat.* 22.3 (1986), pp. 263–285.

[212] A. Jasra, D. A. Stephens, and C. C. Holmes. "On population-based simulation for static inference". *Stat. Comput.* 17.3 (2007), pp. 263–279. Publisher: Springer.

[213] N. Jiang, Y.-L. Luo, and T.-F. Zhang. "Coupled Self-Organized Hydrodynamics and Navier-Stokes models: local well-posedness and the limit from the Self-Organized Kinetic-fluid models". *arXiv preprint arXiv:1712.10134* (2017).

[214] N. Jiang, L. Xiong, and T.-F. Zhang. "Hydrodynamic limits of the kinetic self-organized models". *SIAM J. Math. Anal.* 48.5 (2016), pp. 3383–3411. Publisher: SIAM.

[215] S. Jin, L. Li, and J.-G. Liu. "Random batch methods (RBM) for interacting particle systems". *arXiv preprint: arXiv:1812.10575* (2019).

[216] S. Jin and L. Li. "Random Batch Methods for classical and quantum interacting particle systems and statistical samplings". *arXiv preprint: arXiv:2104.04337* (2021).

[217] A. Joffe and M. Métivier. "Weak convergence of sequences of semimartingales with applications to multitype branching processes". *Adv. in Appl. Probab.* 18.1 (1986), pp. 20–65.

[218] B. Jourdain. "Diffusions with a nonlinear irregular drift coefficient and probabilistic interpretation of generalized Burgers' equations". *ESAIM Probab. Stat.* 1 (1997), pp. 339–355.

[219] B. Jourdain, T. Lelièvre, and B. Miasojedow. "Optimal scaling for the transient phase of Metropolis Hastings algorithms: The longtime behavior". *Bernoulli* 20.4 (2014).

[220] B. Jourdain, T. Lelièvre, and B. Miasojedow. "Optimal scaling for the transient phase of the random walk Metropolis algorithm: The mean-field limit". *Ann. Appl. Probab.* 25.4 (2015).

[221] B. Jourdain and S. Méléard. "Propagation of chaos and fluctuations for a moderate model with smooth initial data". *Ann. Inst. Henri Poincaré Probab. Stat.* 34.6 (1998), pp. 727–766. Publisher: Gauthier-Villars.

[222] A. Jüngel. *Entropy Methods for Diffusive Partial Differential Equations*. Springer, 2016.

[223] M. Kac. "Foundations of kinetic theory". In: *Proceedings of the Third Berkeley Symposium on Mathematical Statistics and Probability*. Vol. 3. University of California Press Berkeley and Los Angeles, California, 1956, pp. 171–197.

[224] M. Kac. "Some Probabilistic Aspects of the Boltzmann Equation". In: *The Boltzmann Equation. Acta Physica Austriaca (Supplementum X Proceedings of the International Symposium "100 Years Boltzmann Equation" in Vienna 4th–8th September 1972)*. Ed. by E. G. D. Cohen and W. Thirring. Springer Vienna, 1973, pp. 379–400.

[225] N. Kantas, A. Doucet, S. S. Singh, and J. M. Maciejowski. "An Overview of Sequential Monte Carlo Methods for Parameter Estimation in General State-Space Models". en. *IFAC Proceedings Volumes* 42.10 (2009), pp. 774–785.

[226] L. Kanzler and C. Schmeiser. "Kinetic Model for Myxobacteria with Directional Diffusion". *arXiv preprint: arXiv:2109.13184* (2021).

[227] I. Karatzas and S. Shreve. *Brownian Motion and Stochastic Calculus*. 2nd ed. Graduate Texts in Mathematics 113. Springer-Verlag New York, 1998.

[228] T. K. Karper, A. Mellet, and K. Trivisa. "Hydrodynamic limit of the kinetic Cucker–Smale flocking model". *Math. Models Methods Appl. Sci.* 25.01 (2015), pp. 131–163.

[229] J. Kennedy and R. Eberhart. "Particle swarm optimization". In: *Proceedings of ICNN'95 - International Conference on Neural Networks*. Vol. 4. Perth, WA, Australia: IEEE, 1995, pp. 1942–1948.

[230] J. Kent, A. M. Ganeiber, and K. V. Mardia. "A new unified approach for the simulation of a wide class of directional distributions". *J. Comput. Graph. Statist.* 27.2 (2018), pp. 291–301.

[231] C. Kipnis and C. Landim. *Scaling Limits of Interacting Particle Systems*. Grundlehren der mathematischen Wissenschaften 320. Springer Berlin Heidelberg, 1999.

[232] P. E. Kloeden and E. Platen. *Numerical Solution of Stochastic Differential Equations*. Applications of Mathematics 23. Springer, Berlin, Heidelberg, 1992.

[233] V. N. Kolokoltsov. *Nonlinear Markov Processes and Kinetic Equations*. Cambridge University Press, 2010.

[234] S. Kusuoka and Y. Tamura. "Gibbs measures for mean field potentials". *J. Fac. Sci. Univ. Tokyo* 31 (1984), pp. 223–245.

[235] D. Lacker. "On a strong form of propagation of chaos for McKean-Vlasov equations". *Electron. Commun. Probab.* 23.45 (2018), pp. 1–11.

[236] D. Lacker. "Hierarchies, entropy, and quantitative propagation of chaos for mean field diffusions". *arXiv preprint: arXiv:2105.02983* (2021).

[237] O. E. Lanford. "Time evolution of large classical systems". In: *Dynamical systems, theory and applications*. Springer, 1975, pp. 1–111.

[238] P. D. Lax. *Linear Algebra and Its Applications*. Second. Wiley Interscience, 2007.

[239] T. Lee. "Bayesian Attitude Estimation With the Matrix Fisher Distribution on SO(3)". *IEEE Trans. Automat. Contr.* 63.10 (2018), pp. 3377–3392.

[240] B. Leimkuhler and C. Matthews. *Molecular Dynamics With Deterministic and Stochastic Numerical Methods*. Interdisciplinary Applied Mathematics 39. Springer International Publishing, 2015.

[241] G. Letta. "Sur les théorèmes de Hewitt-Savage et de de Finetti". *Séminaire de probabilités de Strasbourg* 23 (1989), pp. 531–535.

[242] S. Lojasiewicz. "Sur les trajectoires du gradient d'une fonction analytique". *Seminari di geometria, Univ. Stud. Bologna, Bologna* 1982–1983 (1984), pp. 115–117.

[243] E. Luçon. "Large Population Asymptotics for Interacting Diffusions in a Quenched Random Environment". In: *From Particle Systems to Partial Differential Equations II*. Ed. by P. Gonçalves and A. J. Soares. Springer Proceedings in Mathematics & Statistics 129. Springer, Cham, 2015, pp. 231–251.

[244] L. B. Lucy. "An iterative technique for the rectification of observed distributions". *Astron. J.* 79 (1974), p. 745.

[245] F. Malrieu. "Logarithmic Sobolev inequalities for some nonlinear PDE's". *Stochastic Process. Appl.* 95 (2001), pp. 109–132.

[246] K. V. Mardia. "Statistics of Directional Data". *J. R. Stat. Soc. Ser. B. Stat. Methodol.* 37.3 (1975), pp. 349–393.

[247] K. V. Mardia and P. E. Jupp, eds. *Directional Statistics*. Wiley Series in Probability and Statistics. John Wiley & Sons, Inc., 1999.

[248] D. Matthes and G. Toscani. "On Steady Distributions of Kinetic Models of Conservative Economies". *J. Stat. Phys.* 130.6 (2008), pp. 1087–1117.

[249] H. P. McKean. "Propagation of chaos for a class of non-linear parabolic equations". In: *Stochastic Differential Equations.* Lecture Series in Differential Equations, Session 7, Catholic Univ. Arlington, Va.: Air Force Office of Scientific Research, Office of Aerospace Research, 1967, pp. 41–57.

[250] H. P. McKean. "Propagation of chaos for a class of non-linear parabolic equations". In: *Lecture Series in Differential Equations, Volume 2.* Ed. by A. K. Aziz. Van Nostrand Mathematical Studies 19. Van Nostrand Reinhold Company, 1969, pp. 177–194.

[251] S. Mei, A. Montanari, and P.-M. Nguyen. "A mean field view of the landscape of two-layer neural networks". *Proc. Natl. Acad. Sci. USA* 115.33 (2018), E7665–E7671.

[252] S. Méléard. "Asymptotic Behaviour of some interacting particle systems; McKean-Vlasov and Boltzmann models". In: *Probabilistic Models for Nonlinear Partial Differential Equations.* Ed. by D. Talay and L. Tubaro. Lecture Notes in Mathematics 1627. Springer-Verlag Berlin Heidelberg, 1996.

[253] K. L. Mengersen and R. L. Tweedie. "Rates of convergence of the Hastings and Metropolis algorithms". *Ann. Statist.* 24.1 (1996), pp. 101–121. Publisher: Institute of Mathematical Statistics.

[254] S. Merino-Aceituno. "Isotropic wave turbulence with simplified kernels: Existence, uniqueness, and mean-field limit for a class of instantaneous coagulation-fragmentation processes". *J. Math. Phys.* 57.12 (2016), p. 121501.

[255] N. Metropolis, A. W. Rosenbluth, M. N. Rosenbluth, A. H. Teller, and E. Teller. "Equation of State Calculations by Fast Computing Machines". *J. Chem. Phys.* 21.6 (1953), pp. 1087–1092.

[256] N. Metropolis and S. Ulam. "The Monte Carlo Method". *J. Amer. Statist. Assoc.* 44.247 (1949), pp. 335–341.

[257] S. Mischler and C. Mouhot. "Kac's program in kinetic theory". *Invent. Math.* 193.1 (2013), pp. 1–147. Publisher: Springer.

[258] S. Mischler, C. Mouhot, and B. Wennberg. "A new approach to quantitative propagation of chaos for drift, diffusion and jump processes". *Probab. Theory Related Fields* 161 (2015), pp. 1–59.

[259] Y. S. Mishura and A. Y. Veretennikov. "Existence and uniqueness theorems for solutions of McKean-Vlasov stochastic equations". *arXiv preprint arXiv:1603.02212* (2020).

[260] P. Monmarché. "Elementary coupling approach for non-linear perturbation of Markov processes with mean-field jump mechanims and related problems." *arXiv preprint arXiv:1809.10953* (2018).

[261] J. Morales and D. Poyato. "On the trend to global equilibrium for Kuramoto Oscillators". *arXiv preprint arXiv:1908.07657* (2019).

[262] S. Motsch. "Vicsek_microFlat". *GitHub repository* (2016).

[263] S. Motsch and L. Navoret. "Numerical simulations of a nonconservative hyperbolic system with geometric constraints describing swarming behavior". *Multiscale Model. Simul.* 9.3 (2011), pp. 1253–1275. Publisher: SIAM.

[264] S. Motsch and D. Peurichard. "From short-range repulsion to Hele-Shaw problem in a model of tumor growth". *J. Math. Biol.* 76.1-2 (2018), pp. 205–234.

[265] A. Muntean and F. Toschi, eds. *Collective Dynamics from Bacteria to Crowds: An Excursion Through Modeling, Analysis and Simulation*. CISM International Centre for Mechanical Sciences 553. Springer, Vienna, 2014.

[266] G. Naldi, L. Pareschi, and G. Toscani, eds. *Mathematical Modeling of Collective Behavior in Socio-Economic and Life Sciences*. Modeling and Simulation in Science, Engineering and Technology. Birkhäuser Boston, 2010.

[267] J. Nash. "The Imbedding Problem for Riemannian Manifolds". *Ann. Math.* 63.1 (1956), p. 20.

[268] F. Natterer and F. Wübbeling. *Mathematical Methods in Image Reconstruction*. Vol. 5. SIAM Monographs on Mathematical Modeling and Computation. Society for Industrial and Applied Mathematics, 2001.

[269] Nobel Foundation. *The Nobel Prize in Physics 1985*.

[270] Nobel Foundation. *The Nobel Prize in Physics 2016*.

[271] K. O'Keeffe and C. Bettstetter. "A review of swarmalators and their potential in bio-inspired computing". In: *Micro- and Nanotechnology Sensors, Systems, and Applications XI*. Ed. by M. S. Islam and T. George. Baltimore, United States: SPIE, 2019, p. 85.

[272] K. P. O'Keeffe, H. Hong, and S. H. Strogatz. "Oscillators that sync and swarm". *Nat. Commun.* 8.1 (2017), p. 1504.

[273] K. Oelschläger. "A law of large numbers for moderately interacting diffusion processes". *Zeitschrift für Wahrscheinlichkeitstheorie und Verwandte Gebiete* 69.2 (1985), pp. 279–322.

[274] L. Pareschi and G. Toscani. "Self-Similarity and Power-Like Tails in Nonconservative Kinetic Models". *J. Stat. Phys.* 124.2-4 (2006), pp. 747–779.

[275] A. Paszke, S. Gross, F. Massa, A. Lerer, J. Bradbury, G. Chanan, T. Killeen, Z. Lin, N. Gimelshein, L. Antiga, A. Desmaison, A. Kopf, E. Yang, Z. DeVito, M. Raison, A. Tejani, S. Chilamkurthy, B. Steiner, L. Fang, J. Bai, and S. Chintala. "PyTorch: An Imperative Style, High-Performance Deep Learning Library". In: *Advances in Neural Information Processing Systems*. Ed. by H. Wallach, H. Larochelle, A. Beygelzimer, F. Alché-Buc, E. Fox, and R. Garnett. Vol. 32. Curran Associates, Inc., 2019.

[276] A. Paszke, S. Gross, S. Chintala, G. Chanan, E. Yang, Z. DeVito, Z. Lin, A. Desmaison, L. Antiga, and A. Lerer. "Automatic differentiation in PyTorch". In: *Proceedings of Neural Information Processing Systems*. 2017.

[277] L. Pédèches. "Asymptotic properties of various stochastic Cucker-Smale dynamics". *Discrete Contin. Dyn. Syst.* 38.6 (2018), pp. 2731–2762.

[278] L. Perko. *Differential equations and dynamical systems*. Vol. 7. Springer Science & Business Media, 2013.

[279] A. Perna, B. Granovskiy, S. Garnier, S. C. Nicolis, M. Labédan, G. Theraulaz, V. Fourcassié, and D. J. T. Sumpter. "Individual Rules for Trail Pattern Formation in Argentine Ants (Linepithema humile)". en. *PLoS Computat. Biol.* 8.7 (2012). Ed. by B. Ermentrout, e1002592.

[280] M. J. Piggott and V. Solo. "Geometric Euler–Maruyama Schemes for Stochastic Differential Equations in SO(n) and SE(n)". *SIAM J. Numer. Anal.* 54.4 (2016), pp. 2490–2516.

[281] R. Pinnau, C. Totzeck, O. Tse, and S. Martin. "A consensus-based model for global optimization and its mean-field limit". *Math. Models Methods Appl. Sci.* 27.01 (2017), pp. 183–204.

[282] M. Pulvirenti. "Kinetic limits for stochastic particle systems". In: *Probabilistic Models for Nonlinear Partial Differential Equations*. Ed. by D. Talay and L. Tubaro. Lecture Notes in Mathematics 1627. Springer-Verlag Berlin Heidelberg, 1996.

[283] A. Quarteroni, R. Sacco, and F. Saleri. *Numerical mathematics*. Vol. 37. Springer Science & Business Media, 2010.

[284] A. Rahman. "Correlations in the Motion of Atoms in Liquid Argon". *Phys. Rev. Lett.* 136.2A (1964), A405–A411.

[285] C. W. Reynolds. "Flocks, herds and schools: A distributed behavioral model". In: *Proceedings of the 14th annual conference on Computer graphics and interactive techniques - SIGGRAPH '87*. ACM Press, 1987, pp. 25–34.

[286] W. H. Richardson. "Bayesian-Based Iterative Method of Image Restoration". *J. Opt. Soc. Am.* 62.1 (1972), pp. 55–59. Publisher: OSA.

[287] M. L. Rizzo and G. J. Székely. "Energy distance". *Wiley interdisciplinary reviews: Computational Statistics* 8.1 (2016), pp. 27–38. Publisher: Wiley Online Library.

[288] C. Robert and G. Casella. *Monte Carlo statistical methods*. Springer Science & Business Media, 2013.

[289] C. P. Robert. "The Metropolis–Hastings Algorithm". In: *Wiley StatsRef: Statistics Reference Online*. Ed. by N. Balakrishnan, T. Colton, B. Everitt, W. Piegorsch, F. Ruggeri, and J. Teugels. John Wiley & Sons, 2015.

[290] C. P. Robert and G. Casella. *Monte Carlo Statistical Methods*. Springer Texts in Statistics. Springer, New York, 2004.

[291] V. Rokhlin. "Rapid solution of integral equations of classical potential theory". *J. Computat. Phys.* 60.2 (1985), pp. 187–207.

[292] G. M. Rotskoff and E. Vanden-Eijnden. "Trainability and Accuracy of Neural Networks: An Interacting Particle System Approach". *arXiv preprint: arXiv:1805.00915* (2019).

[293] E. Salamin. *Application of quaternions to computation with rotations*. Tech. rep. Working Paper, 1979.

[294] S. Salem. "A gradient flow approach to propagation of chaos". *Discrete Contin. Dyn. Syst.* 40.10 (2020), pp. 5729–5754.

[295] A. Sarlette, S. Bonnabel, and R. Sepulchre. "Coordinated Motion Design on Lie Groups". *IEEE Trans. Automat. Contr.* 55.5 (2010), pp. 1047–1058.

[296] D. Scherer, P. Dubois, and B. Sherwood. "VPython: 3D interactive scientific graphics for students". *Comput Sci Eng.* 2.5 (2000), pp. 56–62.

[297] C. Schmeiser. *Entropy methods*. 2018.

[298] G. Schou. "Estimation of the concentration parameter in von Mises–Fisher distributions". *Biometrika* 65.2 (1978), pp. 369–377. Publisher: Oxford University Press.

[299] S. Shankar, M. J. Bowick, and M. C. Marchetti. "Topological sound and flocking on curved surfaces". *Phys. Rev. X* 7.3 (2017), p. 031039.

[300] H. Sigurgeirsson, A. Stuart, and W.-L. Wan. "Algorithms for Particle-Field Simulations with Collisions". *J. Comput. Phys.* 172.2 (2001), pp. 766–807.

[301] B. Simon. *Representations of finite and compact groups*. Graduate Studies in Mathematics 10. American Mathematical Soc., 1996.

[302] J. Sirignano and K. Spiliopoulos. "Mean Field Analysis of Neural Networks: A Law of Large Numbers". *SIAM J. Appl. Math.* 80.2 (2020), pp. 725–752.

[303] K. Sone and Y. Ashida. "Anomalous Topological Active Matter". *Phys. Rev. Lett.* 123.20 (2019), p. 205502.

[304] A. Souslov, B. C. Van Zuiden, D. Bartolo, and V. Vitelli. "Topological sound in active-liquid metamaterials". *Nature Phys.* 13.11 (2017), p. 1091.

[305] A.-S. Sznitman. "Équations de type de Boltzmann, spatialement homogènes". *Zeitschrift für Wahrscheinlichkeitstheorie und Verwandte Gebiete* 66 (1984), pp. 559–592.

[306] A.-S. Sznitman. "Nonlinear Reflecting Diffusion Process, and the Propagation of Chaos and Fluctuations Associated". *J. Funct. Anal.* 56 (1984), pp. 311–336.

[307] A.-S. Sznitman. "Topics in propagation of chaos". In: *Éc. Été Probab. St.-Flour XIX—1989*. Springer, 1991, pp. 165–251.

[308] D. Talay and L. Tubaro, eds. *Probabilistic Models for Nonlinear Partial Differential Equations*. Lecture Notes in Mathematics 1627. Springer-Verlag Berlin Heidelberg, 1996.

[309] H. Tanaka. "Some probabilistic problems in the spatially homogeneous Boltzmann equation". In: *Theory and Application of Random Fields, Proceedings of the IFIP-WG 7/1 Working Conference, Bangalore 1982*. Ed. by G. Kallianpur. Lecture Notes in Control and Information Sciences. Springer-Verlag Berlin Heidelberg, 1983, pp. 258–267.

[310] R. C. Tolman. *The principles of statistical mechanics*. Courier Corporation, 1979.

[311] M. Tomasevic. "Propagation of chaos for stochastic particle systems with singular mean-field interaction of L^p-L^q type". *hal preprint: hal-03086253* (2020).

[312] J. Toner and Y. Tu. "Flocks, herds, and schools: A quantitative theory of flocking". *Phys. Rev. E* 58.4 (1998), pp. 4828–4858.

[313] G. Toscani. “Kinetic models of opinion formation”. *Commun. Math. Sci.* 4.3 (2006), pp. 481–496.

[314] C. Totzeck. “Trends in Consensus-based optimization”. *arXiv preprint: arXiv:2104.01383* (2021).

[315] C. Totzeck, R. Pinnau, S. Blauth, and S. Schotthöfer. “A Numerical Comparison of Consensus-Based Global Optimization to other Particle-based Global Optimization Schemes”. *PAMM. Proc. Appl. Math. Mech.* 18.1 (2018).

[316] H. F. Trotter. “Approximation of semi-groups of operators”. *Pacific J. Math.* 8.4 (1958), pp. 887–919.

[317] P. Vanetti, A. Bouchard-Côté, G. Deligiannidis, and A. Doucet. “Piecewise-Deterministic Markov Chain Monte Carlo”. *arXiv preprint arXiv:1707.05296* (2017).

[318] A. Y. Veretennikov. “On ergodic measures for McKean–Vlasov stochastic equations”. In: *Monte Carlo and Quasi-Monte Carlo Methods 2004*. Ed. by H. Niederreiter and D. Talay. 2006, pp. 471–486.

[319] L. Verlet. “Computer "Experiments" on Classical Fluids. I. Thermodynamical Properties of Lennard-Jones Molecules”. *Phys. Rev.* 159.1 (1967), pp. 98–103.

[320] R. Vershynin. “Introduction to the non-asymptotic analysis of random matrices”. In: *Compressed sensing, theory and applications*. Ed. by Y. C. Eldar and G. Kutinyok. Cambridge University Press, 2012, pp. 210–260.

[321] T. Vicsek, A. Czirók, E. Ben-Jacob, I. Cohen, and O. Shochet. “Novel Type of Phase Transition in a System of Self-Driven Particles”. *Phys. Rev. Lett.* 75.6 (1995), pp. 1226–1229.

[322] T. Vicsek and A. Zafeiris. “Collective motion”. *Phys. Rep.* 517.3-4 (2012), pp. 71–140.

[323] C. Villani. “Limite de champ moyen”. *Cours de DEA* (2001).

[324] C. Villani. “A Review of Mathematical Topics in Collisional Kinetic Theory”. In: *Handbook of Mathematical Fluid Dynamics*. Ed. by S. Friedlander and D. Serre. Vol. 1. Elsevier Science, 2002, pp. 71–74.

[325] C. Villani. “Cercignani’s conjecture is sometimes true and always almost true”. *Comm. Math. Phys.* 234.3 (2003), pp. 455–490. Publisher: Springer.

[326] C. Villani. *Topics in Optimal Transportation*. Graduate Studies in Mathematics 58. American Mathematical Society, 2003.

[327] C. Villani. “Hypocoercivity”. *Mem. Amer. Math. Soc.* 202.950 (2009).

[328] C. Villani. *Optimal Transport, Old and New*. Grundlehren der mathematischen Wissenschaften 338. Springer-Verlag Berlin Heidelberg, 2009.

[329] F.-Y. Wang. “Distribution dependent SDEs for Landau type equations”. *Stochastic Process. Appl.* 128 (2018), pp. 595–621.

[330] H. Wang and P. Hoffman. “A unified view on the rotational symmetry of equilibiria of nematic polymers, dipolar nematic polymers, and polymers in higher dimensional space”. *Commun. Math. Sci.* 6.4 (2008), pp. 949–974. Publisher: International Press of Boston.

[331] H. H. Wensink, J. Dunkel, S. Heidenreich, K. Drescher, R. E. Goldstein, H. Lowen, and J. M. Yeomans. “Meso-scale turbulence in living fluids”. *Proc. Natl. Acad. Sci. USA* 109.36 (2012), pp. 14308–14313.

[332] D. Williams. *Probability with Martingales*. Cambridge University Press, 1991.

[333] D. M. Woolley, R. F. Crockett, W. D. I. Groom, and S. G. Revell. “A study of synchronisation between the flagella of bull spermatozoa, with related observations”. *J. Exp. Biol.* 212.14 (2009), pp. 2215–2223.

[334] T. Yang, Y.-F. Li, M. Mahdavi, R. Jin, and Z.-H. Zhou. “Nyström method vs random Fourier features: A theoretical and empirical comparison”. In: *Advances in neural information processing systems*. 2012, pp. 476–484.

[335] H. Zhou and H. Wang. “Stability of equilibria of nematic liquid crystalline polymers”. *Acta Math. Sci.* 31.6 (2011), pp. 2289–2304.